

254

Topics in Current Chemistry

Editorial Board:

**A. de Meijere · K. N. Houk · H. Kessler · J.-M. Lehn · S.V. Ley
S. L. Schreiber · J. Thiem · B. M. Trost · F. Vögtle · H. Yamamoto**

Topics in Current Chemistry

Recently Published and Forthcoming Volumes

Anion Sensing

Volume Editor: Stibor, I.
Vol. 255, 2005

Organic Solid State Reactions

Volume Editor: Toda, F.
Vol. 254, 2005

DNA Binders and Related Subjects

Volume Editors: Waring, M.J., Chaires, J.B.
Vol. 253, 2005

Contrast Agents III

Volume Editor: Krause, W.
Vol. 252, 2005

Chalcogenocarboxylic Acid Derivatives

Volume Editor: Kato, S.
Vol. 251, 2005

New Aspects in Phosphorus Chemistry V

Volume Editor: Majoral, J.-P.
Vol. 250, 2005

Templates in Chemistry II

Volume Editors: Schalley, C.A., Vögtle, F.,
Dötz, K.H.
Vol. 249, 2005

Templates in Chemistry I

Volume Editors: Schalley, C.A., Vögtle, F.,
Dötz, K.H.
Vol. 248, 2004

Collagen

Volume Editors: Brinckmann, J.,
Notbohm, H., Müller, P.K.
Vol. 247, 2005

New Techniques in Solid-State NMR

Volume Editor: Klinowski, J.
Vol. 246, 2005

Functional Molecular Nanostructures

Volume Editor: Schlüter, A.D.
Vol. 245, 2005

Natural Product Synthesis II

Volume Editor: Mulzer, J.
Vol. 244, 2005

Natural Product Synthesis I

Volume Editor: Mulzer, J.
Vol. 243, 2005

Immobilized Catalysts

Volume Editor: Kirschning, A.
Vol. 242, 2004

Transition Metal and Rare Earth Compounds III

Volume Editor: Yersin, H.
Vol. 241, 2004

The Chemistry of Pheromones and Other Semiochemicals II

Volume Editor: Schulz, S.
Vol. 240, 2005

The Chemistry of Pheromones and Other Semiochemicals I

Volume Editor: Schulz, S.
Vol. 239, 2004

Orotidine Monophosphate Decarboxylase

Volume Editors: Lee, J.K., Tantillo, D.J.
Vol. 238, 2004

Long-Range Charge Transfer in DNA II

Volume Editor: Schuster, G.B.
Vol. 237, 2004

Long-Range Charge Transfer in DNA I

Volume Editor: Schuster, G.B.
Vol. 236, 2004

Spin Crossover in Transition Metal Compounds III

Volume Editors: Gülich, P., Goodwin, H.A.
Vol. 235, 2004

Spin Crossover in Transition Metal Compounds II

Volume Editors: Gülich, P., Goodwin, H.A.
Vol. 234, 2004

Spin Crossover in Transition Metal Compounds I

Volume Editors: Gülich, P., Goodwin, H.A.
Vol. 233, 2004

Organic Solid State Reactions

Volume Editor: Fumio Toda

With contributions by

D. Braga · D. D'Addario · S. Giaffreda · F. Grepioni · W. Jones
G. Kaupp · K. Komatsu · L. Maini · A. Matsumoto · M. Polito
M. Sakamoto · J. R. Scheffer · F. Toda · A.V. Trask · W. Xia



Springer

The series *Topics in Current Chemistry* presents critical reviews of the present and future trends in modern chemical research. The scope of coverage includes all areas of chemical science including the interfaces with related disciplines such as biology, medicine and materials science. The goal of each thematic volume is to give the nonspecialist reader, whether at the university or in industry, a comprehensive overview of an area where new insights are emerging that are of interest to a larger scientific audience.

As a rule, contributions are specially commissioned. The editors and publishers will, however, always be pleased to receive suggestions and supplementary information. Papers are accepted for *Topics in Current Chemistry* in English.

In references *Topics in Current Chemistry* is abbreviated Top Curr Chem and is cited as a journal.

Visit the TCC content at springerlink.com

Library of Congress Control Number: 2004110638

ISSN 0340-1022

ISBN 3-540-22982-5 **Springer Berlin Heidelberg New York**

DOI 10.1007/b98357

This work is subject to copyright. All rights are reserved, whether the whole or part of the material is concerned, specifically the rights of translation, reprinting, reuse of illustrations, recitation, broadcasting, reproduction on microfilms or in any other ways, and storage in data banks. Duplication of this publication or parts thereof is only permitted under the provisions of the German Copyright Law of September 9, 1965, in its current version, and permission for use must always be obtained from Springer-Verlag. Violations are liable to prosecution under the German Copyright Law.

Springer is a part of Springer Science+Business Media

springeronline.com

© Springer-Verlag Berlin Heidelberg 2005

Printed in The Netherlands

The use of general descriptive names, registered names, trademarks, etc. in this publication does not imply, even in the absence of a specific statement, that such names are exempt from the relevant protective laws and regulations and therefore free for general use.

Cover design: KunkelLopka, Heidelberg/design & production GmbH, Heidelberg

Typesetting: Fotosatz-Service Köhler GmbH, Würzburg

Printed on acid-free paper 02/3141 xv – 5 4 3 2 1 0

Volume Editor

Prof. Dr. Fumio Toda
Department of Chemistry
Okayama University of Science,
Ridai-cho 1-1
Okayama 700-0005, Japan
toda@chem.ous.ac.jp

Editorial Board

Prof. Dr. Armin de Meijere
Institut für Organische Chemie
der Georg-August-Universität
Tammannstraße 2
37077 Göttingen, Germany
ameijer1@uni-goettingen.de

Prof. Dr. Horst Kessler
Institut für Organische Chemie
TU München
Lichtenbergstraße 4
85747 Garching, Germany
kessler@ch.tum.de

Prof. Steven V. Ley
University Chemical Laboratory
Lensfield Road
Cambridge CB2 1EW, Great Britain
svl1000@cus.cam.ac.uk

Prof. Dr. Joachim Thiem
Institut für Organische Chemie
Universität Hamburg
Martin-Luther-King-Platz 6
20146 Hamburg, Germany
thiem@chemie.uni-hamburg.de

Prof. Dr. Fritz Vögtle
Kekulé-Institut für Organische Chemie
und Biochemie der Universität Bonn
Gerhard-Domagk-Straße 1
53121 Bonn, Germany
voegt@uni-bonn.de

Prof. K.N. Houk
Department of Chemistry and Biochemistry
University of California
405 Hilgard Avenue
Los Angeles, CA 90024-1589, USA
houk@chem.ucla.edu

Prof. Jean-Marie Lehn
Institut de Chimie
Université de Strasbourg
1 rue Blaise Pascal, B.P.Z. 296/R8
67008 Strasbourg Cedex, France
lehn@chimie.u-strasbg.fr

Prof. Stuart L. Schreiber
Chemical Laboratories
Harvard University
12 Oxford Street
Cambridge, MA 02138-2902, USA
sls@slsiris.harvard.edu

Prof. Barry M. Trost
Department of Chemistry
Stanford University
Stanford, CA 94305-5080, USA
bmtrost@leland.stanford.edu

Prof. Hisashi Yamamoto
Arthur Holly Compton Distinguished
Professor
Department of Chemistry
The University of Chicago
5735 South Ellis Avenue
Chicago, IL 60637
773-702-5059, USA
yamamoto@uchicago.edu

Topics in Current Chemistry also Available Electronically

For all customers who have a standing order to Topics in Current Chemistry, we offer the electronic version via SpringerLink free of charge. Please contact your librarian who can receive a password for free access to the full articles by registration at:

springerlink.com

If you do not have a subscription, you can still view the tables of contents of the volumes and the abstract of each article by going to the SpringerLink Homepage, clicking on “Browse by Online Libraries”, then “Chemical Sciences”, and finally choose Topics in Current Chemistry.

You will find information about the

- Editorial Board
- Aims and Scope
- Instructions for Authors
- Sample Contribution

at springeronline.com using the search function.

Preface

Organic reactions in the absence of solvent, so called “Organic Solid-State Reactions”, have been well established as proceeding much more efficiently and faster than solution reactions in many cases, since solid-state reactions are infinitely high-concentration reactions. Organic solid-state reactions proceed even more selectively than solution reactions in some cases, since substrate molecules in solids or crystals are ordered regularly. Solid-state reactions are important not only for their high efficiency and selectivity but also for their simplicity and cleanness. In other words, solid state reactions may be regarded as more economical and ecologically favorable procedures in chemistry.

Organic solid-state reactions are also useful for studying molecular dynamics, since dynamic behavior of molecules in the solid-state can easily be monitored by spectral measurements and X-ray analysis. For example, reaction mechanisms can easily be clarified by studying molecular dynamics in the solid state.

In this volume, thermochemical and photochemical reactions in the solid state which have been studied mainly during the last five years by eight research groups are included. The editor hopes that this volume will contribute to the further development of organic solid-state reactions and solid-state chemistry.

Fumio Toda

Okayama, November 2004

Contents

| | |
|---|-----|
| Thermal and Photochemical Reactions in the Solid-State | |
| F. Toda | 1 |
| Crystal Engineering of Organic Cocrystals by the Solid-State Grinding Approach | |
| A.V. Trask · W. Jones | 41 |
| Intra-Solid and Inter-Solid Reactions of Molecular Crystals: a Green Route to Crystal Engineering | |
| D. Braga · D. D'Addario · S. L. Giaffreda · L. Maini · M. Polito · F. Grepioni | 71 |
| Organic Solid-State Reactions with 100% Yield | |
| G. Kaupp | 95 |
| The Mechanochemical Solid-State Reaction of Fullerenes | |
| K. Komatsu | 185 |
| Photochemical Aspects of Thiocarbonyl Compounds in the Solid-State | |
| M. Sakamoto | 207 |
| Asymmetric Induction in Organic Photochemistry via the Solid-State Ionic Chiral Auxiliary Approach | |
| J. R. Scheffer · W. Xia | 233 |
| Reactions of 1,3-Diene Compounds in the Crystalline State | |
| A. Matsumoto | 263 |
| Author Index Volumes 201–254 | 307 |
| Subject Index | 309 |

Contents of Volume 248

Templates in Chemistry I

Volume Editors: Christoph A. Schalley · Fritz Vögtle · Karl Heinz Dötz
ISBN 3-540-22547-1

Spacer-Controlled Multiple Functionalization of Fullerenes

C. Thilgen · S. Sergeev · F. Diederich

Chromium-Templated Benzannulation and Haptotropic Metal Migration

K. H. Dötz · B. Wenzel · H. C. Jahr

Supramolecular Templating in the Formation of Helicates

M. Albrecht

Hydrogen-Bond-Mediated Template Synthesis of Rotaxanes, Catenanes, and Knotanes

C. A. Schalley · T. Weilandt · J. Brüggemann · F. Vögtle

Template-Controlled Synthesis in the Solid-State

L. R. MacGillivray · G. S. Papaefstathiou · T. Frišćić · D. B. Varshney ·
T. D. Hamilton

Gels as Templates for Nanotubes

J. H. Jung · S. Shinkai

Contents of Volume 249

Templates in Chemistry II

Volume Editors: Christoph A. Schalley · Fritz Vögtle · Karl Heinz Dötz
ISBN 3-540-23087-4

First Considerations: Principles, Classification, and History
D. H. Busch

Macrocycle Synthesis Through Templatation
Z. R. Laughrey · B. C. Gibb

**Macrocycles and Complex Three-Dimensional Structures
Comprising Pt(II) Building Blocks**
A. Kaiser · P. Bäuerle

Templated Synthesis of Interlocked Molecules
F. Aricó · J. D. Badjic · S. J. Cantrill · A. H. Flood · K. C. F. Leung · Y. Liu ·
J. F. Stoddart

Molecular Knots
C. Dietrich-Buchecker · B. X. Colasson · J.-P. Sauvage

Templatation in Noncovalent Synthesis of Hydrogen-Bonded Rosettes
M. Crego-Calama · D. N. Reinhoudt · M. G. J. ten Cate

Imprinted Polymers
A. J. Hall · M. Emgenbroich · B. Sellergren

Thermal and Photochemical Reactions in the Solid State

Fumio Toda (✉)

Department of Chemistry, Okayama University of Science, Ridai-cho 1-1,
 Okayama 700-0005, Japan
toda@chem.ous.ac.jp

| | | |
|----------|--|-----------|
| 1 | Introduction | 1 |
| 2 | Thermal Reactions | 2 |
| 2.1 | Bromination Reactions | 2 |
| 2.2 | Stobbe Condensation and O-Silylation Reactions | 6 |
| 2.3 | Claisen and Cannizzaro Reactions | 9 |
| 2.4 | Robinson Annulation Reactions in a One-Pot Process | 11 |
| 3 | One-Pot Preparative Method of Optically Active Compounds by a Combination of Solid–Solid Reaction and Enantioselective Inclusion Complexation with a Chiral Host in a Water Suspension Medium | 12 |
| 4 | Mechanistic Study of Thermal Solid-State Reactions | 16 |
| 4.1 | Thorpe Reactions | 16 |
| 4.2 | Rap–Stoermer Reactions | 18 |
| 4.3 | Benzoylation Reactions of Phenol and Naphthol Derivatives | 22 |
| 5 | Crystal-to-Crystal Reactions | 25 |
| 5.1 | Crystal-to-Crystal Cyclization Reactions of Allene Derivatives | 26 |
| 5.2 | Racemic Crystal-to-Conglomerate Crystal Transformation Reactions in 2,2′-Dihydroxy-1,1′-binaphthyl-Me ₄ N ⁺ Cl [−] Complex | 28 |
| 5.3 | Enantioselective Reactions | 29 |
| 6 | Photochemical Reactions | 32 |
| 6.1 | Intramolecular Photoreactions | 32 |
| 6.2 | Intermolecular Photoreactions | 36 |
| | References | 39 |

1 Introduction

In this chapter we describe efficient thermal and photochemical reactions in the solid state which have been studied in our research group and published during 1999–2004. Some stereo- and enantioselective reactions in crystalline inclusion compounds are also described, together with their mechanisms, which were studied by spectroscopic and X-ray diffraction techniques.

Thermal and photochemical reactions in the solid state which were studied before 1999 are summarized in reviews [1] and books [2].

2

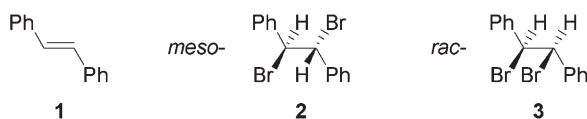
Thermal Reactions

Thermal solid-state reactions were carried out by keeping a mixture of powdered reactant and reagent at room temperature or elevated temperature, or by mixing with pestle and mortar. In some cases, the solid-state reactions proceed much more efficiently in a water suspension medium or in the presence of a small amount of solvent. Sometimes, a mixture of solid reactant and reagent turns to liquid as the reaction proceeds. All these reactions are called solid-state reactions in this chapter. Solid-state reactions were found to be useful in the study of reaction mechanisms, since it is easy to monitor the reaction by continuous measurement of IR spectra.

2.1

Bromination Reactions

The stereochemistry of addition reactions of Br_2 to olefins is difficult to control. For example, the reaction of (*E*)-stilbene (**1**) with Br_2 in CH_2Cl_2 gives a 84:16 mixture of *meso*- (**2**) and *rac*-1,2-dibromo-1,2-diphenylethane (**3**) in 98%



yield. The reaction of **1** with Br_2 vapor gives a 62:38 mixture of **2** and **3** in only 20% yield. However, solid-state reaction of **1** with **7** gave only **2** in 71% yield. For example, after keeping a mixture of powdered **1** and powdered **7** at room temperature for 168 h in the solid state, water was added to the reaction mixture and then the product was isolated by filtration to give **2** in 71% yield (Table 1) [3]. Bromination of chalcone (**4a**) with **7** in the solid state was also found to

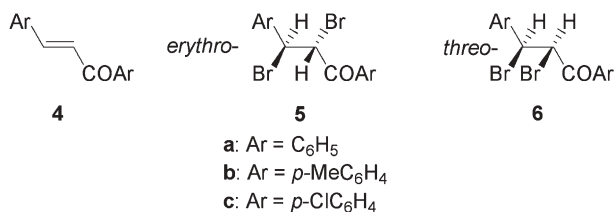


Table 1 Bromination of **1** with Br₂ or **7** under various conditions

| Reagent | Conditions | Reaction time (h) | Yield (%) | 2:3 Ratio |
|-----------------|---------------------------------|-------------------|-----------|-----------|
| Br ₂ | CH ₂ Cl ₂ | 12 | 98 | 84:16 |
| Br ₂ | Gas/solid | 64 | 20 | 62:38 |
| 7 | Solid/solid | 168 | 71 | 100:0 |
| 7 | Water suspension | 15 | 88 | 100:0 |

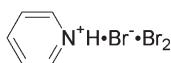
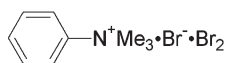
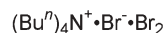
Table 2 Bromination of **4a** with Br₂ or **7** under various conditions

| Reagent | Conditions | Reaction time (h) | Yield (%) | 5a:6a Ratio |
|-----------------|---------------------------------|-------------------|-----------|-------------|
| Br ₂ | CH ₂ Cl ₂ | 0.5 | 90 | 86:14 |
| Br ₂ | Solid/solid | 4 | 89 | 100:0 |
| 7 | Water suspension | 1.5 | 90 | 100:0 |

Table 3 Bromination of **4a** with **7–9** in solid state

| Reagent | Reaction time (h) | Yield (%) | 5a:6a Ratio |
|----------|-------------------|-----------|-------------|
| 7 | 4 | 89 | 100:0 |
| 8 | 4 | 91 | 100:0 |
| 9 | 168 | 83 | 100:0 |

proceed efficiently and stereoselectively, although the solution reaction of **4a** and Br₂ in CH₂Cl₂ gave an 86:14 mixture of *erythro*- (**5a**) and *threo*-2,3-dibromo-1,3-diphenylpropan-1-one (**6a**) (Table 2). For example, when a mixture of powdered **4a** and powdered **7** was kept in the solid state for 4 h, **5a** was obtained exclusively in 89% yield (Table 2). As well as **7**, phenyltrimethylammonium tribromide (**8**)

**7****8****9**

was also effective for the stereoselective bromination of **4a**, but the sterically bulky reagent **9** takes a long time for the reaction to go to completion (Table 3).

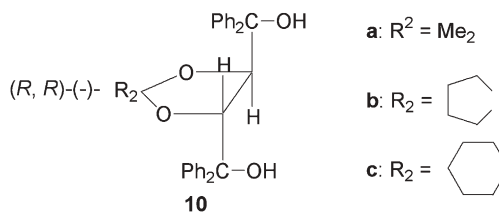
Very interestingly, bromination of the crystalline powder of **1** with **7** in a water suspension medium proceeded much more efficiently. For example, a suspension of powdered **1** and **7** in a small amount of water was stirred at room temperature for 15 h, and the reaction mixture was filtered and air-dried to

Table 4 Bromination of **4a–c** with **7** in a water suspension

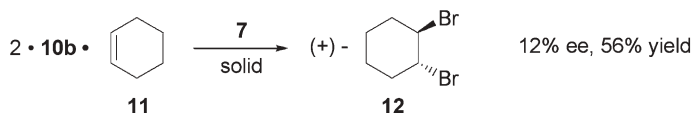
| Chalcone | Time (h) | Yield (%) | 5a:6a Ratio |
|-----------|----------|-----------|--------------------|
| 4a | 1.5 | 90 | 100:0 |
| 4b | 4 | 90 | 100:0 |
| 4c | 2 | 87 | 100:0 |

give **2** in 88% yield (Table 1). Bromination of chalcones **4a–c** was also found to proceed very efficiently and selectively in a water suspension medium. For example, a suspension of powdered **4a** and **7** in a small amount of water was stirred at room temperature for 1.5 h to give **5a** in 90% yield (Table 2). Similar treatment of **4b** and **4c** with **7** in a water suspension gave **5b** and **5c** in 90 and 87% yields, respectively (Table 4) [3]. In these reactions, ammonium bromides (**7–9**) play important roles not only as a reagent for the bromination, but also as a surfactant in the water medium. Water seems to act mainly as a suspension medium of reactant and reagent. However, water also seems to work as a kind of solvent, since solid-state reactions are accelerated in the presence of a small amount of organic solvent [4].

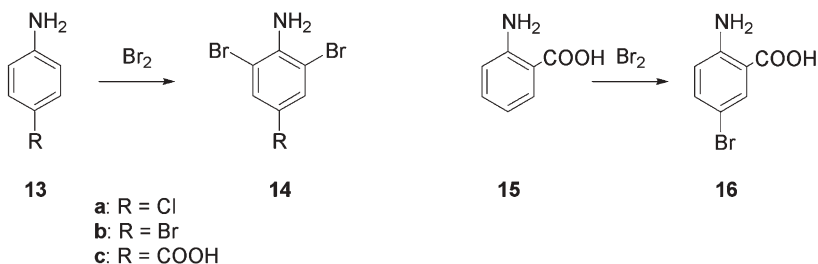
Enantioselective bromination of cyclohexene (**11**) in an inclusion complex with the optically active host compound, (*R,R*)-(-)-*trans*-4,5-bis(hydroxydiphenylmethyl)-2,2-dimethyl-1,3-dioxacyclopentane (**10a**) was accomplished.



When a solution of **10a** and **11** in ether was kept at room temperature for 12 h, a 2:1 inclusion complex of **10a** and **11** was obtained as colorless prisms (m.p. 134–137 °C) in 72% yield. When a powdered mixture of the inclusion crystal and **7** was kept at room temperature in the solid state for 3 days, (+)-*trans*-1,2-dibromocyclohexane (**12**) of 12% ee was obtained in 56% yield by distillation of the reaction mixture [3]. Much more efficient enantioselective reactions in the solid state are described in Sect. 6.



The direct bromination of aniline and phenol derivatives in solution results in polybromination to give a complex mixture. But bromination by gas–solid and solid–solid reactions proceeds more efficiently and selectively. Bromination by gas–solid reaction can be accomplished through a very simple procedure. For example, the powdered crystalline aniline **13** and Br₂ were placed in



Scheme 1

a desiccator in separate flasks and the apparatus was kept overnight at room temperature. The reaction mixture was washed with MeOH and recrystallized from aqueous EtOH to give a pure reaction product. By this procedure, **14a** and **14b** were obtained from **13a** and **13b** in 68 and 63% yields, respectively, although the solution reaction does not give the product (Table 5) [5]. The gas–solid bromination of **13c** and **15** gave **14c** and **16**, respectively, in quantitative yields (Scheme 1; Table 5) [5].

Bromination by solid–solid reaction with **7** or 2,4,4,6-tetrabromocyclohexa-2,5-dienone (**17**) is more effective. After a mixture of equimolar amounts of powdered **13a** and powdered **17** was kept for 10 h at room temperature, the

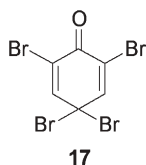
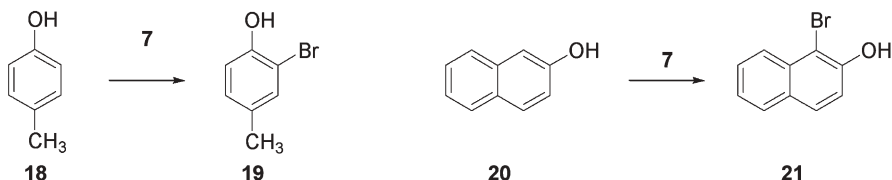


Table 5 Bromination in the solid state

| Reactant | Reagent | Product | Yield (%) | Yield (%) in solution reaction |
|------------|---------------------|------------|-----------|--------------------------------|
| 13a | Br ₂ gas | 14a | 68 | 0 |
| 13b | Br ₂ gas | 14b | 63 | 0 |
| 13c | Br ₂ gas | 14c | 100 | 82 |
| 15 | Br ₂ gas | 16 | 100 | 87 |
| 18 | 7 | 19 | 88 | 0 |
| 20 | 7 | 21 | 98 | 0 |

reaction mixture was washed with MeOH and recrystallized from aqueous EtOH to give **14a** in 87% yield. By similar treatments, **13b** and **15** gave **14b** (87%) and **16** (88%), respectively, in the yields indicated [5].

Solid-state reaction of *p*-cresol (**18**) and 2-naphthol (**20**) with **7** gave **19** (88%) and **21** (98%), respectively, in the yields indicated (Scheme 2), although these products cannot be obtained by solution reaction with Br₂ (Table 5) [5].

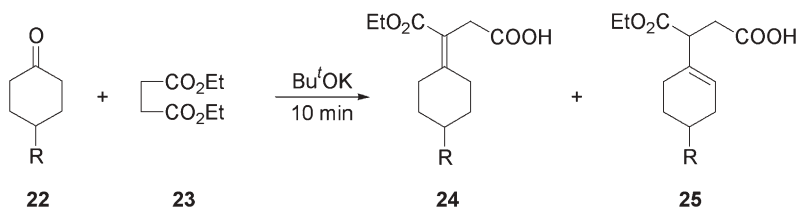


Scheme 2

2.2

Stobbe Condensation and *O*-Silylation Reactions

The Stobbe condensation is an important C–C bond forming reaction. However, when a Stobbe condensation reaction of cyclohexanone (**22a**) and diethyl succinate (**23**) is carried out under usual conditions such as heating under reflux in Bu^tOH in the presence of Bu^tOK, a mixture of cyclohexylidenesuccinic acid (**24a**) and cyclohexenylsuccinic acid (**25a**) is produced (Scheme 3; Table 6) [6]. Interestingly, Stobbe condensation reactions proceed efficiently and selectively in the absence of solvent. For example, reaction of **22a** and **23** in the presence of Bu^tOK at room temperature and at 80 °C gave **24a** (75%) and **25a** (92%), respectively, in the yields indicated (Table 6). When the solvent-free reactions were carried out at 40 and 60 °C, the **24a**:**25a** ratios were 65:35 and 10:90, respectively, although a solution reaction in Bu^tOH by heating under reflux gave a 27:73 mixture of **24a** and **25a** (Table 6). When the reaction temperature of the similar Stobbe reaction of 4-methylcyclohexanone (**22b**) with **23** was changed from room temperature to 80 °C, the **24b**:**25b** ratios were changed dramatically from 95:5 to 0:100 (Table 6) [7]. This reaction selectivity can be accomplished only under solvent-free conditions, since the Stobbe reaction in the solid state



Scheme 3

a: R = H
b: R = Me

Table 6 Stobbe condensation reaction of **22** and **23** in the solid state

| Cyclohexane | Reaction conditions | | Product | |
|-------------|---------------------|------------------|-----------|-------------|
| | Solvent | Temperature (°C) | Yield (%) | 24:25 Ratio |
| 22a | Bu ^t OH | Reflux | 84 | 27:73 |
| 22a | – | rt | 75 | 100:0 |
| 22a | – | 40 | 88 | 65:35 |
| 22a | – | 60 | 81 | 10:90 |
| 22a | – | 80 | 92 | 0:100 |
| 22b | – | rt | 55 | 95:5 |
| 22b | – | 80 | 85 | 0:100 |

proceeds both at room temperature and at elevated temperature, although its solution reaction does not proceed at room temperature.

The *O*-silylation reaction of alcohols is important as a protection method of hydroxyl groups. *O*-Silylations of liquid or crystalline alcohols with liquid or crystalline silyl chlorides were found to be possible in the solid state. For example, when a mixture of powdered *L*-menthol (**26**), *tert*-butyldimethylsilyl chloride (**27**), and imidazole (**28**) was kept at 60 °C for 5 h, *O*-*tert*-butyldimethylsilyl *L*-menthol (**29**) was obtained in 97% yield [8] (Scheme 4). Similar treatments of **26** with the liquid silyl chlorides, trimethyl- (**30a**) and triethylsilyl chloride (**30b**), gave the corresponding *O*-silylation products **31a** (89%) and **31b** (89%), respectively, in the yields indicated [8] (Scheme 4). However, *O*-silylation of triisopropyl- (**30c**) and triphenylsilyl chloride (**30d**) proceeded with difficulty even at 120 °C and gave **31c** (57%) and **31d** (70%), respectively, in relatively low yields. Nevertheless, when the solvent-free silylation reactions at 120 °C were carried out using two equivalents of **30c** and **30d**, **31c** (77%) and **31d** (99%) were obtained, respectively, in relatively high yields.

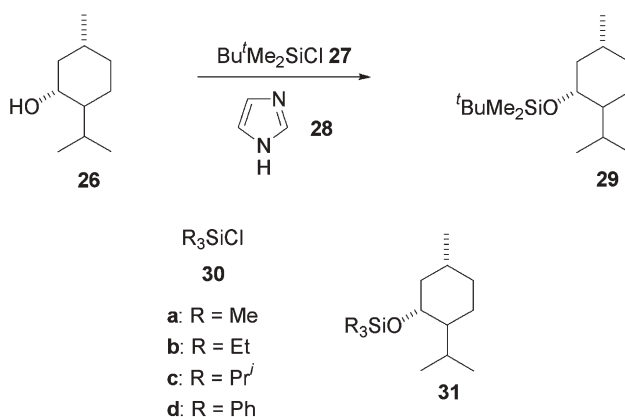
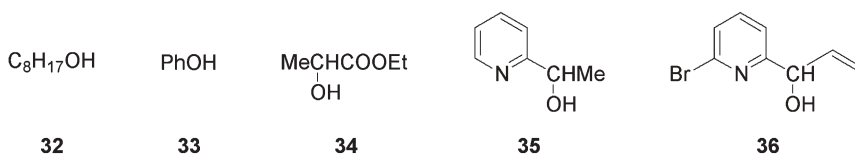
**Scheme 4**

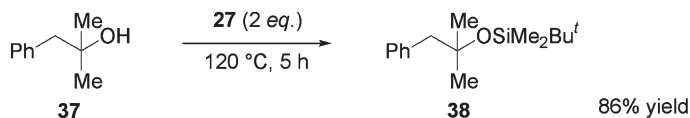
Table 7 Solvent-free *O*-silylation of liquid alcohols

| Alcohol | Silyl chloride | Yield (%) of silyl ether |
|---------|----------------|--------------------------|
| 32 | 27 | 88 |
| 33 | 27 | 78 |
| 34 | 27 | 80 |
| 34 | 30b | 86 |
| 34 | 30c | 78 |
| 35 | 27 | 78 |
| 35 | 27 | 84 |

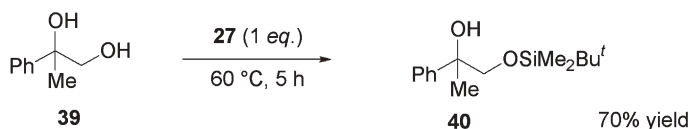
The solvent-free *O*-silylation can also be applied to liquid alcohols. Treatment of liquid alcohols **32**–**36** with various silyl chlorides at 60 °C for 5 h gave the corresponding *O*-silyl ethers in good yields (Table 7). In this case, the steric bulkiness of the alcohol and reagent do not present any significant problem, except in the case of tertiary alcohols.



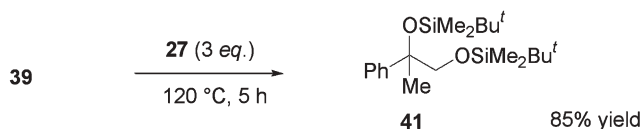
Although the *O*-silylation reaction of the tertiary alcohol 1,1-dimethyl-2-phenylethanol (**37**) with **27** required a reaction temperature of 120 °C and two equivalents of **27**, the *O*-silyl ether **38** was still obtained in 86% yield by the simple solvent-free procedure. By contrast, the sterically hindered hydroxyl group of **37** was not silylated at all by heating with **27** in DMF at 120 °C for 5 h [8].



The solvent-free *O*-silylation reaction can also be accomplished selectively. For example, when 1-methyl-1-phenylethane-1,2-diol (**39**) was treated with **27** at 60 °C for 5 h, its primary hydroxyl group was silylated to give **40** in 70% yield.



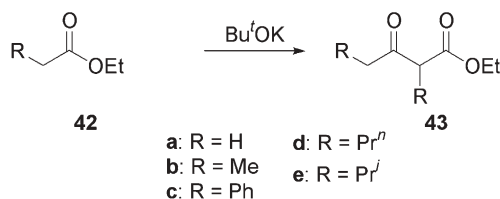
Reaction of **39** with three mol equivalents of **27** at 120 °C for 5 h gave the fully O-silylated product **41** in 85% yield [8]



2.3

Claisen and Cannizzaro Reactions

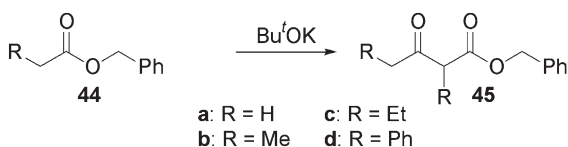
Solvent-free Claisen reactions were found to proceed efficiently. Particularly, the solvent-free Claisen reactions of esters substituted with sterically bulky groups proceeded very efficiently, although these reactions did not occur in solution. When a mixture of ethyl acetate (**42a**) and Bu^tOK was kept at 80 °C for 20 min, condensation product **43a** was obtained in 73% yield (Scheme 5). However, reaction of **42a** and EtONa in EtOH by heating under reflux for 8 h gave **43a** in 45% yield. The solvent-free reaction has some advantage in comparison to the solution reaction. Similar solvent-free reactions of **42b–d** with Bu^tOK gave the corresponding condensation products, **43b** (60%), **43c** (73%), and **43d** (61%) in the yields indicated. The efficiency of the same reaction in solution is much poorer. For the ester substituted with a sterically bulky group, the difference in efficiency becomes larger. Solvent-free reaction of ethyl 3-methylbutanoate (**42e**) with Bu^tOK for 1 h gave **43e** in 33% yield, although solution reaction by heating under reflux for 48 h did not give any **43e** and **42e** was recovered unchanged [9].



Scheme 5

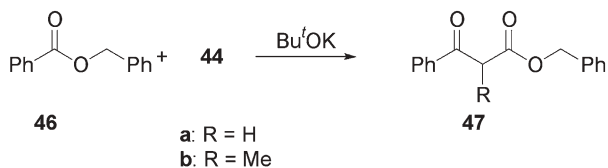
A similar steric effect was observed in the reaction of benzyl carboxylate (**44**). When **44a–d** were treated with Bu^tOK under solvent-free conditions at around 100 °C for 30 min, the corresponding condensation products **45a** (75%), **45b** (66%), **45c** (64%), and **45d** (84%) were obtained in the yields indicated [9] (Scheme 6). When the same reactions of **44a–d** and Bu^tOH were carried out in toluene under reflux for 16 h, no condensation product was obtained and **44a–d** were recovered unchanged. In solution reactions, exchange of the alkoxy group occurs among the substrate, reagent, and solvent. Therefore, the alkoxy groups of the ester, metal alkoxide, and alcohol used as a solvent should be identical.

In the solvent-free reactions, however, a strong base such as Bu^tOK can be used for any kind of ester substrate, since such exchange does not occur. This is also a considerable advantage.



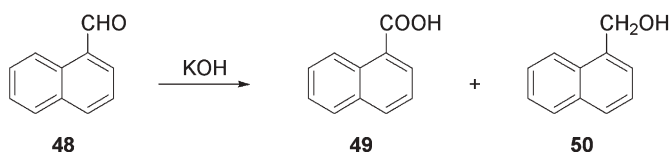
Scheme 6

The cross-condensation reaction of benzyl benzoate (**46**) and **44** was carried out under solvent-free conditions. Treatment of a 1:1 mixture of **46** and **44a** with Bu^tOK at 120 °C for 1 h gave the cross-condensed product **47a** in 42% yield (Scheme 7). Similar reaction of **46** with **44b** gave **47b** in 45% yield. Because heating of **46**, **44**, and Bu^tOK in toluene under reflux for 16 h did not give any product, it is clear that the solvent-free reaction is again effective for the cross-condensation. In these cases, self-condensation of **44** itself did not occur probably because of the high reactivity of **46** [9].

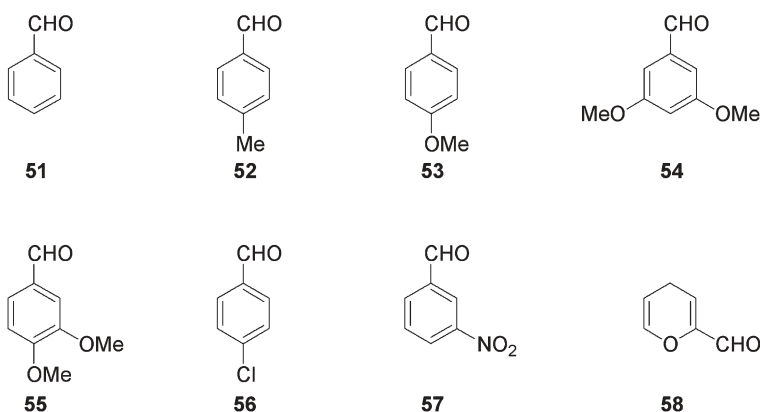


Scheme 7

After a mixture of powdered 1-formylnaphthalene (**48**) and powdered KOH was kept at 100 °C for 5 min, water was added to the reaction mixture, which was filtered to give 1-(hydroxymethyl)naphthalene (**50**), after Kugelrohr distillation, in 38% yield. The filtrate was acidified with concentrated HCl and filtered to



give 1-naphthoic acid (**49**) in 41% yield [9]. For liquid aldehydes, a similar method can be applied. When the alcohol formed by the solvent-free reaction is an oily material, the product was extracted with ether. Finally, treatment of aldehydes **51**–**58** by these procedures gave the corresponding alcohols and acids in the yields indicated in Table 8. In the case of crystalline *m*-nitrobenzaldehyde (**57**), the yield of *m*-nitrobenzoic acid exceeded 50%, probably due to air oxidation of **57** during the reaction at 80 °C. When the reaction was carried out at

**Table 8** Solvent-free Cannizzaro reactions

| Aldehyde | Reaction conditions | | Yield (%) | |
|----------|---------------------|------------|-----------|---------|
| | Temperature (°C) | Time (min) | Acid | Alcohol |
| 48 | 100 | 5 | 41 | 38 |
| 51 | rt | 10 | 43 | 39 |
| 52 | 80 | 3 | 51 | 18 |
| 53 | 80 | 5 | 46 | 38 |
| 54 | 100 | 5 | 49 | 41 |
| 55 | 100 | 30 | 46 | 27 |
| 56 | rt | 10 | 48 | 45 |
| 57 | rt | 10 | 53 | 33 |
| 58 | 0 | 10 | 40 | 36 |

room temperature in nitrogen atmosphere under ultrasound irradiation, *m*-nitrobenzoic acid and *m*-nitrobenzyl alcohol were obtained in 43 and 33% yields, respectively.

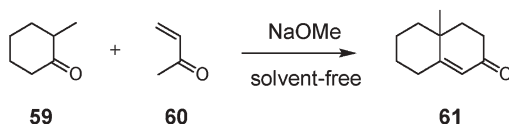
The solvent-free Cannizzaro reaction has some advantages. In addition to simplicity and cleanness of the procedure, the solvent-free reaction proceeds much faster than a solution reaction. For example, reaction of **51** in 60% aqueous NaOH takes 24 h to complete [10], although the solvent-free reaction is completed within 5 min [9].

2.4

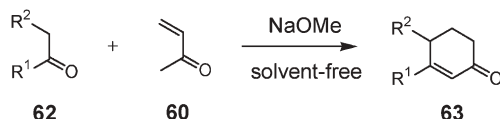
Robinson Annellation Reactions in a One-Pot Process

Ecologically and economically valuable solvent-free Robinson annellation reactions, which proceed efficiently in a one-pot process at room temperature, have been reported [10]. For example, 2-methylcyclohexanone (**59**), methyl vinyl

ketone (**60**), and NaOMe were well mixed with an agate mortar and pestle and the mixture was kept at room temperature for 3 h. From the reaction mixture, 4,4a,5,6,7,8-hexahydro-4a-methyl-2(3*H*)-naphthalenone (**61**) was obtained in 25% yield. The solvent-free Robinson annelation reaction in a one-pot process has some advantages. Namely, the procedure is much simpler and the yield of product is higher than that of the solution reaction.



Reactions of acyclic ketones **62a–e** and **60** in the absence of solvent in the one-pot processes gave the corresponding product **63a** (27%), **63b** (12%), **63c** (45%), **63d** (15%) and **63e** (15%) in the yields indicated (Scheme 8). These yields are higher than those of **63a** (17%), **63b** (8%), **63c** (29%), **63d** (5%) and **63e** (8%) obtained by solution reaction [11].



- a: $\text{R}^1=\text{Ph}$; $\text{R}^2=\text{Me}$
 b: $\text{R}^1=\text{Ph}$; $\text{R}^2=\text{Et}$
 c: $\text{R}^1=\text{R}^2=\text{Ph}$
 d: $\text{R}^1=p\text{-MeC}_6\text{H}_4$; $\text{R}^2=\text{Ph}$
 e: $\text{R}^1=p\text{-BrC}_6\text{H}_4$; $\text{R}^2=\text{Ph}$

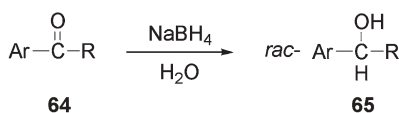
Scheme 8

3

One-Pot Preparative Method of Optically Active Compounds by a Combination of Solid–Solid Reaction and Enantioselective Inclusion Complexation with a Chiral Host in a Water Suspension Medium

Some solid–solid reactions were shown to proceed efficiently in a water suspension medium in Sect. 2.1. When this reaction, which gives a racemic product, is combined with an enantioselective inclusion complexation with a chiral host in a water suspension medium, a unique one-pot preparative method of optically active product in a water medium can be constructed. Some such successful examples are described.

When a suspension of acetophenone (**64a**) (1 g, 8.3 mmol) and NaBH₄ (1 g, 25 mmol) in water (10 ml) was stirred at room temperature for 2 h, *rac*-**65a** was produced (Scheme 9). To the water suspension medium of *rac*-**65a** was added



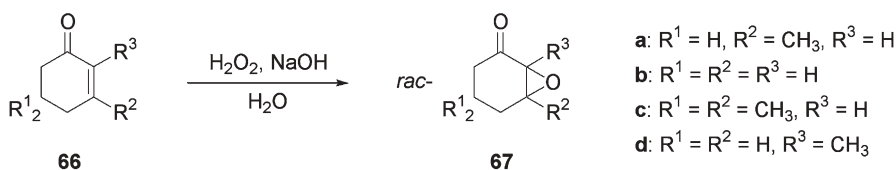
Scheme 9

- a: Ar = C₆H₅, R = CH₃
 b: Ar = C₆H₅, R = CH₂CH₃
 c: Ar = C₆H₅, R = CH₂CH₂CH₃
 d: Ar = C₆H₅, R = CF₃
 e: Ar = 2-pyridyl, R = CH₃
 f: Ar = 3-pyridyl, R = CH₃
 g: Ar = 4-pyridyl, R = CH₃
 h: Ar = 2-furyl, R = CH₃
 i: Ar = 2-thiophenyl, R = CH₃

the optically active host compound (**10a**) (3.87 g, 8.3 mmol), and the mixture was stirred for 3 h to give a 2:1 inclusion complex of **10a** with (–)-**65a**. Heating the filtered inclusion complex in vacuo gave (–)-**65a** of 95% ee (0.42 g, 85% yield). From the filtrate left after separation of the inclusion crystals, (+)-**65a** of 77% ee (0.35 g, 70% yield) was obtained by extraction with ether [12]. By the same procedure, optically active **65b** and **65e–i** were prepared (Table 9). *Rac*-**65c,d** did not form an inclusion complex with the hosts **10a–c**. Although *rac*-**65f,g** formed 1:1 inclusion complexes with **10c**, no enantiomeric resolution occurred.

The enantioselective inclusion complexation of the reaction product with **10a–c** in aqueous medium is more efficient than that by the recrystallization method. For example, inclusion complexation of *rac*-**65e** with **10a,b** did not occur by recrystallization from an organic solvent; however, enantioselective complexation occurred efficiently in aqueous medium to give finally optically active **65e** [12].

When a mixture of 30% H₂O₂ (2.61 g, 23 mmol), 8 N NaOH (30 ml), 3-methyl-2-cyclohexen-1-one (**66a**) (2.5 g, 23 mmol), and water (10 ml) was stirred at room temperature for 3 h, *rac*-**67a** was produced (Scheme 10). To the water suspension of *rac*-**67a** was added **10b** (3.7 g, 7.6 mmol), and the mixture was stirred for 48 h to give a 1:1 inclusion complex of **10b** with (–)-**67a**. Heating the filtered inclusion complex in vacuo gave (–)-**67a** of 97% ee (0.88 g, 61% yield). From the filtrate left after separation of the inclusion complex, (+)-**67a** of 48% ee (1.43 g, 99%) was obtained by extraction with ether. By the same procedure, optically active **67b–d** were obtained (Table 10). In the case of **67b** and **67c**, (+)-**67b** and (+)-**67c** were obtained in an enantiopure state by using **10b** and (S,S)-(-)-1,6-bis(*o*-chlorophenyl)-1,6-diphenylhexa-2,4-diene-1,6-diol (**68**) as a chiral host compound, respectively (Table 10) [12].



Scheme 10

Table 9 Result of one-pot preparation method of optically active *sec*-alcohols (**65a**, **65b**, **65e-i**) by a combination of reduction of ketone and enantiomeric resolution in a water suspension medium

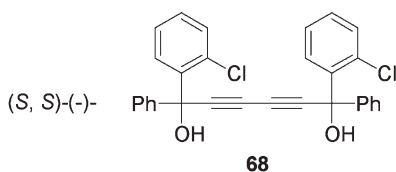
| Host | Ketone | Inclusion complex | | From complex | | From filtrate | | |
|------|--------|-------------------|---------|--------------|----------------------------|---------------|-----------|----------------------------|
| | | Host:guest | Product | Yield (%) | Enantiomeric purity (% ee) | Product | Yield (%) | Enantiomeric purity (% ee) |
| 10a | 64a | 2:1 | (-)-65a | 85 | 95 | (+)-65a | 70 | 77 |
| 10a | 64b | 2:1 | (-)-65b | 96 | 62 | (+)-65b | 50 | 52 |
| 10a | 64e | 3:1 | (-)-65e | 26 | 76 | (+)-65e | 156 | 18 |
| 10b | 64e | 2:1 | (-)-65e | 44 | 99 | (+)-65e | 134 | 40 |
| 10c | 64e | 1:1 | (-)-65e | 92 | 88 | (+)-65e | 76 | 62 |
| 10a | 64f | 1:1 | (+)-65f | 88 | >99 | (-)-65f | 86 | 73 |
| 10b | 64f | 1:1 | (+)-65f | 86 | 96 | (-)-65f | 82 | 66 |
| 10c | 64f | 1:1 | rac-65f | 78 | 0 | rac-65f | 86 | 0 |
| 10a | 64g | 1:1 | (+)-65g | 82 | 47 | (-)-65g | 78 | 26 |
| 10b | 64g | 1:1 | (+)-65g | 80 | 77 | (-)-65g | 82 | 36 |
| 10c | 64g | 1:1 | rac-65g | 90 | 0 | rac-65g | 80 | 0 |
| 10a | 64h | 2:1 | (-)-65h | 76 | 93 | (+)-65h | 96 | 50 |
| 10a | 64i | 2:1 | (-)-65i | 84 | 86 | (+)-65i | 61 | 43 |

Table 10 Result of one-pot preparation method of optically active epoxides (**67a–d**) by a combination of epoxidation of cyclohexenone and enantiomer resolution in a water suspension medium

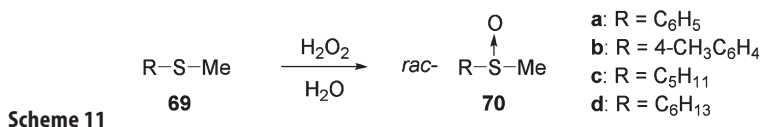
| Host | Cyclo-hexenone | Inclusion complex | | From complex | | From filtrate | | | |
|------|----------------|-------------------|--|--------------|-----------|----------------------------|---------|-----------|----------------------------|
| | | Host:guest | | Product | Yield (%) | Enantiomeric purity (% ee) | Product | Yield (%) | Enantiomeric purity (% ee) |
| 10a | 66a | 1:1 | | (-)-67a | 61 | 97 | (+)-67a | 99 | 48 |
| 10c | 66a | 1:1 | | (-)-67a | 56 | 97 | (+)-67a | 79 | 34 |
| 10b | 66b | 1:1 | | (+)-67b | 38 | 100 | (-)-67b | 78 | 51 |
| 68 | 66c | 1:1 | | (+)-67c | 57 | 100 | (-)-67c | 62 | 87 |
| 10b | 66d | 2:1 | | (-)-67d | 63 | 63 | (+)-67d | 96 | 47 |

Table 11 Result of one-pot preparation method of optically active sulfoxides (**64a–d**) by a combination of oxidation of sulfide and enantiomeric resolution in a water suspension medium

| Host | Sulfide | Inclusion complex | | From complex | | From filtrate | | | |
|------|---------|-------------------|--|--------------|-----------|----------------------------|---------|-----------|----------------------------|
| | | Host:guest | | Product | Yield (%) | Enantiomeric purity (% ee) | Product | Yield (%) | Enantiomeric purity (% ee) |
| 10c | 69a | 1:1 | | (+)-70a | 82 | 57 | (-)-70a | 73 | 54 |
| 10c | 69b | 1:1 | | (+)-70b | 75 | 98 | (-)-70b | 89 | 78 |
| 10c | 69c | 1:1 | | (-)-70c | 70 | 96 | (+)-70c | 80 | 55 |
| 10c | 69d | 3:2 | | (-)-70d | 55 | 49 | (+)-70d | 100 | 31 |



When a mixture of methyl phenyl sulfide (**69a**) (1 g, 8.1 mmol), 30% H_2O_2 (1.84 g, 16.2 mmol), and water (10 ml) was stirred at room temperature for 24 h, *rac*-**70a** was produced (Scheme 11). To the water suspension medium of *rac*-**70a** was added **10c** (2 g, 4 mmol), and the mixture was stirred for 15 h to give a 1:1 inclusion complex of **10c** with (+)-**70a**. Heating the filtered complex in vacuo gave (+)-**70a** of 57% ee (0.45 g, 82% yield). From the filtrate left after separation of the inclusion complex, (–)-**70a** of 54% ee (0.4 g, 73% yield) was obtained by extraction with ether. By the same procedure, optically active **70b–d** were also prepared (Table 11). In the case of (+)-**70b** and (–)-**70c**, the efficiency of the enantiomeric resolution was very high.



Since the optically active host remaining after separation of the optically active guest from its inclusion complex by distillation can be used again and again, this one-pot method in water is an ecological and economical method [12].

4

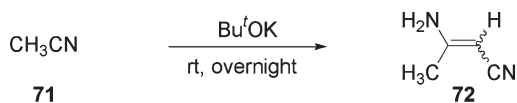
Mechanistic Study of Thermal Solid-State Reactions

Since solid-state reactions can easily be monitored by continuous measurement of spectra, it is easy to study the mechanism of the reactions. For this purpose, IR spectroscopy is the most useful, because IR spectra can be measured simply as Nujol mulls or directly for any mixture of solid–solid, solid–liquid, or liquid–liquid by using the ATP (attenuated total reflection) method. Some such examples of the mechanistic study are described.

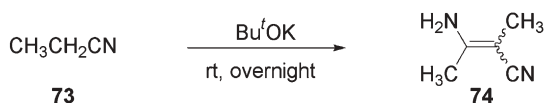
4.1

Thorpe Reactions

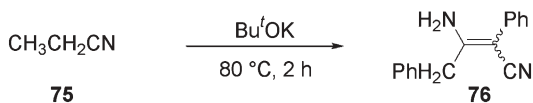
It has been established that Thorpe reactions proceed efficiently under solvent-free conditions. For example, when a mixture of acetonitrile (**71**) and powdered Bu^tOK was kept at room temperature overnight, a 1:1 mixture of (*E*)- and (*Z*)-



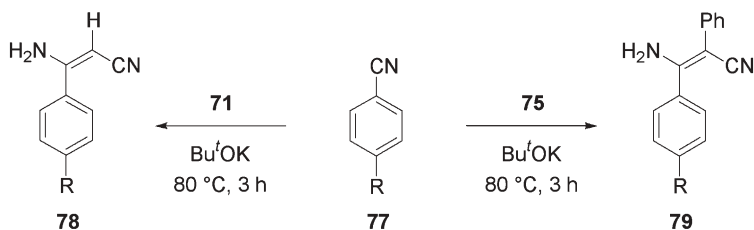
enamines (**72**) was obtained in 48% yield [13]. The same treatment of propionitrile (**73**) with powdered Bu^tOK gave a 1:1 mixture of (*E*)- and (*Z*)-**74** in 65%



yield. Solvent-free Thorpe reaction of benzyl cyanide (**75**) at 80 °C was completed within 2 h to give a 4:1 mixture of (*E*)- and (*Z*)-enamines (**76**) [13]. This reaction procedure can be applied to cross-Thorpe reactions. When a mixture



of powdered *p*-methylbenzonitrile (**77b**), two molar amounts of **71**, and two molar amounts of powdered Bu^tOK was heated at 80 °C for 3 h, (*E*)-**78b** was obtained as the sole isolable product in 74% yield (Scheme 12). In the solvent-free cross-reaction, self-condensation reaction of **71** did not occur. The cross-condensation of benzonitrile (**77a**) with **71** gave (*E*)-**78a** in 70% yield. The same reaction of **77a** and **77b** with **75** gave (*E*)-**79a** and (*E*)-**79b** in 70 and 62% yields, respectively [13].

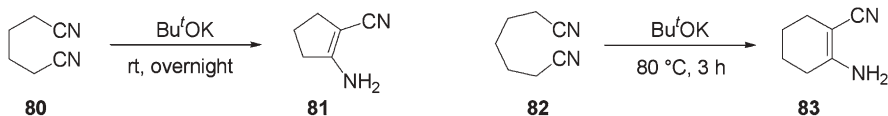


a: R = H
b: R = CH₃

Scheme 12

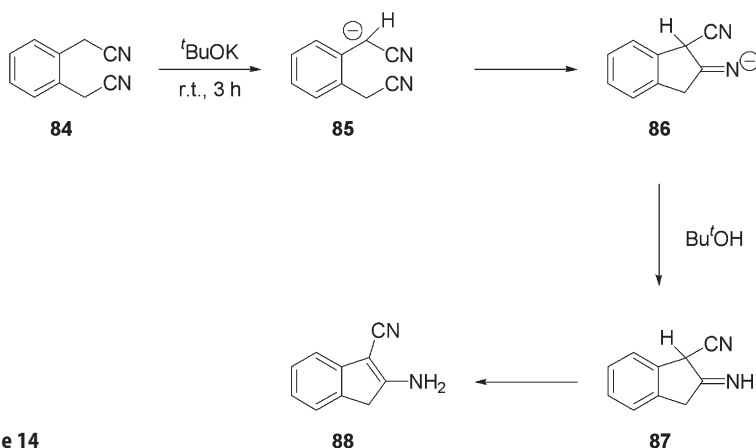
The intramolecular Thorpe reaction can also be carried out under solvent-free conditions. When a mixture of powdered adiponitrile (**80**) and Bu^tOK was kept at room temperature for 3 h, cyclization product **81** was obtained as a

white crystalline powder in 74% yield [13] (Scheme 13), although the solution reaction gives a dimeric product [14]. By the same procedure, pimelonitrile (**82**) and *o*-di(cyanomethyl)benzene (**84**) gave **83** and **88** as white crystalline powders in 83 and 97% yields, respectively.



Scheme 13

Until recently the products of all nitrile cyclizations by the Thorpe reaction had been formulated as imines, although the products were found in 1955 to be better written as the enamine structure. In order to verify the reaction mechanism of the Thorpe reaction, the solid-state reaction of **84** and Bu^tOK was monitored by measurement of IR spectra in Nujol mulls. As the reaction proceeds (Scheme 14), the CN absorption of **84** at 2250 cm^{-1} decreases and a new CN absorption of the imine intermediate (**87**) arises at 2143 cm^{-1} . As **87** is converted into **88** by a proton migration, the CN absorption of **87** at 2143 cm^{-1} disappears, and only the CN absorption of **88** at 2189 cm^{-1} remains finally [13].

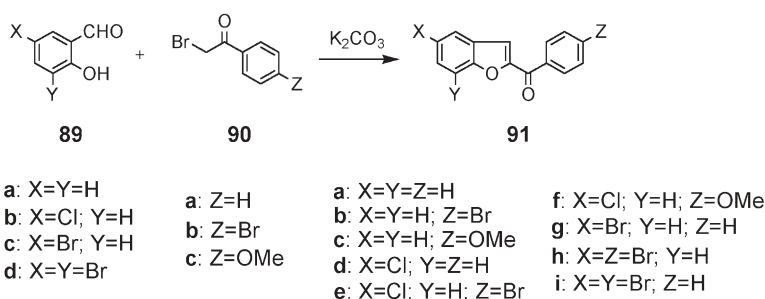


Scheme 14

4.2

Rap–Stoermer Reactions

Rap–Stoermer reactions are useful for the preparation of 2-benzoylbenzofuran derivatives (**91**) by a base-assisted condensation of salicylaldehydes (**89**) with phenacyl bromides (**90**) (Scheme 15). However, these reactions are not very



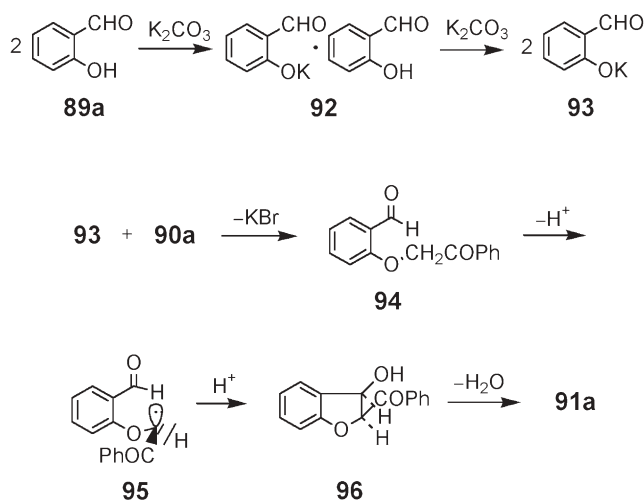
Scheme 15

efficient in solution, and the yield of products is not very high. For example, heating of a solution of **89b**, **90b**, and K_2CO_3 in EtOH under reflux for 3 h gave **91b** in 70% yield [15]. In this case, the solvent must be removed from the reaction mixture by evaporation and the residue must be worked up for isolation of the product. By contrast, solvent-free reactions proceed efficiently under much simpler conditions to give products in almost quantitative yield. For example, a mixture of **89a** and an equimolar amount of **90a** and K_2CO_3 was heated at 80 °C for 1 h, and the reaction mixture was washed with water to give **91a** in 98% yield. Similar reactions of various salicylaldehydes (**89a–d**) and phenacyl bromides (**90a–c**) at 80–100 °C for 1 h gave the corresponding 2-benzoylbenzofuran derivatives (**91a–i**) in almost quantitative yields (Table 12) [16].

In order to clarify the reason why the Rap–Stoermer reaction proceeds so efficiently under solvent-free conditions, the K_2CO_3 -assisted reaction of **89a** and **90a** was studied by IR spectral monitoring in Nujol mulls [16]. Firstly, the potassium salt formation of **89a** was studied (Scheme 16). One minute after mixing of **89a** with twice the molar amount of K_2CO_3 , a $\nu C=O$ absorption band (B) appeared at 1692 cm^{-1} (spectrum II in Fig. 1), although **89a** itself shows $\nu C=O$ absorption (A) at 1664 cm^{-1} (spectrum I in Fig. 1). After 10 min, B disappeared and a new $\nu C=O$ absorption band (C) appeared at 1670 cm^{-1} (spectrum III in

Table 12 K_2CO_3 -assisted solvent-free Rap–Stoermer reaction (1 h)

| Aldehyde | Reagent | Reaction temperature (°C) | Product | Yield (%) |
|------------|------------|---------------------------|------------|-----------|
| 89a | 90a | 80 | 91a | 98 |
| 89a | 90b | 80 | 91b | 95 |
| 89a | 90c | 80 | 91c | 98 |
| 89b | 90a | 80 | 91d | 99 |
| 89b | 90b | 100 | 91e | 93 |
| 89b | 90c | 100 | 91f | 97 |
| 89c | 90a | 80 | 91g | 98 |
| 89c | 90b | 100 | 91h | 94 |
| 89d | 90a | 100 | 91i | 93 |



Scheme 16

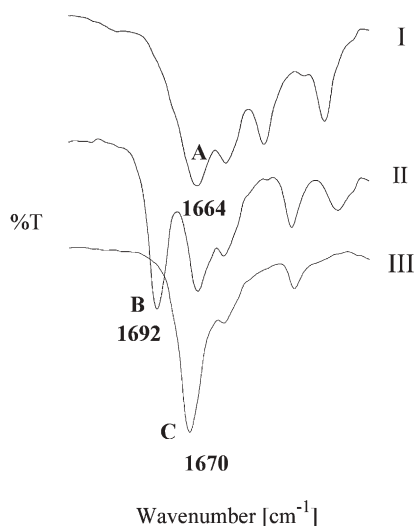


Fig. 1 IR spectra of a mixture of **89a** and twice the molar amount of K_2CO_3 in Nujol mulls. I Pure **89a** for reference; II 1 min after mixing; III 10 min after mixing

Fig. 1). The absorption (C) was assigned to $\nu\text{C}=\text{O}$ in the potassium salt (**93**) by comparison of the spectrum III with that of an authentic sample. Absorption band B was assigned to $\nu\text{C}=\text{O}$ in a 1:1 complex (**92**) of **89a** with **93**, by comparison of the spectrum II with that of an authentic sample, prepared by mixing **89a** with half the molar amount of K_2CO_3 . Unfortunately, the structure of **92** could not be determined, since **92** did not form suitable crystals for X-ray analysis. Treatment of **92** with K_2CO_3 in the solid state gave **93**.

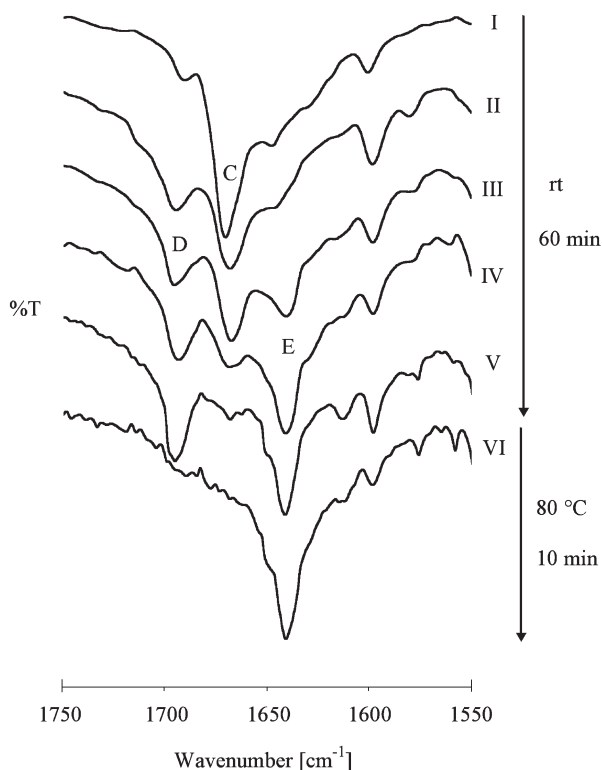


Fig. 2 IR monitoring of the K_2CO_3 -assisted solvent-free reaction of **89a** with **90a** by spectroscopic measurements in Nujol mulls. I–IV measured every 15 min

Secondly, the reaction of **89a**, **90a**, and K_2CO_3 under solvent-free conditions was monitored by IR spectral measurement. A mixture of **89a**, an equimolar amount of **90a**, and twice the molar amount of K_2CO_3 initially showed $\nu C=O$ absorption (C) at 1670 cm^{-1} , assigned to the formation of **93**; this absorption decreased gradually and new $\nu C=O$ absorption bands appeared at 1696 cm^{-1} (D) and 1641 cm^{-1} (E) (Fig. 2). After 60 min, the C absorption band disappeared and the D and E absorptions increased. After further reaction at $80\text{ }^\circ\text{C}$ for 10 min, the D absorption disappeared and only the E absorption remained in the spectrum (VI in Fig. 2). The spectrum VI is identical to that of the final product **91a**. The appearance of the D absorption band together with a strong OH absorption band at 3465 cm^{-1} suggests production of a ketoalcohol intermediate.

In order to isolate the ketoalcohol intermediate, the following experiment was carried out. A mixture of **89a** (1 g, 8.2 mmol), **90a** (0.77 g, 5 mmol), and K_2CO_3 (1.38 g, 10 mmol) was stored at room temperature for 3 h, and the crude reaction product was added to a 1:1 mixture of ether and water. From the ether solution, *cis*-2-benzoyl-3-hydroxy-2,3-dihydrobenzofuran (**96**) was obtained (0.18 g, 15% yield). Compound **96** showed its $\nu C=O$ absorption at 1696 cm^{-1} .

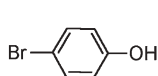
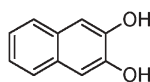
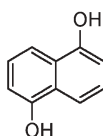
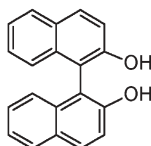
Heating of **96** under solvent-free Rap–Stoermer reaction conditions easily gave **91a** [16] (Scheme 16).

The *cis* configuration of **96** was elucidated by X-ray structure analysis. The data suggest that the cyclization reaction of the anion **95** generated from **94** to **91a** proceeds stereoselectively in the solid state [16].

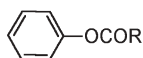
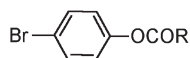
4.3

Benzoylation Reactions of Phenol and Naphthol Derivatives

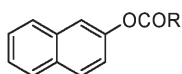
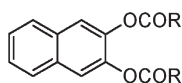
Benzoylation reactions of phenols (**33**, **97**) and naphthols (**20**, **98–100**) can be accomplished very efficiently by heating with benzoyl chloride (**101**) under-

**97****98****99****100**

a: *rac*-form
b: (*R*)-(+)-form
c: (*S*)-(–)-form

**101****102****103**

solvent-free conditions. For example, a mixture of 2-naphthol (**20**) and an equimolar amount of *p*-methylbenzoyl chloride (**101b**) was heated at 60 °C for 2 h under magnetic stirring. The reaction mixture was washed with aqueous Na₂CO₃ and water, and air dried to give pure 2-naphthyl *p*-methylbenzoate (**104b**) as a

**104****105**

white powder in 97% yield [17]. By the same simple procedure, **20** and **97–100** were reacted with **101** to give the corresponding benzoates in good yields [17].

In order to clarify the reaction mechanism of the solvent-free benzoylation process, the reactions of **20** and **98** with **101b** at 80–100 °C were monitored by continuous measurements of IR spectra as Nujol mulls (Figs. 3 and 4). First, the reaction of **20** with **101b** at 80 °C was studied. Initially, on mixing of powdered **20** and **101b**, no significant new νOH absorption appeared, and only two $\nu\text{C}=\text{O}$ absorptions of **101b** appeared at 1775 and 1740 cm^{-1} (I in Fig. 3). After 10 min of mixing, new νOH and $\nu\text{C}=\text{O}$ absorptions appeared at 3450 and 1710 cm^{-1} , respectively (II in Fig. 3). As the reaction proceeded, a $\nu\text{C}=\text{O}$ absorption appeared at 1720 cm^{-1} , in addition to the $\nu\text{C}=\text{O}$ absorption at 1710 cm^{-1} (II–IV in Fig. 3). When the reaction mixture was further heated at 80 °C for 10 min, the νOH absorption at 3450 cm^{-1} and $\nu\text{C}=\text{O}$ absorptions at 1775, 1740, and 1710 cm^{-1} disappeared and only the $\nu\text{C}=\text{O}$ absorption at 1720 cm^{-1} remained (VI in Fig. 3). The spectrum VI is identical to that of the final product **104b**. The appearance of the νOH and $\nu\text{C}=\text{O}$ absorptions at relatively low frequencies 3450 and 1720 cm^{-1} , respectively, during the reaction process suggests the formation of a complex of **20** and **104b**. Hydrogen bond formation between the OH hydrogen of **20** and the C=O oxygen of **104b** would shift their absorptions to lower frequencies. Recrystallization of **20** and **104b** from ether gave their 1:1 complex, which shows absorptions at 3450 and 1710 cm^{-1} . Finally, the

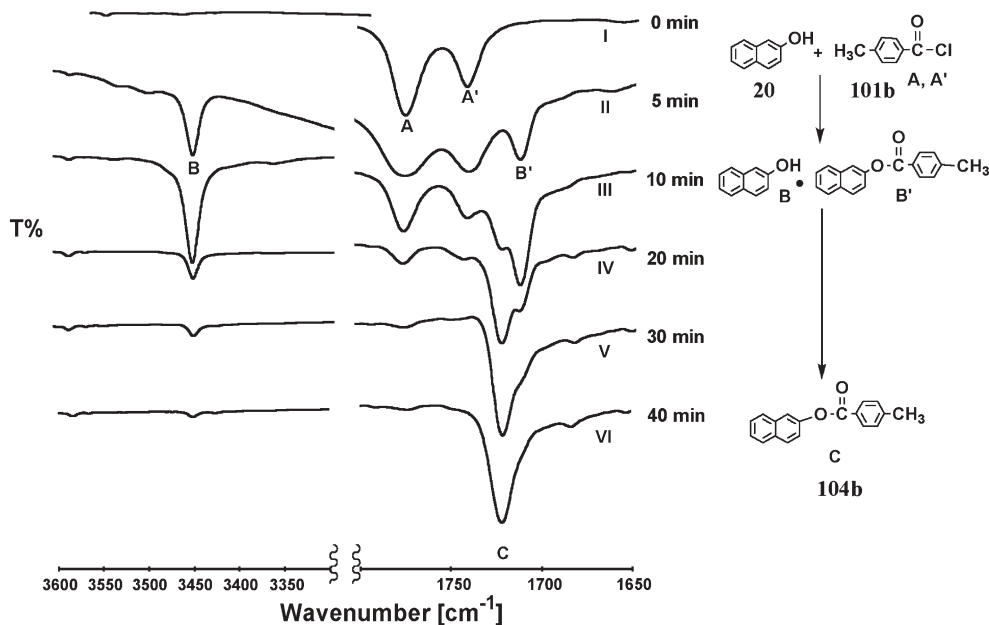


Fig. 3 Monitoring for 40 min of the solvent-free benzoylation of **20** with **101b** at 80 °C by IR spectral measurements in Nujol mulls

1:1 complex of **20** and **104b** was found to be an intermediate of the benzylation reaction. However, the complex did not form crystals appropriate for X-ray analysis [17].

Secondly, the solvent-free benzylation reaction of **98** with **101b** at 100 °C was monitored by IR spectral measurements (Fig. 4). Initially, on mixing **98** and **101b**, the νOH of **98** and $\nu\text{C=O}$ of **101b** appeared at 3500 (A) and 3450 (A'), and 1775 and 1740 cm^{-1} , respectively (I in Fig. 4). As the benzylation reaction proceeded, new νOH absorptions appeared at 3487 (B), 3338 (C), and 3385 cm^{-1} (B'), and the original νOH absorptions of **98** at 3500 (A) and 3450 cm^{-1} (A') disappeared after 6 min (II and III in Fig. 4). After 20 min, only the 3338 cm^{-1} (C) absorption remained as the sole νOH absorption, and the 1740 cm^{-1} absorption remained the strongest $\nu\text{C=O}$ absorption (VI in Fig. 4). The 3388 cm^{-1} absorption (C) is assigned to the νOH of the monoester, 2-hydroxy-3-naphthyl *p*-methylbenzoate (**108b**) by comparison of the spectrum with that of an authentic sample. When the reaction mixture was further heated at 100 °C for 90 min, the νOH absorption disappeared and only the $\nu\text{C=O}$ absorption of the final product **105b** at 1740 cm^{-1} remained (VIII in Fig. 4). The appearance of the new νOH and $\nu\text{C=O}$ absorptions at 3467 (B) and 3335 (B') and 1730 cm^{-1} , respectively, during the course of the reaction (II–VII in Fig. 4) suggests the formation of a complex (**109b**) of **98** and **105b**. In order to confirm the forma-

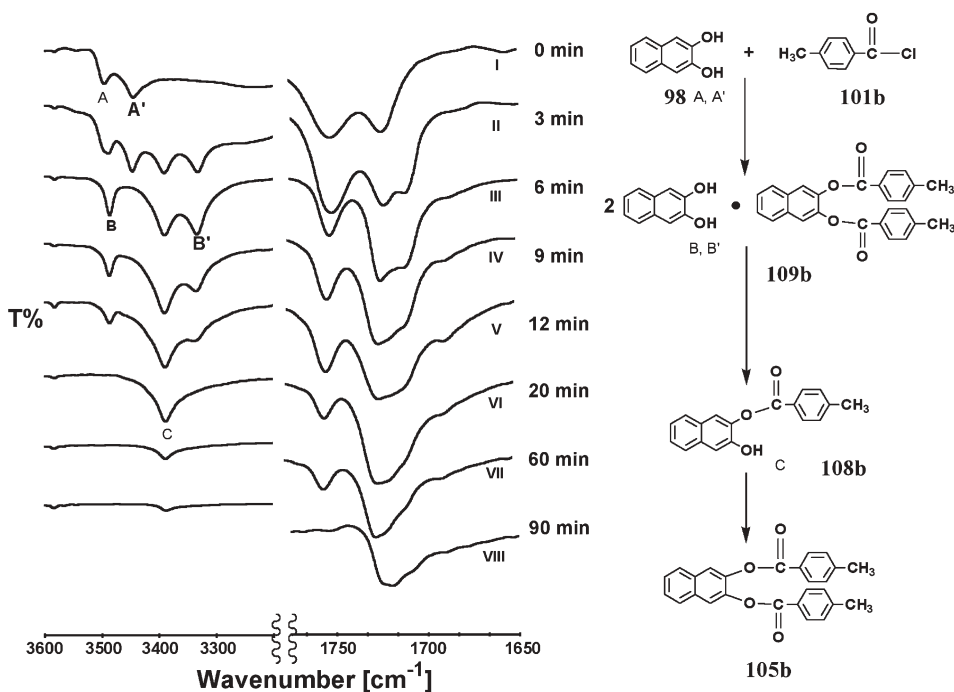
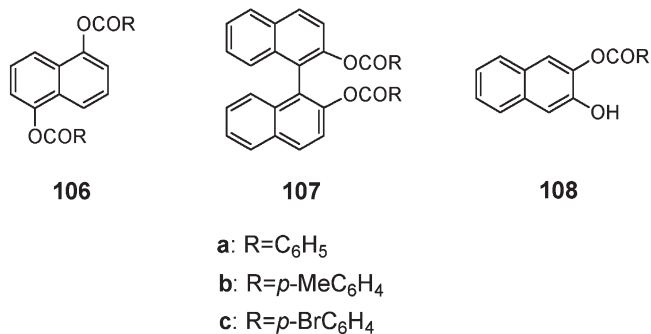


Fig. 4 Monitoring for 90 min of the solvent-free benzylation of **98** with **101b** at 100 °C by IR spectral measurements in Nujol mulls



tion of the complex **109b** (Fig. 5) as an intermediate, both components were recrystallized from ether to give the 2:1 complex as colorless plates. The IR spectrum of the intermediate was identical with that of the initially observed 2:1 complex (**109b**). The crystal structure of **109b** was elucidated by X-ray analysis [17]. By these IR spectroscopic studies, the mechanism of the benzylation reaction under solvent-free conditions was fully clarified. It is interesting that even a fundamental organic reaction, such as the benzylation reaction of **98**, does not proceed through simple stepwise benzylation of its two hydroxyl groups.

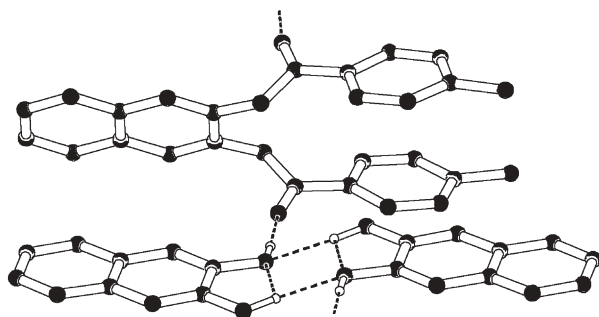


Fig. 5 A basic part of the hydrogen bonding network in **109b**. Hydrogen atoms on carbon are omitted for clarity

5

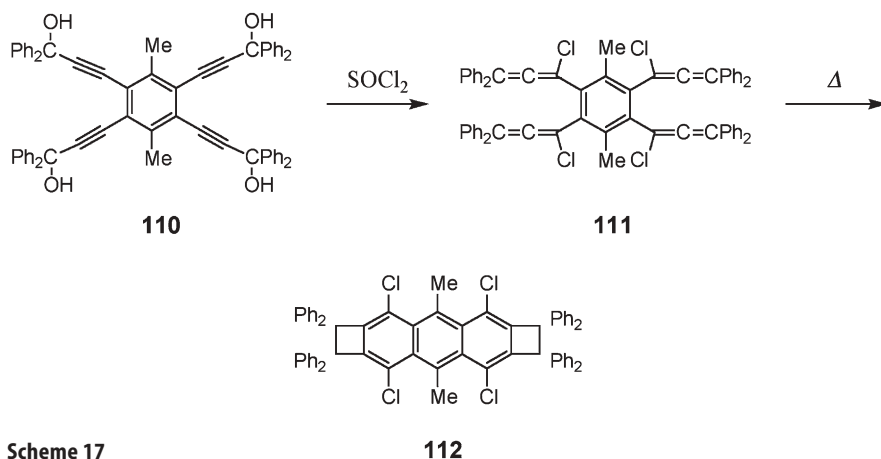
Crystal-to-Crystal Reactions

As typical examples of crystal-to-crystal thermal reactions, the cyclization of allene derivatives to four-membered ring compounds and the transformation of a racemic complex into a conglomerate complex are described.

5.1

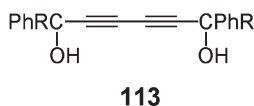
Crystal-to-Crystal Cyclization Reactions of Allene Derivatives

Treatment of 2,3,5,6-tetrakis(3-hydroxy-3,3-diphenyl-1-propynyl)-*p*-xylene (**110**) with SOCl_2 gave 2,3,5,6-tetrakis(1-chloro-3,3-diphenyl-1,2-propadienyl)-*p*-xylene (**111**) as colorless prisms through a propargylic rearrangement (Scheme 17). By heating at 180 °C for 1 h, a single crystal of **111** was converted into the crystal of the cyclization product **112** [18, 19]. Although the crystal of **112** was not a single crystal any more, it is very clear that the conversion of **111** into **112** occurs by a crystal-to-crystal reaction. It is interesting that the thermal cyclization reaction of **111** into **112**, which should be accompanied by a molecular motion of allene moieties, occurs easily in a crystal. It is also interesting that the **112**, which has the strained cyclobutane rings constructed with the extremely long $\text{sp}^3\text{-sp}^3$ bond of around 1.720 Å, can easily be obtained by the crystal-to-crystal reaction [18, 19].

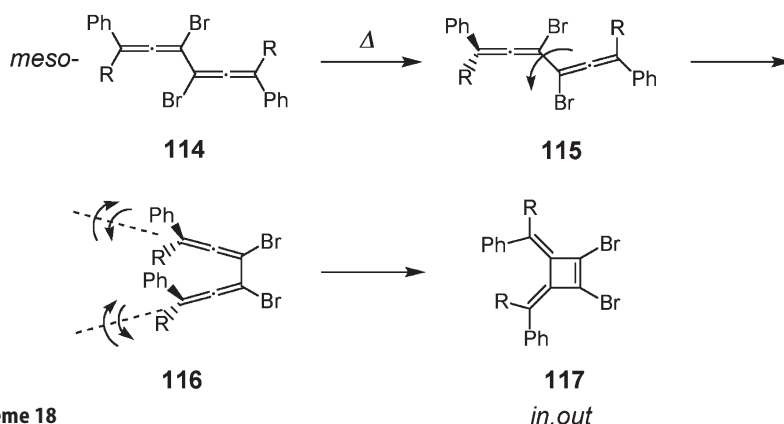


Scheme 17

The thermal solid-to-solid cyclization reaction of diallene derivatives also proceeds stereospecifically. Reaction of 1,6-diphenyl-1,6-di(*p*-tolyl)hexa-2,4-diyne-1,6-diol (**113**) with HBr gave *meso*- (**114**) and *rac*-3,4-dibromo-1,6-di-

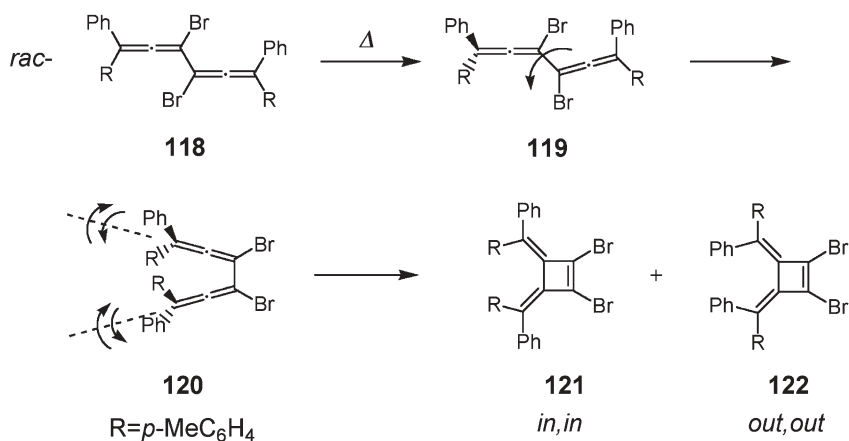


phenyl-1,6-di(*p*-tolyl)hexa-1,2,4,5-tetraene (**118**). Heating colorless crystals of **114** at 150 °C for 1 h gave *in,out*-1,2-dibromo-3,4-bis(phenyl-*p*-tolylmethylene)cyclobutene (**117**) in quantitative yield [19, 20] (Scheme 18). Similarly,



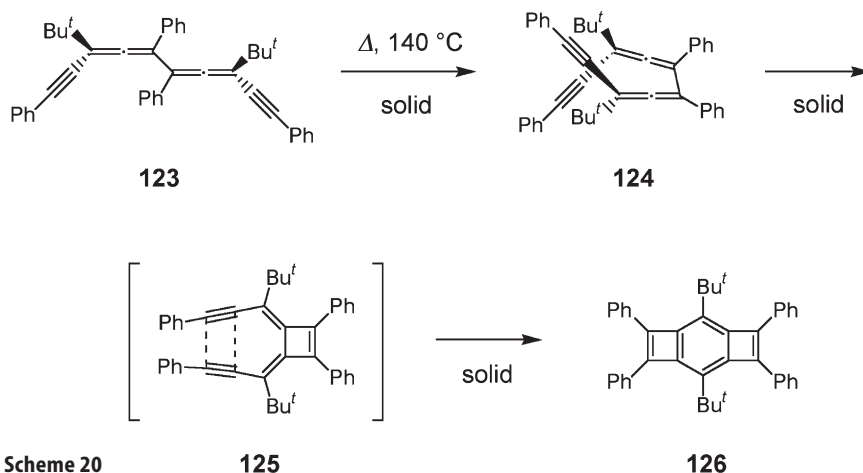
Scheme 18

heating colorless crystals of **118** at 150 °C for 1 h gave the *in,in*- (**121**) and *out,out*-isomers (**122**) of **117** in a 1:1 ratio (Scheme 19). Since no liquid state was observed during the cyclization reactions of **114** and **118**, the reaction in the crystal is a real crystal-to-crystal reaction. An X-ray analysis showed that **114** and **118** have an *s-trans* conformation in the crystal [21]. In order to cyclize to **117** and to **121** and **122**, **114** and **118** should first isomerize to their *s-cis* isomers **116** and **120**, respectively, in the crystal. The conformational change from the *s-trans* form to the *s-cis* form requires a rotation of the sterically bulky 1,1-diarylbisallene moiety around the single bond connecting the two allene groups in the crystalline state as indicated. Furthermore, thermal conversion of the *s-cis*-diallenes to the corresponding dimethylenecyclobutenes should also be accompanied by a molecular motion of the sterically bulky 1,1-diarylbisallene groups. These dynamic motions of the molecules in the crystalline state occur stereospecifically, namely, through a [2+2] conrotatory ring closure [19–21].



Scheme 19

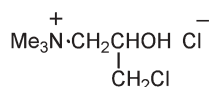
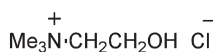
When colorless crystals of *rac-s-trans*-3,8-di-*tert*-butyl-1,5,6,10-tetraphenyl-deca-3,4,6,7-tetraene-1,9-diyne (**123**) were heated at 140 °C for 2 h, the ben-zodicylobutadiene derivative (**126**) was produced as green crystals. As shown in the sequence (Scheme 20), **123** is first isomerized to its *s-cis*-isomer (**124**), and intramolecular thermal reaction of the two allene moieties through a [2+2] conrotatory cyclization gives the intermediate **125**, which upon further thermal reaction between acetylene moieties gives the final product **126** [19, 22]. This is another example of the crystal-to-crystal reaction.



5.2

Racemic Crystal-to-Conglomerate Crystal Transformation Reactions in 2,2'-Dihydroxy-1,1'-binaphthyl-Me₄N⁺Cl⁻ Complex

Rac-2,2'-dihydroxy-1,1'-binaphthyl (**100a**) can easily be resolved by inclusion complexation not only with chiral ammonium salts such as (+)-*N*-benzylcinchonidinium chloride [23], (*S*)-(-)-**127b**, and (*R*)-(+)-*N*-(3-chloro-2-hydroxypropyl)-*N,N,N*-trimethylammonium chloride (**127c**) [24], but also with racemic ammonium salts such as **127a** [25]. Furthermore, **100a** can easily be resolved

**127****128****129**

a: *rac*-form

b: (*S*)-(-)-form

c: (*R*)-(+)-form

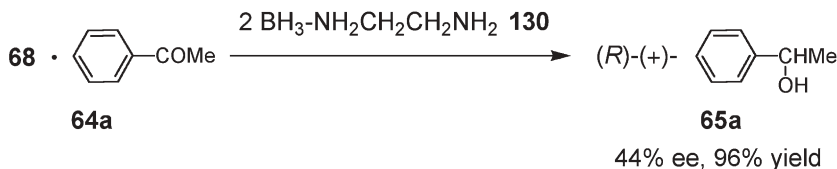
by complexation with achiral ammonium salts such as *N*-(2-hydroxyethyl)-*N,N,N*-trimethylammonium chloride (**128**) or tetramethylammonium chloride (**129**) [25]. In the case of the complexation of **100a** with **127a**, mutual resolution of both the components can be done very efficiently to give optically pure **100b**, **100c**, **127b**, and **127c** at once [25].

Interestingly, **129** forms both racemic and conglomerate complex crystals with **100**, and the former complex is transformed into the conglomerate complex by heating at 100 °C for 30 min or by exposure to MeOH vapor at room temperature for 30 min. This is the first finding of the transformation of a racemic crystal to a conglomerate crystal by heating or contact with a solvent vapor. The mechanism of this transformation in the solid state is now under investigation [25, 26].

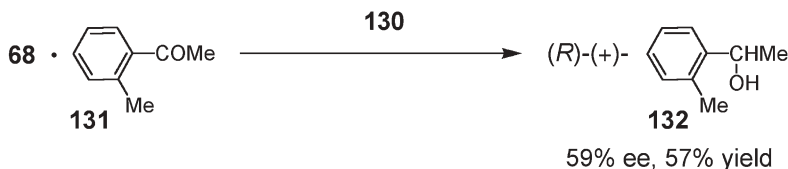
5.3

Enantioselective Reactions

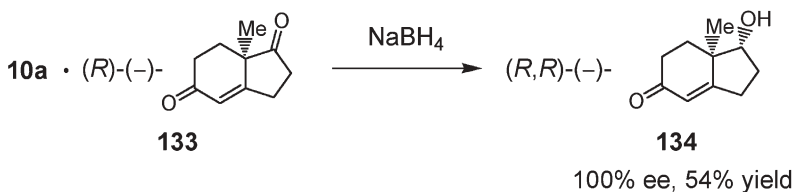
Enantioselective Br₂ addition to cyclohexene (**11**) was accomplished by the solid-state reaction of a 2:1 inclusion complex of **10b** and **11** with **7**, although the optical yield was low (Sect. 2.1). However, some successful enantioselective solid-state reactions have been reported. For example, reaction of a 1:1 complex of **68** and acetophenone (**64a**) with borane-ethylenediamine complex (**130**) in the solid state gave the (*R*)-(+)-2-hydroxyethylbenzene (**65a**) of 44% ee in 96% yield



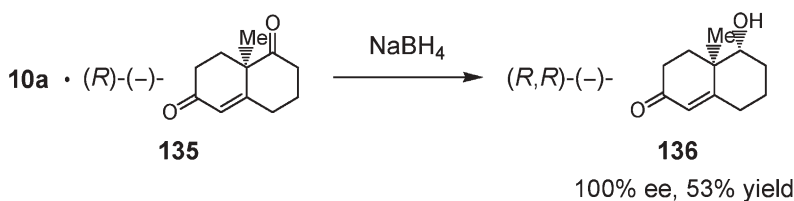
yield. By the same procedure, *o*-methylacetophenone (**131**) gave (*R*)-(+)-**132** of 59% ee in 57% yield [27].



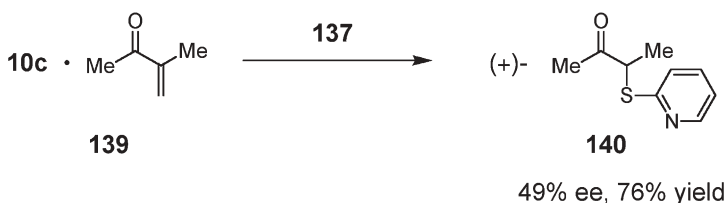
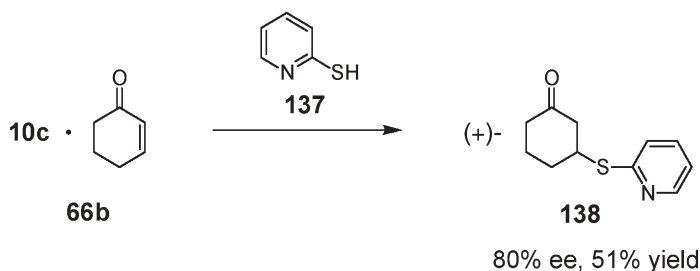
By complexation of the *rac*-bicyclic diketone (*rac*-**133**) with **10a**, (*R*)-(-)-**133** was included enantioselectively to give a 1:1 complex of **10a** and enantiomerically pure (*R*)-(-)-**133**. Treatment of the complex with NaBH₄ in the solid state gave (*R,R*)-(-)-**134** of 100% ee in 54% yield [28]. Not only enantioselective but also regioselective reduction of the cyclopentanone moiety of **133** occurred. X-ray



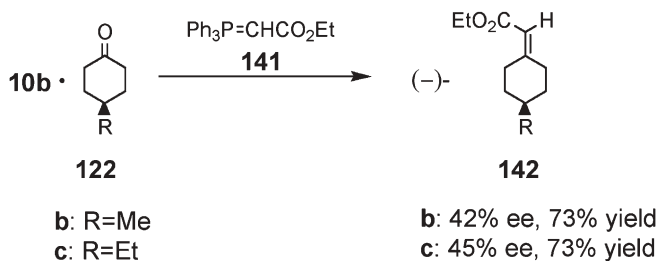
analysis of the complex of **10a** and $(R)-(-)-133$ showed that the cyclohexenone moiety is masked by forming a hydrogen bond with the hydroxyl group of **10a** [29]. By a similar method, reduction of a 1:1 complex of **10a** and enantiomerically pure $(R)-(-)-135$ gave $(R,R)-(-)-136$ of 100% ee in 53% yield [28].



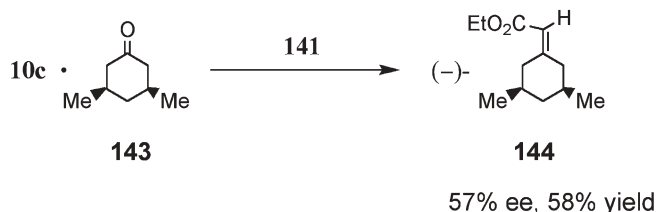
An enantioselective Michael addition reaction was also accomplished in an inclusion complex with a chiral host compound. Treatment of a 1:1 complex of **10c** and **66b** with 2-mercaptopyridine (**137**) in the solid state gave $(+)-138$ of 80% ee in 51% yield. By a similar method, 3-methyl-3-buten-2-one (**139**) gave $(+)-140$ of 49% ee in 76% yield [30].



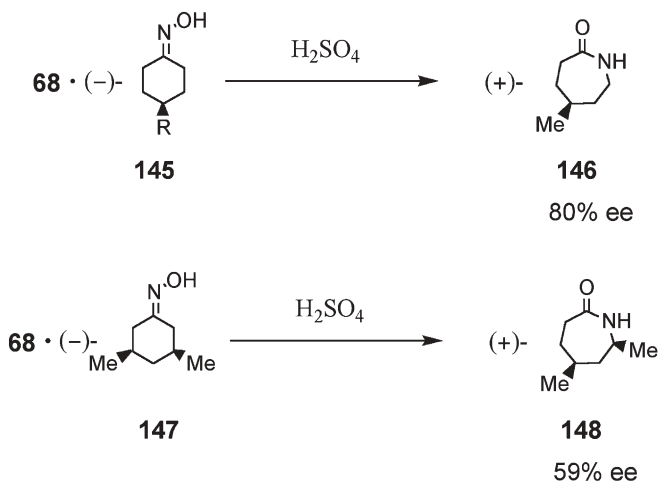
An enantioselective Wittig reaction was accomplished by the solid-state reaction of a 1:1 complex of **10b** and **122** or **10c** and **143** with **141**, which gives



the corresponding (-)-olefin **142** or **144**, respectively, in the optical and chemical yields indicated [31]. Optically active oximes **145** and **147** were obtained



as inclusion compounds by an enantioselective complexation of their racemic compounds with **68**. Beckmann rearrangement of these oximes **145** and **147** occurred stereospecifically in the crystalline complex by treatment with H_2SO_4 to give the (+)-lactams **146** and **148**, respectively, in the optical yields indicated [32].



Much more efficient enantioselective solid-state reactions can be accomplished by photochemical reactions. Some new results are summarized in the following section.

6

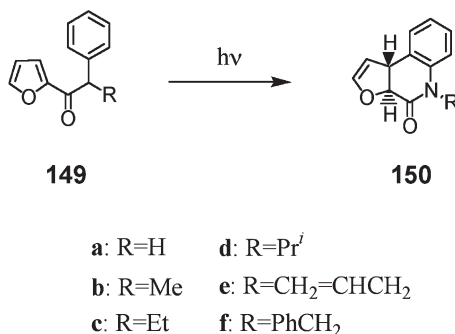
Photochemical Reactions

It is not easy to control the steric course of photoreactions in solution. Since molecules are ordered regularly in a crystal, it is rather easy to control the reaction by carrying out the photoreaction in a crystal. However, molecules are not always arranged at an appropriate position for efficient and stereoselective reaction in their crystals. In these cases inclusion chemistry is a useful technique, as it can be employed to position molecules appropriately in the host–guest structure. Chiral host compounds are especially useful in placing prochiral and achiral molecules in suitable positions to yield the desired product upon photoirradiation. Some controls of the steric course of intramolecular and intermolecular photoreactions in inclusion complexes with a host compound are described.

6.1

Intramolecular Photoreactions

Enantiocontrol of the photocyclization of *N*-alkylfuran-2-carboxyanilides (**149**) to *trans*-dihydrofuran derivatives (**150**) (Scheme 21) was accomplished by carrying out the reaction in an inclusion complex crystal of **149** with the chiral host **10a–c**. Although **149a** did not form an inclusion complex with **10a–c**, **149b–f** formed inclusion complexes in the ratios indicated in Table 13. Irradiation of these powdered inclusion complexes in a water suspension gave optically active **150b–f** in the chemical and optical yields summarized in Table 13 [33]. Optical yields of **150c** and **150e,f** were very high. In the case of **149e**, two kinds of inclusion complexes with the host **10b** were formed with the different host–guest ratios 1:1 and 2:1. Interestingly, photoirradiation of the 1:1



Scheme 21

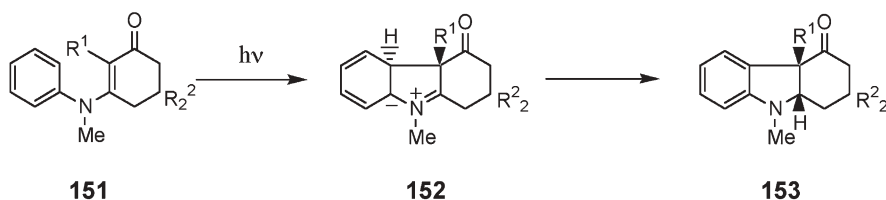
Table 13 Photoreaction of **149b–f** in their 1:1 inclusion complexes with **10a–c**

| Host | Guest | Ratio | Irradiation time (h) | Product | Yield (%) | |
|------------|-------------|-------|----------------------|------------------|-----------------------|----|
| | | | | | Optical purity (% ee) | |
| 10b | 149b | 1:1 | 40 | (–)- 150b | 25 | 8 |
| 10c | 149c | 2:1 | 120 | (+)- 150c | 41 | 99 |
| 10c | 149d | 1:1 | 143 | (+)- 150d | 16 | 52 |
| 10a | 149e | 1:1 | 96 | (+)- 150e | 20 | 93 |
| 10b | 149e | 1:1 | 77 | (–)- 150e | 50 | 96 |
| 10b | 149e | 2:1 | 48 | (+)- 150e | 86 | 98 |
| 10c | 149e | 2:1 | 50 | (+)- 150e | 77 | 98 |
| 10c | 149f | 1:1 | 120 | (–)- 150f | 72 | 98 |

and 2:1 complexes gave (–)-**150e** and (+)-**150e**, respectively (Table 13). This is an example of the formation of different enantiomers from a prochiral guest included by the same host in different ratios. X-ray analysis of the 1:1 complex showed that the prochiral molecules of **149e** are arranged in the inclusion cavity in a chiral form so as to give (*S,R*)-(–)-**150e** by photocyclization [33].

In the case of the inclusion complexation between **10c** and **149e**, the two inclusion compounds **10c–149e** (1:1) and **10c–149e** (2:1) were formed by mixing of powdered **10c** and **149e** in 1:1 and 2:1 ratios, respectively. Irradiation of the 1:1 and 2:1 complexes gave the same product (–)-**150e** in 49% and 54% ee, respectively. However, recrystallization of **10c** and **149e** from toluene gave only the 2:1 complex, and its photoreaction gave (+)-**150e** of 98% ee in 77% yield (Table 13) [33].

Enantiocontrol of the photocyclization of *N*-methyl-*N*-phenyl-3-amino-2-cyclohexen-1-one (**151a,b**) to the corresponding *N*-methylhexahydro-4-carbazolones (**153a,b**) via the dipolar ionic intermediate (**152a,b**) (Scheme 22) was also accomplished by photoirradiation of 1:1 inclusion complexes of **151a,b** with the chiral hosts **10a–c**. Of the complexes prepared, **10a–151a**, **10a–151b**,



a: $R^1=H$; $R^2=Me$

b: $R^1=Me$; $R^2=H$

Scheme 22

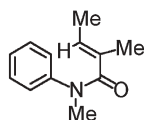
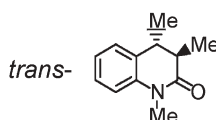
Table 14 Photoreaction of **151a,b** in their 1:1 inclusion complexes with **10a–c**

| Host–guest complex | Irradiation time (h) | Product | Conver- | Yield (%) | Optical |
|------------------------------|----------------------|----------------------|----------|-----------|---------------|
| | | | sion (%) | | purity (% ee) |
| 10a–151a | 16 | (+)- 153 | 29 | 6 | 97 |
| 10c–151a (prisms) | 11.5 | (+)- 153a | 9 | 54 | 87 |
| 10c–151a (needles) | 100 | No reaction occurred | | | |
| 10a–151b | 23 | (-)- 153b | 86 | 43 | 94 |
| 10b–151b | 13 | (-)- 153b | 64 | 20 | 85 |
| 10c–151b | 12 | (-)- 153b | 46 | 26 | 62 |

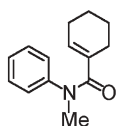
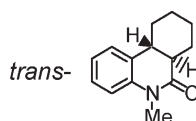
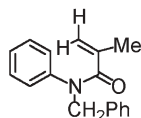
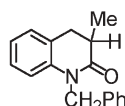
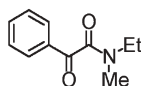
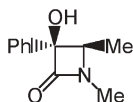
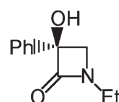
10b–151b, **10c–151a**, and **10c–151b** complexes gave the corresponding optically active cyclization products by photoirradiation in a water suspension medium in the chemical and optical yields summarized in Table 14 [34]. Interestingly, however, inclusion complexation of **10c** and **151a** formed two 1:1 complexes **10c–151a** as colorless prisms and needles. Although complexation of **10c** and **151a** by recrystallization of these compounds from a solvent gave a mixture of the two dimorphous crystals, if one piece of seed crystal of the **10c–151a** (prisms) is added during the recrystallization, the **10c–151a** (prisms) can be obtained in a large quantity and vice versa. Upon photoirradiation, **10c–151a** (prisms) gave (+)-**153a** of 87% ee and **10c–151a** (needles) was recovered unchanged (Table 14) [34].

X-ray structures of **10c–151a** (prisms) and **10c–151a** (needles) were analyzed and compared. In the former complex, the shortest contact between the aromatic carbon and cyclohexenyl carbon which are going to bind is 3.161(4) Å. In the latter complex, however, those two carbons are too distant to permit reaction [34].

Photoirradiation of the powdered 1:1 complex of **10b** and *N*-methyl-*N*-[(*E*)-methylmethacryloyl]anilide (**154**) gave (–)-**155** of 98% ee in 46% yield [35].

**154****155**

This reaction was proven to proceed in a partial single crystal-to-single crystal manner [35, 36]. However, irradiation of a 1:1 complex of **10c** with **154** gave (+)-**155** of 95% ee in 29% yield [37]. By a similar method, **156**, **158**, and **160** gave

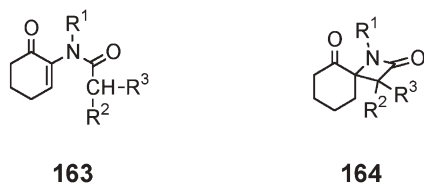
**156****157****158****159****160****161****162**

the corresponding optically active cyclization products in the chemical and optical yields indicated in Table 15 [37]. Very interestingly, irradiation of **160** in the inclusion complexes with **10b** and **10c** gave (–)-**161** and (+)-**162**, respectively, in almost enantiomerically pure forms. In the complex with **10b** and **10c**, ethyl and methyl groups reacted to give (–)-**161** and (+)-**162**, respectively. The reason for the difference was studied by X-ray analysis [37].

Irradiation of a 2:1 complex of **10c** and **163a** for 8 h gave (–)-**164a** of 97% ee in 52% yield [38]. Similar irradiation of a 1:1 complex of **10b** and **163b** for 20 h

Table 15 Enantioselective photocyclization of anilides and glyoylamide in their 1:1 inclusion complexes with **10b** or **10c**

| Host | Guest | Irradiation time (h) | Product | | |
|------------|------------|----------------------|-----------------|-----------|-----------------------|
| | | | | Yield (%) | Optical purity (% ee) |
| 10b | 154 | 150 | (–)- 155 | 46 | 98 |
| 10c | 154 | 150 | (+)- 155 | 29 | 95 |
| 10b | 156 | 50 | (+)- 157 | 62 | 70 |
| 10c | 156 | 50 | (–)- 157 | 70 | 98 |
| 10b | 158 | 15 | (–)- 159 | 64 | 98 |
| 10c | 158 | 15 | (+)- 159 | 41 | 8 |
| 10b | 160 | 53 | (–)- 161 | 21 | 99 |
| 10c | 160 | 58 | (+)- 162 | 48 | 98 |



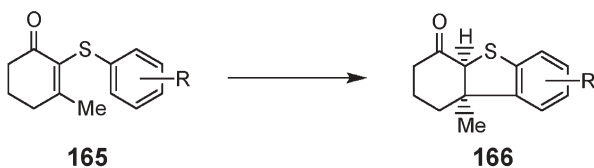
a: $R^1 = \text{PhCH}_2$, $R^2 = \text{Ph}$, $R^3 = \text{H}$

b: $R^1 = \text{PhCH}_2$, $R^2 = \text{Me}$, $R^3 = \text{H}$

c: $R^1 = \text{Pr}^i$, $R^2, R^3 = \text{Cyclopentyl}$

gave (–)-**164b** of 71% ee in 81% yield. Irradiation of a 1:1 complex of **10a** and **163c** for 13 h gave (–)-**164c** of 99.9% ee in 94% yield [38].

Irradiation of 2-arylthio-3-methylcyclohexen-1-ones (**165a–g**) (Scheme 23) in a 1:1 complex with **10b** for 30 h gave the corresponding (+)-cyclization products **166a** (52%), **166b** (68%), **166c** (72%), **166d** (75%), **166e** (81%), **166f** (70%), and **166g** (83%), respectively, in the enantiomeric excesses indicated and in good yields [39].



a: $R = \text{H}$

e: $R = o\text{-Cl}$

b: $R = p\text{-Me}$

f: $R = p\text{-Br}$

c: $R = o\text{-Me}$

g: $R = o\text{-Br}$

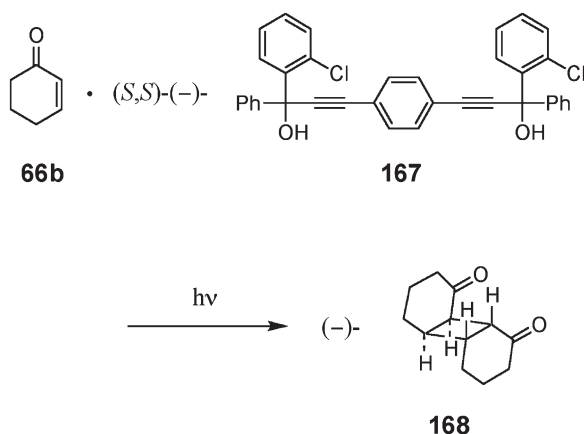
d: $R = p\text{-Cl}$

Scheme 23

6.2

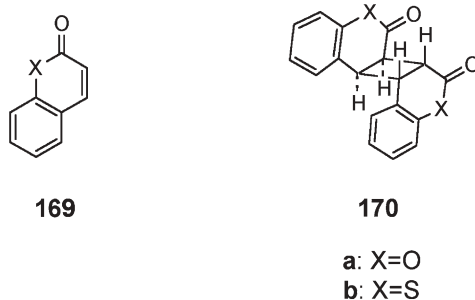
Intermolecular Photoreactions

Photoirradiation of both neat and benzene solutions of 2-cyclohexenone (**66b**) gives a complex mixture of photodimers [40]. However, photoirradiation of a 1:1 complex of **66b** with the chiral host (S,S)-(–)-1,4-bis[3-(*o*-chlorophenyl)-3-hydroxy-3-phenylprop-1-ynyl]benzene (**167**) in the solid state (Scheme 24) gave (–)-*anti*-head-to-head dimer **168** of 46% ee in 75% yield [40]. This reaction was found to proceed in a single crystal-to-single crystal manner. The mechanism of the reaction was studied by X-ray crystal structural analysis [41].



Scheme 24

Single crystal-to-single crystal enantioselective photodimerizations of coumarin (**169a**) and thiocoumarin (**169b**) were found to proceed efficiently in



inclusion complexes with **10a** and **10b**, respectively [42]. By these reactions, (-)-*anti*-head-to-head dimers **170a** and (+)-*anti*-head-to-head dimer **170b** were obtained in optically pure forms. In order to clarify the mechanism of the single crystal-to-single crystal reaction, X-ray analysis was carried out twice for the **10a**–**169a** complex crystal before and after the irradiation. Before the irradiation, two **169a** molecules are arranged in the complex at very close positions as shown in Fig. 6. After the irradiation, the molecule of the photodimer **170a** produced is arranged at almost the same position as the two **169a** molecules had been before the irradiation (Fig. 7). By the photodimerization from **169a** to **170a**, no big change of the crystalline cavity occurred in the complex [42]. This is the reason for the single crystal-to-single crystal reaction. X-ray structural study of the **169b**–**10c** complex before and after the irradiation led to the same conclusion [42].

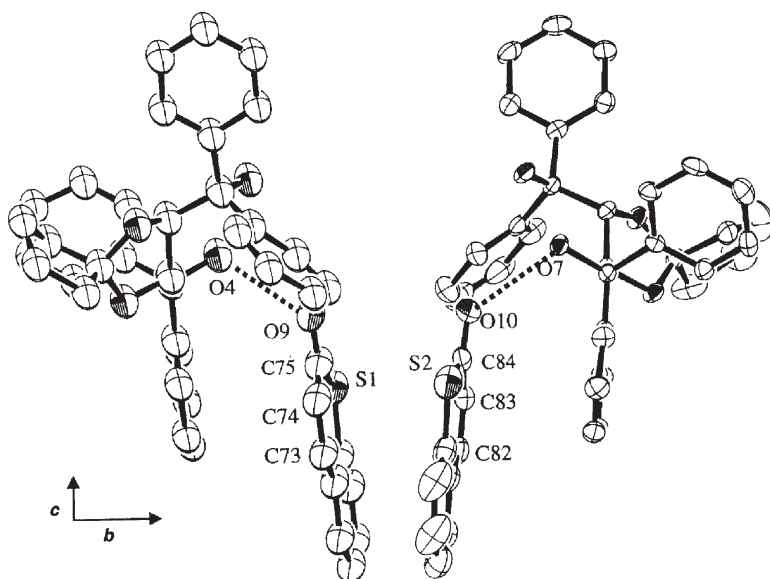


Fig. 6 ORTEP drawing of molecular structure of a 1:1 complex of **169b** with **10b** viewed along the *a*-axis. All hydrogen atoms are omitted for clarity. The hydrogen bonding is shown by dotted lines

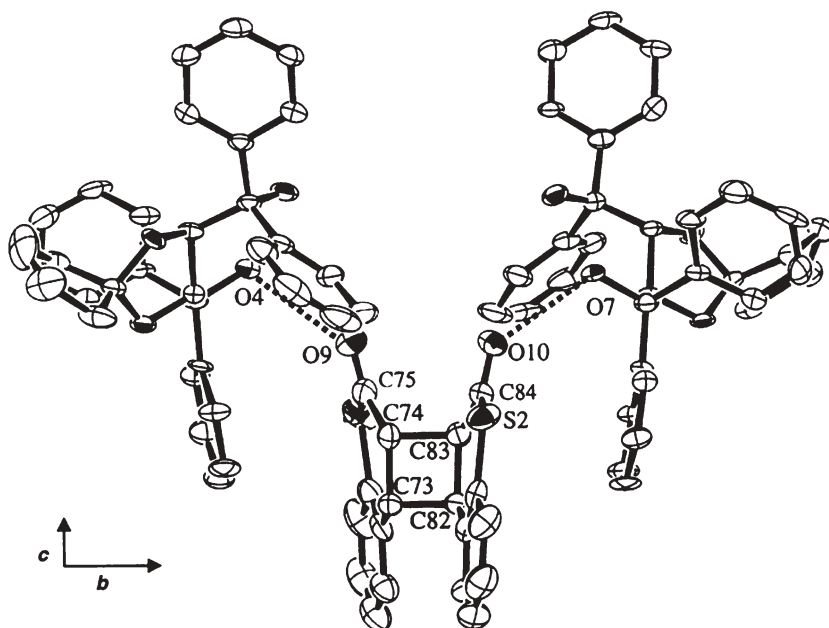


Fig. 7 ORTEP drawing of molecular structure of a 2:1 complex of (+)-**170b** with **10b** viewed along the *a*-axis. All hydrogen atoms are omitted for clarity. The hydrogen bonding is shown by dotted lines

Acknowledgements The author is grateful to his coworkers whose names appear in the references. The author would also like to thank PhD students Kazuhiro Yoshizawa and Shinya Hirano for their technical assistance in the preparation of this chapter.

References

1. Toda F (1988) *Top Curr Chem* 149:211; Toda F (1995) *Acc Chem Res* 28:480; Tanaka K, Toda F (2000) *Chem Rev* 100:1025
2. Toda F (ed) (2000) *Organic Solid-State Reactions*. Kluwer, Dordrecht; Toda F, Bishop R (eds) (2004) *Separations and Reactions in Organic Supramolecular Chemistry*. Wiley, New York
3. Tanaka K, Shiraishi R, Toda F (1999) *J Chem Soc Perkin Trans 1* 3069
4. Shan N, Toda F, Jones W (2002) *Chem Commun* 2374
5. Toda F, Schmeyers J (2003) *Green Chem* 5:701
6. Johnson WS, Davis CE, Hunt RH, Stork G (1948) *J Am Chem Soc* 70:3021; Johnson WS, Schneider WP *Org Synth Coll Vol IV*:132
7. Tanaka K, Sugino T, Toda F (2000) *Green Chem* 2:303
8. Hatano B, Toyota S, Toda F (2001) *Green Chem* 3:140
9. Yoshizawa K, Toyota S, Toda F (2001) *Tetrahedron Lett* 42:983
10. Miyamoto H, Kanetaka S, Tanaka K, Yoshizawa K, Toyota S, Toda F (2000) *Chem Lett* 888
11. Cumming WM, Hopper IV, Wheeler TS (1950) *Synth Org Chem* 190
12. Miyamoto H, Yasaka S, Takaoka R, Tanaka K, Toda F (2001) *Enantiomer* 6:51
13. Yoshizawa K, Toyota S, Toda F (2002) *Green Chem* 4:68
14. Thompson QE (1958) *J Am Chem Soc* 80:5483
15. Buu-Hoi N, Saint-Ruf G, Loc TB, Xuong ND (1957) *J Chem Soc* 2593
16. Yoshizawa K, Toyota S, Toda F, Csoeregh I (2003) *Green Chem* 5:353
17. Nakamatsu S, Yoshizawa K, Toyota S, Toda F, Matijasic I (2003) *Org Biomol Chem* 1:2231
18. Tanaka K, Takamoto N, Tezuka Y, Kato M, Toda F (2001) *Tetrahedron* 57:3761
19. Toda F (2000) *Eur J Org Chem* 1377
20. Toda F, Tanaka K, Tamashima T, Kato M (1988) *Angew Chem Int Ed Engl* 37:2724
21. Kaupp G, Schmeyers J, Kato M, Toda F (2002) *J Phys Org Chem* 15:148
22. Boese R, Benet-Buchholz J, Stange A, Tanaka K, Toda F (1999) *Chem Commun* 319
23. Tanaka K, Okada T, Toda F (1993) *Angew Chem Int Ed Engl* 32:1147
24. Toda F, Yoshizawa K, Hyoda S, Toyota S, Chatziefthimiou S, Mavridis IM (2004) *Org Biomol Chem* 2:449
25. Yoshizawa K, Toyota S, Toda F (2004) *Tetrahedron* 7767
26. Yoshizawa K, Toyota S, Toda F (2004) *Chem Commun* 1844
27. Toda F, Mori K (1989) *J Chem Soc Chem Commun* 1245
28. Toda F, Kiyoshige K, Yagi M (1989) *Angew Chem Int Ed Engl* 28:320
29. Bond DR, Bourne SA, Nassimbeni LR, Toda F (1989) *J Cryst Spec Res* 19:809
30. Toda F, Tanaka K, Sato J (1993) *Tetrahedron Asymm* 4:1771
31. Toda F, Akai H (1990) *J Org Chem* 55:3446
32. Toda F, Akai H (1990) *J Org Chem* 55:4973
33. Toda F, Miyamoto H, Kanemoto K, Tanaka K, Takahashi Y, Takenaka Y (1999) *J Org Chem* 64:2096
34. Toda F, Miyamoto H, Tamashima T, Kondo M, Ohashi Y (1999) *J Org Chem* 64:2690
35. Tanaka K, Kakinoki O, Toda F (1992) *J Chem Soc Chem Commun* 1053
36. Hosomi H, Ohba S, Tanaka K, Toda F (2000) *J Am Chem Soc* 122:1818
37. Ohba S, Hosomi H, Tanaka K, Miyamoto H, Toda F (2000) *Bull Chem Soc Jpn* 73:2085

38. Toda F, Miyamoto H, Inoue M, Yasaka S, Matijasic I (2000) *J Org Chem* 65:2728
39. Toda, F, Miyamoto H, Kikuchi S, Kuroda R, Nagami F (1996) *J Am Chem Soc* 118:11315
40. Lam EY, Valentine D, Hammond GS (1967) *J Am Chem Soc* 89:3482
41. Tanaka K, Mizutani H, Miyahara I, Hirotsu K, Toda F (1999) *CrystEngComm* 3
42. Tanaka K, Toda F, Mochizuki E, Yasui N, Kai Y, Miyahara I, Hirotsu K (1999) *Angew Chem Int Ed* 38:2523; Tanaka K, Mochizuki E, Yasui N, Kai Y, Miyahara I, Hirotsu K, Toda F (2000) *Tetrahedron* 56:6853

Crystal Engineering of Organic Cocrystals by the Solid-State Grinding Approach

Andrew V. Trask · William Jones (✉)

University of Cambridge, Department of Chemistry, Lensfield Road, Cambridge CB2 1EW, UK
wj10@cam.ac.uk

| | | |
|---|--|----|
| 1 | Introduction | 42 |
| 2 | A Historical Perspective | 43 |
| 3 | Cocrystals Produced Exclusively by the Grinding Approach | 53 |
| 4 | A Recent Enhancement to the Grinding Approach | 59 |
| 5 | Structure Determination from Powder XRD Data | 64 |
| 6 | Concluding Remarks | 68 |
| | References | 69 |

Abstract Crystal engineering of organic cocrystals is gaining interest across a variety of disciplines. The solid-state grinding approach to preparing cocrystals is an alternative to the traditional method of solution crystallisation, and possesses several distinct advantages. This review first demonstrates that the approach of solid-state cocrystal preparation is well established in the literature by providing a brief historical account of its applications. Several cases are then examined in which certain cocrystal materials can be prepared only by solid-state grinding methodologies. These examples underscore the importance of this approach in the search for new cocrystal materials. This is particularly advantageous when searching for new cocrystal stoichiometries. The focus then turns to a recent modification of the solid-state grinding process, in which small quantities of solvent are introduced either to increase solid-state cocrystallisation kinetics or to provide polymorph control – the latter having particular significance in the pharmaceutical field. Finally, a significant analytical advancement with direct implications for the field of solid-state cocrystal preparation is considered by examining recent examples of crystal structure determination from powder X-ray diffraction data.

Keywords Solid-state grinding · Cocrystal formation · Crystal engineering · Pharmaceutical materials · Polymorphism

Abbreviations

XRD X-ray diffraction

1

Introduction

One flourishing area in the field of crystal engineering is based upon the formation of crystalline molecular complexes, or cocrystals. Cocrystals may be defined as materials which contain two or more discrete molecular entities in the crystal lattice. Crystal engineering, when applied to cocrystal systems, generally involves the design and study of new materials in order to widen the knowledge base of successful engineering strategies, and the application of that knowledge to provide cocrystals with specific properties for a multitude of applications. Crystal engineering is actively applied within a variety of scientific disciplines as diverse as materials science, nanotechnology and the pharmaceutical industry [1].

In designing a cocrystal, it is necessary to evaluate the potential intermolecular interactions that a given molecule may exhibit. Due to their robust and directional nature, hydrogen bonds are a valuable tool in cocrystal synthesis. Hydrogen bonds of varying strengths may be employed, including the traditional $\text{OH}\cdots\text{O}$ and $\text{OH}\cdots\text{N}$ strong hydrogen bonds and the weaker $\text{CH}\cdots\pi$ or $\text{CH}\cdots\text{Cl}$ variety. Other intermolecular associations which may be employed in cocrystal design include halogen–halogen, nitro–nitro and $\pi\cdots\pi$ interactions, among others [2–4].

Cocrystals are often prepared by a traditional solution crystallisation approach such as solvent evaporation, cooling, or anti-solvent addition. There are a number of reasons for the popularity of the solution-based approach. Solution crystallisation can yield large, well-formed single crystals, from which one may easily evaluate crystal habit and surface features. Analysis of the diffraction pattern of a single crystal is typically the best means of obtaining an absolute crystal structure determination. Further, solution crystallisation is an established and effective purification step.

There are, however, several accompanying drawbacks to the solution-based approach to cocrystal formation. The solubility of the starting components is one obstacle, as a suitable solvent for all ingoing materials must be identified before cocrystallisation may occur. Unexpected solvate formation may also pose a problem. The solvent employed in the cocrystallisation may possess the ability to interfere with the desired cocrystal intermolecular interactions, and thus may become incorporated into the crystal lattice. In this way, solvate formation hampers rational cocrystal design. In the case of polymorphic cocrystal systems, it could be the case that solution crystallisation leads to an undesired kinetically controlled metastable polymorph. An additional drawback to cocrystallisation from solution is the typically large volume of solvent necessary to prepare the cocrystals. As cocrystals emerge as products in industrial applications, avoidable waste streams will be increasingly scrutinised as environmentally and fiscally imprudent.

An alternative to the solution-based approach exists in the approach of solid-state grinding. The act of solid-state grinding to induce chemical change,

known as mechanochemistry, has relevance to a variety of fields [5], and has several attractive aspects with regard to forming organic cocrystals. The relative solubility of ingoing components in a particular solvent is not a concern when solid-state grinding is employed, thereby increasing the utility of this technique over the solution approach by greatly easing the burden of experiment design. Solvent-free solid-state cocrystallisation also eliminates the possibility of forming undesired solvates. There is some evidence to indicate that, at least in single-component systems, solid-state grinding leads to the high-melting thermodynamically stable polymorph [6]. Further, the absence of solvent makes this an inherently 'green' approach to forming cocrystals by eliminating large volumes of solvent waste; the minimization of excess crystallisation solvent could help achieve corporate green chemistry targets [7]. Finally, while it is not yet fully understood, there are instances in which certain structures or stoichiometries of cocrystals may only be obtained via the solid state.

Solid-state cocrystallisation also possesses drawbacks. While the field of crystal engineering develops, the primary point of interest upon forming a cocrystal material is often the elucidation of its crystal structure. Single crystal X-ray diffraction (XRD), which requires a crystal of sufficient size, is incompatible with solid-state grinding, which is a particle size reduction technique. Thus, a cocrystal prepared only by solid-state grinding will require alternative, less common means of revealing structural features of interest, such as the hydrogen bond motif that may be present. Other disadvantages to solid-state grinding include the lack of purification that solution crystallisation may provide, and the increase in crystalline disorder which accompanies some materials upon energetic grinding. A grinding-induced change in a compound's degree of crystallinity may lead to changes in its physicochemical properties [8, 9].

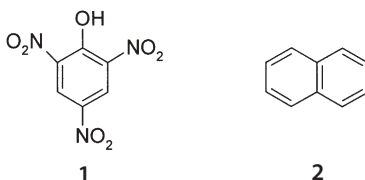
2

A Historical Perspective

Despite its simplicity, the solid-state grinding approach remains less familiar than cocrystal formation from solution. There is, however, ample precedence of the solid-state approach in the literature. Over a century ago, researchers in the field of charge-transfer complexes reported cocrystal formation by grinding [10]. In a paper describing halogen derivatives of quinchrydron, Ling and Baker reported the formation of a tetrachloroquinhydrone by grinding together equal weights of metadichloroquinone and metadichloroquinol, followed by purification from light petroleum.

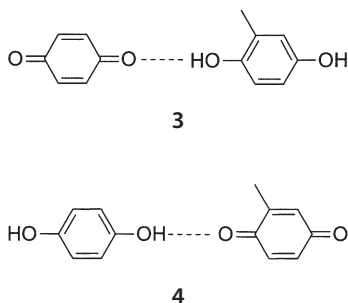
To date, very little research has been directed at understanding the mechanism of organic cocrystal formation by solid-state grinding. Work by Rastogi and co-workers in the 1960s, which was aimed at improving the understanding of the solid-state kinetics of several systems containing picric acid **1**, appeared to suggest that a vapour diffusion mechanism might operate in some of the

systems they studied. One interesting example described solid-state complex formation between **1** and naphthalene **2** in the absence of grinding [11].



The two starting components were packed into a glass capillary from opposite ends until they met in the centre. A coloured reaction product was observed visually after 7 to 10 min at the reactant interface. As time progressed, the product interface was observed to advance in the direction of the picric acid reactant. Further study of this reaction supported a vapour diffusion mechanism, bolstered in part by the observation that complexation proceeds even if a small gap of space exists between the two reactants [12]. The nature of the complex was investigated in additional work, whereby it was proposed that a donor/acceptor π -complex was produced [13]. A crystal structure confirming this deduction was later published [14].

Quinhydrone charge-transfer complexes were the subject of study by Paul, Curtin and co-workers in the 1980s [15–18]. Unsymmetrically substituted quinhydrones, which are very labile in solution with respect to redox self-isomerisation, form asymmetric charge-transfer complexes upon solid-state grinding. For example, 1,4-benzoquinone and 2-methylhydroquinone form the charge-transfer complex **3** upon solid-state grinding with a mortar and pestle.

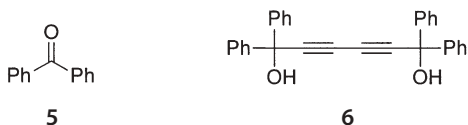


The product of solid-state grinding exhibits no evidence of complex **4**, which would be expected to result following solution-mediated redox isomerisation of the starting components. Solid-state grinding preparation of quinhydrone complexes was later pursued by Guarrera et al. [19].

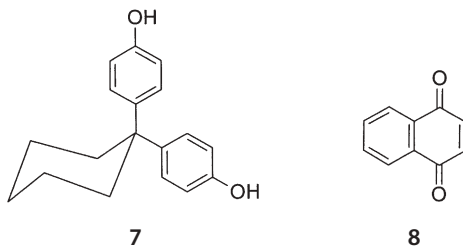
Several examples of solid-state formation of cocrystals without charge-transfer interaction were reported by Toda and co-workers in 1987 [20]. Various or-

ganic reagents were combined in a test tube and agitated with a mechanical test tube shaker for specific lengths of time. A total of seven resulting cocrystal products were formed in this manner.

The amount of time necessary to effect complete cocrystallisation, as judged by IR and melting point, varied significantly. A cocrystallisation between 5 and 6 was deemed complete after only 12 min of solid-state agitation, while the



complexation of 7 and 8 required 48 h of agitation. Interestingly, while many of the complexes could be formed both by solid-state agitation and by solution methods, the cocrystal containing 7 and 8 could not be obtained by solvent crystallisation; this was also the cocrystallisation that required the longest solid-state agitation time.



Beginning in the late 1980s with work directed at understanding the preferences of hydrogen bonds, Etter and co-workers consistently attempted to prepare cocrystals by both solution evaporation and solid-state grinding techniques [21–29]. The sustained effort of the Etter group towards consistently reporting results from both solution and grinding cocrystallisation attempts provided confirmation that the grinding approach was a viable means of generating a variety of hydrogen-bonded cocrystal materials.

In order to illustrate the value of hydrogen bonding in designing acentric organic solids for non-linear optical materials, Etter and Frankenbach studied the 1:1 cocrystal of 4-aminobenzoic acid and 3,5-dinitrobenzoic acid [21]. The carboxylic acid heterodimer hydrogen-bonding pattern (Fig. 1) was confirmed by XRD analysis on a single crystal obtained by evaporation of an equimolar solution in methanol. The same cocrystal material, as determined by powder XRD, was produced by grinding the solid components together for 5 min (grinding was performed in a dental amalgamator).

A cocrystallisation study of the hydrogen bond preferences of 2-amino-pyrimidine 9 by Etter and Adsmond provided further evidence of the utility

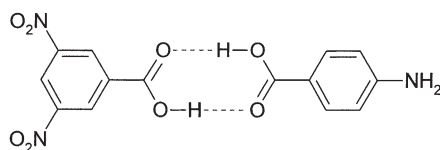
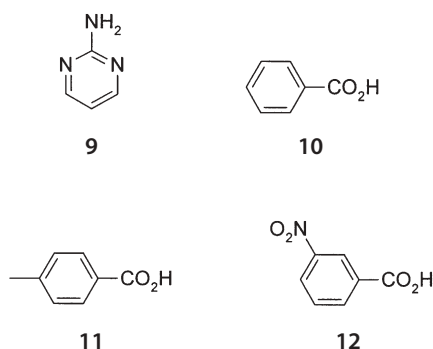


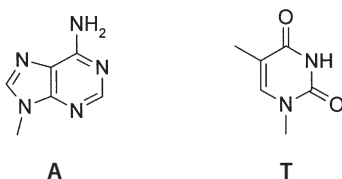
Fig. 1 Carboxylic acid heterodimer formed by solution and solid-state grinding cocrystallisation approaches [21]

of solid-state grinding, especially with regard to stoichiometry selection [23]. A total of 11 cocrystals were reported with different mono- and dicarboxylic acids. Interestingly, both 1:2 and 1:1 cocrystal stoichiometries were observed in cocrystals of **9** with **10**, **11** and **12**. For both solution and solid-state grind-



ing approaches, it was found that the resulting cocrystal stoichiometry could be dictated by the stoichiometry of the ingoing components. Different crystallisation behaviour was observed in one instance with two stoichiometries of a cocrystal with succinic acid; this case is described in the following section.

A further example of interest reported by Etter and co-workers involved the base pair consisting of the pyrimidine 1-methylthymine **T** and the purine 9-methyladenine **A** [28]. These are derivatives of the base pairs found in the



DNA structure. The hydrogen-bonding interaction of the AT base pair was previously described from XRD analysis by Hoogsteen on a single crystal grown from aqueous solution (Fig. 2a) [30]. Etter et al. reported that grinding **A** and

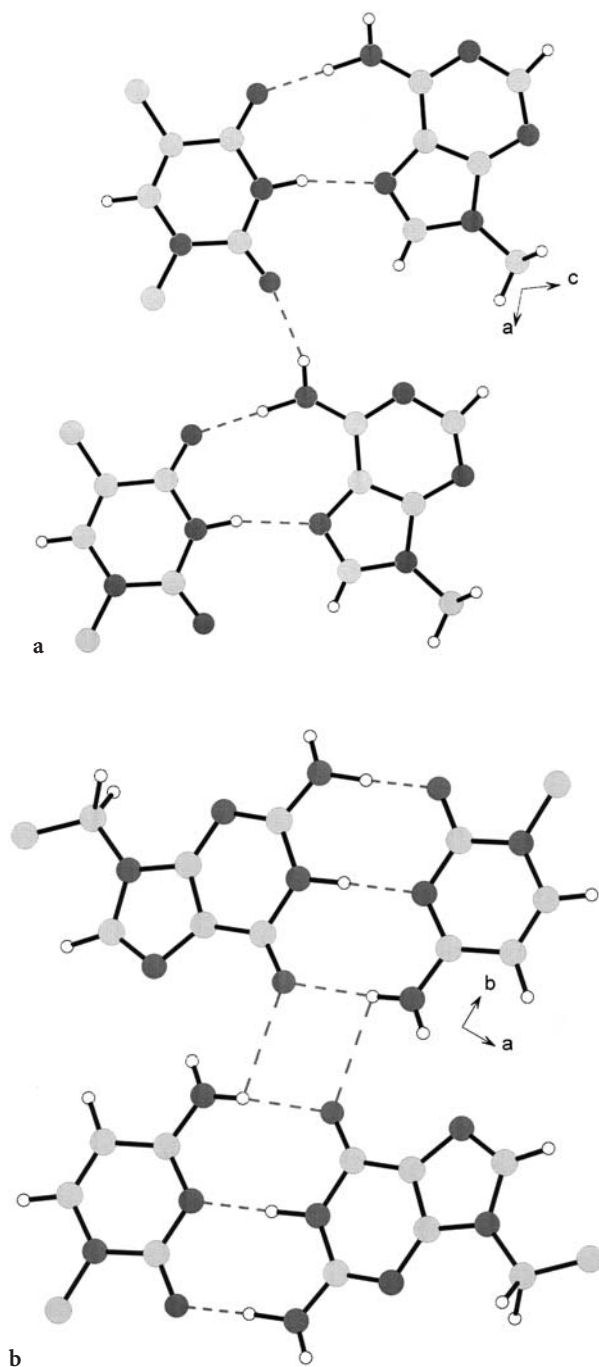
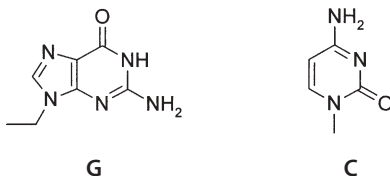


Fig. 2 a AT crystal packing [30] and b CG crystal packing [31] (some methyl hydrogens are absent from both reported crystal structures)

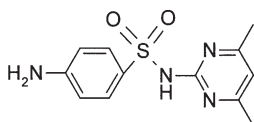
T together in the solid state for 20 min produced a material which had the same powder XRD pattern as that calculated from the known crystal structure AT. By comparison, however, an interesting distinction exists with an analogous base pair involving 9-ethylguanine G and 1-methylcytosine C, which had also



been grown from solution and characterised by single crystal XRD (Fig. 2b) [31]. While AT formed after grinding for only 20 min, CG showed no cocrystallisation after intermittent grinding and heating for up to 7 days. This is surprising, particularly in light of the increased number of hydrogen bonds that are possible in the CG base pair as compared to the AT pair. This illustration underscores a lack of full understanding of the factors which influence successful solid-state grinding.

Resulting from their efforts at using the grinding approach with a variety of cocrystal systems, Etter and co-workers related two factors which appeared to be important determinants of cocrystal formation by solid-state grinding. Etter et al. state that “at least one of the components should have some volatility at the temperature of the grinding experiments, and the product dimers should have a stronger intermolecular hydrogen bond than any of the hydrogen bonds in the structures of the two starting materials” [25]. The comment regarding volatility, which calls to mind the findings of Rastogi et al. [12], is experimentally supported by the observation of Etter et al. that the yield of a solid-state cocrystallisation may be improved by heating the product following grinding [25]. The heating was always at least 50 °C below the melting temperature of either starting component, and no melting or fusing of the particles was observed. While this topic appears not to have been further explored, it is interesting to consider the possibility that ‘activation’ of a cocrystallisation mixture may also be accomplished by other methods, such as the input of ultrasound [32] or microwave energy.

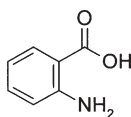
Cocrystallisation has gained recent interest in application to pharmaceuticals [33–35]. The ability to tailor the physiochemical properties of a drug substance via complexation is highly desirable for bioavailability, stability and processing considerations. In 1995, Caira and co-workers demonstrated the pharmaceutical application of cocrystallisation via solid-state grinding by systematically studying a range of different pharmaceutical cocrystals [36]. Cocrystals of the sulfa drug sulfadimidine 13 (also known as sulfamethazine) with various carboxylic acids were prepared from solution, and crystal structures were obtained [37, 38]. It was then demonstrated that six of the cocrystals



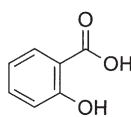
13

could be prepared by grinding with mortar and pestle or with a ball mill. The cocrystals formed by grinding exhibited identical powder XRD patterns to those grown from solution.

A remarkable preference was demonstrated for one particular cocrystal, the sulfadimidine:anthranilic acid (**13:14**) cocrystal. In a grinding competition experiment, a sulfadimidine:salicylic acid (**13:15**) cocrystal, for which the crystal structure had been previously determined [39], was ground in the presence of anthranilic acid **14**. The result was a displacement of salicylic acid **15** by



14



15

anthranilic acid **14** as the cocrystal partner of sulfadimidine **13**. Because of the common hydrogen-bonding pattern in both cocrystals (Fig. 3), the authors base their explanation for the preference on the intermolecular bonding of the ingoing homomeric acid crystals. Salicylic acid **15** is observed to pack with familiar carboxylic acid dimers, while the particular polymorph of anthranilic acid **14** employed in the experiment consists of an unusual helical packing of un-ionised and zwitterionic molecules. The preferential formation of the sulfadimidine:anthranilic acid (**13:14**) cocrystal is attributed to an increased reactivity of the pure anthranilic acid material due to its presumably less stable hydrogen-bonding pattern.

This elegant demonstration of the displacement of one cocrystallisation partner with another via solid-state grinding may indicate the possibility of a more general application. A new route may exist to obtaining novel cocrystals whereby one first produces an intermediate cocrystal, or precursor, containing a cocrystallising agent which may then be displaced by a second cocrystallising agent en route to the desired product. While this has not yet been widely demonstrated with organic cocrystals, a similar methodology has been demonstrated in the field of layered inorganic solids. In order to generate an isopoly-metalate pillared clay, a precursor is first prepared in which a large organic anion is inserted between brucite layers. The precursor is then subjected to polymetalate exchange to allow the even larger heptamolybdate or decavanadate anion to intercalate within the solid [40–42].

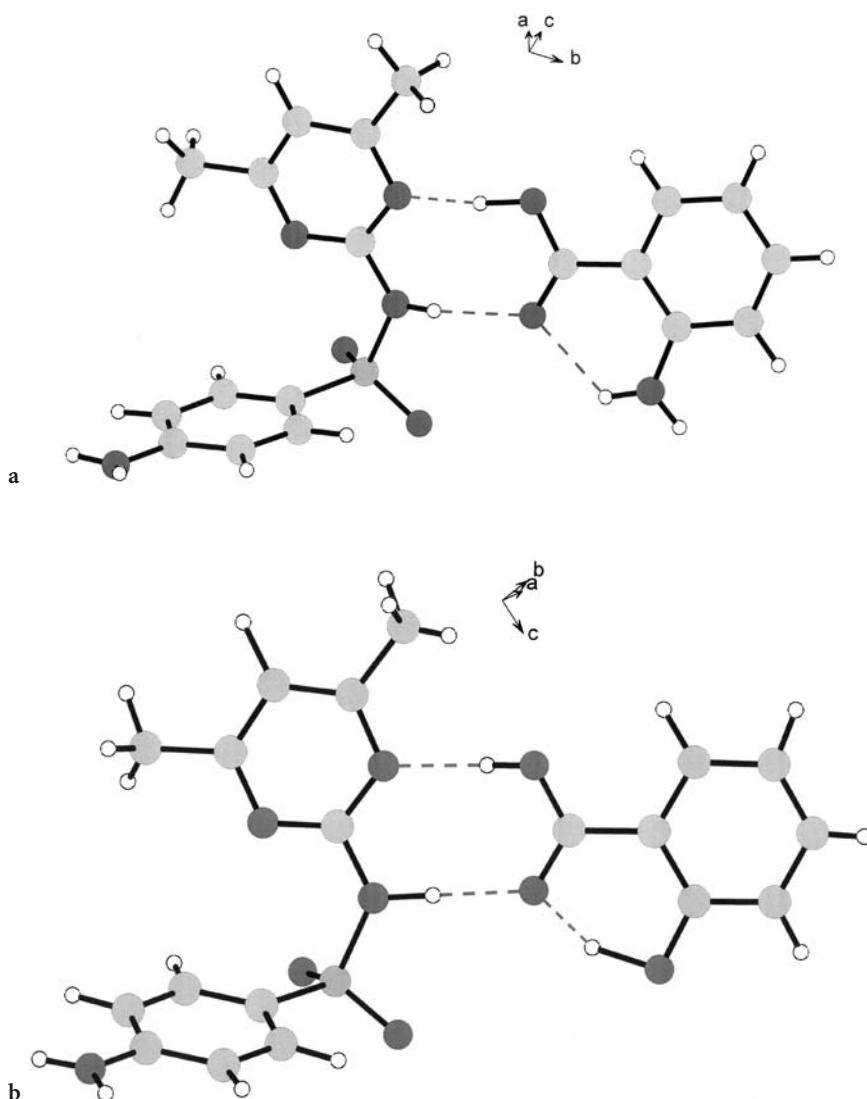
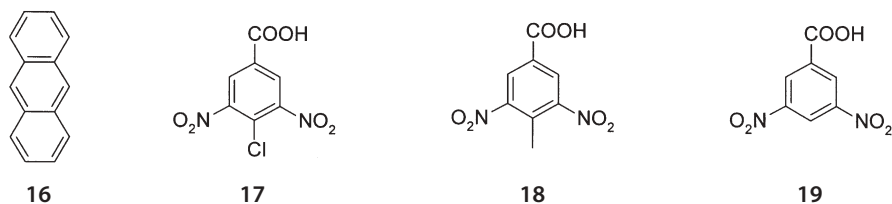


Fig. 3 Hydrogen bonding motif of a sulfadimidine:anthranilic acid (13:14) [37] and b sulfadimidine:salicylic acid (13:15) [39]

As mentioned above, Caira et al. implicated the stability of an ingoing cocrystallisation component as a factor in the preferential formation of a sulfadimidine cocrystal [36]. A year later, in a detailed structural analysis of three anthracene **16** cocrystals, Pedireddi et al. concluded that the ability of potential constituents to satisfy a network of hydrogen bonds dictated solid-state cocrystal formation [43]. Cocrystallisations of anthracene **16** with 4-chloro-3,5-dinitrobenzoic acid **17**, 3,5-dinitro-4-methylbenzoic acid **18** and 3,5-dinitrobenzoic



acid **19** were attempted by solution precipitation and by solid-state grinding. Solid-state grinding led to cocrystallisation of **17:16** and **18:16** but not **19:16**. Solution precipitation also yielded **17:16** and **18:16**. A cocrystal of **16** and **19** resulted from solution precipitation from benzene only.

Crystal structures of the three cocrystal materials were solved by single crystal XRD. The inability of a **19:16** cocrystal to form by solid-state grinding was revealed by the fact that a benzene molecule was incorporated into the cocrystal structure formed from solution. Hydrogen bonding of the **17:16** and **18:16** cocrystals is nearly identical (Fig. 4a,b). In each, a planar hexagonal hydrogen-bonded ring composed of **17** or **18** surrounds the anthracene **16**. In order to maintain favourable contacts around the ring, the following three

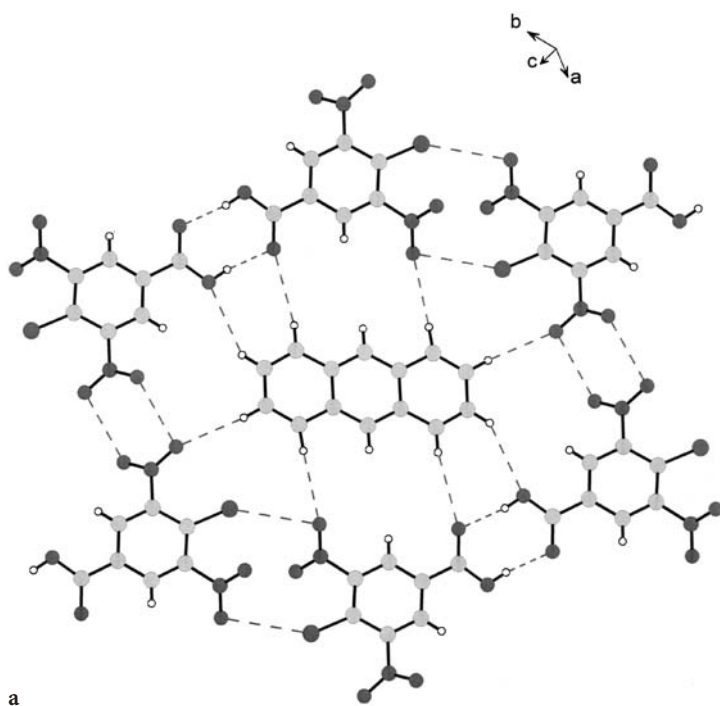
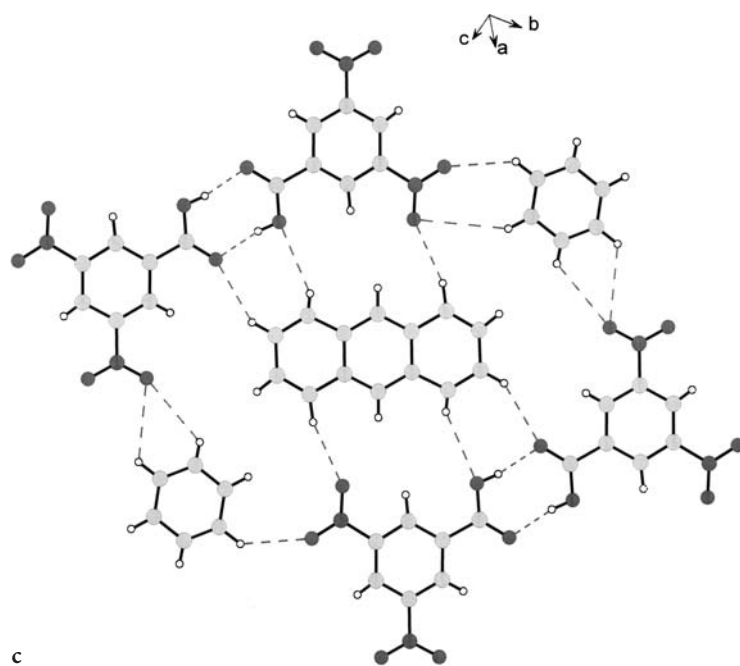
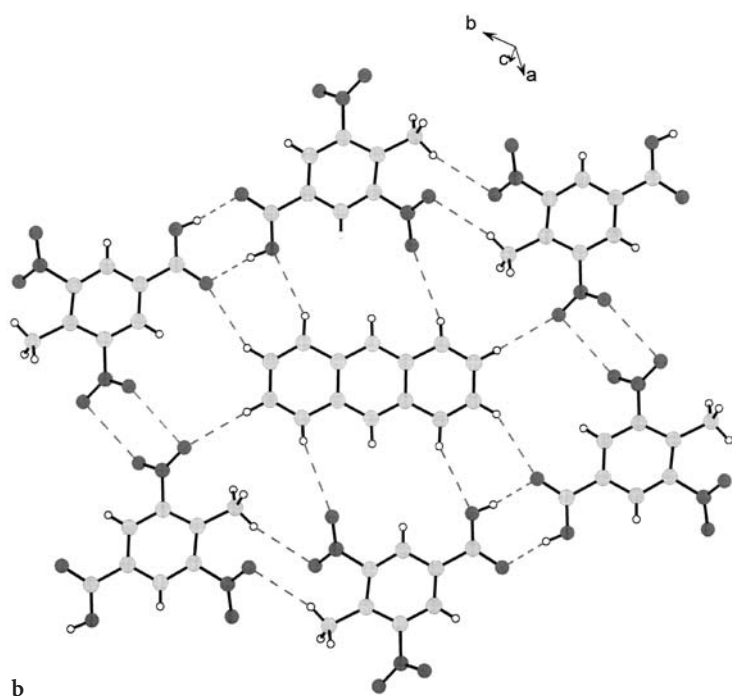


Fig. 4 Crystal packing diagrams of **a** **17:16** and **b** **18:16**, both with 2:1 stoichiometry, and **c** **19:16**:benzene with 2:1:1 stoichiometry (*dashed lines* represent hydrogen bonds and close contacts) [43]

**Fig. 4** (continued)

interactions are necessary for the cocrystal involving **18**: carboxylic acid dimer, O \cdots O close contact of nitro groups, and C–H \cdots O hydrogen bonding between the methyl and a nitro. In the case of **17**, a Cl \cdots O interaction replaces one of the C–H \cdots O hydrogen bonds.

Lacking a *meta* constituent, it is clear that **19** alone cannot satisfy an analogous ring of continuous intermolecular interactions around anthracene. Hence, no cocrystallisation occurred by solid-state grinding, and the incorporation of a benzene solvent molecule upon solution evaporation was necessary to permit cocrystallisation (Fig. 4c). The authors thus attributed the lack of cocrystal formation by solid-state grinding to an inability of reactants to satisfy the desired intermolecular interactions, rather than the relative stability of reactants.

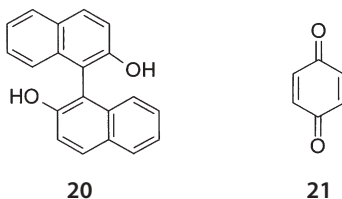
A selection from early reports on the solid-state grinding cocrystallisation approach has been offered here. The quantity and scope of solid-state grinding cocrystallisation examples continues to grow today. Interest is also turning towards varied constituent types, such as organometallic cocrystals [44–46]. Additionally, the use of grinding as a means of inducing chemical reactivity has been demonstrated by Toda and others to be of tremendous utility [47–49]. It is anticipated that as interest grows with respect to cocrystals and green chemistry practices alike, so too will the field of cocrystal formation by solid-state grinding continue to develop.

3

Cocrystals Produced Exclusively by the Grinding Approach

One great attraction of preparing cocrystals by solid-state grinding is that, in certain cases, cocrystals unobtainable by other methods may be prepared. The number of reported instances of these cases is small, but may grow as the field of solid-state cocrystal preparation widens. From the standpoint of novel materials design, these cases are of great interest in that they may lead to understanding, prediction and exploitation of this phenomenon.

An illustrative example was provided by the work of Kuroda and co-workers [50]. They reported that different methods of preparation resulted in distinct cocrystal products in their work with racemic bis- β -naphthol (BN) **20** and benzoquinone (BQ) **21**. Upon solid-state grinding with a mortar and pestle, a 1:1.5 BN:BQ cocrystal resulted, termed form I. In contrast, from a solution of ether and hexane, a cocrystal containing **20** and **21** in a 1:1 BN:BQ ratio resulted,



termed form II. Further, cooling a mixture of the two components from the melt resulted in a third cocrystal, form III.

Several of the experimental details were varied in order to elucidate a possible mechanism for the variation in products derived from the different techniques. The starting ratio of components was varied without successfully producing form II by grinding, showing that the formation of form I occurred independently of the starting ratio. Additional experiments were performed to demonstrate that the grinding procedure was not affected by light, oxygen, or static charge. It was also illustrated that either mixing without grinding or exposure of solid **20** to **21** vapour did not induce cocrystallisation. Coupled with the observation that a third cocrystal form was obtained from the melt of these materials, the experiments seem to highlight the importance of solid–solid interaction and grinding-induced crystal cleavage during the cocrystallisation process.

It was fortunate that in one case of solution crystallisation, a few crystals of the grinding product, form I, were found as a minor component, which allowed for structure determination of both form I and form II by single crystal XRD. A crystal structure of the material from the melt is not available. The asymmetric unit of form I contains one **20** and two **21** molecules, one of which rests on a centre of symmetry. The expected O–H \cdots O hydrogen bond between the hydroxyl of **20** and the carbonyl of **21** is observed, although one of the four total carbonyls does not participate in any hydrogen bonding. This results in a discrete hydrogen bond chain consisting of five alternating participants (see Fig. 5). In the structure of form II, which contains three each of **20** and **21** in the asymmetric unit, all hydrogen-bonding donors and acceptors are satisfied. This provides an infinite chain of hydrogen bond connectivity, as viewed in Fig. 6. π -Stacking interactions seem to play a role in both structures, as the BQ rings are always stacked between BN rings.

Whether the difference in hydrogen bonding between the cocrystal structures has a role in their crystallisation preferences is not clear. The authors suggested that crystal shearing together with molecular diffusion may have a role in the preference for form I formation by grinding. A structural confirmation of the shearing hypothesis, however, is not readily apparent from the crystal structures. In viewing the packing of a unit cell of both cocrystals, a cleavage plane may be envisaged in each structure. In viewing form I along the *c* axis, one may identify planes parallel to the *a* axis across which no hydrogen bonding occurs (Fig. 7). Similarly, when viewed from an appropriate angle, the unit cell of form II shows what may be interpreted as non-polar cleavage planes (Fig. 8). From this analysis, it is possible that both crystals may possess the capability for shearing. Thus, an examination of unit cell packing alone is not sufficient to explain the crystallisation behaviour of these cocrystals. As the authors suggested, further investigation into the solid-state cocrystallisation mechanism will provide a foundation for exciting future work.

The example illustrated above is unusual, in that the crystal structures of the cocrystals from both solution and grinding have been determined and hence

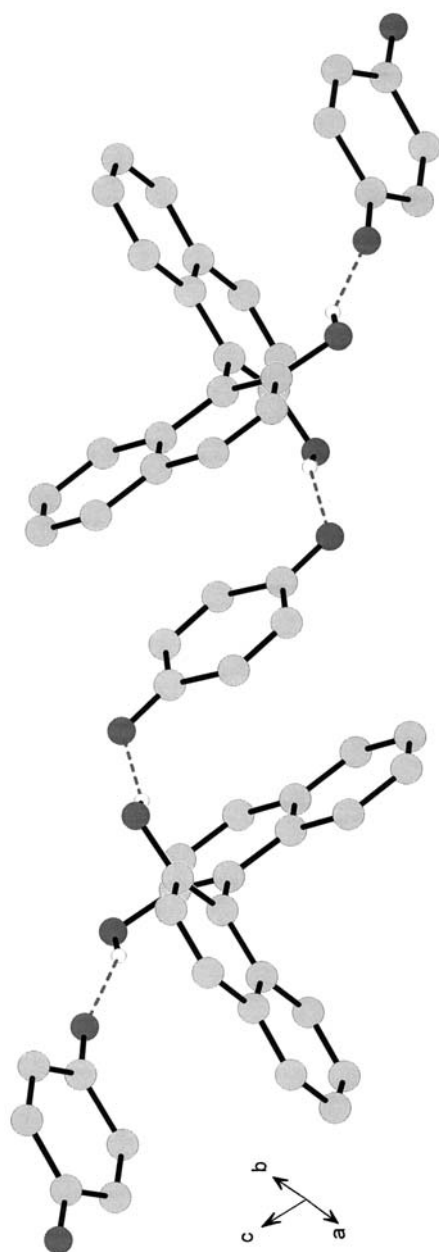


Fig. 5 Form I cocrystal of 20:21 showing discrete hydrogen-bonded unit (non-hydroxyl hydrogens removed for clarity) [50]

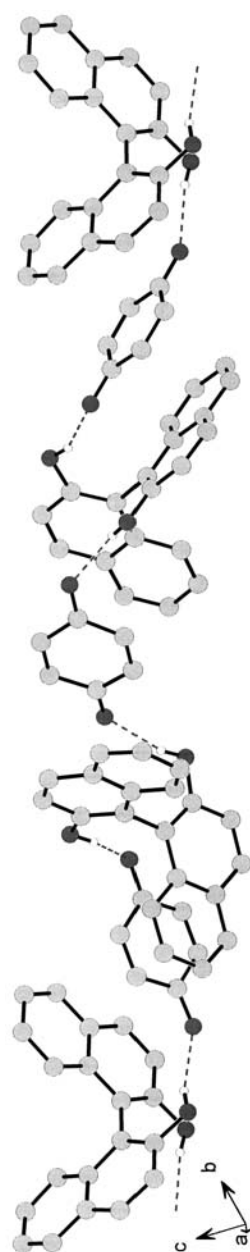


Fig. 6 Form II cocrystal of 20:21 showing infinite chain of hydrogen bonding (non-hydroxyl hydrogens removed for clarity) [50]

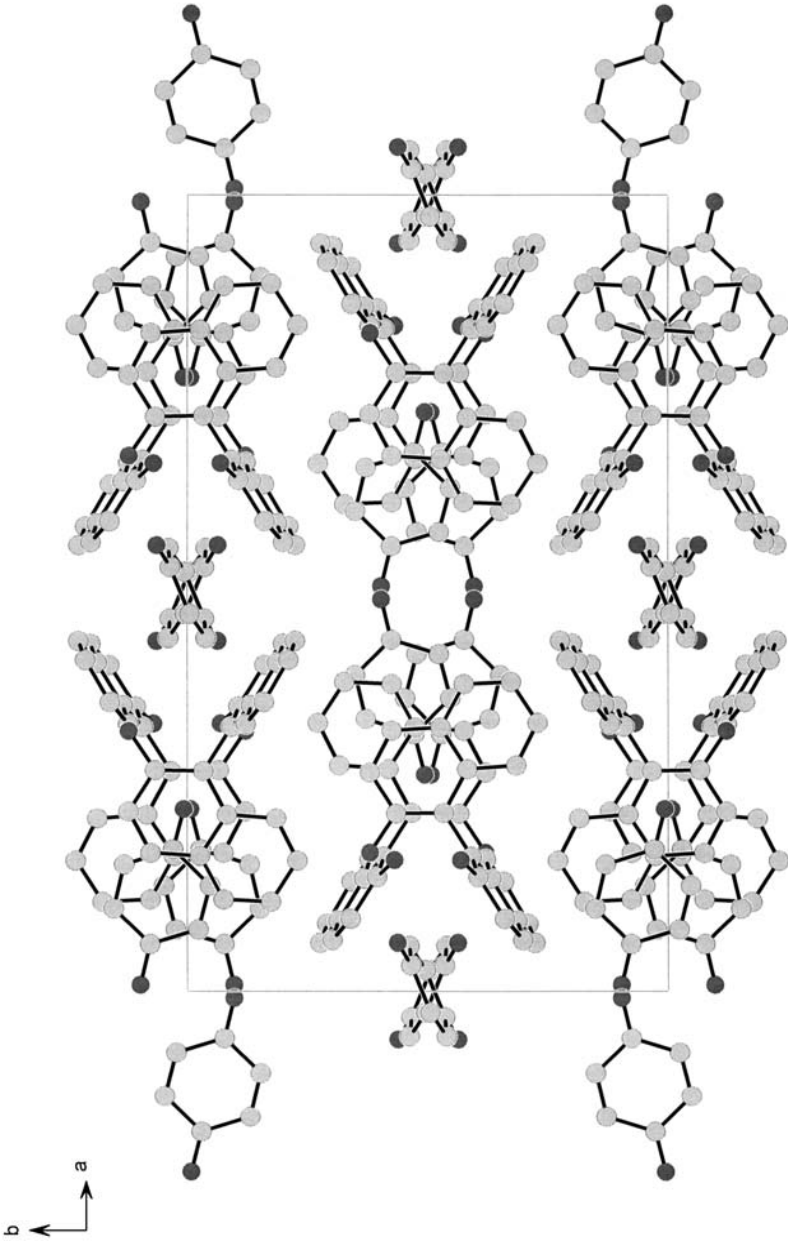


Fig. 7 Form I unit cell packing of cocrystal 20:21 – possible cleavage planes are projected horizontally [50]

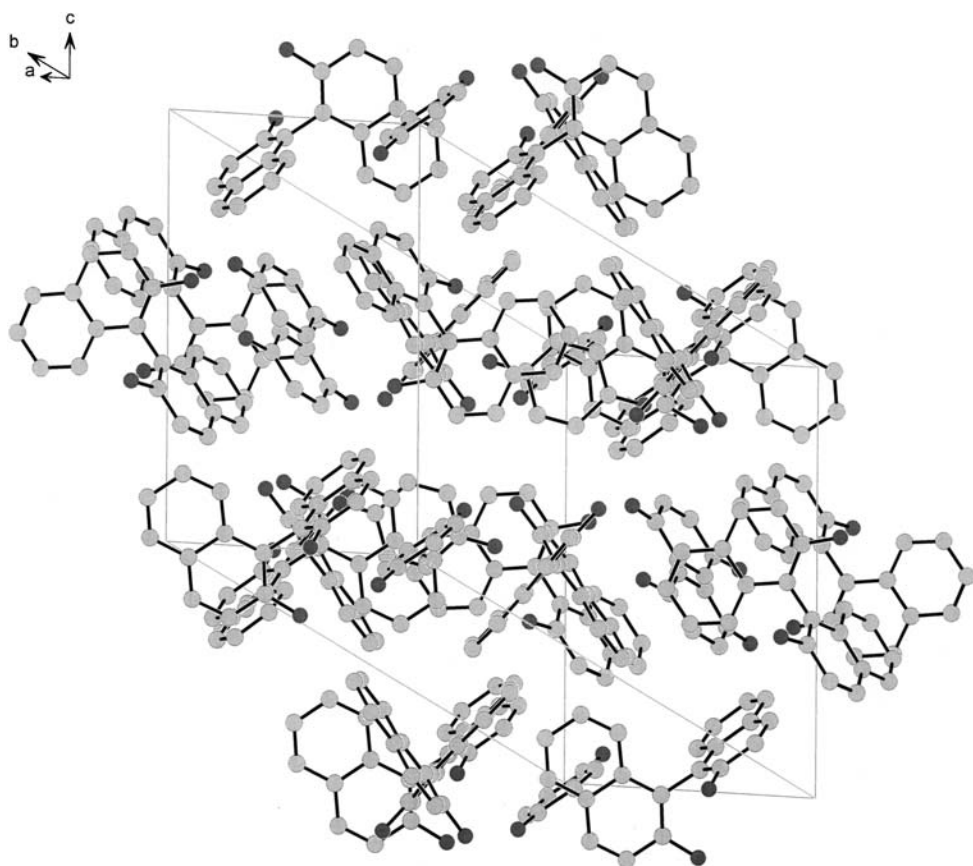
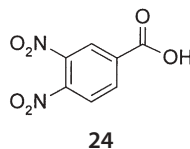
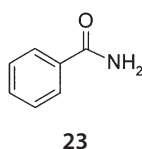
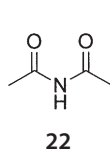


Fig. 8 Form II unit cell packing of cocrystal 20:21, showing potential cleavage planes projected horizontally [50]

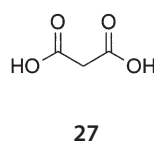
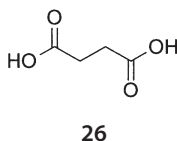
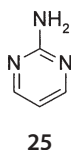
may be studied. Typically this is not the case, particularly for materials produced only by grinding. Etter and co-workers frequently prepared cocrystals by multiple methods, including grinding, solution evaporation and crystallisation from the melt. Often the same cocrystal was obtained by all techniques. However, there were certain instances in which grinding afforded a unique cocrystal product.

Etter and Reutzel conducted a series of experiments designed to understand the hydrogen bonding preferences of acyclic imides [27]. They identified two cocrystals containing the compound diacetamide 22, which could only be prepared by the solid-state grinding approach. The first is a 1:1 cocrystal of 22 and benzamide 23. A crystal structure was not determined; however, infrared spectroscopy, solid-state NMR and melting range characterization data were reported. The second material obtainable only by solid-state grinding is a 1:1 cocrystal containing diacetamide 22 and 3,4-dinitrobenzoic acid 24. A crystal structure is also unavailable for this compound. The authors offer the expla-



nation of disparate solubilities for why these two compounds could not be formed from solution.

In contrast, solubility was not an issue in a second case of a product obtained only from grinding. In work with Adsmond on cocrystals of 2-aminopyrimidine 25, Etter found that by grinding the base 25 with succinic acid 26, two cocrystal



stoichiometries were obtained, 1:1 and 2:1 base:acid [23]. The outcome depended upon the ingoing starting material ratio. Solution crystallisation, conversely, yielded only the 1:1 product. The crystal structure of the product obtained only by grinding is not known, so a structure-based rationalisation of this observation is difficult. It may be possible that a certain preference for the 1:1 stoichiometry exists in solution, which is not as dominant during solid-state grinding.

Interestingly, in the same work [23] Etter and Adsmond reported two polymorphs of a 1:1 cocrystal containing 25 and malonic acid 27. Both crystallised from solution, but only one was obtainable from solid-state grinding. Contrary to the examples mentioned above, this instance suggests that solution crystallisation may at times offer more product diversity than grinding.

Hollingsworth et al. demonstrated the utility of the grinding approach in preparing a cocrystal material not initially accessible from solution [51, 52]. The researchers aimed to prepare a series of cocrystals with α,ω -dinitriles of the formula $\text{NC}(\text{CH}_2)_n\text{CN}$ with urea, with varying aliphatic chain lengths (n). Success was achieved in growing from solution a number cocrystals of different chain lengths; however, the $n=3$ (glutaronitrile) derivative could not be prepared from solution. Solid-state grinding of the two components, on the other hand, allowed for cocrystal formation with greater than 98% yield. When growth from solution was re-attempted, with the introduction of cocrystal seeds from the grinding experiment, the solution growth was successful and a single crystal of this compound was grown, thereby enabling crystal structure determination. This case establishes that the initial use of solid-state grinding for the preparation of cocrystal seeds may allow subsequent solution growth of novel cocrystal materials. The method was also demonstrated to apply to organometallic cocrystal systems [53, 54].

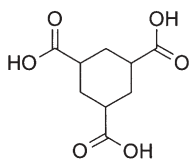
At the moment, the aforementioned examples serve as curious exceptions to the general trend that most cocrystals can be produced by both the grinding and solution approaches. However, as research continues in this field, it is hoped that an improved understanding will develop regarding the different mechanisms of these cocrystallisation approaches. With a better understanding in hand, novel solid-state materials for various uses may eventually arise as a consequence.

4

A Recent Enhancement to the Grinding Approach

The technique of solid-state grinding by mortar and pestle to induce cocrystal formation has been known for at least a century [10], and unlike many scientific techniques, this basic approach has seen little advancement since that time. Notwithstanding the development of more sophisticated mechanical grinders, grinding solids together with a mortar and pestle is still performed today exactly as it was then. Recent reports, however, have introduced a new variable into the process. The addition of a small amount of a particular solvent to the grinding process has been termed ‘solvent-drop grinding’, and has been shown to influence the cocrystallisation process in two specific ways: reaction kinetics and polymorph control.

Shan et al. first illustrated this solid-state enhancement technique in the context of cocrystals of the compound cyclohexane-1,3*cis*,5*cis*-tricarboxylic acid (CTA) **28** [55]. CTA readily formed phase-pure cocrystal material with hexamethylenetetramine (HMTA) **29** upon grinding for 20 min (as judged from powder XRD data).



28



29

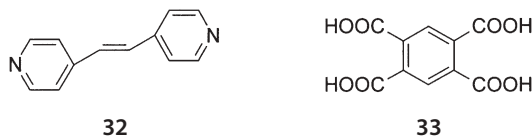
The same was not true of a cocrystal of CTA **28** with 4,4'-bipyridine (Bipy) **30**. The structure of a cocrystal containing these two components was determined by single crystal XRD, using crystals grown from methanol [56]. When the ingoing powders were ground together without solvent, only partial formation of this cocrystal occurred after 1 h of grinding. The kinetics of the cocrystallisation, however, could be accelerated by introducing approximately 0.05 ml of methanol (i.e. two drops from a pipette) to the two powders before grinding commenced. In this case of the CTA:Bipy (**28:30**) cocrystal, the kinetics were increased so that the pure cocrystal was obtained in 20 min.

A second illustration of such reaction acceleration was reported using CTA **28** and 4,7-phenanthroline (fPh) **31** [55]. A 1:2 CTA:fPh (**28**:**30**) cocrystal, known



to precipitate readily from a methanol solution, was observed by powder XRD only as a minor component after grinding for a considerable period of time. The addition of two drops of methanol, water, ethyl acetate, or acetonitrile were all shown to accelerate this cocrystal formation. At least one of the components was soluble in each of these solvents. To demonstrate that solubility was a factor in this phenomenon, the researchers noted that the addition of cyclohexane, in which neither material was soluble, did not noticeably improve the reaction rate.

Solvent-drop grinding was next applied as an eco-friendly modification to a previously described preparation of a crystalline organic inclusion compound. Initial work had demonstrated solution-mediated supramolecular organisation and solid-state topochemically controlled reactivity in a system involving 1,2-bis(4-pyridyl)ethylene (bpe) **32** and 1,2,4,5-benzenetetracarboxylic acid (bta) **33** [57]. A single crystal of a 2:1 bpe:bta **32**:**33** cocrystal was



obtained from a dimethyl sulfoxide (DMSO) solution of the starting components, and its structure was determined (Fig. 9). UV-irradiation of this cocrystal induced [2+2] photodimerisation between adjacent bpe molecules in the

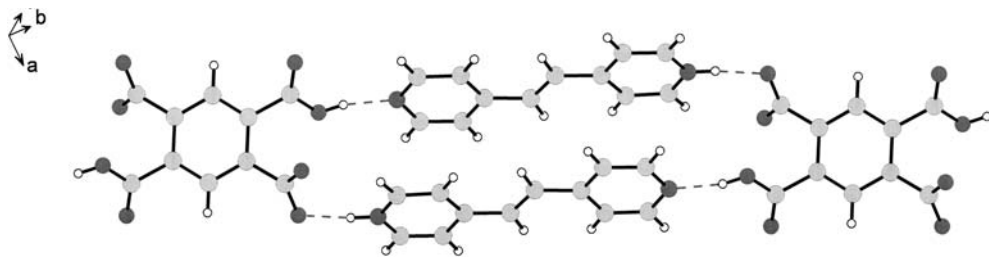
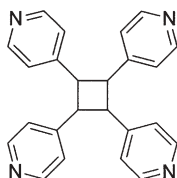


Fig. 9 Crystal packing of bpe:bta (**32**:**33**) cocrystal material, showing topochemical alignment of bpe molecules prior to UV radiation-induced solid-state dimerisation [57]

solid state to produce *rctt*-tetrakis(4-pyridyl)cyclobutane (tpcb) **34**. Following a DMSO recrystallisation of the irradiated product, single crystals of a novel



34

cocrystalline inclusion compound were isolated and were shown to contain 1:1 tpcb:bta **34:33** with disordered DMSO and water molecules in the supramolecular channels (Fig. 10).

A 'green' modification to this process, utilising the approach of solvent-drop grinding, was then demonstrated [58]. It was found that the initial cocrystal material (Fig. 9) containing bpe **32** and bta **33** could not be prepared by grinding the starting components for 2 h. However, the addition of several drops of the solvent methanol permitted complete cocrystallisation in 20 min, as determined by a comparison of the powder XRD pattern of the ground material to the pattern simulated from the known cocrystal structure. The cocrystal was irradiated as before to induce solid-state dimerisation. The irradiated mater-

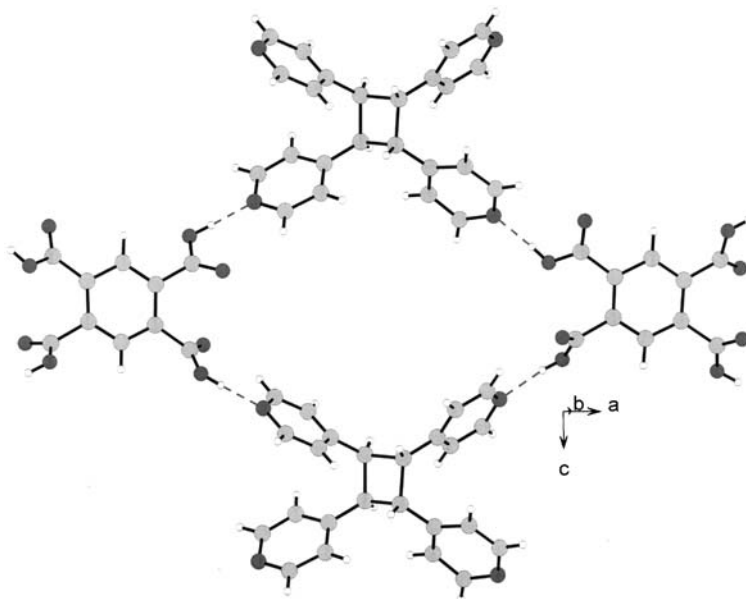
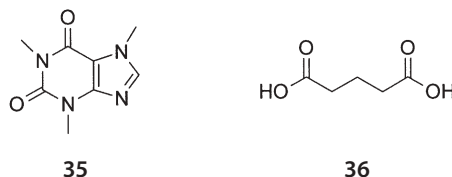


Fig. 10 Crystal packing of tpcb:bta (**34:33**) cocrystal material; disordered water and DMSO molecules have been omitted from supramolecular cavity [57]

ial was then subjected to 20 min of solvent-drop grinding with DMSO to produce the desired organic inclusion compound as before (Fig. 10). This was an efficient demonstration of the value of solvent-drop grinding in providing 'greener' routes to novel supramolecular materials.

The utility of the solvent-drop grinding approach was recently extended by Trask et al. with a cocrystal system containing the model pharmaceutical



compound caffeine **35** and glutaric acid (GA) **36** [59]. Evaporation of a solution containing both components produced single crystals of two habits. Rod-like crystals were solved as monoclinic form I; block-like crystals were solved as triclinic form II. Both exhibited 1:1 stoichiometry; with identical chemical composition, the two cocrystals were designated polymorphs.

The hydrogen bonding scheme is identical in both crystals as seen in Fig. 11 and Fig. 12. The molecules pack so as to provide what may be aptly described as a hydrogen-bonded comb, with a GA **36** backbone and caffeine **35** teeth. In fact, the major difference between the two polymorphs on the secondary level of supramolecular architecture resides in the torsion of the GA **36** aliphatic chain.

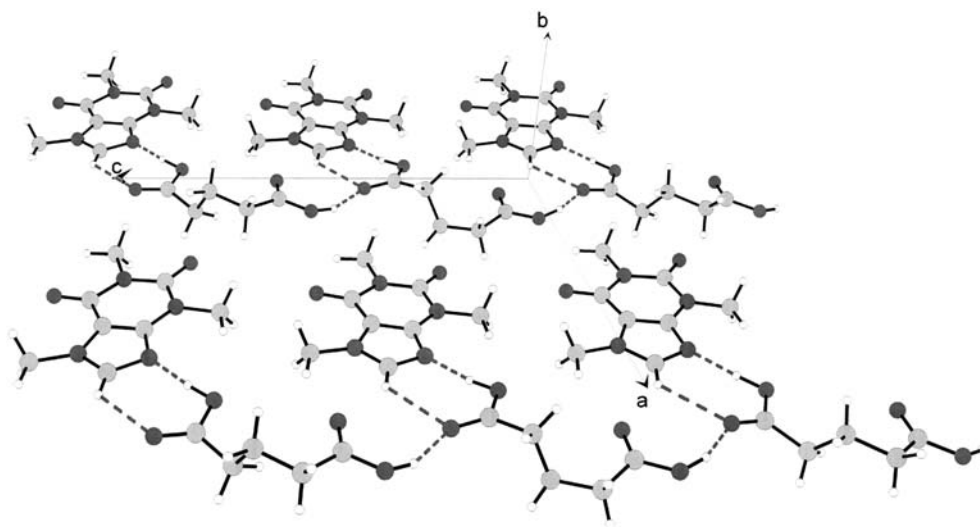


Fig. 11 Caffeine:glutaric acid (**35:36**) form I crystal packing, showing two hydrogen-bonded combs [59]

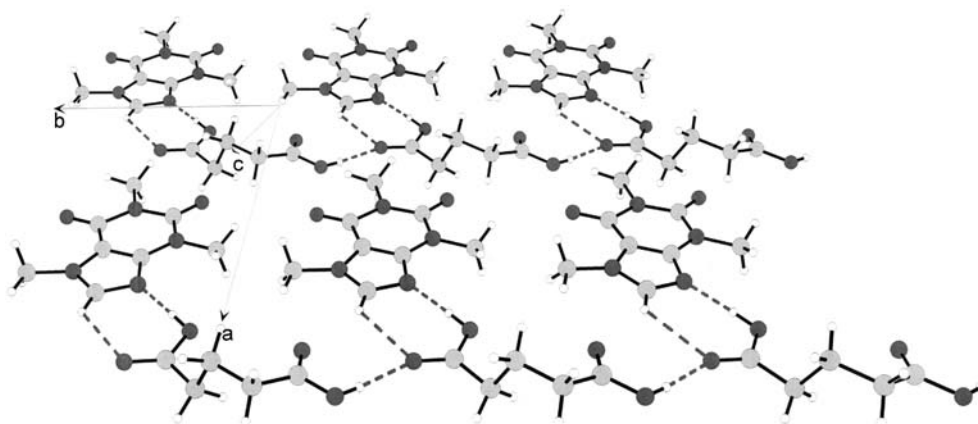


Fig. 12 Caffeine:glutaric acid (35:36) form II crystal packing, showing two hydrogen-bonded combs [59]

Given the identical hydrogen bonding arrangement, it may not be surprising that these two polymorphs precipitated concomitantly. Unexpectedly, however, it was found that application of the solvent-drop grinding approach allowed preparation of each crystal form essentially pure from the other. Grinding equimolar starting components in the absence of solvent produced form I. Similarly, grinding in the presence of a solvent in which neither component was soluble, including cyclohexane, hexane and heptane, also provided form I. Grinding with several drops of a more polar solvent, on the other hand, produced predominantly form II. Such solvents included chloroform, dichloromethane, acetonitrile and water.

A clear explanation for this observation was not offered. However, as a consequence of the space group symmetry, the crystals differ in their tertiary level of supramolecular architecture (see Fig. 13 and Fig. 14). The authors note that this difference affords a potential non-polar cleavage plane in form I but not in form II. As it is form I that preferentially formed in the presence of non-polar solvents, it is possible that this may play a role in the phenomenon.

The examples of this section summarise the recent application of the solvent-drop grinding approach to solid-state cocrystal preparation. The approach has been shown in certain instances to provide for either acceleration of cocrystallisation kinetics or selection of a particular polymorph via solid-state grinding. The approach is attractive, as it appears to incorporate some of the beneficial aspects of solvent participation while maintaining an essentially green, eco-friendly process.

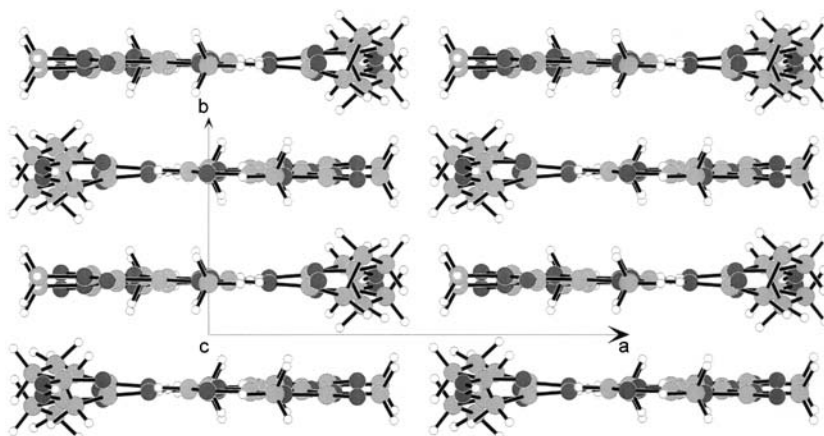


Fig. 13 Form I crystal packing of caffeine:glutaric acid (35:36), as viewed down the length of the hydrogen-bonded combs, showing potential non-polar cleavage plane, projected vertically [59]

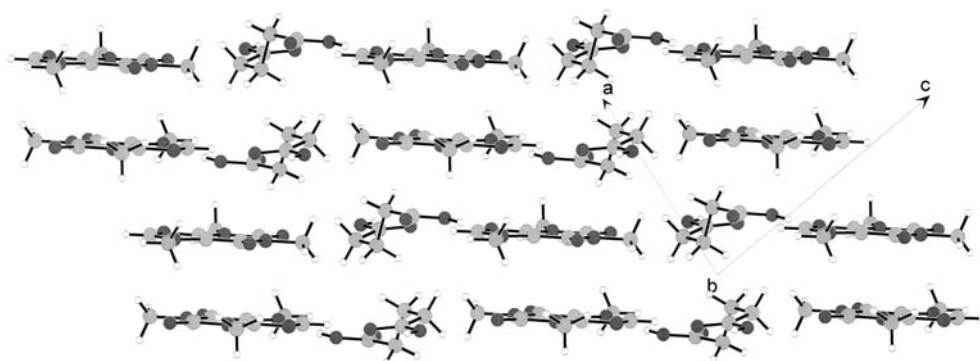


Fig. 14 Form II crystal packing of caffeine:glutaric acid (35:36), as viewed down the length of the hydrogen-bonded combs, showing lack of analogous cleavage plane [59]

5

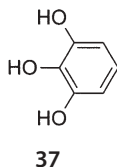
Structure Determination from Powder XRD Data

The solid-state grinding approach to cocrystal formation is simple, easily performed and environmentally friendly. So why is it not the clear favourite for obtaining cocrystal material? The answer may in part pertain to the fact that grinding results in microcrystalline powders, which are unsuitable for single crystal XRD. In other words, the most common means of obtaining a crystal structure is incompatible with solid-state cocrystal preparation. Thus, in order to ascertain the intermolecular interactions and packing features of a particular cocrystal via single crystal XRD, the researcher must grow a suitably sized

crystal of the same structure and stoichiometry from solution. A simulated powder XRD pattern from the solved crystal structure can then be compared to other powdered materials which may have been produced by solid-state grinding.

However, recent advancements in the field of crystal structure determination from powder XRD data may soon change this bias [60]. For some time, researchers have been developing the technique for solving homomeric crystal structures of materials with an increasingly large number of degrees of freedom [61]. Commonly these freedoms exist as molecular torsions or independent molecules in the asymmetric unit. The direct-space approach has seen much recent success in solving structures from powder data. This approach is an iterative process consisting of (1) generating a trial crystal structure independently of the experimental powder diffraction pattern, (2) simulating the powder diffraction pattern of the generated structure, and (3) comparing the simulated pattern to the experimental pattern. The crystal structure corresponding to the best agreement between the two patterns is found by a particular global optimisation strategy such as Monte Carlo, simulated annealing, or genetic algorithm. When the agreement is within an acceptable standard, the crystal structure has been solved.

In 2000 Tremayne and Glidewell claimed the first instance of a structure determination of a cocrystal material by the direct-space approach [62]. Their work involved a 1:1 cocrystal of 1,2,3-trihydroxybenzene **37** and hexamethyl-



enetetramine (HMTA) **29**, which was crystallised from solution but could not be grown as sufficiently sized single crystals. The experimental powder XRD pattern was collected using a monochromated laboratory instrument. The pattern was indexed to a monoclinic cell; its volume was consistent with one molecule each of **37** and **29** in the asymmetric unit. Both molecules **37** and **29** are rigid, so no torsional variables were necessary. However, within the asymmetric unit, each molecule must be described by three positional coordinates (x, y, z) and three rotational coordinates (θ, φ, ψ). This system, therefore, possessed a total of 12 degrees of freedom.

The crystal structure obtained from structure solution and subsequent refinement shows a rational pattern of hydrogen bonding, with each hydroxyl group of **37** participating in an $\text{OH}\cdots\text{N}$ intermolecular hydrogen bond to a tertiary amine of **29** to form a ribbon parallel to the a axis (Fig. 15). Such interactions are consistent with structures obtained from single crystal XRD data on other hydroxyl compounds complexed with HMTA [63].

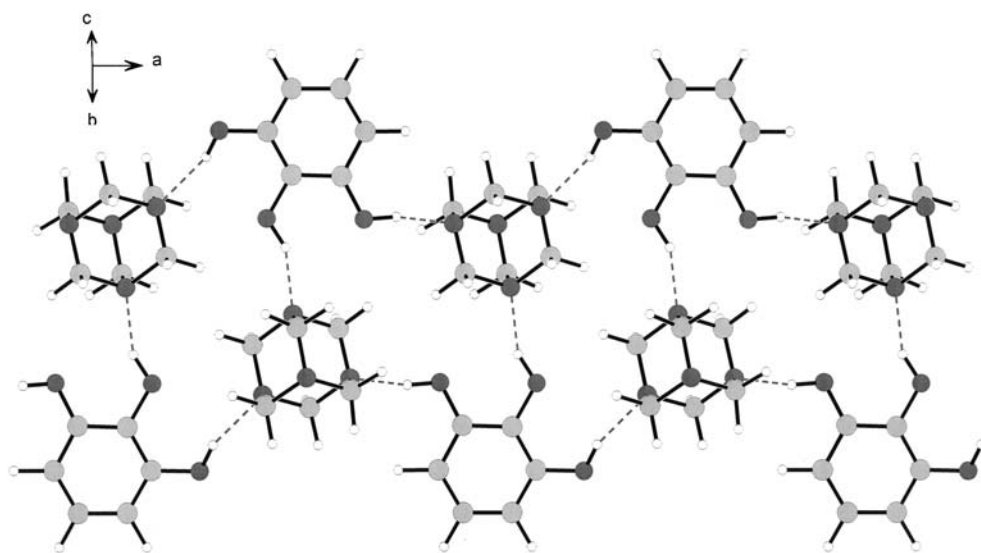


Fig. 15 Hydrogen-bonded ribbons of 37:29; the crystal structure was solved from powder XRD data [62]

The structure solution of the cocrystal of 37 and 29 from powder XRD illustrates the current utility of this approach in the field of crystal engineering. While the material above was prepared from solution crystallisation, it is clear that this approach directly impacts cocrystals prepared by solid-state grinding.

Recently, Harris, Kuroda and co-workers claimed the first example of a direct structure determination of a cocrystal prepared by solid-state grinding [64]. The cocrystal involved was an extension of a system described earlier [50], consisting of the three components benzoquinone (BQ) 21, bis- β -naphthol (BN) 20 and anthracene (AN) 16. The authors noted that this system was yet another example in which solution and grinding approaches yielded different cocrystal products, as judged by their powder XRD patterns. This example highlights the significance of powder XRD structure determination, as the likelihood of obtaining sizable single crystals of this compound appears small.

The stoichiometry of the ground cocrystal material was confirmed by NMR and elemental analysis to be 1:1:0.5 (21:20:16). Interestingly, however, it was reported that a slight excess of BQ 21 was necessary to generate phase-pure material, in order to compensate for partial sublimation during the 60 min of manual mortar and pestle grinding.

Both BQ 21 and AN 16 are rigid structures, but BN 20 contains a molecular torsion about the two naphthol rings. The unit cell volume and the $C2/c$ space group assignment indicated that AN 16 spanned a symmetry element, therefore requiring the evaluation of only one half of that molecule. The crystal structure was confirmed by the resulting agreement between the experimental and simulated powder XRD pattern following Rietveld refinement (Fig. 16).

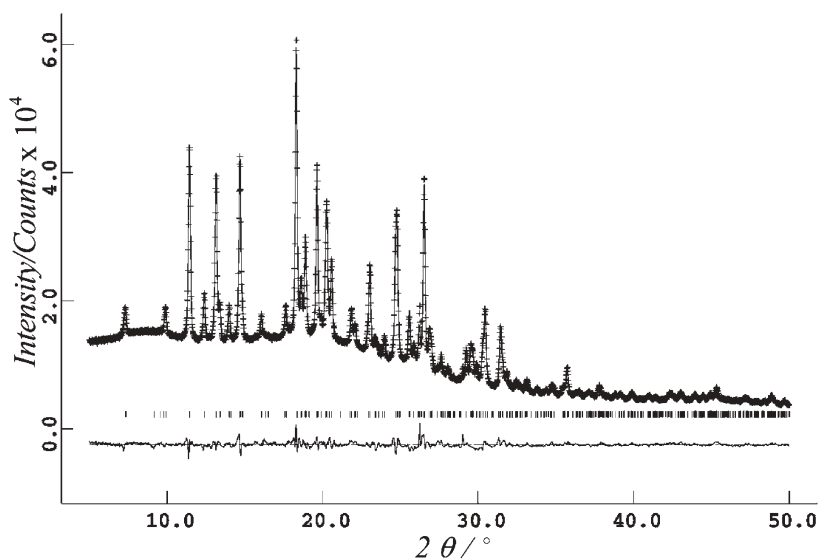


Fig. 16 Experimental (+ marks), calculated (solid line) and difference (lower line) powder X-ray diffraction profiles for the three-component material after final Rietveld refinement, as reported by the authors [64]. (Reprinted with permission from Cheung et al. (2003) *J Am Chem Soc* 125:14658. Copyright 2003 American Chemical Society)

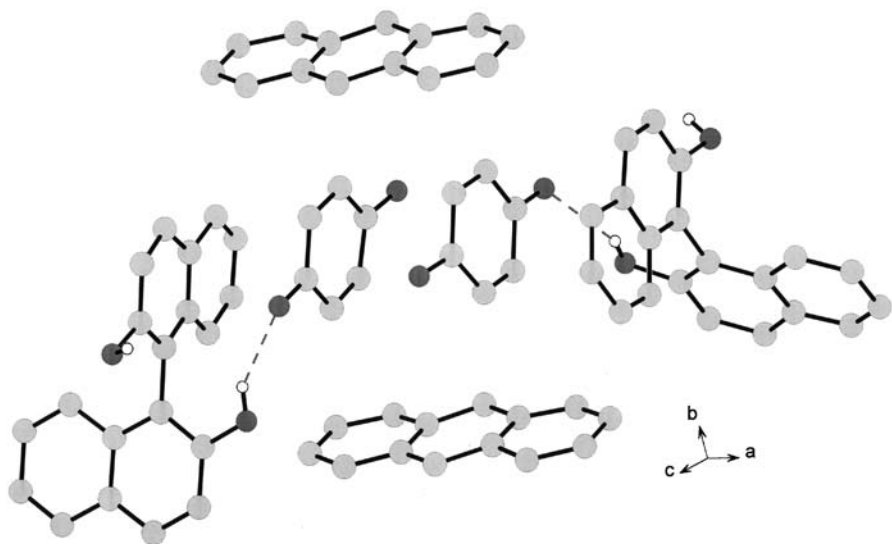


Fig. 17 The intermolecular interactions of the BN:BQ:AN (21:20:16) cococrystal, as solved from powder XRD data (non-hydroxyl hydrogens removed for clarity) [64]

The structure determination allows for an examination of the intermolecular interactions of the three-component cocrystal (Fig. 17). Hydrogen bonding is observed between the carbonyls of BQ 21 and the hydroxyls of BN 20. A four-component π -stacking motif is apparent among two molecules each of BQ 21 and BN 20. Finally, edge-to-face interactions are observed with two molecules each of BQ 21 and AN 16.

Such a detailed understanding of the structural features of these two cocrystals would not have been possible without the advent of the developing technique of powder XRD crystal structure determination. Further progress in this exciting area of research will undoubtedly continue to benefit the advancement of solid-state cocrystal preparation.

6 Concluding Remarks

Crystal engineering is a prospering scientific field, comprised of practitioners with a variety of interests. The field at present remains to some extent in an information-gathering phase. Researchers are producing an abundance of novel cocrystal structures, cataloguing intermolecular interactions, and revealing crystallisation preferences. With evolving computational methodology and clever mining of the Cambridge Structural Database, the ultimate goal of reliable crystal structure prediction will someday be realised. Until then, novel cocrystal structures will be discovered through a process which combines design and chance: while the design of cocrystals using discrete intermolecular interactions, such as hydrogen bonding, is increasingly common, the entire three-dimensional architecture of the cocrystal structure, which often results from weaker, non-directional forces, is quite often left to chance. Because of this present inability to understand and control all contributing forces of the crystallisation process, researchers in search of novel cocrystal materials must increase the diversity of experimental conditions to plumb all chances for success.

A variety of cocrystallisation approaches, including solid-state grinding, will provide the most gainful outcome to a series of cocrystallisation experiments. The solid-state approach is certainly well preceded, but until more research is conducted its mechanism will remain far from well understood. It is simplistic in its application, and its environmental benefits, particularly on a large scale, could provide tremendous cost savings and hazard reduction. In what may someday provide a reliable source of novel materials, the solid-state grinding approach has been demonstrated to produce materials which will not form by traditional solution crystallisation. Enhancement by the solvent-drop method is known to provide increased cocrystallisation kinetics or polymorph control in certain instances. Finally, the arrival of structure determination from powder XRD data is beginning to overcome what may have comprised the most significant deficiency of the grinding approach: an inability to conclusively analyse the intermolecular interactions within the cocrystal produced. As

researchers further demonstrate the utility of solid-state grinding and more thoroughly examine its mechanism in cocrystal formation, its role in the field of crystal engineering will certainly grow.

Acknowledgements The authors gratefully acknowledge funding from the Pfizer Institute for Pharmaceutical Materials Science at the University of Cambridge. AVT additionally wishes to thank the Sidney Sussex North American Foundation for funding.

References

1. Braga D (2003) *Chem Commun* 2751
2. Desiraju GR (1989) *Crystal engineering: the design of organic solids*. Elsevier, Amsterdam
3. Jones W (1997) In: Jones W (ed) *Organic molecular solids: properties and applications*. CRC, New York, p 149
4. Bond AD, Jones W (2002) In: Jones W, Rao CNR (eds) *Supramolecular organization and materials design*. Cambridge University Press, Cambridge, p 391
5. Fernandez-Bertran JF (1999) *Pure Appl Chem* 71:581
6. Chan HK, Doelker E (1985) *Drug Dev Ind Pharm* 11:315
7. Anastas PT, Warner JC (1998) *Green chemistry: theory and practice*. Oxford University Press, Oxford, UK
8. Otsuka M, Kaneniwa N (1983) *Chem Pharm Bull* 31:4489
9. Otsuka M, Kaneniwa N (1984) *Chem Pharm Bull* 32:1071
10. Ling AR, Baker JL (1893) *J Chem Soc* 63:1314
11. Rastogi RP, Bassi PS, Chadha SL (1962) *J Phys Chem* 66:2707
12. Rastogi RP, Bassi PS, Chadha SL (1963) *J Phys Chem* 67:2569
13. Rastogi RP, Singh NB (1966) *J Phys Chem* 70:3315
14. Banerjee A, Brown CJ (1985) *Acta Crystallogr C* 41:82
15. Patil AO, Curtin DY, Paul IC (1984) *J Am Chem Soc* 106:4010
16. Patil AO, Curtin DY, Paul IC (1984) *J Am Chem Soc* 106:348
17. Scheffer JR, Wong YF, Patil AO, Curtin DY, Paul IC (1985) *J Am Chem Soc* 107:4898
18. Patil AO, Pennington WT, Desiraju GR, Curtin DY, Paul IC (1986) *Mol Cryst Liq Cryst* 134:279
19. Guarrera D, Taylor LD, Warner JC (1994) *Chem Mater* 6:1293
20. Toda F, Tanaka K, Sekikawa A (1987) *J Chem Soc Chem Commun* 279
21. Etter MC, Frankenbach GM (1989) *Chem Mater* 1:10
22. Etter MC, Frankenbach GM, Bernstein J (1989) *Tetrahedron Lett* 30:3617
23. Etter MC, Admond DA (1990) *Chem Commun* 8:589
24. Etter MC, Urbanczyklipkowska Z, Ziaebrahimi M, Panunto TW (1990) *J Am Chem Soc* 112:8415
25. Etter MC, Frankenbach GM, Admond DA (1990) *Mol Cryst Liq Cryst* 187:25
26. Etter MC (1991) *J Phys Chem* 95:4601
27. Etter MC, Reutzel SM (1991) *J Am Chem Soc* 113:2586
28. Etter MC, Reutzel SM, Choo CG (1993) *J Am Chem Soc* 115:4411
29. Huang KS, Britton D, Etter MC, Byrn SR (1997) *J Mater Chem* 7:713
30. Hoogsteen K (1963) *Acta Crystallogr* 16:907
31. O'Brien EJ (1967) *Acta Crystallogr* 23:92
32. Ueno S, Ristic RI, Higaki K, Sato K (2003) *J Phys Chem B* 107:4927
33. Remenar JF, Morissette SL, Peterson ML, Moulton B, MacPhee JM, Guzman HR, Almars-son O (2003) *J Am Chem Soc* 125:8456

34. Fleischman SG, Kuduva SS, McMahon JA, Moulton B, Walsh RDB, Rodriguez-Hornedo N, Zaworotko MJ (2003) *Cryst Growth Des* 3:909
35. Bailey Walsh RD, Bradner MW, Fleischman S, Morales LA, Moulton B, Rodriguez-Hornedo N, Zaworotko MJ (2003) *Chem Commun* 186
36. Caira MR, Nassimbeni LR, Wildervanck AF (1995) *J Chem Soc Perkin Trans 2*:2213
37. Caira MR (1991) *J Crystallogr Spectrosc Res* 21:641
38. Caira MR (1992) *J Crystallogr Spectrosc Res* 22:193
39. Patel U, Haridas M, Singh TP (1988) *Acta Crystallogr C* 44:1264
40. Drezdson MA (1988) *Inorg Chem* 27:4628
41. Jones W, Chibwe M (1990) In: Mitchell IV (ed) *Pillared layered solids*. Elsevier, Amsterdam, p 67
42. Newman SP, Jones W (2002) In: Jones W, Rao CNR (eds) *Supramolecular organization and materials design*. Cambridge University Press, Cambridge, p 295
43. Pedireddi VR, Jones W, Chorlton AP, Docherty R (1996) *Chem Commun* 987
44. Nichols PJ, Raston CL, Steed JW (2001) *Chem Commun* 1062
45. Braga D, Maini L, Polito M, Mirolo L, Grepioni F (2002) *Chem Commun* 2960
46. Braga D, Maini L, Polito M, Mirolo L, Grepioni F (2003) *Chem-Eur J* 9:4362
47. Toda F (1994) *J Syn Org Chem Jpn* 52:923
48. Toda F (1995) *Acc Chem Res* 28:480
49. Tanaka K, Toda F (2000) *Chem Rev* 100:1025
50. Kuroda R, Imai Y, Tajima N (2002) *Chem Commun* 2848
51. Hollingsworth MD, Santarsiero BD, Oumar-Mahamat H, Nichols CJ (1991) *Chem Mater* 3:23
52. Hollingsworth MD, Brown ME, Santarsiero BD, Huffman JC, Goss CR (1994) *Chem Mater* 6:1227
53. Braga D, Maini L, Polito M, Mirolo L, Grepioni F (2002) *Chem Commun* 2960
54. Braga D, Maini L, Polito M, Mirolo L, Grepioni F (2003) *Chem-Eur J* 9:4362
55. Shan N, Toda F, Jones W (2002) *Chem Commun* 2372
56. Shan N, Bond AD, Jones W (2002) *Cryst Eng* 5:9
57. Shan N, Jones W (2003) *Tetrahedron Lett* 44:3687
58. Shan N, Jones W (2003) *Green Chem* 5:728
59. Trask AV, Motherwell WDS, Jones W (2004) *Chem Commun* 890
60. Harris KDM, Johnston RL, Cheung EY, Turner GW, Habershon S, Albesa-Jove D, Tedesco E, Kariuki BM (2002) *Crystengcomm* 356
61. Harris KDM, Tremayne M, Kariuki BM (2001) *Angew Chem Int Ed* 40:1626
62. Tremayne M, Glidewell C (2000) *Chem Commun* 2425
63. Coupar PI, Glidewell C, Ferguson G (1997) *Acta Crystallogr B* 53:521
64. Cheung EY, Kitchin SJ, Harris KDM, Imai Y, Tajima N, Kuroda R (2003) *J Am Chem Soc* 125:14658

Intra-Solid and Inter-Solid Reactions of Molecular Crystals: a Green Route to Crystal Engineering

Dario Braga¹ (✉) · Daniela D’Addario · Stefano L. Giaffreda · Lucia Maini · Marco Polito · Fabrizia Grepioni²

¹ Department of Chemistry G. Ciamician, Via F. Selmi 2, University of Bologna, 40126 Bologna, Italy
dario.braga@unibo.it

² Department of Chemistry, Via Vienna 2, University of Sassari, 07100 Sassari, Italy
grepioni@ssmain.uniss.it

| | | |
|---|---|----|
| 1 | Introduction | 72 |
| 2 | Gas–Solid Reactions | 75 |
| 3 | Organometallic Molecules Reacting with Gases | 77 |
| 4 | Intra-Solid Reactions: Reactions Occurring Within Solids | 82 |
| 5 | Inter-Solid Reactions: Reactions Occurring Between Molecular Crystals | 84 |
| 6 | Mechanochemical Complexation | 87 |
| 7 | Conclusions | 89 |
| | References | 91 |

Abstract The thesis developed in this chapter is that reactions taking place between molecular solids or within molecular solids, or involving a molecular solid and a vapour, can be exploited to “make new crystals”, which is the quintessence of crystal engineering. Processes that lead from a crystalline reactant, or mixture of reactants, to a crystalline product without the intervention of solvents will be discussed. The focus will be on solid-state reactions controlled primarily by supramolecular bonding, such as template cycloadditions, formation of inclusion compounds, reactions between molecular crystals via reassembling of non-covalent bonding, and formation of complexes and coordination compounds. It is argued that solvent-free methods, e.g. co-grinding or milling of molecular solids, or reactions of solids with vapours represent viable “green” routes for the preparation of novel molecular and supramolecular solids.

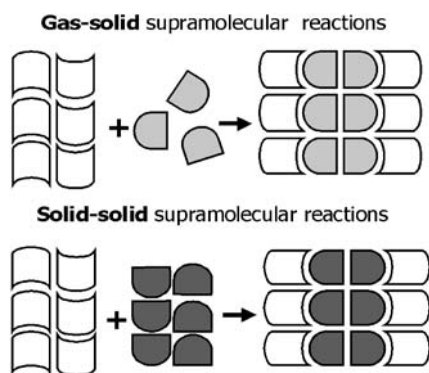
Keywords Solid-state reaction · Crystal engineering · Organometallic molecule · Molecular crystal · Green chemistry

1

Introduction

The paradigm of crystal engineering is the “bottom-up” construction of crystalline assemblies from molecular or ionic components and the exploitation of the resulting materials for physical and chemical applications [1]. The bottom-up paradigm, shared with supramolecular chemistry [2], implies the ability to assemble molecular or ionic components into the desired architecture by engineering a target network of supramolecular interactions. The interactions of choice can be covalent bonds between atoms, but also weaker types of bonds, such as coordination bonds between ligands and metal centres, Coulombic attractions and repulsions between ions, and non-covalent bonds between neutral molecules or ions (van der Waals, hydrogen bonds, etc.) [3]. These bonding interactions, and their combinations, imply very different enthalpic and entropic contributions: from the tiny energies involved in the van der Waals interactions between neutral atoms in neutral molecules to the high energies involved in covalent bond breaking and forming processes [4]. The existence of several, almost equivalent, free-energy minima for the solid-state assembly of the same molecular system carries important implications in studies of crystal polymorphism [5], and needs to be kept in mind by the crystal engineer.

Since crystal engineering is *making* crystals, it is usually thought that the method of choice to grow crystals of a desired material would be a crystallization method, whether from solution or by means of more forceful conditions, such as hydrothermal processes [6]. In this respect, we have argued that reactions between solids as well as those between solids and vapours – as pictorially represented in the cartoon in Scheme 1 – can represent alternative ways to prepare crystals [7]. Since reactions involving solid reactants or occurring between solids and gases do not generally require recovery, storage and disposal



Scheme 1 A cartoon-like representation of the reaction of a molecular solid with a gas (*top*) and of the reaction between two molecular solids (*bottom*) to yield a molecular crystal product

of solvents [8], they are of interest in the field of so-called green chemistry where environmentally friendly processes are actively sought [9]. Furthermore, solvent-less reactions often lead to very pure products and reduce the formation of solvate species [10].

This chapter will deal with both types of processes, namely reactions between solids and reactions between solids and gases. In the first section we will discuss examples of gas–solid reactions between molecular solids (operatively taken as crystals formed by neutral molecules or molecular ions) and vapours of small molecules, while the second section will deal with solid–solid reactions between molecular crystals to yield co-crystals. Even though examples will come mainly from our own work with organometallic molecules, coverage of the work of many scientists in the field will be attempted. The reader should be warned, however, that this chapter has no review-type ambitions.

Both solid–solid and solid–gas types of reactions lead from solid reactants to a solid product without the use of solvents. *Solvent-less processes, however, are not necessarily solid-state processes.* Indeed, it has been argued [8d,e] that many solid-state syntheses cannot be regarded as bona fide solid–solid reactions because they occur with the intermediary of a liquid phase, such as a eutectic phase or a melt, or may require destruction of the crystals prior to reaction. This latter situation is often observed, for instance, in the case of reactions activated by co-grinding, since the heat generated in the course of the mechanochemical process can induce local melting at the interface between the different crystals, or when *kneading*, i.e. grinding in the presence of small amounts of solvent, takes place (vide infra).

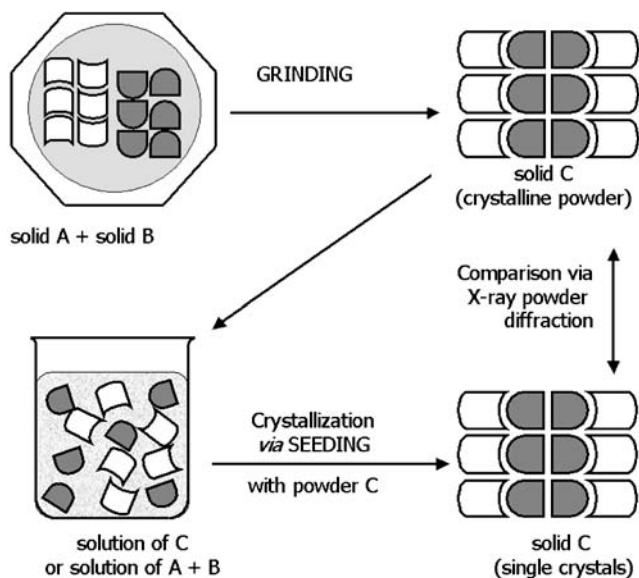
A further distinction has to be made between reactions taking place *within* a molecular crystal and reactions of a molecular crystal “A” with a molecular crystal “B” (see Scheme 2; A and B can also be the same crystal) [7b]. Reactions of the former type, or *intra-solid reactions*, can be either under topochemical control, depending on the proximity of the reactants, or may imply extensive molecular motion within the crystal lattice. Reactions of the second type, or *inter-solid reactions*, can either take place on the crystallite surface or require molecular diffusion through the lattice. Inter-solid reactions are often accompanied by formation of eutectics.

This distinction is, however, only practical. Several reaction types are not easily encompassed in the above description. For instance, Scheffer (see within this book) has provided ample examples of stereocontrolled solid-state reactions [11], while solid-state isomerizations have been studied by Coville and Levendis [12]. These processes can be explained with the reaction cavity concept, i.e. reactivity takes place in a constrained environment generated by the surrounding molecules. Relevant contributions to the field have also derived from the studies of Eckhardt [13] and those of Ohashi and collaborators [14].

We shall thus confine our interest to:

1. Gas–solid reactions and the relationship with solvation processes and the formation of crystal polymorphs and pseudo-polymorphs [15].

solid–solid processes possess the same structure by comparing the observed X-ray powder diffraction pattern with that computed on the basis of the single crystal structure (see Scheme 3). This approach has been used previously by us and by others to determine the structure of many polycrystalline products obtained by “non-solution” methods (grinding, dehydration, thermal treatment).



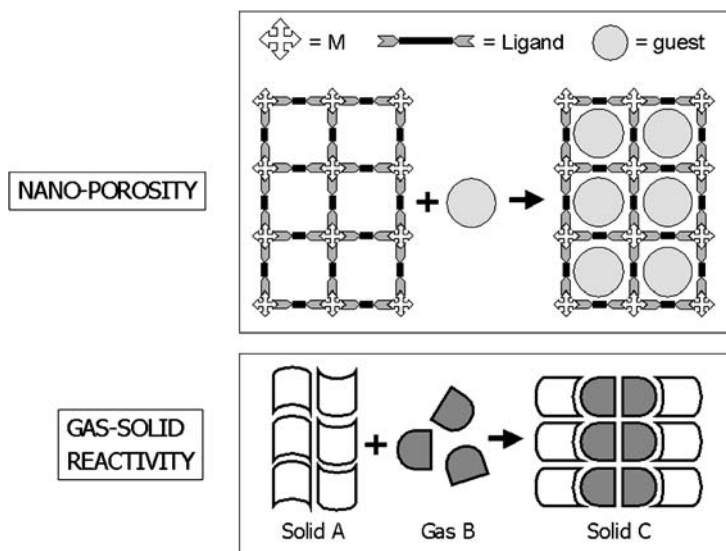
Scheme 3 The solid yielded by mechanical mixing of the reactants can be used to *seed* crystal growth from solution to obtain crystals for single-crystal X-ray diffraction experiments. This procedure allows one to compare the X-ray powder diffraction pattern measured on the mechanochemical sample with that calculated on the basis of the single-crystal experiment for the solids obtained by crystallization via *seeding* of a solution of the ground powder of the adduct

2

Gas–Solid Reactions

In a solid–gas reaction involving a molecular crystal, the reactants are respectively the molecules in the crystalline solid and the molecules in the gas phase and the product is the product crystal, which can be crystalline or amorphous. Vapour uptake to generate a solvate crystal (e.g. hydration) is a related process. In fact the difference between a crystal solvation process and a solid–gas reaction leading to new molecular/ionic species is mainly in the energetic scale of the processes and in the fact that in solvation processes, molecules retain their chemical identity. On this premise there is a relevant analogy between the uptake of small molecules by a nanoporous material [16] and the reaction between a molecular crystal and molecules to yield a co-crystal or a salt (e.g. acid–base

proton transfer). Indeed, both processes can be seen as special types of *supramolecular reactions* whereby non-covalent interactions between guest and host are broken and formed. A comparison is shown in Scheme 4.



Scheme 4 There is a relevant analogy between the uptake of molecules by a nanoporous material and the reaction between a molecular crystal and molecules to yield a co-crystal or a salt

Pellizzari reported in 1884 a study of the reaction of dry ammonia vapours with dried and pulverized phenols and carboxylic acids [17]. However, in spite of this early beginning, a systematic exploration of solvent-less processes of this type was not undertaken until the early 1970s by Paul and Curtin [18–20] and subsequently by others [21].

In the following we shall focus on heterogeneous acid–base reactions. One of the best known case studies is the reaction of crystalline benzoic acid with ammonia to form 1:1 ammonium salts [19, 20]. Crystalline *p*-chlorobenzoic anhydride reacts with gaseous ammonia to give the corresponding amide and ammonium salt [22]; a similar reaction has been investigated in the case of optically active cyclopropanecarboxylic acid crystals [23].

A series of solid-state reactions has been explored by Kaupp et al., in which gaseous amines were reacted with aldehydes to give imines. Analogous reactions with solid anhydrides, imides, lactones or carbonates, and isothiocyanates were used to give, respectively, diamides or amidic carboxylic salts or imides, diamides, carbamic acids, and thioureas [24]. In general the yields were found to be quantitative. Ammonia and other gaseous amines, in particular methylamine, have also been shown to aminolyse thermoplastic polycarbonates [25].

Kaupp et al. also exploited heterogeneous reactions with ClCN and BrCN in the quantitative synthesis of cyanamides, cyanates, thiocyanates and derivatives [26]. Gaseous acids were shown to form salts with strong and weak solid nitrogen bases. Solid hydrohalides are formed quantitatively by reaction with vapours of HCl, HBr and HI; the same applies to di-bases such as *o*-phenylenediamines. The products are much more easily handled than when they are formed in solution. The solid products can in turn be used in reactions with gaseous acetone to form the corresponding dihydrohalides of 1,5-benzodiazepines [27].

Conversion of secondary and tertiary alcohols into the corresponding chlorides has been shown to proceed efficiently when the powdered solid alcohol is exposed to HCl in a desiccator [28]. Solid-state bromination of anilines and phenols with gaseous bromine and solid bromination reagents has been shown to proceed with higher yields than in solution [29].

3

Organometallic Molecules Reacting with Gases

A recent application of the principles outlined above has been reported by us in the organometallic chemistry area [30]. The organometallic sandwich zwitterion $[\text{Co}^{\text{III}}(\eta^5\text{-C}_5\text{H}_4\text{COOH})(\eta^5\text{-C}_5\text{H}_4\text{COO})]$ can be quantitatively prepared from the corresponding dicarboxylic cationic acid $[\text{Co}^{\text{III}}(\eta^5\text{-C}_5\text{H}_4\text{COOH})_2]^+$. The amphoteric behaviour of the zwitterion depends on the presence of one $-\text{COOH}$ group, which can react with bases, and one $-\text{COO}^{(-)}$ group, which can react with acids as shown in Fig. 1.

As a matter of fact, the organometallic zwitterion $[\text{Co}^{\text{III}}(\eta^5\text{-C}_5\text{H}_4\text{COOH})(\eta^5\text{-C}_5\text{H}_4\text{COO})]$ undergoes fully reversible heterogeneous reactions with the hydrated vapours of a variety of acids (e.g. HCl, CF_3COOH , HBF_4 , HCOOH) and bases (e.g. NH_3 , NMe_3 , NH_2Me) [31], with formation of the corresponding salts, as summarized in Fig. 2.

Complete conversion of the neutral crystalline zwitterion into the crystalline chloride salt $[\text{Co}^{\text{III}}(\eta^5\text{-C}_5\text{H}_4\text{COOH})_2]\text{Cl}\cdot\text{H}_2\text{O}$, for instance, is attained in 5 min of exposure to vapours of aqueous HCl 36%. Formation of the salt in the heterogeneous reaction is easily assessed by comparison of the observed X-ray powder diffraction pattern with that calculated on the basis of the single-crystal structure determined previously. Crystalline $[\text{Co}^{\text{III}}(\eta^5\text{-C}_5\text{H}_4\text{COOH})_2]\text{Cl}\cdot\text{H}_2\text{O}$ can be converted back to neutral $[\text{Co}^{\text{III}}(\eta^5\text{-C}_5\text{H}_4\text{COOH})(\eta^5\text{-C}_5\text{H}_4\text{COO})]$ by heating the sample for 1 h at 440 K in an oil bath under low pressure (10^{-2} mbar). A thermogravimetric analysis (TGA) was used to demonstrate that the solid releases one water molecule and one HCl molecule per molecular unit at 394 and 498 K, respectively. The powder diffractogram of the final product corresponds precisely to that of the anhydrous $[\text{Co}^{\text{III}}(\eta^5\text{-C}_5\text{H}_4\text{COOH})(\eta^5\text{-C}_5\text{H}_4\text{COO})]$. The behaviour of the zwitterion towards NH_3 is similar: the neutral system quantitatively transforms into the hydrated ammonium salt $[\text{Co}^{\text{III}}(\eta^5\text{-C}_5\text{H}_4\text{COO})_2]-$

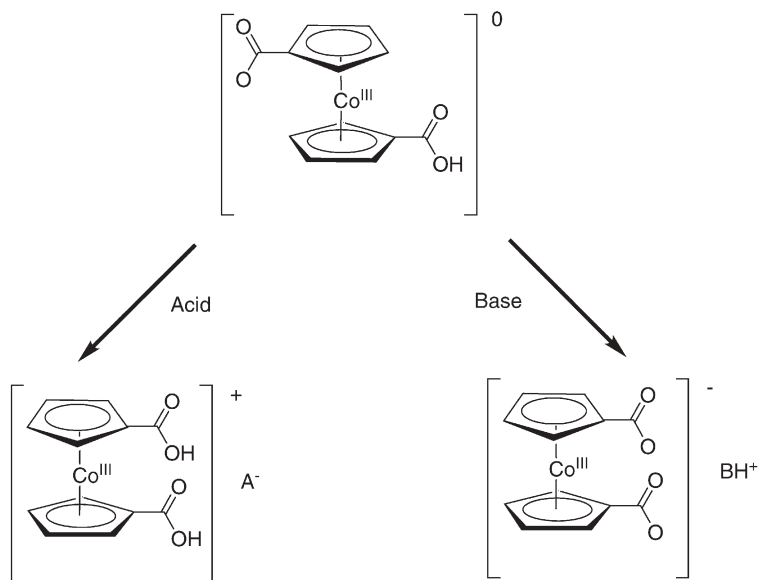


Fig. 1 The amphoteric behaviour of the zwitterion $[\text{Co}^{\text{III}}(\eta^5\text{-C}_5\text{H}_4\text{COOH})(\eta^5\text{-C}_5\text{H}_4\text{COO})]$ depends on the presence of one -COOH group, which can react with bases, and one $\text{-COO}^{(-)}$ group, which can react with acids

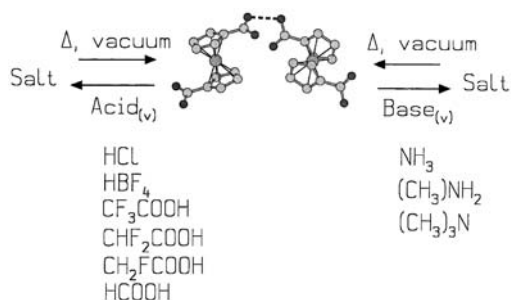


Fig. 2 The zwitterion $[\text{Co}^{\text{III}}(\eta^5\text{-C}_5\text{H}_4\text{COOH})(\eta^5\text{-C}_5\text{H}_4\text{COO})]$ reacts with vapours of acids and bases in reversible solid–gas reactions. Note that the reactions imply profound rearrangements of the hydrogen bonding patterns

$[\text{NH}_4]\cdot 3\text{H}_2\text{O}$ upon 5 min exposure to vapours of aqueous ammonia 30%. Single crystals of the ammonium salt for X-ray structure determination can be obtained if the reaction of the zwitterion with ammonia is carried out in aqueous solution. As in the case of the chloride salt, formation of $[\text{Co}^{\text{III}}(\eta^5\text{-C}_5\text{H}_4\text{COO})_2][\text{NH}_4]\cdot 3\text{H}_2\text{O}$ in the heterogeneous reaction is assessed by comparison of the observed and calculated X-ray powder diffraction patterns. Absorption of ammonia is also fully reversible: upon thermal treatment (1 h at

373 K, ambient pressure) the salt converts quantitatively into the neutral zwitterion.

The material can be cycled through several absorption and release processes of HCl or ammonia, as well as other gaseous acids and bases, without decomposition or detectable formation of amorphous material. The solid-state structures of $[\text{Co}^{\text{III}}(\eta^5\text{-C}_5\text{H}_4\text{COOH})_2]\text{Cl}\cdot\text{H}_2\text{O}$ and of $[\text{Co}^{\text{III}}(\eta^5\text{-C}_5\text{H}_4\text{COO})_2][\text{NH}_4]\cdot 3\text{H}_2\text{O}$ as obtained from single-crystal X-ray diffraction on the sample recrystallized by seeding are shown in Figs. 3 and 4, respectively. It is worth

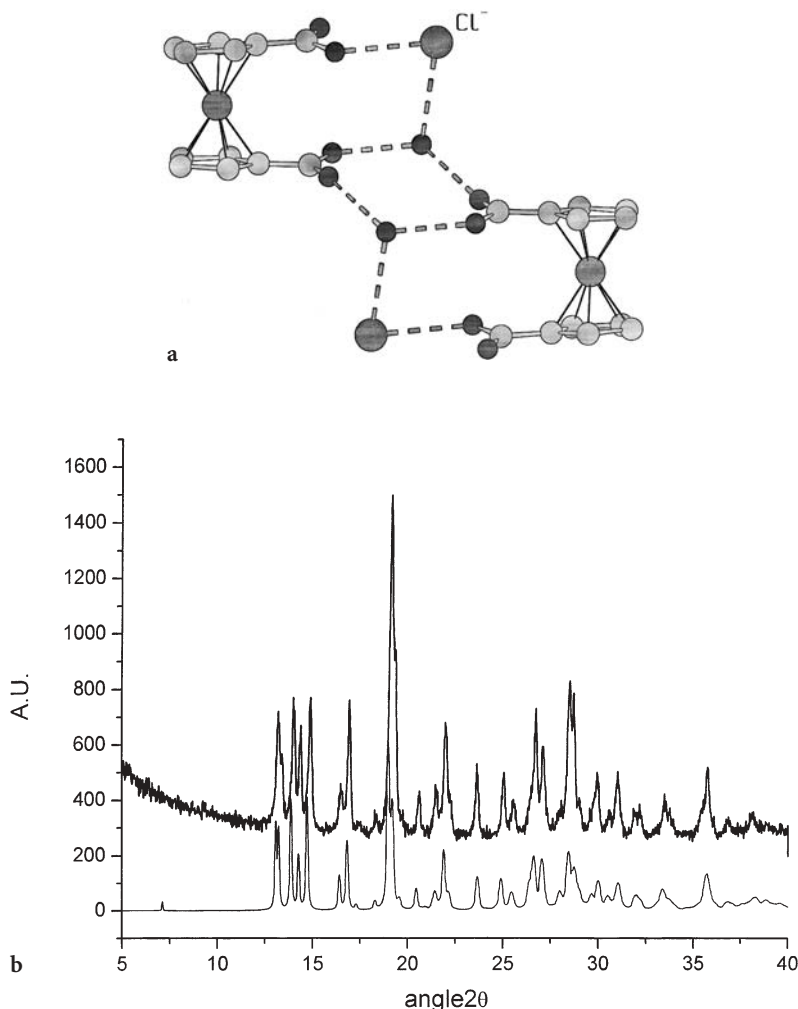


Fig. 3 a The solid-state structure of $[\text{Co}^{\text{III}}(\eta^5\text{-C}_5\text{H}_4\text{COOH})_2]\text{Cl}\cdot\text{H}_2\text{O}$ as obtained from single crystals grown from solution. b The calculated powder diffraction pattern matches the one measured on the powder material recovered from the solid-gas reaction

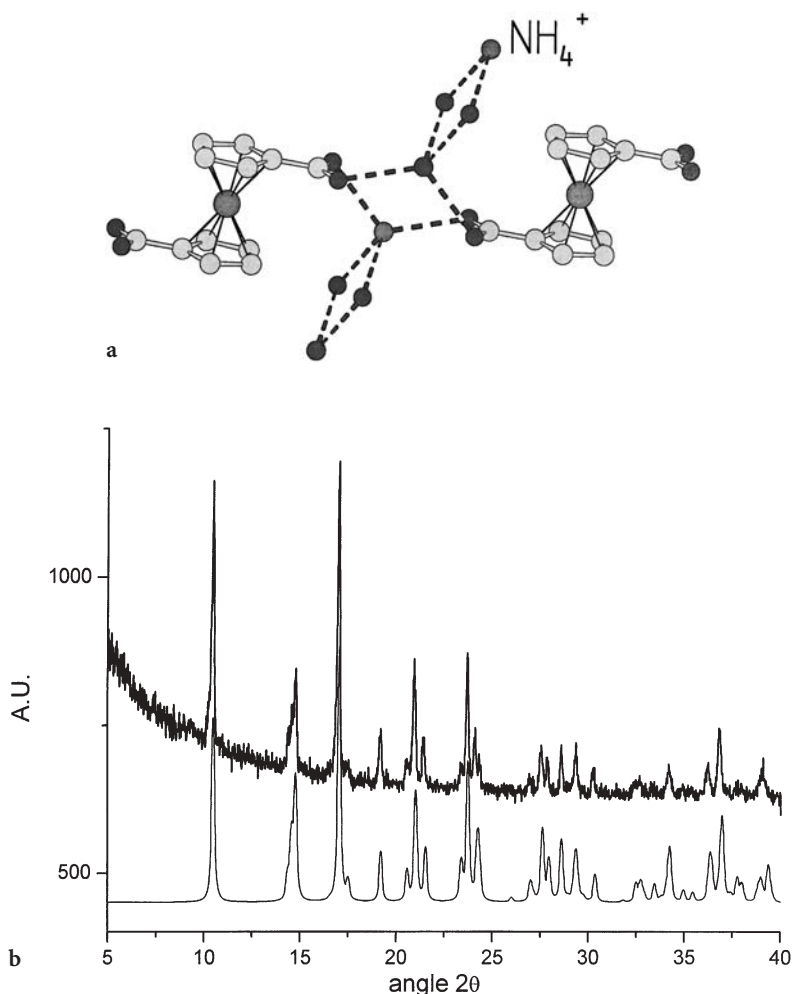


Fig. 4 **a** The structure of $[\text{Co}^{\text{III}}(\eta^5\text{-C}_5\text{H}_4\text{COO})_2][\text{NH}_4]\cdot 3\text{H}_2\text{O}$ as obtained from single crystals grown from solution. **b** The calculated powder diffraction pattern matches the one measured on the powder material recovered from the solid–gas reaction

stressing that the formation of $[\text{Co}^{\text{III}}(\eta^5\text{-C}_5\text{H}_4\text{COOH})_2]\text{Cl}\cdot\text{H}_2\text{O}$ from the anhydrous $[\text{Co}^{\text{III}}(\eta^5\text{-C}_5\text{H}_4\text{COOH})(\eta^5\text{-C}_5\text{H}_4\text{COO})]$ requires that the O–H–O bonds involving the protonated -COOH group and the deprotonated $\text{-COO}^{(-)}$ of neighbouring zwitterion molecules are replaced, upon absorption of HCl, by $(^+)\text{O}-\text{H}-\text{Cl}^{(-)}$ interactions between the -COOH groups on the fully protonated organometallic cation $[\text{Co}^{\text{III}}(\eta^5\text{-C}_5\text{H}_4\text{COOH})_2]^+$ and the $\text{Cl}^{(-)}$ anions. Analogously, formation of $[\text{Co}^{\text{III}}(\eta^5\text{-C}_5\text{H}_4\text{COO})_2][\text{NH}_4]\cdot 3\text{H}_2\text{O}$ implies formation of charge-assisted $(^+)\text{N}-\text{H}-\text{O}^{(-)}$ interactions between the ammonium cation and the deprotonated $\text{-COO}^{(-)}$ groups on the organometallic anion [32].

The reversible heterogeneous solid–gas reactions of single crystals of the neutral organometallic zwitterion $[\text{Co}^{\text{III}}(\eta^5\text{-C}_5\text{H}_4\text{COOH})(\eta^5\text{-C}_5\text{H}_4\text{COO})]$ with moist vapours of NH_3 , HCl and CF_3COOH were also investigated by atomic force microscopy (AFM) (see Fig. 5). It was possible to demonstrate by means of AFM that the reactions proceed well on the (110) and (110) faces where the cleavage planes start [33]. The surface features of the heterogeneous solid-state processes correlate with the crystal packing without formation of liquid phases on the surfaces of the organometallic crystal. All three gases lead to surface passivation in the absence of moisture by the creation of submicroscopic closed covers that prevent further reaction.

$[\text{Co}^{\text{III}}(\eta^5\text{-C}_5\text{H}_4\text{COOH})(\eta^5\text{-C}_5\text{H}_4\text{COO})]$ also reversibly absorbs formic acid from humid vapours [33]. The reaction leads to selective formation of a 1:1 co-crystal, $[\text{Co}^{\text{III}}(\eta^5\text{-C}_5\text{H}_4\text{COOH})(\eta^5\text{-C}_5\text{H}_4\text{COO})][\text{HCOOH}]$, from which the zwitterion can be fully recovered by mild thermal treatment. Complete conversion of the zwitterion into the adduct is attained in 4 h of exposure to hydrated vapours of HCOOH . Single crystals of $[\text{Co}^{\text{III}}(\eta^5\text{-C}_5\text{H}_4\text{COOH})(\eta^5\text{-C}_5\text{H}_4\text{COO})][\text{HCOOH}]$ can be obtained by crystallization from a water solution of HCOOH in which the zwitterion is dissolved. The process was also investigated by ^{13}C CPMAS NMR spectroscopy, confirming that no proton transfer occurs between formic acid and the zwitterion.

The gas–solid reaction can thus be more appropriately described as a special kind of solvation rather than as a heterogeneous acid–base reaction. In the reversible supramolecular reaction the zwitterion reacts with gaseous HCOOH ,

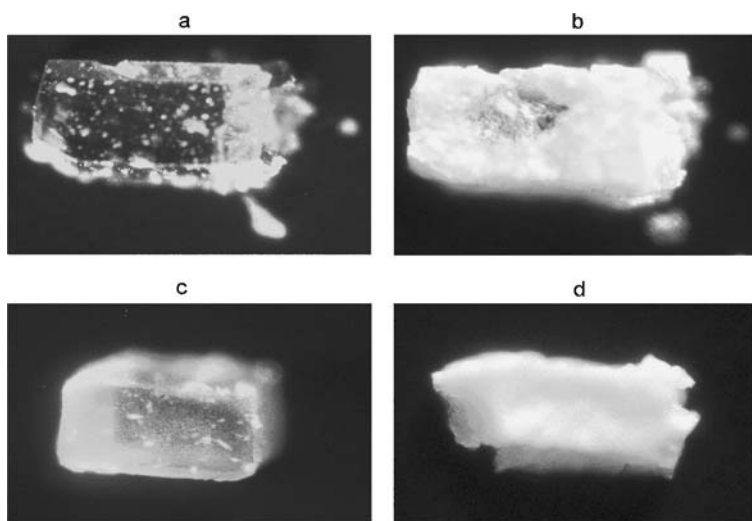


Fig. 5 Micrographs of single crystals of the zwitterion $[\text{Co}^{\text{III}}(\eta^5\text{-C}_5\text{H}_4\text{COOH})(\eta^5\text{-C}_5\text{H}_4\text{COO})]$ before and after treatment of single crystals with moist gases: **a** fresh; **b** after 25 min treatment with 14% HCl (same specimen as in **a**); **c** after 5 min treatment with 0.5% CF_3COOH ; **d** after 10 min treatment with 40% NH_3

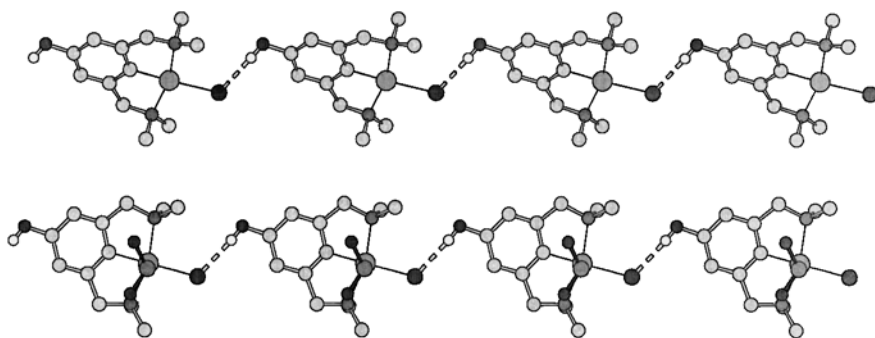


Fig. 6 The organo-platinum(II) complex containing N,C,N tridentate ligands reversibly binds gaseous SO_2 in the solid state. The reversible reaction occurs at the Pt(II) complex by Pt-S bond formation and cleavage. Uptake and release of SO_2 does not destroy the crystalline ordering

O-H...O and C-H...O bonds are disrupted and/or rearranged, while covalent bonds are not affected.

In summary, the organometallic zwitterionic system $[\text{Co}^{\text{III}}(\eta^5\text{-C}_5\text{H}_4\text{COOH})-(\eta^5\text{-C}_5\text{H}_4\text{COO})]$ behaves as a reversible “amphoteric sink” towards a variety of hydrated vapours of acids and bases.

There are other important examples of the utilization of coordination compounds in gas–solid reactions. For reasons of space we cannot review this field of research. It is, however, useful to mention some of the recent results obtained in the quest for new solid-state sensors and traps. Van Koten et al. have shown, for instance, that organo-platinum(II) complexes containing N,C,N tridentate coordinating anion “pincers” reversibly bind gaseous SO_2 in the solid state, leading to quantitative adduct formation [34, 35]. Solid–gas reaction occurs at the Pt(II) complex, which reversibly binds gaseous SO_2 in the solid state by Pt-S bond formation and cleavage. Uptake and release of SO_2 does not destroy the crystalline ordering. The crystalline reagent and product are shown in Fig. 6.

4

Intra-Solid Reactions: Reactions Occurring Within Solids

The purpose of the following section is that of providing an overview of reactions that take place within a crystal, i.e. *intra-solid* reactions. In a way, intra-solid reactions represent an area of chemistry where solid-state and molecular chemical reactivity meet more clearly.

The prototypes of intra-solid reactions are the [2+2] photochemically activated cycloaddition reactions that constitute the basis of Schmidt’s work on topochemical reactions [36]. It is now clear, however, that the topochemical postulate, though correct and of wide applicability, cannot account for many solid-state processes, in particular those implying high molecular or ionic mo-

bility within the crystal lattice, such as many solid–gas and solid–solid reactions that require that molecules travel through the reactant crystal [37]. Crystal homogeneity can also be very important for the success of a solid-state process [38]. Toda [40] and Kaupp [41] were among the first to investigate in a systematic manner non-photochemical organic solid-state reactions for preparative purposes (see this book). True-type topochemical solid-state reactions, very much inspired by those investigated by Schmidt, are now being extensively investigated with remarkable results by MacGillivray et al. [39].

MacGillivray's group has employed rigid bifunctional molecules [42], such as 1,3-dihydroxybenzene and 1,8-naphthalenedicarboxylic acid [42a], as linear templates to organize reactants such as *trans*-1,2-bis(4-pyridyl)ethylene via hydrogen bonds for single and multiple photoinduced [2+2] cycloadditions, for the template-controlled synthesis of a 1,2,3,4-(4-pyridyl)cyclobutane [42b] and also of paracyclophanes [42d]. Very recently, [*n*]ladderanes (*n*=2, 3) have been synthesized in the solid state by UV irradiation of 2(5-methoxyresorcinol)-2(4-pyr-poly-*m*-ene) (*m*=2, 3) [42e].

π-stacking interactions have also been exploited to orientate olefinic moieties in a geometry suitable for photochemical cycloaddition reactions, and have been invoked by Coates et al. to explain the photodimerization and photopolymerization of mono- and diolefins carrying phenyl and perfluorophenyl groups [43]. Matsumoto et al. reported the photodimerization of 2-pyridone in co-crystals with naphthalene-substituted monocarboxylic acids, where the stacking of the naphthalene rings provides carbon–carbon distances appropriate for [4+4] cycloaddition [44].

Feldman and Campbell, on the other hand, used hydrogen-bonding interactions to enforce a particular stereo- and regiochemical outcome of the solid-state photocycloaddition of a naphthoic acid-derived cinnamic acid [45]. In a conceptually similar approach, Scheffer demonstrated that diamines can form double salts with a variety of *trans*-cinnamic acid derivatives. The locking in place of the double bonds steers the solid-state [2+2] photodimerization [46].

In some cases, reactions could be investigated directly on single crystals. For instance, Novak and Enkelman have been able to study photodimerization of cinnamic acid and its thermal reverse reaction on single crystals [47]. Irie et al. have shown that alternate irradiation of single crystals of the diarylethene 1,2-bis(2,4-dimethyl-5-phenyl-3-thienyl)perfluorocyclopentene with ultraviolet and visible lights causes a photochemically reversible color change (from colorless to blue) associated with a reversible intramolecular photocyclization reaction [48a]. More recently [48b], single crystals of four different polymorphic modifications of the diarylethene compound 1,2-bis(2-methyl-5-*p*-methoxyphenyl-3-thienyl)perfluorocyclopentene were subjected to alternate UV/VIS photoirradiation, showing that the photocycloreversion quantum yields were different by as much as four times, depending on the conformation of the closed-ring isomers in the crystals. With the same successful approach [48c] it has also been possible to achieve absolute asymmetric photocyclization of the *achiral* diarylethene derivative 1,2-bis(5-*m*-formyl-phenyl-2-methyl-3-thienyl)-

perfluorocyclopentene in its chiral crystals, with formation of either chiral or closed-ring isomers, depending on the absolute configuration of the crystals.

Toda et al. reported that the topotactic and enantioselective photodimerization of coumarin and thiocoumarin takes place in single crystals without significant molecular rearrangements [49]. Molecular motion needs to be called upon to explain the photochemically activated cycloaddition reaction of 2-benzyl-5-benzylidenecyclopentanone. The dimer molecules, once formed, move smoothly in the reactant crystal to form the product crystal [50]. Harris et al. investigated the reactivity of 10-hydroxy-10,9-boroxophenanthrene in the solid state and the mechanism of the solid-state reaction was characterized by both X-ray diffraction and thermal analysis [51]. It was demonstrated that the solution chemistry of 10-hydroxy-10,9-boroxophenanthrene is different from that in the solid state, where it undergoes dimerization and dehydration to form a monohydrate derivative.

The reader is addressed to the other relevant chapters within this volume of *Topics in Current Chemistry* and to the cited references.

5

Inter-Solid Reactions: Reactions Occurring Between Molecular Crystals

Rastogi et al. carried out pioneering investigations of reactions between solid naphthalene, phenanthrene, anthracene, naphthols and other substituted hydrocarbons and picric acid [52]. M. Etter and collaborators demonstrated that co-crystals of hydrogen-bonded systems could be prepared not only by evaporation of a solution containing stoichiometric amounts of the components, but also by grinding the solid components together [53a]. For example, 9-methyladenine and 1-methylthymine were shown to form co-crystals containing inter-molecular hydrogen-bonded pairs in the solid state by simple grinding of the two pure components. Importantly, the co-crystals could also form in the presence of a third solid component [53b]. In yet another example, it was shown that polymorph interconversion in the case of 2-aminobenzoic acid could also be achieved by grinding [54]. As mentioned in the Introduction the issue of polymorphism is always present in solid-state reactivity studies, in particular when the mechanochemical process may activate phase transition between enantiotropic forms or lead to formation of pseudo-polymorphs via vapour uptake or release [55].

Curtin and Paul [56] contributed substantially also to the investigation of intra-solid reactions between crystals. In this context, Ref. [57] constitutes, together with the other references quoted throughout, a useful entry in the recent literature of organic solid-state reactions, including those activated mechanochemically [57]. An early application to the preparation of charge-transfer systems was reported by Toda and Miyamoto [58].

Braga, Grepioni and collaborators have recently shown [59] that manual grinding of the ferrocenyl dicarboxylic acid complex $[\text{Fe}(\eta^5\text{-C}_5\text{H}_4\text{COOH})_2]$ with

a variety of solid bases, namely 1,4-diazabicyclo[2.2.2]octane, 1,4-phenylenediamine, piperazine, *trans*-1,4-cyclohexanediamine and guanidinium carbonate, generates quantitatively the corresponding organic–organometallic adducts (see Fig. 7). The reaction with phenylenediamine is highlighted. In the case of the adduct $[\text{HC}_6\text{N}_2\text{H}_{12}][\text{Fe}(\eta^5\text{-C}_5\text{H}_4\text{COOH})(\eta^5\text{-C}_5\text{H}_4\text{COO})]$, not only can the base be removed by mild treatment regenerating the structure of the starting dicarboxylic acid, but the same product can also be obtained via a (much slower) vapour uptake process. The processes imply breaking and reassembling of hydrogen-bonded networks, conformational change from *cis* to *trans* of the -COO/-COOH groups on the ferrocene diacid, and proton transfer from acid to base. In some cases it was necessary to resort to seeding, i.e. to the use of a

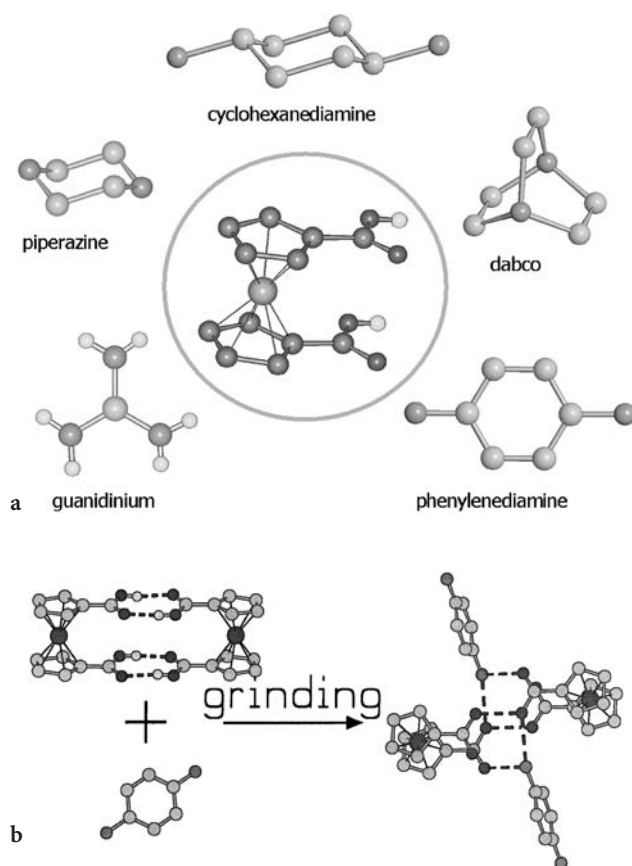


Fig. 7 Manual grinding of the ferrocenyl dicarboxylic acid complex $[\text{Fe}(\eta^5\text{-C}_5\text{H}_4\text{COOH})_2]$ with 1,4-diazabicyclo[2.2.2]octane, 1,4-phenylenediamine, piperazine, *trans*-1,4-cyclohexanediamine and guanidinium carbonate generates quantitatively the corresponding organic–organometallic adducts. The reaction with phenylenediamine highlights that single crystals of the adduct can be grown from solution and used to fully characterize the reaction product

tiny amount of powder of the desired compound, to grow crystals suitable for single-crystal X-ray experiments.

Seeding procedures are commonly employed in the pharmaceutical industries to make sure that the desired crystal form is always obtained from a preparative process [60]. It is important to appreciate that seeding often prevents the formation of kinetically favoured products.

Seeds of isostructural or quasi-isostructural species that crystallize well can also be employed to induce crystallization of unyielding materials [61]. *Heteromolecular seeding* [62], whereby near isostructural compounds can be used to template crystallization in less accessible or elusive desired crystal forms, can be applied. For instance, chiral co-crystals of tryptamine and hydrocinnamic acid were prepared by crystallization in the presence of seeds of different chiral crystals [63]. Of course, unintentional seeding may also alter the crystallization process in an undesired manner [64].

The mechanochemical formation of hydrogen-bonded co-crystals between 4-amino-*N*-(4,6-dimethylpyrimidin-2-yl)benzenesulfonamide and aromatic carboxylic acids was investigated by Caira et al. [65].

The effect of mechanical mixing of solid dicarboxylic acids of variable chain length $\text{HOOC}(\text{CH}_2)_n\text{COOH}$ ($n=1-7$) together with solid 1,4-diazabicyclo[2.2.2]-

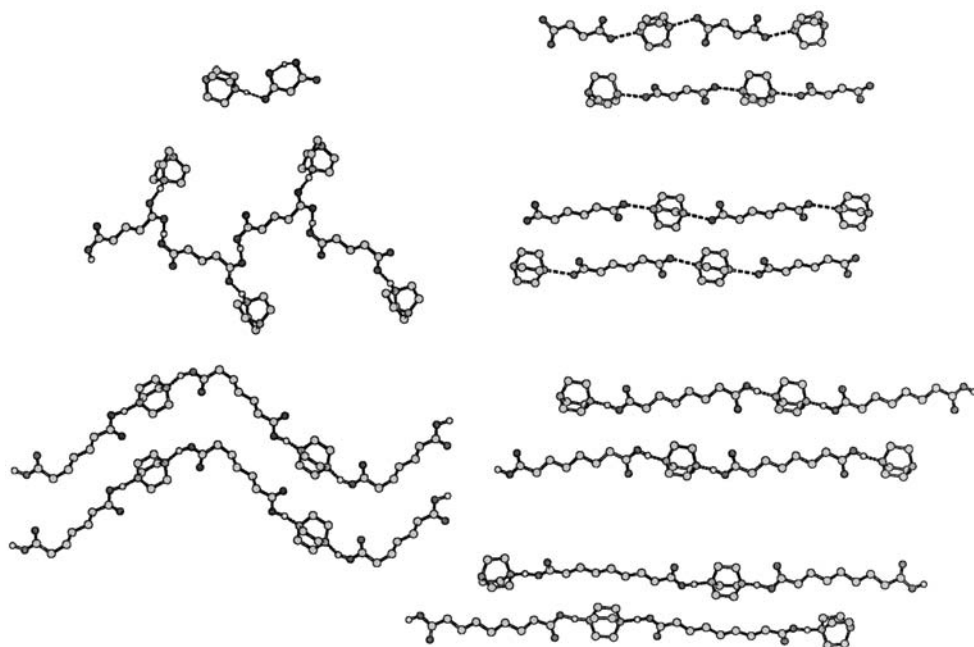


Fig. 8 The solid-state structures of the compounds $[\text{N}(\text{CH}_2\text{CH}_2)_3\text{N}]\text{-H-}[\text{OOC}(\text{CH}_2)_n\text{COOH}]$ ($n=1-7$) obtained by co-grinding the dicarboxylic acid of variable carbon atom chain length with the base $[\text{N}(\text{CH}_2\text{CH}_2)_3\text{N}]$. Single crystals of the adducts can be grown from solution and used to fully characterize the reaction products

octane, $C_6H_{12}N_2$, to generate the corresponding salts or co-crystals of formula $[N(CH_2CH_2)_3N]-H-[OOC(CH_2)_nCOOH]$ ($n=1-7$) has also been investigated [66] (Fig. 8). The reactions implied transformation of inter-acid O–H–O bonds into hydrogen bonds of the O–H–N type between acid and base. The nature (whether neutral O–H–N or charged $(^-)O-H-N^{(+)}$) of the hydrogen bond was established by means of solid-state NMR measurement, the chemical shift tensors of the compounds obtained with chain length from 3 to 7 [66].

In a related study it was shown that the reaction of $[N(CH_2CH_2)_3N]$ with malonic acid $[HOOC(CH_2)COOH]$ in the molar ratio 1:2 yields two different crystal forms of the salt $[HN(CH_2CH_2)_3NH][OOC(CH_2)COOH]_2$ depending on the preparation technique and crystallization speed: the less dense form I, containing malonate anions with intramolecular hydrogen bonds, is obtained by solid-state co-grinding or by rapid crystallization while a denser form II, containing intermolecular hydrogen bonds, is obtained by slow crystallization. Forms I and II do not interconvert, while form I undergoes an order–disorder phase transition on cooling [66b]. These observations led the authors to wonder whether the two forms could be treated as bona fide polymorphs or should be regarded more appropriately as hydrogen bond isomers of the same *solid supermolecule*.

6 Mechanochemical Complexation

The same organometallic zwitterion $[Co^{III}(\eta^5-C_5H_4COOH)(\eta^5-C_5H_4COO)]$ used successfully in the solid–solid reactions described above has also been used in solid–solid reactions with crystalline alkali salts MX ($M=K^+$, Rb^+ , Cs^+ , NH_4^+ ; $X=Cl^-$, Br^- , I^- , PF_6^- though not in all permutations of cations and anions) yielding supramolecular complexes of formula $[Co^{III}(\eta^5-C_5H_4COOH)-(\eta^5-C_5H_4COO)]_2 \cdot M^+X^-$ [67].

The prototype complex $[Co^{III}(\eta^5-C_5H_4COOH)(\eta^5-C_5H_4COO)]_2 \cdot K^+Br^-$ shows that complexation of the alkali cation takes place by encapsulation of the K^+ cations within a cage formed by four zwitterion molecules, dimerized via O–H...O hydrogen bonds, with the Br^- anions forming layers in between the cationic complexes. The reactions imply a profound solid-state rearrangement accompanied by breaking and forming of O–H–O hydrogen-bonding interactions between the organometallic molecules. The solid-state complexation of alkali cations by the organometallic zwitterion has been described as a special kind of solvation process taking place in the solid state (see Fig. 9). For some of the alkali salts the mechanochemical complexation was speeded up by *kneading*, i.e. by grinding the salts in the presence of a catalytic amount of water.

Toda demonstrated that significant improvements in the kinetics of co-crystal formation by grinding could be achieved by the addition of minor amounts of appropriate solvent [68]. As a matter of fact, a very common method in the

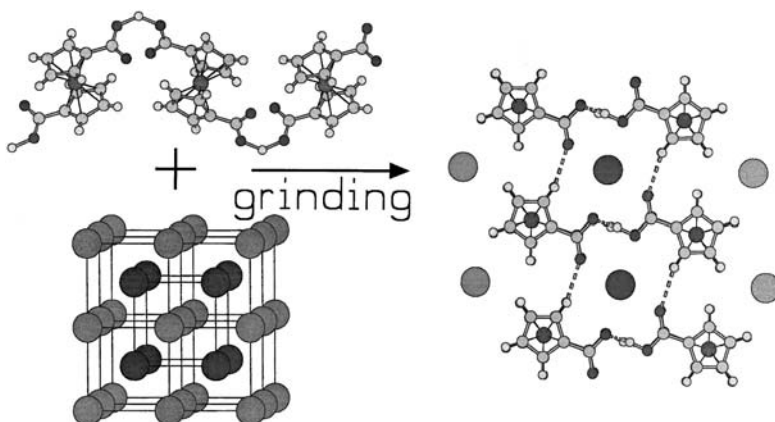


Fig. 9 The organometallic zwitterion $[\text{Co}^{\text{III}}(\eta^5\text{-C}_5\text{H}_4\text{COOH})(\eta^5\text{-C}_5\text{H}_4\text{COO})]$ reacts quantitatively as a solid polycrystalline phase with a number of crystalline alkali salts MX ($\text{M} = \text{K}^+, \text{Rb}^+, \text{Cs}^+, \text{NH}_4^+$; $\text{X} = \text{Cl}^-, \text{Br}^-, \text{I}^-, \text{PF}_6^-$) forming supramolecular complexes of formula $[\text{Co}^{\text{III}}(\eta^5\text{-C}_5\text{H}_4\text{COOH})(\eta^5\text{-C}_5\text{H}_4\text{COO})]_2 \cdot \text{M}^+\text{X}^-$. The example shows the adduct obtained from the reaction with KBr

preparation of cyclodextrin inclusion compounds is the so-called kneading process, viz. the grinding of powdered reactants in the presence of a minimal amount of solvent. Studies of kneading and development of lab/industrial kneaders (mainly of pharmaceutical powders) have been carried out [69]. One may reasonably object that solid-state processes via kneading cannot be considered as true solid–solid processes, since solvent, though in minimal quantity, is involved. We would argue in favour of the “catalytic” function of this solvent in view of the fact that it is not retained within the crystalline products.

The effect of KBr pellet preparation discussed above brings about a well known – and possibly overlooked – class of mechanochemical reactions: those between alkaline halogenides, such as KBr and CsI, used for IR pellets, and species, such as molecules carrying $-\text{COOH}$ groups, which may cause an alteration of the absorption frequencies with respect to those measured in solution or Nujol [70]. The mechanochemical reactions that take place when milling and pressing analytes with KBr to form discs for IR experiments have been recently reviewed by Fernandez-Bertran and Reguera [71].

The interaction of alkali salts with inorganic and organic acids has been extensively studied by the same group. In the case of alkali fluorides it was shown that milling leads to proton transfer and to formation of KHF_2 , while the reactivity of fluorides follows the order $\text{KF} > \text{NH}_4\text{F} > \text{NaF} > \text{LiF}$, CaF_2 [71b,c].

Besides reactions with alkali salts, there are several groups investigating metal–ligand bond formation by mechanochemical methods. For example Orita et al. have shown that the supramolecular self-assembly of a number of complexes can take place under solvent-free conditions, leading to higher-order fabrications of two- or three-dimensional topology and even double

helicates [72]. Balema et al. have shown that the *cis*-platinum complexes *cis*-(Ph₃P)₂PtCl₂ and *cis*-(Ph₃P)₂PtCO₃ can be prepared mechanochemically from solid reactants in the absence of solvent [73]. *Cis*-(Ph₃P)₂PtCl₂ was obtained in 98% yield after ball-milling of polycrystalline PtCl₂ and Ph₃P, while the mechanically induced solid-state reaction of *cis*-(Ph₃P)₂PtCl₂ with an excess of anhydrous K₂CO₃ produced *cis*-(Ph₃P)₂PtCO₃ in 70% yield [73]. The same group also investigated, by means of solid-state ³¹P NMR spectroscopy and powder diffraction, the formation of phosphonium salts during high-energy ball-milling of triphenylphosphine with solid organic bromides [74] as well as the mechanical preparation of phosphorus ylides [75].

Steed, Raston and collaborators explored the use of mechanochemistry in the synthesis of extended supramolecular arrays [76a]. Grinding of Ni(NO₃) with 1,10-phenanthroline (phen) resulted in the facile preparation of [Ni(phen)₃]²⁺ accompanied by a dramatic and rapid colour change. Addition of the solid sodium salt of tetrasulfonatocalix[4]arene (tsc) gives two porous π -stacked supramolecular arrays [Ni(phen)₃]₂[tsc⁴⁻] $\cdot n$ H₂O and the related [Na(H₂O)₄-(phen)][Ni(phen)₃]₄[tsc⁴⁻][tsc⁵⁻] $\cdot n$ H₂O depending on stoichiometry. Grinding copper(II) acetate hydrate with 1,3-di(4-pyridyl)propane gives a gradual colour change from blue to blue-green over ca. 15 min. The resulting material was shown by solid-state NMR spectroscopy to comprise a 1D coordination polymer with water-filled pores. The same host structure, [{Cu(OAc)₂}₂(μ -dpp)]_{*n*}, could be obtained from solutions containing methanol, acetic acid or ethylene glycol guest species [76b].

In a recent study, Fernandez-Bertran et al. used mechanochemical reactions to prepare a number of hemin complexes with amino acids such as arginine, histidine, lysine, methionine and tryptophan. The basic amino acids react with the hemin peripheral propionic acid groups, while arginine is also able to form a pentacoordinated complex at the Fe(III) centre. The reactions were followed by IR and Mossbauer spectroscopies [77a]. The solid-state reaction of hemin with KCN, Na₂S and various substituted imidazoles has also been investigated [77b].

7

Conclusions

In this chapter we have described two classes of solvent-less chemical reactions: those occurring between molecular solids (*inter*-solid reactions) to yield a new crystalline solid, and those occurring between a molecular solid and a gas (solid-gas reactions) to yield a solid product. We have also described solid-state reactions taking place between molecules within a crystal (*intra*-solid reactions). The distinction between intra- and inter-solid reactions carries no implications for the reaction mechanisms, which we have decided not to discuss. Indeed, the mechanical stress produced by grinding or milling together two solids, as in the case of inter-solid reactions, may well generate molecular

diffusion through the cracks and fractures and increased crystal surface area and allow reaction to take place, but may also cause local melting and/or lead to formation of intermediate co-crystalline phases of lower melting point so that the reaction occurs in the liquid state. The process of *kneading* does also imply an intermediary of some sort of liquid phase (a hyper-saturated solution?) wherein reaction, crystal nucleation and crystallization may occur. The relationship between molecular diffusion within solids and vapour molecules in a solid is also conceptually related. To this end, one should also consider the thermodynamic aspects related to the entropy contributions.

In spite of the enormous progress in analytical, spectroscopic and computational methods, the study of solid–solid or solid–gas processes is often a difficult challenge. One of the main disadvantages of solid-state studies, with respect to reactions occurring in solution, is obviously related to the fact that the reaction product, whether generated by a solid–solid, a solid–gas or a kneaded solid–solid process, is in the form of a polycrystalline powder. The characterization of the chemical and physical nature of a polycrystalline powder requires solid-state techniques [78] such as DSC, TGA or XPD, which are not always accessible in routine chemical laboratories. Moreover, the polycrystalline nature of the products prevents the use of single-crystal X-ray diffraction, while *ab initio* structure determination from powder diffraction is not yet amenable to routine work [79]. The lack of structural information can often be overcome if one finds a way to grow single crystals from the powdered material or to obtain single crystals of the same material via a different route or by *seeding* as discussed above. When single crystals are available, comparison between calculated and measured powder diffractograms is possible.

In some cases, for example when hydrogen-bonded systems are investigated, solid-state NMR techniques are extremely valuable [80].

These are probably some of the reasons why work in the field of solid-state chemistry has never been extremely popular, even though it is unquestionable that solvent-free conditions are cheaper (due to the saving in solvents, resources, energy, waste disposal and time) and are highly preferable in the quest for environmentally sustainable processes. It is a fact that the teaching of chemistry is still largely based on the “chemistry in solution paradigm”: organic synthesis (hence organometallic and much of coordination chemistry) takes place in solution. This is not to say that solvent-less reactions are the *panacea* of all problems, but it is a fact that many chemists still look at reactions between solids or between solids and gases as oddities, while mechanical methods are felt to be fundamentally “non-chemical”.

In this contribution we have also underlined an emerging aspect of solid-state chemistry, namely that solvent-free solid-state synthetic procedures can be exploited to construct “bottom-up” new materials from molecular or ionic building blocks. This is at the core of molecular crystal engineering [81]. It is fascinating to think that the *crystal engineer* may free him/herself from operating with solvent to achieve the bottom-up construction of supramolecular materials completely “from solid to solid”.

Acknowledgements Financial support by MIUR (FIRB and COFIN) and by the Universities of Bologna and Sassari is acknowledged. We wish to thank J. Scheffer for useful discussions during his sabbatical stay in Bologna and G. Kaupp for useful suggestions.

References

1. (a) Desiraju GR (ed) (1989) *Crystal engineering: the design of organic solids*. Elsevier, Amsterdam; (b) Dunitz JD (1996) The crystal as a supramolecular entity. In: Desiraju GR (ed) *Perspectives in supramolecular chemistry*. Wiley, Chichester; (c) Braga D, Grepioni F, Orpen AG (eds) (1999) *Crystal engineering: from molecules and crystals to materials*. Kluwer, Dordrecht; (d) Braga D, Grepioni F, Desiraju GR (1998) *Chem Rev* 98:1375; (e) Hollingsworth MD (2002) *Science* 295:2410; (f) Desiraju GR (2001) *Nature* 412:397; (g) Hosseini MW (2003) *Coord Chem Rev* 240:157–166
2. (a) Lehn JM (1990) *Angew Chem Int Ed Engl* 29:1304; (b) Lehn JM (1995) *Supramolecular Chemistry: Concepts and Perspectives*. VCH, Weinheim; (c) Philp D, Stoddard JF (1996) *Angew Chem Int Ed Engl* 35:1154; (d) Steed JW, Atwood JL (eds) (2000) *Supramolecular chemistry*. Wiley, Chichester; (f) Haiduc I, Edelmann FT (eds) (1999) *Supramolecular organometallic chemistry*. Wiley-VCH, Weinheim
3. (a) Whitesides GM, Simanek EE, Mathias JP, Seto CT, Chin DN, Mammen M, Gordon DM (1995) *Acc Chem Res* 28:37; (b) Gans W, Boyens JCA (1997) *Intermolecular interactions*. Plenum, New York; (c) Braga D, Grepioni F (2000) *Acc Chem Res* 33:601; (d) Burrows AD, Chan C-W, Chowdry MM, McGrady E, Mingos DMP (1995) *Chem Soc Rev* 329; (e) Aakeröy CB (1997) *Acta Crystallogr B* 53:569; (f) Steiner T (2002) *Angew Chem Int Ed* 41:48; (g) Desiraju GR (2002) *Acc Chem Res* 35:565; (h) Desiraju GR, Steiner T (1999) *The weak hydrogen bond in structural chemistry and biology*. Oxford University Press, Oxford; (i) Nishio M, Hirota M, Umezawa Y (1998) *The CH/ π interaction: evidence, nature, and consequences*. Wiley-VCH, New York; (j) Domenicano A, Hargittai I (eds) (2002) *Strength from weakness: structural consequences of weak interactions in molecules, supermolecules and crystals*. Kluwer, Dordrecht; (k) Brammer L (2003) *Dalton Trans* 16:3145
4. Dunitz JD, Gavezzotti A (1999) *Acc Chem Res* 32:677
5. Bernstein J (2002) *Polymorphism in molecular crystals*. Oxford University Press, Oxford
6. (a) Finn RC, Rarig RS, Zubieta J (2002) *Inorg Chem* 41:2109–2123; (b) Rao CNR, Natarajan S, Choudhury A, Neeraj S, Ayi AA (2001) *Acc Chem Res* 34:80
7. (a) Braga D (2003) *Chem Commun* 2751; (b) Braga D, Grepioni F (2004) *Angew Chem Int Ed* 43:4002–4011
8. (a) Bradley D (2002) *Chem Br* 42; (b) Tanaka K, Toda F (2000) *Chem Rev* 100:1025; (c) Tanaka K (2003) *Solvent-free organic synthesis*, Wiley-VCH, Weinheim; (d) Cave GWV, Raston CL, Scott JL (2001) *Chem Commun* 2159; (e) Rothenberg G, Downie AP, Raston CL, Scott JL (2001) *J Am Chem Soc* 123:8701
9. Anastas PT, Warner JC (1998) *Green chemistry: theory and practice*. Oxford University Press, New York
10. (a) Kaupp G (2003) *CrystEngComm* 5:117; (b) Boldyrev VV, Tkacova K (2000) *J Mater Synth Proc* 8:121; (c) Fernandez-Bertran JF (1999) *Pure Appl Chem* 71:581
11. See for example: (a) Ariel S, Askari S, Scheffer JR, Trotter J (1989) *J Org Chem* 54:4324; (b) Pokkuluri PR, Scheffer JR, Trotter J, Yap M (1992) *J Org Chem* 57:1486; (c) Cheung E, Kanf T, Scheffer JR, Trotter J (2000) *Chem Commun* 2309; (d) Braga D, Chen S, Filson H, Maini L, Netherton MR, Patrick BO, Scheffer JR, Scott C, Xia WJ (2004) *J Am Chem Soc* 126:3511

12. (a) Coville NJ, Levendis DC (2002) *Eur J Inorg Chem* 3067; (b) Coville NJ, Cheng L (1998) *J Organomet Chem* 149
13. Luty T, Eckhardt CJ (1995) *J Am Chem Soc* 117:2441
14. Ohashi Y (1988) *Acc Chem Res* 21:268
15. Braga D, Grepioni F (2003) In: Desiraju GR (ed) *Crystal design, structure and function. Perspectives in supramolecular chemistry*, vol 7. Wiley, Chichester
16. (a) Li HL, Eddaoudi M, O'Keefe M, Yaghi OM (1999) *Nature* 402:276; (b) Eddaoudi M, Kim J, Rosi N, Vodak D, Wachter J, O'Keefe M, Yaghi OM (2002) *Science* 295:469; (c) Lu JJ, Mondal A, Moulton B, Zaworotko MJ (2001) *Angew Chem Int Ed* 40:2113; (d) Leininger S, Cleiniuk B, Stang PJ (2000) *Chem Rev* 100:853; (e) Fujita M (1999) *Acc Chem Res* 32:53; (f) Abrahams BF, Hoskins BF, Michail DM, Robson R (1994) *Nature* 369:727; (g) Yaghi OM, Li HL, Davis C, Richardson D, Groy TL (1998) *Acc Chem Res* 31:474; (h) Batten SR (2001) *CrystEngComm* 18:1; (i) Subramanian S, Zaworotko MJ (1994) *Coord Chem Rev* 137:357; (j) Carlucci L, Ciani G, Proserpio DM, Sironi A (1995) *J Am Chem Soc* 117:4562; (k) Carlucci L, Ciani G, Proserpio DM, Rizzato S (2002) *CrystEngComm* 22:121; (l) Carlucci L, Ciani G, Proserpio DM (2003) *Coord Chem Rev* 246:247; (m) Rao CNR, Nataraajan S, Vaidhyanathan R (2004) *Angew Chem Int Ed* 43:1466
17. Pellizzari G (1884) *Gazz Chim Ital* 14:362
18. Paul IC, Curtin DY (1975) *Science* 187:19
19. (a) Miller RS, Curtin DY, Paul IC (1971) *J Am Chem Soc* 93:2784; (b) Miller RS, Curtin DY, Paul IC (1972) *J Am Chem Soc* 94:5117; (c) Miller RS, Curtin DY, Paul IC (1974) *J Am Chem Soc* 96:6329; (d) Chiang CC, Lin CT, Wang AHJ, Curtin DY, Paul IC (1977) *J Am Chem Soc* 99:6303
20. Miller RS, Curtin DY, Paul IC (1974) *J Am Chem Soc* 96:6334
21. See for instance: Kaupp G (1996) In: Davies JED (ed) *Comprehensive supramolecular chemistry*, vol 8. Elsevier, Oxford, p 381
22. Lin CT, Paul IC, Curtin DY (1974) *J Am Chem Soc* 96:3699
23. Miller RS, Curtin DY, Paul IC (1974) *J Am Chem Soc* 96:6340
24. Kaupp G, Schmeyers J, Boy J (2000) *Tetrahedron* 56:6899
25. (a) Kaupp G, Kuse A (1998) *Mol Cryst Liq Cryst* 313:36; (b) Kaupp G (1994) *Mol Cryst Liq Cryst* 242:153; (c) Kaupp G, Schmeyers J, Haak M, Marquardt T, Herrmann A (1996) *Mol Cryst Liq Cryst* 276:315
26. Kaupp G, Schmeyers J, Boy J (1998) *Chem Eur J* 4:2467
27. Kaupp G, Pogodda U, Schmeyers J (1994) *Chem Ber* 127:2249
28. (a) Toda F, Takumi H, Akehi M (1990) *J Chem Soc Chem Commun* 1270; (b) Toda F, Okuda K (1991) *J Chem Soc Chem Commun* 1212; (c) Tanaka K, Fujimoto D, Oeser T, Irngartinger H, Toda F (2000) *Chem Commun* 413
29. Toda F, Schmeyers J (2003) *Green Chem* 5:701
30. Braga D, Cojazzi G, Emiliani D, Maini L, Grepioni F (2001) *Chem Commun* 2272
31. Braga D, Cojazzi G, Emiliani D, Maini L, Grepioni F (2002) *Organometallics* 21:1315
32. Kaupp G, Naimi-Jamal MR, Maini L, Grepioni F, Braga D (2003) *CrystEngComm* 5:474
33. Braga D, Maini L, Mazzotti M, Rubini K, Masic A, Gobetto R, Grepioni F (2002) *Chem Commun* 2296
34. Albrecht M, Gossage RA, Lutz M, Speck AL, van Koten G (2000) *Chem Eur J* 6:1431
35. Albrecht M, Lutz Schreurs AMM, Lutz ETHM, Speck AL, van Koten G (2000) *J Chem Soc Dalton Trans* 3797
36. (a) Schmidt GMJ (1971) *Pure Appl Chem* 27:647; (b) Cohen MD (1975) *Angew Chem Int Ed Engl* 14:386; (c) Cohen MD, Schmidt GMJ (1964) *J Chem Soc* 1996; (d) Elgavi GA, Green BS, Schmidt GMJ (1973) *J Am Chem Soc* 95:2058

37. Kaupp G (2003) *CrystEngComm* 5:117
38. Garcia-Garibay MA (2003) *Acc Chem Res* 36:491
39. (a) MacGillivray LR (2000) *CrystEngComm* 7:1; (b) MacGillivray LR (2002) *CrystEngComm* 4:37 (and references therein)
40. See for instance: (a) Toda F (1987) *Top Curr Chem* 140:43; (b) Kaupp G, Matthies D (1986) *Chem Ber* 119:2387
41. (a) Kaupp G, Schmeyers J, Boy J (2001) *Chemosphere* 43:55; (b) Kaupp G, Schmeyers J, Boy J (2000) *Tetrahedron* 56:6899; (c) Kaupp G, Schmeyers J, Kato M, Toda F (2002) *J Phys Org Chem* 15:148; (d) Kaupp G, Schmeyers J, Kato M, Tanaka K, Harada N, Toda F (2001) *J Phys Org Chem* 14:444; (e) Kaupp G (1996) In: Davies JED (ed) *Comprehensive supramolecular chemistry*, vol 8. Elsevier, Oxford, pp 381; (f) Hirano S, Yoshizawa K, Toyota S, Toda F, Urbanczyk-Lipkowska Z (2003) *Mendeleev Commun* 141; (g) Yagi M, Hirano S, Toyota S, Toda F, Giastas P, Marvidis IM (2003) *Heterocycles* 59:735
42. (a) MacGillivray LR, Reid JL, Ripmeester JA (2000) *J Am Chem Soc* 122:7817; (b) Papaefstathiou GS, Kipp AJ, MacGillivray LR (2001) *Chem Commun* 2462; (c) Varshney DB, Papaefstathiou GS, MacGillivray LR (2002) *Chem Commun* 1964; (d) Friščić T, MacGillivray LR 2003 *Chem Commun* 1306; (e) Gao X, Friščić T, MacGillivray LR (2004) *Angew Chem Int Ed* 43:232
43. Coates GW, Dunn AR, Henling LM, Ziller JW, Lobkovsky EB, Grubbs RH (1998) *J Am Chem Soc* 120:3641
44. (a) Odani T, Matsumoto A (2002) *CrystEngComm* 4:467; (b) Matsumoto A, Sada K, Tashiro K, Miyata M, Tsubouchi T, Tanaka T, Odani T, Nagahama S, Tanaka T, Inoue K, Saraghi S, Nakamoto S (2002) *Angew Chem Int Ed* 41:2502
45. Feldman KS, Campbell RF (1995) *J Org Chem* 60:1924
46. (a) Ito Y, Borecka B, Trotter J, Scheffer JR (1995) *Tetrahedron Lett* 36:6083; (b) Ito Y, Borecka B, Olovsson G, Trotter J, Scheffer JR (1995) *Tetrahedron Lett* 36:6087
47. (a) Novak K, Enkelmann V, Wegner G, Wagener KB (1999) *Angew Chem Int Ed* 32:1614; (b) Enkelmann V, Wegner G, Novak K, Wagener KB (1993) *J Am Chem Soc* 115:10390
48. (a) Irie M, Kobatake S, Horichi M (2001) *Science* 291:1769; (b) Morimoto M, Kobatake S, Irie M (2003) *Chem Eur J* 9:621; (c) Yamamoto S, Matsuda K, Irie M (2003) *Angew Chem Int Ed* 42:1636
49. Tanaka K, Toda F, Mochizuki E, Yasui N, Kai Y, Miyahara I, Hirotsu K (1999) *Angew Chem Int Ed* 38:3523
50. Turowska-Tyrk I (2001) *Chem Eur J* 7:3401
51. Greig LM, Kariuki BM, Habershon S, Spencer N, Johnston RL, Harris KDM, Philp D (2002) *New J Chem* 26:701
52. (a) Rastogi RP, Bassi PS, Chadha SL (1963) *J Phys Chem* 67:2569; (b) Rastogi RP, Singh NB (1996) *J Phys Chem* 70:3315; (c) Rastogi RP, Singh NB (1968) *J Phys Chem* 72:4446
53. (a) Etter MC (1991) *J Phys Chem* 95:4601; (b) Etter MC, Reutzel SM, Choo CG (1993) *J Am Chem Soc* 115:4411
54. Ojala WH, Etter MC (1992) *J Am Chem Soc* 114:10228
55. (a) Bernstein J, Davey RJ, Henck JO (1999) *Angew Chem Int Ed* 38:3440; (b) Braga D, Grepioni F (2000) *Chem Soc Rev* 4:229
56. (a) Curtin DY, Paul IC (1973) *Acc Chem Res* 7:217; (b) Chiang CC, Lin CT, Wang AHJ, Curtin DY, Paul IC (1977) *J Am Chem Soc* 99:6303; (c) Patil AO, Curtin DY, Paul IC (1984) *J Am Chem Soc* 106:348
57. Toda F (ed) (2002) *Organic solid-state reactions*. Kluwer, Dordrecht
58. Toda F, Miyamoto H (1995) *Chem Lett* 861
59. (a) Braga D, Maini L, Polito M, Mirolo L, Grepioni F (2002) *Chem Commun* 24:2960; (b) Braga D, Maini L, Polito M, Mirolo L, Grepioni F (2003) *Chem Eur J* 9:4362

60. (a) Threlfall TL (1995) *Analyst* 120:2435; (b) Kubota N, Doki N, Yokota M, Jagadesh D (2002) *J Chem Eng Jpn* 35:1063
61. (a) Seiler P, Dunitz JD (1932) *Acta Crystallogr B* 38:1741; (b) Davey RJ, Blagden N, Potts GD, Docherty R (1997) *J Am Chem Soc* 119:1767
62. Braga D, Cojazzi G, Paolucci D, Grepioni F (2001) *CrystEngComm* 1
63. Koshima H, Miyauchi M (2001) *Cryst Growth Des* 1:355
64. Dunitz J, Bernstein J (1995) *Acc Chem Res* 28:193
65. Caira MR, Nassimbeni LR, Wildervanck AF (1995) *J Chem Soc Perkin Trans 2*:2213
66. (a) Braga D, Maini L, de Sanctis G, Rubini K, Grepioni F, Chierotti MR, Gobetto R (2003) *Chem Eur J* 9:5538; (b) Braga D, Maini L (2004) *Chem Commun* 976
67. Braga D, Maini L, Polito M, Grepioni F (2002) *Chem Commun* 2302
68. Shan N, Toda F, Jones W (2002) *Chem Commun* 2372
69. (a) Watano S, Okamoto T, Tsumari M, Koizumi I, Osako Y (2002) *Chem Pharm Bull* 50:341; (b) Watano S, Furukawa J, Miyunami K, Osako Y (2001) *Adv Powder Technol* 12:427
70. (a) Günzler H, Gremlich HU (2002) *IR spectroscopy*. Wiley-VCH, Weinheim, chap 4; (b) Falk M (1990) *Vibr Spectrosc* 1:69
71. (a) Fernandez-Bertran J, Reguera E (1997) *Solid State Ionics* 93:139; (b) Valor A, Fernandez-Bertran J, Radilla J (2001) *J Fluor Chem* 107:137; (c) Fernandez-Bertran J, Reguera E (1997) *Solid State Ionics* 93:139; (d) Fernandez-Bertran J, Reguera E, Paneque A, Yee-Madeira H, Gordillo-Sol A (2002) *J Fluorine Chem* 113:93; (e) Fernandez-Bertran J, Blanco Pascual J, Hernandez M, Rodriguez R (1988) *React Solid* 5:95; (f) Fernandez-Bertran J (1998) *Solid State Ionics* 112:351
72. Orita A, Jiang LS, Nakano T, Ma NC, Otera J (2002) *Chem Commun* 1362
73. Balema VP, Wiench JW, Pruski M, Pecharsky VK (2002) *Chem Commun* 1606
74. Balema VP, Wiench JW, Pruski M, Pecharsky VK (2002) *Chem Commun* 724
75. Balema VP, Wiench JW, Pruski M, Pecharsky VK (2002) *J Am Chem Soc* 124:6244
76. (a) Nichols PJ, Raston CL, Steed JW (2001) *Chem Commun* 1062; (b) Belcher WJ, Longstaff CA, Neckenig MR, Steed JW (2002) *Chem Commun* 1602
77. (a) Paneque A, Fernandez-Bertran J, Reguera E, Yee-Madeira H (2003) *Syn React Inorg Met* 33:1405; (b) Paneque A, Fernandez-Bertran J, Reguera E, Yee-Madeira H (2003) *Struct Chem* 14:551
78. Cheetam AK, Day P (1987) *Solid state chemistry techniques*. Clarendon, Oxford
79. (a) Harris KDM, Tremayne M (1996) *Chem Mater* 8:2554; (b) Harris KDM, Tremayne M, Kariuki BM (2001) *Angew Chem Int Ed* 40:1626
80. See for example: (a) Garcia-Viloca M, Gelabert R, Gonzalez Lafont A, Moreno M, Lluich JM (1997) *Phys Chem A* 101:8727; (b) Nakanaga T, Buchhold K, Ito F (2003) *Chem Phys* 288:69; (c) Lorente P, Shenderovich IG, Golubev NS, Denisov GS, Buntkowsky G, Limbach HH (2001) *Magn Reson Chem* 39:S18; (d) Gu ZT, Mcdermott A (1993) *J Am Chem Soc* 115:4282; (e) Gu ZT, Zambrano R, Mcdermott A (1994) *J Am Chem Soc* 116:6368; (f) Facelli JC, Gu ZT, Mcdermott A (1995) *Mol Phys* 86:865; (g) Aguilar Parrilla A, Claramunt RM, Lopez C, Sanz D, Limbach HH, Elguero J (1994) *J Phys Chem* 98:8752
81. See for instance: Braga D, Desiraju GR, Miller J, Orpen AG, Price S (2002) *CrystEngComm* 4:500

Organic Solid-State Reactions with 100% Yield

Gerd Kaupp (✉)

University of Oldenburg, Organic Chemistry 1, P.O. Box 2503, 26111 Oldenburg, Germany
kaupp@kaupp.chemie.uni-oldenburg.de

| | | |
|------|---|-----|
| 1 | Introduction | 97 |
| 2 | Experimental Techniques | 100 |
| 3 | Single Electron and Oxygen Atom Transfer | 102 |
| 4 | Salt Formation | 103 |
| 5 | Complexation | 109 |
| 6 | Geometrical Isomerization | 114 |
| 7 | Hydrogenation | 117 |
| 8 | Addition of Halogens | 118 |
| 9 | Addition of Halogenohydrides | 121 |
| 10 | Addition of Nucleophiles | 125 |
| 11 | Elimination | 128 |
| 12 | Alkylation | 129 |
| 13 | Aliphatic Substitutions | 130 |
| 13.1 | Hydroxyls and Phenoxides | 130 |
| 13.2 | Thiols and Thiolates | 134 |
| 13.3 | Amines and Amide Anions | 136 |
| 13.4 | Enols | 139 |
| 13.5 | Radicals | 140 |
| 13.6 | Ring-Opening Substitution of Acid Derivatives | 140 |
| 14 | Aromatic Substitution | 143 |
| 15 | Diazotization | 144 |
| 16 | Sandmeyer Reaction | 146 |
| 17 | Azo Coupling | 147 |
| 18 | Amine Condensations | 152 |

| | | |
|------|------------------------------------|-----|
| 18.1 | Imine Formation | 152 |
| 18.2 | Secondary Amines | 157 |
| 18.3 | Diamines | 157 |
| 18.4 | Cyclizing Condensation | 158 |
| 19 | Knoevenagel Condensation | 161 |
| 20 | Michael Addition | 162 |
| 21 | Linear Dimerization | 162 |
| 22 | Cycloaddition | 164 |
| 23 | Cyclization | 168 |
| 24 | Rearrangement | 170 |
| 25 | Cascade Reactions | 172 |
| 26 | Reduction | 176 |
| 27 | Oxidation | 177 |
| 28 | Conclusion | 179 |
| | References | 180 |

Abstract Environmentally benign gas–solid, solid–solid, and intracrystalline (thermal and photochemical) reactions that give 100% yield of only one product are summarized for almost all important reaction types. Their mechanistic background is evaluated on the basis of supermicroscopic studies and crystal packing analyses, which helps in predicting good solid-state performance on the basis of phase rebuilding, phase transformation, and crystal disintegration and in engineering solid-state reactions in the case of difficulties. This allows one to profit from the bargain of the crystal packing for reactions with unsurpassed atom economy, in most cases without any auxiliary or purifying workup necessity, mostly close to room temperature and with short reaction times. The experimental techniques are described in some detail including the scale-up. Preparative use is made of known and new reactions, and many products cannot be prepared by any other technique or they are only stable in the solid state, but they are quantitatively obtained and ready for further syntheses due to their very high reactivity. “Solvent-free” reactions that pass through a liquid phase are generally excluded, but some comparisons with important quantitative stoichiometric melt reactions are made. Numerous new solid-state reactions are described here for the first time.

Keywords Gas–solid reaction · Solid–solid reaction · Intracrystalline reaction · Phase rebuilding mechanism · Solid-state cascade reaction · 100% yield

Abbreviations

| | |
|--------|--|
| AFM | Atomic force microscopy |
| B3LYP | An ab initio routine in DFT calculations |
| DDQ | Dichlorodicyano- <i>para</i> -benzoquinone |
| DFT | Density functional theory |
| DSC | Differential scanning calorimetry |
| GID | Grazing incidence diffraction |
| i.d. | Internal diameter |
| rpm | Revolutions per minute |
| r.t. | Room temperature |
| SNOM | Scanning near-field optical microscopy |
| TADDOL | Tetraaryl-2,2-dimethyl-1,3-dioxolan-4,5-dimethanol |
| TBAB | Tetrabutylammonium bromide |
| TEMPO | Tetramethylpiperidiny- <i>N</i> -oxyl |
| THF | Tetrahydrofuran |

1**Introduction**

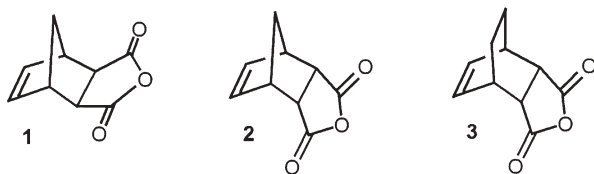
Waste-free environmentally benign solid-state reactions mean 100% yield of one product without any necessity for purifying workup by recrystallization, chromatography, etc. They have therefore the highest possible atom economy. This does not exclude gas–solid reactions, which frequently use excess reactive gas that is removed at the end of reaction by collection in a cold trap, or which require a solid catalyst or a drying agent that has to be removed by a simple quantitative extraction procedure. Even quantitative protonic salt formation is covered. Essentially quantitative liberation of the organic acid or the organic base therefrom may require treatment with water. Furthermore, quantitative stoichiometric reactions involving salts, with the necessity of removing the simple stoichiometric coproduct salt (e.g., NaCl, that can be simply washed out), remain environmentally benign and are not excluded. Not relevant, however, are so-called quantitative reactions at less than any specified conversion below 100% or nonstoichiometric solid–solid reactions that may provide quantitative conversion (100% yield with respect to the minor component) but require removal of the excess reagent using solvent. Polymerizations that require removal of residual monomers or oligomers are excluded. At present there are no microwave-accelerated reactions known that would meet the selection criteria.

Solid-state reactions are known from thermal intracrystalline conversions (isomerizations or loss of volatile fragments), photoreactions, gas–solid reactions, and solid–solid reactions. As all of these relate strictly to the crystal packing (unifying solid-state mechanism) and are not separated in the various sections. Also, nontopotactic (normal) and topotactic (very rare) reactions are not separated in different sections.

Pure solid-state reactions are more frequently waste-free than melt reactions with increased risk of incompleteness or side reactions. We select here only

quantitative examples of gas–solid reactions, stoichiometric solid–solid reactions, and intracrystalline reactions as these are particularly typical, and we are well aware that many previously nonquantitative solid-state reactions might be transformed to 100%-yield reactions by application of suitable techniques that derive from the mechanistic knowledge gained from submicroscopic AFM studies. These investigations show strict correlation with the crystal packing, because molecular migrations within the crystal using cleavage planes (along easy paths!) are required for all reactions with significant change in the molecular shape upon reaction. The geometrical change upon chemical reaction or conformational change creates so much internal pressure that the molecules have to move out of the lattice (rarely to a suitable crystallographic void or channel – but not “reaction cavity” – in the lattice) directly upon the event. Such molecular migrations are easily traced at the crystal surface with AFM or in suitable cases with depth-dependent GID. The types of surface features have been exhaustively imaged [1]. The three-step solid-state mechanism of (1) phase rebuilding, (2) phase transformation, and (3) crystal disintegration is amply demonstrated. It becomes multistep in reaction cascades, of course. That means, one observes at first gradually growing characteristic features, then abruptly enormous changes of surface features, and shortly thereafter disintegration of the original crystal with creation of fresh surface. This ingenious mechanism has been repeatedly termed “the phase rebuilding mechanism”.

The interplay of crystal packing, migrational aptitudes, and solid-state reactivity may be demonstrated with the reactivities of the Diels–Alder cycloadducts of maleic anhydride and cyclopentadiene (1 and 2) or cyclohexadiene (3).



Figures 1, 2, and 3 show stereoscopic views of their crystal packing. It is clearly seen that the *exo*-bicyclo[2.2.1]anhydride 1 has a hardly interlocked monolayer structure and so does the *endo* isomer 2 except for slight interpenetrations. These structural features facilitate molecular migrations upon chemical reaction, whereas the bicyclo[2.2.2] anhydride 3 exhibits strong interlocking, preventing molecular migrations.

If the crystals of 1 are exposed to bromine vapor, addition to the C=C double bond occurs without difficulty, as the molecules can anisotropically migrate along the cleavage plane and the quantitatively obtained *trans* adduct does not include large amounts of bromine. The gas–solid addition of 2 is more complicated. The initially formed crystalline adduct keeps large quantities of additional bromine and eliminates HBr upon standing and in solution by forming lactones. Thus, mixtures of products arise because consecutive reactions

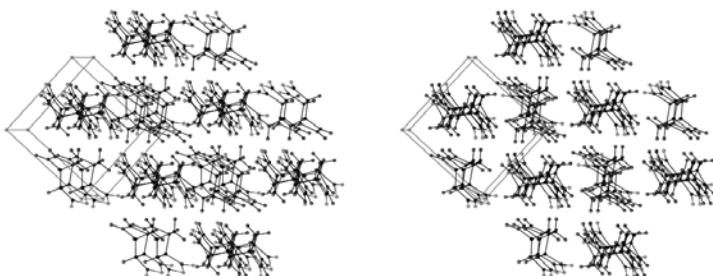


Fig. 1 Stereoscopic representation of the molecular packing of *exo*-bicyclo[2.2.1]hept-5-ene-2,3-dicarboxyanhydride (1) on its (001) face (rotated around y by 5° for a better view) showing the hardly interpenetrated monolayered structure

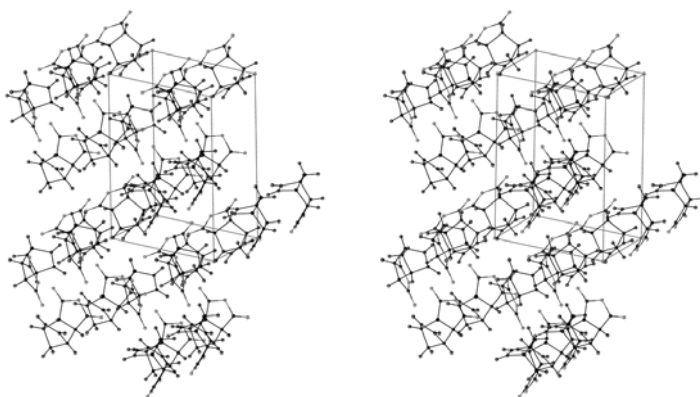


Fig. 2 Stereoscopic representation of the molecular packing of *endo*-bicyclo[2.2.1]hept-5-ene-2,3-dicarboxyanhydride (2) on its (111) face showing the slightly interpenetrating monolayered structure

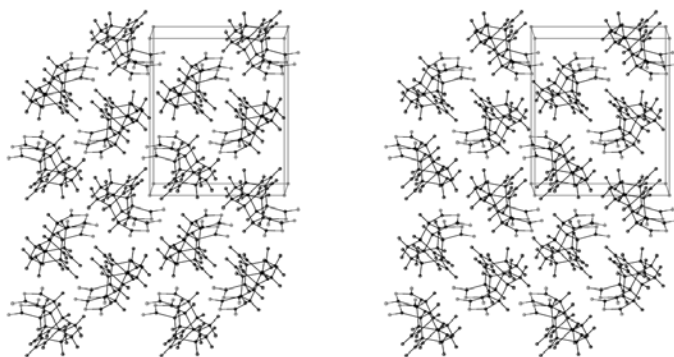


Fig. 3 Stereoscopic representation of the molecular packing of *endo*-bicyclo[2.2.2]oct-5-ene-2,3-dicarboxyanhydride (3) on its (100) face showing interpenetrating strongly inter-locked layers

prevent a clean result in that case. As expected, the behavior of **3** is totally different. If crystals of **3** experience diluted bromine vapor, no addition to the C=C double bond occurs at 22 °C (and upon removal of included Br₂ at 22–50 °C in a vacuum) as long as the crystals do not melt by the uptake of excessive Br₂. The bromine is included by the solid up to about 0.4 equivalents without melting. The lattice of **3** opens at best the possibility of forming minor internal channels or cages for the inclusion of some bromine, but not for the accommodation of a possible dibromide in the absence of possibilities for migration. Therefore, no addition occurs in the solid state of **3** even though some bromine is accommodated by inclusion.

Melt or intermediate melt reactions are excluded from this review as much as possible because these do not (fully) profit from the initial crystal packing. They can nevertheless be of preparative importance or be preferable in particular instances if the products crystallize directly from the melt during reaction and thus produce a quantitative yield [2]. Nevertheless, these different types of solvent-free reactions should be sharply separated for the sake of consistent wording. Solid–solid should not only mean that the reactants were solids but also that profit was made from the crystal packing, which is only possible if there were no liquids upon mixing and during the reaction period.

2

Experimental Techniques

Solid-state reactions may be very efficient as they avoid solvents or liquid phases and profit from crystal structure. In most cases of gas–solid reactions the crystals must not be finely ground or milled and the gas must be gradually added in order to calm down the reaction at room temperature or below. Solid–solid reactions require repeated contacts over and over again. This is more easily and thoroughly obtained by milling rather than by grinding, sonication, or resting. Liquids or intermediate liquids are observed or excluded by visual, microscopic, or supermicroscopic inspection. It may be necessary to cool down or (rarely) to slightly heat in order to avoid liquid phases. There are, of course, limits to the cooling down, as the reactions will freeze out at too low temperatures and not all of them can be executed at –80 °C, for example. The possibility of “solidifying” liquid reagents by salt formation and complexation is far from being exhausted. However, these techniques introduce auxiliaries that slightly detract from atom economy even though a 100% yield may be valuable and worth the effort.

Gas–solid reactions that run to completion require vacuum-tight glassware. In lab-scale syntheses the flask containing the crystals is evacuated and the reactive gases are let in at the desired pressure, speed, or amount at room temperature or with cooling or heating of the flask. Stirring or shaking is necessary if a product gas is liberated in order to mix the gases. Vapors of volatile liquids should be applied at a stoichiometric ratio as there may be the risk of lique-

faction if excess vapor dissolves the solid. Ultrasound application (from a cooled cleaning bath) may overcome rare problems with product disintegration (e.g., 177). If this does not help, in very rare cases of persistent product layers (e.g., 104b) milling and cautious application of the reacting gas at low pressure and low temperature cannot be avoided for a quantitative conversion. These engineering techniques overcome problems with step 3 of the solid-state mechanism but they are rarely required. Larger-scale gas–solid reactions use loosely packed columns and gas flow. Heat is removed or added by admixed air or inert gas at the appropriate ratio while increasing the reacting gas proportion toward the end. However, highly diluted reactive gases may create a sharp reaction front through the column. Both stream bed and suspension or fluidized beds can be chosen. Volume increase during reaction has to be taken into account [3–5].

For complete solid–solid reactions with 100% yield in stoichiometric mixtures, ball-milling is the first choice [3, 6–9]. If double-walled milling chambers are used the possibility of cooling/heating can be used which appears quite important. Continuous cogrinding and a final sonication for solid–solid reactions should only be used if milling is not possible. As ball-milling of molecular crystals or salts [9–11] does not induce “mechanochemistry” (breaking of regular molecular bonds cannot occur, with the exception of weak bonds of explosives, but intermolecular interactions and van der Waals attractions or H bonds can be broken, and the surface is increased by crystal disintegration), the moderate efficiency of swing-mills with a cooling/heating device is sufficient [3, 12]. High milling efficiency in rotor-mills for larger-scale milling (up to the kilogram scale and beyond) [6–8] increases the contact rate. It is also essential for tribochemistry (mechanochemistry if strong σ bonds in polymers or infinite covalent crystals are broken with formation of local plasma at the freshly broken crystal surfaces, for example at silica or silicon) with totally different reactivities in plasma chemistry with virtually all kinds of organic additives [6, 8] which, however, is not the subject of this review.

Mechanistic investigations of gas–solid and solid–solid reactions as well as their proper engineering require identifiable crystal surfaces for atomic force microscopy (AFM) and scanning near-field optical microscopy (SNOM) [1, 3, 13–15] in combination with X-ray diffraction data, which are the basis of crystal packing analyses [1, 3, 16–18].

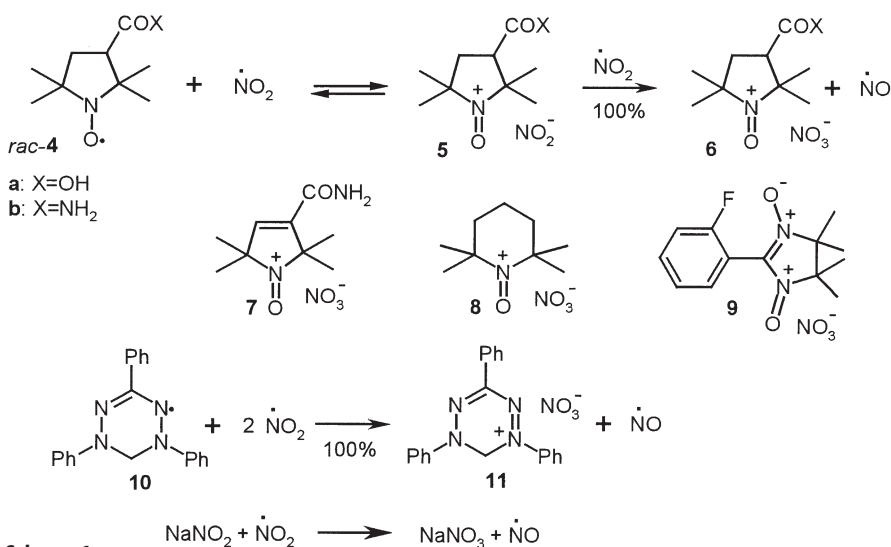
Spectroscopic analyses of solid-state reactions must first use solid-state techniques (IR, UV/Vis, Raman, luminescence, NMR, ESR, CD, X-ray powder diffraction, DSC, etc.) in order to secure the solid-state conversion, before the solution techniques (detection of minor side products, specific rotation, etc.) are applied.

Environmentally friendly sustainable gas–solid and solid–solid or intrasolid thermal reactions proceed with 100% yield without side products. Simple couple products such as H_2O , or gases or inorganic salts, can be removed without application of solvents (salts may alternatively be washed out with water). In all of these cases genuine solvent-free reactions or syntheses are achieved with unsurpassed atom economy, as these do not require purifying workup (such as

crystallization, chromatography, etc.). It is therefore most important to run solid-state reactions to total conversion and starting with stoichiometric mixtures of reactants in the solid–solid version. Hard to remove catalysts are rarely required and should be avoided, if possible.

3 Single Electron and Oxygen Atom Transfer

Probably the most simple, although hardly recognized, chemical processes are single-electron transfer reactions that lead to stable products, for example 6–8 [19], 9 [20], and 11 [19] (Scheme 1). The oxidations of stable nitroxyl or verdazyl radicals by NO_2 are of that type by necessity and they lead to quantitative yields of the nitrosonium nitrates [19]. Clearly, a second reaction type, the exchange of an oxygen atom between a nitrite anion and nitrogen dioxide is coupled in all cases. This latter reaction type can be separately studied by the interaction of NO_2 gas with sodium nitrite crystals [19]. Even the nitrogen monoxide formed in the single-electron transfer reactions can be purified from nitrogen dioxide by storing over solid sodium nitrite. For large-scale production of NO by this technique, milling of the NaNO_2 is essential due to some difficulties with the crystal disintegration step [6].



Scheme 1

Also, the tribromides or fluorides of 6–9 and 11 can be quantitatively synthesized by similar one-electron transfer to bromine [20] or xenon difluoride in the solid state [1]. Further inorganic solid-state one-electron redox reactions have also been reported [6].

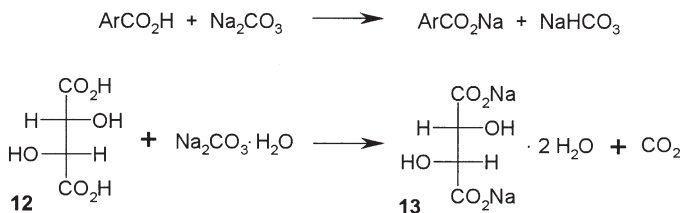
The ease of the synthesis may be disclosed by the experimental procedure. An evacuated 100-mL flask was filled with N₂O₄/NO₂ to a pressure of ca. 650 mbar (296 mg, 6.4 mmol NO₂). The sampling flask was connected to an evacuated 1-L flask, which was then connected to an evacuated 10-mL flask that was cooled to 5 °C and contained the nitroxyl **4a** or **4b**, or the nitroxyl precursor to **7** (500 mg, 2.70 mmol). After 1 h, the cooling bath was removed and excess NO₂ and NO were condensed in a cold trap at 77 K for further use. The yield was 665 mg (100%) of pure **6a**, **6b**, or **7** [19]. Similarly, 2-g quantities of tetramethylpiperidine-*N*-oxyl (TEMPO) or 0.2 g of the ferromagnetic 2-fluorophenyl-tetramethylnitronyl nitroxide stable radical [21] were reacted at –10 °C (initial pressure of NO₂ 0.03 bar) or 5 °C (0.3 bar NO₂) in 12 h with a quantitative yield of pure **8** or **9**, respectively [19].

4

Salt Formation

Salt formation in the solid state may be achieved by solid–solid or gas–solid neutralization. The preparation of sodium or potassium salts of carboxylic acids by grinding or milling them with NaOH or KOH is not very practical due to the enormous heat development. The use of Na₂CO₃ or K₂CO₃ is helpful in this respect. However, it is hard to get complete reaction with benzoic acid or salicylic acid to the neat sodium salt upon comilling at a 2:1 ratio, as the solid-state reaction of sodium hydrogen carbonate with these aromatic acids is uncomfortably slow (hours) [22]. There is, however, a claim of “rapid and complete neutralization” in a planetary ball-mill at 60 g acceleration [23]. The technical importance of solid-state neutralizations derives from the energy savings by avoiding large amounts of water. Such processes can be executed in large horizontal ball-mills. For example, 200-g batches have been executed in the neutralization of L-(+)-tartaric acid (**12**) with sodium carbonate monohydrate in a 2-L ball-mill under near ambient conditions, and disodium tartrate dihydrate (**13**), a food additive, is directly obtained in quantitative yield (Scheme 2). If sodium hydrogen carbonate is stoichiometrically used, sodium hydrogen tartrate hydrate for the preparation of carbonated lemonades is quantitatively obtained [6].

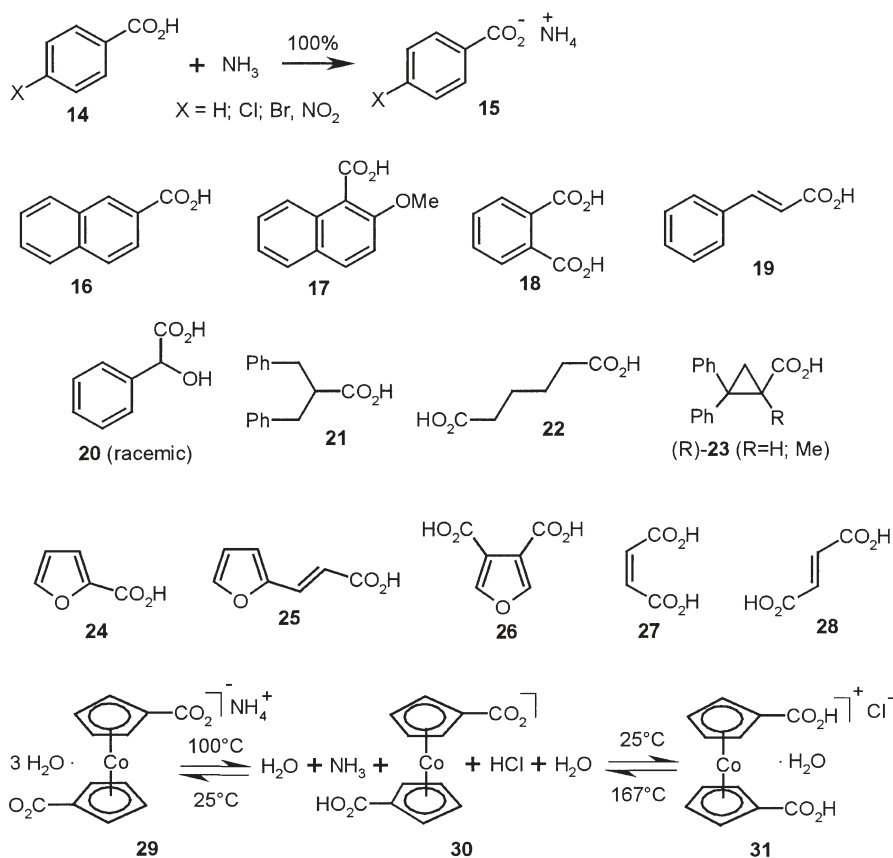
The preparation in 200-g batches works as follows [6]. A horizontal water-cooled 2-L high-grade steel ball-mill (Simoloyer CM01) is charged with 2 kg of



Scheme 2

steel balls (0.5 g), 200 g of L-(+)-tartaric acid and the precise stoichiometric amount of sodium carbonate monohydrate taking into account its actual water content. The carbon dioxide that is formed during milling at 1,300 rpm is released through a pressure valve and if gas production ceases, the outmilling is started intermittently at 300 and 800 rpm under gravity or in an autobatch arrangement by an internal air cycle through a cyclone of a connected separation/classification system (Simoloyer VS01a). The latter equipment is particularly advantageous as it allows for automatic reloading for the next batches prior to complete powder collection. The yield of the solid powder **13** is quantitative.

The gas–solid neutralizations found more interest than the solid–solid variant. The quantitative reactions of gaseous ammonia with solid benzoic and related acids were interpreted by a concept of “gas permeability of the crystal” in order to explain anisotropic reaction fronts in single crystals [24]. Also, the ammonium salts of the aromatic or aliphatic mono- and dicarboxylic acids **16–21** (Scheme 3) formed the corresponding salts with 100% yield. The need for molecular migrations immediately upon reaction was not considered at that



Scheme 3

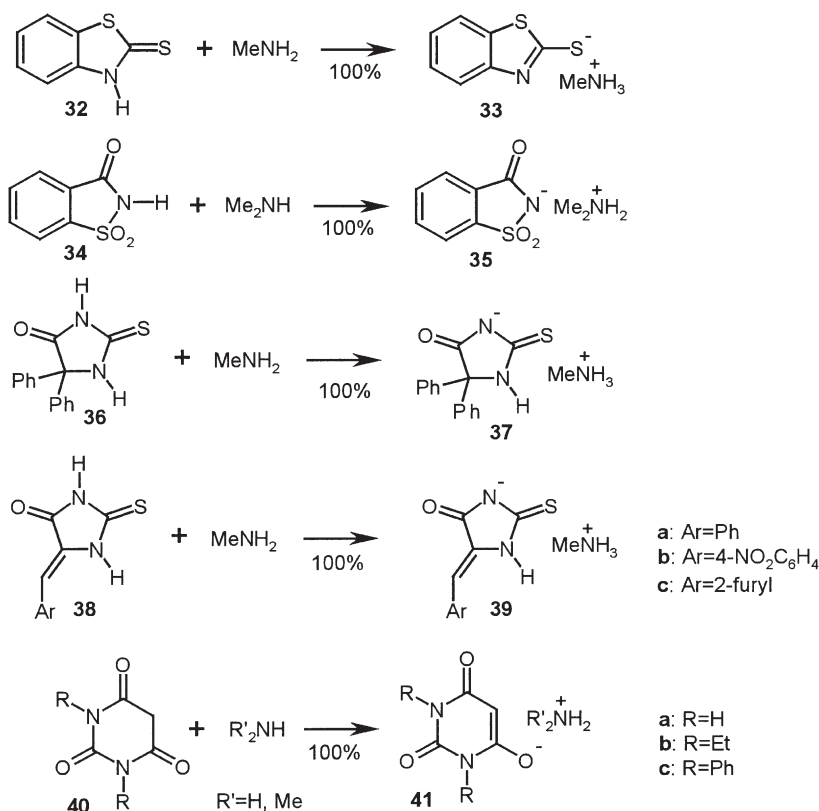
time, and indeed unexplainable anisotropies emerged with the acids **22**, **23**, and **14** ($X=Br$) [25, 26] that can only be understood on the basis of the experimentally supported three-step solid-state mechanism, including far-reaching molecular migrations [Sect. 1; 1, 3]. For example, AFM measurements have clarified the anisotropies in the reactions of **22** with ammonia and have pointed out the differences to the behavior of **24** also with respect to the migrational aptitudes in the crystals [1, 27].

Particularly rapid are the quantitative salt formations of gaseous ammonia with 2-furancarboxylic (**24**), 2-furylacrylic (**25**), and 3,4-furandicarboxylic acid (**26**), and maleic (**27**) or fumaric acid (**28**) (bis-ammonium salts) (Scheme 3). Applications in removal of ammonia from atmospheric gases appear promising [22, 28].

The solid amphoteric Co(III) complex **30**, which crystallizes in hydrogen-bridged chains with the *transoid* arrangement of the ligands, protonates moist ammonia gas and quantitatively forms the hydrated salt **29** which keeps the *transoid* ligands' conformation (Scheme 3). If, however, **30** is protonated with gaseous moist HCl the crystalline hydrated salt **31** is quantitatively formed. The *cisoid* conformation of the ligands in crystalline **31** enforces a new hydrogen-bridged chain structure. This is shown by the X-ray crystal structures of **29**, **30**, and **31** and powder diffraction data. The effects of the chain structure for the stereospecific gas–solid reactions have been elucidated with AFM. The clear-cut results correlate the surface features formed with the crystal structures. The single crystals heavily disintegrate upon reaction and the neutral product **30** is re-formed upon heating of **29** or **31** [29]. Clearly, the conformational reversal of **30**→**31** or of **31**→**30** is the result of chemical reactions combined with particular crystal properties. This is to be distinguished from crystal phase transitions that are not within the scope of this article. Similarly, protonation of **30** with the vapor of trifluoroacetic acid enforces the *cisoid* conformation in the salt, though without additional water. On the other hand, the vapor of tetrafluoroboric acid forms a salt with **30** in which a different chain structure in the *transoid* conformation is obtained [30].

Very weak acids such as 2-mercaptobenzothiazole (**32**) [27], saccharine (**34**), 5,5-diphenylthiohydantoin (**36**) [31], or 5-ylidene-thiohydantoins (**38**) [32] form salts with methylamine gas (Scheme 4). Such quantitatively formed salts (**33**, **35**, **37**, **39**) cannot be obtained in solution. This new possibility of reaction was studied and interpreted with AFM [1, 27]. Even C–H acids such as barbituric acids **40**, which crystallize as the triketo tautomers, form the ammonium barbiturates **41** with gaseous bases such as ammonia or dimethylamine with great ease [32].

Equally important is the salt formation of solid bases with gaseous acids. An example has been cited above (**30**→**31**). This type of reaction is quite general. Strong and very weak bases react quantitatively and the gas–solid technique does not have problems with moisture. Amino acids such as L-phenylalanine, D-penicillamine (**42**), DL-penicillamine, L-cysteine, L-leucine, L-proline, DL-tyrosine and others are quantitatively converted into their hydrohalides with

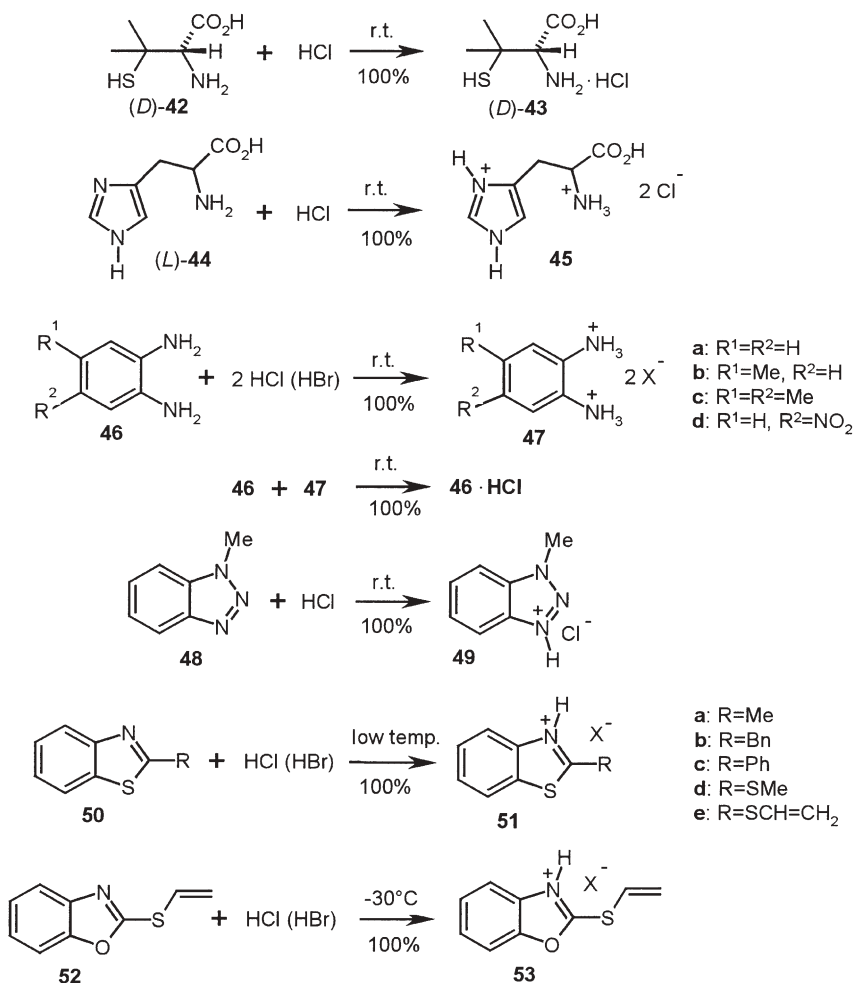


Scheme 4

gaseous HCl or HBr in preparative runs (Scheme 5). Several of these amino acids react thoroughly without pregrinding. However, there may be surface passivation effects if the amino acids (in particular glycine and alanine) were previously exposed to ambient air. In those cases anhydrous premilling will enable the slightly exothermic complete salt formation [22]. It is remarkable that the usually three-dimensional hydrogen-bond networks (except α - and β -polymorphs of glycine) are broken up by the protonations so that molecular migrations become possible and disintegration of the crystals ensues. A bis-hydrochloride is obtained if solid L-histidine (**44**) reacts with HCl gas. Anisotropic molecular migrations that relate to the crystal packing have been shown with AFM [1, 27].

Preparative applications have been found with the anhydrous bis-hydrochlorides of various *o*-phenylenediamines **46**. These were produced at the 50-g scale and all of these were required for enabling gas-solid condensation reactions with acetone [5]. If the monohydrochlorides of the *o*-phenylenediamines are required, the dihydrochlorides **47** are simply milled with a stoichiometric amount of the corresponding free solid diamine **46** in order to get

a pure product with quantitative yield. The benzotriazole **48** gives a quantitative yield of the hydrochloride **49** (Scheme 5), which on heating to 210 °C provides a liquid mixture of **48** and 2-methyl-2*H*-benzotriazole in an 87:13 ratio. Similarly, solid 1-phenyl-1*H*-benzotriazole quantitatively adds HCl. On the other hand, solid 2-phenyl-2*H*-benzotriazole does not form a salt with gaseous HCl [22].

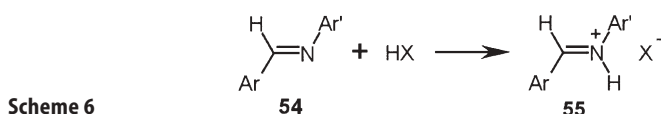


Scheme 5

Liquid bases may be solidified at low temperatures prior to being exposed to gaseous HCl, HBr, or HI. Once quantitatively formed the solid salts are surprisingly stable under ambient conditions [5]. The benzothiazoles **50** (with the exception of **50c**) are liquids and require cooling down to -10, -30, or -45 °C for

solidification prior to the application of the reactive gases. Interestingly, *S*-vinyl-benzothiazole (**50e**) and -benzoxazole (**52**) form the salts with HCl and HBr but do not undergo addition to the double bond [33] (Scheme 5). Furthermore, creatinine hydrochloride and hydrobromide are quantitatively obtained by gas–solid reaction and have much better quality than samples from solution reactions [28].

The gas–solid technique is particularly attractive in the synthesis of extremely sensitive hydrohalogenides of Schiff bases (e.g., **54**) as the exclusion of moisture is automatically achieved. Some of these salts include additional HX, which cannot be completely removed by evacuation and the phenolic compounds keep a second mole of HX that cannot be evaporated (Table 1, Scheme 6) [9].



The characteristic melting points and IR frequencies of **55** indicate well-defined compounds. The second molecule HX in the salts **d**, **d'**, **e**, **e'** is probably firmly included, forming hydrogen bonds to the available oxygen atoms. These salts are easily obtained and should be versatile building blocks in solid-state reactions or reactions in dry aprotic solvents [9].

While the stoichiometric salt formations with HX are clear-cut if the acid cannot be removed simply by evacuation, there may be questions of salt formation versus complexation in solid–solid reactions between acids and bases. This point has been suitably addressed with IR spectroscopy and X-ray powder diffraction studies of solid carboxylic acids and amine bases of varying strengths that were ground or milled together [34]. Yields are not given, but it may be assumed that quantitative reactions occurred in all stoichiometric mixtures.

Table 1 Iminium hydrohalogenides (**55**), their m.p., C=N⁺ vibrational frequency, and titrated HX content

| | Ar | Ar' | X | m.p. | ν (cm ⁻¹) | HX ratio |
|-----------|---|-----------------------------------|----|---------|---------------------------|----------|
| a | C ₆ H ₅ | C ₆ H ₅ | Cl | 189–190 | 1662 | 1.14 |
| b | 4-ClC ₆ H ₄ | 4-MeC ₆ H ₄ | Cl | 219–223 | 1659 | 1.26 |
| b' | 4-ClC ₆ H ₄ | 4-MeC ₆ H ₄ | Br | 248–249 | 1655 | 1.09 |
| c | 4-NO ₂ C ₆ H ₄ | 4-MeC ₆ H ₄ | Cl | 212–214 | 1670 | 1.00 |
| c' | 4-NO ₂ C ₆ H ₄ | 4-MeC ₆ H ₄ | Br | 241–243 | 1663 | 0.98 |
| d | 4-HOC ₆ H ₄ | 4-MeC ₆ H ₄ | Cl | 252–253 | 1659 | 1.93 |
| d' | 4-HOC ₆ H ₄ | 4-MeC ₆ H ₄ | Br | 280–281 | 1658 | 1.94 |
| e | 3-MeO, 4-HOC ₆ H ₄ | 4-ClC ₆ H ₄ | Cl | 205–207 | 1652 | 2.04 |
| e' | 3-MeO, 4-HOC ₆ H ₄ | 4-ClC ₆ H ₄ | Br | 239–239 | 1650 | 2.05 |

Unfortunately the authors argue that they were performing “mechanochemical” reactions with mechanical energy input for the salt formation or complexation to occur, rather than just creating the required contacts between reacting crystals. Furthermore, they did not exclude moisture, reported intermediate liquid phases in various cases, and did not separate out any real solid-state reactions that might have been achieved. It is therefore not possible to discuss the results in more detail here.

5 Complexation

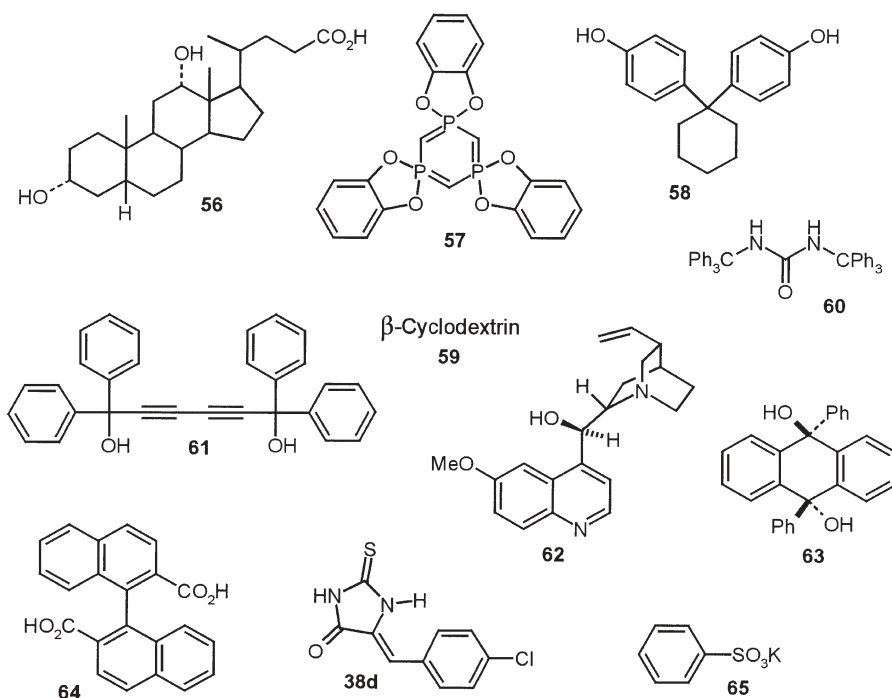
Solid-state complexations occur both as imbibition of gases into crystals of hosts or by comilling of the solid partners. In both cases, the host lattice will be changed unless the original host lattice exhibits large and accessible (via channels) cages, such as in zeolites. This has been repeatedly shown by the detection of long-range anisotropic molecular migrations with the sensitivity of AFM. Unlike crystallization of molecular complexes from solvents, the solid-state technique may lead to higher loaded complexes that cannot be obtained from solution. A large number of gas–solid complexations have been observed in the research groups of Kaupp [28], Nassimbeni [35], Toda [36], and Weber [37]. Numerous host types are reported in [38], but their potential imbibition properties still await exploration, as all inclusion experiments were executed from solutions. However, gas–solid imbibitions have particular advantages and applications.

Of particular interest are exceedingly efficient imbibitions of acetone vapor into solid hosts at very low partial pressures (down to the detection limit), so that these reactions may be used for atmospheric detoxifications [5, 28].

Solid-state complexes are not always composed at simple ratios of the components if crystallized from solution. Such a composition may change further upon gas imbibition into crystals with usually higher uptake of the volatile component. On the other hand, as the crystal packing changes upon imbibition the three steps of phase rebuilding, phase transformation, and crystal disintegration are a prerequisite and if one of these fails there will be no reaction. This has been nicely shown by AFM studies, which correlate the surface features with the initial crystal structure, and by crystal structure investigations after complex formation [5]. Some typical examples of acetone vapor imbibition are listed in Table 2 together with the carbonyl frequencies ($\nu_{C=O}$) of the included acetone, which indicate the degree of polar interaction. The guest acetone is taken up by various host crystals with guest/host ratios that considerably exceed the values of the crystallized inclusion complexes. However, desoxycholic acid (**56**) does not include from the gas phase [5]. The inclusion ratios are stable upon completion of the reactions. The desorption temperatures under atmospheric pressure are high enough and in a comfortable range for collecting very diluted acetone gas in columns of host crystals and for recovery of the

Table 2 Some results with gas–solid imbibitions of acetone [28]

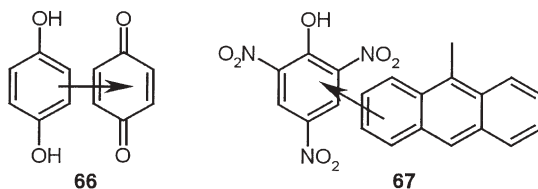
| Host | Acetone/host (imbibed) | $\nu_{(C=O)}$ (cm ⁻¹) | Desorption temperature (°C) | Acetone/host (crystallized) |
|--------------------|---------------------------|-----------------------------------|--------------------------------|--------------------------------|
| 56 | – | – | – | 0.58 ^[37] |
| 57 | 0.48 | 1716 | 146 | 0.20 |
| 58 | 0.61 | 1701 | 63 | 0.58 |
| 59 | 2.56 | 1705 | 143 | 1.55 |
| 60 | 0.97 | 1711 | 121 | 0.76 |
| 61 ^[36] | 2.0 ^[39] | 1702 | 70 | 2.0 |



acetone by heating. A number of coexisting imbibitions of volatile solvents as ambient vapor mixtures (e.g., acetone, *t*-Bu₂O, THF, dioxane, cyclohexane, etc.) or separations of volatile liquids via the gas phase are known or can be developed [5, 28]. Host 61 imbibes acetone to a 1:2 host/guest ratio [36], and sharp decay occurs at 70 °C [39]. Interestingly, host 63 imbibes two acetone molecules per diol host molecule. However, in that case a threshold pressure, which increases with increasing temperature, was found [35]. This disqualifies system 63 for the collection of minute quantities of acetone. Conversely, hosts 57–61 appear suitable for applications in the field of gas sensors [28].

Numerous gas–solid imbibitions are known (molar ratio; desorption temperature): vapors of hexane are taken up by **57** (0.15; 175 °C) and **62** (0.13), not by **56**, **59**, or **60**; heptane by **57** (0.20); cyclohexane by **57** (0.29; 128 °C), **62** (0.19), not by **56**, **59**, or **60**; methylcyclohexane by **57** (0.26); benzene by **56** (0.31; 98 and 148 °C), **57** (0.23; 107 °C), **59** (1.59; 110 °C), **60** (1.19; 104 °C), **62** (0.49; 75 °C), **64** (0.92; 110 and 154 °C); toluene by **56** (0.38; 160 °C), **57** (0.27; 155 °C), **59** (0.72; 100 °C), **60** (0.14; 93 °C), **62** (0.52; 77 °C), **54** (0.50; 92 °C); dichloromethane by **57** (0.44; 147 °C), **59** (1.43; 125 °C), **60** (0.93; 117 °C), **61** (2.0) [39], not by **56**; furan by **57** (0.21; 131 °C), **59** (1.48; 120 °C), **62** (0.25; 75 °C), not by **56** or **60**; tetrahydrofuran by **56** (0.39; 162 °C), **57** (1.40), **58** (0.40), **59** (1.70; 129 °C), **64** (0.95; 115 °C); dioxane by **38d** (34; 123 °C); methyl *t*-butyl ether by **57** (1.00 at flow; 106 °C), **58** (0.20; 70 °C); ethyl acetate by **57** (0.40; 145 °C); methanol by **59** (4.11; 130 °C), **60** (1.14; 116 °C), **64** (0.56; 126 and 140 °C), not by **56**; ethanol by **56** (0.80; 132 °C), **59** (2.76; 132 °C), **60** (1.50; 123 °C), **64** (1.80; 90 and 135 °C); dinitrogen tetroxide by **65** (0.33; 80 and 160 °C). All data are for room temperature [28]. The inclusion efficiencies differ from those found by clathration in solution but are frequently higher or comparable. Sometimes inclusion is not reported from solution and there are only three cases of liquid-state inclusion that do not occur by the gas–solid technique (**56** and dichloromethane, acetone, and methanol), probably due to the low inclusion rate of that host. The stable compounds have reproducible composition, are not covalently bound, and liberate the gases sharply upon heating to the desorption temperatures. The selectivities are remarkable and if the amount of vapor component stays below the capacity of the host, all of it is included down to the detection limit. Actually, the mentioned gases can be eliminated from ambient atmosphere. Only host **56** is too slow for that purpose and only host **38d** requires removal of moisture prior to inclusion [28]. Importantly, the data offer the separation of vapors by gas–solid imbibition and coexisting inclusion mixtures of compounds are also obtained [28].

Solid–solid complexes are usually easily and quantitatively obtained upon grinding or better, milling. This has been shown with the formation of numerous charge-transfer sandwich complexes such as quinhydrones (**66**) or picrates (**67**) [22]. Numerous one plus one combinations of essentially planar donors and acceptors provide the homogeneous complexes most easily upon milling.



Two examples are depicted (milling of picrates should be preceded by a negative explosion test of a small sample with a hammer on an anvil). On the other hand, the combination anthracene and anthraquinone did not form the charge-

transfer complex upon milling or from solution but only from the rapidly cooled melt [15]. This brown complex separates slowly (several months) into anthracene and anthraquinone upon standing at room temperature in a complete solid-state reaction.

A big advantage of the solid–solid technique is the possibility of obtaining complexes that are not obtainable from solution. It must, however, be shown that uniform complexes rather than microcrystalline mixtures occur. Apart from X-ray powder diffraction (which does not properly account for very small crystallites), proof is obtained by solid-state spectroscopy (IR, UV, luminescence) or, in the case of stable radicals, by magnetic susceptibility measurements. The 1:1 and 2:1 complexes **68**–**72** were prepared by stoichiometric milling and relevant physical properties are collected in Table 3 [20].

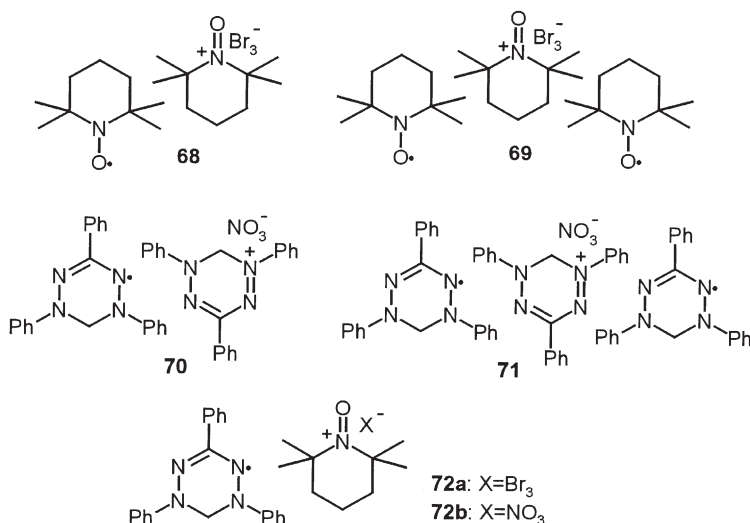
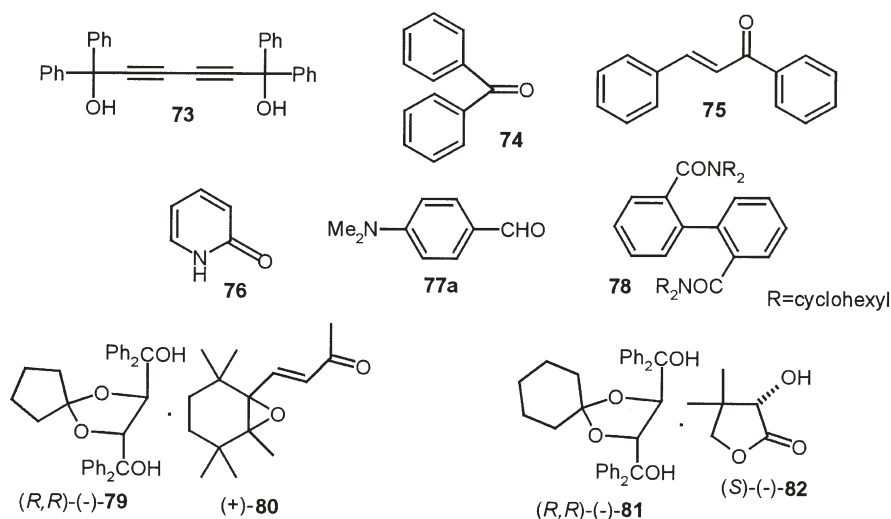


Table 3 Physical constants of the radicals TEMPO (tetramethylpiperidiny-*N*-oxyl), 1,3,5-triphenylverdazyl (**10**), and their complexes with the oxidized cation salts

| Compound | m.p. (DSC endotherms) (°C) | <i>C</i> (emu K mol ⁻¹) | Θ (K) | Magnetic interaction |
|--------------------|----------------------------|-------------------------------------|-------|----------------------|
| TEMPO | 36–38 | 0.38 | –5.9 | Antiferromagnetic |
| Verdazyl 10 | 142–143 | 0.38 | –9.9 | Antiferromagnetic |
| 68 | 115/161 | 0.0034 | –0.21 | Antiferromagnetic |
| 69 | 114/150 | 0.60 | –5.7 | Antiferromagnetic |
| 70 | 174 | 0.094 | –0.12 | Antiferromagnetic |
| 71 | 139 | 0.20 | –3.3 | Antiferromagnetic |
| 72a | 158 | 0.0079 | –0.25 | Antiferromagnetic |
| 72b | 146/150 | 0.071 | –0.09 | Antiferromagnetic |

It is seen from Table 3 that **68**, **69**, and **72b** have two DSC endotherms, the first without melting, the second with melting and decomposition. Interestingly, the Curie constants (2–300 K range) differ markedly and are much larger in the 2:1 complexes **69** and **71** with considerable short-range order as compared to all of the 1:1 complexes, which exhibit only weak antiferromagnetic interactions between the spins. The large decrease of the magnetic susceptibility in all 1:1 complexes suggests a near-resonant charge transfer from stable radical to cation, with equal distribution of the spin over both partners that become chemically identical if the anion is symmetrically located. There is also a marked influence of the anion in **72**. Evidently, the interactions of the resonant complexes with the additional radicals do not prevent short-range spin alignment. All Weiss constants in Table 3 are negative.

Solid-solid inclusions of tetraarylhexadiynediols (e.g., **73**) and TADDOLS (e.g., **79**, **81**) have been summarized in [40–42]. Most of these authors used



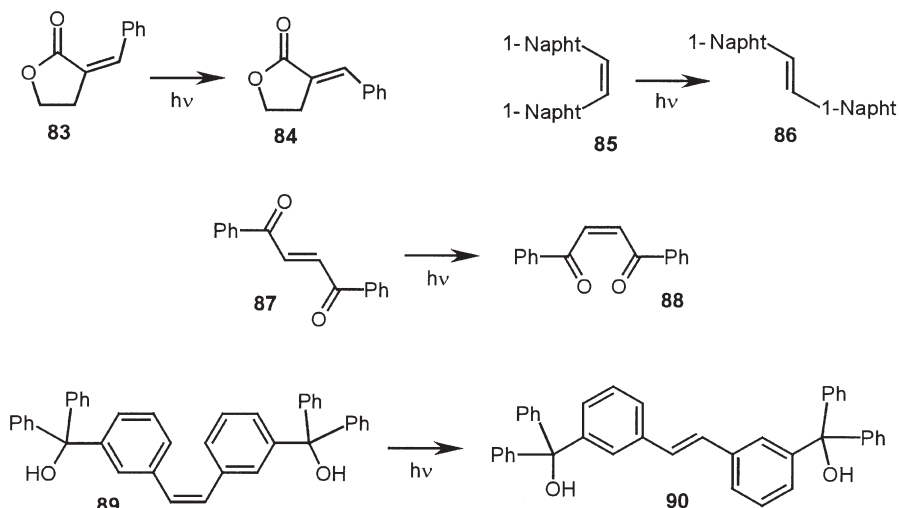
crystallizations from solution or slurry techniques for chiral resolutions. Less studied are solid-solid techniques in the preparation of these and related inclusion reactions. Benzophenone (**74**, 1 mole), chalcone (**75**, 2 mole), 2-pyridone (**76**, 2 mole), *p*-dimethylaminobenzaldehyde (**77a**, 2 mole) [43], or the bisamide **78** (1 mole) [40] are included by the diacetylene upon grinding. Furthermore, (+)-β-ionone oxide [(+)-**80**] has been quantitatively included by (*R,R*)-(-)-**79** upon grinding at room temperature. The quantitative inclusion of (*S*)-(-)-**82** by (*R,R*)-(-)-**81** required heating of coground solid mixtures to 80 °C [44] or comilling at 25–30 °C [22]. For the latter case and in the solid-state inclusion of (*S*)-(-)-**82** by (*R,R*)-(-)-**79**, AFM investigations [44] indicated low-distance solid-to-solid sublimation on the double layers with surface passiva-

tion that has to be broken for quantitative conversions in both cases by the above means, or by addition of water which partly dissolves the guest, a slurry technique that was also used to separate the racemate of pantolactone **82** by enantioselective inclusion [45]. But only AFM and the milling experiments deal with true solid-state reactions. Also cholesterol and oxalic acid give the 1:1 complex upon comilling [22].

The first gas–solid imbibitions of chiral molecules by the host (*S*)-1,2-dihydroxy-1,1-diphenylpropane were not highly enantioselective [46] and can therefore not be discussed here.

6 Geometrical Isomerization

E/Z isomerizations are usually not expected in the solid state. They have been widely studied in solutions or in liquids. This includes thermal, catalytic, and photolytic processes and *E/Z* isomerization was also observed in competition with biphotonic excimer laser photodecompositions [47]. Most of the *E/Z* isomerizations in the solid state have been photochemically observed [48], but mostly not as uniform quantitative reactions. If these isomerizations cannot be performed under selective conditions of irradiation (an exception is **83/84**) [49], the only chance to have these reactions uniform with 100% yield is a very efficient isomerization (according to the phase rebuilding mechanism) that leads to an isomeric product with heavily interlocked crystal lattice. Under such circumstances side reactions of the substrate and photoconversions of the product are prohibited (including the back reaction, of course). Four favorable cases

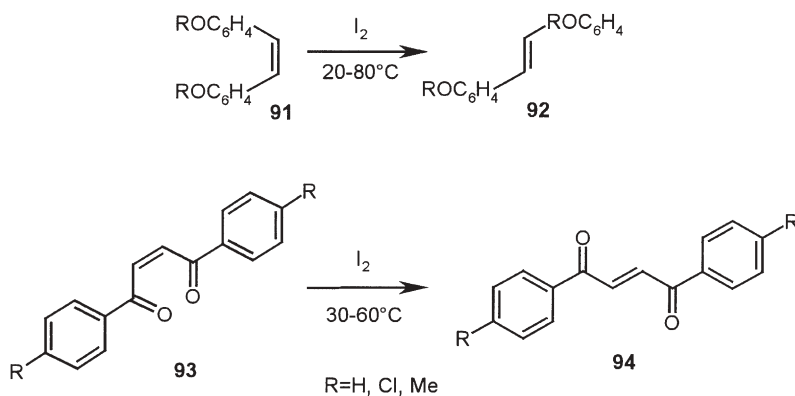


Scheme 7

are known with the reactions of **83** to give **84** (selective irradiation at 365 nm; photodimers of **84** occur at $\lambda > 300$ nm irradiation) [49]), **85** to give **86** [50] (the product lattice is interlocked [1]), **87** ($P2_1/c$) to give **88** ($P2_1$) ($E \rightarrow Z$; the bent product molecules **88** pack in crossing mono- and bilayers with interlocked stacks [51]), and **89** to give **90** (neat or acetone complex; $T < -15$ °C; colloidal particles formed in a macroscopically unchanged crystal [52]) (Scheme 7).

The reactions of **83**, **87**, and **89** have been studied by AFM. The first two of them showed the common long-range anisotropic molecular migrations, but not the third one with the extremely large substituents. The question of the chemical mechanism, i.e., the decision between space-intensive internal rotation or a volume-conserving hula-twist mechanism [53] (which keeps the substituents in their planes while only one C–H unit translocates), could not be experimentally decided. While it might be possible to envisage a cooperative counterclockwise half-rotation on both sides of the double bond in **83** and **85**, these possibilities are excluded for **87** and **89** [48]. Hula-twist expects different initial product conformers, but their distinction was hampered by the molecular migrations and in **89/90** by the lack of X-ray diffraction signal [52], despite retention of the single-crystal shape. The latter case profited from void space in the structure, ready to accommodate the very large geometric change. It should be noted that completion of these E/Z isomerizations may require many photons if internal filtering becomes more and more prominent toward the end, while the yield approaches the 100% margin.

The enormous amount of overactivation in photochemistry is not always required for solid-state *cis-trans* isomerizations. There are also some thermal E/Z isomerizations of crystalline olefins that are catalyzed by iodine. For example, crystalline *cis*-stilbenes **91** can be isomerized to give *trans*-stilbenes **92** without intervening liquid phases (Scheme 8). The isomerizations follow first-order kinetics with various rate constants for 4-MeO, two modifications of 2-MeO, 2-EtO, 2-*n*-PrO, and 2-*i*-PrO substitution. The activation energies vary from 20 to 32 kcal mol⁻¹ but could not be interpreted [54]. Similarly, *cis*-1,2-diben-



Scheme 8

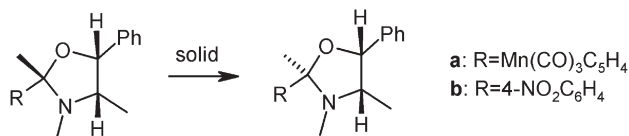
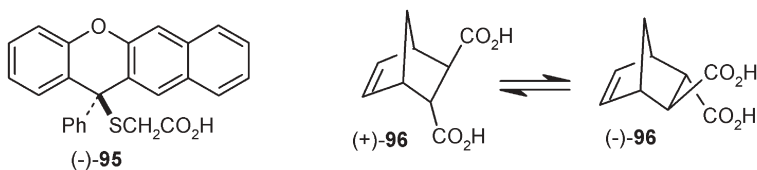
zoylethene **88** (**93**, R=H) and its substitution products **93** give **87** and **94**, respectively, when gently heated with iodine vapor [55]. After apparent induction periods, as evidenced by S-shaped conversion curves (the induction periods were not appreciated in the text of the publication), first-order rate constants and activation energies between 17 and 21 kcal mol⁻¹ were listed [55]. Mechanistic interpretation was not possible. Unlike the reported dibenzoylethenes, an *E/Z* isomerization of *cis*-chalcone could not be catalyzed by iodine vapor in the solid state [56].

Furthermore, the conclusion that the formation of the *meso* dibromide upon gas–solid addition of bromine to *cis*-stilbene “is due to *cis*-*trans* isomerization prior to or during addition” [54, 56] cannot be accepted without further proof, as there is also the possibility for *cis* addition [58–61].

Racemizations in the crystalline state have a long history. It is known that L- α -amino acids slowly racemize in the solid state [62]. As this also happens in solid proteins the implications are manifold, not only in pure chemistry but also in biochemistry, nutrition, food technology, and geology. Therefore, techniques have been developed to determine the DL ratio of amino acids down to 0.1% and inversion rate constants have been determined under acid hydrolysis conditions [63]. One could think of very slow deamination and readdition of the amine or an enolization mechanism. However, such reactions can also be induced by photolysis or radiolysis from natural sources [64].

Significantly faster is the solid-state racemization of the thioglycolic acid derivative **95** (Scheme 9). A solid sample lost its specific rotation upon standing from -42.3° to -36.9° in 2 months and to -13.9° after 14 months. It is noted that such racemization was more rapid when the acid was exposed to light [57]. A heterolytic dissociation/recombination mechanism appears suitable.

The racemization of Diels–Alder adducts in the solid state appears to proceed via diradical or complete cycloreversion. For example, (+)-**96** racemizes in the solid state from 130 to 155 °C ($\Delta H^\ddagger=40.0$ kcal mol⁻¹; $\Delta S^\ddagger=14$ cal mol⁻¹ K⁻¹) to give (–)-**96** (Scheme 9), whereas the melt reaction (eutectic temperature is 165 °C) from 176 to 194 °C has much lower activation parameters ($\Delta H^\ddagger=$



Scheme 9 (2*S*,4*S*,5*R*)-**97**

(2*R*,4*S*,5*R*)-**98**

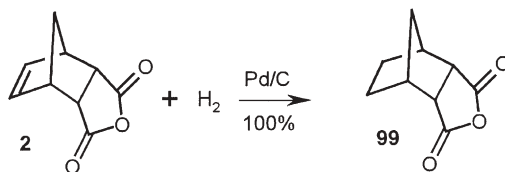
29.7 kcal mol⁻¹; $\Delta S^\ddagger = -6.9$ cal mol⁻¹ K⁻¹) [65]. Racemizations in both the solid and the melt follow strictly first-order kinetics [65]. The extrapolated rate in the melt state is about ten times higher than that in the solid state in this unimolecular reaction.

Chiral N/O-acetals may racemize in the solid state when water of crystallization is present. Examples are the epimerizations of the oxazolidines **97** that contain water from their preparation by stereoselective condensation. Thus, the kinetically preferred products **97a,b** (which are admixed to the thermodynamically more stable products **98a,b**) epimerize within some weeks in the solid state to give enantiopure **98a,b** [66] (Scheme 9). It appears that the N/O-acetal hydrolyses and recloses. Solid-state racemizations are quantitative if the 1:1 equilibrium between the enantiomers is obtained. Therefore they do not really fulfill the criterion of only one product. Numerous examples in the organo-metallic field are listed in [67] and [68].

7

Hydrogenation

Solid-state catalytic hydrogenations in the absence of any solvent can be easily and quantitatively performed in ball-mills that allow for evaporation and filling with gases. For example, the Diels–Alder adduct of maleic anhydride and cyclopentadiene **2** hydrogenates readily upon milling with palladium on charcoal in an atmosphere of hydrogen in 200-g batches to give **99**, which is easily sublimed off from the catalyst [22] (Scheme 10).



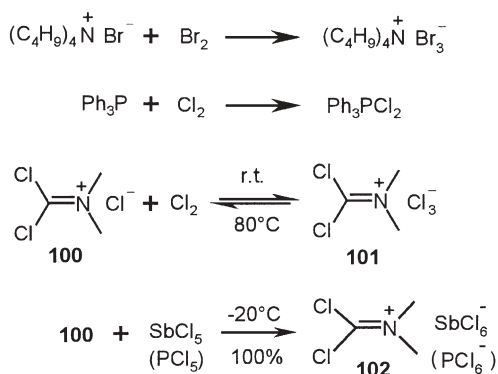
Scheme 10

These hydrogenations are rapid and quantitative. Conversely, the gas–solid hydrogenations of alkenes that were doped by platinum metal compounds on their recrystallization may be incomplete as, for example, the hydrogenation of *trans*-cinnamic acid or *N*-vinylisatin [58, 61], which should be milled for completion. Furthermore, the “spillover technique” by mixing powders of substrate and catalyst followed by application of hydrogen and several hours or days rest [69, 70] appears inappropriate for quantitative conversions. Milling is, however, not applicable if volatile liquids have to be constantly pumped off [69] or if the products become liquid or sticky [70].

8

Addition of Halogens

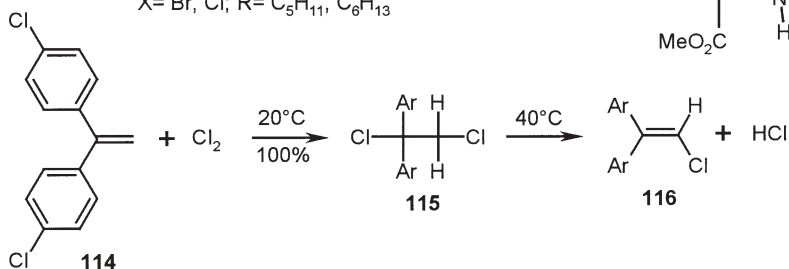
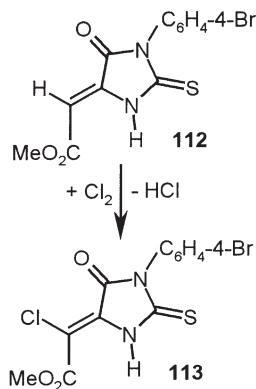
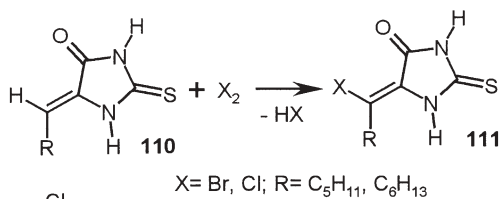
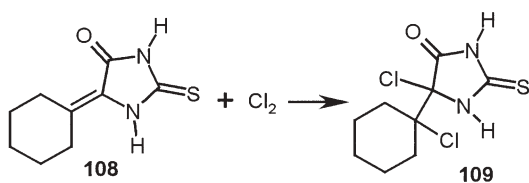
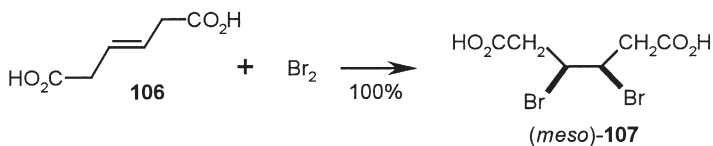
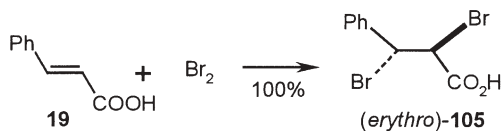
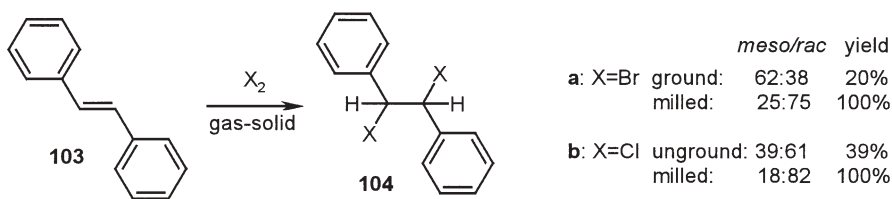
The addition of bromine to quaternary ammonium bromides to provide the tribromides is most easily achieved in a reaction column with the solid while a stream of air carries the required amount of bromine (Scheme 11). Thus, in the case of tetrabutylammonium bromide (TBAB), a sharp yellow reaction front is obtained while bromine is quantitatively added and the pure bromination agent TBABr_3 is obtained. Small runs can be quantitatively performed with 0.5 bar bromine vapor and the unground crystals of TBAB [28]. Equally simple is the gas–solid addition of chlorine to triphenylphosphane to give triphenylphosphane dichloride [28].



Scheme 11

Also, the extremely labile trichloride **101** of Viehe salt **100** is reversibly and quantitatively obtained in the solid state [9]. This latter reaction is related to the solid–solid syntheses of the extremely reactive hexachloroantimonates or -phosphates (**102**) of the Viehe salt by its milling with antimony pentachloride or phosphorus pentachloride [9] (Scheme 11). Furthermore, the labile adduct of chlorine to benzyldiene aniline is obtained at -20°C in a solid-state reaction.

The claims of exclusive formation of *rac*-stilbene dichloride upon gas–solid addition of chlorine to *trans*-stilbene (**103**) [71] and of *meso*-stilbene dibromide in the gas–solid addition of bromine to *trans*- or *cis*-stilbene [54] could not be verified. Scheme 12 shows the results of more detailed studies indicating the *meso/rac* ratios on the solid-state chlorination and bromination of *trans*-stilbene (**103**) and some variations when the crystal size was changed [58, 60–61]. There is a risk of partial transient liquefaction if the chlorine is added too rapidly, due to initially heavy reaction. But even at the start with a stoichiometric amount of chlorine at 0.1 bar and 0°C , a persistent product layer forms on the unground crystal powder of **103** that cannot be disintegrated by the ultrasound of a cleaning bath at 20°C for 60 h (only 7% conversion with *meso/rac* ratio of 11:89 under these conditions) [22]. It is therefore unavoidable to mill the crystals of **103** to sizes $<1\ \mu\text{m}$ in order to overcome these rare diffi-

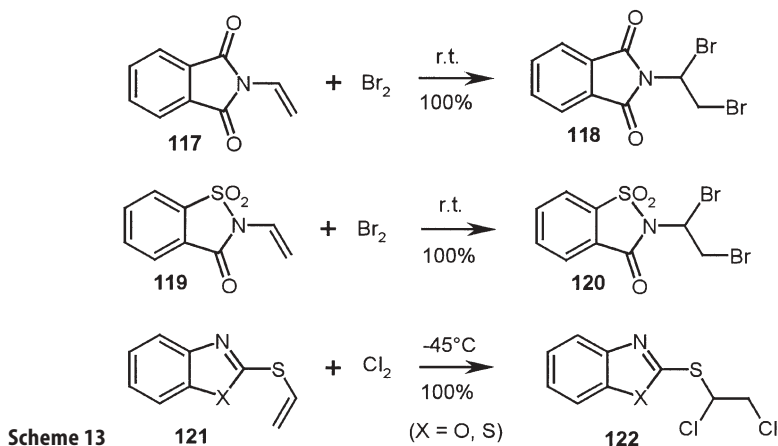


Scheme 12

culties in the disintegration step. Anisotropic molecular migrations within the crystal of **103** upon halogen addition have been recorded by AFM [59]. The early solid-state addition of bromine to *trans*-cinnamic acid [72] was revisited and provided a quantitative yield of the *erythro* dibromide **105**, with both the α - and β -modifications of **19** [59, 73]. The anisotropic molecular migrations within the crystals have been explored by AFM [59, 73]. Various substituted cinnamic acids (*m*-NO₂; *m*-Cl, α -phenyl) in different crystal modifications were reported to yield quantitatively the corresponding *trans* adducts, as detected by the weight increase of 20-mg samples [54]. No NMR spectra were reported. A large-scale quantitative yield of the *meso* dibromide **107** was also reported [54].

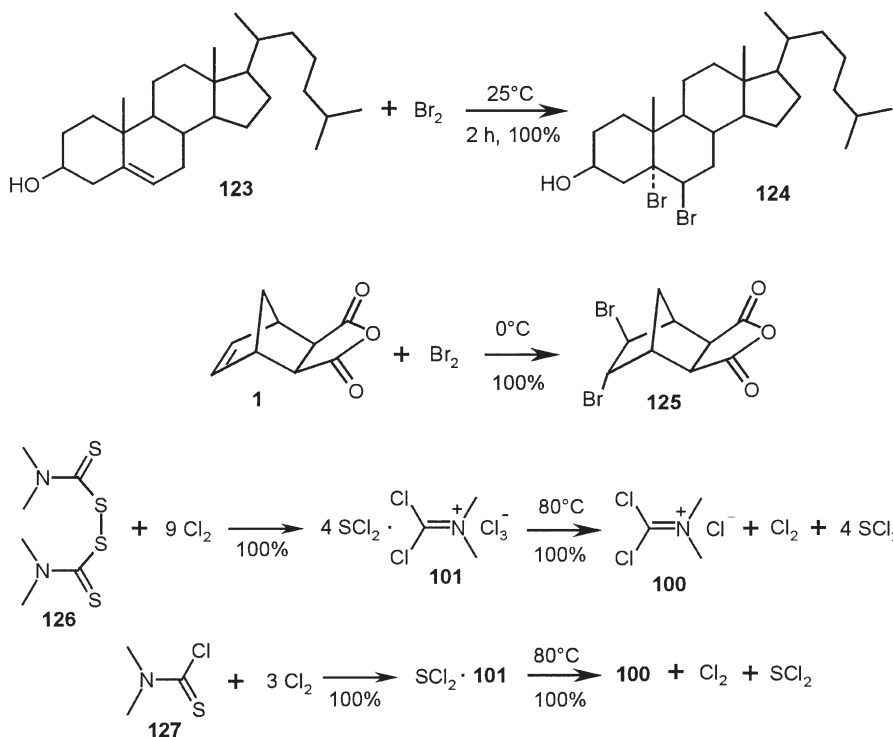
The chlorine adduct to the tetrasubstituted exocyclic double bond in **108** is quantitatively obtained by gas–solid reaction [27]. Conversely, related trisubstituted double bonds lose HX after the gas–solid halogen addition such as in the reactions of **110** and **112** that give **111** and **113**, respectively [28] (Scheme 12). The completion of these solid-state eliminations (Sect. 11) is faster at 100 °C. The product **113** is an interesting substrate for the synthesis of orotic acids. Furthermore, the production of **116** from solid **114** and chlorine gas proceeds with 100% yield via the intermediate adduct **115** [58, 60–61] (Scheme 12).

A number of highly reactive dihalogenides **118**, **120**, and **122**, far too reactive to be synthesized by conventional techniques, have been quantitatively obtained in pure form by halogen gas addition to solid *N*-vinyl and *S*-vinyl compounds at the appropriate temperatures [33, 61, 74] (Scheme 13).



Unsubstituted solid alicyclic alkenes have also been exposed to bromine vapor and gave 100% of pure *trans* dibromides, as in the case of cholesterol (**123**) [75] and the (milled) *exo* adduct **1** [22] (Scheme 14). The products **124** and **125** cannot be obtained with the same good quality from solution reactions.

Interestingly, the chlorination of dimethylthiocarbamoyl compounds such as **126** and **127** to give the trichloride of Viehe salt (**101**) can be performed as a



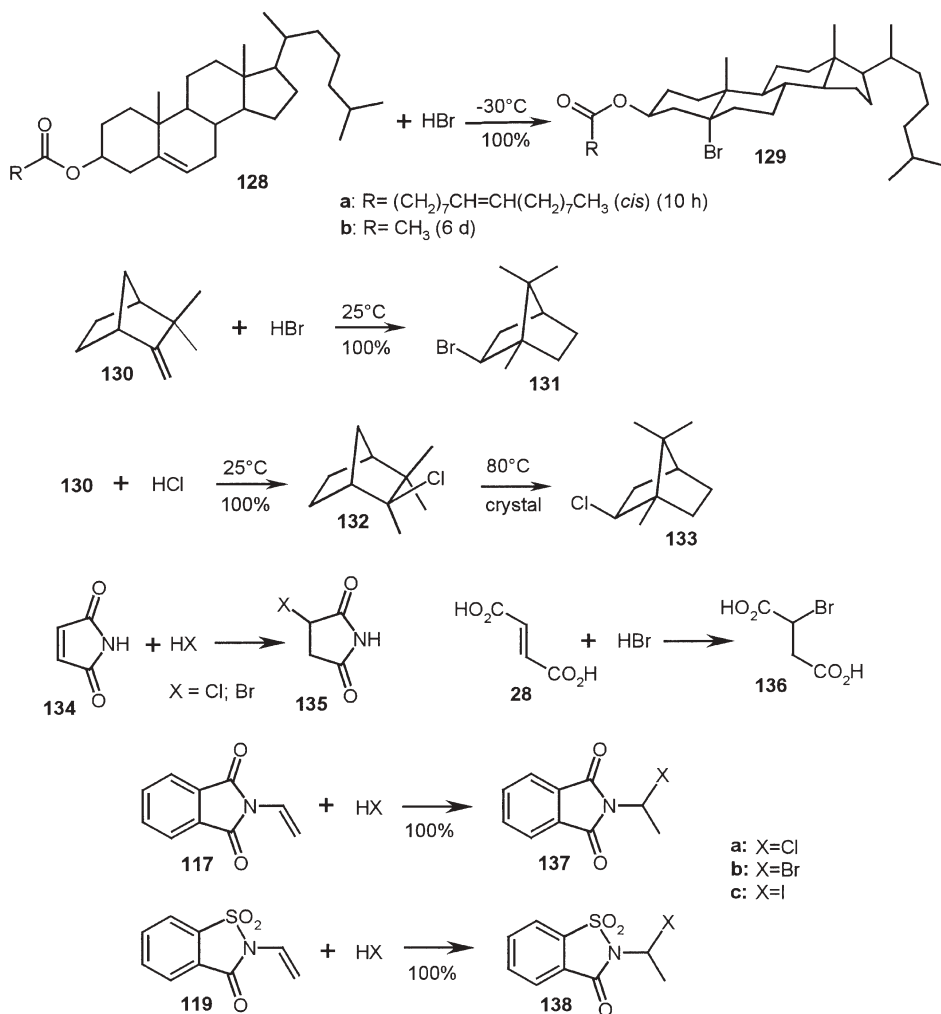
Scheme 14

quantitative gas–solid reaction, as the volatile sulfur dichloride is included in the solid product [9] (Sect. 5). Both SCl₂ and excess Cl₂ can be removed at 80 °C in a vacuum. We thus have easy access to pure Viehe salt by the gas–solid technique. Tetramethylthiocarbamoyl disulfide (**126**; 1.20 g, 5.00 mmol) or dimethylthiocarbamoyl chloride (**127**; 1.24 g, 10.0 mmol) was reacted in an evacuated 1-L flask with Cl₂ (1 bar, 45 mmol). After 10 h, all Cl₂ was consumed to form solid **101** with included SCl₂. This product was heated to 80 °C for 2 h in a vacuum with a cold trap (77 K) condensing the liberated Cl₂ and SCl₂. The yield of pure **100** was 1.62 g (100%) in both cases (Scheme 14).

9

Addition of Halogenohydrides

Various unsubstituted solid alkenes are able to quantitatively add gaseous halogenohydrides. Prominent examples are the cholesterol esters **128** that give stereospecifically the bromides **129** at –30 °C [75, 75a] and camphene (**130**) that gives stereospecifically the rearranged bromide **131** or the elusive camphene hydrochloride (**132**) with 100% yield [11] (Scheme 15). The quantitative solid–



Scheme 15

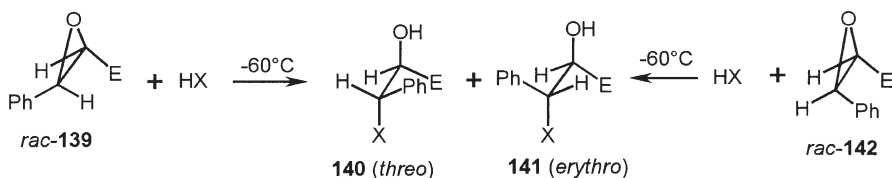
state [1,2/2,1]-rearrangement [76] (Wagner–Meerwein rearrangement) of 132 to give 133 is obtained at 80 °C (6 h) or at room temperature (3 years). The same rearrangement in solution is rapid, but it is possible to secure the purity of solid 132 by extrapolation back to time zero with ^1H NMR measurements.

Gaseous HCl adds to maleimide (134). Even more general are quantitative additions of HBr, which succeed with maleimide (134), maleic anhydride, fumaric acid (28), and maleic acid [28].

Very reactive (and probably not accessible from solution reactions) are the quantitatively obtained products 137 and 138 by the addition of gaseous HX to the *N*-vinyl compounds 117 and 119 [33, 61, 74] (Scheme 15). Also, *N*-vinylpyrrolidinone adds HBr probably quantitatively as a solid at -40°C in the

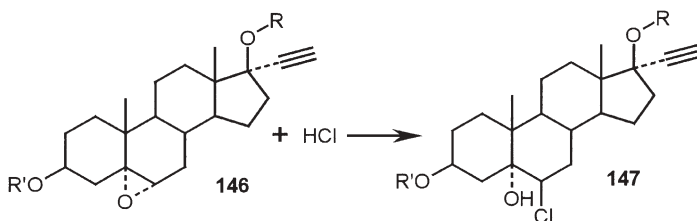
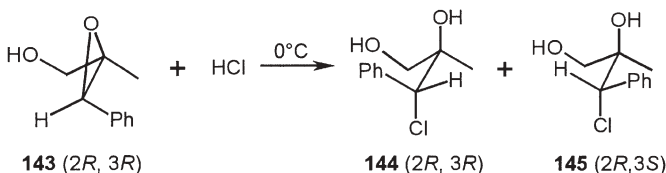
Markovnikov orientation. However, the product is too labile for storage at room temperature and must be reacted further at low temperature (examples are substitutions with methylthiol that work also with **137** and **138** [33]). Upon warming to room temperature the product *N*-(1-bromoethyl)pyrrolidinone releases HBr and forms the linear dimer (*E*)-1,1'-(3-methyl-1-propene-1,3-diyl)-bis(2-pyrrolidinone) that is most easily obtained by this technique [58].

Numerous solid oxiranes quantitatively add gaseous HCl or HBr even at low temperatures. These reactions are stereoselective; the ratio of the front to back side reaction of the protonated oxirane certainly depends on the stabilization of the intended carbocation [77]. This is worked out by the data in Scheme 16

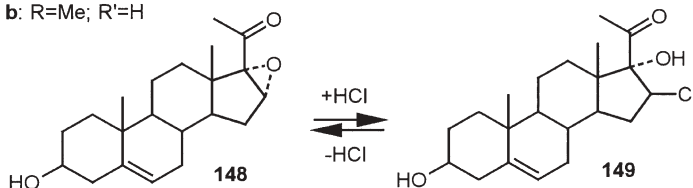


E=CO₂CH₃
 a: X=Cl
 b: X=Br

| | front side | backside |
|-------------|------------------|------------------|
| 139a | 140a (73) | 141a (27) |
| 139b | 140b (74) | 141b (26) |
| 142a | 141a (71) | 140a (29) |
| 142b | 141b (65) | 140b (35) |
| 143 | 144 (74) | 145 (26) |



a: R=H; R'=COMe
 b: R=Me; R'=H

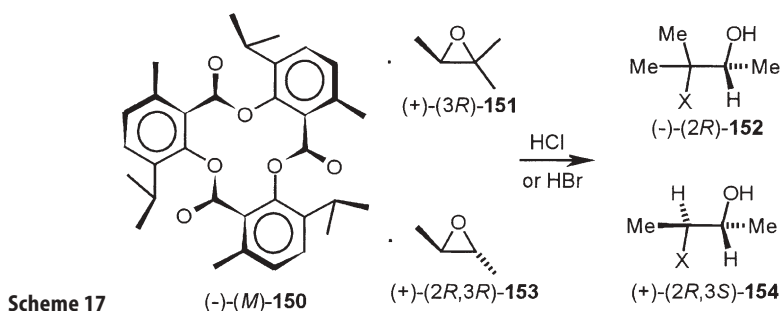


Scheme 16

for *rac*-139 and *rac*-142 that give the products 140 and 141 in the given proportions. Similarly, the epimer ratio 144:145 upon reaction of (2*R*,3*R*)-143 is 74:26 and the configuration at the 2-position is conserved. The experimental procedure for *rac*-139 is as follows: liquid *rac*-139 (500 mg, 2.80 mmol) was crystallized by cooling to -60°C in a 100-mL flask under vacuum. HCl gas (1 bar, 4.5 mmol) was let in through a vacuum line. After 15 h at -60°C the excess gas was pumped off and 600 mg (100%) yellow crystals (73:27 mixture of 140a and 141a) were obtained that melted at room temperature. Pure 140a (m.p. $65\text{--}67^{\circ}\text{C}$) was obtained by crystallization from *n*-hexane, though involving heavy losses.

The marked stereoselectivities and clean solid-state reactions of oxiranes were used for synthetic purposes in the steroid field. The stereospecifically obtained *trans*-chlorohydrins 147 ensue quantitatively from the crystalline 5 α ,6 α -epoxides 146 with gaseous HCl [77]. Similarly, the crystalline 16 α ,17 α -epoxide 148 reacts with gaseous HCl to yield exclusively the *trans*-chlorohydrin 149 which easily loses HCl to re-form the starting epoxide 148. Therefore, an equilibrium situation is reached in that case [77] (Scheme 16).

The gas–solid addition of HCl or HBr to simple alkylated oxiranes requires their inclusion. (–)-(*M*)-Tri-*o*-thymotide (150) (*P*₃,21) selectively enclathrates the oxiranes 151 or 153 with 13–14% ee for (+)-(3*R*)-151 or 51–55% ee for (+)-(2*R*,3*R*)-153. Isolated molecules in the chiral cages of 150 react stereoselectively with HCl or HBr gas to give the products 152 and 154, respectively, in almost stereopure form according to the optical rotations after quantitative reaction under the influence of the chiral environment [78] (Scheme 17). The host lattice is preserved during the reactions, but destroyed during liberation of the product molecules.

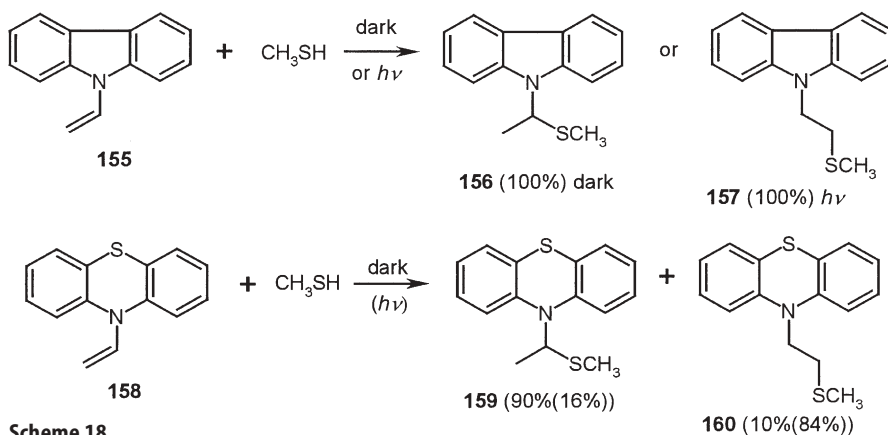


The hydrohalogenide additions to oxiranes are ether cleavages, of course. A further example for this reaction type is the quantitative reaction of solid 2,4,6-trimethoxy-*s*-triazine with HCl gas at 100°C to give cyanuric acid and methyl chloride [22].

10

Addition of Nucleophiles

Neutral gaseous nucleophiles such as water vapor are attacking hydrolyzable polar double bonds of all kinds (e.g., cyanates, isocyanates, iminium salts, etc.); however, these reactions tend to remain located at the surface due to its passivation (which allows the handling of such compounds in ambient air) or they form liquid layers. No quantitative reaction of the gas–solid type that may occur in a reasonable time (weeks) can be cited. More successful are solid-state addition reactions of thiols and amines. Methylthiol has been added to various *N*-vinyl compounds in the gas–solid variant, both thermally and photochemically, and the change in orientation has been studied [33]. The reactions of **155** are fully specific. Quantitative yields of **156** (Markovnikov orientation) were obtained in the dark and of **157** (*anti*-Markovnikov orientation) under irradiation. Similar reactions of **158** exhibit considerable selectivities for the orientation in the dark or under irradiation and mixtures of regioisomers are obtained, the yields of which add up to 100% as indicated in Scheme 18. The experimental procedures were as follows. Crystalline *N*-vinylcarbazole (**155**, 5.2 mmol, 0 °C) or *N*-vinylphenothiazine (**158**, 1.8 mmol, r.t.) was exposed to 20 or 10 mmol CH₃SH (0.9 bar) for 18 h or 2 days in the dark. Irradiations were similarly performed in a 250-mL round-bottomed flask under 0.9 bar CH₃SH with a 500-W water-cooled tungsten lamp (**155**: 5.2 mmol, 2 h, 0 °C; **158**: 1.8 mmol, 11 h, r.t.). The purity of the products was determined by ¹H NMR spectroscopy.



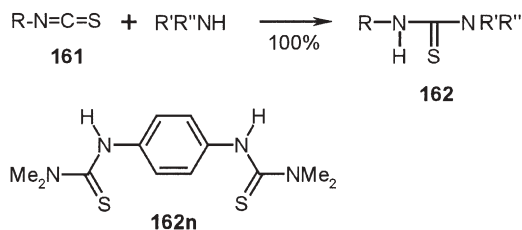
Scheme 18

Numerous further synthetic applications can be envisaged. Amines add to heterocumulenes. For example, the isothiocyanates **161** give a great number of thioureas in quantitative yield with gaseous or solid primary and secondary amines that are listed in Table 4 [12]. All thioureas are obtained with 100% yield directly in pure form (Scheme 19).

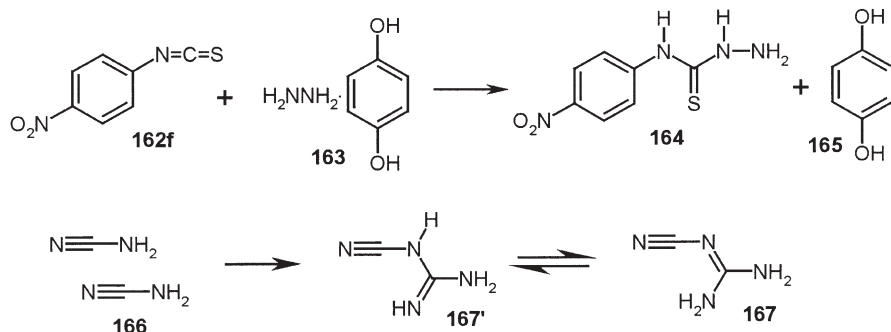
Table 4 Variations in the synthesis of **162**

| | R | R'/R'' | T (°C) | Type ^a |
|----|----------------------|-----------|--------|-------------------|
| a: | Ph | H/H | -30 | gs |
| b: | 4-BrPh | Me/H | r.t. | gs |
| c: | 4-BrPh | Me/Me | r.t. | gs |
| d: | 1-Naph | Me/H | r.t. | gs |
| e: | 1-Naph | Me/Me | r.t. | gs |
| f: | 4-NO ₂ Ph | Me/H | r.t. | gs |
| g: | 4-NO ₂ Ph | Me/Me | r.t. | gs |
| h: | Me | H/H | 0 | gs |
| i: | Me | Me/H | 0 | gs |
| j: | Me | Me/Me | 0 | gs |
| k: | Me | 4-MeOPh/H | r.t. | mo |
| l: | Me | 4-BrPh/H | r.t. | mo |
| m: | Me | 4-ClPh/H | r.t. | mo |
| n: | 4-S=C=N-Ph | Me/Me | r.t. | gs |

^a gs: gas-solid; mo: ground in a mortar.

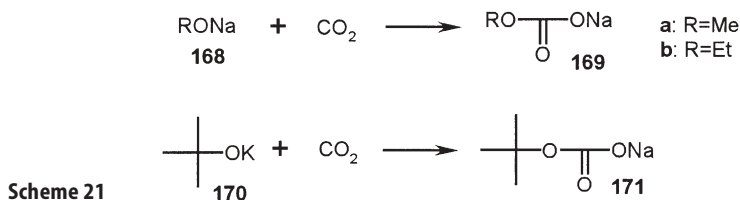
**Scheme 19**

A further variation is the reaction of isothiocyanates (e.g., **162f**) with hydrazine that has been “solidified” by inclusion into the host hydroquinone (**163**). Ball-milling of the solids leads to a quantitative reaction and the auxiliary **165** is washed away with water [79] (Scheme 20).

**Scheme 20**

The solid-state dimerization of cyanamide (**166**; m.p. 46 °C) to give cyano-guanidine (**167**; m.p. 205 °C) upon storage at room temperature represents an addition of the amino group to the triple bond. Thus, it happened in the author's lab that a 1-kg supply of dry crystalline **166** was unwillingly stored at ambient temperature for more than one year and was thereafter completely transformed to crystalline **167**. However, 25 g of crystalline **166** in a sealed bottle were also completely transformed to **167** after 5 years in a refrigerator at 4 °C. The corresponding melt reaction of **166** in a DSC scan at 5 °C min⁻¹ was completed in the range of 125–155 °C with an exothermic peak at 146 °C, following the melting endotherm of **166** and followed by the melting endotherm of **167**. The tautomerism has been decided in favor of **167**, as ab initio DFT calculations at the B3LYP/6–31G* level predict the best possible rotamer of **167'** to be higher in energy by 13.2 kcal mol⁻¹ [22] (Scheme 20).

A great multitude of quantitative solid-state additions between anionic nucleophiles and appropriate double bonds can be envisaged, but the field is not explored. The potential may be demonstrated with larger-scale additions of alkoxides (**168**, **170**) to carbon dioxide gas (Scheme 21). Versatile carbonic acid half ester salts (**169**, **171**) ensue for diverse preparative applications in alkylations, carboxylations, and acylations [4, 80]. The experimental technique may be cited. A chromatography column (diameter 4 cm, height 60 cm) with a D3-frit and gas outlet through a drying tube was charged upon glass wool with commercial 97.5% **168a** (250 g, 4.63 mol), 95% **168b** (250 g, 3.68 mol), or 95% **170** (250 g, 2.23 mol) and covered with glass wool. Initially a mixture of CO₂ (250 mL min⁻¹) and N₂ (2.25 L min⁻¹) was applied from the bottom. It created a warm zone of about 50 °C that passed the column in about 1 h. After that, the N₂ stream was halved and the reaction continued until the heat production ceased and such halving was repeated twice again. Finally the N₂ flow was removed and the now cold column left closed with pure CO₂ overnight. The weight increase (without correction for losses due to initially present ROH contents) was 191 g (97%), 154 g (95%), and 90 g (92%), and the fill volume increase 29, 45, and 56%, respectively. The pH values of aqueous solutions of the products varied from 8.5 to 9. Titration after decomposition with aqueous H₂SO₄ gave content values between 97 and 102% of the versatile reagents **169a**, **169b**, or **171**.

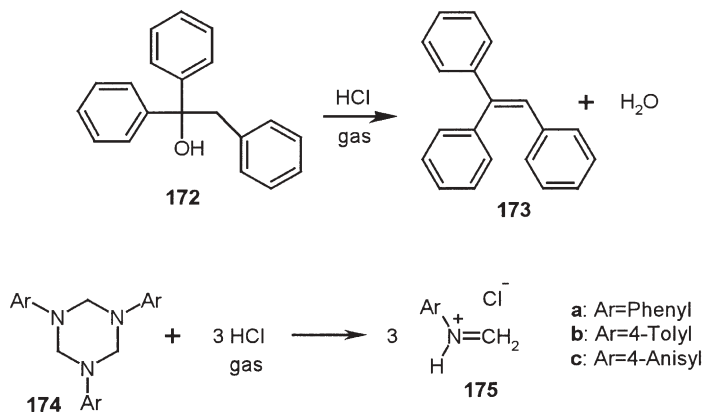


Michael additions to electron-poor alkenes are treated separately in Sect. 20.

11 Elimination

Eliminations belong to one of the most diverse reaction types [76] and numerous solvent-free pyrolyses (sometimes quantitative melt reactions) provided useful syntheses [58, 81–87]. However, quantitative solid-state eliminations are rare (examples are found in the halogenations of **110**, **112**, and **114** (Scheme 12)). If an elimination reaction cannot be performed purely thermally or photochemically, usually a catalyst or other auxiliary has to be added and it is then no longer waste-free.

The dehydration of solid alcohol **172** provides a 100% yield of solid triphenylethylene **173** upon the catalytic action of HCl gas in a desiccator [88] (Scheme 22). Further examples of that type may have provided liquefied product.



Scheme 22

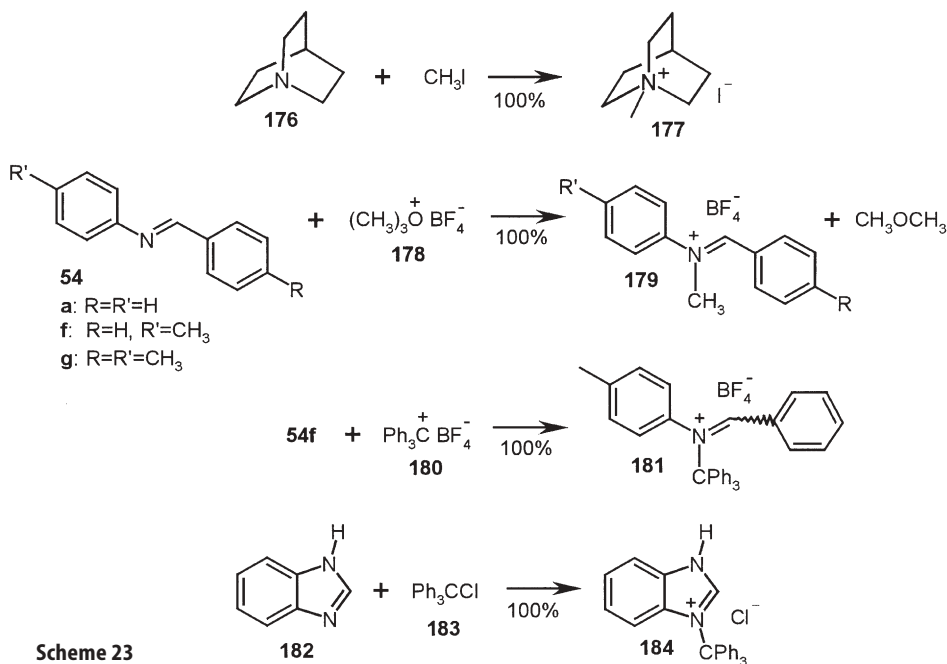
N-arylmethylenimine hydrochlorides are new highly reactive reagents that only exist in the solid state. They are easily and quantitatively obtained by *cyclo*-[1,2,(3)4,(5)6] elimination [76] (also termed [2+2+2] cycloreversion) of the hexahydrotriazine under the action of gaseous HCl at low temperature [10]. The hexahydrotriazines **174a–c** (3.00 mmol) were cooled to -18 , -10 , and -10 °C, respectively, in an evacuated 500-mL flask. HCl gas (500 mL, 1 bar) was let in through a vacuum line in six portions during 2 h or continuously through a stopcock in 3 h. Excess gas was evaporated after thawing to 4 °C and 8 h rest. Yellow **175a**, orange **175b**, and brown **175c** solids were obtained with quantitative yield (Scheme 22). The versatile iminium salts **175** are only stable in the solid state and should be used for aminomethylations soon after their preparation. Gas–solid or solid–solid hydrolysis produces the corresponding Troeger’s bases [10, 89].

A cyclizing elimination of water is described in Sect. 13.2: heating of **220** gives quantitatively **221** in the solid state (Scheme 28).

12

Alkylation

Solid tertiary amines and imines may be quantitatively alkylated by gas–solid and solid–solid techniques. Methylation of quinuclidine (**176**) to give the methoiodide **177** is achieved waste-free by exposure of **176** to a stoichiometric amount of methyl iodide vapor (Scheme 23). Difficulties with the disintegration of the crystals of **177** from those of **176** (reaction step 3) are overcome by ultrasound treatment from a cleaning bath at 20 °C [22]. Numerous applications of this technique to tertiary amines can be envisaged. However, solid Troeger's base (with interlocked layers, i.e., no possibility for molecular migrations) is not alkylated by methyl iodide vapor unless an excess of the vapor is applied to induce intermediate (partial) liquefying of the solid [22].

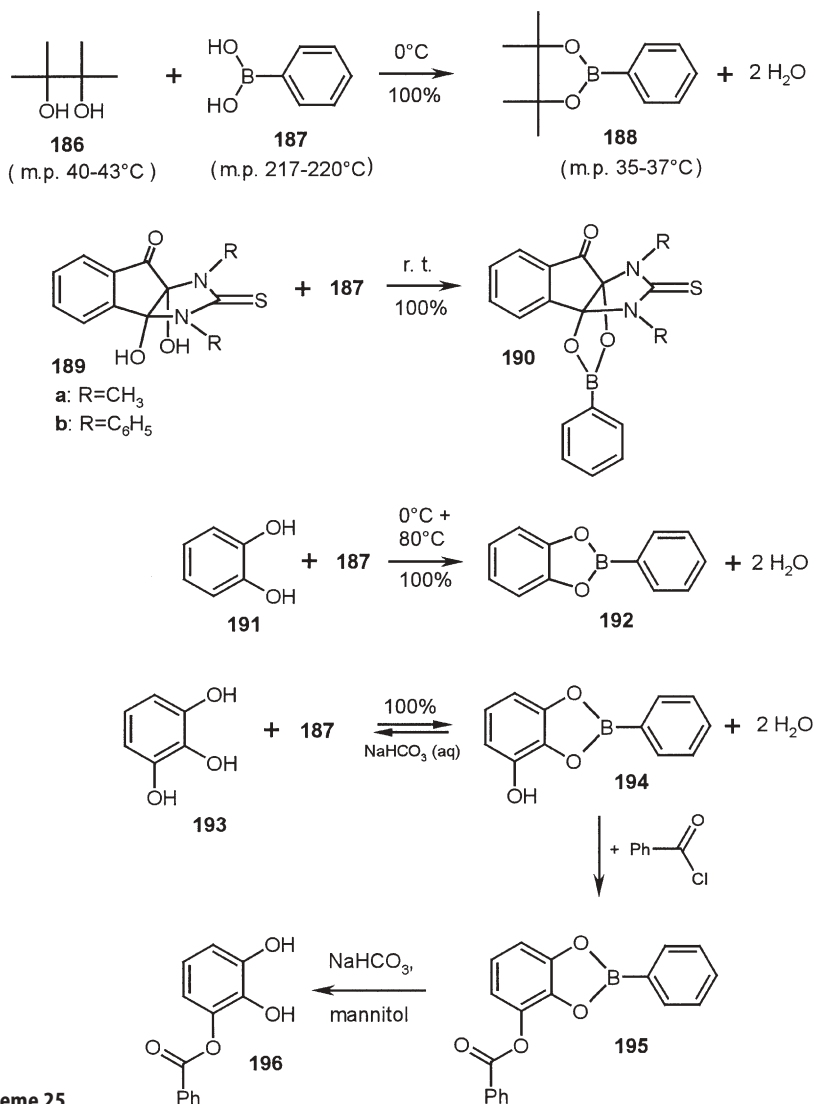


Scheme 23

Of particular interest are quantitative syntheses of extremely deliquescent and reactive alkyliminium salts by milling of solid imines with oxonium salts (**178**), triphenylmethylium tetrafluoroborate (**180**), or triphenylmethyl chloride (**183**) (dry atmosphere in these cases). The sensitive salts **179**, **181**, and **184** are formed in pure form without any waste by an easy experimental technique [10]. Precisely weighed samples of **178** (ca. 2 mmol), **180** (ca. 1 mmol), or **183** (1.00 mmol) were placed in a ball-mill under argon together with the precise equivalent of **54a,f,g**, or **54f**, or **182**, respectively. The Teflon gasket was closed

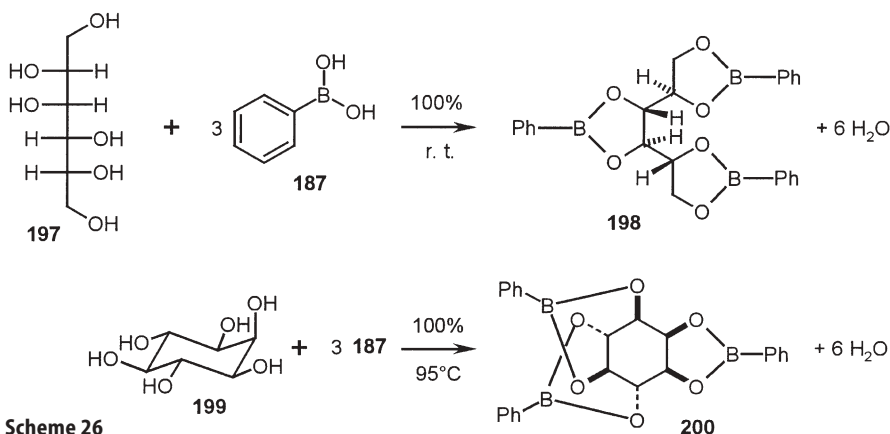
These are powerful protection reactions. An example is given for the synthesis of 1-benzoyl-pyrogallol (**196**) starting with pyrogallol (**193**) that is quantitatively converted to its borolic ester (**194**) by stoichiometric milling with **187**. The free hydroxy group in **194** is benzoylated to give the derivatized borolic ester **195**, which is finally deprotected by treatment with mannitol in aqueous sodium hydrogen carbonate [90]. Generally, the deprotection of borolic esters succeeds under very mild conditions.

Very profitable are solid-state reactions of polyols. D-Mannitol (**197**) reacts quantitatively at room temperature with three molecules of phenylboronic acid



Scheme 25

(**187**) in the ball-mill to give the 1:2,3:4,5:6 product **198** with 2*R*,3*R*,4*R*,5*R* configuration as a nonsticky powder [90] (Scheme 26). This fully protected manitol is now available with great ease as the water can be removed by drying in a vacuum at 80 °C. The same is true for the stoichiometric synthesis of the fully protected *myo*-inositol *rac*-**200**. It is obtained by milling of **199** with three molecules of **187** at 95 °C. The *meso* compound **199** provides specifically the racemate of **200** with one five-membered and two six-membered rings. In both syntheses the six equivalents of the couple product water are taken up by the crystal lattice of the tris-borolic esters [90]. These fully specific reactions in highly complicated lattices with multiple hydrogen bonds are remarkable.

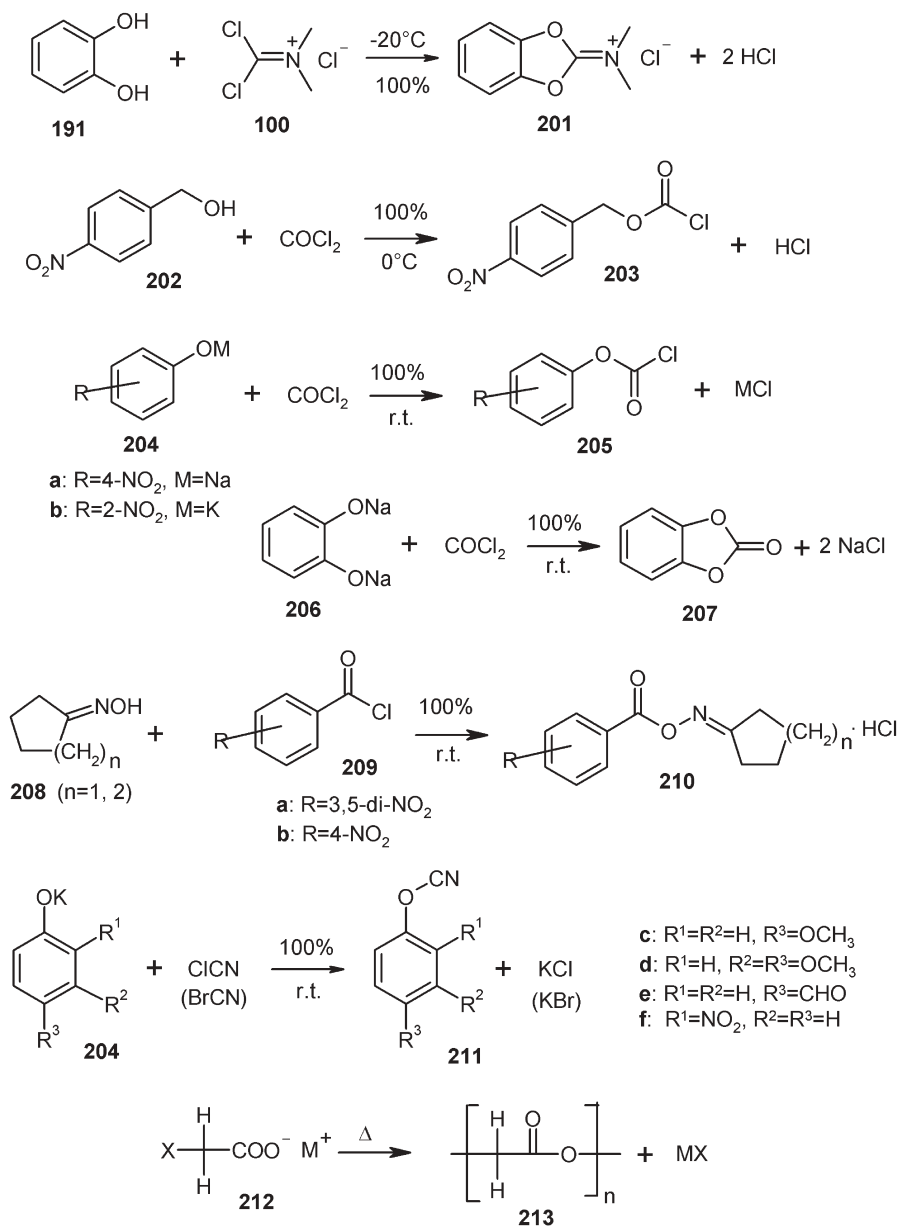


Scheme 26

Highly reactive ketene iminium salts such as **201** are easily accessible, for example, by stoichiometric milling of **191** with **100** [9] (Scheme 27). Also, the quantitative gas–solid reactions of benzylic alcohols (**202**) or alicyclic alcohols like 1*S*-(–)-borneol and phenolates (**204**) with phosgene are of high preparative importance [91]. If the disodium salt of pyrocatechol (**206**) is reacted with phosgene the carbonate **207** arises. Reactions with the poisonous phosgene are particularly safely handled if solvents are avoided. The quantitative esterifications of high-melting alcohols or phenolates are attractive examples, as only HCl or sodium (potassium) chloride are formed as easily removable stoichiometric coproducts. Stoichiometric co-milling of cholesterol and oxalic acid at 90 °C gives 100 % of the diester and H_2O [22]. Versatile oxime esters **210** are obtained by milling of oximes (**208**) and acid chlorides (**209**) [91].

Also, the hard to get in pure form cyanates (**211**) have been quantitatively obtained by reacting cyanogen chloride (gas–solid) or cyanogen bromide (solid–solid) with phenolates, washing away the salts and drying [92] (Scheme 26).

True solid-state reactions without liquids are exothermically obtained upon heating of halogenoacetate salts (**212**) to 100–200 °C. Quantitative yields of polyglycolide matrices (**213**) with cubic holes after washing with water (when the MX dissolved away) were obtained [93] (Scheme 27).

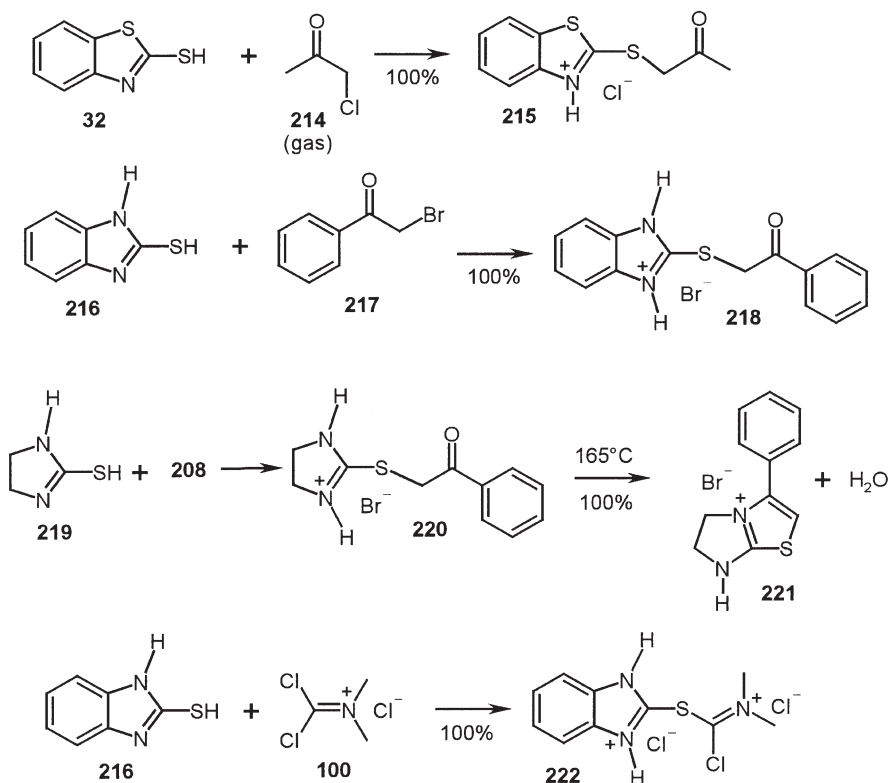


Scheme 27
 M: Na K Na Ag K
 X: Cl Cl Br Br I

13.2

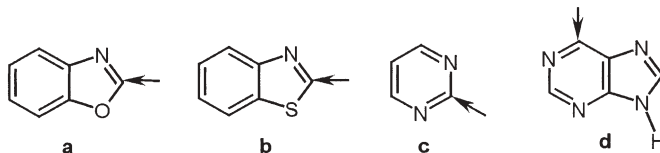
Thiols and Thiolates

Thiols and thiolates are particularly versatile in quantitative solid-state substitutions. Thus, the solid heterocyclic thiols **32**, **216**, and **219** react with gaseous (**214**) and solid (**217**) acyl halides to give the thiuronium salts **215**, **218**, and **220** [10] (Scheme 28). The thiuronium salt **220** undergoes an interesting cyclization reaction with loss of water upon heating to 165 °C for 1 h. A quantitative yield of **221** is obtained without melting [10]. The solid–solid reaction (milling) of Viehe salt (**100**) with **216** gives the highly substituted doubly charged thiuronium salt **222** at room temperature, again waste-free [10].



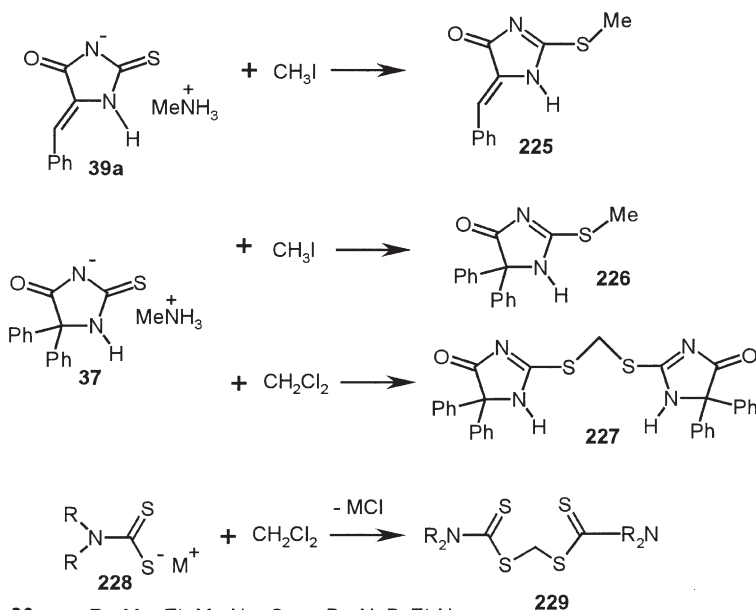
Scheme 28

For the quantitative synthesis of thiocyanates by reaction with cyanogen chloride or cyanogen bromide it is essential to start with thiolates instead of thiols. The product salts are then removed by washing of the products with water. Thus, the various heterocyclic thiocyanates **224a–d** are easily obtained in pure form by either gas–solid (ClCN) or solid–solid (BrCN) reaction [92] (Scheme 29).



Scheme 29

Volatile alkyl halogenides such as methyl iodide, methylene chloride etc., react quantitatively with the solid methylamine salt of 5-benzylidene- (39a) [32] and 5,5-diphenylthiohydantoin (37) to form the anticonvulsive solids 225 and 226 in quantitative yield [28] (Scheme 30). Unlike the solution reaction, only the S-alkylation occurs under gas-solid conditions. Furthermore, various dialkylamidodithiolate salts 228 react readily with dichloromethane at 80 °C. The salts with the quaternary cations react at room temperature and it is also possible to catalyze the reaction of the sodium salt by admixture of 10% of the corresponding “phase transfer bromides” [28]. These reactions have been tuned for removal of dichloromethane from loaded air streams [28].

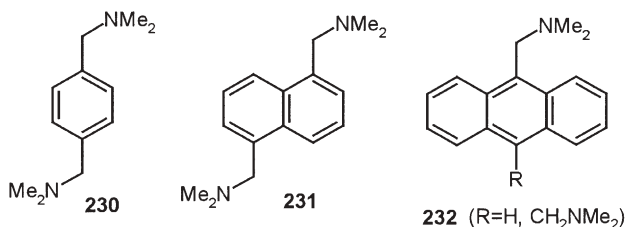
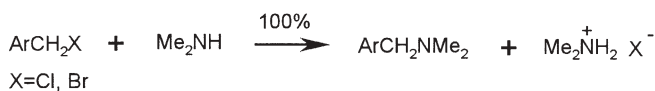


Scheme 30

13.3

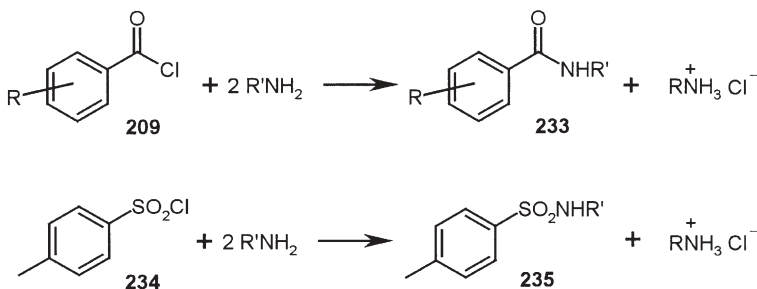
Amines and Amide Anions

Solid benzylic halogens are easily substituted with gaseous dialkylamines. Monoalkylamines are less suitable for uniform reactions due to secondary substitution of the initial product by the benzylic halide present. Some characteristic 100% yield conversions are listed in Scheme 31. The benzene (**230**) and naphthalene derivatives (**231**) started from the solid bromides, the anthracene derivatives (**232**) from the solid chlorides [22].



Scheme 31

Quantitative stoichiometric gas–solid or solid–solid (these at 0 °C) acylations of amines with acid chlorides are varied (Scheme 32). However, for a clean reaction the liberated hydrochloric acid has to be neutralized by an additional gaseous or solid base that may also be a second mole of the amine. The reactions are performed in an evacuated flask or in a ball-mill, respectively. There are only minimal losses of the amides or sulfonamides upon removal of the stoichiometric coproduct with water [91]. The solid–solid reactions can be turned into sustainable 100% yield processes with optimal atom efficiency by milling stoichiometric 1:1:1 mixtures of acid chloride, aniline derivative, and K_2CO_3



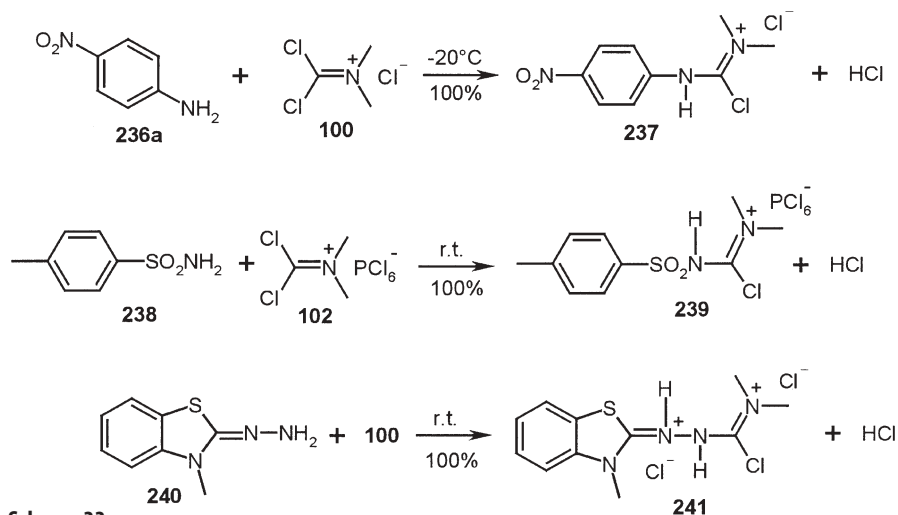
Scheme 32

Table 5 Quantitative acylations of amines by gas–solid and solid–solid reactions

| Acid chloride | Amine | m.p. (°C) | Amide | m.p. (°C) |
|---------------------|--|-----------|-------|-----------|
| 209a: R=3,5-dinitro | NH ₃ | gas | 233a | 175 |
| 209a: R=3,5-dinitro | MeNH ₂ | gas | 233b | 145 |
| 209a: R=3,5-dinitro | EtNH ₂ | gas | 233c | 123 |
| 209b: R=4-nitro | NH ₃ | gas | 233d | 140 |
| 209b: R=4-nitro | MeNH ₂ | gas | 233e | 214 |
| 209b: R=4-nitro | EtNH ₂ | gas | 233f | 149 |
| 209a: R=3,5-dinitro | 4-MeC ₆ H ₄ NH ₂ | 41–46 | 233g | 283 |
| 209a: R=3,5-dinitro | 4-MeOC ₆ H ₄ NH ₂ | 57–60 | 233h | 237 |
| 209a: R=3,5-dinitro | 4-ClC ₆ H ₄ NH ₂ | 68–71 | 233i | 235 |
| 209a: R=3,5-dinitro | 4-BrC ₆ H ₄ NH ₂ | 62–64 | 233j | 249 |
| 209a: R=3,5-dinitro | 1-NaphNH ₂ | 48–50 | 233k | 270 |
| 209b: R=4-nitro | 4-MeC ₆ H ₄ NH ₂ | 41–46 | 233l | 200 |
| 209b: R=4-nitro | 4-MeOC ₆ H ₄ NH ₂ | 57–60 | 233m | 195 |
| 209b: R=4-nitro | 4-ClC ₆ H ₄ NH ₂ | 68–71 | 233n | 229 |
| 209b: R=4-nitro | 4-BrC ₆ H ₄ NH ₂ | 62–64 | 233o | 245 |
| 209b: R=4-nitro | 1-NaphNH ₂ | 48–50 | 233p | 173 |
| 234 | NH ₃ | gas | 235a | 137 |
| 234 | MeNH ₂ | gas | 235b | 77 |
| 234 | EtNH ₂ | gas | 235c | 63 |

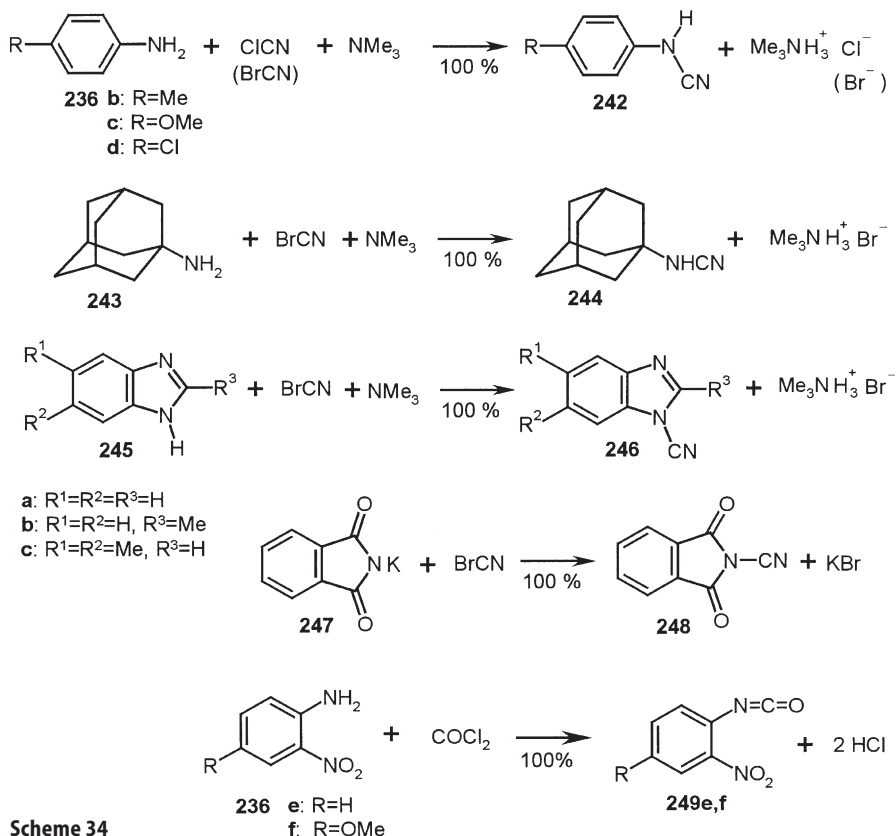
followed by aqueous washings [22]. The quantitatively obtained amides **233** or **235** are listed in Table 5 [91].

The solid-state reactions of Viehe salt (**100**) with primary amine functionalities (**236**, **238**, **240**) leads to highly substituted iminium salts in quantitative



yield without waste. Thus, compounds **237**, **239**, and **241** are easily prepared (Scheme 33). The mill is charged under dry atmosphere [9].

The solid-state reactions of cyanogen chloride or cyanogen bromide with the primary and secondary amines **236**, **243**, and **245** require the addition of an inert base such as trimethylamine if quantitative reactions are desired. Solid volatile BrCN may be reacted via the gas phase in the chosen setup that gives quantitative yields of the cyanamides **242**, **244**, and **246** after removal of the amine salts [92] (Scheme 34). The crystalline substrate **236a–c**, **243**, or **245a–c** (10 mmol) was placed in a 500-mL flask which was evacuated and filled with a 1:1 mixture of ClCN and trimethylamine (11.7 mmol each), or it was placed in an evacuated 250-mL wide-necked flask connected to a 250-mL wide-necked flask with freshly sublimed BrCN (1.17 g, 11.0 mmol). Trimethylamine (0.5 bar, 11.7 mmol) was added through a vacuum line. A magnetic spin bar was rotated in the flask in order to mix the gases and the system was left overnight at room temperature. Excess gas was pumped to a cold trap at 77 K. The trimethylammonium chloride (bromide) was removed by washing with water. The yield of **242**, **244**, or **246** was quantitative in all cases. Furthermore, the reaction of ball-

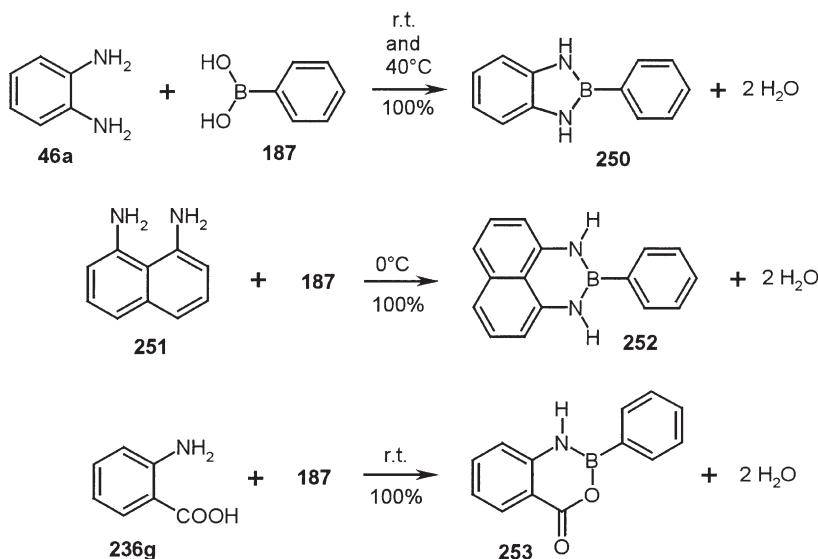


Scheme 34

milled potassium phthalimide (**247**) with BrCN gas in a vacuum provides a quantitative yield of the cyanimide **248** [92]. These appear to be the best and most convenient procedures for the preparation of these pure compounds.

The gas–solid reactions of anilines with phosgene experience similar difficulties as the corresponding solution reactions, giving product mixtures of carbamoyl chlorides, isocyanates, and diarylureas. It was, however, possible to get product specificity by reacting *o*-nitroanilines with gaseous phosgene. Thus, **236e,f** provide quantitative yields of the isocyanates **249e,f** without producing wastes as the couple product HCl can be collected for further use [91] (Scheme 34).

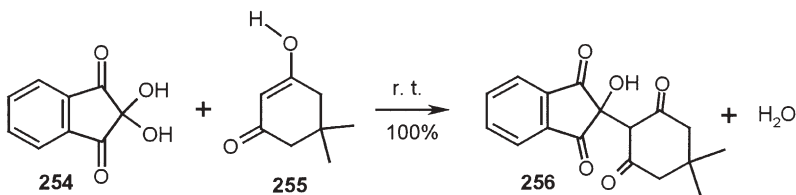
Interestingly, primary aromatic amino groups substitute the hydroxyl groups of phenylboronic acid with great ease in the solid state. Cogrinding of **46a** and **187** followed by heating to 40 °C leads to a quantitative yield of **250**. The compounds **252** and **253** are quantitatively obtained by ball-milling of **251** (0 °C) or **236g** (r.t.) with **187** [90] (Scheme 35). Both the amino and the carboxyl group participate in the reaction of anthranilic acid. The products lose the water of reaction at 80, 50, and 80 °C, respectively, in a vacuum without melting. These are protection reactions. The diamines or anthranilic acid can be recovered by mild hydrolysis.



Scheme 35

13.4 Enols

Solid enols such as dimedone (**255**) are able to substitute one of the hydroxyl groups of ninhydrin (**254**) upon milling and give a quantitative yield of the



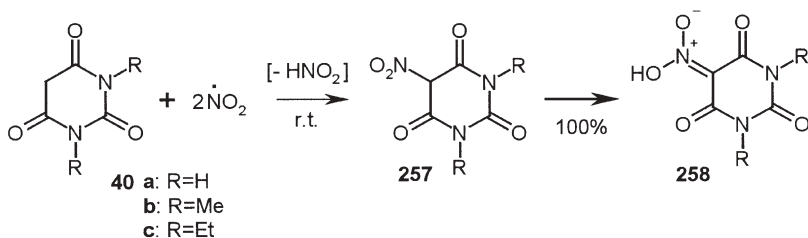
Scheme 36

tertiary alcohol **256** [94] (Scheme 36). This appears to be a rare reaction type which merits further exploration.

13.5

Radicals

Free radicals may substitute C–H bonds. Gaseous NO_2 (0.3 bar) has been tested with solid barbituric acids (**40a–c**). Reactions with 100% yield arise after 4 h exposure and the dried products (80 °C) assume the *aci*-nitro forms **258a–c** [19] (Scheme 37). A very large field for preparative use appears to be opened with these and related waste-free reactions. The couple product N_2O_3 can be collected for further use.



Scheme 37

13.6

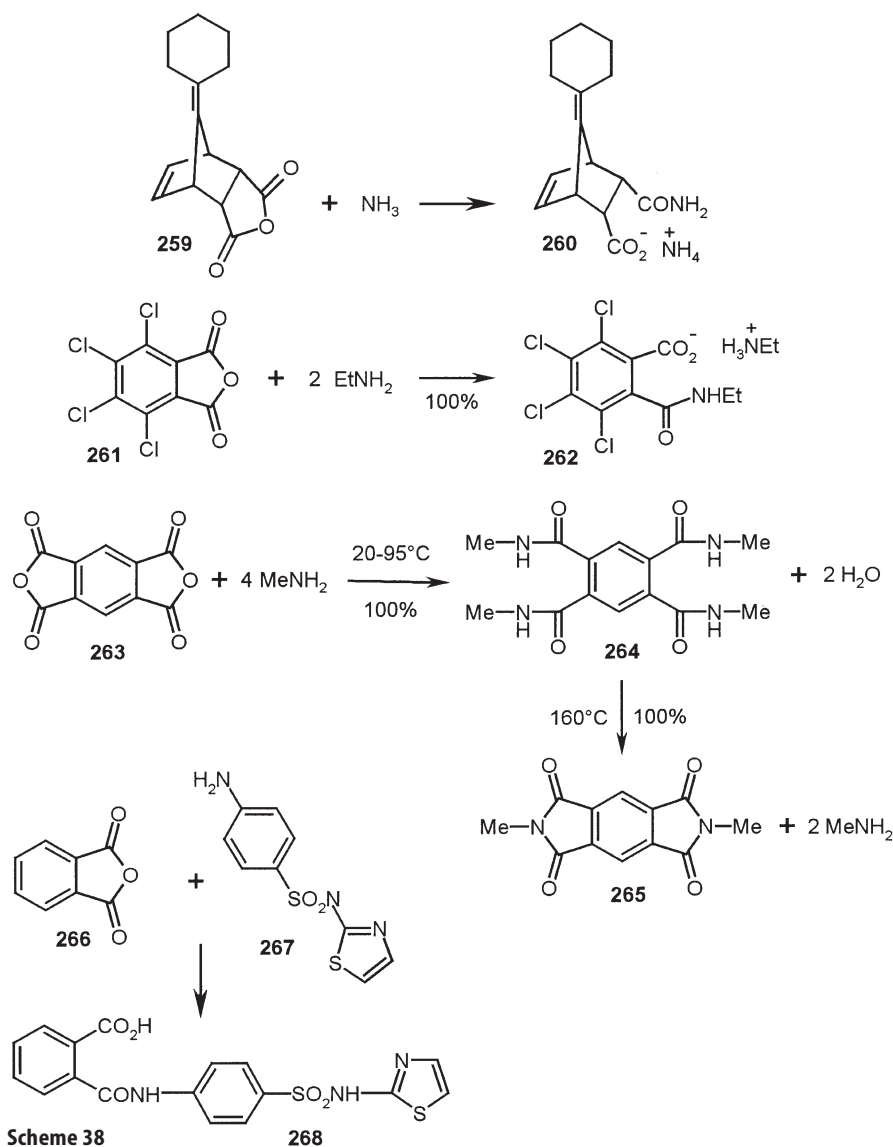
Ring-Opening Substitution of Acid Derivatives

Most important are quantitative solid-state reactions of cyclic carbonic acid derivatives with gaseous or solid amines. These give open-chain amides that can be recycled in various cases to new products of preparative interest.

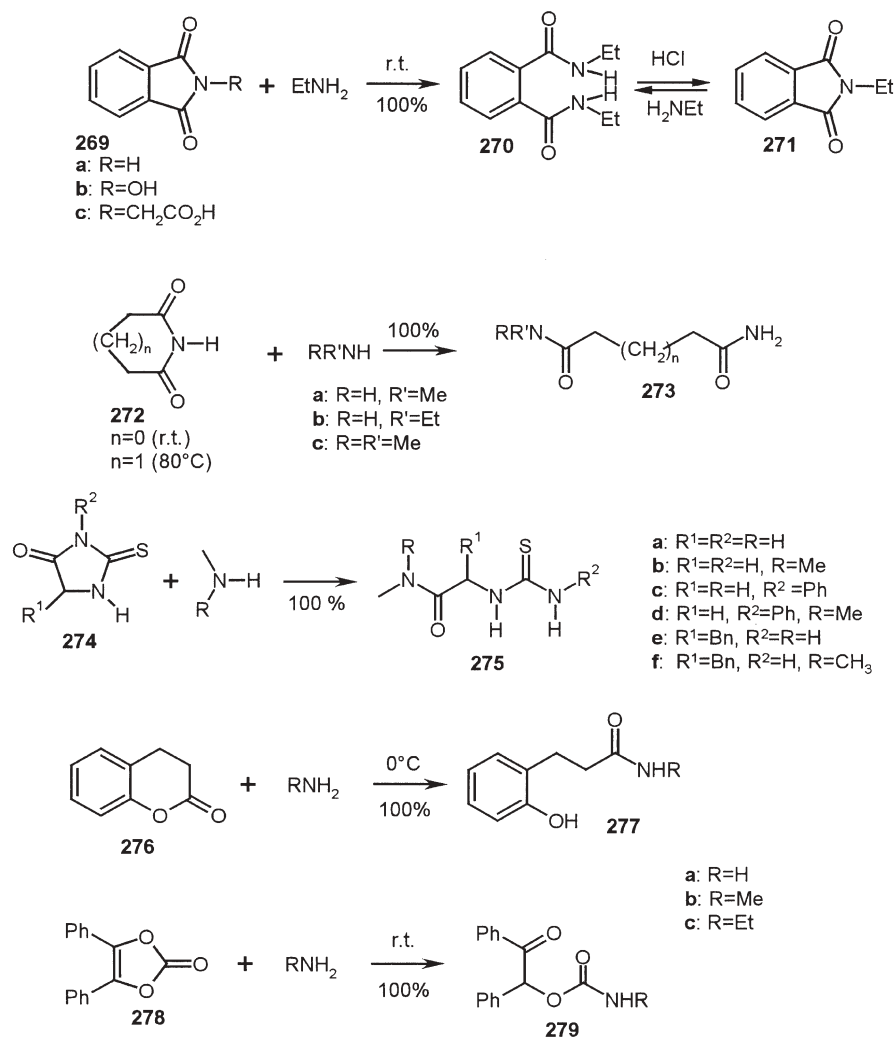
Solid cyclic carboxylic anhydrides react with gaseous ammonia to give ammonium salts with quantitative yield. This has been observed with the labile Diels–Alder adduct **259** [25] (Scheme 38). Aliphatic amine vapors are equally able to open anhydride rings to form the amide salts from where the free amide acids can be obtained in 100% yield. The reaction of **261** with ethylamine to give **262** is an example of a large-scale preparative application [11–12]. Conversely, solid pyromellitic bis-anhydride (**263**) and methylamine vapor react exothermally (rise to 95 °C) and quantitatively to yield the tetraamide **264**. Interest-

ingly, **264** cyclizes in a thermal solid-state reaction at 160 °C to give the bis-imide **265** also with 100% yield [12].

The antibacterial sulfonamide phthalazole **268** is obtained free of imide and bisamide side products (that occur upon reaction in solution or in the melt) if stoichiometric solid-state milling of the reactants **266** and **267** is performed for the acylation [95] (Scheme 38). Numerous solid arylamines and heterocyclic amines react correspondingly with phthalic anhydride upon stoichiometric milling and provide 100% yield without any workup requirement [22].



Similarly, solid cyclic imides are attacked by gaseous aliphatic amines and lead to open-chain diamides. For example, **269a–c** react with ethylamine gas to give a 100% yield of the diamide **270**, which can be quantitatively cyclized to the *N*-ethylimide **271** by the action of gaseous HCl [12]. As expected, the solid alicyclic imides **272** behave correspondingly and yield the bis-amides **273** in an easy waste-free procedure [12] (Scheme 39).



Scheme 39

A number of solid thiohydantoin **274** react quantitatively and specifically at the C(=O)–N bond with gaseous aliphatic amines to give the versatile [96] thioureido-acetamides **275** [31]. These reactions proceed equally well with sec-

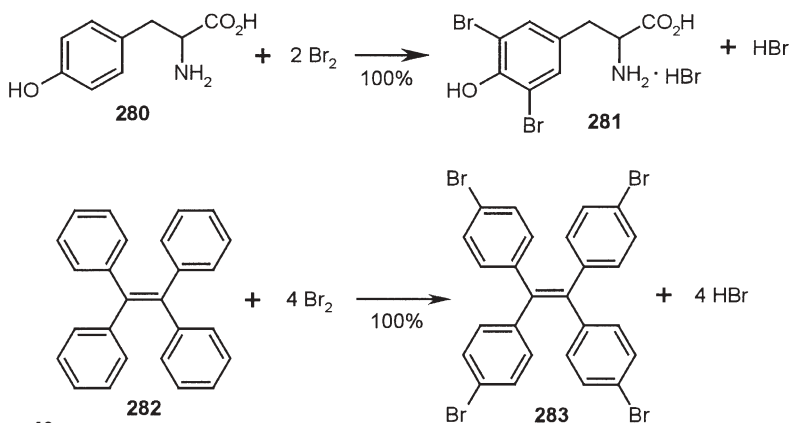
ondary and allyl or propargyl amines, and 29 preparative 100% yield gas–solid conversions have been realized [32].

Solid lactones or cyclic carbonates form linear hydroxy amides upon reaction with gaseous ammonia, methylamine, or ethylamine. For example, the compounds **277a–c** and (ketonized) **279a–c** are quantitatively formed at 0 °C and room temperature, respectively, without melting [12] (Scheme 39).

14

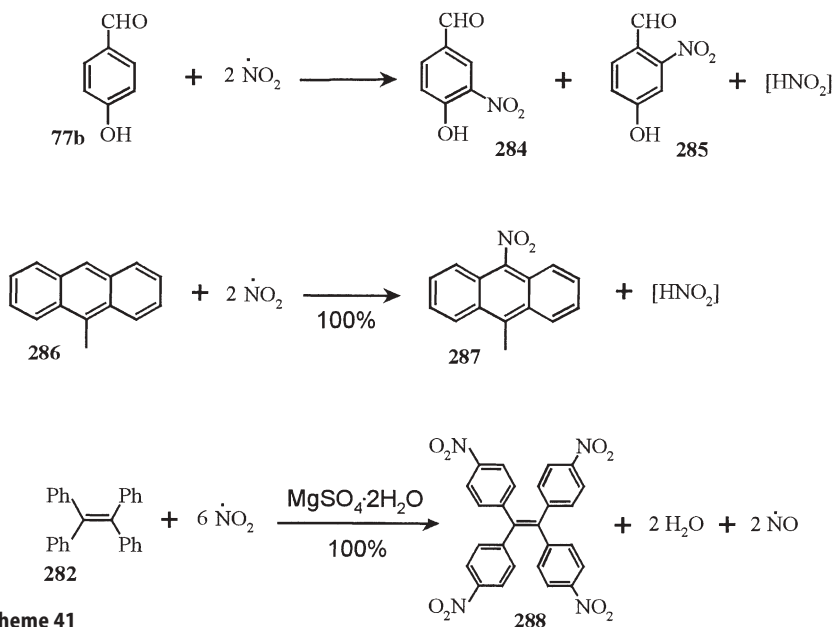
Aromatic Substitution

A very old gas–solid bromination of tyrosine (**280**) [97] has been revisited and it gave a quantitative yield for the reaction of *rac*-**280** [22]. The doubly brominated hydrobromide *rac*-**281** is spectroscopically pure after removal of included gases at 50 °C in a vacuum. Quite spectacular is the specific and quantitative waste-free gas–solid tetrabromination of tetraphenylethylene (**282**), which shows some signs of autocatalysis and requires rotation of the flask around a horizontal axis at room temperature for 12 h as the reactant and product gases require mixing [60]. The isomer-free tetrabromide **283** is an attractive starting point for dendrimer syntheses and inclusion studies (Scheme 40). Also 4-bromoantipyrin hydrobromide is quantitatively obtained from antipyrin(hydrobromide) and bromine vapor [22].



Scheme 40

Aromatic gas–solid nitrations with NO_2 gas are not always regiospecific. The reaction of 4-hydroxybenzaldehyde (**77b**) at 0.3 bar of reacting gas gave a 100% yield of a 82/18 mixture of **284** and **285** [19] (Scheme 41). On the other hand, 9-methylantracene (**286**) provides a quantitative yield of compound **287**. Highly spectacular is the quantitative yield of the pure tetra-*p*-nitro derivative **288** upon application of gaseous NO_2 to **282** in the presence of the drying agent $\text{MgSO}_4 \cdot 2\text{H}_2\text{O}$ for removal of the water of reaction that cannot be accommodated



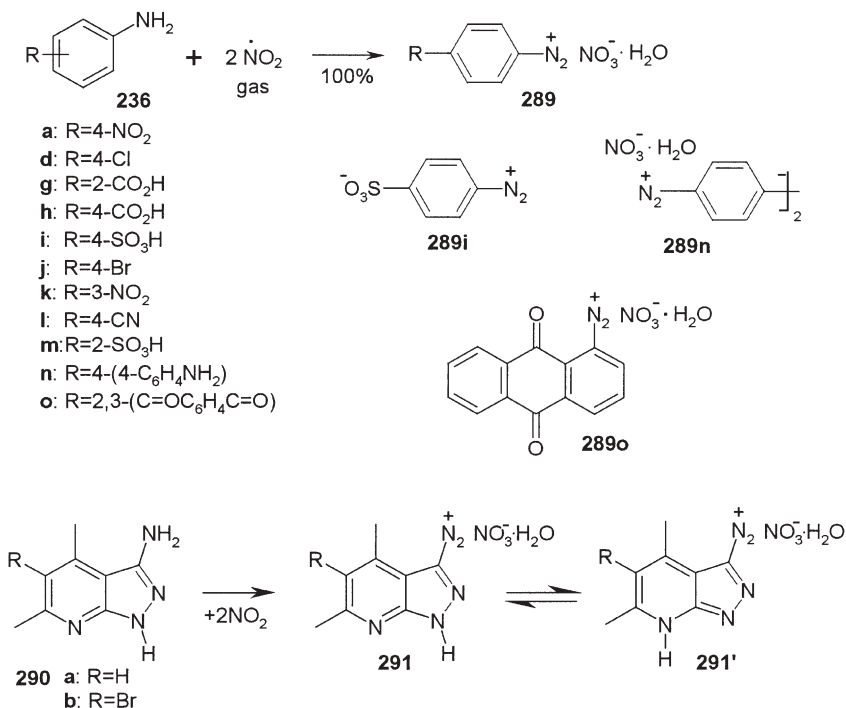
Scheme 41

by the crystal in this case [19]. The yield is 100% if the magnesium salt is dissolved away with water after reaction. The couple product NO can be used in further reactions after reduction of excess NO₂ by NaNO₂ (cf. Sect. 2). For larger-scale runs the use of a flow apparatus is advisable, which allows for circulation of the gas and admixing of the calculated amount of oxygen to oxidize the NO formed for use in the running reaction.

Azo couplings in the solid state are treated in Sect. 17.

15 Diazotization

Solid diazonium salts are explosive upon heating (at least at their melting point) and upon shock (hammer on anvil, grinding over sharp edges, or milling) and should be handled with great care. The easiest way to obtain diazonium nitrates in hydrated form is the action of gaseous NO₂ on solid aniline derivatives. These exothermic diazotizations are waste-free by avoiding strong acid solutions and by 100% yield throughout despite the multistep processes within the crystals [98–100]. A great variety of diazonium nitrates have been prepared. Even very highly substituted heterocycles such as **290** give a quantitative yield of the diazonium salt without nitrosation at one of the other nitrogen atoms (Scheme 42). The prescription should be closely followed for safety reasons:



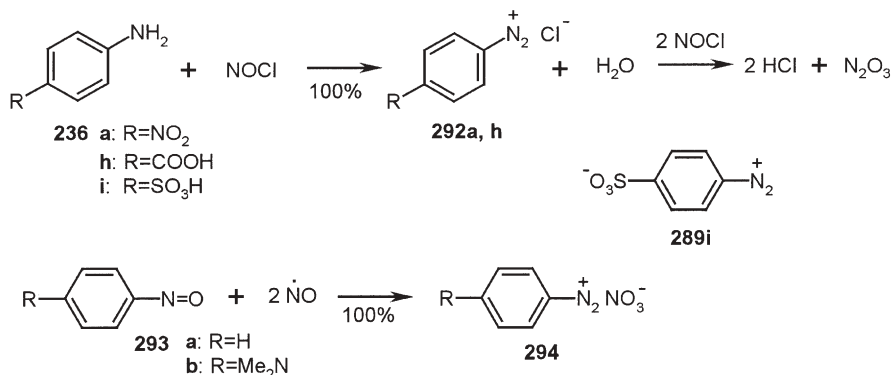
Scheme 42

Caution: solid diazonium salts explode upon heating to the melting point and upon shock or grinding at sharp edges. Do not ball-mill!

The solid aniline derivatives **236** (2.0 mmol; 1.0 mmol of **236n**) were treated with NO_2 gas in an evacuated 50-mL flask at 0°C (**236h,o** at room temperature). NO_2 (460 mg, 10 mmol) from a 250-mL flask was applied through a stopcock in five small portions, each after the brown color of the previous portion had disappeared. Finally, the excess gas was let in and the reaction completed by 6 h rest. Excess gas was recovered by cooling the 250-mL flask to 77 K. Quantitative conversion to the diazonium nitrate hydrates **289/291** (except with **289a** where not all of the water could be accommodated by the crystal: 92%) was secured by weight, spectroscopy, and quantitative coupling with β -naphthol. Compounds **289i,m** were freed from HNO_3 and water at $5 \cdot 10^{-4}$ Torr (12 h) and were obtained as zwitterions. Compound **289a** was purified by washing with ethyl acetate in order to remove unreacted **236a**, a technique that should be applied in all cases where the aniline derivative **236** contained nonpolar impurities that are most easily removed at that stage. Thus, the synthesis of **289o** started with **236o** of 97% purity. Compound **289o** was obtained in pure form by two washings with ethyl acetate. Density functional theory calculations (DFT) at the B3LYP/6-31G* level predict **291a** to be more stable than **291a'** by the

minute amount of $0.53 \text{ kcal mol}^{-1}$. Therefore an equilibrium is assumed but the crystal might prefer one of these tautomers [100] (Scheme 42).

The need for solid anhydrous diazonium chlorides can be complied with gas–solid reactions using NOCl as the reactive gas, and anhydrous diazonium nitrates are obtained by reacting solid aromatic nitroso compounds with nitrogen monoxide gas (Scheme 43). The alternative by reacting solid arylidene anilines with gaseous nitrogen monoxide to give diazonium nitrates and aryl aldehydes did not give quantitative but only good yields [99]. Again, the prescriptions should be closely followed for safety reasons:



Scheme 43

Caution: solid diazonium salts explode upon heating, shock, and grinding at sharp edges!

The solid aniline **236** (1.00 mmol) in an evacuated 250-mL flask was connected via vacuum line to a 250-mL flask that was filled with NOCl (1 bar, 11 mmol). After 24 h, the gases were condensed back into the gas reservoir at 77 K, absorbed in water, and neutralized with NaOH for disposal. The yellow-orange crystals **292a,h** or **289i** were quantitatively obtained.

The nitrosobenzenes **293a,b** (2.00 mmol) in an evacuated 250-mL flask were connected via vacuum line with a 250-mL flask containing NO (1 bar, 11 mmol) that had been freed from traces of NO₂ by storing over 4-chloroaniline. After 24 or 48 h rest in a refrigerator at 4 °C, excess gas was recovered in a cold trap at 77 K. Pure **294** was quantitatively obtained.

16

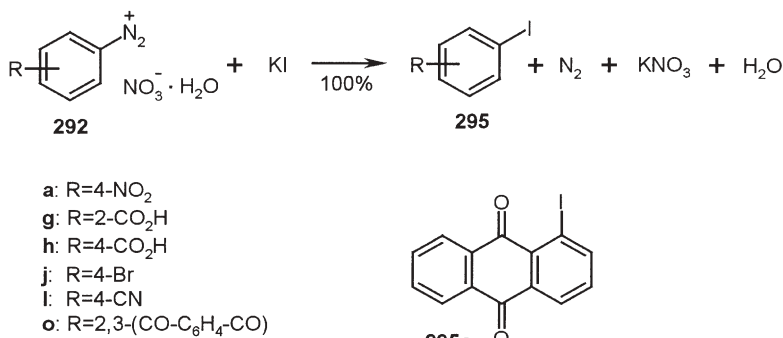
Sandmeyer Reaction

Solid diazonium salts are well suited for reactions in the solid state. They rapidly react with potassium iodide when coground in an agate mortar (without sharp edges!) and give a quantitative yield of the solid aryl iodide after

removal of the potassium salt by washing with water [99]. This is well superior to the normal Sandmeyer technique in solution that provides side products and requires purifying workup of the product mixtures. For safety reasons the prescription should be carefully followed:

Caution: solid diazonium salts are heat- and shock-sensitive; do not ball-mill!

Potassium iodide (830 mg, 5.0 mmol) was finely ground in an agate mortar and the diazonium salt **292** (0.50 mmol) added in five portions and coground for 5 min each. After a 24-h rest with occasional grinding, the diazonium band in the IR spectrum had completely disappeared. The potassium salts were removed by washing with cold water. The yield of pure aryl iodide **295** was 100% throughout (Scheme 44).



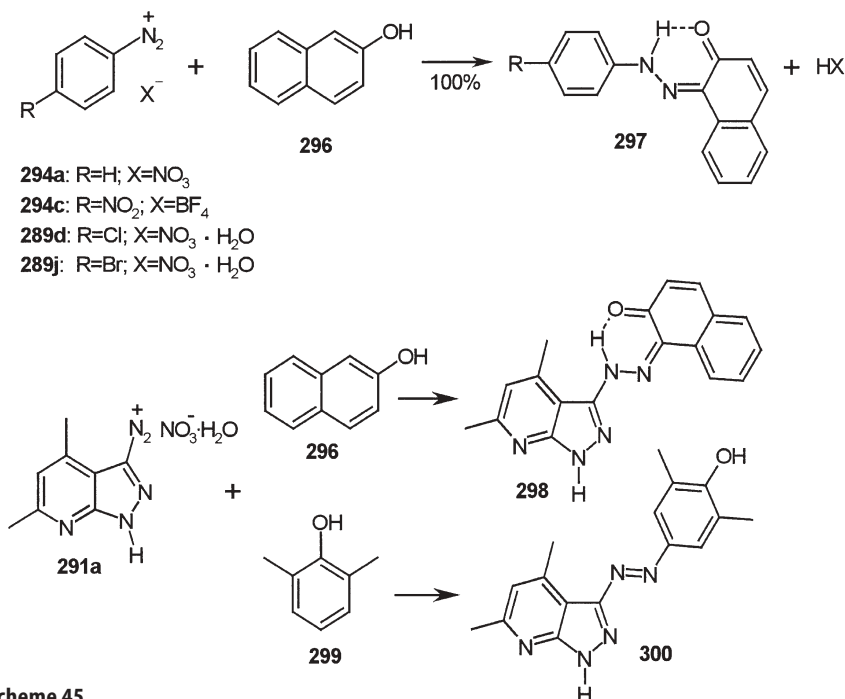
Scheme 44

17 Azo Coupling

Equally popular are azo couplings of diazonium salts that keep the nitrogen atoms in the product. The solid–solid version is very suitable with appropriate phenols such as **296** and **299**. The waste-free and quantitatively obtained “azo dye” salts can be neutralized. The free dyes have the hydrazone structure (**297**, **298**) or the azo structure (**300**) [99–100] (Scheme 45). The prescription should be carefully followed for safety reasons:

Caution: these reactions might occur violently; use a smooth agate mortar and do not ball-mill!

Solid diazonium salt **294** or **289** (0.50 mmol) and β -naphthol (**296**; 0.60 mmol) were separately ground in agate mortars and cautiously mixed. In the case of **289j** the drying agent $\text{MgSO}_4 \cdot 2\text{H}_2\text{O}$ (0.50 mmol) was added to the mixture. The mixtures were rested for 24 h in test tubes and were then exposed to ultra-

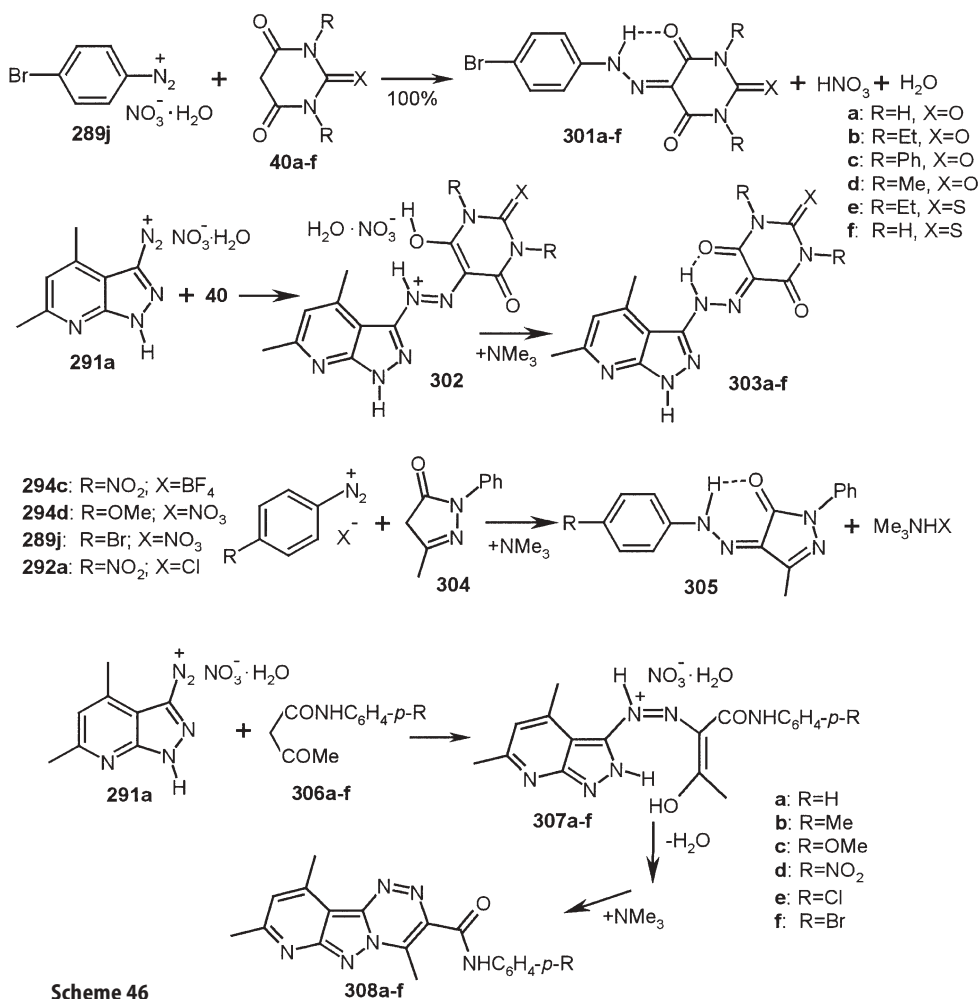


sound for 24 h in a cleaning bath at 20 °C. The quantitatively obtained azo dye salts **297**·HX were neutralized and freed from excess **296** by washing with 0.5 N -NaOH (20 mL) and water (20 mL). The yields of the neutral dyes with the hydrazono structure **297** were 100, 98, 99, and 99%, respectively. The analogous procedure was applied for the syntheses of **298** and **300**, giving 100 and 98% yield, respectively, after the washings [100].

Azo couplings with C–H acidic compounds such as barbituric acids (**40**) or pyrazolones (**304**) proceed equally quantitatively in the solid state. However, in some combinations a basic catalyst has to be added in the form of gaseous trimethylamine in order to speed up the reaction. The free azo dyes occur in the hydrazono form after washing away the unavoidable stoichiometric salts [99–100] (Scheme 46). The prescription should be carefully followed for safety reasons:

Caution: solid diazonium salts are heat- and shock-sensitive; do not ball-mill!

The barbituric acid derivative **40a–f** (0.50 mmol) was ground in an agate mortar. Solid diazonium salt **289j** (0.50 mmol) was added and coground in five portions for 5 min each. Most of the diazonium band at 2280 cm^{−1} had disappeared, but completion of the reaction was achieved by 24 h ultrasound application in a test tube. After neutralization (0.5 N NaOH, 20 mL), washing (H₂O), and



Scheme 46

drying, the quantitatively obtained products **301a-f** assume the hydrazono structure.

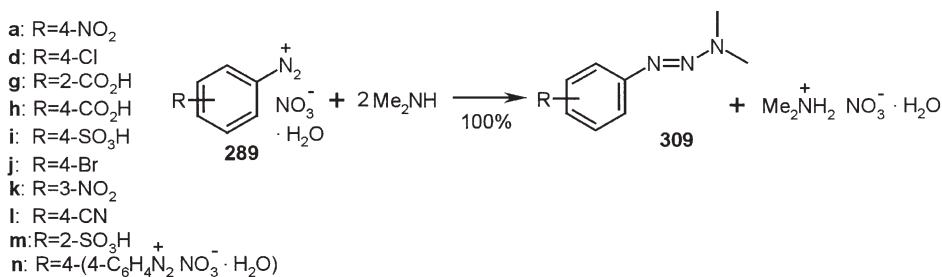
Similarly, the barbituric acids **40a-f** (1.00 mmol) were coground with five portions of **291a** (1.00 mmol in total). The mixture was transferred to a 100-mL flask which was then evacuated. Me_3N (0.5 bar) was let in. After 12 h at room temperature, excess gas was recovered in a remote trap at 77 K. The salt was washed away with water (20 mL) and the residual solid dried. The yields were 100, 100, 100, 100, 98, and 99%, respectively.

The pyrazolone **304** (1.00 mmol) and the solid diazonium salt **294c,d**, **289j**, or **292a** (1.00 mmol) were cautiously coground in an agate mortar for 5 min. The mixture was transferred to a 100-mL flask which was then evacuated. Me_3N (0.5 bar) was let in. After 12 h at room temperature, excess gas was recovered

in a remote trap at 77 K. The salt was washed away with water (20 mL) and the residual solid dried. The yield was 98–99% of pure **305** with the hydrazono structure in all cases.

An interesting cyclization reaction has been observed after the solid-state coupling of diazonium salt **291a** with the acetoacetanilides **306a–f** (Scheme 46). Thus, quantitative yields of the pyridopyrazolotriazines **308a–f** occur with 100% yield (except **308b,c** where there is a loss of 1% by the washings) upon the action of trimethylamine on the intermediate **307a–f** [100]. The experimental technique (2.00 mmol runs) is the same as with the syntheses of **303a–f**.

Azo couplings of diazonium salts with primary or secondary amines give triazenes which are normally hard to get in pure form. It is, however, quite easy to get triazenes with aliphatic or aromatic amines if solid-state techniques are applied that give rise to pure products in quantitative yield [98–100]. The dimethyltriazenes **309** have been quantitatively obtained by very cautious addition of gaseous dimethylamine (exothermic!) [98] (Scheme 47). Extreme care has to be taken for safety reasons:



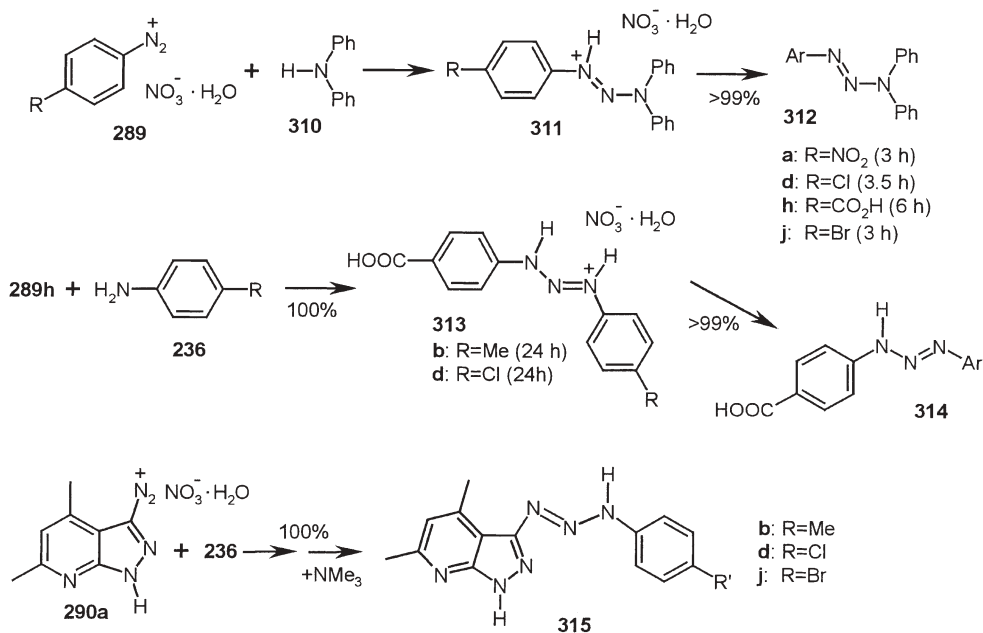
Scheme 47

Caution: these reactions may occur violently; use protecting shield!

The diazonium nitrate (**289**, 0.70 mmol; **289n**, 0.35 mmol), the zwitterion (**289i,m**; 0.70 mmol), or 4-nitrophenyldiazonium tetrafluoroborate (**294c**·BF₄; 0.70 mmol) in an evacuated 250-mL flask was cautiously treated with dimethylamine (**289g–i,m** and **294c**·BF₄ at room temperature; **289a,d,e,j,k,n** at 0 °C): slow application was obtained by connecting to an evacuated flask with 70 mg (1.56 mmol) Me₂NH cooled to 77 K and then removing the liquid nitrogen bath, for security reasons behind a protecting shield. After the consumption of the amine, the slight excess of gas was condensed back to the other flask and a quantitative reaction was secured by weighing. The triazenes **309** were extracted from the dimethylammonium salts with dry EtOAc and evaporated. The purity was checked with m.p. and by spectroscopic techniques.

The reactions of solid diazonium salts with solid aromatic amines are less violent and the aryldiphenyltriazene salts **311** or the 1,3-bis-aryltriazene salts **313** and **315**·HNO₃ are quantitatively obtained upon cautious cogrinding

(Scheme 48). From there, neutralization leads to the free triazenes **312**, **314**, and **315** with insignificant losses (<1%) [99–100]. The compounds **315** are almost isoenergetic with their tautomers as formed by 1,3-H shift to the other N atom according to DTF calculations at the B3LYP/6–31G* level [100]. The precautions during grinding should be followed for safety reasons:



Scheme 48

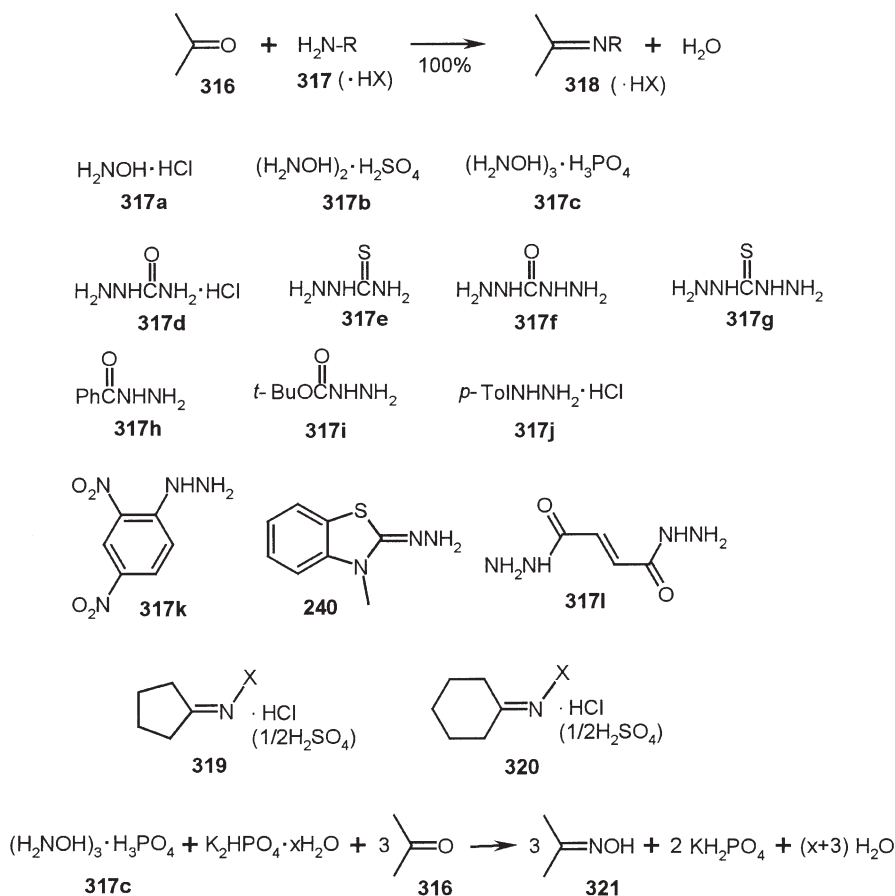
Caution: solid diazonium salts are heat- and shock-sensitive; do not ball-mill!

Diphenylamine (**310**; 1.00 mmol) or substituted aniline (**236b,d**; 1.00 mmol) was ground in an agate mortar. The diazonium salt (**289a,d,h,j**; 1.00 mmol) was added in five portions and coground for 5 min. To complete the reaction, the solid mixture was transferred to a test tube and then exposed to ultrasound in a cleaning bath, the temperature of which was maintained at 20–25 °C for the time given, when all of the diazonium band in the IR had disappeared. The triazenum salts **311** or **313** were obtained quantitatively. The free triazene bases **312** or **314** were obtained by trituration of their salts with 0.1 N NaOH (20 mL), filtering, washing (H₂O), and drying. The yield was >99% in all cases. Compound **315** was quantitatively obtained by the corresponding procedure.

18 Amine Condensations

18.1 Imine Formation

Previously, the derivatization of primary amine functions by their reaction with carbonyl compounds in solution required strong acid catalysis and removal of the water of reaction from the equilibrium with production of much dangerous waste. It is therefore of high interest that many of these reactions can be performed waste-free by gas–solid or solid–solid technology which provides 100% yield of the product. This was exemplified with a great number of condensations using gaseous acetone (Scheme 49) [5, 28]. In some cases (**317a,b,c,d,j**) solid salts of the liquid-free bases had to be used, but all of the solid hydrazine derivatives



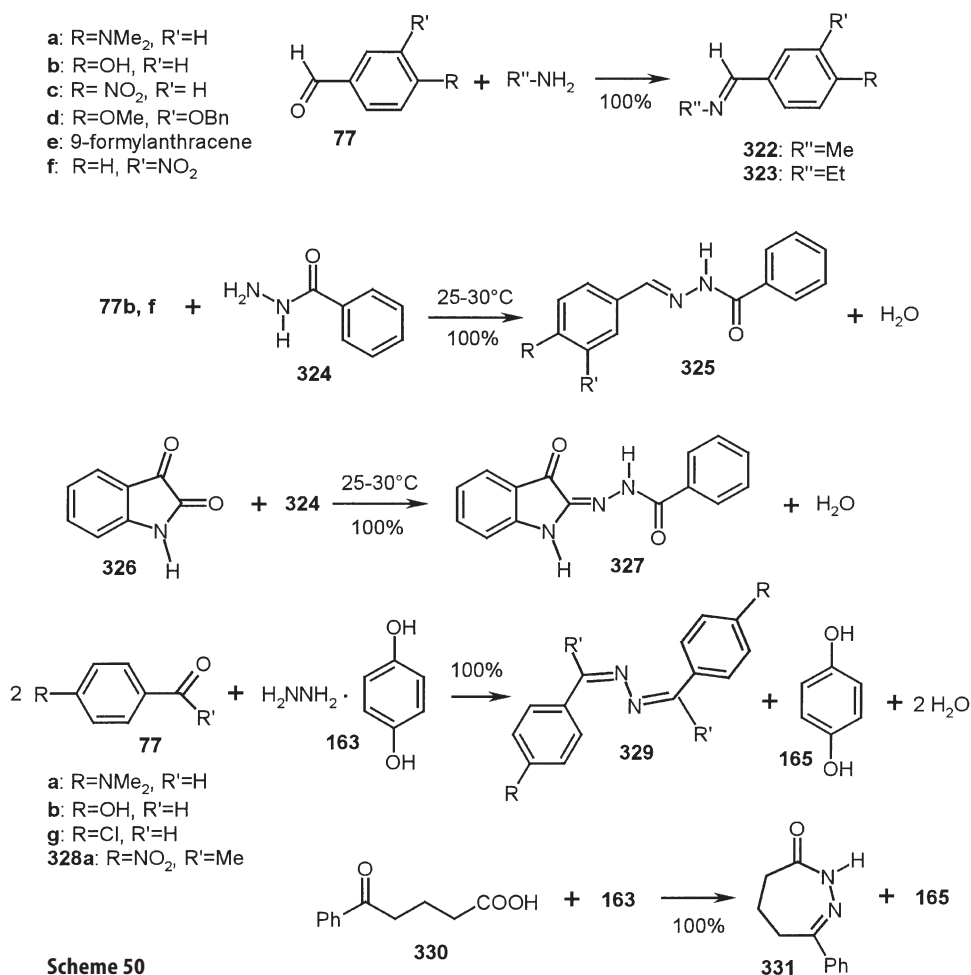
Scheme 49

did not require any catalyst and formed the free imine compounds **318** directly. The acetone gas is applied to an evacuated flask containing the solid carbonyl reagent **317** ($\cdot\text{HX}$) with an overnight rest. Similarly, the oxime, carbodihydrazone, semicarbazone, and thiosemicarbazone salts of cyclopentanone or cyclohexanone (**319** and **320**) can be quantitatively obtained as monohydrates by the gas–solid technique [28].

Importantly, the volatile carbonyl compounds are consumed down to the detection limit by most of the solid reagents **317** from gas mixtures in dynamic systems. Therefore, volatile carbonyl compounds can be removed if they are present in spoiled atmosphere. A larger-scale process has been devised for the rapid removal of acetone down to the detection limit using columns charged with hydroxylamine phosphate (**317c**) and pH adjusted such that free acetone oxime product is directly expelled together with the water at 80 °C and high flow rates [5, 28]. Apart from the quantitative synthesis of **321**, which is also the easiest way to synthesize pure free acetone oxime (**321**), this experiment simulates an exhaust gas purification down to zero emission. The experimental procedure describes the larger-scale process (Scheme 49). Two heatable glass tubes ($l=50$ cm, i.d.=2 cm) fitted with glass frits were each loaded with 53.1 g (0.269 mol) of ground ($0.14\text{ m}^2\text{ g}^{-1}$) hydroxylaminium phosphate (**317c**) and 51.9 g (0.269 mol) of unground ($0.10\text{ m}^2\text{ g}^{-1}$) $\text{K}_2\text{HPO}_4\cdot\text{H}_2\text{O}$. Both tubes were externally heated to 80 °C. Air (1 L min^{-1}) was passed through 46.9 g (0.807 mol) of acetone (**316**) and then over the solids from the top of the tubes. All of the acetone (at a load of ca. 78 g m^{-3}) had reacted within 10 h. Behind the second column was a condenser flask in an ice bath and a filter of activated carbon (5 g; $645\text{ m}^2\text{ g}^{-1}$) to catch the last traces of free acetone oxime (**321**) which escaped condensation. The product **321** and the water of reaction and crystal water were continuously expelled in gaseous form from the columns and condensed out at 0 °C. Only after >75% conversion did acetone start to escape from the first column and the second column started to react (at $<50\text{ g m}^{-3}$ acetone load, such escape started at >90% conversion). After passing all of the acetone, column 1 had reacted to 94% and column 2 to 6%. The condensate consisted of water (18.5 g, 96%) and of crystalline acetone oxime **321** (58.7 g, 99.3%). The missing 400 mg (0.7%) of uncondensed **321** was efficiently and completely absorbed by the activated carbon at the exhaust (400 mg of **321** are absorbed by 3 g of activated carbon). The acetone oxime **321** was separated from water by continuous azeotropic removal with *t*-butyl methyl ether. The reacted column was contracted by less than 10% and contained crystalline KH_2PO_4 in analytically pure form as a useful couple product.

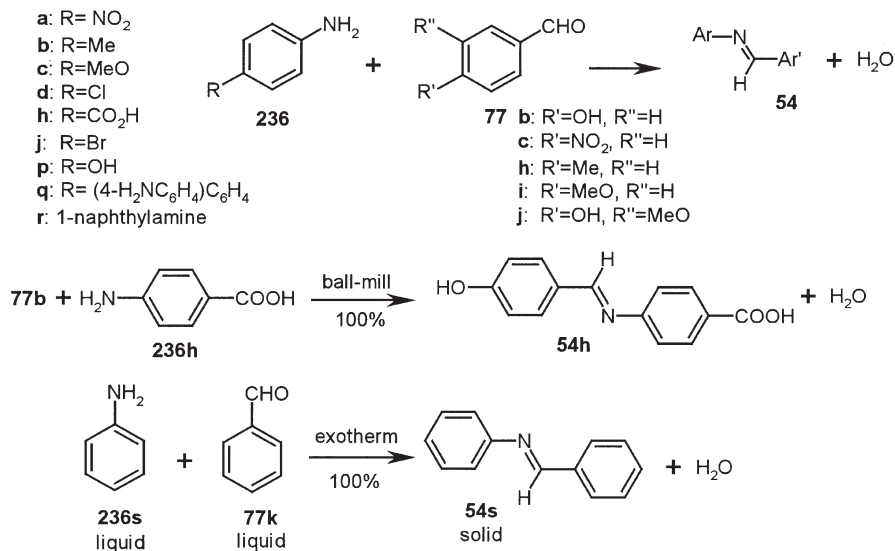
Solid aromatic aldehydes (**77a–e,j**) react quantitatively with aliphatic amines (0.25 bar) at room temperature (**77b** at 0 °C) to give the solid *N*-alkylazomethines **322** and **323** without melting, which are dried at 80 °C in a vacuum. The yield is 100% throughout [12] (Scheme 50).

Similarly, benzhydrazide (**324**) and “solidified” hydrazine (**163**) react quantitatively in the solid state with aldehydes, ketones, and other carbonyl compounds. Thus, quantitative yields of the hydrazones **325** and fully specific **327**



are obtained upon stoichiometric milling of the components [10]. This works also with the “solid” hydrazine and 77, 328a, and 330. The azines 329 and the cyclic hydrazone (331) (by reaction of both the carbonyl and the carboxyl group) are obtained in pure form after aqueous washing to remove the auxiliary 165, which is recycled [79].

Solid anilines (236) and solid aromatic aldehydes (77) give the benzyldiene anilines 54 upon grinding with 100% yield after drying at 80 °C; 20 combinations were performed [101–102] (Scheme 51). A semibatch large-scale experiment of 236h with 77b yields quantitatively the hydrated imine 54h that can be dried as well [7]. The reaction of aniline (236s) with benzaldehyde (77k) cannot be run as a solid-state reaction. However, it should be mentioned that the stoichiometric liquid–liquid reaction proceeds with 100% yield because it profits from direct crystallization of the product 54s upon reaction. This technique can



Scheme 51

be used large-scale and it so supersedes all waste-producing previous techniques (including 900-W microwave activation of 106+93 mg of the adsorbed reagents) in all respects that it must be shown here [2].

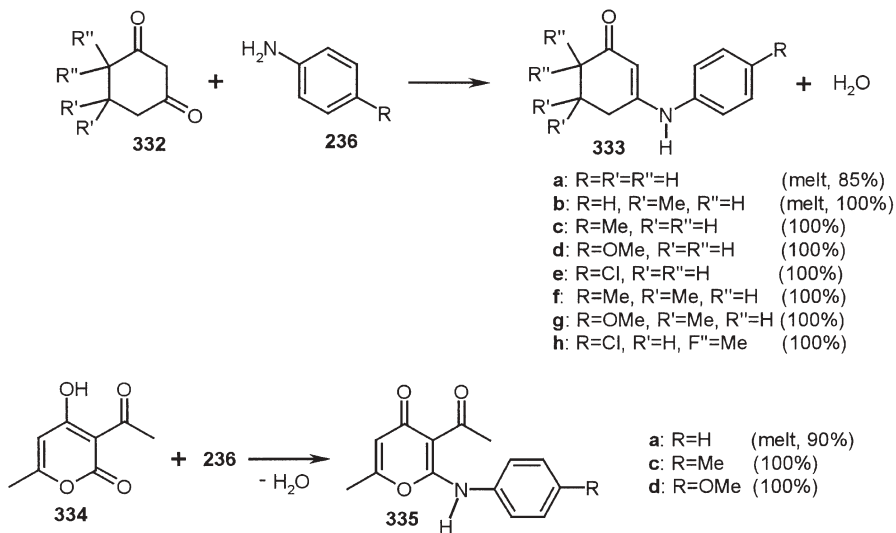
The experimental procedures are not complicated. All small-scale reactions were performed by grinding together 10 mmol of the pure aniline derivative 236 with 10 mmol of the pure aldehyde 77 in a mortar and keeping the mixture at room temperature. Some mixtures liquefied intermediately at room temperature, but most of these could be run without melting at lower temperatures. It should be noted that the liquid-state synthesis of some of the imines 54 starting with low-melting reagents may be more practical as the yield is also quantitative in these exceptional cases. The completion of the reactions was checked by IR spectroscopy in KBr. The water produced in the reaction was removed at 80 °C in a vacuum. The yield of 54 was 100% at 100% conversion in the 20 studied combinations of 236 and 77. Chemical analysis was carried out by IR and NMR spectroscopy, which gave the expected peaks and signals. Thin-layer chromatography and comparison of melting points with literature data confirmed the purity of the products 54.

A stoichiometric 1:1 mixture (200 g) of the loosely premixed commercial crystals of 236h and 77b, both at >99% purity, were fed to a stainless-steel 2-L horizontal ball-mill (Simoloyer) equipped with a hard-metal rotor, steel balls (2 kg; 100Cr6; 5-mm diameter), and water cooling. The temperature was 15 °C at the walls with a maximum of 19 °C in the center of the mill. The rotor was run at 900 rpm (the power was 610 W) for 15 min for quantitative reaction. A 100% conversion and 100% yield was indicated by m.p., IR spectrum, chemical analyses, and DSC experiments. The product 54h·H₂O was milled out for

10 min leaving some holdup, but a quantitative recovery was obtained from the second batch and so on. For quantitative recovery of the powdered material in the last batch, an internal air cycle for deposition through a cyclone should be used. The hydrate water was removed from **54h**·H₂O by heating to 80 °C in a vacuum. A melt reaction is not possible in this case due to the high melting points involved and severe decomposition above 180 °C.

For the stoichiometric liquid–liquid large-scale synthesis a flat steel pan (31×44 cm²) was charged with benzaldehyde (**77k**) (99.5%; 848 g, 7.95 mol) and aniline (**236s**) (99.5%; 744 g, 7.95 mol) (Scheme 51). The liquids were mixed at 18 °C. The temperature rose to a maximum of 32 °C and fell back to 24 °C when crystallization started with another increase in temperature to a maximum of 35 °C within 12 min when crystallization was virtually complete and water of reaction separated. Next day, the wet crystal cake was crunched with an ordinary household grain mill and dried in a vacuum at room temperature to give 1.438 kg (100%) of pure benzylidene-aniline (**54s**).

An interesting synthetic approach to cyclic enamine ketones is provided by waste-free and quantitative solid-state reaction of the anilines **236** with cyclic 1,3-diketones such as **332** or enolized **334** (Scheme 52). The enamine ketones **333c–h** are quantitatively obtained in the solid state by milling at room temperature. The melt reaction (80 °C) for **333a** is not quantitative, but **333b** arises with 100% yield from the melt reaction [10]. All of the solid-state reactions give 100% yield, as usual.



Scheme 52

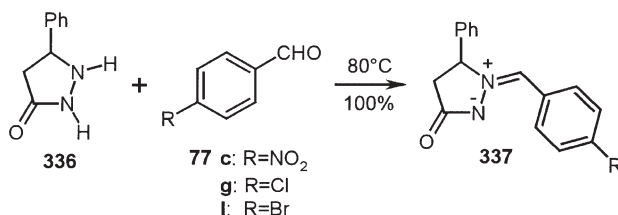
Very exciting is the reaction specificity with dehydracetic acid **334** in the stoichiometric milling reaction. Only **335c,d** is obtained. Also, a rather good

selectivity is observed in the (by necessity) melt reaction (80 °C) with aniline (236s) giving a 90% yield of 335a (Scheme 52) [10].

18.2

Secondary Amines

Solid-state condensation reactions of secondary amines are not yet well developed. However, an interesting condensation of the pyrazolidinone (336) with aromatic aldehydes 77 gives a quantitative access to the azomethinimines 337 by cogrinding and heating to 80 °C [103] (Scheme 53).



Scheme 53

Furthermore, (L)-proline and paraformaldehyde give (L)-N-hydroxymethylproline (as the iminium carboxylate + H₂O) upon large scale milling and stoichiometric millings of imidazole (0 °C) or benzimidazole (r. t.) with (HCHO)_n quantitatively provide the corresponding solid 1-imidazolylmethanols [22].

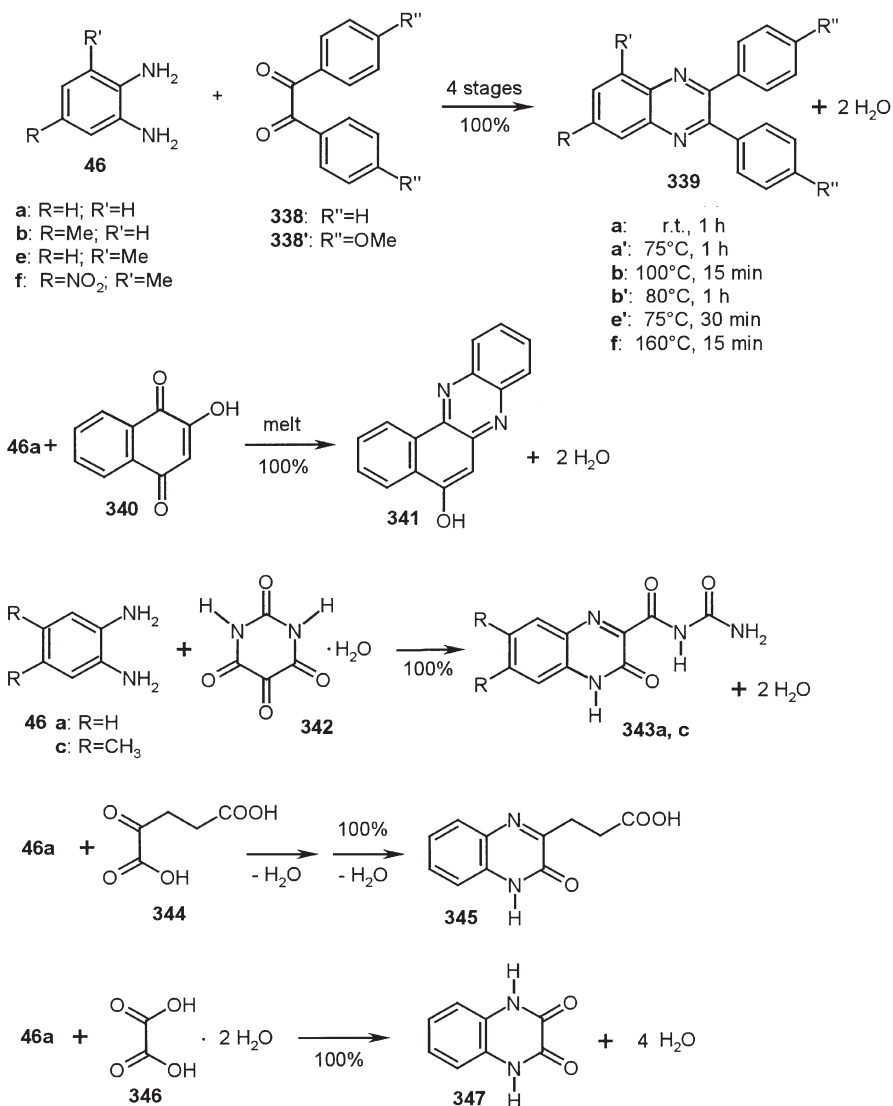
18.3

Diamines

Aromatic 1,2-diamines (46) condense readily with 1,2-diketones, α -keto amides, α -keto acids, or oxalic acid and provide quantitative yields in the solid state. For example, benzils (338) react with *o*-phenylenediamines (46) at room temperature upon milling and drying (Scheme 54). All products 339 are also obtained with 100% yield by heating to the temperatures given after initial stoichiometric cogrinding. Similarly 340 and 46a (70 °C, 15 min) give quantitatively compound 341 [104].

The reaction of alloxane hydrate (342) and 46a,c gives 100% yield of the products 343a,c upon milling at room temperature [104]. The solid-state reaction of 2-oxoglutaric acid (344) and 46a similarly gives a quantitative yield of the quinoxalinone 345 in the solid state upon heating of coground mixtures for 30 min to 120–125 °C [104].

The solid-state reactivity of the carboxylic function was demonstrated with oxalic acid dihydrate (346) and *o*-phenylenediamine (46a) (Scheme 54). A 100% yield of quinoxalinedione (347) is easily obtained upon cogrinding of the components and heating of the high-melting salt thus formed in a vacuum to 150 °C for 8 h, to 180 °C for 30 min, or to 210–220 °C for 10 min [104]. Compound 347 is ready for further interesting condensation reactions [104].



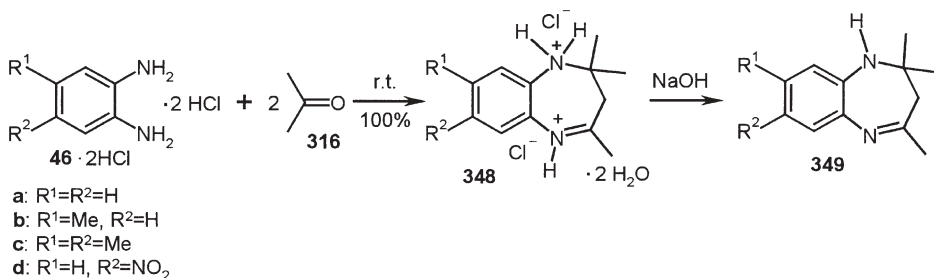
Scheme 54

18.4

Cyclizing Condensation

1,2-Diamines, aminothiols, and aminoalcohols are well suited for quantitative solid-state cyclizing condensations with simple aldehydes and ketones. As yet only quantitative gas–solid reactions with acetone and solid–solid reactions with paraformaldehyde (that will monomerize upon the milling) have been profited from. An early remarkable reaction type involving two molecules of

acetone (**316**) and one molecule of *o*-phenylenediamine dihydrochlorides (**46**) has been found to produce 1,4-benzodiazepine derivatives **349** in quantitative yield (except the synthesis of **349d**; 71%) upon gas–solid interaction of the reactants and neutralization of the salts **348** [5] (Scheme 55). This cascade reaction (cf. Sect. 25) is treated here as no other quantitative cyclizing condensations of 1,2-diamines with ketones are known to date, and all condensations of **46** with acids in melts at 220 °C to give benzimidazoles [105, 106] ended up with medium to good yields at best.



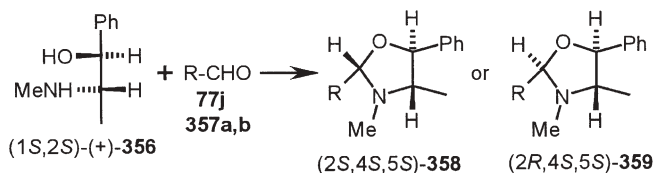
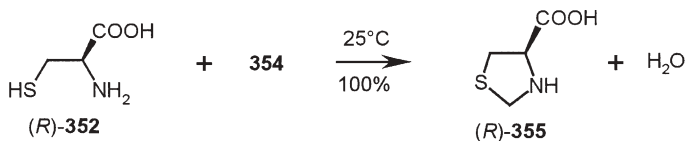
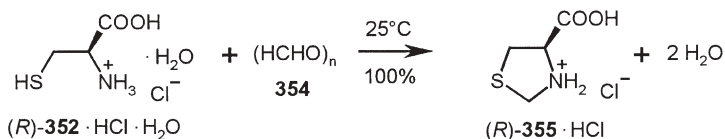
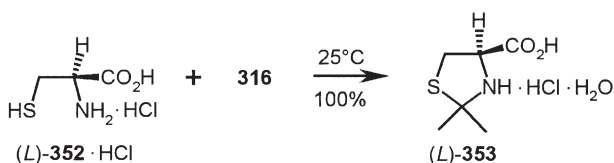
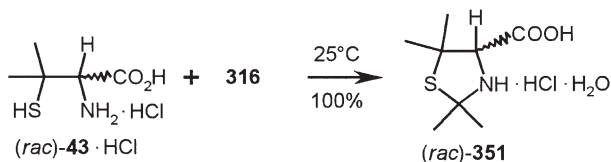
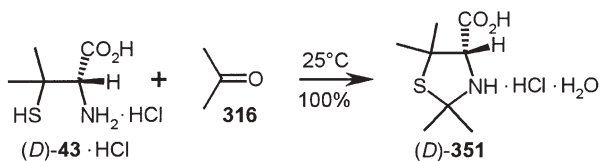
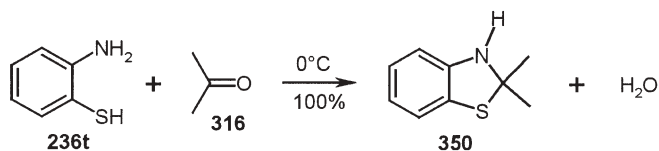
Scheme 55

A larger-scale synthesis of compound **349a** has been published [5]. The salt **46**·2HCl (20 g, 80 mmol) was placed in a 10-L desiccator and after evacuation it was connected to a 100-mL flask containing 9.3–11.6 g (160–200 mmol) of acetone, which had previously been degassed in a vacuum and cooled with liquid nitrogen. Upon removal of the cooling bath the acetone evaporated slowly into the desiccator. After 12 h, excess gas was condensed back to the flask (77 K) and a 100% yield of **348a**·2H₂O was obtained. The free base **349a** was liberated with NaOH in water.

2-Aminothiophenol (**236t**) reacts quantitatively to give the five-membered compound **350** [5] (Scheme 56). On the other hand, D- and *rac*-penicillamine hydrochloride (**43**·HCl) (but not the free bases) give the D- and *rac*-thiazolidine hydrochloride hydrates (**351**) with 100% yield if acetone (**316**) vapors are applied to them. The same is true for L-cysteine hydrochloride (**352**·HCl) giving the thiazolidine L-**353**·HCl·H₂O [5].

Various crystalline states of cysteine, cysteine hydrochloride, and cysteine hydrochloride hydrate have been tested for solid-state reactivity. Thus, (*R*)-**352** and (*R*)-**352**·HCl·H₂O were also reactive in the solid-state. This was verified by quantitative solid–solid reactions with paraformaldehyde (**354**) in stoichiometric ball-milling experiments at room temperature giving 100% yield of (*R*)-**355** [12] or (*R*)-**355**·HCl [10] after drying.

Similarly, quantitative yields are obtained when solid (1*S*,2*S*)-(+)-pseudoephedrine (**356**) is reacted with prochiral organic and organometallic solid aldehydes **77j** or **357a,b** to give one of the epimeric oxazolidines **358** or **359** as a consequence of true solid-state reactions upon milling (Scheme 56). The epimer configurations have not been assigned. If (1*R*,2*S*)-(–)-ephedrine is



de values for **358** or **359**:

j: vanillyl; 100% de

a: R=C₅H₅FeC₅H₄; 98% de

b: R=C₅H₅RuC₅H₄; 100% de

Scheme 56

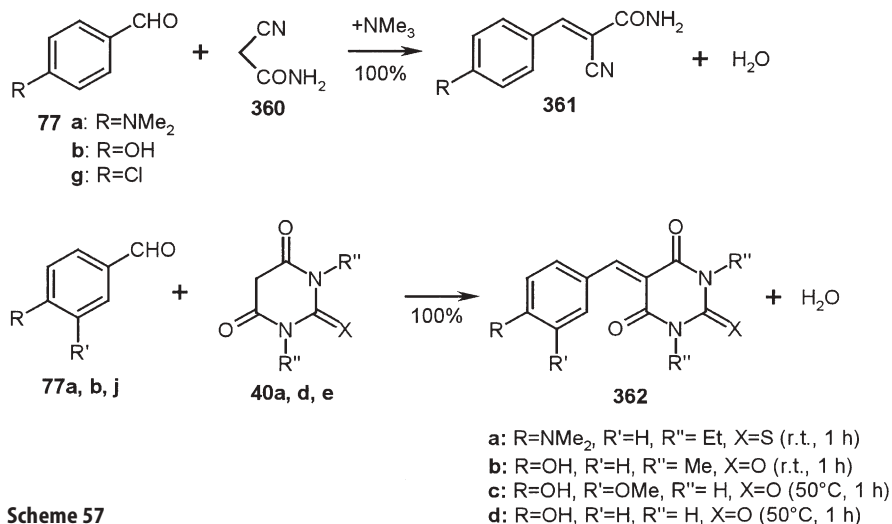
similarly reacted with **357b**, a 1:1 mixture of (2*S*,4*S*,5*R*)-**97** ($R=C_5H_5RuC_5H_4$) and (2*R*,4*S*,5*R*)-**98** ($R=C_5H_5RuC_5H_4$) ensues with 100% yield in a solid-state reaction [66].

19

Knoevenagel Condensation

Quantitative Knoevenagel condensations of aldehydes with active methylene compounds are most desirable due to the frequent use of the electron-poor alkenes that arise [107]. But previous techniques use catalysts and produce dangerous wastes even if highly energy-consuming microwave irradiation upon polar solid supports is additionally used.

The solid-state reaction of **77a,b,g** with cyanoacetamide (**360**) is too slow at room temperature even upon ball-milling. It is therefore best choice to put briefly milled stoichiometric mixtures in a vacuum and apply the easily removable gaseous catalyst trimethylamine for completion of condensation in the solid state and to obtain a 100% yield of **361a,b,g** after evaporation of the catalyst [107] (Scheme 57). Melt reactions of these reactants perform less efficiently due to inferior yield. The reason for the low reactivity is not elucidated but it is not encountered in the solid-state condensations by milling of **77a,b,j** with various (thio)barbituric acids **40** at 20–50 °C to give quantitative yields of the products **362a–d** after drying (80 °C in a vacuum) [107]. The corresponding reaction of 1,3-indandione and **77c** ($R=NO_2$) is performed at 80 °C [22].



Scheme 57

Two large-scale procedures show the synthetic potential. A stoichiometric mixture of **77b** and **40d** (200 g per batch) was milled in a water-cooled (14 °C)

horizontal ball-mill (2 L, Simoloyer, Zoz GmbH) with 2-kg steel balls (5-mm diameter) for 1 h at 1,000 rpm. The product **362b** was milled out at 600–1,000 rpm. A 100% yield (recovery) was obtained in the second batch etc. The purity of **362b** was checked by IR, ^1H and ^{13}C NMR, and m.p. (297 °C) after drying in a vacuum at 80 °C.

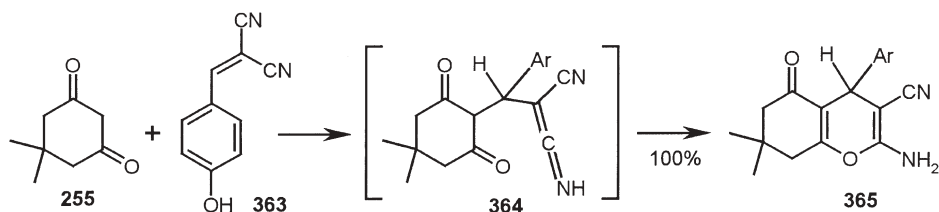
Similarly, **77b** and **40a** reacted with quantitative yield in the 2-L ball-mill that was not water cooled while care was taken that the interior temperature did not rise above 50 °C (1 h per 200-g batch) to quantitatively yield **362d**, m.p. 299–301 °C.

Numerous solvent-free Knoevenagel condensations with malononitrile, methylcyanoacetate, dimedone (**255**), and Meldrum acid proceeded with high to quantitative results with intermediate melt or full melt at higher temperatures but with direct crystallization [107].

20

Michael Addition

Electron-poor alkenes are suitable starting points for Michael additions. For example, the arylidene malononitrile **363** adds quantitatively to solid dimedone (**255**) upon milling at 80 °C followed by heating of the yellow powder to 100 °C. The initial Michael adduct **364** is not isolated, as it cyclizes in the solid state to give the pyrone **365** with 100% yield [107] (Scheme 58). The potentials for waste-free solid-state chemistry are manifold indeed and deserve further exploration.



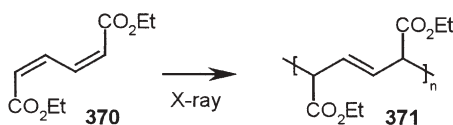
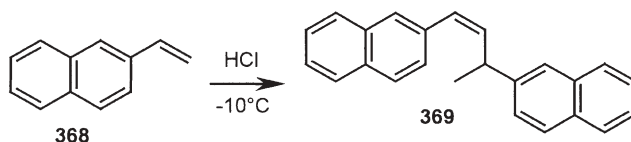
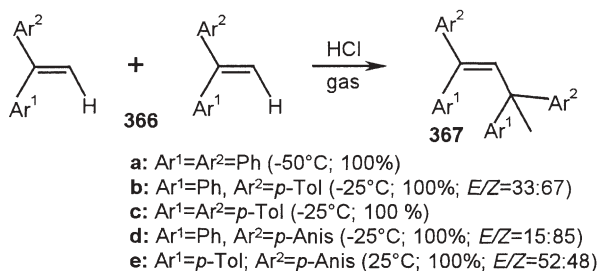
Scheme 58

21

Linear Dimerization

The first solid-state linear dimerization was observed with *N*-vinylpyrrolidone. It was first quantitatively converted to its Markovnikov HBr addition product (by application of HBr gas at –40 °C), which upon warming to room temperature lost HBr and formed (*E*)-1,1'-(3-methyl-1-propene-1,3-diyl)bis-(2-pyrrolidinone), but the yield was less than 100% [58]. Interestingly, such head-to-tail dimerizations of alkenes lead to shrinking and that may create reactivity even if the crystal lattice does not allow for molecular migrations due

to 3D-interlocked packing. Such a situation is encountered with solid 1,1-diarylethenes (**366**) that crystallize in 3D-interlocked structures and therefore do not add HCl or HBr gas. However, they dimerize linearly head-to-tail and the concomitant shrinking has been nicely shown with AFM measurements [3, 60]. Some of the preparatively important quantitative linear dimerizations of solid **366** to give **367** are collected in Scheme 59. Similarly, the gas–solid catalyzed dimerization of 2-vinylnaphthalene (**368**) gives a 100% yield of **369** with a *cis* double bond [22]. The *cis* arrangement of the hydrogen atoms is secured by the ^1H NMR coupling constant (6.8 Hz) of the neighboring hydrogen atoms. The linear dimerizations can also be catalyzed by HBr or BF_3 gas.



Scheme 59

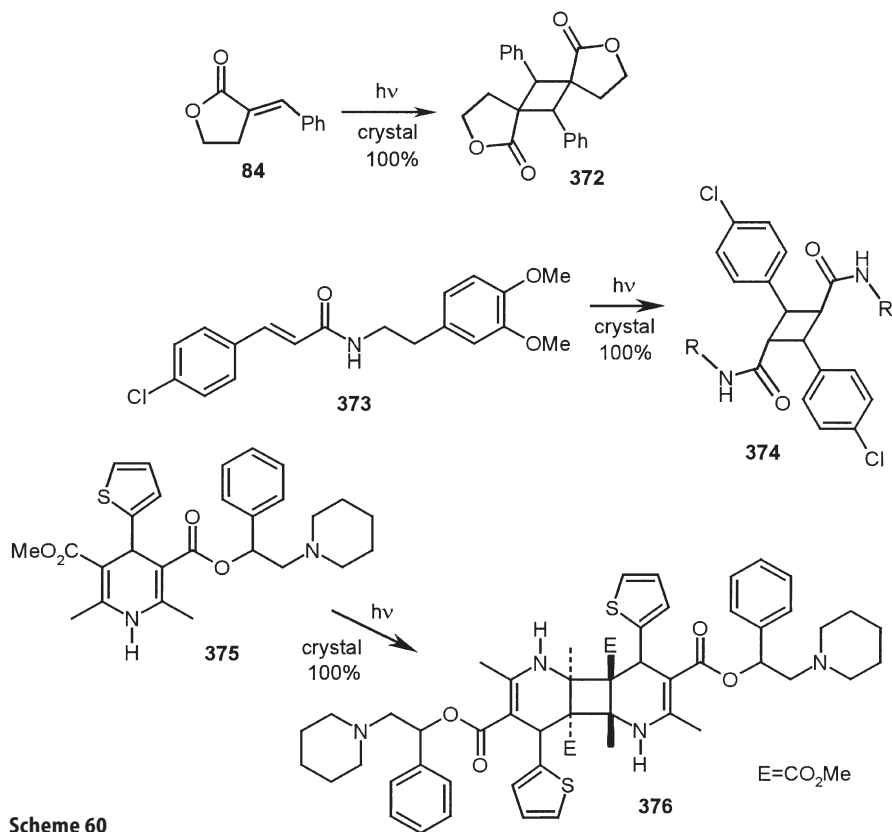
There may be situations in the crystal packing of alkenes or dienes in which the spacing and period are the same for monomer and intended polymer, so that no molecular migrations would be necessary upon reaction. That is the criterion for topotactic processes. Such a situation is encountered in specially selected single crystals of *cis,cis*-diethylmuconate (**370**). When a qualified single crystal of **370** was exposed to slow X-ray irradiation a single crystal of the polymer **371** was obtained almost free of monomer impurities (Scheme 59). Topotacticity is assured by the crystal packing in monomer and polymer, both with spacing and period of 3.8 Å. The effective cross-sectional area was decreased by only 3% and the crystal structure was not changed by the radiolysis. Therefore, no molecular movements were required and the linear polymerization proceeded smoothly [108].

22

Cycloaddition

Most solid-state cycloadditions are photochemical and of the [2+2] type. Numerous early solid-state photodimerizations are listed in [109]. More recent examples are listed in [110]. Important polar effects engineer the crystal packing [111], but the yields are at best close to quantitative. Even the selectivities may be poor and interesting product mixtures may arise [112–114]. However, there are some quantitative photochemical cyclobutane syntheses. The quantitative head-to-tail photodimerization of the benzylidenelactone **84** to give **372** [115] (Scheme 60) exhibits the anisotropic molecular migrations, as has been shown by AFM scrutiny [113]. The conversion of **373** to **374** was described as a quantitative single-crystal-to-single-crystal reaction [116]. Interestingly, while the photolysis of **375** in solution gives only dehydrogenation, irradiation of the crystals provides a 100% yield of **376** [117].

The photolytic synthesis of **372** proceeds as follows: α -Benzylidene- γ -butyrolactone (1.0 g, m.p. 115–117 °C) was evenly spread on the inner wall of a

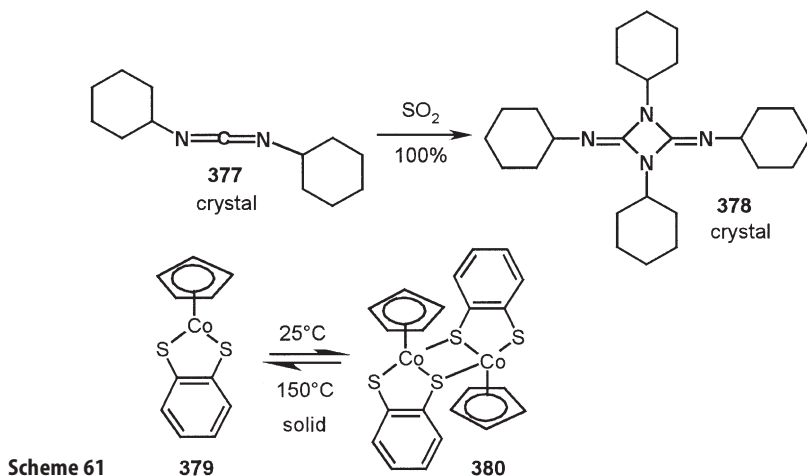


Scheme 60

mirrored Dewar vessel (diameter 14 cm, height 20 cm) with some dichloromethane. After heating to 80 °C for 1 h the dry crystalline film was irradiated from within for 5 h with a Hg high-pressure lamp (Hanovia 450 W) through a 5% solution of benzophenone in benzene (5 mm; $\lambda > 380$ nm) under cooling with running water at 30–35 °C. The yield of the head-to-tail *anti* dimer **372** was 100% (m.p. 242 °C).

It may be suspected that the genuinely topotactic (as secured by the molecular precision of the AFM [18]) photodimerization of 2-benzyl-5-benzylidenecyclopentanone [118] might be a good candidate for a quantitative preparative photodimerization to give the head-to-tail *anti*-[2+2] dimer. Early quantitative solid-state [2+2] photodimerizations (most of the published mechanistic interpretations of which can no longer be accepted) are listed in [110]. These deal with the *anti* dimerization of acenaphthylene-1,2-dicarboxylic anhydride, the head-to-head *syn* dimerization of acenaphthylene-1-carboxylic acid, the *syn* dimerization of 5,6-dichloroacenaphthylene, and the thermally reversible head-to-tail *anti* dimerization of seven (*E*)-2,6-di-*t*-butyl-4-(2-arylethenyl)pyrylium-trifluoromethanesulfonates. All of these reactions proceed fully specific. On the other hand, quantitative photoconversions of a 1:1 mixed crystal of ethyl and propyl α -cyano-4-[2-(4-pyridyl)ethenyl]cinnamates gives mixtures of diesters with one ($\lambda > 410$ nm) or two cyclobutane rings (no cutoff filter).

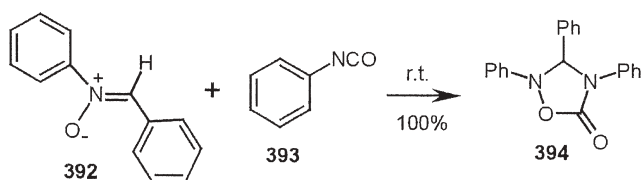
The thermal [2+2] dimerization of solid dicyclohexylcarbodiimide **377** requires the action of gaseous sulfur dioxide at 0 °C as an easily removable catalyst. The interesting heterocyclic compound **378** is quantitatively obtained [33] (Scheme 61).



of the *endo* adduct **3** [120] (Scheme 62). Also the solid–solid stoichiometric additions of **381** with the fulvenes **383a,b** provide quantitatively and exclusively the *endo* adducts (**384**) by milling at 30 °C [120]. Similarly, the *endo* adduct **386** is obtained by milling of *o*-benzoquinone **385** (prepared in situ according to Scheme 73) and the fulvene **383a** [22]. Further quantitative solid-state Diels–Alder additions occur with 9-methylantracene **286** (favorable layered structure) and fumarodinitrile (**387**) [22]. This addition to give **388** is incomplete below 60 °C due to softening in the ball-mill probably due to slow phase transformation resulting in an undercooled microliquid. At 60 °C (not at 50 °C) the solid-state reaction is complete giving the product as a powder in 100% yield. The *trans* arrangement of the cyano groups is secured by the ^1H NMR coupling constant (4.9 Hz) of the neighboring hydrogen atoms. While this thermal behavior is certainly of mechanistic importance, from a preparative point of view it is easier to perform the quantitative melt reaction at 80 °C or above also with 100% yield in this case.

No problems are encountered if 9-methylantracene (**286**) is milled with maleic anhydride (**381**, X=O) or maleimide (**381**, X=NH) at room temperature. The solid adducts **389** form quantitatively [120]. Interestingly, anthracene does not undergo the corresponding solid-state Diels–Alder additions under these conditions. The reason must be sought in the crystal packing. 9-Methylantracene crystallizes in double layers with well-developed cleavage planes, whereas anthracene exhibits a scaly molecular arrangement with interlocked monolayers but not well-behaved cleavage planes. However, anthracene undergoes Diels–Alder reactions in preformed charge-transfer complex crystals such as **390**. The adduct **391** forms quantitatively upon heating single crystals of the complex **390** [121] (Scheme 62). But the authors' claim of first-order kinetics that was invoked in order to "substantiate" an assumed topotactic reaction is completely unjustified (obvious data mistreatment). The reported data clearly indicate zero-order kinetics and there are also obvious signs of crystal disintegration. No AFM study has been tried, which would have given the answer to the mechanistic question with molecular precision (cf. Sect. 1, 2).

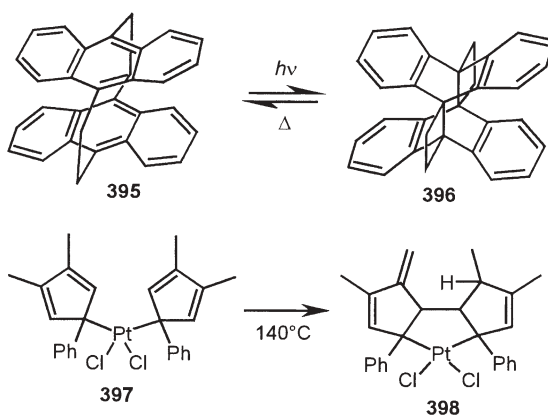
1,3-Dipolar additions are a fertile field in quantitative solid-state chemistry. For example, solid diphenylnitrone (**392**) adds phenylisocyanate vapor (**393**) at room temperature to give a 100% yield of the interesting heterocyclic compound **394** (Scheme 63) [22].



Scheme 63

Quantitative [4+4] additions and quantitative ene additions in the solid state are still rare. Useful models are the very first example of a photo/thermo-

chemical cycle photochrome [122], which is fully topotactic as proven by AFM with molecular precision [13]. The golden-yellow crystals of **395** were exposed to glass-filtered daylight and thus formed the colorless “dimer” structure **396** with quantitative yield. If **396** was heated to 30 °C in the dark for 5 h, compound **395** was quantitatively re-formed in a topotactic manner without change of the crystal shape even on the nanoscopic scale as shown by AFM [13]. Numerous cycles were performed without loss using single crystals of **395/396** (Scheme 64).

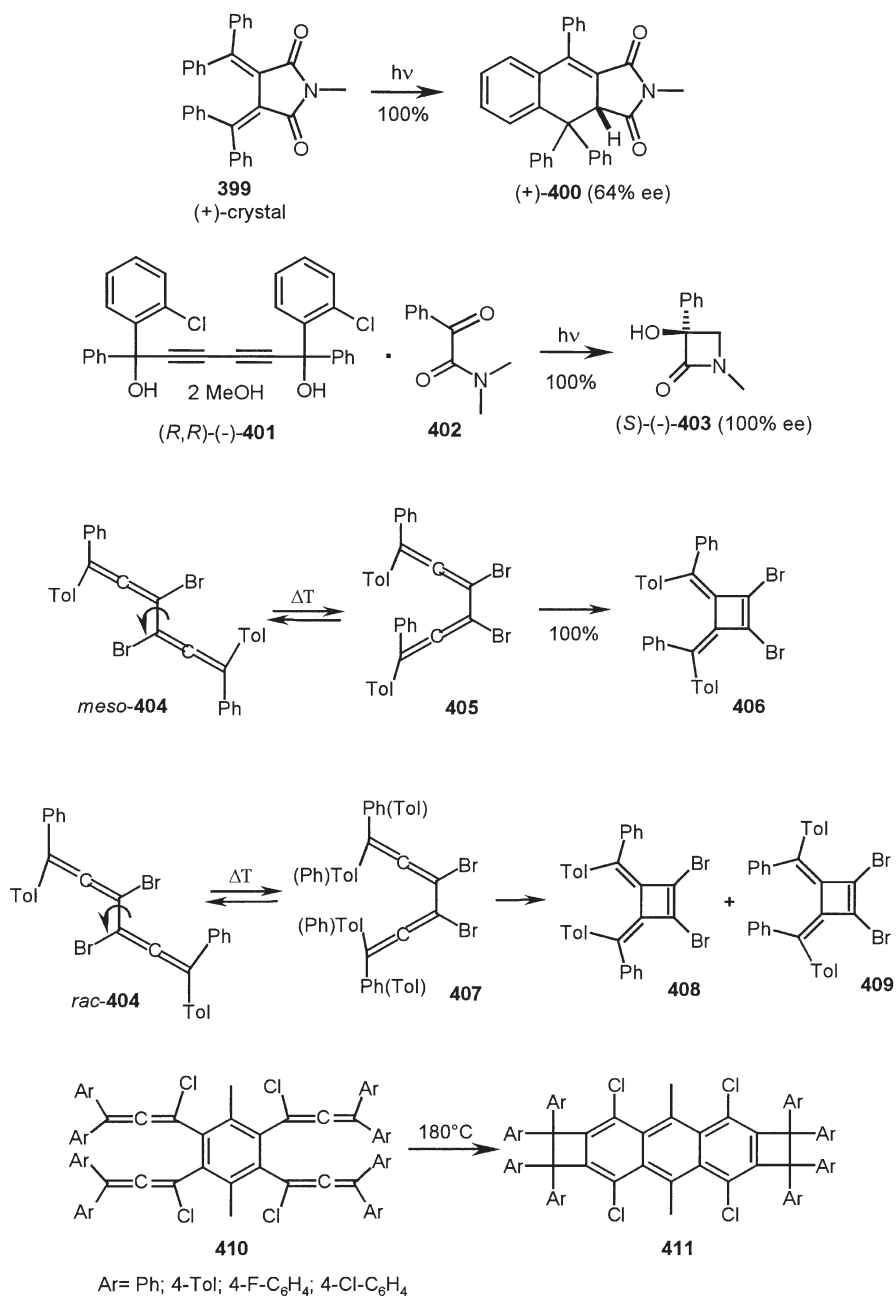


Scheme 64

A quantitative solid-state ene addition between two ligands of the platinum complex **397** gives the rearranged platinum complex **398** upon extensive heating to 140 °C [123]. This rearrangement reaction (cf. Sect. 24) is treated here, as it is the only known quantitative solid-state “ene addition” to date. Further quantitative solid-state [4+4] additions and higher vinyllogs, as well as ene additions also of the intermolecular type, await detection both as thermal and photochemical reactions.

23 Cyclization

Several intramolecular eliminative cyclizations have been noted in previous sections (149 → 148; 220 → 221; 264 → 265; 270 → 271; 307 → 308). The following cyclizations (Scheme 65) occur without elimination similar to 364 → 365. Chiral (+)-crystals of the *s-cis*-enforced tetraphenylbutadiene **399** photocyclize with 100% yield to give (+)-**400**. The (+)-enantiomer prevails with 64% ee. The corresponding (–)-crystal of **399** prefers (–)-**400**, correspondingly [124]. Clearly, this is a fine example of an absolute asymmetric synthesis [125]. Chiral hosts may also induce enantioselectivity. Thus, the guest **402** photocyclizes to give enantiospecifically the β-lactone (*S*)-(–)-**403** with 100% yield when included in the host (*R,R*)-(–)-**401** [126] (Scheme 65).



Scheme 65

Various bisallenenes have been quantitatively cyclized by heating in the solid state. The space demand is extremely high for *s-trans*-configured samples within crystals and not all reactions proceed with quantitative yield, as is also rationalized by AFM studies [127]. Both *meso*-**404** and *rac*-**404** cyclize stereospecifically upon heating to 135 or 125 °C for 90 min to give the bismethylene-cyclobutenes **406** or **408**+**409** (1:1 ratio) with 100% yield [128] (Scheme 65). There cannot be any doubt that the *s-cis* conformers **405** and **407** are intermediates. The space-conserving hula-twist-like mechanism for the formation of these *s-cis*-bisallenenes is more plausible than internal rotation mechanisms around the single bond within the crystal [48]. However, there is also the necessity for molecular migration as the geometric change is considerable. These points have been clarified by detailed crystal packing analyses on the basis of X-ray crystal structure and AFM data which detected anisotropic molecular migrations [129].

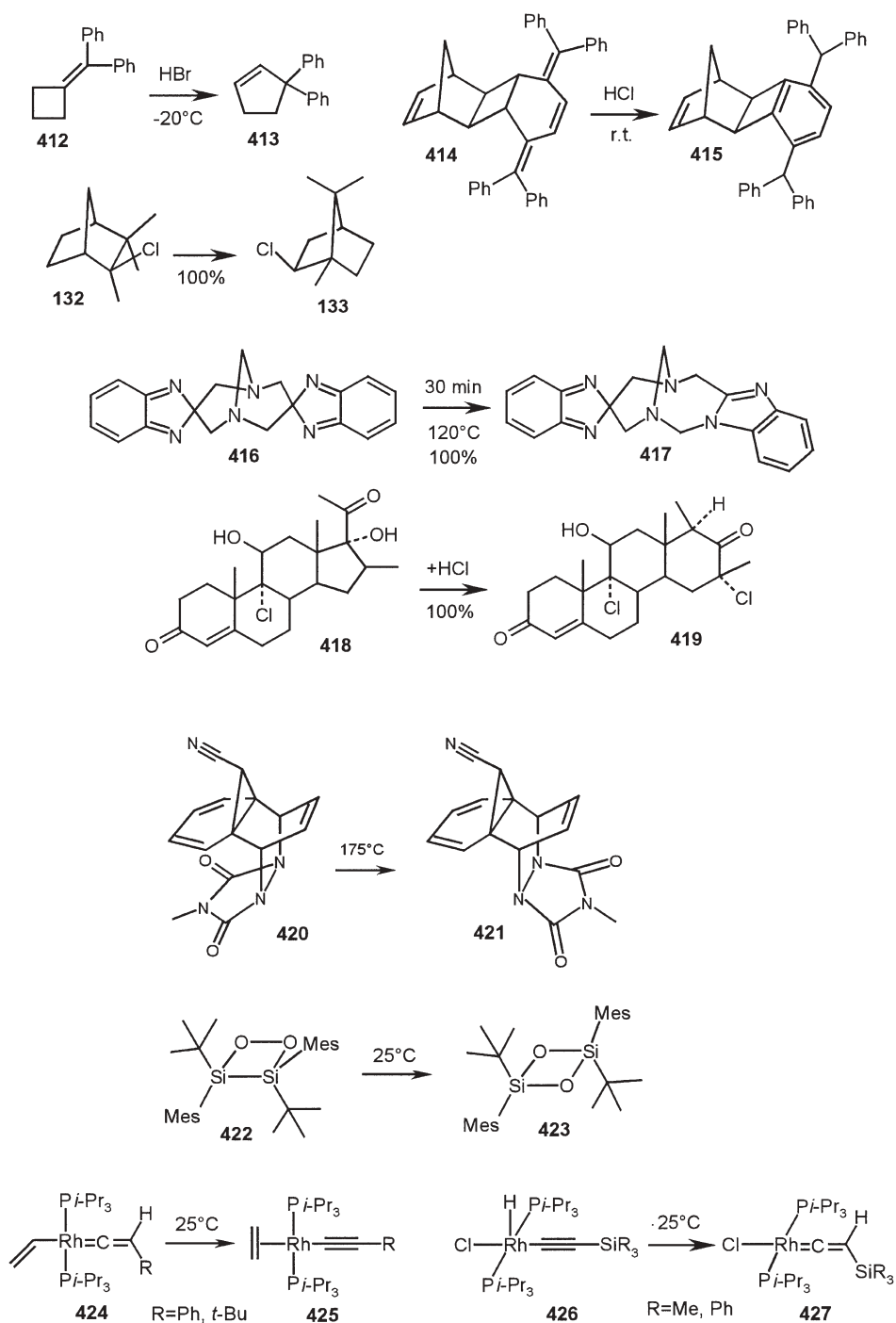
The even more involved quantitative transformation of **410** to give **411** requires four cyclization steps within the crystal. These cyclizations can be performed on a hot stage at 180 °C for 30 min and the macroscopic shape of the crystals does not change at least for the octaphenyl case [130]. Importantly, the tetraphenyl-substituted benzocyclobutene bonds of **411** exhibit the extraordinary length of 1.726 Å [130], which is the world record for sp^3 - sp^3 single bonds [131] (Scheme 65).

24 Rearrangement

Acid-catalyzed [1,3]-hydrogen shifts may occur quantitatively in the solid state. Thus, the conversions of **412** to give **413** (this requires [1,3]-H shift and additional [1,2/2,1] rearrangement) and **414** to give **415** (two [1,3]-H shifts) have been realized under HBr and HCl catalysis as gas-solid reactions [120] (Scheme 66). Thermal rearrangements in crystals are comparatively rare. The crystalline camphene hydrochloride (**132**) rearranges slowly upon standing (quantitative after <3 years at r.t. or 6 h at 80 °C) in a solid-state Wagner–Meerwein rearrangement ([1,2/2,1]-rearrangement) [76] without melting to give pure **133** [11].

A quantitative uncatalyzed [1,5]-shift reaction has been realized in the solid state with the symmetric bis-spiro compound **416** to yield the unsymmetric isomer **417** [132]. The acyloin compound **418** with a 16β -methyl substituent undergoes a substitutive rearrangement with HCl gas to give stereospecifically product **419** with 100% yield [133] (Scheme 66). The most probable mechanism starts with acid-catalyzed migration of the 13,17-bond, enolization, vinylogous substitution of OH by Cl, and 1,3-H shift. This unprecedented reaction did not occur in CH_2Cl_2 . Several further solid-state acyloin-type substitutive rearrangements are known in the steroid field; however, these do not provide one single product with quantitative yield [133].

A thermal solid-state N–N double inversion between kinetically stable invertomers (*exo/endo* isomerism) was studied by high-temperature X-ray dif-



Scheme 66

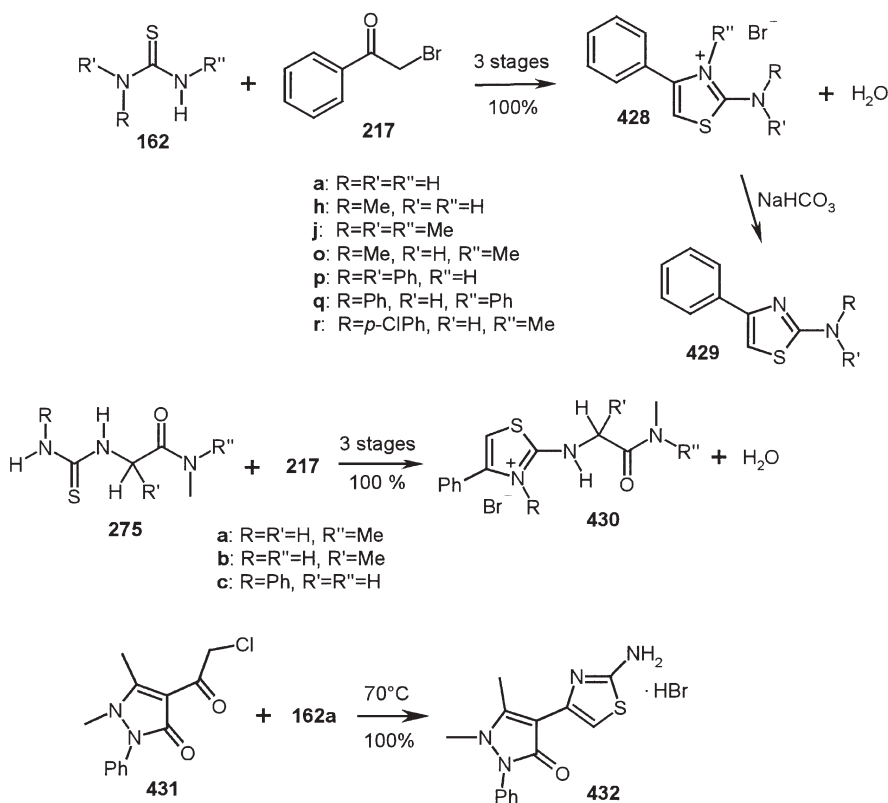
fraction. The conversion of the less stable isomer of the Diels–Alder product **420** into the more stable isomer **421** occurred at 175 °C from single crystal to polycrystalline material [134] (Scheme 66). The rearrangement of the 1,2-disiladioxetane **422** into the 1,3-disiladioxetane **423** occurs in the crystal (also in solution) at room temperature and below. It is stereospecific with retention of the configuration at silicon [135]. The crystalline vinyl(vinylidene)rhodium complexes **424** rearrange on standing at room temperature and form the alkynyl(ethene) complexes **425**. Conversely, the corresponding η^3 -2,3,4-*trans*-butadienyl complexes are obtained in benzene solution at 50 °C [136]. Furthermore, the quantitative rearrangement of the rhodium complex **426** to give **427** is stereoselective [137]. Further reactions of that type are reported [137].

25

Cascade Reactions

It is highly rewarding that solid-state reactions with 100% yield of one product are not restricted to single reaction steps. Several multistep reactions have already been described in the preceding sections (for example diazotizations). Reaction cascades imply a sequence of separate reaction steps preferably of different type. For example, in the reaction of 2-chloromethylbenzimidazole with hexamethylenetetramine to give 7*H*,16*H*-8,17-methano-9*H*,18*H*-dibenzimidazolo[1,2-*c*:1',2'-*h*][1,3,6,8]tetrazecine (an isomer of compound **417**) eight new bonds must be formed in a solvent-free melt reaction at 120–160 °C [132]. While such extreme reaction cascades have not yet been observed in the solid state, it is nevertheless surprising that numerous cascade reactions occur in the solid state and give 100% yield. This fact stresses convincingly the occurrence and necessity of molecular migrations upon chemical reaction within the crystal. An already great number of 2- to 5-cascades proceed with quantitative yield without melting in the solid state, and the phase rebuilding mechanism as detected by AFM is the same as for one-step reactions except that it becomes multistep in the phase rebuilding stage. These unusual reactions are of unmatched atom economy.

Most of the now synthetically used quantitative cascade reactions involve an initial substitution step. That is quite clear for the reactions of acyl halides with thioureas to give 2-aminothiazolium salts. The 3-cascade consists of substitution to form the thiuronium salt, specific cyclization with the more nucleophilic of the amino groups, and elimination of water. In all reported cases, the water of reaction is taken up by the product crystal and it can be removed by heating to about 80 °C in a vacuum. For example, if the thioureas **162** and phenacyl bromide **217** are stoichiometrically ball-milled at room temperature for 30 min, quantitative yields of the pure products **428** are obtained in all cases after drying at 0.01 bar at 80 °C [10] (Scheme 67). The free bases **429** can be obtained by trituration of **428** with NaHCO₃ solution. Furthermore, the thioureido-acetamides **275** react correspondingly with **217** to give quantitative yields of the salts **430** from which the free bases can be obtained by NaHCO₃ trituration [96].



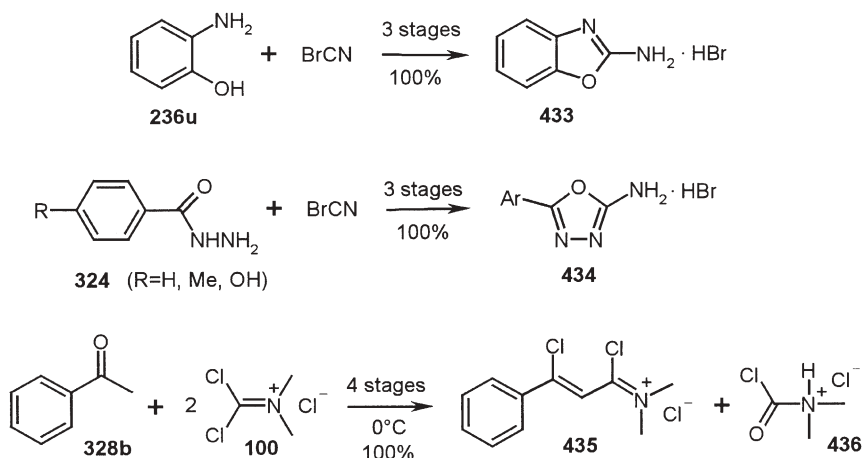
Scheme 67

An extension of the technique is the milling of the heterocyclic chloroacetyl derivative **431** with thiourea (**162a**) at 70°C , which gives a quantitative yield of the salt **432** [138].

The interaction of cyanogen bromide vapors with solid *o*-hydroxyaniline (**236u**) or the solid benzhydrazides **324** at room temperature provides the 2-aminobenzoxazole (**433**) or the 2-amino-5-aryl-aminoxadiazole salts **434** [92] (Scheme 68). These 3-cascades imply formation of the cyanamide, its cyclization, and tautomerization.

The quantitative solid-state reaction of Viehe salt (**100**) with acetophenone (**328b**) by stoichiometric comilling at 0°C leads to the highly labile iminium salt **435** and the couple product **436** [9]. A 4-cascade is assumed consisting of substitution (Cl by enol-C of **328b**), reaction of the oxygen with a second molecule of **100**, chlorine migration, and elimination of **436**.

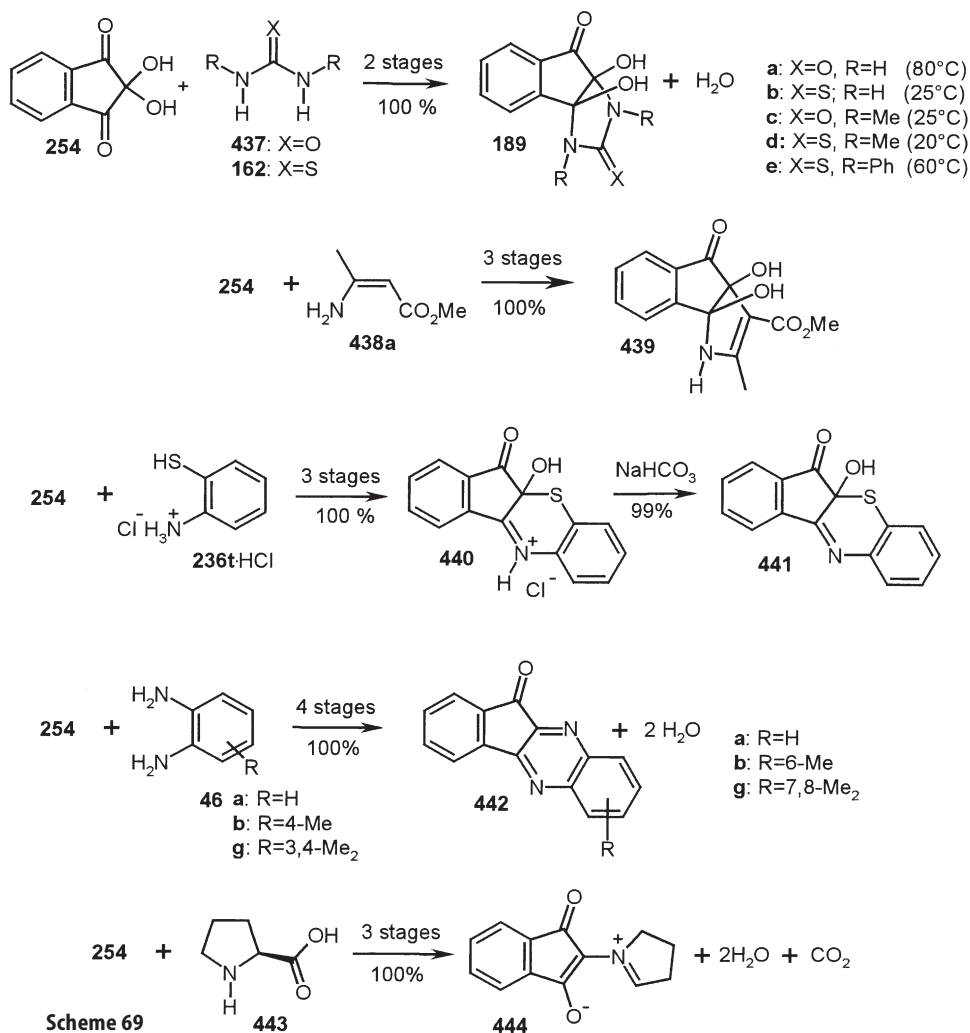
The easy access of a hydroxy group of ninhydrin (**254**) to its substitution and the presence of the carbonyl groups makes this highly reactive compound an interesting starting point for cascade reactions with amino compounds. These have been mechanistically investigated with AFM on six different faces of **254** and strictly relate to the crystal packing [94].



Scheme 68

The reactions of (thio)ureas with ninhydrin (**254**) are 2-cascades (substitution and addition) to give stable *N/O*-semiacetals (**189**) with 100% yield by stoichiometric milling at the temperatures given in Scheme 69 and drying at 140 °C in a vacuum. The 3-cascades of **254** with **438a** or the hydrochloride of **236t** provide the products **439** and **440** with 100% yield. In both cases the amino group adds to a carbonyl group of **254**, there is a substitution step (enamine or SH replacing OH), and tautomerization or elimination of water, respectively. The 4-cascades of **254** with the *o*-phenylenediamines **46a,b,g** are fully regio-specific and also quantitative upon milling at –5 °C and drying at 80 °C in a vacuum. This is an easy access to **442** with well-defined substitution. A reasonable sequence of events is addition to C=O, substitution of OH, and two eliminations of water [94]. It is remarkable that the *N/O*-semiacetals **189a,b** and **439** do not eliminate water under ordinary and rather sharp conditions. On the other hand, the six-membered rings in **440** and **442** exhibit the double bonds as a consequence of elimination of water already during the solid-state reactions. The reaction of ninhydrin with the secondary amino acid L-proline (**443**) is of particular interest as the 3-cascade (substitution, elimination, decarboxylation) provides the versatile azomethine ylide **444** with 100% yield both in small and in large runs [8], whereas tedious solution syntheses gave yields of 82% at best in small runs with difficult purification procedures required [139].

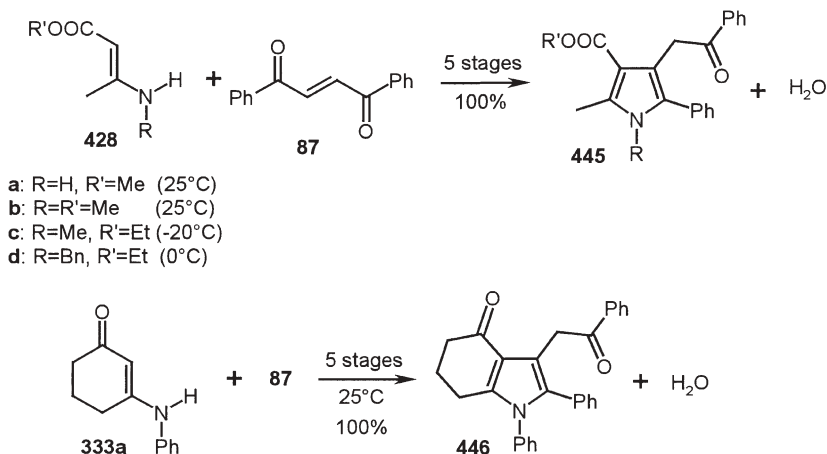
The large-scale procedure demonstrates the breakthrough in sustainable chemistry by profiting from the bargain of the crystal packing. A stoichiometric mixture of ninhydrin (**254**) and L-proline (**443**) (200 g) was milled in a 2-L horizontal ball-mill (Simoloyer) with steel balls (100Cr6, 2 kg, diameter 5 mm) at 1,100 rpm for 40 min until the liberation of CO₂ was complete. The temperature varied from 15 °C at the water-cooled walls to 21 °C in the center. The power was 800 W. Quantitative reaction to give **444** (Scheme 69) was secured by weight (146 g, 100%) and by spectroscopic techniques. The product was not



separated in a cyclone but the milling-out toward the end was completed with 4×250 mL of water. This part of the highly disperse (<1 μm) pure azomethine ylide **444** was obtained after centrifugation and drying in a vacuum. The combined water phase contained 0.2 g of **444** [8].

The solid-state interaction of enamines (**428**, **333a**) with *trans*-1,2-dibenzoyl ethene (**87**) provides quantitative yields of the pyrrole derivatives **445** or **446** [140]. These remarkable 5-cascades consist of initial vinylogous Michael addition, enol/keto tautomerism, imine/enamine tautomerism, cyclization, and elimination, all within the crystal without melting. A waste-free extraordinary atom economy is achieved that cannot nearly be obtained in solution. The milling times are unusually long here (3 h) but it's certainly worth the effort

as no purifying workup is required. The milling temperatures are listed in Scheme 70. Only in the reaction of **428c** was the elimination of water not complete upon milling and had to be finalized by short heating to 150 °C. Drying of the products **445** and **446** was performed at 80 °C in a vacuum.



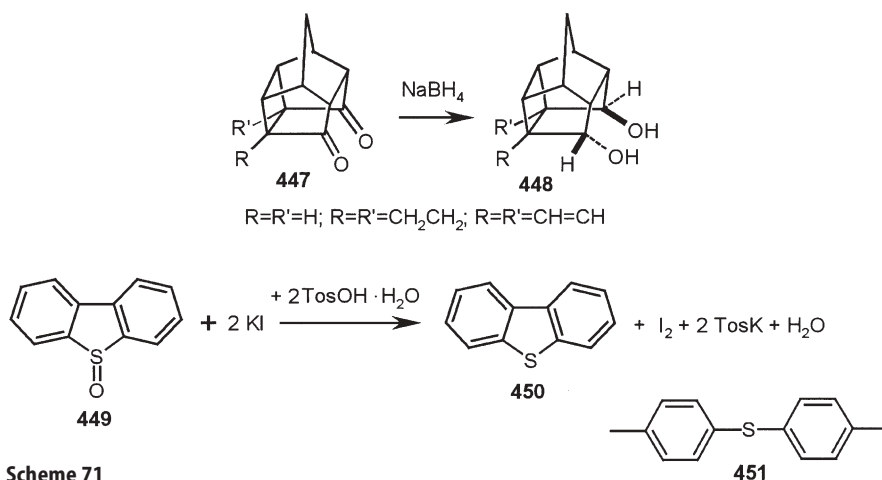
Scheme 70

Also quantitative is the solid-state oxidation (DDQ) of O,O'-diacetyl-dihydroindigo to give N,N'-diacetylindigo [22]. There are a number of further solid-state cascade reactions or solvent-free cascade reactions that cannot be treated here in detail because their yield is not quantitative or because they proceed as melt reactions. But some useful examples may be mentioned here. The gas-solid hydrolysis of *N*-arylmethylenimines (**175**) yields Troeger's base derivatives [10]. The isothiocyanate function can be transferred to aromatic aniline derivatives from 1,2-diisothiocyanatobenzene with the concomitant formation of 2-mercaptobenzimidazole (first milling at r.t. then sublimation at 100–120 °C in a vacuum) [22]. 2-Aminophenylthiol (**236t**) or thioureido-acetamides (**275**) were reacted with dimethylacetylenedicarboxylate to form benzothiazepinone derivatives [84] or iminomethylenethiazolidinones [96]. Unsubstituted five- to seven-membered lactams yield spiroaminals/aminoalkylimines at 270 °C in the presence of LiOH in preparatively useful reaction cascades [141].

26 Reduction

There are numerous preparatively useful solid-state reductions with potential for quantitative conversion and yield [142]. It appears, however, that these have not been tried under more favorable conditions in ball-mills. The stereospecific reductions of **447** to give **448** used enormous excessive amounts of reducing

agent (NaBH_4 , 21-fold) in order to achieve 100% yield upon grinding and agitating (7 days) [143] (Scheme 71). It is to be expected that proper solid-state techniques may avoid such waste of time and reagent.



Scheme 71

Solid-state reductions of sulfoxides such as **449** have been performed with potassium iodide and *p*-toluenesulfonic acid monohydrate [144]. Dibenzothiophene (**450**) or similarly bis-4-tolylsulfide (**451**) are obtained with 100% yield.

The interaction of hydrogen with organometallic complexes is reviewed in [68].

27 Oxidation

A review on solvent-free oxidation procedures with numerous oxidizing agents is given in [142]. However, the solid-state oxidations did not find much preparative interest or were not conducted to completion (see, however, the one-electron transfer reactions of stable radicals in Sect. 3) or the removal of the stoichiometrically reduced coproduct caused losses in the yield. The quantitative solid–solid oxidation of L-cysteine (**352**) by iodine to give L,L-cystine dihydroiodide (**452**) (in moist air deliquescence occurs) can serve as a precedent for countless useful and benign solid-state oxidations [22] (Scheme 72). 2-Mercaptobenzothiazole (**32**) was oxidized by nitrosonium nitrates such as **8** to give **453** and **454** upon milling. This reaction has also been mechanistically studied by AFM [1] and SNOM [15]. While solid 2-mercaptobenzothiazole (**32**) is not efficiently oxidized by solid iodine, its methylamine salt **33** is quantitatively oxidized by milling with iodine and gives **453** with 100% yield after washing with water and drying [22].

pyrocatechol (**191**) is quantitatively oxidized by milling with **456**. The highly reactive *o*-benzoquinone (**385**) is most easily reacted with solid addition partners directly in the mill. For example, diphenylfulvene **383a** was comilled to form the addition product **386** that could be extracted from DDQH (**458**) in quantitative yield [22]. Hydroquinone is oxidized by **456** and parabenzoquinone (**459**) easily sublimed off for isolation.

Nitroarylbenzhydrols (**460**) can be quantitatively oxidized by gaseous nitrogen dioxide to quantitatively give the aldehydes **77**, whereas long-chain solid primary aliphatic alcohols (**461**) provide the carboxylic acids **462** under these conditions and secondary alcohols with sufficiently high melting point give ketones. For example, benzoin (**463**) gives benzil (**338**) with 100% yield [91] (Scheme 73).

Numerous oxidative additions to organometallic complexes occur with 100% yield in the solid state. A review is given in [68]. Well-guided combustion reactions of solids proceed almost quantitatively and may be relevant despite the gaseous products.

28 Conclusion

Quantitative waste-free solid-state reactions are far from being fully appreciated. The numerous known and new examples for almost all important reaction types that are collected in this review clearly demonstrate the environmental and preparative use, as well as the mechanistic background that is so important for further exploration. Clearly, there are some crystallographic conditions and the melting points of reactants and products must not be too low. But it can be confidently assumed that the solids described here will also be amenable to further solid-state reaction types. If the solid-state equipment (vacuum facilities, mortar, mill, ultrasound cleaning bath) is not available one can always try to perform the solid–solid reactions as melt reactions at much higher temperatures, and a quantitative yield might be obtained in some exceptional cases, but unfortunately not in most cases. That is to say the profit of having a quantitative yield with 100% of pure product in a short time at low temperatures without workup requirement by using the benefits of the crystal packing is lost in melt reactions. There may, however, still be advantages of stoichiometric melt reactions over solution reactions. But milling may also be suitable and possible if very insoluble and low viscosity liquid partners are stoichiometrically reacted. Such reactions are, however, omitted in this review. Fortunately, the solid-state techniques supersede all other techniques in terms of sustainability, avoiding wastes, energy savings, time savings, work savings, ease of execution, safety, and unmatched performance in the synthesis of highly sensitive products. Furthermore, numerous products that cannot be obtained by any other technique become available now. If solid-state reactions don't work for the reasons that are discussed in this review, one should try to engineer them by using the

developed principles. Further exploration is worth the effort and unavoidable if people get acquainted with the new principles of solid-state reactivity [1, 3] and start to appreciate the avoidance of solvents and other auxiliaries including purifying workup, just by profiting from the bargain benefits of the crystal structure packing and if they trust that scale-up is possible, such as has been demonstrated in various instances.

There is still much to explore. For example, quantitative solid-state Wittig and Grignard reactions await exploration (see less than quantitative examples in [67]). First experiments are promising, but the authors did not yet care for running the reactions to completion or they did not assess the solid state even though interesting stereoselectivities emerged (review in [67]).

Material for a complete students' course has been widely spread by the OECD. This can also be downloaded from the author's homepage for use in students' education for really sustainable syntheses in the future [145].

References

1. Kaupp G (1996) In: Davies JED, Ripmeester JA (eds) *Comprehensive supramolecular chemistry*, vol 8. Elsevier, Oxford, pp 381–423 (and 21 color plates)
2. Kaupp G (2001) *Angew Chem Int Ed* 40:4508
3. Kaupp G (2003) *CrystEngComm* 5:117
4. Kaupp G, Matthies D, de Vrese C (1989) *Chem Ztg* 113:219
5. Kaupp G, Pogodda U, Schmeyers J (1994) *Chem Ber* 127:2249
6. Kaupp G, Naimi-Jamal MR, Ren H, Zoz H (2003) *Process chemical and pharmaceutical engineering worldwide* 4:24; long version: <http://vmg01.dnsalias.net/vmg/process-worldwide/download/102327/Long-Version.doc>
7. Kaupp G, Schmeyers J, Naimi-Jamal MR, Zoz H, Ren H (2002) *Chem Eng Sci* 57:763
8. Kaupp G, Naimi-Jamal MR, Ren H, Zoz H (2002) *Chem Tech* 31:58
9. Kaupp G, Boy J, Schmeyers J (1998) *J Prakt Chem* 340:346
10. Kaupp G, Schmeyers J, Boy J (2000) *J Prakt Chem* 342:269
11. Kaupp G, Schmeyers J, Boy J (2001) *Chemosphere* 43:55
12. Kaupp G, Schmeyers J, Boy J (2000) *Tetrahedron* 56:6899
13. Kaupp G (1995) *Adv Photochem* 19:119
14. Kaupp G, Herrmann A, Haak M (1999) *J Phys Org Chem* 12:797
15. Kaupp G, Herrmann A (1997) *J Phys Org Chem* 10:675
16. Kaupp G, Haak M (1998) *Mol Cryst Liq Cryst* 313:193
17. Kaupp G (2001) *Int J Photoenergy* 3:55
18. Kaupp G (2002) *Curr Opin Solid State Mater Chem* 6:131
19. Kaupp G, Schmeyers J (1995) *J Org Chem* 60:5494
20. Nakatsuji S, Takai A, Mizumoto M, Anzai H, Nishikawa K, Morimoto Y, Yasuoka N, Boy J, Kaupp G (1999) *Mol Cryst Liq Cryst* 334:177
21. Nakatsuji S, Anzai H (1997) *J Mater Chem* 7:2161
22. Kaupp G (unpublished results)
23. Dushkin AV, Rykova ZU, Shaktshneider TP, Boldyrev VV (1994) *Int J Mechanochem Mech Alloying* 1:48
24. Miller RS, Curtin DY, Paul IC (1974) *J Am Chem Soc* 96:6329

25. (a) Miller RS, Curtin DY, Paul IC (1974) *J Am Chem Soc* 96:6340; (b) Chiang CC, Lin CT, Wang AHJ, Curtin DY, Paul IC (1977) *J Am Chem Soc* 99:6303
26. Butler LG, Cory DG, Dodey KM, Miller JB, Gerroway AN (1992) *J Am Chem Soc* 114:125
27. Kaupp G, Schmeyers J, Haak M, Marquardt T, Herrmann A (1996) *Mol Cryst Liq Cryst* 276:315
28. Kaupp G, Pogodda U, Bartsch K, Schmeyers J, Ulrich A, Reents E, Juniel M (1993) *Min-derung Organischer Luftschadstoffemissionen mittels Gas/Festkörper-Reaktionen. Bericht des Bundesministers für Forschung und Technologie 01VQ9027*, 31. 3. 1993; available from Technische Informationsbibliothek, Welfengarten 1B, 30167 Hannover, Germany
29. Kaupp G, Naimi-Jamal MR, Maini L, Grepioni F, Braga D (2003) *CrystEngComm* 5:474
30. Braga D, Cojazzi G, Emiliani D, Maini L, Grepioni F (2002) *Organometallics* 21:1315
31. Kaupp G, Schmeyers J (1993) *Angew Chem Int Ed Engl* 32:1587
32. Schmeyers J (1995) PhD thesis, University of Oldenburg
33. Kaupp G, Lübben D, Sauerland O (1990) *Phosphorus Sulfur Silicon* 53:109
34. Fernandez-Bertran J, Alvarez JC, Reguera E (1998) *Solid State Ionics* 106:129
35. Barbour LJ, Caira MR, Nassimbeni LR (1993) *J Chem Soc Perkin Trans II* 2321
36. Bond DR, Johnson L, Nassimbeni LR, Toda F (1991) *J Solid State Chem* 92:68
37. Weber E, Czugler M (1988) *Top Curr Chem* 149:45
38. MacNicol DD, Toda F, Bishop R (eds) (1996) *Comprehensive supramolecular chemistry*, vol 6. Elsevier, Oxford
39. Pogodda U (1995) PhD thesis, University of Oldenburg
40. Tanaka K, Toda F (2000) *Chem Rev* 100:1025
41. Seebach D, Beck AK, Heckel A (2001) *Angew Chem Int Ed* 40:92
42. Toda F in [38], pp 463–516
43. Toda F, Tanaka K, Sekikawa A (1987) *J Chem Soc Chem Commun* 279
44. Kaupp G, Schmeyers J, Toda F, Takumi H (1996) *J Phys Org Chem* 9:795
45. Toda F, Sato A, Tanaka K, Mak TCW (1989) *Chem Lett* 873
46. Weber E, Wimmer C, Llamas-Saiz AL, Foces-Foces C (1992) *J Chem Soc Chem Commun* 733
47. Kaupp G, Sauerland O (1991) *J Photochem Photobiol A Chem* 56:375
48. Kaupp G (2002) *Photochem Photobiol* 76:590
49. Kaupp G, Haak M (1996) *Angew Chem Int Ed Engl* 35:2774
50. Aldoshin SM, Alfimov MV, Atovmyan LO, Kaminsky VF, Razumov VF, Rachinsky AG (1984) *Mol Cryst Liq Cryst* 108:1
51. Kaupp G, Schmeyers J (2000) *J Photochem Photobiol B Biol* 59:15
52. Tanaka K, Hiratsuka T, Ohba S, Naimi-Jamal MR, Kaupp G (2000) *J Phys Org Chem* 16:905
53. Liu RSH, Hammond GS (2001) *Chem Eur J* 7:4537
54. Hadjoudis E, Schmidt GMJ (1972) *J Chem Soc Perkin Trans II* 1060
55. Hadjoudis E (1973) *Israel J Chem* 63
56. Hadjoudis E (1986) *Mol Cryst Liq Cryst* 134:237
57. Wallis ES, Adams FH (1933) *J Am Chem Soc* 55:3838
58. Kaupp G, Matthies D (1987) *Chem Ber* 120:1897
59. Kaupp G (1994) *Mol Cryst Liq Cryst* 242:153
60. Kaupp G, Kuse A (1998) *Mol Cryst Liq Cryst* 313:361
61. Kaupp G, Matthies D (1988) *Mol Cryst Liq Cryst* 161:119
62. Dose K (1981) *Orig Life* 11:165

63. Liardon R, Ledermann S, Ott U (1981) *J Chromatogr* 203:385
64. Bonner WA, Blair NE, Lemmon RM (1979) *Orig Life* 9:279
65. Pincock RE, Tong MM, Wilson KR (1971) *J Am Chem Soc* 93:1669
66. Khruscheva NS, Loim NM, Sokolov VI, Makhaev VD (1997) *J Chem Soc Perkin Trans I* 2425
67. Kaupp G (2005) Stereoselective thermal solid-state reactions. In: Toda F (ed) (*preliminary*) *Organic solid-state reactions*. Wiley-VCH, Weinheim, *in preparation*
68. Coville NJ, Cheng L (1998) *J Organomet Chem* 571:149
69. Sabra F, Bassus J, Lamartine R (1990) *Mol Cryst Liq Cryst* 186:69
70. Lamartine R, Perrin R, Thozet A, Perrin M (1983) *Mol Cryst Liq Cryst* 96:57
71. Miller RS, Curtin DY, Paul IC (1972) *J Am Chem Soc* 94:5117
72. Schmitt A (1863) *Justus Liebigs Ann Chem* 127:319
73. Kaupp G (1994) *J Vac Sci Technol B* 12:1952
74. Kaupp G, Matthies D (1986) *Chem Ber* 119:2387
75. Kaupp G, Seep C (1988) *Angew Chem Int Ed Engl* 27:1511
- 75a. The reported coloration by HCl and HBr gas could not be reproduced with pure (from lanolin) or sublimed cholesterol
76. Kaupp G (1988) *Top Curr Chem* 146:57
77. Kaupp G, Ulrich A, Sauer G (1992) *J Prakt Chem* 334:383
78. Gerdil R, Barchietto G (1994) *Helv Chim Acta* 77:691
79. Kaupp G, Schmeyers J (2000) *J Phys Org Chem* 13:388
80. Kaupp G (1991) *Merck Spectrum* 3:42
81. Kaupp G, Knichala B (1985) *Chem Ber* 118:462
82. Kaupp G, Frey H, Behmann G (1985) *Synthesis* 555
83. Kaupp, Hunkler GD, Zimmermann I (1982) *Chem Ber* 115:2467
84. Kaupp Gründken GE, Matthies D (1986) *Chem Ber* 119:3109
85. Kaupp G, Matthies D (1987) *Chem Ber* 120:1741
86. Kaupp G (1984) *Chem Ber* 117:1643
87. Kaupp G (1985) *Chem Ber* 118:4271
88. Toda F, Takumi H, Akehi M (1990) *Chem Commun* 1270
89. Kaupp G (2004) Träger's base derivatives. In: *Encyclopedia of supramolecular chemistry*. Marcel Dekker, New York, pp 1516–1524
90. Kaupp G, Stepanenko VA, Naimi-Jamal MR (2003) *Eur J Org Chem* 9:4156
91. Boy J (1999) PhD thesis, University of Oldenburg
92. Kaupp G, Schmeyers J, Boy J (1998) *Chem Eur J* 4:2467
93. Eppe M, Krischnick H (1996) *Chem Ber* 129:1123
94. Kaupp G, Naimi-Jamal MR, Schmeyers J (2002) *Chem Eur J* 8:594
95. Chuev VP, Lyagina LA, Ivanov EY, Boldyrev VV (1989) *Dokl Acad Nauk SSSR* 307:1429
96. Schmeyers J, Kaupp G (2002) *Tetrahedron* 58:7241
97. von Gorup-Besanez E (1863) *Justus Liebigs Ann Chem* 125:281
98. Kaupp G, Herrmann A (1997) *J Prakt Chem* 339:256
99. Kaupp G, Herrmann A, Schmeyers J (2002) *Chem Eur J* 8:1395
100. Kaupp G, Metwally MA, Amer FA, Abdel-latif E (2003) *Eur J Chem* 1545
101. Schmeyers J, Toda F, Boy J, Kaupp G (1998) *J Chem Soc Perkin Trans II* 989
102. Schmeyers J, Toda F, Boy J, Kaupp G (2001) *J Chem Soc Perkin Trans II* 132
103. Kaupp G, Naimi-Jamal MR, Schmeyers J (unpublished results)
104. Kaupp G, Naimi-Jamal MR (2002) *Eur J Org Chem* 1368
105. Ebana T, Yokota K, Takada Y (1978) *Hokkaido Daigaku Kogakubu Kenkyu Hokoku* 89:127; *Chem Abstr* (1979) 91:157660
106. Reddy VP, Prasunamba PL, Reddy PSN, Ratnam CV (1983) *Indian J Chem B* 22:917

107. Kaupp G, Naimi-Jamal MR, Schmeyers J (2003) *Tetrahedron* 59:3753
108. Tashiro K, Zadorin AN, Saragai S, Kamae T, Matsumoto A, Yokoi K, Aoki S (1999) *Macromolecules* 32:7946
109. Kaupp G (1975) Dimerisierungen und cycloadditionen zwischen ungleichen olefinen. In: Houben-Weyl, Methoden der organischen chemie, vol IV/5a. Thieme, Stuttgart, chaps C.4 and C.5
110. Kaupp G (1995) Cyclobutane synthesis in the solid phase. In: Horspool WM (ed) *CRC Handbook of organic photochemistry and photobiology*. CRC, Boca Raton, chap 4
111. Kaupp G, Frey H, Behmann G (1988) *Chem Ber* 121:2135
112. Kaupp G, Zimmermann I (1981) *Angew Chem Int Ed Engl* 20:1018
113. Kaupp G (1994) *J Microsc* 174:15
114. Kaupp G (1994) *Mol Cryst Liq Cryst* 252:259
115. Kaupp G, Jostkleigrewe E, Hermann HJ (1982) *Angew Chem Int Ed Engl* 21:435
116. Ohba S, Ito Y (2003) *Acta Cryst B* 59:149
117. Marubayashi N, Ogawa T, Hamasaki T, Hirayama N (1997) *J Chem Soc Perkin Trans II* 1309
118. Nakanishi H, Jones W, Thomas JM, Hursthouse MB, Motevalli M (1981) *J Phys Chem* 85:3636
119. Miller EJ, Brill TB, Rheingold AL, Fultz WC (1983) *J Am Chem Soc* 105:7580
120. Kaupp G (2000) *ACS Int Chem Congress of Pacific Basin Societies*. Honolulu, Hawaii Org, 1253
121. Kim JH, Hubig SM, Lindeman SV, Kochi JK (2001) *J Am Chem Soc* 123:4951
122. Kaupp G (1973) *Liebigs Ann Chem* 844
123. Wilson WL, Rahn JA, Alcock NW, Fischer J, Frederick JH, Nelson JH (1994) *Inorg Chem* 73:109
124. Toda F, Tanaka K (1994) *Supramol Chem* 3:87
125. Kaupp G, Haak M (1993) *Angew Chem Int Ed Engl* 32:694
126. Kaftory M, Yagi M, Tanaka K, Toda F (1988) *J Org Chem* 53:4391
127. Kaupp G, Schmeyers J, Kato M, Tanaka K, Harada N, Toda F (2001) *J Phys Org Chem* 14:444
128. Toda F, Tanaka K, Tamashima T, Kato M (1998) *Angew Chem Int Ed* 37:2724
129. Kaupp G, Schmeyers J, Kato M, Tanaka K, Toda F (2002) *J Phys Org Chem* 15:1
130. Tanaka K, Takamoto N, Tezuka Y, Kato M, Toda F (2001) *Tetrahedron* 57:3761
131. Kaupp G, Boy J (1997) *Angew Chem Int Ed Engl* 36:48
132. Kaupp G, Sailer K (1996) *J Prakt Chem* 338:47
133. Kaupp G, Jaskulska E, Sauer G, Michl G (1994) *J Prakt Chem* 336:686
134. Kaftory M (1983) *J Am Chem Soc* 105:3832
135. McKillop KL, Gillette GR, Powell DR, West R (1992) *J Am Chem Soc* 114:5203
136. Wiedemann R, Wolf J, Werner H (1995) *Angew Chem Int Ed Engl* 34:1244
137. Werner H, Rappert T, Baum M, Stark A (1993) *J Organomet Chem* 459:319
138. Kaupp G, Amer FA, Metwally MA, Abdel-latif E (2003) *J Heterocyclic Chem* 40:963
139. Johnson AW, McCaldin DJ (1958) *J Chem Soc* 817
140. Kaupp G, Schmeyers J, Kuse A, Atfeh A (1999) *Angew Chem Int Ed* 38:2896
141. Denisenko SN, Pasch E, Kaupp G (1989) *Angew Chem Int Ed Engl* 28:1381
142. Tanaka K (2003) *Solvent-free organic synthesis*. Wiley-VCH, Weinheim
143. Marchand AP, Reddy GM (1991) *Tetrahedron* 47:6571
144. Fujiki K, Kurita S, Yoshida E (1996) *Synth Commun* 26:3619
145. Kaupp G, Schmeyers J, Naimi-Jamal MR (2001) A practical students course: environmentally benign chemical syntheses. Case study for distribution by OECD. Also available at <http://kaupp.chemie.unioldenburg.de>

The Mechanochemical Solid-State Reaction of Fullerenes

Koichi Komatsu (✉)

Institute for Chemical Research, Kyoto University, Uji, Kyoto 611-0011, Japan
komastu@scl.kyoto-u.ac.jp

| | | |
|-----|---|-----|
| 1 | Introduction | 185 |
| 2 | Solid-State Fullerene Reactions | 187 |
| 2.1 | Complex Formation | 187 |
| 2.2 | Dimerization and Trimerization | 188 |
| 2.3 | [4+2] Cycloaddition | 193 |
| 2.4 | 1,3-Dipolar Addition | 197 |
| 2.5 | Nucleophilic Addition | 200 |
| 3 | Conclusion | 203 |
| | References | 204 |

Abstract More than a decade has passed since fullerenes became available to researchers in almost all fields of science. The explosive development of study on the chemical functionalization of fullerenes has led to a wide variety of fullerene derivatives. However, most of these reactions have been carried out in the liquid phase, and curiously enough the solid-state reaction (or solid–solid reaction) of fullerenes has been developed only in recent years. This chapter focuses on the solid-state reaction of fullerenes, particularly the reaction which was conducted under what is called “high-speed vibration milling” conditions. It will be shown how this reaction technique is pertinent for the creation of fullerene derivatives with novel structures, and how efficient this method is for certain reactions compared with the liquid-phase reaction.

Keywords Fullerenes · Mechanochemistry · Dimerization · Cycloaddition · Nucleophilic addition

1 Introduction

For the solid-state reaction to take place, the reactants have to be vigorously mixed by applying external mechanical energy. Thus, the solid-state reaction may be called mechanochemistry. Mechanochemistry has been used mostly for inorganic solids (for example, for alloying, interaction of soft metals with ceramics, activation of minerals for catalysis, and so on) [1, 2] and for inor-

ganic–organic composite materials [3]. However, application of this method to purely organic reactions had not been well developed before the pioneering and systematic work by Toda and coworkers [4], as described in the previous chapters. The solid-state reactions are attractive not only because of the simplicity of the procedure, but also particularly from the viewpoint of environmental protection because there is no need for the use of harmful organic solvents.

As the procedure for mechanochemical solid-state reactions, the simplest is grinding using a mortar and pestle. When a longer reaction time is required, ball milling is used [5]. In the case when higher energy is necessary, the so-called Wiggle-Bug-type mill is more efficient. This is a rapidly vibrating mixer-mill, frequently used in the laboratory for the purpose of milling crystals of KBr into fine powder to be pressed to form a pellet for IR spectral measurement of organic compounds. The main part of this type of mill, which we refer to as a “high-speed vibration mill” or “HSVM” in this article, is essentially a stainless-steel capsule and a milling ball, which are rapidly vibrated at the speed of 3,500 rpm (for our home-built mill) or 1,700 rpm (for a commercial mill). Based on the observation of phase transformation of inorganic material such as BeF_2 and B_2O_3 , pressures as high as 10–20,000 bars are considered to be generated and applied to the particles during the milling process by the use of a HSVM [6].

The chemical reactions are usually driven by the action of external activation such as heat, photoirradiation, microwave irradiation, and so on. In the case of mechanochemical solid-state reactions, the mechanical energy, such as that caused by stress, friction, and shear deformation, is considered as the important external activator. Organic reactions are generally conducted in solution, whereas in the mechanochemical reactions any solvent is eliminated and thus the reacting species are free from solvation. These two unusual factors, i.e., the generation of local high pressure caused by mechanical energy and the absence of solvation, are expected to cause some novel reactions, which cannot take place in liquid-phase reactions. These reaction conditions are also considered to be ideal for the reaction of fullerenes, which are hardly soluble in common organic solvents.

Fullerenes, among which the representative and most abundant is the I_h symmetrical C_{60} with 30 double bonds and 60 single bonds, are known to behave as electron-deficient polyenes rather than aromatic compounds [7]. The energy level of the triply degenerate LUMO of C_{60} is almost as low as those of *p*-benzoquinone or tetracyanoethylene. Thus, a wide variety of reactions have been reported for C_{60} such as nucleophilic addition, [4+2] cycloaddition, 1,3-dipolar addition, radical and carbene additions, metal complexation, and so on [7]. Fullerene C_{60} also undergoes supramolecular complexation with various host molecules having electron-donating ability and an adequate cavity size [8].

When subjected to solid-state organic reactions under HSVM conditions, fullerenes have been found to give both the expected and unexpected products as shown in the next sections and in review articles [9].

2

Solid-State Fullerene Reactions

2.1

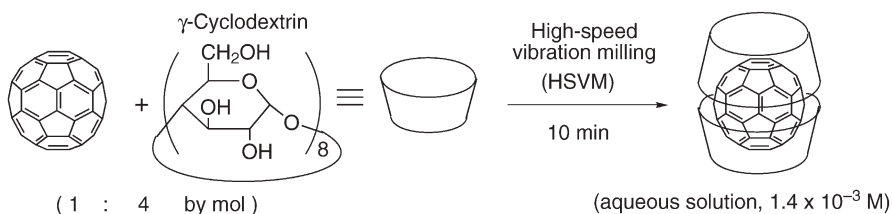
Complex Formation

It had been reported that fullerene C_{60} forms a water-soluble complex with γ -cyclodextrin by heating with an excess amount of γ -cyclodextrin in water [10] or in a mixture of refluxing water and toluene for a long time, such as 30 h [11]. The isolated complex is considered to have the C_{60} structure bicapped with γ -cyclodextrin in a molar ratio of 1:2 [11], and the complex dissolved in water to give a solution of C_{60} with a concentration of nearly 10^{-4} mol L^{-1} [10, 11]. Fullerene C_{60} was also solubilized in water by complexation with a sulfocalix[8]arene, i.e., calix[8]aryloxy-49,50,51,52,53,54,55,56-octakis(propene-3-sulfonate). The concentration of this complex in water is estimated as 5×10^{-4} mol L^{-1} [12]. Complex formation between fullerene and various calixarenes has also been reported [8].

In contrast to the high temperature required for the liquid-phase treatment described above, the ball milling of C_{60} with an excess of γ -cyclodextrin for 20 h conducted at room temperature afforded a mixture containing C_{60} - γ -cyclodextrin complex, which can give an aqueous solution of C_{60} in a concentration of 1.5×10^{-4} mol L^{-1} [13]. It was also reported that simple kneading of C_{60} and γ -cyclodextrin for 1 h with dropwise addition of hexane can give the 1:1 and 1:2 complexes according to the ratio of the starting materials [14]. The formation of water-soluble complexes of C_{60} and solid amines by grinding was also reported [15].

The complexation of fullerenes and γ -cyclodextrin was found to take place more efficiently by the use of a HSVM. Thus, when C_{60} was vigorously shaken with 4 molar equivalents of γ -cyclodextrin for only 10 min by HSVM and the resulting mixture dissolved in 4 mL of water, a magenta-colored solution of C_{60} was obtained by filtration with a membrane filter (Scheme 1) [16]. The concentration of C_{60} was 1.4×10^{-3} mol L^{-1} , which is the highest value for C_{60} dissolved in water. When this aqueous solution was let stand for 2 weeks, the C_{60} - γ -cyclodextrin 1:2 complex was obtained as purple crystals.

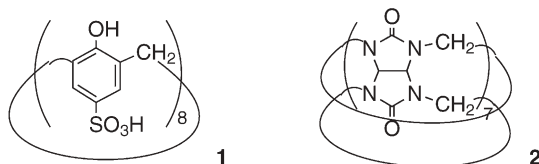
The similar HSVM treatment of C_{70} with γ -cyclodextrin also gave a solution of C_{70} in water at a concentration of 7×10^{-4} mol L^{-1} , which is one order of mag-



Scheme 1 The HSVM reaction of C_{60} with γ -cyclodextrin

nitude higher than the solution obtained by boiling C_{70} in a concentrated aqueous solution of γ -cyclodextrin for several hours [17].

Other than γ -cyclodextrin, sulfocalixarene **1** [16] and cucurbit[7]uril **2** [18] are also effective in complexation with C_{60} by use of the solid-state HSVM method.

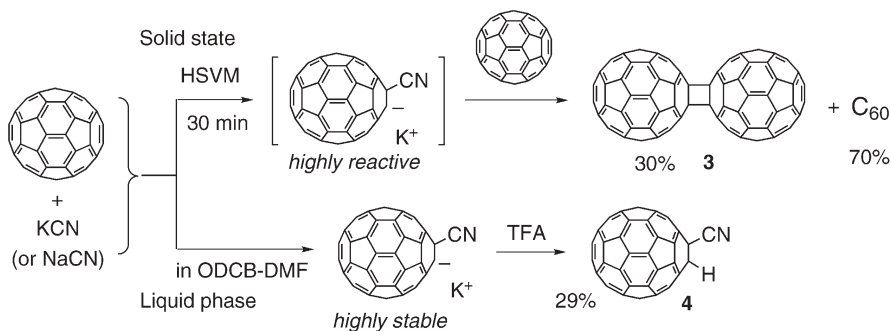


2.2

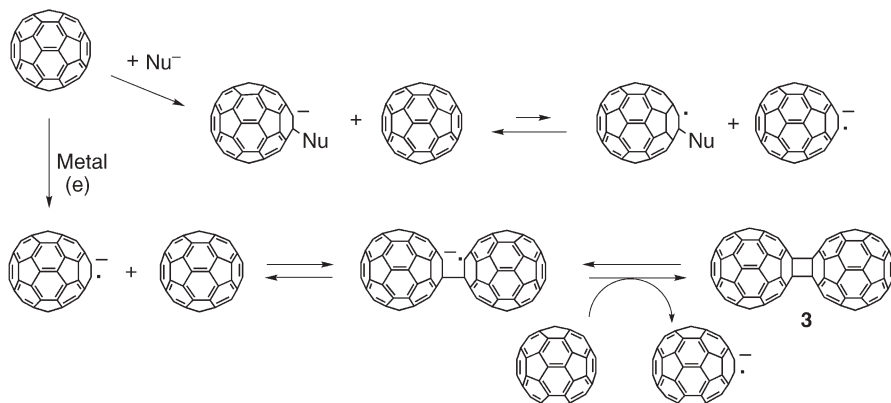
Dimerization and Trimerization

Since there are 30 double bonds to react in fullerene C_{60} , the [2+2] cycloaddition of C_{60} molecules at these bonds results in the formation of so-called fullerene polymers [19]. Although it seemed important to clarify the structure and properties of the most basic unit of these polymers such as dimers and trimers, the method for preparation of these polymers such as high-pressure/high-temperature treatment or photoirradiation was not suitable to stop the [2+2] reaction at the stage of dimerization or trimerization.

On the other hand, the mechanochemical solid-state reaction was found to be the most suitable for this purpose. Thus, when the solid-state reaction was conducted for C_{60} in the presence of one equivalent or less of KCN under the HSVM conditions for 30 min, a clean reaction took place to give the [2+2] fullerene dimer C_{120} (**3**) in 30% yield while 70% of C_{60} was recovered unchanged (Scheme 2) [20]. It is to be noted that no cyanated fullerene such as **4** was obtained in comparison to the result of a liquid-phase reaction in *o*-dichlorobenzene (ODCB)-DMF [21]. This is apparently ascribed to the difference in reactivity of the initially formed cyanated C_{60} anion with or without solvation.



Scheme 2 The reaction of C_{60} with KCN in the solid state and in the liquid phase

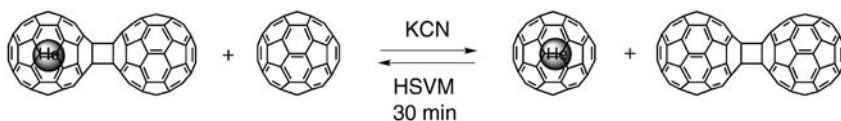


Scheme 3 Possible mechanism for the dimerization of C_{60} in the solid state

Since this dimerization also took place by the action of a catalytic amount of alkali metals [22, 23], the reaction was supposed to proceed through the formation of the fullerene radical anion as shown in Scheme 3 [23, 24]. Effective catalysts for the dimerization of C_{60} under the HSVM conditions for 30 min were metals such as Li (yield of **3**, 28%), Na (32%), K (29%), Mg (18%), Al (22–34%), Fe (15%), Zn (11–19%), and Cu (10%), potassium salts such as KCN (29%), KOH (28%), KOAc (27%), K_2CO_3 (15%), and KSCN (7%), and solid amines such as 4-aminopyridine (43%), 3,4-diaminopyridine (38%), 4-(dimethylamino)pyridine (29%), and imidazole (32%) [23, 24].

The time dependence of this KCN-catalyzed dimerization of C_{60} under the HSVM conditions, and also of the HSVM treatment of the dimer **3** under the same conditions, indicated that the reaction reaches a kind of equilibrium state after the reaction time of 30 min as shown in Fig. 1. The relative amount of C_{60} and dimer **3** (7:3) at the apparent equilibrium state reflects the relative thermodynamic stability of C_{60} and dimer **3** [23].

The establishment of the equilibrium state is also confirmed by a scrambling experiment using the dimer **3** with one of the C_{60} cages labeled by ^3He encapsulation. As shown in Scheme 4, the HSVM treatment of unlabeled (empty) C_{60} with labeled **3** for 30 min in the presence of KCN as a catalyst resulted in scrambling of labeled C_{60} in both monomer and in dimer **3** in a ratio of 3:7, as examined by ^3He NMR spectroscopy [23]. The structure of



Scheme 4 Scrambling of ^3He -containing C_{60} between C_{60} and C_{120} under HSVM; integrated peak ratio of $^3\text{He}@C_{60}$ and $^3\text{He}@C_{120}$ = 7:3 by ^3He NMR

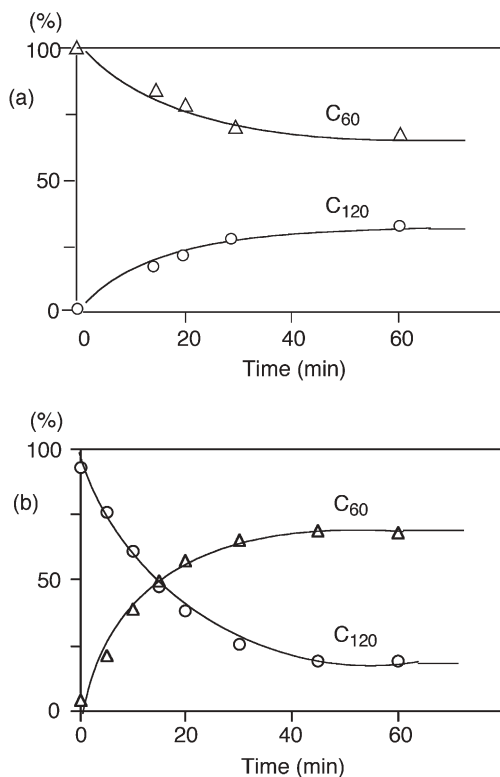


Fig. 1 Time dependence of the components of the reaction mixture for the HSVM treatment of **a** C_{60} with KCN and **b** C_{120} (3) with KCN

dimer 3 was determined by X-ray crystallography to be a dumbbell shape as shown in Fig. 2 [20].

Subsequently, the formation of dimer 3 was also attained in a higher yield of 80% by heating the 1:2 cocrystals of C_{60} and bis(ethylenedithio)tetrathiafulvalene at 200 °C under a high pressure of 5 GPa [25]. Simple grinding of a mixture of C_{60} and K_2CO_3 was also reported to give dimer 3 in 15% yield [26]. It was also reported that, when this grinding was conducted for C_{70} with K_2CO_3 ,

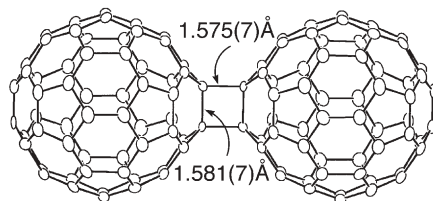
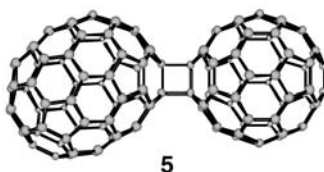
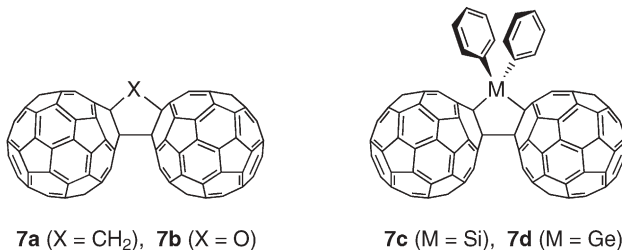


Fig. 2 The X-ray crystallographic structure of fullerene dimer C_{120} (3)

The solid-state reaction of C₆₀ with one equivalent of C₇₀ in the presence of 4-aminopyridine under the HSVM conditions for 30 min afforded a cross dimer of these two fullerenes, C₁₃₀ (**5**), albeit in a low yield (3%) [27]. The ¹³C NMR and UV-vis spectral analyses of the product indicated that only an isomer having a C₆₀ cage attached to the 1,2-junction bond of C₇₀ was selectively produced by this reaction, in addition to C₁₂₀ (**3**).



In addition to the dumbbell-type structure **3**, fullerene dimer structures having the two fullerene cages connected by a single bond and a methylene or an oxa bridge such as **7a** and **7b** are possible, and have been actually reported



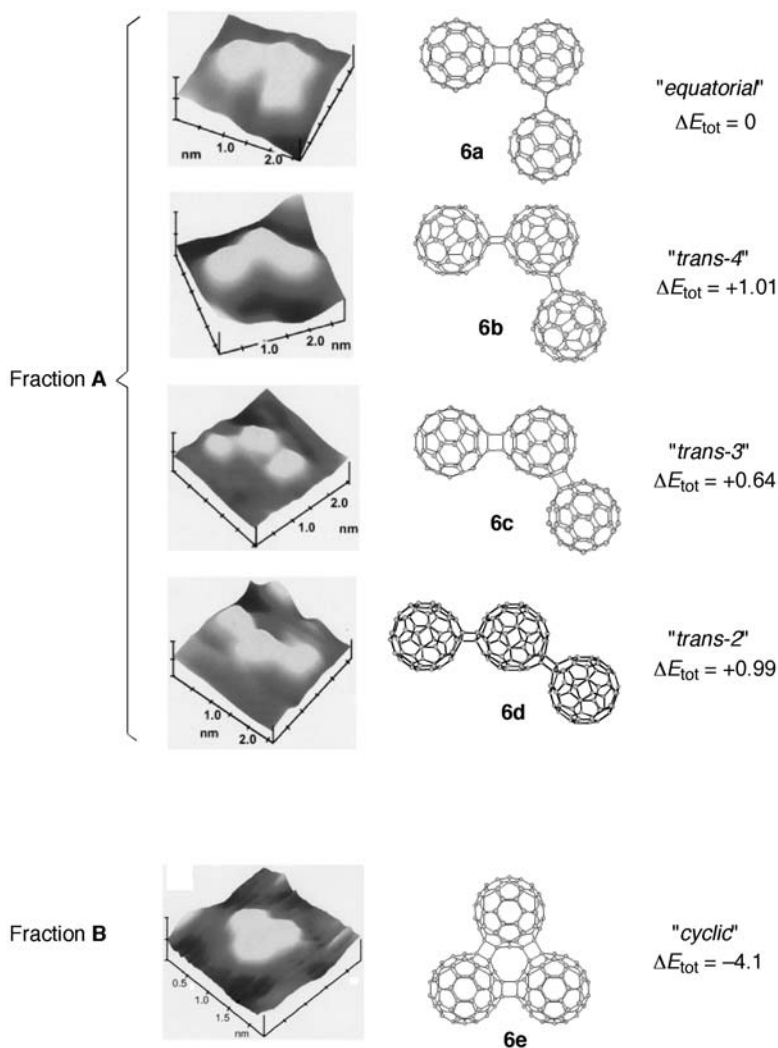


Fig. 3 STM images of fraction A containing fullerene trimers **6a–6d** and fraction B containing **6e**, together with the calculated energy relative to that of “equatorial” isomer

to be formed by thermal reactions of solid precursors [30, 31]. On the other hand, the solid-state reaction under the HSV conditions was found to be applicable to the synthesis of this type of C₆₀ dimer connected by a silicon or germanium bridge **7c** or **7d** [32, 33]. Thus, the HSV reaction of C₆₀ with dichlorodiphenylsilane or dichlorodiphenylgermane, and lithium powder, in a molar ratio of 1:4:6 or 1:4:10 for 30 min afforded **7c** in 7.5% yield with unchanged C₆₀ (67%) [32] or **7d** in 9% yield with unchanged C₆₀ (37%) [33], respectively. Upon electrochemical reduction of these two dimers, the two C₆₀

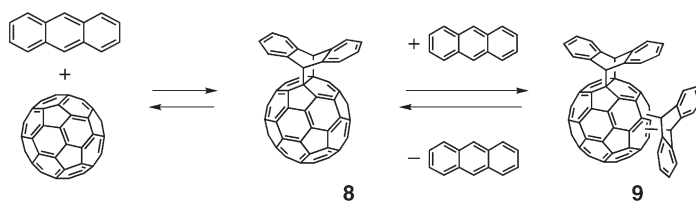
cages were found to be reduced not at the same time but in a stepwise manner, indicating the presence of electronic interaction between the two cages in both **7c** and **7d**.

2.3

[4+2] Cycloaddition

The reactions described in the previous section are assumed to proceed with one-electron transfer as a key step. On the other hand, [4+2] cycloaddition reactions, which should proceed in a concerted manner in solution, were also found to proceed efficiently for fullerene C_{60} under the HSVM solid-state reaction conditions.

As a typical example, the HSVM reaction of C_{60} with anthracene was examined in detail. In solution with heating, the reaction is supposed to reach an equilibrium state, where unreacted C_{60} , monoadduct **8**, and bisadduct **9** coexist (Scheme 5) [34]. For example, the reaction even at such a high temperature as 200 °C in a naphthalene solution for 48 h afforded **8** in only 39% yield with unchanged C_{60} being recovered in 42% yield [34a]. In contrast, the HSVM reaction of C_{60} with 1.2 equivalents of anthracene for 1 h afforded **8**, **9**, and unchanged C_{60} in 55, 19, and 12% isolated yields, respectively [35]. It is of interest to see if an apparent equilibrium state similar to that in the liquid-phase reaction can also be reached in the solid-state reaction. The time dependence of the HSVM reaction of C_{60} and 1.2 equivalents of anthracene, producing **8** and **9**, is shown in Fig. 4a [35]. Apparently the time-dependence curve for the formation of **8** reaches a plateau with almost 60% yield at the reaction time of 30 min. The reverse reaction, i.e., the dissociation of adduct **8**, was also found to take place under the HSVM conditions, and its time dependence also indicates that the time–dissociation curve appears to reach a plateau after about 30 min, again leaving nearly 60% of the starting material **8** unchanged as shown in Fig. 4b. Thus, a kind of equilibrium state appears to be attained even under the present heterogeneous solid-state reaction conditions [35].



Scheme 5 Equilibrated reaction of C_{60} with anthracene

The crystalline monoadduct **8** has been reported to undergo a regiospecific thermal disproportionation into a solid 1:1 mixture of C_{60} and the *trans*-1 bisadduct isomer **9a** (Scheme 6) [36]. However, bisadducts **9** obtained under the HSVM conditions were a mixture of positional isomers [35].

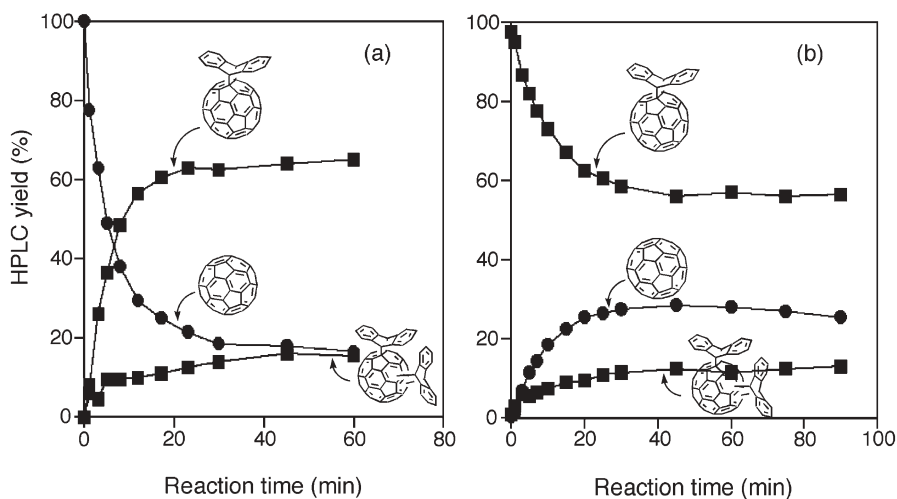
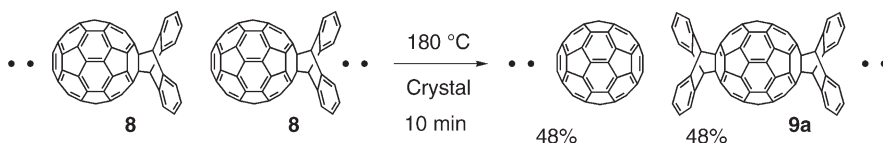


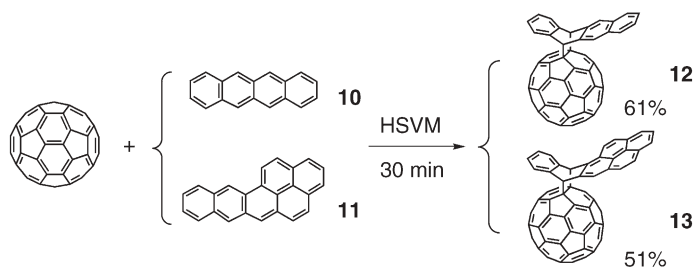
Fig. 4 Time dependence of **a** HSVM reaction of C_{60} with anthracene (1.2 equiv) and **b** HSVM treatment of 1:1 C_{60} -anthracene adduct **8**



Scheme 6 Thermal disproportionation reaction of C_{60} -anthracene adduct **8** in crystal

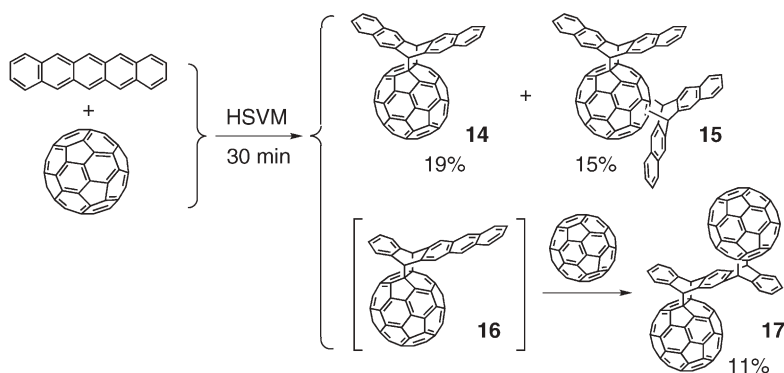
The solid-state HSVM reaction of C_{60} with tetracene (**10**) and with naphtho[2,3-*a*]pyrene (**11**) afforded the corresponding [4+2] cycloadducts **12** and **13** in 61 and 51% yield, respectively (Scheme 7) [35].

In the case of the reaction of C_{60} with pentacene, the solution-phase reaction in refluxing toluene for 72 h gave only the monoadduct **14** and bispentacene



Scheme 7 Solid-state HSVM reactions of C_{60} with tetracene (**10**) and with naphtho[2,3-*a*]pyrene (**11**)

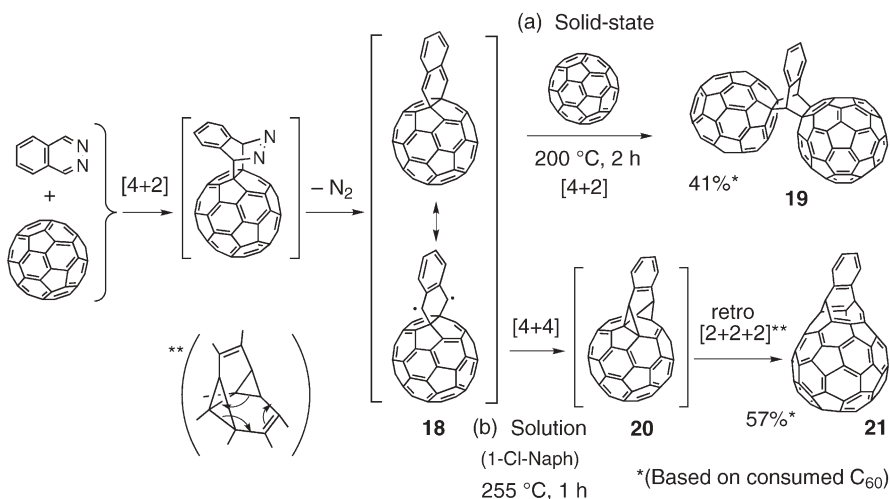
adducts **15** in 59 and 13% yield, respectively, in accordance with the generally known highest reactivity at 6,13-carbons of pentacene [37]. In sharp contrast, the HSVM reaction of C_{60} with an equimolar amount of pentacene for 1 h afforded not only the adducts **14** and **15** in 19 and 15% yield, respectively, but also the bisfullerene adduct **17** in 11% yield [35]. The formation of **17** apparently indicates that C_{60} successfully trapped the thermodynamically less favored monoadduct **16** formed by the cycloaddition of C_{60} at 5,14-carbons (Scheme 8).



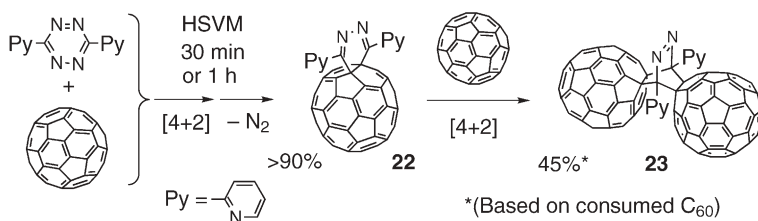
Scheme 8 Solid-state HSVM reactions of C_{60} with pentacene

As was described in Sect. 2.2, the mechanochemical solid-state reaction using HSVM is characteristic in giving a product totally different from that obtained from the liquid-phase reaction. Another example is the reaction of C_{60} with phthalazine, i.e., 2,3-diazanaphthalene. This reaction afforded bisfullerene compound **19** with two C_{60} cages incorporated in a benzobicyclo[2.2.2]octene framework under the solid-state HSVM conditions followed by heating, while the reaction gave an open-cage benzofullerene derivative **21** when heated at 255 °C in a 1-chloronaphthalene solution [38]. These reactions are considered to proceed via a common intermediate **18** as shown in Scheme 9. Thus, the intermediate **18**, formed by the first [4+2] reaction of the starting materials and following nitrogen elimination, is subjected to the second [4+2] cycloaddition with one of the C_{60} molecules surrounding **18** in place of solvent molecules to give bisfullerene compound **19** in the solid-state reaction (route a). In contrast, when **18** is formed in solution and surrounded by solvent molecules, the highly reactive butadiene unit of the orthobenzoquinodimethane structure in **18** undergoes an intramolecular formal [4+4] reaction with the fullerene diene system to give **21** via the retro [2+2+2] reaction of the second intermediate **20** (route b) in the liquid-phase reaction.

A quite similar type of solid-state [4+2] reaction was also observed between C_{60} and an equimolar amount of di(2-pyridyl)-1,2,4,5-tetrazine under the HSVM conditions for 1 h (Scheme 10). The reaction was very clean and the ^1H and ^{13}C NMR spectra of the resulting brown powder exhibited signals corre-



Scheme 9 Reaction of C₆₀ with phthalazine **a** in the solid state and **b** in solution

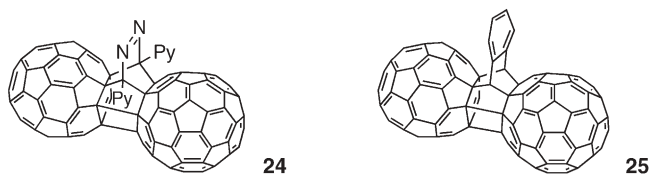


Scheme 10 Solid-state HSVM reactions of C₆₀ with 3,6-di(2-pyridyl)-1,2,4,5-tetrazine

sponding to 1:1 adduct **22** as a single product only contaminated by a small amount (5%) of unreacted C₆₀ [39]. The isolated yield of **22** was larger than 90%, and this is to be compared with 50–60% yield when the same reaction was conducted in refluxing toluene [40].

On the other hand, when the HSVM reaction was conducted between the same reactants in a 2:1 molar ratio and the resulting mixture was further heated at 150 °C for 2 h, a similar reaction to Scheme 9 took place to give bisfullerene compound **23** with two C₆₀ cages incorporated in a 2,3-diazadiazabicyclo[2.2.2]oct-2-ene framework in 27% yield along with 40% of recovered C₆₀ [41].

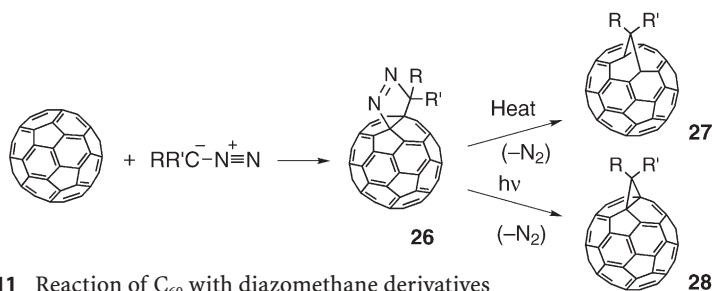
Both of the bisfullerene compounds **19** and **23** undergo the intramolecular [2+2] reaction in chloroform and in ODCB, respectively, to give **24** [38] and **25** [41] quantitatively under irradiation by visible light. In these newly formed bisfullerene compounds, the electronic interaction between two C₆₀ cages was found to be greater than that in **19** and **23**, as examined by electrochemical measurements, due to the closely fixed geometry.



2.4

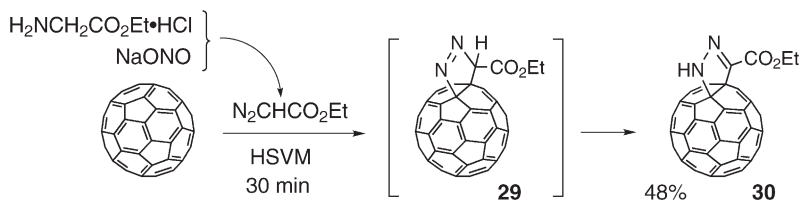
1,3-Dipolar Addition

The 1,3-dipolar addition reaction of fullerene with diazo compounds is one of the most studied reactions in the early stage of the research on fullerene chemistry [7]. The reaction in solution first affords rather labile fulleropyrazoline derivative **26**, which is readily converted to the so-called 5,6-open (a bond originally shared by five- and six-membered rings cleaved) fulleroid (**27**) or 6,6-closed (a bond shared by two six-membered rings remaining closed) methanofullerene derivatives (**28**) by heat (e.g., refluxing in toluene) or photoirradiation (UV light), respectively (Scheme 11) [7a].



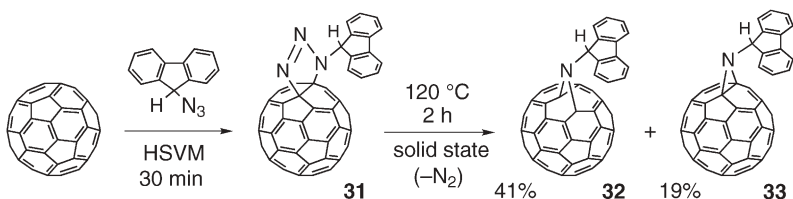
Scheme 11 Reaction of C_{60} with diazomethane derivatives

The feasibility of this reaction under mechanochemical conditions was examined in the following manner. When a mixture of C_{60} , glycine ethyl ester hydrochloride, and sodium nitrite in a molar ratio of 1:1:2 was vigorously milled under the HSVM conditions for 30 min, ethyl diazoacetate, which was formed in situ, immediately reacted with C_{60} to give fulleropyrazoline, i.e., fullerene-fused 2-pyrazoline **30**, in 48% yield (87% yield based on consumed C_{60}) [42]. Pyrazoline **30** was apparently formed by isomerization of 1-pyrazoline **29** formed as the product of direct 1,3-dipolar addition of ethyl diazoacetate to C_{60} (Scheme 12). Actually the reaction of C_{60} with an equimolar amount of ethyl diazoacetate itself conducted under the HSVM conditions for only 6 min gave 2-pyrazoline **30** in 45% yield, together with a mixture of methanofullerene **28** ($R=H$, $R'=CO_2Et$) and fulleroids **27a** ($R=H$, $R'=CO_2Et$) and **27b** ($R=CO_2Et$, $R'=H$) in 19% yield (in a ratio of 1:2.7:1.3) [42]. The formation of **27a**, **27b**, and **28** is ascribed to the reaction of (ethoxycarbonyl)carbene with C_{60} [42].



Scheme 12 Reaction of C_{60} with ethyl diazoacetate under HSVM conditions

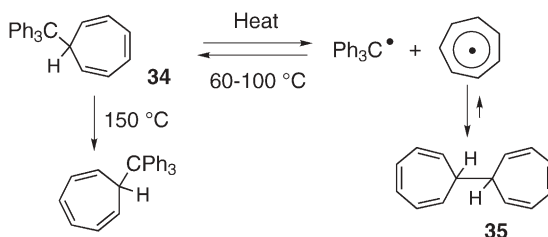
Similarly, the reaction of C_{60} with organic azides takes place in solution by heating at 60 °C to give derivatives of fullerotriazoline, which can then be converted to 5,6-open and 6,6-closed azafullerenes in 24 and 4% yields, respectively, by heating the solution at 100 °C [43]. In comparison, the solid-state HSVM reaction of C_{60} with 9-fluorenyl azide for 30 min afforded fullerotriazolines **31** in 62–76% yield [9b]. Then, heating the fullerotriazoline **31** in the solid state at 120 °C for 2 h gave the *N*-(9-fluorenyl) derivatives of 5,6-open and 6,6-closed azafullerenes **32** and **33** in 41 and 19% yields, respectively (Scheme 13), which are much higher than those in the liquid-phase reaction.



Scheme 13 Reaction of C_{60} with 9-fluorenyl azide under HSVM conditions

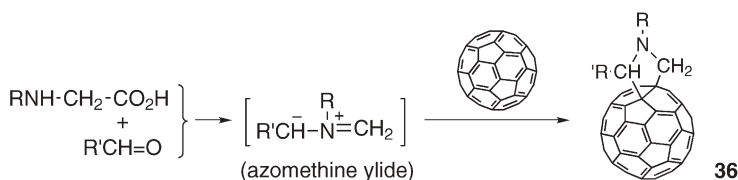
One may raise a question as to the temperature of the reactants generated in the reaction capsule during the milling using HSVM. From the fact that the intermediate fullerotriazolines **31** could be isolated from the reaction of C_{60} with organic azides without appreciable occurrence of nitrogen elimination, the inside temperature of the HSVM capsule apparently does not reach such a high temperature as 120 °C. As another probe to estimate the temperature of the inside of the vibration capsule, the behavior of a thermally labile compound, 7-triphenylmethylcycloheptatriene (**34**), was examined under the HSVM conditions. Compound **34** is known to undergo a thermal 1,5-hydride shift at around 150 °C [44] and also radical dissociation and recombination to give bitropyl (**35**) at 60–100 °C (Scheme 14) [45]. After **34** was treated under the HSVM conditions for 30 min, however, it was recovered without any change [23]. This finding indicates that the inside temperature of the capsule does not rise higher than 60 °C.

Another typical example of 1,3-dipolar addition is the reaction of fullerenes with an azomethine ylide intermediate, which can be readily generated by the reaction of *N*-substituted glycines or other amino acids with aldehydes or



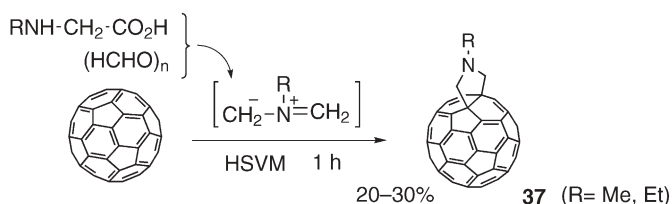
Scheme 14 Thermal reaction of 7-triphenylmethylcycloheptatriene (**34**)

ketones, giving the fulleropyrrolidine **36**. This is known as the Prato reaction and is apparently the most versatile and widely used method to functionalize fullerenes (Scheme 15) [46].



Scheme 15 Reaction of C_{60} with azomethine ylide; the Prato reaction

The Prato reaction was also found to take place in the solid-state reaction. Thus, the reaction of C_{60} with *N*-methyl- or *N*-ethylglycine in the presence of paraformaldehyde or with various substituted benzaldehydes was examined under the HSVM conditions (1 h), and was found to give a moderate yield (20–30%) of fulleropyrrolidine **37** together with around 50% recovery of C_{60} (Scheme 16) [47]. The effect of the molar ratio of the reagents was examined in detail and a C_{60} :glycine:aldehyde ratio of 1:1:1 to 1:2:2 was found to be optimum.

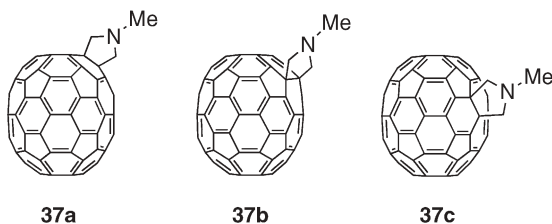


Scheme 16 Solid-state Prato reaction of C_{60} under HSVM conditions

It was also found that the HSVM reaction of C_{60} with *N*-methylglycine can proceed even without the presence of any carbonyl compound to give *N*-methylfulleropyrrolidine **36a** ($\text{R}=\text{Me}$) in 20–30% yield [47]. In this reaction, the fullerene dimer C_{120} (**3**) was also formed in a yield comparable to that of **36a**

(R=Me), suggesting that this reaction involves electron transfer as an important key step.

A similar solid-state reaction using C_{70} instead of C_{60} for 1 h afforded three positional isomers of fulleropyrrolidine **37a**, **37b**, and **37c** in a ratio of 47:36:16



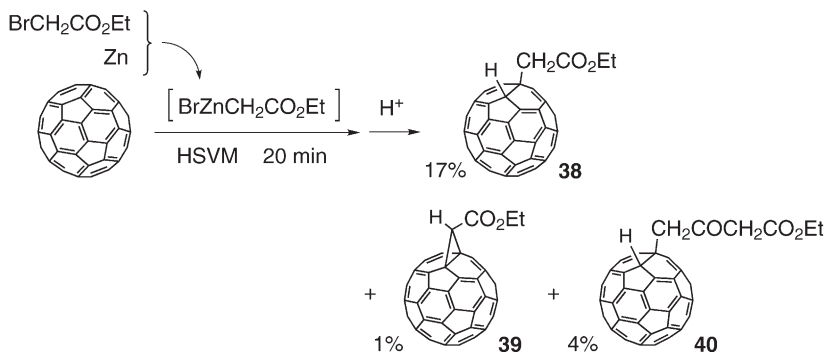
in a total yield of 41%. This ratio reflects the highest reactivity of the double bond near the pole at the 1,2-positions with the greatest curvature, as has been observed in other reactions of C_{70} [7a].

2.5

Nucleophilic Addition

Reflecting its electronegative character, C_{60} readily undergoes nucleophilic additions with various nucleophiles [7]. Apparently the most fundamental C–C bond forming reaction is the reaction with alkyllithium or Grignard reagents, giving the monoalkylated derivative of 1,2-dihydro- C_{60} after protonation of the initially formed alkyl- C_{60} carbanion [48].

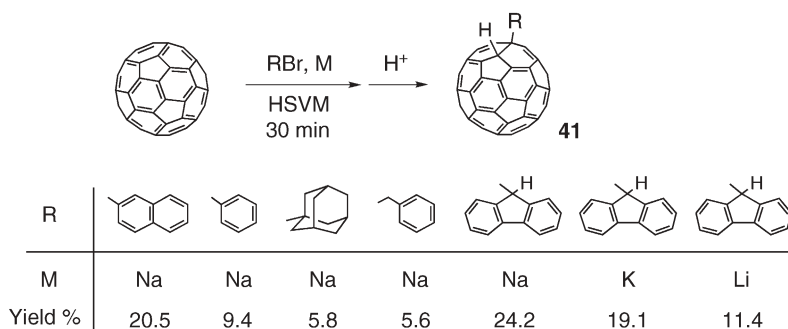
As an example of the solid-state C–C bond forming reaction with a nucleophile, a Reformatsky-type reaction was conducted with C_{60} . Thus, a mixture of C_{60} , ethyl bromoacetate, and zinc powder in a molar ratio of 1:5:20 was vigorously milled under the HSVM conditions for 20 min. After the mixture was treated with trifluoroacetic acid, the expected adduct **38** was obtained in 17%



Scheme 17 Solid-state reaction of C_{60} with an organozinc reagent under HSVM conditions

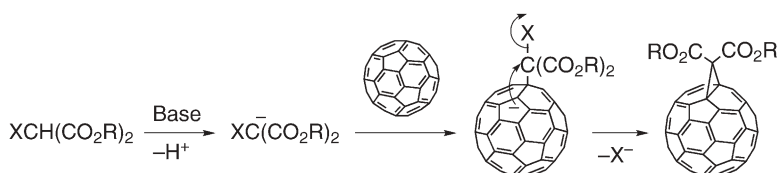
yield (63% based on consumed C_{60}) together with very small amounts of by-products such as **39** (fullerocyclopropane) and **40** in 1 and 4% yield, respectively (Scheme 17) [49]. The product **40** was apparently formed by the addition of organozinc reagent, $BrZnCH_2CO_2Et$, to **38**, and can be taken as an indication for the formation of such an organometallic reagent under the present solid-state reaction conditions.

The solid-state reaction was also conducted for C_{60} with alkyl or aryl bromides (RBr) in the presence of alkali metals (M) in the molar ratio of 1:2–3:4–6 under the HSVM conditions for 30 min. After the reaction mixture was treated with trifluoroacetic acid, the main product was isolated and identified as the alkyl or aryl derivative of 1,2-dihydro- C_{60} **41**, obtained in the rather modest yield of 6–24% with 13–49% recovery of C_{60} (Scheme 18) [50].



Scheme 18 Solid-state alkylation and arylation reaction of C_{60} under HSVM conditions

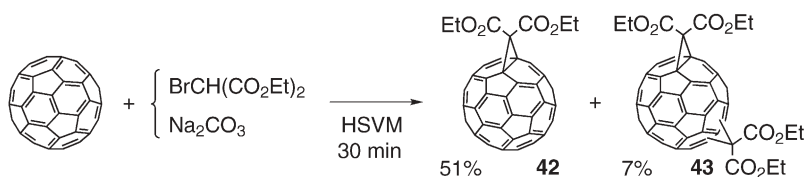
The nucleophilic addition of a carbon nucleophile generated by deprotonation of α -halogenated malonic acid esters or α -halogenated β -diketones to C_{60} and following intramolecular nucleophilic substitution leads to the clean cyclopropanation of C_{60} , which is known as the Bingel reaction (Scheme 19) [51]. This is another example of a most widely used method for functionalization of fullerenes as versatile as the Prato reaction [7, 46]. The active methylene compounds can be used in the presence of carbon tetrabromide to generate α -bromo carbonyl compounds in situ. In typical liquid-phase reactions, the most frequently used base for the deprotonation is DBU (1,8-diazabicyclo[5.4.0]undec-7-ene). Although inorganic base such as NaH was used



Scheme 19 Cyclopropanation of C_{60} ; the Bingel reaction

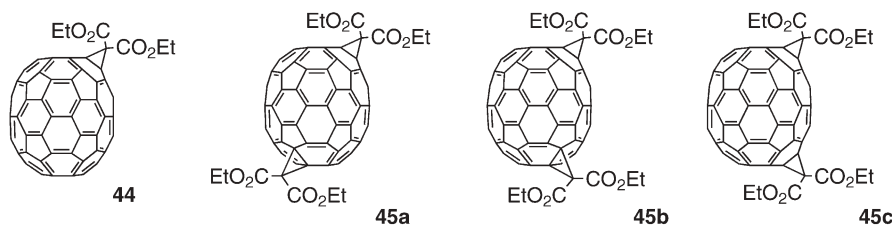
in the early reports, there has been no report as to the use of weaker inorganic bases.

The feasibility of conducting this Bingel reaction in the solid state was examined under the HSVM conditions. When the HSVM reaction was attempted with C_{60} , diethyl bromomalonate, and DBU, no desired product was obtained. However, when the organic base (DBU) was replaced by inorganic base (Na_2CO_3), and a mixture of C_{60} , diethyl bromomalonate, and Na_2CO_3 in a 1:1:1 molar ratio was vigorously milled under the HSVM conditions for 30 min, the cyclopropanated fullerene **42** was obtained in 51% yield (86% based on consumed C_{60}) along with 7% (12% based on consumed C_{60}) of bis-cyclopropanated product **43** (Scheme 20) [52]. Other inorganic weak bases such as $NaHCO_3$, $NaOAc$, $Ca(OH)_2$, and $Na_2B_4O_7$ were as effective as Na_2CO_3 [53]. When K_2CO_3 was used, a larger amount of bis-cyclopropanated product **43** was obtained, but the reason is not clear yet [53]. These conditions are also applicable to the cyclopropanation of C_{70} , giving the mono- and bis-cyclopropanated C_{70} in almost the same yields as for the reaction of C_{60} . Among the various isomers of monoadducts, the 1,2-adduct **44** was obtained selectively (74% yield when $NaOAc$ was used as a



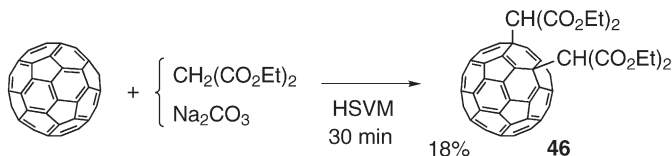
Scheme 20 Solid-state Bingel reaction of C_{60} under the HSVM conditions

base), while three positional isomers **45a**, **45b**, and **45c** were obtained as bis-cyclopropanated products in a ratio of 1.3:2.8:1 (29% total yield when K_2CO_3 was used as a base) [53].



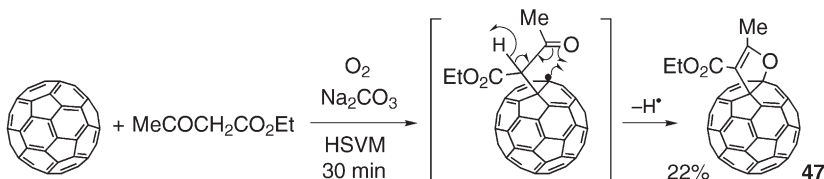
In contrast, when the reaction was conducted using diethyl malonate instead of bromomalonate in the presence of Na_2CO_3 under the HSVM conditions, there was obtained not the cyclopropanated product but a C_{60} derivative having two bis(ethoxycarbonyl)methyl groups at the 1,4-positions **46** in 18% yield (82% based on consumed C_{60}) (Scheme 21) [52]. Previously it was reported that

a reaction of C_{60} with lithium fluorenyl in THF gave the similar 1,4-bis(9-fluorenyl) adduct when a small amount of oxygen was present in the reaction system to cause one-electron oxidation of the initially formed functionalized C_{60} anion to its radical [54]. The similar radical addition process seemed to be operating in this solid-state reaction, since no such addition reaction took place when the solid-state reaction was conducted under conditions in which air was strictly eliminated.



Scheme 21 Solid-state reaction of C_{60} with diethyl malonate and base under HSVM conditions

When ethyl acetoacetate was employed instead of diethyl malonate in a similar solid-state reaction, dihydrofuran-fused C_{60} derivative **47** was obtained in 22% yield (49% based on consumed C_{60}). Again, the initially formed anion is supposed to be oxidized by oxygen to the corresponding radical, which undergoes intramolecular cyclization with release of a hydrogen radical as shown in Scheme 22 [52].



Scheme 22 Solid-state reaction of C_{60} with ethyl acetate and base under HSVM conditions

3 Conclusion

This chapter has dealt with a solid-state reaction (or solid–solid reaction) which was conducted by the use of what is called the “high-speed vibration milling (HSVM)” technique. This technique is characteristic in its simplicity of operation, efficiency of the reaction (most of the reactions being completed within 30 min), and the complete elimination of the use of any solvent. In some limited examples the reactant was a liquid and thus, in the strict sense of the word, the term “solid–solid reaction” is not correct and the term “solvent-free reaction” would be better used in those cases. However, even in such cases the driving force for the reaction is considered to be the local high pressure generated by vigorous milling. This HSVM reaction technique is also unique

in providing compounds which can never be obtained in the liquid-phase reaction, as typically exemplified by the selective formation of fullerene dimer C_{120} (3).

The substrates subjected to the HSVM reactions have so far been mostly fullerenes. This is partly because the present method is particularly suited to these carbon allotrope materials, which are hardly soluble in common organic solvents. It has been reported that no damage in the C_{60} molecule is observed within the HSVM reaction time of 30 min [55]. It is true that the introduction of this technique of the solid-state HSVM reaction to organic chemistry is so new that not much work has been done yet to clarify the scope and limitations for the application of this technique to organic reactions in general. However, some limited examples indicated that the Michael addition of chalcones to ethyl acetate [56] or to other active methylene compounds [57] under the HSVM conditions with K_2CO_3 as a catalyst proceeds almost quantitatively, and also the HSVM treatment of diethyl bromomalonate with KOH gives tetrakis(ethoxy-carbonyl)ethene as a single product in high yield [53]. Many other organic reactions are expected to take place under these conditions, and wide applicability of the present method will be demonstrated in the future. By proper choice of the apparatus and methodology, the solid-state reaction has great potential to be more widely used as an ideal procedure for organic reactions which are environmentally benign, and it also enables the creation of novel materials.

References

1. (a) Heinicke G (1984) *Tribochemistry*. Hanser, Munich; (b) Brice DW, O'Hare D (eds) (1992) *Inorganic materials*. Wiley, Chichester; (c) Boldyrev VV (1993) *Solid State Ionics* 63:537; (d) Gilman JJ (1996) *Science* 274:65; (e) Gielen M, Willen R, Wrackmeyer B (eds) (1999) *Solid-state organometallic chemistry, methods and applications*. Wiley, Chichester
2. (a) Aylmore MG, Lincoln FJ, Cosgriff JE, Deacon GB, Gatehouse BM, Sandoval CA, Spiccia L (1996) *Eur J Solid State Inorg Chem* 33:109; (b) Gaffet E, Bernard F, Niepce J-C, Charlot F, Gras C, Le Caër G, Guichard J-L, Delcroix P, Mocellin A, Tillement O (1999) *J Mater Chem* 9:305; (c) Fernández-Bertran JF (1999) *Pure Appl Chem* 71:581
3. Imamura H, Takesue Y, Tabata S, Shigetomi N, Sakata Y, Tsuchiya S (1999) *Chem Commun* 2277
4. (a) Toda F (1993) *Synlett* 303; (b) Toda F (1995) *Acc Chem Res* 28:480
5. (a) Rowlands SA, Hall AK, McCormick PG, Street R, Hart RJ, Ebell GF, Donecker P (1994) *Nature* 367:223; (b) Field LD, Sternhell S, Wilton HV (1997) *Tetrahedron* 53:4051
6. Dachille F, Roy R (1960) *Nature* 186:34
7. (a) Hirsch A (1994) *The chemistry of the fullerenes*. Thieme, Stuttgart; (b) Hirsch A (1995) *Synthesis* 895; (c) Taylor R (ed) (1995) *The chemistry of fullerenes*. World Scientific, Singapore; (d) Diederich F, Thilgen C (1996) *Science* 271:317; (e) Rubin Y (1997) *Chem Eur J* 3:1009; (f) Hirsch A (ed) (1999) *Fullerenes and related structures*. Top Curr Chem 199, Springer, Berlin Heidelberg New York
8. For typical examples: (a) Atwood JL, Koutsantonis GA, Raston CL (1994) *Nature* 368:229; (b) Suzuki T, Nakashima K, Shinkai S (1994) *Chem Lett* 699; (c) Williams RM, Zwier JM,

- Verhoeven (1994) *J Am Chem Soc* 116:6965; (d) Haino T, Yanase M, Fukazawa Y (1997) *Angew Chem Int Ed Engl* 36:259; (e) Barbour LJ, Orr GW, Atwood JL (1997) *Chem Commun* 1439; (f) Tsubaki K, Tanaka K, Kinoshita T, Fuji K (1998) *Chem Commun* 895
9. (a) Braun T (1997) *Fullerene Sci Technol* 5:1291; (b) Komatsu K, Murata Y, Wang G-W, Tanaka T, Kato N, Fujiwara K (1999) *Fullerene Sci Technol* 7:609
 10. (a) Andersson T, Nilsson K, Sundahl M, Westman G, Wennerström O (1992) *J Chem Soc Chem Commun* 604; (b) Andersson T, Westman G, Wennerström O, Sundahl M (1994) *J Chem Soc Perkin Trans II* 1097; (c) Constable EC (1994) *Angew Chem Int Ed Engl* 33:2269
 11. Yoshida Z, Takekuma H, Yakekuma S, Matsubara Y (1994) *Angew Chem Int Ed Engl* 33:1597
 12. Williams RM, Verhoeven JW (1992) *Recl Trav Chim Pays-Bas* 111:531
 13. Braun T, Buvári-Barcza Á, Barcza L, Konkoly-Thege I, Fodor M, Migali B (1994) *Solid State Ionics* 74:47
 14. Zhang D-D, Liang Q, Chen J-W, Li M-K, Wu S-H (1994) *Supramol Chem* 3:235
 15. Mohan H, Priyadarsini KI, Tyagi AK, Mittal JP (1996) *J Phys B At Mol Opt Phys* 29:5015
 16. Komatsu K, Fujiwara K, Murata Y, Braun T (1999) *J Chem Soc Perkin Trans I* 2963
 17. Andersson T, Sundahl M, Westman G, Wennerström O (1994) *Tetrahedron Lett* 35:7103
 18. Constabel F, Geckeler KE (2004) *Tetrahedron Lett* 45:2071
 19. Eklund PC, Rao AM (eds) (1999) *Fullerene polymers and fullerene polymer composites*. Springer, Berlin Heidelberg New York
 20. Wang G-W, Komatsu K, Murata Y, Shiro M (1997) *Nature* 387:583
 21. Keshavarz K-M, Knight B, Srdanov G, Wudl F (1995) *J Am Chem Soc* 117:11371
 22. Lebedkin S, Gromov A, Giesa S, Gleiter R, Renker B, Rietschel H, Krätschmer W (1998) *Chem Phys Lett* 285:210
 23. Komatsu K, Wang G-W, Murata Y, Tanaka T, Fujiwara K, Yamamoto K, Saunders M (1998) *J Org Chem* 63:9358
 24. Komatsu K, Fujiwara K, Tanaka T, Murata Y (2000) *Carbon* 38:1529
 25. Iwasa Y, Tanoue K, Mitani T, Izuoka A, Sugawara T, Yagi T (1998) *Chem Commun* 1411
 26. Forman GS, Tagmatarchis N, Shinohara H (2002) *J Am Chem Soc* 124:178
 27. Komatsu K, Fujiwara K, Murata Y (2000) *Chem Commun* 1583
 28. Komatsu K, Fujiwara K, Murata Y (2000) *Chem Lett* 1016
 29. Kunitake M, Uemura S, Ito O, Fujiwara K, Murata Y, Komatsu K (2002) *Angew Chem Int Ed* 41:969
 30. Smith AB III, Tokuyama H, Strongin RM, Furst GT, Romanow WJ (1995) *J Am Chem Soc* 117:9359
 31. Lebedkin S, Ballenweg S, Gross J, Taylor R, Krätschmer W (1995) *Tetrahedron Lett* 36:4971
 32. Fujiwara K, Komatsu K (2002) *Org Lett* 4:1039
 33. Murata Y, Han A, Komatsu K (2003) *Tetrahedron Lett* 44:8199
 34. (a) Komatsu K, Murata Y, Sugita N, Takeuchi K, Wan TSM (1993) *Tetrahedron Lett* 34:8473; (b) Schlueter JA, Seaman JM, Taha S, Cohen H, Lykke KR, Wang HH, Williams JM (1993) *J Chem Soc Chem Commun* 972; (c) Tsuda M, Ishida T, Nogami T, Kurono S, Ohashi M (1993) *J Chem Soc Chem Commun* 1296
 35. Murata Y, Kato N, Fujiwara K, Komatsu K (1999) *J Org Chem* 64:3483
 36. Kräutler B, Müller T, Maynollo J, Gruber K, Kratky C, Ochsenbein P, Schwarzenbach D, Bürgi H-B (1996) *Angew Chem Int Ed Engl* 35:1204
 37. Mack J, Miller GP (1997) *Fullerene Sci Technol* 5:607
 38. Murata Y, Kato N, Komatsu K (1999) *J Org Chem* 66:7235
 39. (a) Komatsu K, Murata Y, Kato (2000) In: Maggini M, Guldi D (eds) *Fullerenes 2000*, vol 9. Functionalized fullerenes. Electrochem Soc, Pennington, p 20; (b) Murata Y, Suzuki M, Rubin Y, Komatsu K (2003) *Bull Chem Soc Jpn* 76:1669

40. Miller GP, Tetreau MC (2000) *Org Lett* 2:3091
41. Murata Y, Suzuki M, Komatsu K (2001) *Chem Commun* 2338
42. Wang G-W, Li Y-L, Peng R-F, Liang Z-H, Liu Y-C (2004) *Tetrahedron* 60:3921
43. For example, see Grösser T, Prato M, Lucchini V, Hirsch A, Wudl F (1995) *Angew Chem Int Ed Engl* 34:1592
44. Nozoe T, Takahashi K, Yamamoto H (1969) *Bull Chem Soc Jpn* 42:3277
45. Okamoto K, Komatsu K, Kinoshita T, Shingu H (1970) *Bull Chem Soc Jpn* 43:1901
46. (a) Maggini M, Scorrano G, Prato M (1993) *J Am Chem Soc* 115:9798; (b) Prato M, Maggini M (1998) *Acc Chem Res* 31:519
47. Wang G-W, Zhang T-H, Hao E-H, Jiao L-J, Murata Y, Komatsu K (2003) *Tetrahedron* 59:55
48. (a) Hirsch A, Soi A, Karfunkel HR (1992) *Angew Chem Int Ed Engl* 31:766; (b) Hirsch A, Grösser T, Skiebe A, Soi A (1993) *Chem Ber* 126:1061
49. Wang G-W, Murata Y, Komatsu K, Wan TSM (1996) *Chem Commun* 2059
50. Tanaka T, Komatsu K (1999) *Synth Commun* 29:4397
51. Bingel C (1993) *Chem Ber* 126:1957
52. Wang G-W, Zhang T-H, Li Y-J, Lu P, Zhan H, Liu Y-C, Murata Y, Komatsu K (2003) *Tetrahedron Lett* 44:4407
53. Peng R-F, Wang G-W, Shen Y-B, Li Y-J, Zhang T-H, Liu Y-C, Murata Y, Komatsu K (2004) *Synth Commun* 34:1309
54. Murata Y, Komatsu K, Wan TSM (1996) *Tetrahedron Lett* 37:7061
55. Braun T, Rausch H, Biró LP, Zsoldos É, Ohmacht R, Márk L (2003) *Chem Phys Lett* 375:522
56. Zhang Z, Dong Y-W, Wang G-W, Komatsu K (2004) *Chem Lett* 168
57. Zhang Z, Dong Y-W, Wang G-W, Komatsu K (2004) *Synlett* 61

Photochemical Aspects of Thiocarbonyl Compounds in the Solid-State

Masami Sakamoto (✉)

Department of Applied Chemistry and Biotechnology, Faculty of Engineering,
Chiba University, Chiba, Japan
sakamotom@faculty.chiba-u.jp

| | | |
|-----|--|-----|
| 1 | Introduction | 207 |
| 2 | Photoreactions of Thiocarbonyl Compounds in the Solid State | 208 |
| 2.1 | [2+2] Thietane Formation in the Solid State | 208 |
| 2.2 | Hydrogen Abstraction by Thiocarbonyl Groups in the Solid State | 218 |
| 2.3 | Oxidation of Thiones in the Solid State | 225 |
| 2.4 | Solid-State Photoreactions of Conjugated Thiones | 226 |
| 3 | Concluding Remarks | 231 |
| | References | 231 |

Abstract The field of organic solid-state photochemistry has become popular, and has been extended in recent years to a variety of new systems. In this chapter, the solid-state photochemical aspects of thiocarbonyl compounds are reviewed, which show considerably high photochemical reactivity toward [2+2] cycloaddition and hydrogen abstraction reactions. Excited thioimides react with alkenes in the solid state to give thietane-fused heterocycles. Thiones and thioimides abstract hydrogen intramolecularly in the solid state to make a new C–C bond. Oxidation of thiones by the solid–gas reaction gave the corresponding ketones. Some achiral materials crystallized in chiral space groups, and absolute asymmetric syntheses were performed using the chiral crystalline environment. These reactions can now be regarded as an important branch of organic chemistry. Furthermore, insight into the reaction mechanism that directly connects with X-ray crystallographic analysis is also described.

Keywords Thiocarbonyl · Solid-state photoreaction · [2+2] Cycloaddition · Hydrogen abstraction · Asymmetric synthesis · Chiral crystal

1 Introduction

The photochemistry of thiocarbonyl compounds has been extensively studied over the past three decades, and a variety of photochemical reactions are developed [1–8]. One of the earliest photochemical reactions of thiones is the reaction with oxygen [9]. Schönberg and Stephenson reported a detailed study of the photodimerization of thiophosgene and the wavelength-dependent pho-

tooxidation and reduction of thiones [10, 11]. Since then, systematic investigations on thiocarbonyl compounds have established that they undergo a wide variety of reactions, such as cycloaddition, cyclization, dimerization, oxidation, and reduction. Like thioketones, other thiocarbonyl compounds, thioesters, thioamides, and thioimides show considerably high photochemical reactivity toward [2+2] cycloaddition and hydrogen abstraction by the thiocarbonyl sulfur [12, 13]. Especially, a number of examples of photochemical [2+2] cycloaddition with various alkenes are applied to make a new C–C bond.

According to the progress of X-ray structural analysis and crystal engineering, many solid-state photochemical reactions of thiones have been developed. Especially, nitrogen-containing thiocarbonyl compounds, thioamides and thioimides, are in general stable and show good crystallinity. Recently, many interesting photochemical reactions in the solid state have been reported [14–19]. The solid-state photochemical reactions provide not only synthesis of sulfur-containing compounds, but also give important mechanistic information in geometrical considerations. Furthermore, in some cases absolute asymmetric syntheses under a chiral crystal environment could be performed, and optically active compounds were synthesized from achiral materials without any outside chiral source [20–26]. In this chapter, recently developed solid-state photochemical reactions of thiocarbonyl compounds are reviewed.

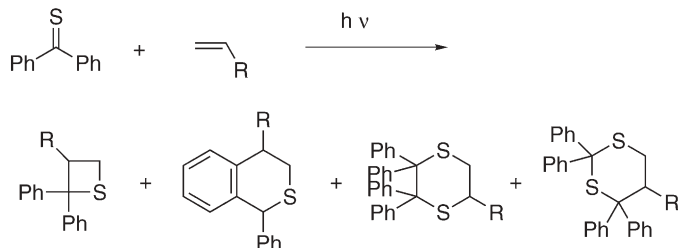
2

Photoreactions of Thiocarbonyl Compounds in the Solid State

2.1

[2+2] Thietane Formation in the Solid State

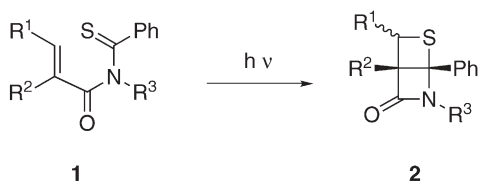
Kaiser and Wulfers reported the first example of a thietane formation reaction involving photolysis of thiobenzophenone with olefins [27]. Since then a large number of systems have been reported. Thiobenzophenone and related compounds, xanthione and related compounds, the α,β -unsaturated thiones such as thiocoumarin, and adamantanethione have been most thoroughly examined. The wavelength dependence of these reactions has been systematically investigated in order to ascertain differences, if any, in the photochemistry of the thione S_2 and T_1 states. Scheme 1 shows one example of photocycloaddition of



Scheme 1

thiobenzophenone with alkenes. This research has been thoroughly reviewed by de Mayo, Ramamurthy, Coyle, and Rao [4, 5, 7, 28]. There is no example for the photochemical [2+2] cycloaddition of thioketones in the solid state; however, nitrogen-containing thiocarbonyl compounds, such as thioamide and thioimides, effectively undergo cycloaddition reaction to thietanes in solution and also in the solid state [19].

Sakamoto et al. reported an interesting example involving the solid-state photoreaction of *N*-(α,β -unsaturated carbonyl)thiobenzamides **1** leading to thietane-fused β -lactam **2** (Scheme 2) [29–31].



1a : $\text{R}^1 = \text{H}$, $\text{R}^2 = \text{Me}$, $\text{R}^3 = \text{Ph}$

1b : $\text{R}^1 = \text{H}$, $\text{R}^2 = \text{Me}$, $\text{R}^3 = i\text{-Pr}$

1c : $\text{R}^1 = \text{Me}$, $\text{R}^2 = \text{Me}$, $\text{R}^3 = \text{Ph}$

1d : $\text{R}^1 = \text{H}$, $\text{R}^2 = \text{Me}$, $\text{R}^3 = i\text{-Pr}$

Scheme 2

Four monothioimides **1a–d** were investigated for their solid-state photochemical behavior. All monothioimides except **1b**, which did not give available crystals, were subjected to X-ray single crystal analysis. Figure 1 shows the Ortep drawing of **1a** (Fig. 1a), **1c** (Fig. 1b), and **1d** (Fig. 1c).

Conformations of monothioimides are described as so-called (*E,E*), (*E,Z*), (*Z,E*), and (*Z,Z*) based on the planar sp^2 nitrogen atom as shown in Fig. 2. In

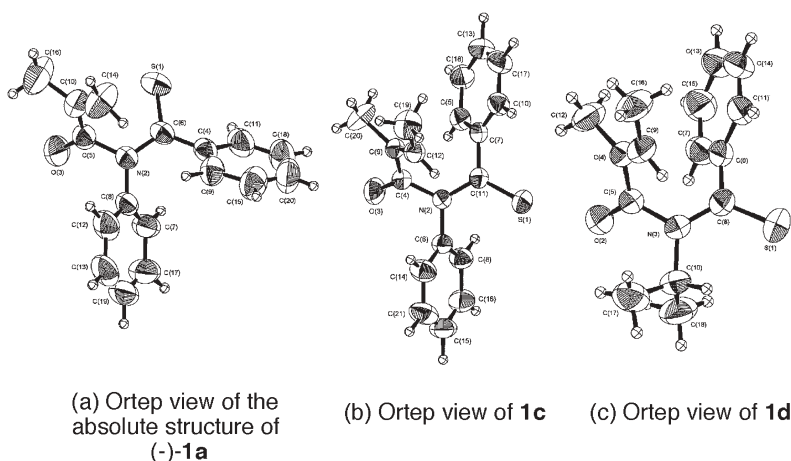


Fig. 1 Ortep drawing of (–)-**1a**, **1c**, and **1d**

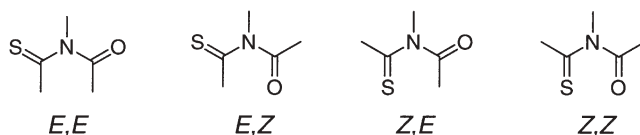


Fig. 2 Conformation of acyclic monothioimides

homogeneous conditions, the conformational interconversion occurs freely, and the photochemical reaction proceeds from the preferable conformation. However, the conformational factors may play a more important role in the photochemical reactivity in the crystalline state.

Monothioimides in the (*E,E*) and (*Z,E*) conformation should be used for the photochemical cycloaddition leading to thietane. In these conformations it is expected that each reacting site, which will make a new bond, is placed closely. The X-ray crystallographic analyses revealed the molecular conformation in the crystal. The monothioimide **1a** forms the (*Z,E*) conformation (Fig. 1a), and tigloyl derivatives **1c** (Fig. 1b) and **1d** (Fig. 1c) are doped in the (*E,E*) conformation in the crystal. The imide plane is remarkably twisted from the ideal sp^2 nitrogen atom as shown in Table 1. The imide chromophore slips out considerably from the ideal plane. The twist angle of $C=O$, which is defined as an average of the torsion angles of $C1-N-C4-C5$ and $C2-N-C4-O$, is in the range of 38.7 – 55.7° and is much greater than that of the $C=S$ moiety (16.8 – 24.7°). This structure is consistent with the lone pair electrons of the nitrogen atom being conjugated through the thiocarbonyl rather than through a carbonyl group. The alkenyl group is slightly twisted to the amide carbonyl (20.1 – 32.1°). Fortunately, the direction of inclination is preferred to the cyclization with the thiocarbonyl group in all cases.

One of the most important parameters to determine the reactivity is the distance between the thiocarbonyl sulfur (S) and the alkenyl carbon atom (C6) in Table 1, because a new bond will be formed between these two atoms at the initial step of the photoprocess. The actual distance of the (*Z,E*)-conformation imide **1a** is 3.59 \AA , which is closely placed and is almost the same as the sum of the van der Waals radii 3.50 \AA . In the (*E,E*) conformation, the atomic distances are longer than that of **1a**, and are 4.13 \AA for **1c** and 4.32 \AA for **1d**. For the second step of cyclization, the atomic distance between the thiocarbonyl carbon (C2) and the alkenyl carbon (C5) is in the range from 3.00 to 3.11 \AA , which is much smaller than the sum of the van der Waals radii 3.40 \AA . From this geometrical consideration of the site of the new bond formation, it is expected that the reaction leading to thietane will smoothly progress.

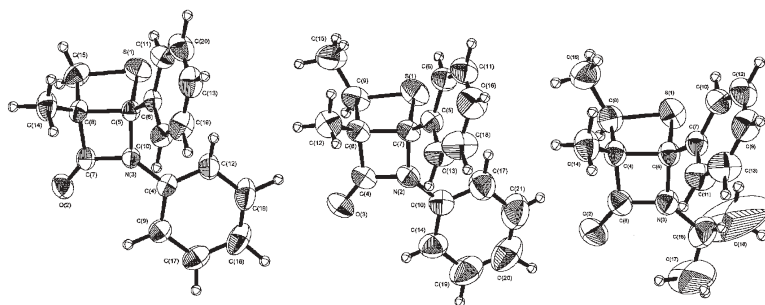
X-ray crystallographic analysis also revealed that the crystal of thioamide **1a** was chiral, the space group $P2_12_12_1$. The absolute configuration of (–)-rotatory crystals of **1a**, where the optical rotation was assigned on the basis of CD spectra in a KBr pellet, was determined by the X-ray anomalous scattering method as (–)-(*M*)-**1a** for the helicity. When (–)-rotatory crystals were irradiated at 0°C until the reaction conversion reached 100% yield, the asymmetric induction in

^{a)} Twist angle of C=S is defined as follows: $\tau=1/2(\omega_1+\omega_2)$, where ω_1 and ω_2 are torsion angles of C1-N-C2-C3 and C4-N-C2-S, respectively. ^{b)} Twist angle of C=O is defined as follows: $\tau=1/2(\omega_1+\omega_2)$, where ω_1 and ω_2 are torsion angles of C1-N-C4-C5 and C2-N-C4-O, respectively. ^{c)} Twist angle of C=C is defined as follows: $\tau=1/2(\omega_1+\omega_2)$, where ω_1 and ω_2 are torsion angles of N-C4-C5-C7 and O-C4-C5-C6, respectively. ^{d)} Distance of S---C6 is the distance between the S and C6 atoms. A new bond will be formed between these two atoms. ^{e)} Distance of C2---C5 is the distance between the C2 and C5 atoms.

Sakamoto et al. also reported the solution photochemistry for **1a–d**, which gave the corresponding thietane-fused β -lactams **2a–d** as shown in Table 2 [30, 31]. For tigloyl derivatives **1c** and **1d**, β -lactams were obtained as a mixture of two stereoisomers (entries 6 and 8). The *anti* isomers were preferably formed, in ratios of 0.8 and 0.7, respectively. In the solid-state photoreaction of

Table 2 Photochemical reaction of *N*-(α,β -unsaturated carbonyl)thiobenzamides **1a–d** under various conditions

| Entry | Thioimide | Conditions | Temp. (°C) | Yield of 2 | <i>Syn/anti</i> | ee (%) |
|-------|-----------|------------|------------|-------------------|-----------------|--------|
| 1 | 1a | Benzene | 15 | 77 | – | 0 |
| 2 | 1a | Solid | 0 | 75 | – | 10 |
| 3 | 1a | Solid | –45 | 70 | – | 40 |
| 4 | 1b | Benzene | 15 | 73 | – | 0 |
| 5 | 1b | Solid | 0 | 93 | – | 0 |
| 6 | 1c | Benzene | 15 | 80 | 0.8 | 0 |
| 7 | 1c | Solid | 0 | 92 | 10 | 0 |
| 8 | 1d | Benzene | 15 | 80 | 0.7 | 0 |
| 9 | 1d | Solid | 0 | 95 | 22 | 0 |



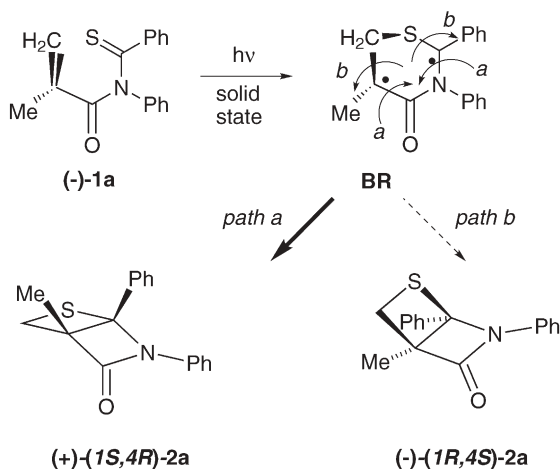
(a) Ortep drawing of the absolute structure of (+)-(1*S*,4*R*)-**2a** (b) Ortep drawing of **2c** (c) Ortep drawing of **2d**

Fig. 3 Ortep drawing of β -lactams **2a**, **2c**, and **2d**

1b, chemoselective reaction occurred, and the β -lactam **2b** was obtained in 93% yield (entry 5). In the cases of **1c** and **1d**, *syn* isomers of **2c** and **2d** were obtained stereospecifically, which reflected the stereochemistry of the tigloyl group of the starting monothioimides **1c** and **1d** (entries 7 and 9). Furthermore, chemoselective reaction was also observed in **1d** (entry 9).

In most cases, the solid gradually changed to amorphous according to the progress of the photoreaction. However, crystal-to-crystal transformation was observed in the photoreaction of **1d**. Orange prismatic crystals gradually decolorized upon irradiation; finally, colorless prisms were obtained.

Scheme 3 shows the mechanism for the thietane formation, in which the six-membered 1,4-biradical **BR** is appropriate. There are two ways of cyclization to thietane **2**, and each pathway gives an enantiomeric structure of thietanes, (1*S*,4*R*)- or (1*R*,4*S*)-**2**, respectively. The absolute structure of (–)-(*M*)-**1a** and the major isomer (+)-(1*S*,4*R*)-**2a** was determined by X-ray structural analysis using



Scheme 3 The dynamic structural changes in the crystal

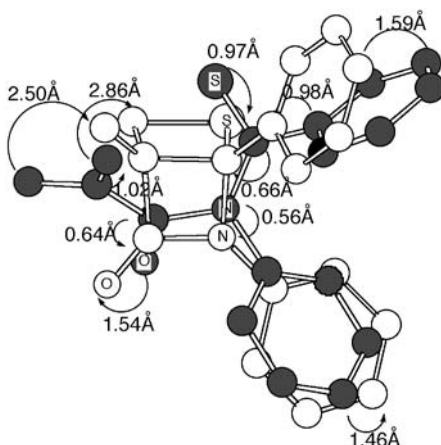


Fig. 4 A front view of the superimposed structure of (-)-(M)-1a (black circle) and (+)-(1S,4R)-2a (empty circle) obtained by X-ray structural analysis using Overlay program in Chem3D

an anomalous scattering method. Figure 4 shows the superimposed structure of both absolute structures, which was drawn with the overlay program included in CSC Chem3D. The sulfur and the alkenyl carbon atoms are closely placed to make the C–S bond easily, and subsequent cyclization of biradical BR needs the rotation of the radical center like *path a* to yield (1S,4R)-2a. The molecular transformation from (-)-1a to (+)-2a needs considerable molecular rearrangement involving the rotation of the methacryl group.

Figures 5 and 6 also show each overlay structure of the tigloyl derivatives 1c–2c and 1d–2d, in which all structures are determined by X-ray structural

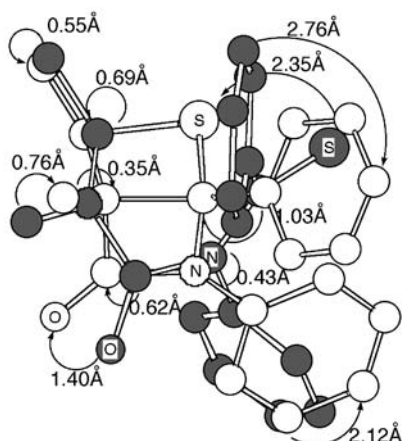


Fig. 5 A front view of the superimposed structure of **1c** (black circle) and **2c** (empty circle) obtained by X-ray structural analysis using Overlay program in Chem3D

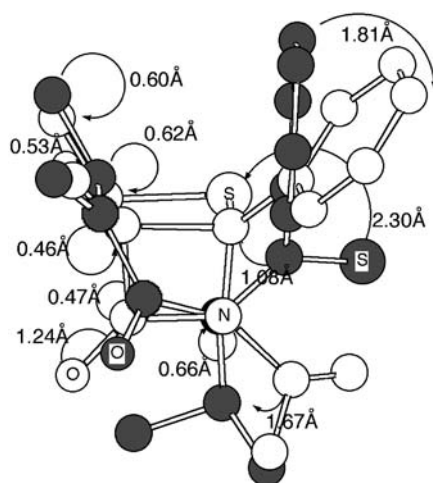


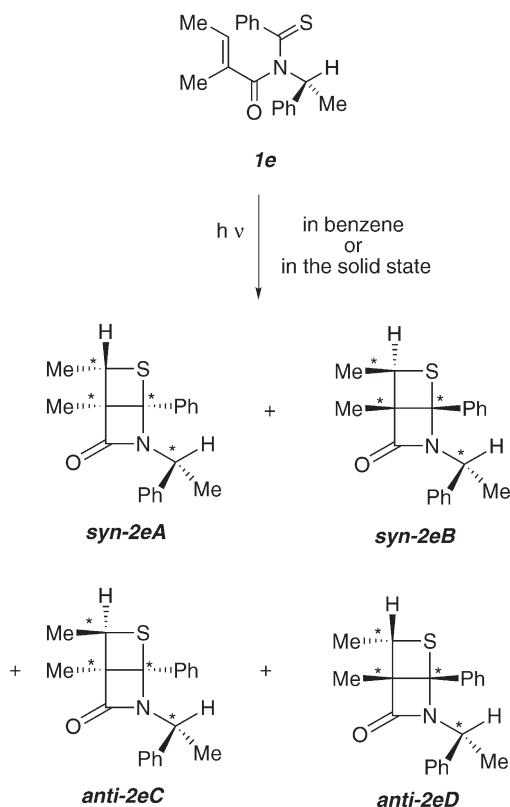
Fig. 6 A front view of the superimposed structure of **1d** (black circle) and **2d** (empty circle) obtained by X-ray structural analysis using Overlay program in Chem3D

analyses. In all cases, recrystallized crystals **2c** and **2d** were used. The atom distance between the alkenyl carbon and the thiocarbonyl sulfur is longer than that of **1a** as shown in Table 1; however, the atomic shift subsequently followed by cyclization is comparatively small (Fig. 5). The thiocarbonyl carbon changed the angle according to the change in the hybrid orbital from sp^2 to sp^3 by the bond formation; nevertheless, less atomic shift is observed for other chromophores. In the case of **1d**, a further small atomic shift is observed in the solid-state photoreaction as shown in Fig. 6, in which a crystal-to-crystal transfor-

mation was maintained throughout the reaction without phase separation, and this fact resulted in the stereospecific formation of *syn*-2c and -2d.

The photoreaction of **1a** in the crystalline state performed an absolute asymmetry synthesis using the chiral crystalline environment. Like this example, achiral materials are capable of crystallizing in chiral space groups by spontaneous resolution, and this chirality can be a source of asymmetry to induce optical activity in the products of chemical reactions carried out in the solid state [22–26]. However, these examples are very rare. On the other hand, it is known that chiral space groups are obligatory for optically active compounds. For chemical reactions carried out in the solid state, the chiral handle exerts a second asymmetric influence that is not present in isotropic solvents. Sakamoto et al. reported a diastereospecific [2+2] thietane formation reaction involving the photochemistry of *N*-[(*R*)-1-phenylethyl]-*N*-tigloylthiobenzamide in the solid state [32]. Having a chiral auxiliary as a substituent on the nitrogen atom affords an opportunity for desymmetrization of the thietane ring.

When monothioimide **1e** was irradiated in a benzene solution, [2+2] thietane formation proceeded, producing four β -lactams, *syn*-2e (A and B) and *anti*-2e (C and D) (Scheme 4). However, diastereoselectivity in the thietane formation



Scheme 4

Table 3 Chemo- and diastereo-selectivity for the photochemical reaction of the mono-thioimide **1e**

| Conditions | Temp. | Conversion | <i>Syn:anti</i> of 2e | <i>Syn/anti</i> of 2e | de of <i>syn-2e</i> (%) |
|------------|-------|------------|------------------------------|------------------------------|-------------------------|
| Benzene | 15 | 98 | (24:24):(26:26) | 0.9 | 0 |
| Solid | 15 | 100 | (73:17):(6:3) | 8.7 | 61 |
| Solid | -78 | 9 | (94:4):(0:0) | ∞ | 93 |
| Solid | -78 | 19 | (93:7):(0:0) | ∞ | 86 |
| Solid | -78 | 90 | (81:13):(3:2) | 19 | 71 |

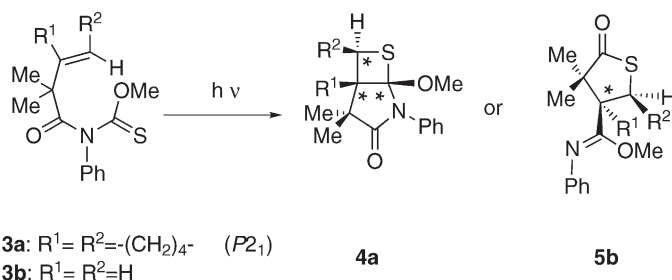
was not observed, and four β -lactams were obtained in almost equal yields (Table 3).

In contrast to the solution photochemistry, irradiation of the crystals of **1e** provided remarkably high diastereoselectivities in the formation of **2e**. The temperature at which the reaction occurs is important in determining diastereoselectivity. At 15 °C, the de of *syn-2e* was 61% and the ratio of *syn/anti* was 8.7, which was the reverse of that in the solution reaction (*syn/anti*=0.9). The solid-state photoreaction proceeded even at -78 °C, and with higher diastereoselectivity. At low conversion (9%), only *syn* isomers (de=93%) were obtained, and 71% de was observed even at 90% conversion.

In the reactant **1e**, the distances between the sulfur atom and the reacting alkenyl carbon and between the thiocarbonyl carbon and the alkenyl carbon are 4.29 and 3.00 Å, respectively. It is surprising that the cyclization proceeds in this situation in which the interatomic distance between the sulfur atom and the reacting alkenyl carbon is much larger than the sum of the van der Waals radii. Furthermore, the imide moiety is highly twisted from a plane, where the twist angle τ of the C(=O)-N bond is 40.8° and that of the C(=S)-N bond is 19.9°. The aromatic ring twists at 55.3° relative to the thiocarbonyl bond and the torsional angle is 38.9°.

Sakamoto et al. also reported a similar solid-state [2+2] thietane formation of *N*-acylthiocarbamates, which reaction was followed by ring reconstruction in some cases [33]. Recrystallization of *O*-methyl-*N*-(β,γ -unsaturated carbonyl)-*N*-phenylthiocarbamates **3a,b** from a hexane solution yielded colorless crystals; however, single crystals for X-ray crystallographic analysis could not be obtained. On the other hand, thiocarbamate **3b** afforded prismatic single crystals, and the X-ray crystallographic analysis indicated the chiral space group *P2*₁. It was revealed that the conformation of the imide chromophore is (*E,E*), and remarkably twisted from the ideal imide plane. The twist angle of the C(=O)-N is 47.4° and is much greater than that of the C(=S)-N moiety (19.4°).

Irradiation of a benzene solution of **3a** gave tricyclic thietane **4a** in 83% yield (Scheme 5 and Table 4, entry 1). The solid-state photolysis also gave racemic **4a** in 81% yield when the reaction conversion was 80% (entry 2). The solid-state reaction proceeded even at -78 °C (entry 3).



Scheme 5

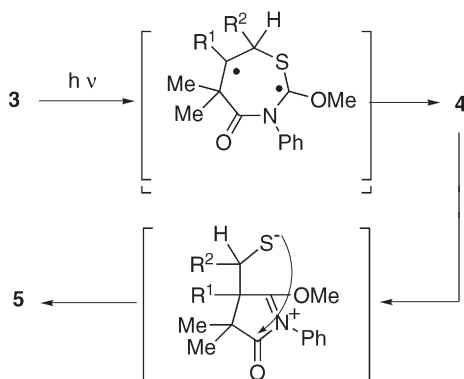
Table 4 Photochemical reaction of **3** in benzene and the solid- state

| Entry | Substrate | Conditions | Reaction temp. (°C) | Conv. (%) | Yield (%) | | ee (%) 4a or 5b |
|-------|-----------|------------|---------------------|-----------|-----------|----------|----------------------------------|
| | | | | | 4 | 5 | |
| 1 | 3a | Benzene | 20 | 100 | 83 | 0 | 0 |
| 2 | 3a | Solid | 0 | 80 | 81 | 0 | 0 |
| 3 | 3a | Solid | -78 | 50 | 85 | 0 | 0 |
| 4 | 3b | Benzene | 20 | 100 | 0 | 90 | 0 |
| 5 | 3b | Solid | 0 | 78 | 0 | 85 | 10 |
| 6 | 3b | Solid | -78 | 84 | 0 | 84 | 20 |
| 7 | 3b | Solid | -78 | 15 | 0 | 90 | 31 |

When thiocarbamate **3b** was irradiated in a benzene solution, thiolactone **5b** was isolated in 90% yield (entry 4). The solid-state photolysis also gave thiolactone **5b** in 85% yield when the reaction conversion was 78% (entry 4).

The stereoselective generation of the chiral center is exemplified by the formation of **5b** at the C4 position, and optically active **4b** was obtained in 10% ee. The solid-state photoreaction also proceeded at -78 °C and an optically active compound which showed a better ee value was formed, 20% ee at 84% conversion (entry 6) and 31% ee at 15% conversion (entry 7). The space group of the crystal of **3a** could not be determined because **3a** did not afford single crystals suitable for X-ray crystallography; however, the production of racemic **4a** shows that the crystals are achiral (entries 2 and 3).

A plausible mechanism for the formation of **4** is rationalized on the basis that photolysis of **3** results in [2+2] cyclization to thietane **4** and is subsequently followed by rearrangement to thiolactone **5** (Scheme 6). Ring opening of the initially formed thietane **4** leads to a zwitterion, which is facilitated by lone pair electrons of nitrogen and oxygen atoms, and nucleophilic reaction of the thiolate anion to carbonyl carbon gives **5**. For the tricyclic thietane **4a**, nucleophilic addition of the thiolate anion is difficult, and results in the formation of stable thietane **4a**.



Scheme 6

From the X-ray structural analysis of the starting thionocarbamate **3b**, the distance between the thiocarbonyl sulfur atom and the alkenyl carbon and between the thiocarbonyl carbon and the alkenyl carbon is 4.69 and 3.00 Å, respectively. The fact that the reaction proceeded under these restricted conditions, in which the distance of each reacting site is longer than the sum of the van der Waals radii (3.5 Å), is accounted for by the fact that the initial reaction occurred in the defect of the crystalline lattice, with the later reaction occurring in increasingly defective regions. Furthermore, two plausible factors are responsible for the relatively low enantiomeric excess of **3b**.

2.2

Hydrogen Abstraction by Thiocarbonyl Groups in the Solid State

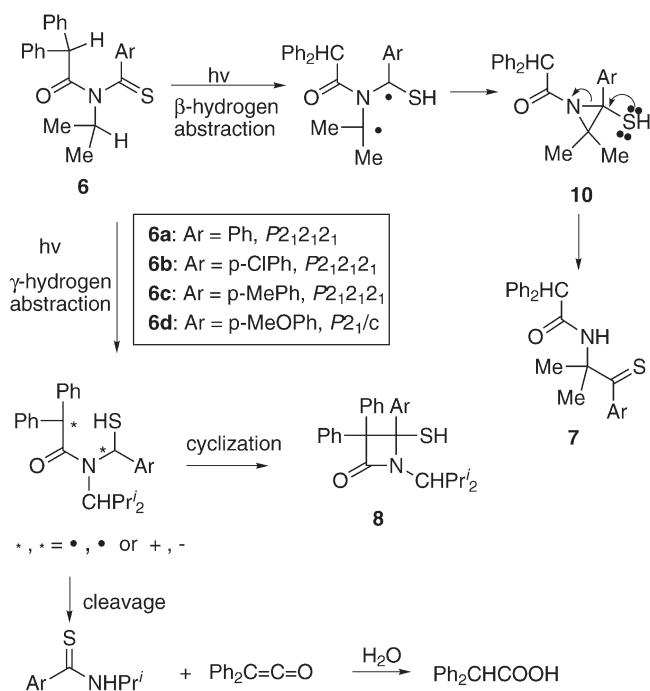
Ketones generally abstract hydrogen more rapidly from their $n\pi^*$ excited states, and the partially filled electronic orbital initiates this process [34, 35]. Thiocarbonyls differ substantially from carbonyl compounds both in terms of electronic configuration of the reactive excited states and the mode of attack of the thiocarbonyl chromophore on hydrogen-bearing substrates. Since $n\pi^*$ and $\pi\pi^*$ excited states differ in the spatial properties of the orbitals involved in abstraction, and since the larger sulfur atom should be capable of abstraction over greater distances than oxygen, it follows that ketones and thiones should exhibit significantly different hydrogen atom abstraction geometries.

Scheffer is interested in determining the geometric requirements for intramolecular hydrogen atom abstraction through application of the solid-state structure–reactivity correlation method [21]. In this method, the chemical reactivity of a series of closely related compounds is determined and correlated with structural data for the same compounds as measured by X-ray crystallography. Such studies have provided information on the geometric requirements for intermolecular [2+2] photocycloaddition [36], as well as for the process of intramolecular hydrogen atom abstraction by the oxygen atom of a photoexcited ketone [21, 34].

In analyzing their reactivity, he considered the following ground state parameters to be the most important in determining reactivity: the distance between O and H; O...H–O angle; the C=O...H angle; and the dihedral angle that the O–H vector makes with respect to the nodal plane of the carbonyl π system. Thiocarbonyls abstract hydrogen from both the upper $\pi\pi^*$ state (S_2) and the lower $n\pi^*$ state (T_1), and the abstracted hydrogen can add at either the C or the S atom of the thiocarbonyl chromophore. This chapter outlines the photochemical hydrogen abstraction of organic molecules containing a thiocarbonyl chromophore in the solid state.

Sakamoto et al. provided the first example of hydrogen abstraction by thiocarbonyl sulfur in the solid state [37, 38]. Irradiation of *N*-diphenylacetyl-*N*-isopropylthioaroylamides **6** in the solid state gave thioketones **7** (β -hydrogen abstraction products by thiocarbonyl sulfur), mercaptoazetidin-2-ones (γ -hydrogen abstraction products by thiocarbonyl sulfur), and aroylthioamides (γ -hydrogen abstraction products by thiocarbonyl sulfur followed by cleavage).

Irradiation of the powdered crystals of **6a–d** with a high-pressure mercury lamp under argon at 0 °C showed a different photochemical behavior from that in benzene solution. Contrary to the photochemical results in solution media in which azetidin-2-ones **8** (γ -hydrogen abstraction products) were formed as major products, thioketones **7** (β -hydrogen abstraction products) were obtained as major components in the solid-state photoreactions (Scheme 7). The



Scheme 7

9

propensity is clearly shown in the low-temperature photolysis. When the monothioimides **6** were irradiated at $-45\text{ }^{\circ}\text{C}$, the red color faded out during the course of the irradiation time and colorless crystals were obtained. The photolysate gradually turned to a purple color derived from thioketones **7** on warming up to room temperature. Colorless intermediates for thioketones are assignable to 2-mercaptoaziridines **10** which are stable at low temperature.

All monothioimides have essentially identical crystalline state conformations as shown in Fig. 7. The preferred conformation of these monothioimides has the (*E,E*) geometry in the crystalline state, which is favorable to photochemical β -hydrogen transfer by the thiocarbonyl group.

It was confirmed that the hydrogen abstraction of **6** from both the β and γ positions proceeds from the $n\pi^*$ triplet excited state of thiocarbonyl. Adopting the Kasha model of the $n\pi^*$ excited state (*n*-orbital), the ideal value of Δ should be 90° . For $\pi\pi^*$ abstraction, Δ should be less than 90° , since the π -electrons do

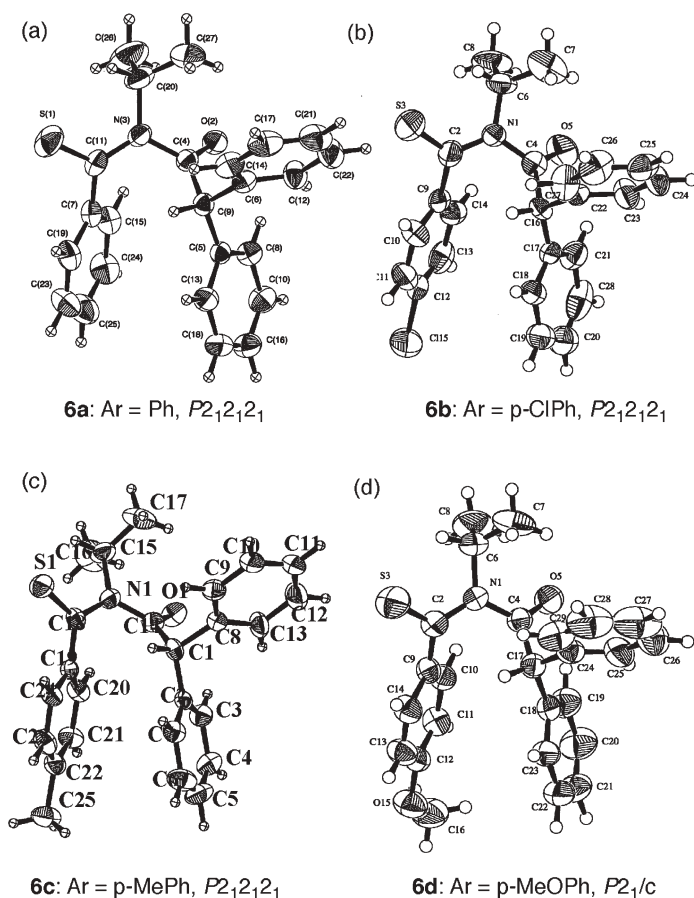



Fig. 7 Ortep drawing of the molecules **a 6a**, **b 6b**, **c 6c**, and **d 6d**

not lie directly above the heteroatom but are displaced toward carbon. The C–H...S angle θ is expected to be optimum at 180° for both types of excited states, and, finally, it is likely that the ideal value of d is independent of excited state configuration and should be close to the sum of the van der Waals radii for S and H, 3.00 \AA .

Table 5 summarizes the geometrical parameters for hydrogen abstraction determined by X-ray single crystal analysis. In the monothioimides **6a–d**, the distance between the thiocarbonyl sulfur atom and the hydrogen atom lies in the range of $2.37\text{--}2.58 \text{ \AA}$, which is considerably shorter than the sum of the van der Waals radii of the sulfur atom and the hydrogen atom, 3.0 \AA . From this value, it is apparent that these reactants are positioned for β -hydrogen transfer in the crystalline state. On the other hand, the $\text{C}=\text{S}\cdots\text{H}_\gamma$ distances ($3.72\text{--}3.84 \text{ \AA}$) are considerably greater than the sum of the van der Waals radii. Actually, in the case of **6a–d**, hydrogen abstraction by the sulfur atom takes place for distances $0.72\text{--}0.84 \text{ \AA}$ longer than the sum of the van der Waals radii. However, the photoreactivity in the solid state cannot be determined by only the intramolecular parameter; the reorientation to permit reaction and the fit in the surrounding crystal lattice are also important. More striking is that the crystals of **6a**, **6b**, and **6c** are orthorhombic of chiral space group $P2_12_12_1$ (Scheme 7), and the photoproducts **8a–c** obtained in the solid-state photoreaction are optically active.

Next, the trapping of unstable mercaptoaziridines **10** was tried by acetylation since they should be optically active. After the powdered monothioimides **6a–c** were irradiated at -45°C , the photolysate was dissolved in toluene at

Table 5 Ideal and experimental values of d , Δ , Θ , and ω



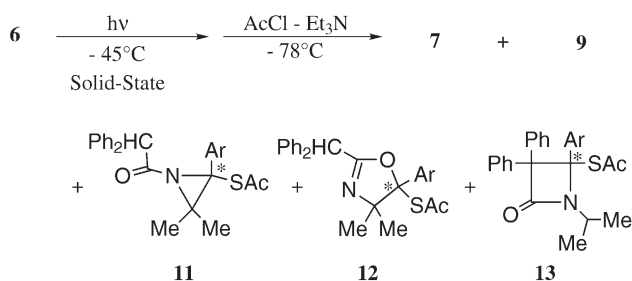
| | β -Hydrogen | | | | γ -Hydrogen | | | | Ideal |
|----------------------------------|-------------------|-----------|-----------|-----------|--------------------|-----------|-----------|-----------|-------|
| | 6a | 6b | 6c | 6d | 6a | 6b | 6c | 6d | |
| $d \text{ (\AA)}$ | 2.57 | 2.52 | 2.68 | 2.37 | 3.79 | 3.84 | 3.74 | 3.72 | 3.0 |
| $\Delta \text{ (}^\circ\text{)}$ | 69.9 | 70.4 | 63.6 | 69.3 | 33.2 | 29.0 | 34.9 | 32.6 | 90 |
| $\theta \text{ (}^\circ\text{)}$ | 114.0 | 116.3 | 119.5 | 124.4 | 120.2 | 125.0 | 130.0 | 123.3 | 180 |
| $\omega \text{ (}^\circ\text{)}$ | 0.8 | 7.3 | 19.6 | 10.0 | 46.4 | 52.0 | 33.6 | 51.5 | 0 |

d , the $\text{C}=\text{S}\cdots\text{H}$ distance; Δ , the $\text{C}=\text{S}\cdots\text{H}$ angle; θ , the $\text{C-H}\cdots\text{S}$ angle and ω , the angle by which the abstracted hydrogen lies above or below the mean plane of the carbonyl group.

Table 6 Solid-state photoreaction of **6** followed by acetylation

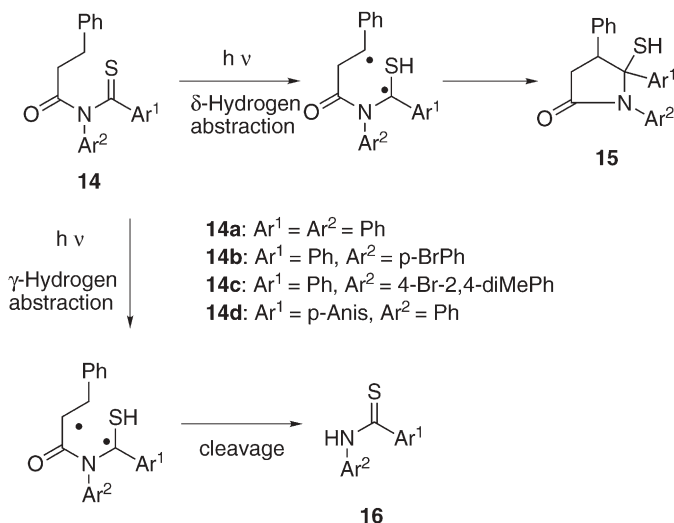
| | | 7 | 9 | 11 | | 12 | | 13 | |
|----|--------------|--------------|--------------|--------------|-----------|--------------|-----------|--------------|-----------|
| 6 | Conv. (%) | Yield (%) | Yield (%) | Yield (%) | ee (%) | Yield (%) | ee (%) | Yield (%) | ee (%) |
| 6a | 70 | 15 | 15 | 39 | 84 | 10 | 50 | 16 | 20 |
| 6b | 80 | 10 | 18 | 37 | 70 | 13 | 40 | 19 | 13 |
| 6c | 40 | 12 | 18 | 35 | 88 | Trace | – | 29 | 40 |

–78 °C, and then three molecular equivalents of acetyl chloride and triethylamine were added. Three types of acetylated materials, **11**, **12**, and **13**, were isolated accompanied by a small amount of thioketone **7** and thioamide **9** (Scheme 8 and Table 6). All of the acetylated materials showed optical activity. For the reaction of **6a**, 84% ee of 2-(acetylthio)aziridine **11a**, 50% ee of 4-(acetylthio)oxazoline **12a**, and 20% ee of 4-(acetylthio)oxazolidin-2-one **13a** were obtained in 39, 10, and 16% yields, respectively. In the reaction of **6b,c**, the corresponding optically active materials **11–13** were obtained as shown in Table 9. The formation of oxazoline **12** involves the rearrangement of *N*-acyl aziridines, which occurs by intramolecular attack of the carbonyl oxygen at the ring carbon to cause rupture of the system.

**Scheme 8**

Sakamoto et al. also reported that acyclic monothioimides of general structure **14a,d** gave δ -lactams **15a,d** via δ -hydrogen abstraction and substituted thiobenzanilides **16** when irradiated in solution using a 1,000-W high-pressure mercury lamp (Scheme 9) [39]. They suggested that the thiobenzanilides are formed through Norrish type II-like γ -hydrogen abstraction and 1,4-biradical cleavage.

Scheffer et al. carried out photolyses of monothioimides in the solid state with a 450-W high-pressure mercury lamp. In a carefully controlled run, photolysis of monothioimides **14a–d** in the solid state with rigorous exclusion of moisture led to no reaction [40, 41]. When no special attempts were made to

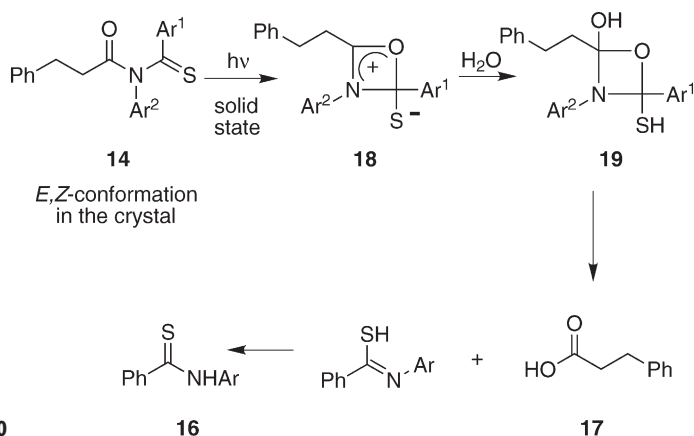


Scheme 9

exclude moisture, however, irradiation of compound **14a**, either as a powder or a single crystal, led exclusively to the same two photoproducts, **16a** and 3-phenylpropionic acid, which were each formed in 9% isolated yield. Concomitant with the photochemical studies, the crystal and molecular structures of the monothioimides were determined by a direct method, single crystal X-ray diffraction. The results showed that compounds **14a–d** adopt conformations in the solid state for which γ - or δ -hydrogen abstraction is most unlikely. All four monothioimides have essentially identical solid-state conformations typified as (*E,Z*) conformation. In this conformation, the shortest $\text{C}=\text{S}\cdots\text{H}_\gamma$ contact is 5.06 Å, considerably greater than the sum of the van der Waals radii for sulfur and hydrogen (3.00 Å). The nearest δ -hydrogen is even further away at 6.33 Å. These facts indicate that the distances are too great to allow abstraction of either γ - or δ -hydrogen atoms.

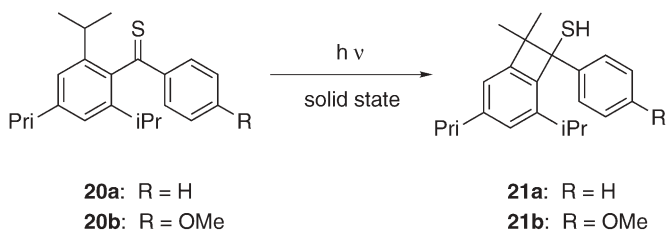
They proposed a mechanism as shown in Scheme 10, because they found close contact between the oxygen atom of the $\text{C}=\text{O}$ group and the carbon atom of the $\text{C}=\text{S}$ group in a range of 2.77–2.86 Å. These contacts are well below the sum of the van der Waals radii for oxygen and carbon (3.22 Å). Thus, in the crystalline state, the oxygen atom is ideally positioned for excited-state nucleophilic attack on the $\text{C}=\text{S}$ double bond, and this process may be the first step of the mechanism by which thiobenzanilides are formed in this medium. This would lead reversibly to the 1,3-oxazetidinium ion **18**, which could react with water present in the medium and then break down, via species **19**, to the enol of thiobenzanilide **16** and 3-phenylpropanoic acid **17**.

Scheffer et al. also reported hydrogen abstraction of thioketones in the solid state [42]. The $n\pi^*$ and $\pi\pi^*$ excited states differ in the spatial properties of the orbitals involved in abstraction, and it follows that ketones and thiones should exhibit significantly different hydrogen atom abstraction geometries.



Scheme 10

2,4,6-Triisopropylthiobenzophenone **20a** and its *p*-methoxy derivative **20b** were chosen for study (Scheme 11). Like thiobenzophenone, thiones **20** show well-separated absorption maxima in the visible (600 nm, $n\pi^*$) and UV (320 nm, $\pi\pi^*$) regions of the spectrum. In contrast, photolysis of freeze-pump-thaw-deoxygenated solutions of thiones **20a** and **20b** in benzene through Pyrex (>290 nm) afforded excellent chemical yields (ca. 70%) of the benzocyclobutenethiol derivatives **21a** and **21b**. The same photoreaction could be brought about in the crystalline state at a much-reduced rate.



Scheme 11

The photochemical results indicate that hydrogen abstraction proceeds from the $\pi\pi^*$ singlet excited state of thiones **20a** and **20b**, and was followed by photocyclization. Four parameters serve to define the geometry of intramolecular hydrogen atom abstraction: d , Δ , θ , and ω , which have the values shown in Table 5. Table 7 summarizes the ideal values of d , Δ , θ , and ω for each type of excited state along with the crystallographically derived experimental values for compounds **20a,b**.

As can be seen from the table, the abstraction distance d is indeed significantly greater for sulfur than for oxygen [21, 35]. Both excited states are able to tolerate ω angles that diverge from the ideal by 40–50°. The major angular difference between the $n\pi^*$ and $\pi\pi^*$ geometrical parameters lies in the values

Table 7 Ideal versus experimental value of d , Δ , θ , and ω

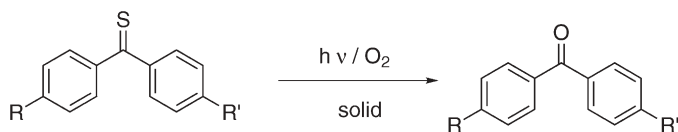
| Entry | Compound | d (Å) | Δ (°) | θ (°) | ω (°) |
|-------|----------------------|---------|--------------|--------------|--------------|
| 1 | n, π^* (ideal) | 3.00 | 90 | 180 | 0 |
| 2 | π, π^* (ideal) | 3.00 | <90 | 180 | 90 |
| 3 | 20a | 3.06 | 52 | 118 | 51 |
| 4 | 20a | 3.28 | 47 | 119 | 46 |
| 5 | 20b | 3.07 | 52 | 125 | 50 |
| 6 | 20b | 3.27 | 50 | 108 | 49 |

of Δ , which are much closer to 90 Å for the $n\pi^*$ absorptions. The Δ value may be more acute for $\pi\pi^*$ absorptions owing to the localization of π -electron density, in this case closer to the center of the C=S bond.

2.3

Oxidation of Thiones in the Solid State

Ramamurthy et al. reported a unique gas–solid reaction activated by light which involves the photochemical oxidation of diaryl thioketones **22a–k** in the solid state (Scheme 12 and Fig. 8). Only six thiones (**22a–d, g, h**) were oxidized to the corresponding ketones, and the rest were photostable, whereas all thiones were readily oxidized in solution [43]. A comparison of the molecular packing of the above five thioketones is quite revealing in rationalizing their photoreactivity in the solid state. For the reacting thioketones there is a channel along the shortest crystallographic axis with the reactive thiocarbonyl chromophore (C=S) directed toward the channel. In the case of stable thioketones, the packing arrangement reveals no such channel in any direction in the unit cell. The cross-sectional area is fairly large. The primary step of oxidation requires interaction between an excited thioketone and ground-state oxygen. For the oxidation to be efficient, oxygen should be able to diffuse into successive layers of thioketones. The absence of a channel in **22e, 22f**, and **22i–k** might then be responsible for their photostability. However, the presence of the thiocarbonyl chromophore at the crystal surface is not sufficient for oxidation to occur. It is also essential that the thiocarbonyl groups are arranged in a tight fashion so that oxidation of one molecule exposes another close neighbor to an oxygen molecule. This is evident from the differences in reactivity among the five thioketones being considered. Although in all the five cases the presence of a

**Scheme 12****22****23**

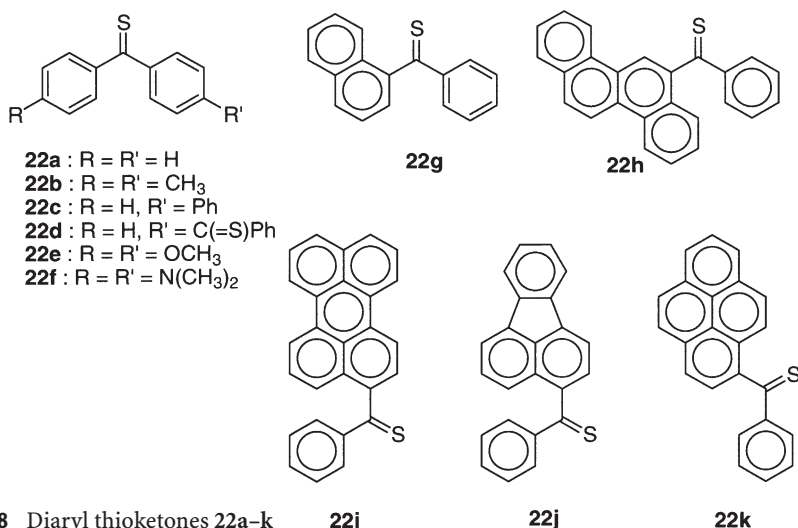


Fig. 8 Diaryl thioketones 22a–k

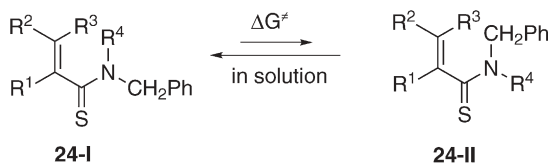
thiocarbonyl chromophore at the crystal surface could be identified, the above-mentioned disposition of reactive chromophores is present only in the reactive thioketones.

2.4

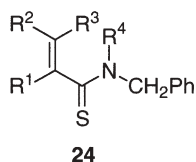
Solid-State Photoreactions of Conjugated Thiones

Sakamoto et al. reported the X-ray crystallographic data and the solid-state photoreaction of eight *N,N*-disubstituted α,β -unsaturated thioamides **23a–h**, which involves hydrogen abstraction by the alkenyl carbon atom conjugated with thiocarbonyls (Fig. 9) [44–46].

Asymmetrically substituted thioamides **24e–h** exist in equilibrium between rotamers **24-I** and **24-II**. The ¹H NMR spectrum of *N*-benzyl-*N*-methylmethacrylthioamide **24e** showed the distribution of **24e-I**:**24e-II** was 55:45 (Scheme 13 and Table 8) [47]. The free energy of activation of the rotational barrier was measured by the temperature-dependent ¹H NMR spectra in DMSO at various temperatures. The free energy of activation of the rotation of the (C=S)–N bond could be estimated as 22.7 kcal mol^{–1}. Furthermore, Table 8 shows the ratio of **I**:**II**, and all three thioamides **24f–h** favor the conformation **I** with the situation that a benzyl group was placed closely to the thiocarbonyl group on



Scheme 13



| thioamide | R ¹ | R ² | R ³ | R ⁴ | space group |
|------------|------------------------------------|----------------|----------------|--------------------|---|
| 24a | Me | H | Me | CH ₂ Ph | <i>P</i> 2 ₁ /a |
| 24b | H | Me | Me | CH ₂ Ph | <i>P</i> 2 ₁ 2 ₁ 2 ₁ |
| 24c | -(CH ₂) ₄ - | H | H | CH ₂ Ph | <i>P</i> 2 ₁ |
| 24d | -(CH ₂) ₅ - | H | H | CH ₂ Ph | <i>P</i> 2 ₁ /n |
| 24e | Me | H | H | Me | <i>P</i> 2 ₁ 2 ₁ 2 ₁ |
| 24f | Me | H | H | <i>i</i> -Pr | <i>P</i> 2 ₁ /n |
| 24g | Me | H | Me | <i>i</i> -Pr | <i>C</i> c |
| 24h | -(CH ₂) ₄ - | H | H | <i>i</i> -Pr | <i>P</i> 2 ₁ /c |

Fig. 9 *N,N*-disubstituted α,β -unsaturated thioamides **23a–h**

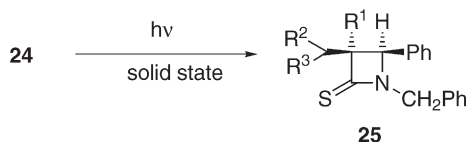
Table 8 Free energy of activation for bond rotation and the conformational distribution of thioamides **24** in solution

| Thioamide | ΔG^* (kcal/mol) | 24-I:24-II |
|------------|-------------------------|-------------------|
| 24a | – | Symmetry |
| 24b | – | Symmetry |
| 24c | – | Symmetry |
| 24d | – | Symmetry |
| 24e | 22.7 | 55:45 |
| 24f | 19.5 | 80:20 |
| 24g | 19.3 | 81:19 |
| 24h | 18.4 | 75:25 |

account of the steric demands. The estimated free energies of activation lie in the range of 18.4–19.5 kcal mol^{–1}.

When the solid sample of **24a** was irradiated at 0 °C, the crystals gradually changed to amorphous. At this point, the generation of **25a** was not observed (Scheme 14 and Table 9, entry 1), and only a mixture of (*E*) and (*Z*) isomers (*Z/E*=1.5) was obtained [47, 48]. Prolonged irradiation gave β -thiolactam **25a** in 54% yield (entry 2).

X-ray crystallographic analysis revealed that the crystals of thioamide **24b** are chiral and the space group was *P*2₁2₁2₁. When the crystals were irradiated



Scheme 14

Table 9 Photochemical reaction of **24** in the solid-state

| Entry | 24 | Conv. (%) | Yield of 25 (%) | ee of 25 (%) |
|-------|------------|----------------|------------------------|---------------------|
| 1 | 24a | 0 ^a | 0 | 0 |
| 2 | | 100 | 54 | 0 |
| 3 | 24b | 81 | 55 | 55 |
| 4 | | 17 | 95 | 74 |
| 5 | 24c | 100 | 81 | 81 |
| 6 | | 20 | 97 | 97 |
| 7 | 24d | 100 | 100 | 0 |

^a (*E,Z*) isomerization occurred (*Z/E*=1/1.5).

at 0 °C until the reaction conversion reached 81% yield, the asymmetric induction in **25b** was obtained in 55% ee (entry 3). According to the suppression of the reaction conversion yield from 81 to 17%, the enantiomeric purity rose to 74% ee (entry 4). The solution photochemistry gave an intractable mixture accompanied with 28% of **25b**. In the solid-state media, a topochemical reaction proceeded and high product selectivity was also achieved.

In the solid-state photoreaction of **24c**, a more chemoselective reaction occurred and only β -thiolactam **25c** was obtained almost quantitatively. Of particular importance is the finding that the solid-state photoreaction of **24c** involves a crystal-to-crystal nature where the optically active β -thiolactam **25c** is formed in specific yield. Furthermore, the X-ray crystallographic analysis revealed that the crystals of **24c** are chiral, and the space group is *P2*₁. Irradiation of crystals at 0 °C exclusively gave optically active β -thiolactam **25c**, in 81% yield at 100% conversion (entry 5). As expected, the thiolactam **25c** showed optical activity (81% ee). This reaction exhibited good enantioselectivity throughout the whole reaction, where a small difference was observed in the ee value from 97 to 81% ee with increasing conversion from 20 to 100% (entries 5 and 6). The solid-state photoreaction also proceeded without phase separation even after 100% reaction conversion. The crystal-to-crystal nature of the transformation was confirmed by X-ray diffraction spectroscopy.

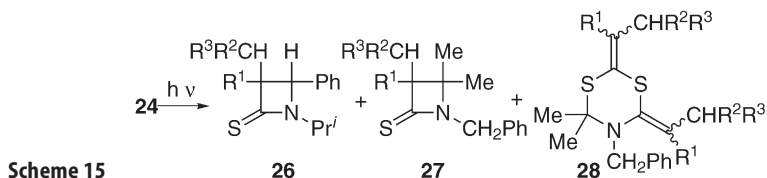
Photolysis of cycloheptenecarbothioamide **24d** in the solid state also gave the corresponding β -thiolactam in specific yield (entry 7). As the X-ray crystallographic analysis revealed, the crystal is racemic (Fig. 9), and the isolated β -thiolactam was obtained as racemate.

Recrystallization of **24e** from hexane yielded yellow crystals, which were analyzed by X-ray crystallography. The conformation of the thioamide chro-

mophore is so-called *Z* in which the alkenyl group is placed far from the benzyl group. The thioamide **24e** also crystallized in a chiral space group, $P2_12_1$. When powdered thioamide **24e** was irradiated in the solid state at 0 °C up to 17% conversion, optically active β -thiolactam **25e** (31% ee) was isolated. The solid unfortunately changed to amorphous at around 20% conversion. The solid-state photoreaction did not proceed at lower temperature (–50 °C).

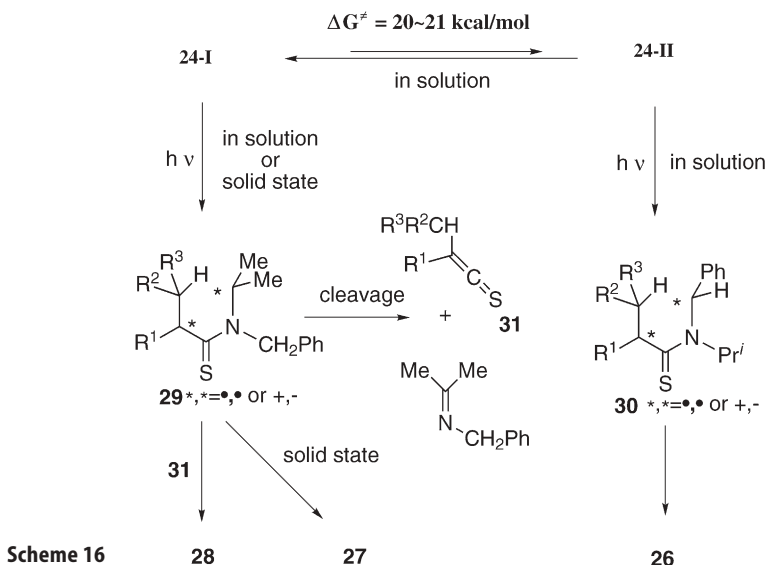
Recrystallization of thioamides **24f–h** gave colorless or slightly yellow prismatic crystals [49]. All three thioamides were subjected to X-ray single crystal analysis, and it was revealed that they prefer the same conformation **24-I** in which a benzyl group was placed close to the thiocarbonyl group, the same as the major isomer in solution. The alkenyl double bonds are perpendicular to the thioamide group, and twist in the range of 87.9° to 100.5°.

When thioamides **24f–h** were irradiated in benzene with a high-pressure mercury lamp, *N*-isopropyl- β -thiolactam **26** and 1,3,5-dithiazine **28** were obtained (Scheme 15 and Table 10, entries 1, 3, and 5). Considerably different photochemical behavior was observed between that in solution and in the solid state. Powdered thioamide **24f** was irradiated in the solid state at 0 °C until 19% conversion, because the solid changed to amorphous at around 20% conversion. In this case, only dithiazine **28f** was obtained as the sole photoproduct (entry 2). On the contrary, photolysis of **24g** gave a new type of β -lactam **27g** as a main product in 88% yield in addition to dithiazine **28g** (12%); the β -lactam **26g** was not detected at all (entry 4). Photochemical (*E,Z*) isomerization of (*Z*)-**24g** was also observed in the early stage of the reaction, where the ratio of the photostationary state was *Z/E*=1.9. In the case of **24h**, β -thiolactam **27h** was ob-



tained as a main product in 56% yield accompanied by **28c**; the structural isomer **26h**, which was isolated in solution photochemistry, was not observed (entry 6).

Scheme 16 shows a plausible mechanism for the formation of β -thiolactams **26**, **27**, and dithiazine **28**. Thioamides **24a,f–h** are composed of two conformers **24-I** and **24-II** in solution, where the conformer **I** slightly predominates over conformer **II**. γ -Hydrogen abstraction by the alkenyl carbon from the isopropyl group in conformer **I** resulted in the formation of a diradical **29**, which subsequently cleaves to a thioketene **31** and isopropylidenebenzylamine. Cycloaddition of **29** with the thioketene **31** gives dithiazine **28**. In this case, intermediate **29** formed by hydrogen abstraction from the isopropyl group did not cyclize to β -lactams in solution medium. On the other hand, conformer **II** abstracts the benzyl hydrogen atom leading to intermediate **30**, and subsequently cyclization takes place to β -thiolactam **26**. It seems that intermediate **29** does not cyclize in solution because of the steric repulsion for C–C bond formation.



The most important parameter to determine the reactivity for hydrogen abstraction in the solid state is d_{C-H} , the distance between the abstracted hydrogen atom and the abstracting carbon atom. Except for the case of **24e**, the actual distances are in the range from 2.58 to 2.84 Å, which are closely placed and are within the sum of van der Waals radii 2.90 Å. Scheffer et al. reported the geometrical parameter of hydrogen abstraction by the C=C double bond from their $\pi\pi^*$ excited state and suggested that hydrogen abstraction occurs within 2.90 Å of the distance between the alkenyl carbon atom and the hydrogen atoms **21**.

In the case of **24e**, the distance between the nearest benzyl hydrogen and the alkenyl β -carbon is 4.52 Å, which is much longer than the sum of the van der

Waals radii of two atoms (2.90 Å). Nevertheless, each reaction site is far apart; the hydrogen abstraction from the benzyl group proceeds and the product was obtained in optically active form. In this case, another mechanism besides the direct intramolecular hydrogen abstraction from the benzyl group may be involved, like intermolecular hydrogen abstraction or hydrogen shift.

In the solid-state photochemical reaction of *N,N*-disubstituted α,β -unsaturated thioamides **24**, a crystal-to-crystal nature was observed in **24c**; furthermore, absolute asymmetric transformation in the chiral crystalline environment was performed in the photoreaction of **24b**, **24c**, and **24e**.

3

Concluding Remarks

Solid-state photochemical reaction has been extended in recent years to a variety of new systems such that it can now be regarded as an important branch of organic chemistry. Now the field of organic solid-state photochemistry has become popular. The solid-state aspects of thiocarbonyl compounds are reviewed in this chapter, which show considerably high photochemical reactivity toward [2+2] cycloaddition and hydrogen abstraction reactions. These reactions are very useful to make a new C–C bond, and especially the photochemical reaction of thioamides and thioimides provides a useful synthesis of nitrogen-containing heterocycles. The fantastic diversity of molecular organization in the crystals provides not only a limitless variety of new chemical reactions, but also deep insight into the reaction mechanism which is directly connected with X-ray crystallographic analysis.

References

1. Ohno A (1971) *Int J Sulfur Chem* B6:183
2. Oae S (ed) (1977) *Thiones in organic sulfur*. Plenum, New York, p 189
3. Coyle JD (1975) *Chem Soc Rev* 4:523,
4. Coyle JD (1985) *Tetrahedron* 41:5393
5. de Mayo P (1976) *Acc Chem Res* 9:52
6. Turro NJ, Ramamurthy R, Cherry W, Farneth W (1978) *Chem Rev* 78:125
7. Ramamurthy V (1985) In: Padwa A (ed) *Organic photochemistry*, vol 7. Marcel Dekker, New York, pp 231–329
8. Itoh Y (1998) *Synthesis* 1
9. Gattermann L, Shultze H (1986) *Chem Ber* 29:2944
10. Shönberg A, Stephenson A (1933) *Chem Ber* 66B:567
11. Shönberg A, Mostafa A (1943) *J Chem Soc* 275
12. Ramamurthy V (1986) *Tetrahedron* 42:5753
13. Ramamurthy V, Venkatesan K (1987) *Chem Rev* 87:433
14. Machida M, Oda K, Sato E, Kanaoka Y (1986) *J Synth Org Chem Jpn (Yuki Gosei Kagaku Kyokai-shi)* 44:1071

15. Sakamoto M, Fujita T, Watanabe S, Nishio T (1994) *J Synth Org Chem Jpn* (Yuki Gosei Kagaku Kyokai-shi) 52:685
16. Nishio T, Sakamoto M (1995) *Rev Heteroatom Chem* 12:23
17. Sakamoto M, Nishio T (1995) *Rev Heteroatom Chem* 12:53
18. Sakamoto M, Nishio T (2003) *Heterocycles* 59:399
19. Sakamoto M, Nishio T (2004) In: Chapman OL (ed) *CRC handbook of organic photochemistry and photobiology*, 2nd edn. CRC, Boca Raton, 106:1
20. Green BS, Lahav M, Rabinovich D (1979) *Acc Chem Res* 12:191
21. Scheffer JR, Garcia-Garibay M, Nalamasu O (1987) In: Padwa A (ed) *Organic photochemistry*, vol 8. Marcel Dekker, New York, p 249
22. Vaida M, Popovitz-Biro R, Leiserowitz L, Lahav M (1991) In: Ramamurthy V (ed) *Photochemistry in organized and constrained media*. VCH, New York, p 249
23. Sakamoto M (1997) *Chem Eur J* 3:384
24. Koshima H, Matsuura T (1998) *J Synth Org Chem Jpn* (Yuki Gosei Kagaku Kyokai-shi) 56:268
25. Feringa BL, Van Delden R (1999) *Angew Chem Int Ed* 38:3419–3438
26. Sakamoto M (2004) In: Inoue Y, Ramamurthy V (eds) *Chiral photochemistry*. Marcel Dekker, New York (in press)
27. Kaiser ET, Wulfers TF (1964) *J Am Chem Soc* 86:1897
28. Rao VP (1992) *Sulfur Rep* 12:359
29. Sakamoto M, Hokari N, Takahashi M, Fujita T, Watanabe S, Iida I, Nishio T (1993) *J Am Chem Soc* 115: 818
30. Sakamoto M, Takahashi M, Mino T, Fujita T (2001) *Tetrahedron* 57:6713
31. Sakamoto M, Yanase T, Fujita T, Watanabe S, Aoyama H, Omote Y (1991) *J Chem Soc Perkin Trans I* 403
32. Sakamoto M, Takahashi M, Hokari N, Fujita T, Watanabe S (1994) *J Org Chem* 59:3131
33. Sakamoto M, Takahashi M, Arai T, Shimizu M, Yamaguchi K, Mino T, Watanabe S, Fujita T (1998) *J Chem Soc Chem Commun* 2315
34. Wagner PJ, Park BS (1991) In: Padwa A (ed) *Organic photochemistry*, vol 11. Marcel Dekker, New York, p 227
35. Wagner PJ (1983) *Acc Chem Res* 16:461
36. Schmidt GMJ (1971) *Pure Appl Chem* 27:647
37. Sakamoto M, Takahashi M, Shimizu M, Fujita T, Nishio T, Iida I, Yamaguchi K, Watanabe S (1995) *J Org Chem* 60:7088
38. Sakamoto M, Aoyama H, Omote Y (1984) *J Org Chem* 49:1837
39. Sakamoto M, Tohnishi M, Fujita T, Watanabe S (1991) *J Chem Soc Perkin Trans I* 347
40. Fu TY, Scheffer JR, Trotter J (1994) *Tetrahedron Lett* 35:3235
41. Fu TY, Scheffer JR, Trotter J (1998) *Acta Cryst C* 54:103
42. Fu TY, Scheffer JR, Trotter J (1996) *Tetrahedron Lett* 37:2125
43. Arjunan P, Ramamurthy V, Venkatesan K (1984) *J Org Chem* 49:1765
44. Sakamoto M, Takahashi M, Kamiya K, Yamaguchi K, Fujita T, Watanabe S (1996) *J Am Chem Soc* 118:10664
45. Sakamoto M, Takahashi M, Arai W, Mino T, Yamaguchi K, Fujita T, Watanabe S (2000) *Tetrahedron* 56:6795
46. Sakamoto M, Kimura M, Shimoto T, Fujita T, Watanabe S (1990) *J Chem Soc Chem Commun* 1214
47. Sakamoto M, Takahashi M, Kamiya K, Arai W, Yamaguchi K, Fujita T, Watanabe S (1998) *J Chem Soc Perkin Trans I* 3731
48. Kinbara K, Saigo K (1996) *Bull Chem Soc Jpn* 69:779
49. Sakamoto M, Takahashi M, Arai W, Kamiya K, Yamaguchi K, Fujita T, Watanabe S (1999) *J Chem Soc Perkin Trans I* 3633

Asymmetric Induction in Organic Photochemistry via the Solid-State Ionic Chiral Auxiliary Approach

John R. Scheffer (✉) · Wujiong Xia

Department of Chemistry, University of British Columbia, 2036 Main Mall, Vancouver, BC, Canada V6T 1Z1

scheffer@chem.ubc.ca; xiawj@chem.ubc.ca

| | |
|---|-----|
| 1. Introduction | 233 |
| 1.1 Absolute Asymmetric Synthesis | 234 |
| 1.2 Asymmetric Induction in the Photochemistry of Crystalline Host–Guest Assemblies | 237 |
| 1.3 The Use of Chirally Modified Zeolites in Photochemical Asymmetric Synthesis | 241 |
| 1.4 Chiral Auxiliary-Mediated Asymmetric Synthesis in the Crystalline State | 244 |
| 1.4.1 Covalent Chiral Auxiliary-Induced Asymmetric Induction in Solid-State Organic Photochemistry | 245 |
| 1.4.2 Ionic Chiral Auxiliary-Induced Asymmetric Induction in Solid-State Organic Photochemistry | 246 |
| 1.4.3 Comparison of the Solid-State Ionic Chiral Auxiliary Method of Asymmetric Synthesis with the Pasteur Resolution Procedure | 258 |
| References | 260 |

Abstract After a brief introduction and summary of various methods of asymmetric induction in organic photochemistry, the main part of the review covers the solid-state ionic chiral auxiliary approach to asymmetric photochemical synthesis. Application of this technique to the Norrish type II reaction, as well as to the di- π -methane and oxa-di- π -methane photorearrangements, and the *cis,trans*-photoisomerization of diarylcyclopropane derivatives is presented and discussed.

Keywords Asymmetric induction · Organic photochemistry · Solid state · Ionic chiral auxiliaries · Crystal structure–reactivity correlations

1 Introduction

Solid-state chemistry has attracted widespread interest and attention owing to its several advantages compared to reactions conducted in solution: increased reaction selectivity, the opportunity to correlate chemical behavior with detailed structural information obtained through X-ray crystallography, access to “latent” reactivity different from that observed in solution, simplicity in process

and handling, and low environmental impact [1]. Photochemical reactions are particularly well suited for study in the solid state because they can be conducted at ambient temperature or below, where the crystals do not melt, and light is able to penetrate deep within the crystal lattice. One aspect of organic solid-state photochemistry that has received a great deal of attention recently concerns its use in asymmetric synthesis. Nevertheless, compared to the extremely well-developed field of asymmetric synthesis in the ground state, asymmetric synthesis in the excited state is still in its early stages [2]. There are at least two reasons for this: first, photochemical reactions tend to be low activation energy processes originating from high-energy excited states, which makes it difficult to achieve significant kinetic differentiation between diastereomeric transition states leading to enantiomeric photoproducts; a second reason is that organic photochemistry is often incompatible with the type of chiral auxiliaries used in ground-state asymmetric synthesis, many of which are transition metal complexes with highly conjugated π -bond-containing ligands. The problem with such species is that they tend to absorb light in the same wavelength region as the reactants, and even when the reactants can be selectively excited, the chiral auxiliaries can act as quenchers, hydrogen atom donors, or electron transfer agents, thus effectively shutting down the desired photoreaction.

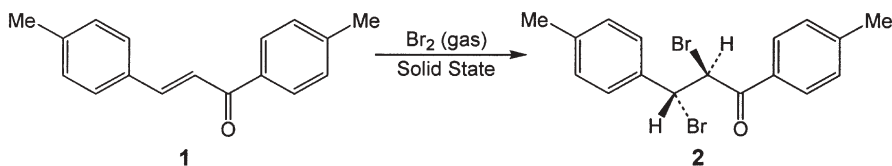
In this review, we begin with a brief discussion of the methods used by others to achieve asymmetric induction in organic photochemistry. For the most part, despite some very elegant advances in solution on enantioselective intermolecular [2+2] photocycloaddition reactions [3] and *cis* to *trans* cycloalkene photoisomerizations [4], the most general and successful approach to photochemical asymmetric synthesis to date has been with reactions carried out in the solid state. The reason for this is that, unlike the situation in solution, molecules in crystals are held in fixed conformations and intermolecular packing arrangements, which, if chiral, lead through least-motion processes to highly enantioenriched photoproducts. The realization that the crystalline state could be used to achieve high levels of asymmetric induction came out of early work on “absolute” asymmetric synthesis, which is briefly outlined below. This is followed by brief sections on asymmetric synthesis using crystalline host–guest assemblies and chirally modified zeolites. The bulk of the review, however, covers our own work on ionic chiral auxiliary-induced asymmetric synthesis in solid-state organic photochemistry.

1.1

Absolute Asymmetric Synthesis

Absolute asymmetric synthesis refers to the situation in which an asymmetric induction occurs in the absence of an externally imposed source of chirality [5]. Such reactions are invariably carried out in the crystalline state, where the asymmetric influence governing the enantioselectivity derives from the spontaneous crystallization of an achiral compound in a chiral space group. This phenomenon, which is analogous to the spontaneous crystallization of racemates as

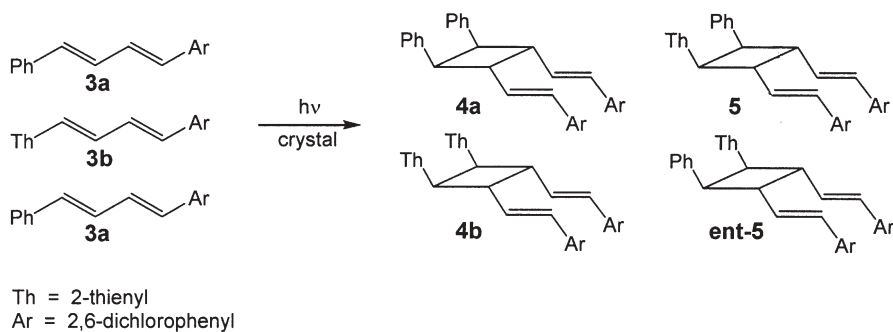
enantiomerically pure conglomerates à la Pasteur, is rare but well documented [6] and was first used in an absolute asymmetric synthesis in 1969 by Penzien and Schmidt [7]. These authors crystallized 4,4'-dimethylchalcone (**1**) from ethyl acetate in the chiral space group $P2_12_12_1$ and then exposed single crystals of this material to bromine vapor in a gas-solid reaction. The corresponding chiral *trans*-dibromide **2** was formed in enantiomeric excesses ranging from 6 to 25%.



Single crystals of compounds such as 4,4'-dimethylchalcone that adopt chiral space groups are characterized by being enantiomorphous, that is, they are either right-handed or left-handed, and the molecules that make up the lattice have homochiral conformations and packing arrangements. Molecular conformation rather than crystal packing was identified as the source of chirality in the solid-state chalcone bromination [8]. This ketone crystallizes in a highly twisted, homochiral conformation in which one face of the carbon-carbon double bond is intramolecularly more hindered than the other. As a result, bromine attacks from the less hindered face, leading to a predominance of one enantiomer over the other. Support for this interpretation came from the finding that gas-solid bromination of alkenes that crystallize in chiral space groups, but which have less highly twisted double bonds, leads to racemic products [9]. The role of the crystal lattice in this reaction is thus one of preorganizing and immobilizing the molecules in conformations favoring the formation of one enantiomer over the other; intermolecular steric effects between lattice neighbors play little or no role in governing enantioselectivity. We shall encounter many additional examples of such conformation-controlled asymmetric syntheses in subsequent sections of this review.

The first photochemical absolute asymmetric synthesis employing chiral crystals was reported by Elgavi, Green, and Schmidt in 1973 [10]. These authors showed that crystals of 1-(2,6-dichlorophenyl)-4-phenyl-*trans,trans*-1,3-butadiene **3a** and the corresponding thienyl analog **3b** are isomorphous, both adopting the chiral space group $P2_12_12_1$ with nearly identical crystallographic cell constants and four molecules per unit cell. The crystal structure of diene **3a** showed that double bonds of adjacent molecules in the lattice are parallel with an interplanar separation of 4.0 Å, ideal for intermolecular [2+2] photocycloaddition. In accord with the crystal structure, irradiation of dienes **3a** and **3b** in the solid state led to the mirror-symmetric dimers **4a** and **4b**, respectively (Scheme 1).

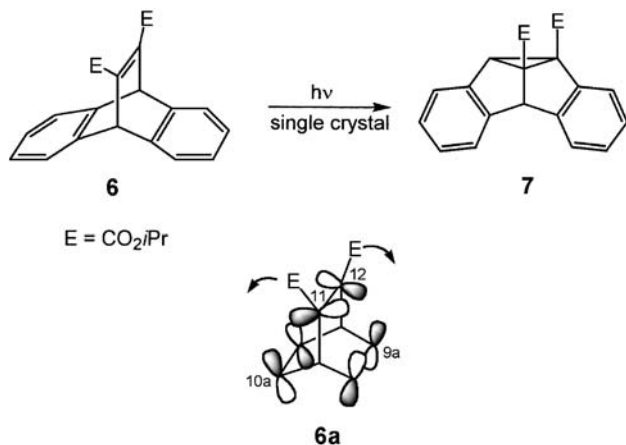
Photodimers **4a** and **4b** are achiral, thus precluding the possibility of absolute asymmetric induction. The mixed dimer **5**, however, is chiral, and in a



Scheme 1 The first photochemical absolute asymmetric synthesis

very clever experiment it was shown that photolysis of mixed single crystals containing both **3a** and **3b** led to dimer **5** with an ee of approximately 70%. The amount of mixed dimer **5** in the photoproduct mixture could be maximized by selectively exciting diene **3b**, which prevents formation of **4a**, and by using mixed crystals with a **3a:3b** ratio of 85:15, which minimizes the formation of dimer **4b**. The enantioselectivity in this reaction was ascribed to deformation of diene **3b** upon excitation, resulting in an unequal interaction between molecule **3b** and its **3a** nearest neighbors on either side.

In addition to bimolecular [2+2] photocycloaddition reactions similar to the one discussed above [11], absolute asymmetric syntheses employing spontaneously grown chiral crystals have been studied for a number of unimolecular photorearrangement reactions as well. The first report of such an investigation dealt with the photoisomerization of dibenzobarrelene diester **6** to the corresponding dibenzosemibullvalene compound **7** [12], an example of the well-known di- π -methane (Zimmerman) photorearrangement. Achiral diester **6** crystallizes spontaneously from cyclohexane in the now familiar chiral space



group $P2_12_12_1$, and when large, carefully grown single crystals of this substance were irradiated to less than 25% conversion, photoproduct **7** was found to be formed in greater than 95% enantiomeric excess, an ee considerably greater than any reported up to that time for an absolute asymmetric synthesis.

In a study similar to that carried out for the gas–solid bromination of dimethylchalcone [8], a crystallographic correlation of the absolute conformation of dibenzobarrelene derivative **6** with the absolute configuration of its photoproduct **7** revealed that the enantioselectivity of this photorearrangement is governed primarily by the molecular conformation of the reactant [13]. As depicted in the equation, compound **6** crystallizes in a conformation in which the C11–C12 double bond is significantly twisted. As a result, initial carbon–carbon bond formation resulting from overlap of the shaded orbitals, which leads to one enantiomer of **7**, is favored over bond formation between the unshaded orbitals leading to the other enantiomer. Furthermore, bond formation between the shaded orbitals is favored sterically, since the bulky ester groups move apart from one another (arrows, structure **6a**). In the alternative, unobserved pathway, the ester groups would be driven toward one another, thus increasing the steric interaction between them.

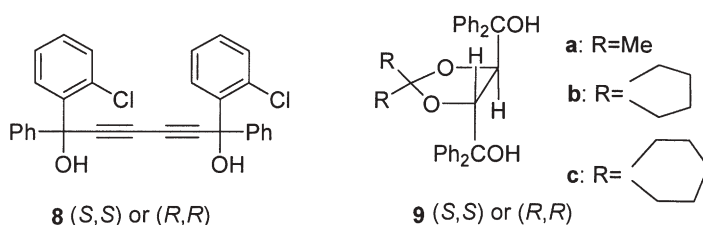
With this we conclude our discussion of chiral crystal-induced absolute asymmetric synthesis. The last 15 years have seen a substantial number of additional absolute asymmetric syntheses reported, primarily unimolecular in nature [14], but in this review, rather than trying to be comprehensive, we have taken a historical approach, with an emphasis on the basic principles involved. Despite the obvious appeal of “getting something for nothing,” it seems fair to conclude that chiral crystal-induced absolute asymmetric synthesis will not become a general synthetic method. The primary drawback is that the great majority of achiral organic compounds do not crystallize in chiral space groups [6], and at the moment, there is no reliable method of predicting when they will, nor any known way of forcing them to do so. In the absence of crystal chirality, of course, there is no asymmetric influence favoring the formation of one enantiomer over the other, and the reaction products, if chiral, are formed as racemates.

1.2

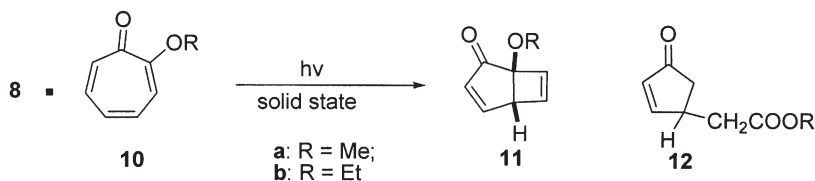
Asymmetric Induction in the Photochemistry of Crystalline Host–Guest Assemblies

Secure in the knowledge that the photoreactions of chiral crystals are capable of producing highly enantioenriched products, the obvious next step was to devise ways of guaranteeing chiral space groups, rather than relying on the occasional kindness of nature. The solution to this problem is relatively straightforward. Taking advantage of the fact that enantiomerically pure compounds necessarily crystallize in chiral space groups, all that is required is to introduce an element of homochirality into the crystalline assembly. This can be accomplished by cocrystallizing the reactant with a second, enantiomerically pure

compound that is photochemically inert and can be removed after reaction. Most commonly, the external chiral auxiliary in this approach takes the form of an optically pure host coordinatoclathrate compound. Coordinatoclathrate host compounds tend to be bulky and pack inefficiently with voids, and they generally possess functional groups that can coordinate to guest molecules through hydrogen bonding or some other noncovalent attractive interaction. When such compounds are synthesized in optically pure form, they can be co-crystallized with achiral guests, and irradiation of the guests in the homochiral environment of the host–guest crystal can lead to asymmetric induction. This approach to photochemical asymmetric synthesis has been pioneered and extensively investigated by Toda, Tanaka, and coworkers [15, 16], who used the optically pure C2 symmetric host molecules **8** and **9** among others.



An example of the use of this approach in the disrotatory photocyclization of tropolone alkyl ethers is shown in Scheme 2. Thus, irradiation of the 1:1 complex of α -tropolone alkyl ether **10a** with host compound **8** in the solid state gave photoproducts **11a** of 100% ee and **12a** of 91% ee in 11 and 26% yields, respectively [17].

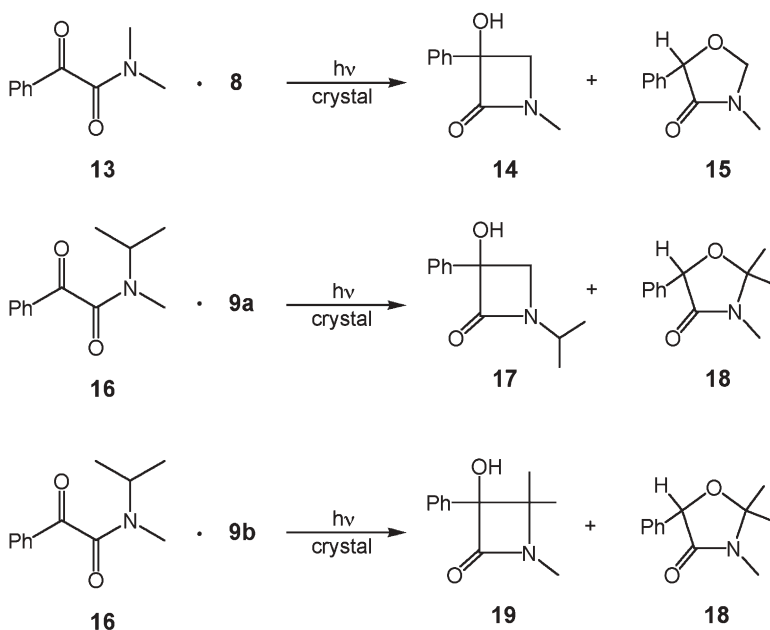


Scheme 2 Asymmetric induction in the disrotatory photocyclization of tropolone ethers

Similar irradiation of the 1:1 complex of tropolone ether **10b** and host compound **8** led to photoproducts **11b** (100% ee) and **12b** (72% ee) in 12 and 14% yields, respectively. The authors interpreted these reactions as follows: disrotatory electrocyclic closure of tropolone derivative **10** to afford photoproduct **11** in the inclusion crystals occurs in only one direction owing to the steric hindrance of host **8**. This interpretation appeared to be reasonable based on an examination of the X-ray crystal structure study of the inclusion complex [18]. Formation of keto-ester **12** takes place by a more complex mechanism

involving secondary photorearrangement of product **11** followed by reaction with water and retro-Claisen ring opening. The authors suggested that small amounts of water present in the crystalline complex are responsible for the formation of photoproduct **12** and that its low ee compared to that of photoproduct **11** is due to photodienol formation and reketonization. An unanswered question raised in this work concerns the reason for the low chemical yields observed.

A second example of the use of optically pure coordinatocathrate hosts in controlling the enantioselectivity of photochemical reactions in the crystalline state is found in the case of the α -oxoamide derivative **13**, which forms a crystalline 1:1 complex with host (*S,S*)-**8** [18, 19]. Irradiation of these crystals led to the β -lactam derivative (–)-**14** in 90% yield and a reported ee of 100% (Scheme 3). The X-ray crystal structure of the complex showed that oxoamide **13** adopts a helical conformation that favors the formation of a single enantiomer of photoproduct **14**. The reaction is thus conformationally controlled in a way exactly analogous to the examples discussed earlier in the review.

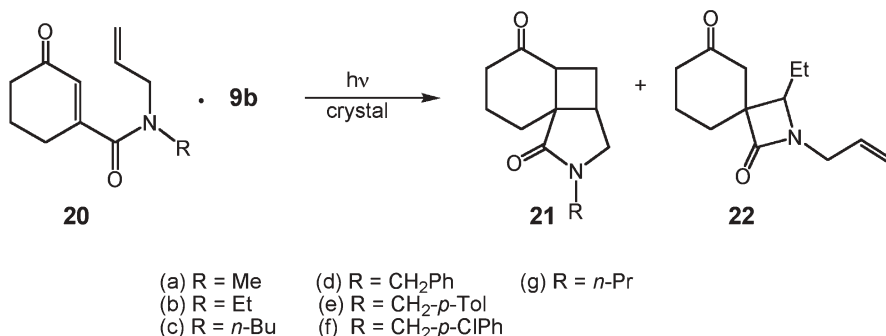


Scheme 3 Asymmetric synthesis using optically pure coordinatocathrate hosts

Compound **13** is only one of a number of differently substituted α -oxoamides investigated by Toda et al. Depending on the optically pure host molecule used, yields and enantiomeric excesses of the corresponding β -lactams varied widely, and in some instances new photoproducts were observed. For example, irradiation of the crystalline complex formed between α -oxoamide **13** and host **9b**

afforded β -lactam **14** in only 40% yield with an ee of 67% [20]. A second photoproduct was formed in 55% yield in this reaction, which proved to be oxazolidinone **15** (Scheme 3). This compound is also chiral and was formed in an ee of 100%. Also unusual were the results of photolyzing the crystalline complexes formed between α -oxoamide **16** and host diols **9a** and **9b** [21]. Here, despite the fact that crystallography showed that α -oxoamide **16** has the same conformation in both complexes, irradiation led to two different β -lactams, **17** (11% yield, 100% ee) and **19** (17% yield, 61% ee). Remarkably, each photolysis gave the same oxazolidinone **18** (20% yield, 39% ee in the complex with **9a** and 71% yield and 43% ee in the complex with **9b**). Thus while these reactions are very interesting and can give rise to high levels of asymmetric induction for certain host–guest combinations, further work is required to come to a general understanding of how host structure determines which photoproduct will be formed and the degree of asymmetric induction.

In principle, the approach outlined above for the α -oxoamides can be applied to any reaction, ground or excited state, which converts an achiral reactant into a chiral product, and Toda, Tanaka, and coworkers have investigated a wide variety of such processes [15, 16]. A complete discussion of their work is beyond the scope of this review, and we illustrate the general approach taken with one final example. As shown in Scheme 4, irradiation of crystalline complexes of ene-diones **20a–f** with chiral host (*R,R*)-(-)-**9b** led to cyclized products **21a–f** in the variable yields and ee values indicated in Table 1 [22]. Remarkably, for reasons that were not clear (there was no accompanying X-ray crystallography), the *R*=*n*-propyl derivative **20g** was found to give a completely different photoproduct, spiro compound **22** (69% yield, 97% ee, stereochemistry unknown), a result that once again illustrates the rather capricious nature of the use of chiral hosts for asymmetric induction.



Scheme 4 Asymmetric induction in an intramolecular [2+2] photocycloaddition reaction using optically pure coordinatoclathrate host **9b**

We close this section with a brief discussion of the advantages and disadvantages of using optically pure coordinatoclathrate hosts for photochemical

Table 1 Photoproduct yields and enantiomeric excesses from irradiation of crystalline complexes of ketones **20a–f** with optically pure host **9b**

| Compound photolyzed | Yield of product 21 (%) | Enantiomeric excess (%) |
|---------------------|--------------------------------|-------------------------|
| 20a | 17 | 68 |
| 20b | 30 | 67 |
| 20c | 25 | 53 |
| 20d | 87 | 100 |
| 20e | 56 | 100 |
| 20f | 42 | 100 |

asymmetric synthesis. On the negative side, the hosts are relatively time consuming and expensive to prepare, and their presence in the reaction mixture complicates the separation and purification of the photoproducts. More significant is the fact that the method is restricted to reactants that form crystalline inclusion complexes with the hosts. Statistics on this point are unavailable, since failures are not reported, but there is little doubt that this is a significant limitation. Finally, coordinatoclathrate complexes tend to be rather low melting, since they are the result of relatively weak interactions between host and guest. Low melting points are anathema in the field of solid-state chemistry, as crystal melting leads to loss of the three-dimensional periodicity of the lattice and results in solution-like chemical behavior. On the positive side, the hosts can be recovered from the reaction mixtures and reused. In addition, the method allows a wide range of guests to be investigated, the major requirement being the ability of the guest to hydrogen bond to the host.

1.3

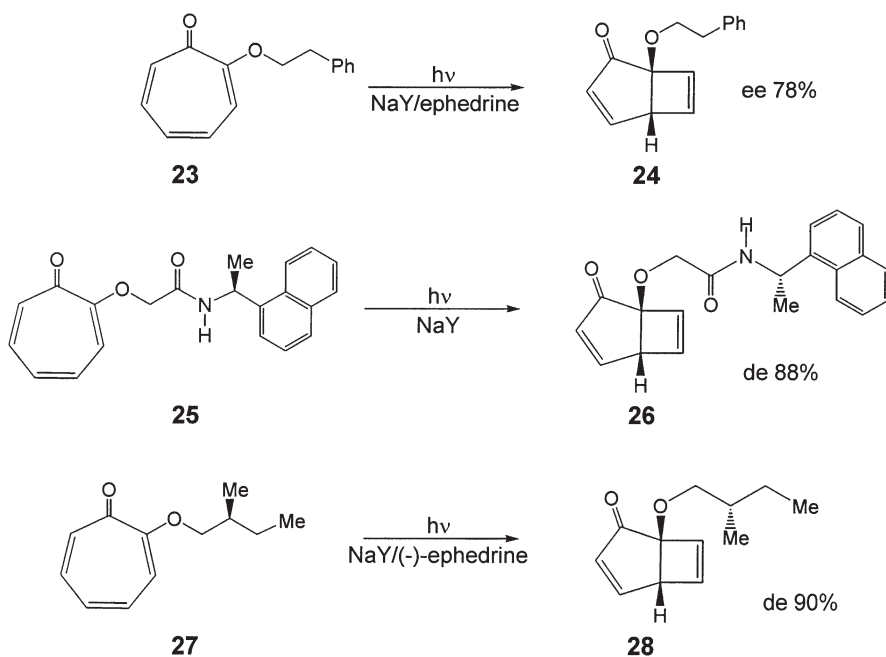
The Use of Chirally Modified Zeolites in Photochemical Asymmetric Synthesis

As we have seen, one of the main reasons why reactions in crystals lead to high levels of asymmetric induction is that the constituent molecules can be organized in homochiral fixed conformations and intermolecular orientations that are predisposed to formation of a single product enantiomer. With this in mind, it was natural to seek other ways of preorganizing molecules in restricted environments for the purpose of asymmetric synthesis, and one approach that has shown a good deal of promise is the use of chirally modified zeolites. The great majority of this work has been carried out by Ramamurthy and coworkers at Tulane University [23], and a brief summary is given below.

Zeolites are crystalline aluminosilicates with porous, framework structures made up of linked $[\text{SiO}_4]^{4-}$ and $[\text{AlO}_4]^{5-}$ tetrahedra that form channels and cages of discrete size [24]. The framework structures of zeolites bear a net negative charge, which must be balanced by positively charged species, typically alkali or alkaline earth metal cations; these cations may be exchanged for one another under appropriate experimental conditions. Zeolites are capable of

accommodating organic compounds within their interstices, access to which is through an opening or window whose size is generally smaller than that of the cavities; the dimensions of this window determine the size of the molecules that can be adsorbed.

The zeolites most often used as hosts for chemical studies are the faujasite type Y zeolites, which are achiral. This, of course, means that any chiral products formed from an achiral precursor within the cavity of such zeolites will be racemic. For this reason, the zeolites must be “chirally modified” prior to use. The initial approach used by Ramamurthy et al. to solve this problem was to employ a “chiral inductor” – a photochemically inert, optically pure compound such as ephedrine, which, when absorbed by the zeolite, renders it chiral. This was accomplished by stirring hexane solutions of the chiral inductors in the presence of anhydrous NaY zeolite, followed by filtration and thorough washing with hexane. The vacuum-dried complexes were then transferred to a hexane solution of the compound to be photolyzed and again stirred, filtered, washed, and dried. The resulting doubly loaded zeolite assemblies were then irradiated as dry powders or, more commonly, as powders suspended in hexane. This methodology was applied to a number of different photorearrangement reactions with mixed success. Best results (78% ee) were obtained with the 2-phenylethyl ether of tropolone (compound **23**), which afforded the corresponding valence isomer **24** upon irradiation in the zeolite NaY with



Scheme 5 Examples of the zeolite chiral inductor and chiral auxiliary methods for photochemical asymmetric synthesis

ephedrine as the chiral inductor (Scheme 5) [25]. Other photoreactions conducted under similar conditions, however, gave significantly lower ee values (15–50%) [23].

As pointed out by Ramamurthy and coworkers, the problem with the chiral inductor procedure is that a substantial number of zeolite cages remain singly occupied, and these can only lead to racemic photoproducts. While modest increases in ee could be achieved by increasing the loading level of the chiral inductors, a better approach to guaranteeing close proximity between chiral inductor and reactant was to link the two together by a covalent bond. This was termed the chiral auxiliary method [23]. An example is shown in Scheme 5 in which the tropolone ether derivative **25** bearing an optically pure chiral auxiliary side chain undergoes disrotatory photocyclization in the zeolite NaY with a diastereomeric excess (de) of 88% [26]. The importance of carrying out this reaction in the restricted space of the zeolite interior is shown by the fact that irradiation of compound **25** in isotropic liquid media gave a de of only 10%. Ramamurthy and coworkers have explored the generality of the zeolite chiral auxiliary method with a number of different examples and shown that diastereomeric excesses of >70–80% can be obtained routinely for systems that give very low de values in solution [23].

In an extension of the above work, Ramamurthy et al. investigated a combination of the chiral inductor and chiral auxiliary approaches by photolyzing zeolite assemblies containing both chiral auxiliary-containing substrates and external chiral inductors – in effect providing two asymmetric influences for the reaction under study. When this approach was applied to optically pure tropolone (*S*)-2-methylbutyl ether (**27**, Scheme 5) in zeolite NaY, the de of the cyclization photoproduct **28** increased from 53% in the absence of an external chiral inductor to 90% in the presence of (–)-ephedrine [27]. Interestingly, when (+)-ephedrine was used as the external chiral inductor, the de of the opposite diastereomer was 70%, a result that was interpreted as indicating the involvement of two types of cages – one that contains the reactant alone and another that contains the reactant and a chiral inductor. According to this picture, if all the photoreactions had occurred in a single type of cage, switching the chiral inductors should have led to equal and opposite de values. While the 90% de obtained above is encouraging, the combined use of chiral auxiliaries and chiral inductors is unpredictable and sometimes leads to de values that are lower than those obtained using chiral auxiliaries alone [23]. As a result, the generality of this approach remains to be established.

We close this section with a few general comments regarding the use of zeolites in asymmetric organic photochemistry. The procedure is not functional group dependent and appears to be limited only by molecular size, i.e., to compounds that are able to pass through the zeolite pore openings (ca. 8 Å in diameter for NaY). Best results (de of 70–80%) are obtained using covalent chiral auxiliaries, which of course require prior installation and subsequent removal. A final point is that reactions in zeolites cannot be investigated easily by standard techniques such as X-ray crystallography and NMR spectroscopy.

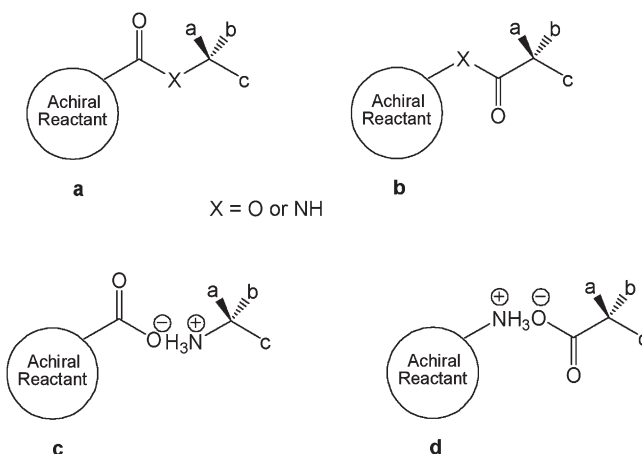
As a result, the underlying factors responsible for asymmetric induction are, at present, mainly a matter of speculation, and the chemist wishing to use the method must be prepared for considerable trial and error experimentation.

1.4

Chiral Auxiliary-Mediated Asymmetric Synthesis in the Crystalline State

We turn now to a presentation of our own research on the use of built-in or internal chiral auxiliaries for asymmetric induction in photochemical reactions in the crystalline state [28]. This work is a natural outgrowth of the work of Toda and coworkers on the use of external chiral host compounds for the same purpose discussed in Sect. 2.2. In both cases, the primary role of the chiral auxiliary is to guarantee the presence of a chiral space group for the ensuing solid-state photochemical reaction.

In general, there are two ways in which a chiral auxiliary can be attached to a photoreactant: covalently and ionically. In the covalent type, the optically pure

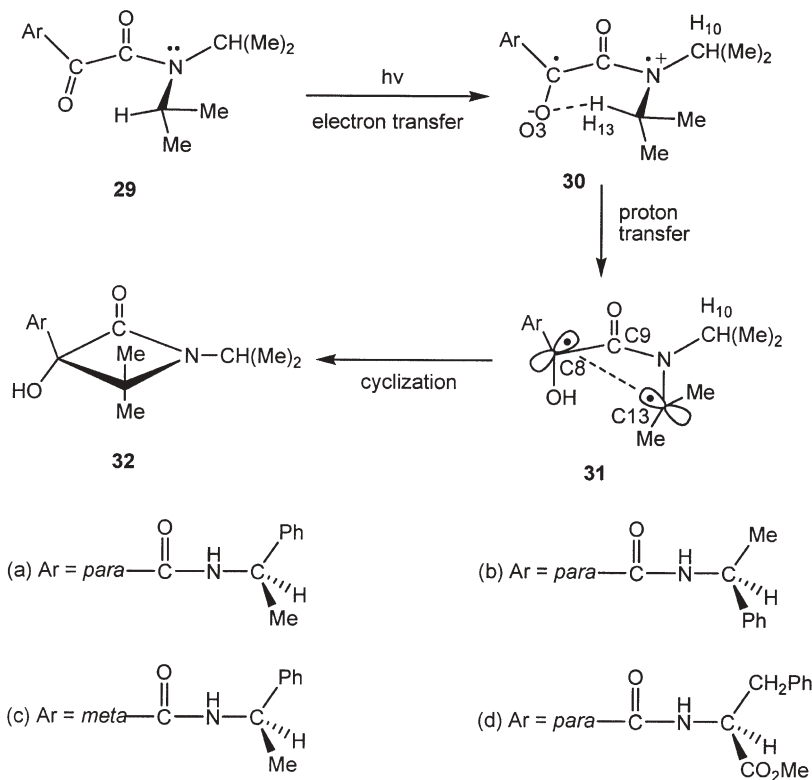


auxiliary is tethered to the achiral reactant by a covalent bond, typically via ester or amide formation between a carboxylic acid and an alcohol or an amine. There are two possible arrangements: one in which the alcohol or amine is the chiral auxiliary (a) and another in which the chiral auxiliary is derived from an optically pure carboxylic acid (b). In the ionic case, the attachment is by means of a salt bridge between a carboxylate anion and an ammonium ion. Here again, either the ammonium ion (c) or the carboxylate anion (d) can serve as the chiral auxiliary. These ions are the ionic chiral auxiliaries referred to in the title of this chapter.

1.4.1

Covalent Chiral Auxiliary-Induced Asymmetric Induction in Solid-State Organic Photochemistry

We present one example using covalent chiral auxiliaries and discuss it briefly. Natarajan, Wang, Ramamurthy, Scheffer, and Patrick reported an investigation of asymmetric induction in the photochemical conversion of α -oxoamides into β -lactam derivatives [29]. Their work dealt with compounds such as oxoamides **29a–d** (Scheme 6) in which the aryl group bears an optically pure amide substituent. Owing to the presence of the covalent chiral auxiliary, these compounds are required to crystallize in chiral space groups, and irradiation of such compounds in the solid state led to the corresponding diastereomerically enriched β -lactam derivatives **32a–d** with de's ranging from 76–99% (Table 2).



Scheme 6 Covalent chiral auxiliary-induced asymmetric synthesis of β -lactams

The mechanism of β -lactam formation is thought to involve photoinduced electron transfer from nitrogen to the benzoyl group followed by transfer of a tertiary γ -proton from one of the isopropyl groups to the carbonyl oxygen

Table 2 Asymmetric induction in the solid-state photochemistry of compounds **29a–d**

| Compound | Conversion (%) | de of 32 (%) |
|------------|----------------|---------------------|
| 29a | 98 | >99 |
| 29b | 97 | >99 |
| 29c | 17 | 80 |
| 29d | 80 | 76 |

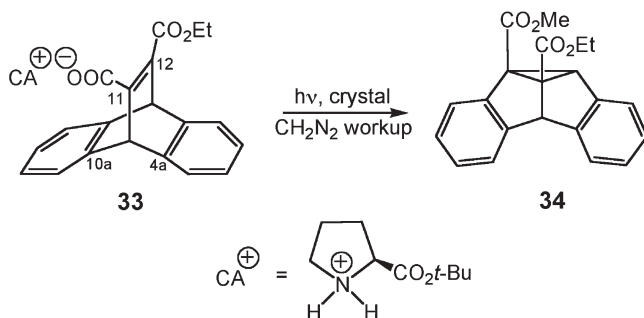
(Scheme 6) [30]. This generates 1,4-hydroxybiradical **31**, which closes to cyclobutanol **32**. The chirality of the photoproduct is determined not only by which of two γ -protons (H13 or H10) is transferred, but also by the stereochemistry of biradical closure. In the crystalline state, γ -hydrogen H13 lies at a shorter distance from O3 than H10, and as a result, H13 is more favorably disposed for proton transfer. The stereochemistry of biradical closure can also be interpreted in terms of molecular conformation. Scheme 6 shows that least-motion closure of biradical **31** should lead to the (*R*) absolute configuration at the newly generated chiral center, while formation of the (*S*) enantiomer would require rotation about the C8–C9 bond to bring the back lobe of the p-orbital on C8 into proximity with C13. Such a process, with its concomitant large-amplitude motions of the aryl substituent, is topochemically forbidden in the rigid, close-packed environment of the crystal.

1.4.2

Ionic Chiral Auxiliary-Induced Asymmetric Induction in Solid-State Organic Photochemistry

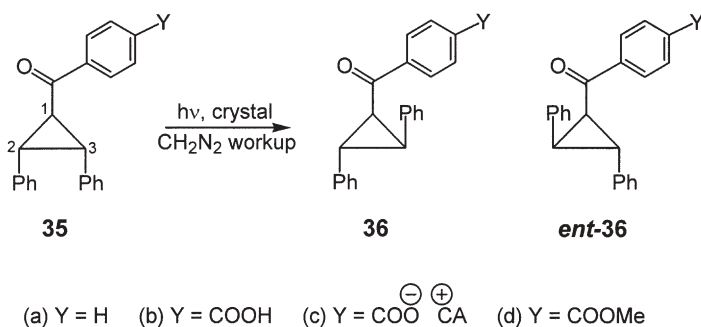
The great majority of our work on asymmetric induction in the crystalline state has been with ionic rather than covalent chiral auxiliaries. There are two main reasons for this choice: (1) at the time this work was begun, in 1990, the use of ionic chiral auxiliaries in asymmetric synthesis was unknown; and (2) because of their relatively high melting points, ionic materials are ideally suited for studies in the crystalline state. High melting points enable the reactions to be carried out to higher degrees of conversion without crystal melting, an important consideration if the method is to be synthetically useful. Additional considerations were the ease of introduction and removal of the ionic auxiliaries and the ready availability of a wide variety of optically pure amines and carboxylic acids from the chiral pool.

The first reported use of ionic chiral auxiliaries in asymmetric synthesis was the work of Gudmundsdottir, Scheffer, and Trotter on the di- π -methane photorearrangement of the dibenzobarrelelene system **33** [31]. Of a number of chiral auxiliaries tested, best results were obtained with proline *tert*-butyl ester, which led to dibenzosemibullvalene derivative **34** in an enantiomeric excess of 95% at 40% conversion following diazomethane workup. By determining the ab-



solute configuration of diester **34** and correlating this with the absolute conformation of salt **33** as determined by X-ray crystallography, it was found that the reaction is conformationally controlled in the same way as for dibenzobarrelene **6** discussed earlier [32]. Thus the C11-C12 double bond of salt **33** is twisted in such a way that, for steric and orbital overlap reasons, initial bond formation is preferred between C11 and C4a rather than C11 and C10a. Once again, therefore, we see that conformational preorganization through crystallization determines enantioselectivity.

A second example of the use of ionic chiral auxiliaries for asymmetric synthesis is found in the work of Chong et al. on the *cis,trans* photoisomerization of certain cyclopropane derivatives [33]. Based on the report by Zimmerman and Flechtner [34] that achiral *trans,trans*-2,3-diphenyl-1-benzoylcyclopropane (**35a**, Scheme 7) undergoes very efficient ($\Phi=0.94$) photoisomerization in solution to afford the racemic *cis,trans* isomer **36a**, the corresponding *p*-carboxylic acid **35b** was synthesized and treated with a variety of optically pure amines to give salts of general structure **35c** (CA=chiral auxiliary). Irradiation of crystals of these salts followed by diazomethane workup yielded methyl ester **36d**, which was analyzed by chiral HPLC for enantiomeric excess. The results are summarized in Table 3.



Scheme 7 Photoisomerization of salts of *trans,trans*-2,3-diphenyl-1-benzoyl-cyclopropane-*p*-carboxylic acid

Table 3 Enantiomeric excesses of compound **36d** resulting from irradiation of salts **35c** in the crystalline state followed by diazomethane workup

| Chiral auxiliary | Conversion (%) | Yield (%) ^a | ee (%) ^b |
|---|----------------|------------------------|---------------------|
| 1- <i>p</i> -bromophenylethylamine | 25 | 99 | 99 (+) |
| | 33 | 95 | 96 (+) |
| | 50 | 70 | 92 (+) |
| α,α -diphenyl-2-pyrrolidinemethanol | 25 | 99 | 99 (–) |
| | 38 | 85 | 96 (–) |
| <i>cis</i> -1-amino-2-indanol | 33 | 99 | 91 (+) |
| <i>N</i> -benzyl-1-phenylethylamine | 32 | 99 | 76 (–) |
| 2-amino-1-phenyl-1,3-propanediol | 18 | 99 | 54 (–) |

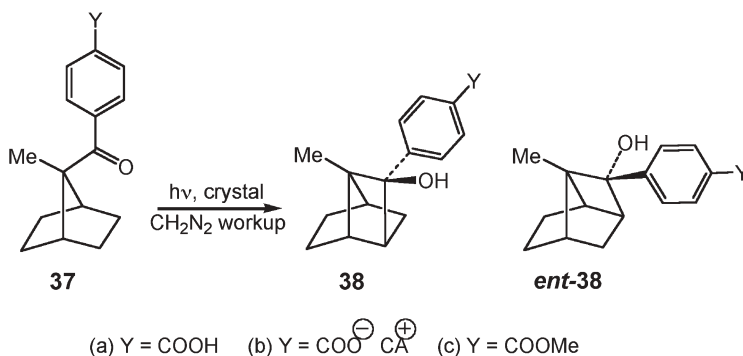
^a Proportion of **36** or *ent*-**36** other than starting material in the converted photoproduct mixture; conversions were kept to $\leq 50\%$ in order to minimize the formation of unidentified side products.

^b The designations (+) and (–) indicate the sign of rotation of the predominant enantiomer at the sodium D line; the absolute configuration was not determined.

Three of the salts gave ee values greater than 90%. There was, however, a slight decrease in ee with increasing conversion, a feature that has been found to be characteristic of asymmetric induction in the solid state, and is presumably due to the generation of lattice defects as the reactants are converted into products. Also typical was the finding that not all ionic chiral auxiliaries gave high ee values. We shall have more to say about this shortly. Finally, a control experiment showed that irradiation of the salts in solution led to racemic **36**. This, too, is typical and highlights the critical importance of carrying out the reactions in the solid state and avoiding conditions that could lead to crystal softening or melting. Unless otherwise mentioned, all the salts discussed in this review gave racemic products when irradiated in solution.

Although direct crystallographic evidence was scanty, the enantioselectivity of the *cis,trans* photoisomerization of salts **35c** in the crystalline state was once again attributed to conformational factors. Earlier theoretical work by Sevin and Chaquin had shown that the preference for photoinduced C1-C2 versus C1-C3 cleavage in cyclopropyl ketones is a function of which bond overlaps better with the p-orbital on the carbonyl carbon [35]. Thus crystallization and immobilization of the reactants in a conformation favoring cleavage of one bond over the other followed by rotation about the C2-C3 bond and reclosure was suggested as the origin of the asymmetric induction in these reactions.

The photochemical reaction that has been most thoroughly investigated from the ionic chiral auxiliary point of view is the well-known Norrish/Yang type II reaction. One example, taken from the work of Patrick, Scheffer, and Scott [36], deals with derivatives of 7-methyl-7-benzoylnorbornane-*p*-carboxylic acid (**37a**, Scheme 8). This compound was treated with a variety of optically pure amines to afford the corresponding 1:1 salts (**37b**), and in an



Scheme 8 Asymmetric induction in the Yang photocyclization reaction.

exceptionally clean reaction, irradiation of these salts in the crystalline state followed by diazomethane workup led to cyclobutanol **38c** as the sole product. Table 4 lists the chiral auxiliaries used and the enantiomeric excess obtained in each case.

The results outlined in Table 4 are remarkable in that the ee values remain high at high conversions. In the case of the (*R*)- and (*S*)-1-phenylethylamine salts, this is due to the fact that the photorearrangement is a single crystal-to-single crystal process, i.e., one in which the photoproduct fits into the crystal lattice of the reactant such that a solid solution of the two components is maintained in all proportions during the transformation. Reactions of this type are highly prized in solid-state chemistry because they allow the reacting crystal to be monitored by X-ray crystallography at the beginning, midpoint, and end of the transformation.

Figure 1 shows the X-ray crystal structure of the (*R*)-(+)-1-phenylethylamine salt of keto-acid **37a** prior to reaction and following 70% conversion to the corresponding cyclobutanol **38b**. The structure of the mixed crystal is

Table 4 Enantiomeric excess of cyclobutanol **38c** resulting from irradiation of crystalline salts **37b**

| Chiral auxiliary | Conversion (%) | ee (%) ^a |
|---|----------------|---------------------|
| (<i>R</i>)-(+)-1-phenylethylamine | 100 | 98 (–) |
| (<i>S</i>)-(–)-1-phenylethylamine | 100 | 97 (+) |
| (1 <i>S</i> ,2 <i>R</i>)-(–)-1-amino-2-indanol | 94 | 96 (+) |
| (1 <i>S</i> ,2 <i>S</i>)-(+)-2-amino-3-methoxy-1-phenyl-1-propanol | 88 | 95 (–) |
| (<i>R</i>)-(–)-2-amino-1-butanol | 100 | 84 (–) |

^a The designations (+) and (–) indicate the sign of rotation of the predominant enantiomer at the sodium D line; the absolute configuration was not determined.

particularly interesting, as it shows the close structural similarity between the reactant and product. This similarity, implying a minimum of atomic and molecular motion during the rearrangement, is presumably the factor responsible for the single crystal-to-single crystal behavior. From Fig. 1, it is apparent that the high ee derives from selective abstraction of the closer γ -hydrogen atom, which is situated 2.60 Å from the carbonyl oxygen, a distance significantly less than the sum of the van der Waals radii for oxygen and hydrogen (2.72 Å). In contrast, the other γ -hydrogen is a relatively distant 3.43 Å from the carbonyl oxygen. Once again, therefore, enantioselectivity originates from preorganization and immobilization of the reactant in a conformation favoring formation of one of two possible enantiomers.

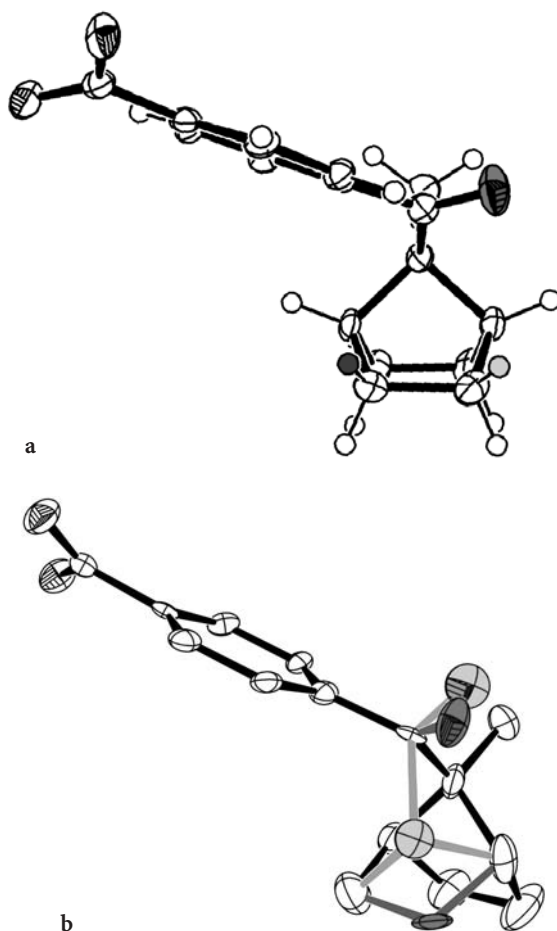
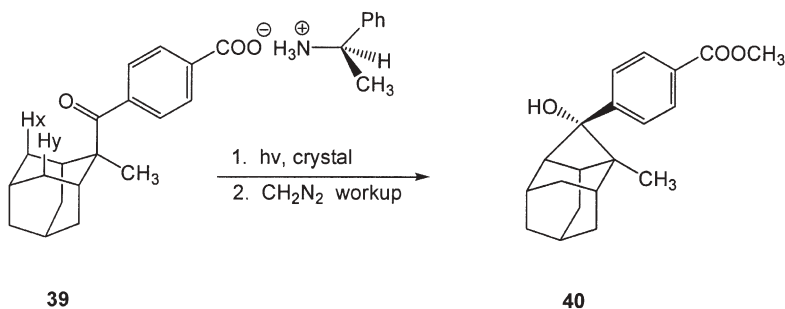


Fig. 1 a Crystal structure of the carboxylate anion portion of the (*R*)-(+)-1-phenylethylamine salt of keto-acid 37a before irradiation, and b after 70% conversion to the corresponding cyclobutanol (ionic chiral auxiliary not shown)

Single crystal-to-single crystal reactions are quite rare in solid-state organic photochemistry, and we were fortunate to discover a second example in the Yang photocyclization of the 1-phenylethylamine salt of 2-methyl-2-benzoyl-*p*-carboxylic acid **39** [37].



When crystals of this salt were irradiated, there was no visible change in the appearance of the crystals, but diazomethane workup of the photolyzed crystals showed that methyl ester **40** had been formed as the sole product with an ee of 82% at 82% conversion. Accordingly, a single crystal of salt **39** was subjected to X-ray diffraction analysis and then irradiated for a sufficient time (2 h) to convert it quantitatively into photoproduct, whereupon a second data set was collected. Both data sets refined successfully in space group $P2_12_12_1$ to final *R* values of 4.6 and 4.9%, thus verifying that the photorearrangement is indeed a single crystal-to-single crystal process. Figure 2 shows the molecular structures of the salts before and after photolysis. The reactant and product have similar shapes and sizes as indicated by a root mean-square error of only 0.53 Å calculated for the overlap of the two structures. This is undoubtedly the reason for the single crystal-to-single crystal nature of the reaction, i.e., the photoproduct fits very well into the lattice site of the reactant.

The X-ray analyses reveal that, as in the case of salt **37b**, enantio- and diastereoselectivity in the solid-state photochemistry of salt **39** are conformationally

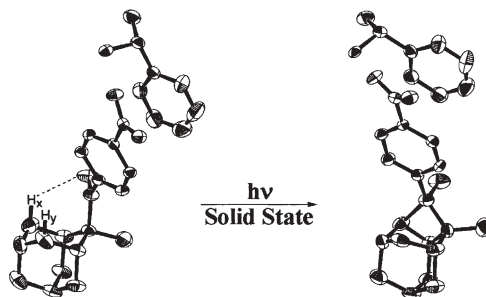
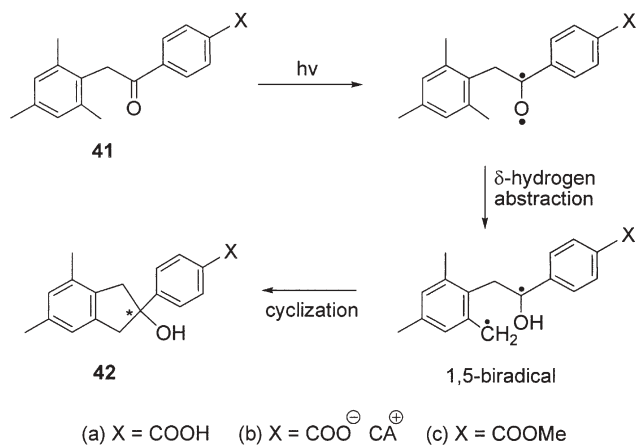


Fig. 2 X-ray crystal structure of salt **39** prior to (*left*) and following (*right*) photolysis in the solid state

determined. Salt **39** crystallizes in a conformation that situates one of the diastereotopic γ -hydrogen atoms (H_X , 2.60 Å) much closer to the ketone oxygen than the other (H_Y , 3.59 Å). Abstraction of H_X forms a 1,4-hydroxybiradical intermediate well suited for least-motion closure (retention) to the observed *endo*-aryl cyclobutanol; formation of the unobserved *exo* diastereomer requires an approximate 180° rotation of the C(OH)Ar group (inversion) prior to closure, a large-amplitude motion that is topochemically forbidden in the crystalline state.

A closely related example involving a seven-membered transition state (δ) hydrogen atom abstraction in the crystalline state is shown in Scheme 9. Based on earlier work by Wagner and coworkers [38], Cheung, Rademacher, Scheffer, and Trotter prepared carboxylic acid **41a** and treated it with a variety of optically pure amines to form chiral salts **41b** [39]. Irradiation of crystalline samples of the salts followed by workup with ethereal diazomethane afforded the chiral in-



Scheme 9 Photocyclization of α -mesitylacetophenone derivatives

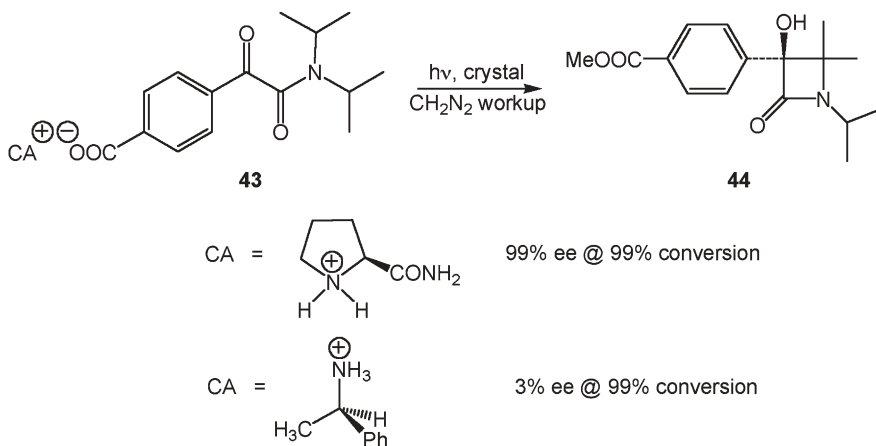
Table 5 Enantioselectivity in the solid-state photolysis of salts **41b**

| Amine | Temp. (°C) | Conv. (%) | ee (%) |
|--------------------------------------|------------|-----------|--------|
| (S)-(-)- α -Methylbenzylamine | rt | 69 | 69 |
| | -20 | 61 | 83 |
| (R)-(+)- α -Methylbenzylamine | rt | 53 | 66 |
| | rt | 18 | 92 |
| | -20 | 74 | 75 |
| (1R,2S)-(-)-Norephedrine | rt | 56 | 82 |
| | -19 | 21 | 95 |
| (1S,2R)-(+)-Norephedrine | rt | 80 | 80 |
| | rt | 12 | 90 |
| | -19 | 30 | 98 |

danol derivative **42c**. The results of enantiomeric excess studies are summarized in Table 5. In several cases ee values of over 90% could be obtained. An increase in conversion led to decreasing ee values owing to the breakdown of the ordered crystal lattice as starting material converts to photoproduct. However, as shown in Table 5, lowering the temperature could be used to compensate this effect to a certain extent. Table 5 also reveals that, as expected for a well-behaved system, either enantiomer of the photoproduct could be prepared as desired by simply using the optical antipode of the ionic chiral auxiliary. This is a general feature of the ionic chiral auxiliary approach to asymmetric synthesis.

The enantioselectivity in these reactions is once again thought to be governed by conformational factors. Salts of general structure **41b** possess two diastereotopic *ortho* methyl groups from which δ -hydrogen abstraction can occur to form the 1,5-biradical intermediate. Crystallographic studies revealed that the salts crystallize in conformations that situate the carbonyl oxygen closer to one methyl group than the other, and assuming that rotations at the biradical stage around the single bonds between the carbonyl group and the mesityl ring are topochemically forbidden in the crystalline state, this accounts for the enantioselectivity observed in the formation of indanol **42c**.

It is important to mention again at this point that a general feature of the solid-state ionic chiral auxiliary approach to asymmetric synthesis is that not all chiral auxiliaries lead to high enantiomeric excesses. A case in point is found in the work of Natarajan et al. on the α -oxoamide-containing salts **43** (Scheme 10) [29]. Like the nonionic α -oxoamides discussed previously (Sect. 2.2), these compounds undergo photocyclization to β -lactam derivatives, and while the prolinamide salt behaves perfectly, leading to β -lactam **44** in 99% ee at 99% conversion, the corresponding 1-phenylethylamine salt affords nearly racemic photoproduct (3% ee at 99% conversion). The reason for this difference is



Scheme 10 Ionic chiral auxiliary-induced asymmetric induction in α -oxoamide photochemistry

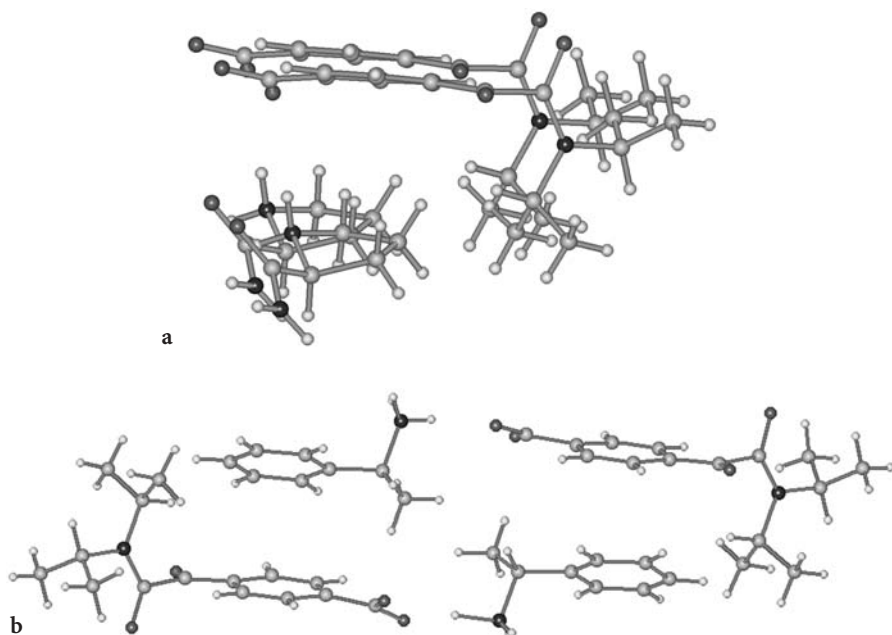
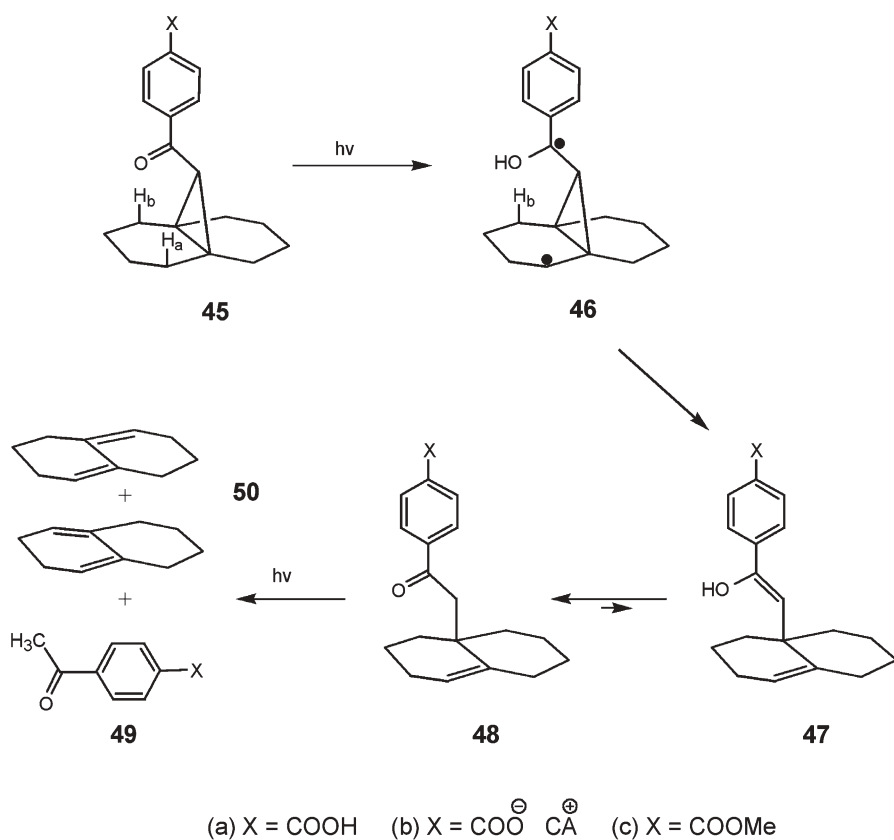


Fig. 3 Prolinamide (a) and 1-phenylethylamine (b) α -oxoamide salts. In the former, the anions are homochiral, while in the latter the anions have a near-mirror-image relationship

apparent from the X-ray crystal structures of the two salts (Fig. 3). In the prolinamide salt (Fig. 3a), which gives high ee, the carboxylate anions crystallize in a uniform, homochiral conformation that leads to a single enantiomer of the photoproduct. In contrast, crystals of the 1-phenylethylamine salt (Fig. 3b) contain equal amounts of two independent carboxylate anion conformers that have a near-mirror-image relationship. As a result half of the anions in the crystal react to give one enantiomer of the photoproduct and the other half lead to its optical antipode, thus accounting for the low ee observed.

Interestingly, the ee in the case of the 1-phenylethylamine salt is not zero, as might be expected if the two independent anions were perfect enantiomers. That they do not have a perfect mirror-image relationship was established by inverting one computationally and superimposing it on the other [29]. When the optically pure chiral auxiliary is taken into consideration, the crystal can be thought of as being composed of a 1:1 mixture of diastereomeric salts that react at slightly different rates, thus giving rise to a small but measurable ee. This mode of crystallization, termed “conformational enantiomerism” [40], may represent an attempt on the part of the crystal to achieve the packing efficiency of a racemic compound. To date, six additional examples of this phenomenon have been identified, including one example in the α -mesitylacetophenone system discussed earlier [38]. In each case, reduced ee values were found when crystals containing conformational enantiomers were irradiated.

Turning now to asymmetric induction in the Norrish-type II cleavage reaction, we note that this process shares the same first step as the Yang photocyclization reactions discussed above, namely γ -hydrogen abstraction to form a 1,4-hydroxy biradical intermediate. In the second step, the C2-C3 bond is cleaved to form an enol (which subsequently ketonizes) along with a $\Delta^{3,4}$ alkene. Chong and Scheffer chose the achiral tricyclo[4.4.1.0]undecane ring system **45** as the target to test for asymmetric induction in this type of reaction (Scheme 11) [41]. Salts of general structure **45b** were prepared by reacting achiral carboxylic acid **45a** with optically pure amines. Irradiation of the salts in the crystalline state caused efficient Norrish-type II cleavage to give chiral olefin **48b**. The enantiomeric excesses of ester **48c** obtained in the solid state following diazomethane workup varied from 63 to 95% as shown in Table 6.



Scheme 11 The ionic chiral auxiliary approach to asymmetric induction in a Norrish-type cleavage reaction

It is interesting to note that although in principle ketone **48** can undergo secondary Norrish type II cleavage to give a mixture of methyl 4-acetylbenzoate

Table 6 Solid-state photolysis of chiral salts **45b**

| Optically pure amine | Conversion (%) ^a | ee (%) ^b |
|---|-----------------------------|---------------------|
| (1 <i>S</i> ,2 <i>S</i>)-(+)-pseudoephedrine | >98 | 95 (+) |
| (<i>R</i>)-(-)-1-cyclohexylethylamine | >98 | 91 (-) |
| (<i>S</i>)-(-)-1- <i>p</i> -tolylethylamine | 75 | 73 (-) |
| (<i>S</i>)-(-)-1-phenylethylamine | >98 | 65 (-) |
| (<i>R</i>)-(+)-1-phenylethylamine | >98 | 63 (+) |
| (<i>R</i>)-(+)-2-phenylpropylamine | >98 | 70 (-) |

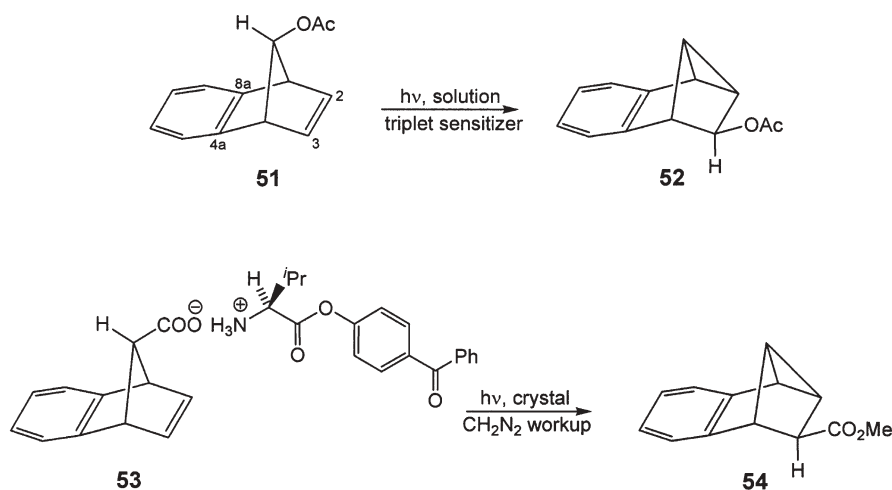
^a Conversion based on NMR.^b Sign of rotation at the sodium D line shown in parentheses; absolute configuration unknown.

(**49**) and hexahydronaphthalenes **50**, only traces of these photoproducts were formed in the crystalline state. The reason is that in the solid state enol **47** ketonizes very slowly to compound **48**. This was demonstrated experimentally by photolyzing crystals of keto-ester **45c** and showing that enol **47c** could be detected by FTIR from the disappearance of the ketone stretch at 1666 cm⁻¹ and the appearance of the OH stretch at 3400 cm⁻¹. Based on its IR spectrum, the enol persisted for days in the solid state at room temperature under nitrogen. In solution, on the other hand, where ketonization of enol **47c** is rapid, irradiation of keto-ester **45c** leads predominantly to cleavage products **49** and **50**.

The successful asymmetric induction in these reactions can once again be explained by a conformational effect. Although direct X-ray crystallographic evidence is lacking in this case, molecular mechanics calculations indicate that the minimum energy conformation of ketones of general structure **45** is one in which the carbonyl oxygen is much closer to H_a (2.5 Å) than H_b (3.3 Å). Because organic compounds generally crystallize in or near their minimum energy conformations, the observed stereoselectivity can be attributed to preferential abstraction of the more favorably located diastereotopic γ-hydrogen atom in the initial step of the photoreaction. This appears to be a general feature of Norrish/Yang type II reactions that give high ee values in the crystalline state.

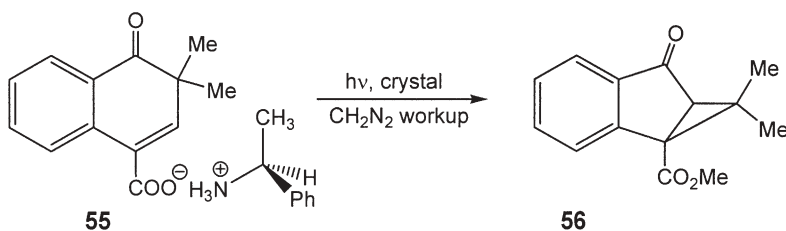
To this point, all the examples presented have been ones in which the origin of the asymmetric induction has been unimolecular in nature, that is, the molecules adopt homochiral conformations in the solid state that favor the formation of one enantiomer over the other, usually through the close intramolecular approach of reactive centers; bimolecular crystal packing effects appear to play little or no role in governing the stereochemical outcome of such reactions. This raises the interesting question of whether the solid-state ionic chiral auxiliary approach to asymmetric synthesis could be made to work for conformationally unbiased reactants, i.e., those possessing symmetrical, conformationally locked structures. Two such cases are presented and discussed below.

The first of these concerns the solid-state photochemistry of symmetrical benzonorbornadiene derivatives. Extensive studies in solution have shown that such compounds undergo triplet-sensitized di- π -methane photorearrangement to chiral, tetracyclic products, an example being the **51** to **52** conversion shown in Scheme 12 [42]. The configuration of the photoproduct in such transformations is governed by the direction of initial benzo-vinyl bridging, i.e., C2-C8a versus C3-C4a. Given the rigidity of the benzonorbornadiene framework, there can be no conformational bias favoring one of these pathways over the other. To test asymmetric induction in this type of system, salt **53** was prepared and irradiated in the crystalline state [43]. A notable feature of this salt is that the ionic chiral auxiliary contains a benzophenone unit, which acts as a triplet energy sensitizer for the reaction. This represents the first use of a chiral sensitizer in a solid-state photoreaction. In the event, photolysis of crystals of salt **53** at -20°C followed by the usual diazomethane workup afforded ester **54** in a gratifying 92% ee at 100% conversion. Because crystals of salt **53** were not suitable for X-ray diffraction, the exact nature of the structural factors responsible for asymmetric induction could not be determined.



Scheme 12 Benzonorbornadiene photochemistry

The second salt studied for which conformational bias in the enantiodifferentiating step was expected to be small was the benzocyclohexadienone derivative **55**. Compounds of this type are known to undergo what is formally an oxadi- π -methane photorearrangement [44], and salt **55** was no exception, affording cyclopropyl ketone **56** upon irradiation in the crystalline state and diazomethane workup [45]. The ee in which this photoproduct was formed at room temperature was 81% at 25% conversion and 71% at 80% conversion. As usual, lowering the temperature raised the ee (at -78°C , the ee was 87% at 30%



conversion), but the reaction was significantly slower. Five other ionic chiral auxiliaries chosen at random failed to give ee values above 50%, even at reduced temperatures.

Crystals of salt **55** were once again unsuitable for X-ray diffraction studies, but molecular mechanics calculations on the corresponding methyl ester showed that the benzocyclohexadiene framework is essentially planar. As a result, it is unlikely that conformational factors play a significant role in determining the absolute stereochemistry of this reaction. The last two examples (salts **53** and **55**) demonstrate that crystal packing can serve as the controlling stereochemical factor in the ionic chiral auxiliary approach to asymmetric synthesis. Such effects are undoubtedly present in conformationally biased systems as well, and it is interesting to speculate that another source of low ee values in these cases (other than conformational enantiomerism) may be that conformational factors favor one enantiomer while crystal packing effects favor the other. In the happy situation in which both effects operate in the same direction, high ee values are observed.

1.4.3

Comparison of the Solid-State Ionic Chiral Auxiliary Method of Asymmetric Synthesis with the Pasteur Resolution Procedure

In principle, any of the compounds synthesized by using the solid-state ionic chiral auxiliary approach could also have been prepared in enantiomerically enriched form by irradiating their achiral precursors in solution to form a racemic mixture and then resolving them by using the classical Pasteur resolution procedure [46]. This sequence is shown in the lower half of Fig. 4. The top half of Fig. 4 depicts the steps involved in the solid-state ionic chiral auxiliary method. The difference between the two approaches is one of timing. In the ionic chiral auxiliary procedure, the photochemical step comes after salt formation between the achiral reactant and an optically pure amine, while in the Pasteur procedure, the photochemical step comes first and is followed by treatment of the resulting racemic mixture with an optically pure amine. Both methods, however, rely on the crystalline state for their success; Pasteur resolution uses fractional crystallization to separate the diastereomeric salts, and the ionic chiral auxiliary method gives good ee values only in the crystalline state.

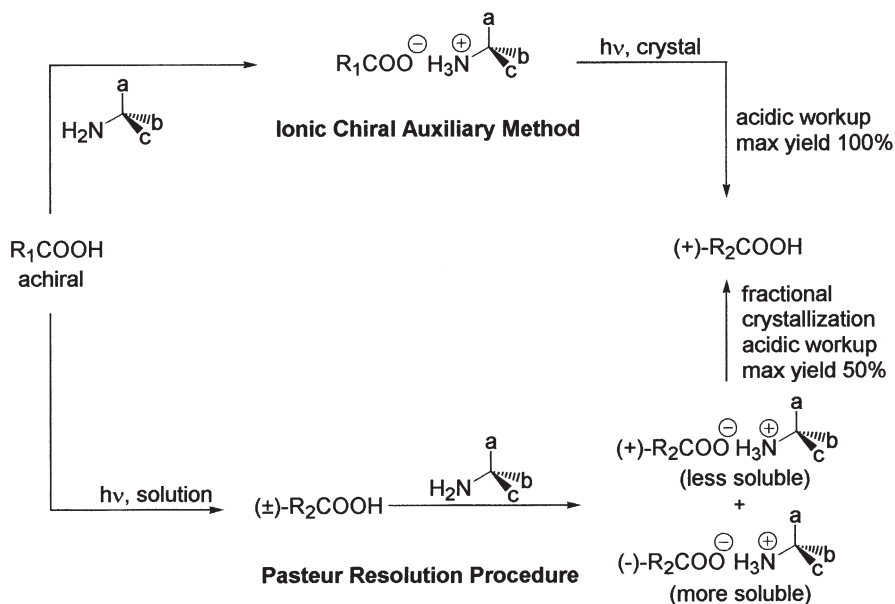


Fig. 4 Comparison of the solid-state ionic chiral auxiliary method of asymmetric synthesis with the Pasteur resolution procedure

Like other methods of asymmetric synthesis, the solid-state ionic chiral auxiliary procedure has an advantage over Pasteur resolution in terms of chemical yield. The maximum amount of either enantiomer that can be obtained by resolution of a racemic mixture is 50%, and in practice the yield is often considerably less [47]. In contrast, the ionic chiral auxiliary approach affords a single enantiomer of the product, often in chemical and optical yields of well over 90%. Furthermore, either enantiomer can be obtained as desired by simply using one optical antipode or the other of the ionic chiral auxiliary.

The success of the solid-state ionic chiral auxiliary approach to asymmetric synthesis can be analyzed both thermodynamically and kinetically. We have seen that conformationally flexible reactants that have average planes of symmetry in solution crystallize in chiral conformations upon salt formation with optically pure amines. This thermodynamic aspect of the process biases the ensuing photochemistry toward a single diastereomer of the salt by, for example, favoring abstraction of one of two diastereotopic γ -hydrogen atoms (γ -hydrogens that were enantiotopic prior to salt formation). On the other hand, in the case of conformationally inflexible reactants (e.g., salts 53 and 55), conformational bias introduced at the crystallization stage does not play a significant role in determining which enantiomer of the photoproduct will be formed following removal of the chiral auxiliary. In such cases, the preference for formation of one diastereomeric salt over the other is best viewed as a kinetic discrimination between diastereomeric transition states whose energies differ as a

result of unequal steric interactions between the reactant and its lattice neighbors [48].

This completes our brief survey of the use of ionic chiral auxiliaries in solid-state photochemical asymmetric synthesis. As in previous sections of this review, our aim has been to set forth the principles of the method with a few well-chosen examples rather than provide comprehensive coverage. The procedure has been successfully applied to a wide variety of photorearrangement reactions, a summary of which and further details can be found in two recent review articles [28]. We close with a short discussion of the advantages and disadvantages of the method in the wider context of asymmetric synthesis. A significant disadvantage is that only compounds possessing acidic or basic functional groups can be investigated, since these are required for attachment of the ionic chiral auxiliaries. It may be possible in the future to expand the scope of the method by designing chiral auxiliaries that can be attached to complementary functional groups on the photoreactants via well-established hydrogen bonding motifs. Another limitation, common to all asymmetric induction methods involving crystals, is the requirement for the reactant to crystallize in a reactive conformation. The Norrish type II photochemistry of acyclic aralkyl ketones, for example, cannot be investigated in the solid state because such compounds crystallize in extended conformations in which the γ -hydrogen is far removed from the oxygen atom of the carbonyl group. Fortunately, because most conformationally flexible molecules crystallize in or near their lowest energy conformations, molecular mechanics calculations give a good indication of the conformation to be found in the solid state.

On the positive side, the ionic nature of the salts guarantees crystallinity with high melting points, which, as pointed out earlier, allows higher conversions without melting. Other advantages of the ionic chiral auxiliary method include ease of introduction and removal of the chiral auxiliary and the availability of a wide variety of chiral auxiliaries, many of which are derived from the optically pure amines and carboxylic acids provided by the chiral pool. On balance, there can be little doubt that the solid-state ionic chiral auxiliary method is among the most general and useful methods of asymmetric synthesis in organic photochemistry.

Acknowledgements Financial support by the Natural Sciences and Engineering Research Council of Canada (NSERC) is gratefully acknowledged. Acknowledgment is also made to the donors of the Petroleum Research Fund, administered by the American Chemical Society, for partial support of this research.

References

1. (a) Ramamurthy V (ed) (1991) *Photochemistry in organized and constrained media*. VCH, New York; (b) Ramamurthy V, Schanze KS (eds) (2000) *Molecular and supramolecular photochemistry*, vol 5. Marcel Dekker, New York
2. (a) Everitt SRL, Inoue Y (1999) In: Ramamurthy V, Schanze KS (eds) *Molecular and supramolecular photochemistry*, vol 3. Marcel Dekker, New York, p 71; (b) Pete JP (1996)

- Adv Photochem 21:135; (c) Inoue Y (1992) Chem Rev 92:471; (d) Buschmann H, Scharf HD, Hoffmann N, Esser P (1991) Angew Chem Int Ed Engl 30:477; (e) Rau H (1983) Chem Rev 83:535
3. Grosch B, Bach T (2004) In: Horspool W, Lenci F (eds) CRC handbook of organic photochemistry and photobiology, 2nd edn. CRC, Boca Raton, chap 61
 4. Mori T, Inoue Y (2004) In: Horspool W, Lenci F (eds) CRC handbook of organic photochemistry and photobiology, 2nd edn. CRC, Boca Raton, chap 16
 5. Caswell L, Garcia-Garibay M, Scheffer JR, Trotter J (1993) J Chem Ed 70:785
 6. Jacques J, Collet A, Wilen SH (1981) Enantiomers, racemates and resolutions. Wiley, New York
 7. Penzien K, Schmidt GMJ (1969) Angew Chem Int Ed Engl 8:608
 8. Green BS, Rabinovich D, Shakked Z (1981) Acta Crystallogr B 37:1376
 9. Green BS, Lahav M, Rabinovich D (1979) Acc Chem Res 12:191
 10. Elgavi A, Green BS, Schmidt GMJ (1973) J Am Chem Soc 95:2058
 11. (a) Hasegawa M, Chung CM, Murro N, Maekawa Y (1990) J Am Chem Soc 112:5676; (b) Chung CM, Hasegawa M (1991) J Am Chem Soc 113:7311
 12. Evans SV, Garcia-Garibay M, Omkaram N, Scheffer JR, Trotter J, Wireko F (1986) J Am Chem Soc 108:5648
 13. Garcia-Garibay M, Scheffer JR, Trotter J, Wireko F (1989) J Am Chem Soc 111:4985
 14. Reviews: (a) Sakamoto M (1997) Chem Eur J 3:684; (b) Sakamoto M (2004) In: Inoue Y, Ramamurthy V (eds) Chiral photochemistry. Marcel Dekker, New York, chap 11 (in press)
 15. Toda F, Tanaka K, Miyamoto H (2001) In: Ramamurthy V, Schanze KS (eds) Molecular and supramolecular photochemistry, vol 8. Marcel Dekker, New York, chap 6
 16. Tanaka K, Toda F (2002) In: Toda F (ed) Organic solid-state reactions. Kluwer, p 109
 17. (a) Toda F, Tanaka K (1986) J Chem Soc Chem Commun 1429; (b) Toda F, Tanaka K, Yagi M (1987) Tetrahedron 43:1493
 18. Kaftory M, Yagi M, Tanaka K, Toda F (1988) J Org Chem 53:4391
 19. Toda F, Tanaka K, Omata T, Nakamura K, Oshima T (1983) J Am Chem Soc 105:5151
 20. Toda F, Miyamoto H, Matsukawa R (1992) J Chem Soc Perkin Trans I 1461
 21. Hashizume D, Uekusa H, Ohashi Y, Matsugawa R, Miyamoto H, Toda F (1994) Bull Chem Soc Jpn 67:985
 22. Toda F, Miyamoto H, Kikuchi S (1995) J Chem Soc Chem Commun 621
 23. (a) Joy A, Ramamurthy V (2000) Chem Eur J 6:1287; (b) Sivaguru J, Natarajan A, Kaanumalle LS, Shailaja J, Uppili S, Joy A, Ramamurthy V (2003) Acc Chem Res 36:509
 24. Breck DW (1974) Zeolite molecular sieves: structure, chemistry and use. Wiley, New York
 25. Joy A, Scheffer JR, Ramamurthy V (2000) Org Lett 2:119
 26. Kaanumalle L, Sivaguru J, Arunkumar N, Karthikeyan S, Ramamurthy V (2003) Chem Commun 116
 27. Joy A, Uppili S, Netherton MR, Scheffer JR, Ramamurthy V (2000) J Am Chem Soc 122:728
 28. Reviews: (a) Scheffer JR (2001) Can J Chem 79:349; (b) Scheffer JR (2004) In: Inoue Y, Ramamurthy V (eds) Chiral photochemistry. Marcel Dekker, New York, chap 12 (in press)
 29. Natarajan A, Wang K, Ramamurthy V, Scheffer JR, Patrick B (2002) Org Lett 4:1443
 30. Chesta CA, Whitten DG (1992) J Am Chem Soc 114:2188. Studies favoring a mechanism involving direct hydrogen atom transfer to form the 1,4-hydroxybiradical intermediate have recently been reported by Wang R, Chen C, Duesler E, Mariano PS (2004) J Am Chem Soc 126:1215
 31. Gudmundsdottir AD, Scheffer JR (1990) Tetrahedron Lett 31:6807
 32. Gudmundsdottir AD, Scheffer JR, Trotter J (1994) Tetrahedron Lett 35:1397

33. Chong KCW, Sivaguru J, Shichi T, Yoshimi Y, Ramamurthy V, Scheffer JR (2002) *J Am Chem Soc* 124:2858
34. Zimmerman HE, Flechtner TW (1970) *J Am Chem Soc* 92:6931
35. Sevin A, Chaquin P (1982) *J Org Chem* 90:4145
36. Patrick BO, Scheffer JR, Scott C (2003) *Angew Chem* 42:3775
37. Leibovitch M, Olovsson G, Scheffer JR, Trotter J (1998) *J Am Chem Soc* 120:12755
38. Wagner PJ, Meador MA, Zhou B, Park BS (1991) *J Am Chem Soc* 113:9630
39. Cheung E, Rademacher K, Scheffer JR, Trotter J (2000) *Tetrahedron* 56:6739
40. Cheung E, Kang T, Netherton MR, Scheffer JR, Trotter J (2000) *J Am Chem Soc* 122:11753
41. Chong KCW, Scheffer JR (2003) *J Am Chem Soc* 125:4040
42. Tufariello JJ, Rowe DW (1971) *J Org Chem* 36:2057
43. Janz KM, Scheffer JR (1999) *Tetrahedron Lett* 40:8725
44. Schultz AG (1995) In: Horspool W, Song PS (eds) *CRC handbook of organic photochemistry and photobiology*, 1st edn. CRC, Boca Raton, chap 58
45. Cheung E, Netherton MR, Scheffer JR, Trotter J (1999) *Tetrahedron Lett* 40:8737
46. Pasteur L (1853) *CR Acad Sci* 37:162
47. Eliel EL, Wilen SH (1994) In: *Stereochemistry of organic compounds*. Wiley, New York, chap 7
48. Cheung E, Netherton MR, Scheffer JR, Trotter J (1999) *J Am Chem Soc* 121:2919

Reactions of 1,3-Diene Compounds in the Crystalline State

Akikazu Matsumoto (✉)

Department of Applied Chemistry, Graduate School of Engineering, Osaka City University,
Sugimoto, Sumiyoshi-ku, Osaka 558-8585, Japan
matsumoto@a-chem.eng.osaka-cu.ac.jp

| | | |
|-----|---|-----|
| 1 | Introduction | 264 |
| 2 | Photodimerization | 265 |
| 2.1 | Crystal Engineering Renaissance | 265 |
| 2.2 | Photodimerization of 1,3-Diene Compounds | 268 |
| 3 | Topochemical Polymerization | 272 |
| 3.1 | Features and Mechanism of Polymerization of 1,3-Diene Compounds | 272 |
| 3.2 | The 5 Å Rule as the Polymerization Principle | 279 |
| 3.3 | Topochemical Polymerization of Other Monomers | 284 |
| 3.4 | Stacking Control in the Crystals | 286 |
| 3.5 | Hydrogen Bond Network | 287 |
| 3.6 | Halogen–Halogen Interactions | 289 |
| 3.7 | CH/π Interactions | 291 |
| 3.8 | Supramolecular Control of Stereochemistry of Polymers | 292 |
| 4 | Photoisomerization | 297 |
| 4.1 | One-Way <i>EZ</i> Photoisomerization of 1,3-Diene Compounds | 297 |
| 4.2 | Mechanism of <i>EZ</i> Isomerization in Constrained Media | 299 |
| 5 | Conclusions | 302 |
| | References | 302 |

Abstract Stereospecific polymerization and *EZ* isomerization as well as classic [2+2] cyclo-dimerization are observed during the photoreaction of 1,3-diene compounds in the solid state. In this article, the features and mechanism are described for the solid-state photo-reactions of 1,3-diene compounds including the ester, ammonium, and amide derivatives of muconic and sorbic acids as well as several other 1,3-diene compounds. Recently, comprehensive studies on the topochemical polymerization of 1,3-diene compounds have been carried out to reveal the solid-state reaction mechanism of the polymerization and the structure and properties of the resulting polymer crystals. The polymerization proceeds when the monomer molecules are stacked with an appropriate stacking distance in the crystals, to provide stereoregular polymers with a 1,4-*trans* repeating structure. Topochemical polymerization principles and the design of organic crystals for controlling solid-state polymerization of 1,3-diene compounds are discussed on the basis of the crystallographic data. Supramolecular architecture enables us to control the stereochemistry as well as the other

chain structures of diene polymers. One-way *EZ* isomerization of 1,3-diene compounds in constrained media is also described.

Keywords Crystal engineering · Solid-state photoreaction · Topochemical polymerization · Controlled radical polymerization · Dimerization · Isomerization · Topotactic reaction

1

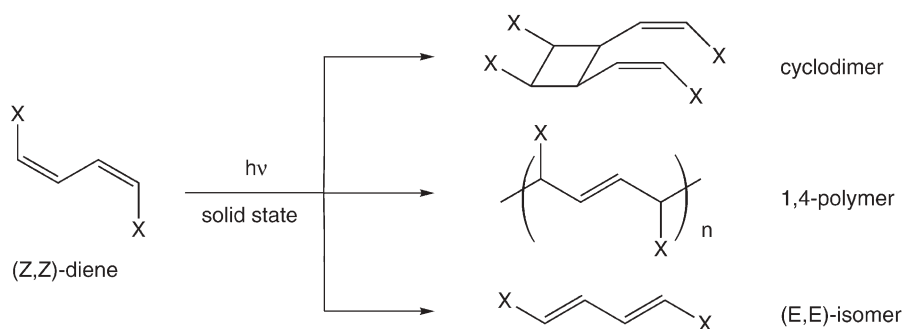
Introduction

Chemical reactions in the solid state have intrinsic features different from those for reactions performed in solution or in the gaseous state. For example, solid-state organic reactions often provide a high regio- or stereoselectivity because the reactions and the structure of a product are determined by the crystal structure of the reactant, i.e., the reaction proceeds under crystalline lattice control [1–8]. When the reactant molecules are themselves crystalline (molecular crystals) or are included in host crystals (inclusion compounds), the rate and selectivity of the reaction are different from those obtained in an isotropic reaction medium.

Topochemical reactions promise to yield products with highly controlled structures, but few successful polymerizations via a topochemical process have been reported [9, 10]. In the late 1960s, two typical examples of topochemical polymerization were discovered: stepwise [2+2] photopolymerization of 2,5-styrylpyradine and its analogous diolefins [11] and thermal or radiation polymerization of diacetylenic derivatives [12]. Thirty years later, Matsumoto et al. discovered the topochemical polymerization of various kinds of conjugated 1,3-diene monomers giving a highly stereoregular polymer in the form of polymer crystals [13, 14]. When a (*Z,Z*)-muconic ester was photoirradiated in the crystalline state, a *meso*-diisotactic 2,5-*trans* (tritactic) polymer was produced, in contrast to the formation of an atactic polymer by conventional radical polymerization in an isotropic state. Thereafter, comprehensive investigation has been carried out for the design of monomers, the crystal structure analysis of monomers and polymers, and polymerization reactivity control, in order to reveal the entire features of the topochemical polymerization of 1,3-diene monomers [15, 16].

Solid-state photoreaction pathways are dependent on the structure of 1,3-diene compounds as the reactant (i.e., molecular packing in the crystals); cyclodimer, 1,4-polymer, or *EE* isomer is produced depending on the structure of the substituent X and the molecular packing in the crystals, as shown in Scheme 1 and Table 1. Here, the stereochemical structure of the products is highly regulated during the photoreactions in the crystalline state.

In this article, the features and mechanism of the crystal-to-crystal reactions of 1,3-diene compounds are described on the basis of the molecular packing structure and intermolecular interactions in the crystals for starting materials and products. The dimerization and isomerization of unsaturated compounds as well as addition polymerization via a chain reaction mechanism are ideal solid-state reactions, because they produce no leaving group during the reac-



Scheme 1 Possible pathways for the solid-state photoreactions of (Z,Z)-diene compounds

Table 1 Stereospecific solid-state photoreaction of (Z,Z)-muconic acid derivatives depending on the structure of alkyl substituents^a

| R | X=CO ₂ R | X=CONHR | X=CO ₂ ⁻ +H ₃ NR |
|-----------------|---------------------|----------------|---|
| H | Cyclodimerization | – | – |
| Methyl | Isomerization | – | No reaction |
| Ethyl | Polymerization | No reaction | Isomerization |
| <i>n</i> -Butyl | No reaction | Isomerization | Isomerization |
| Decyl | Isomerization | Isomerization | Polymerization |
| Dodecyl | Isomerization | Polymerization | Polymerization |
| Isopropyl | No reaction | Isomerization | Isomerization |
| Cyclohexyl | Isomerization | No reaction | Isomerization |
| Benzyl | Isomerization | No reaction | Polymerization |

^a See Scheme 1 for the chemical structure of substrates and photoproducts. The photoirradiation was carried out with a high-pressure mercury lamp at room temperature.

tion, and can be carried out in a quantitative yield with a minimum movement of the groups and atoms in the crystals. The solid-state reactions of 1,3-diene compounds provide us with much information regarding the crystal engineering and solid-state organic chemistry.

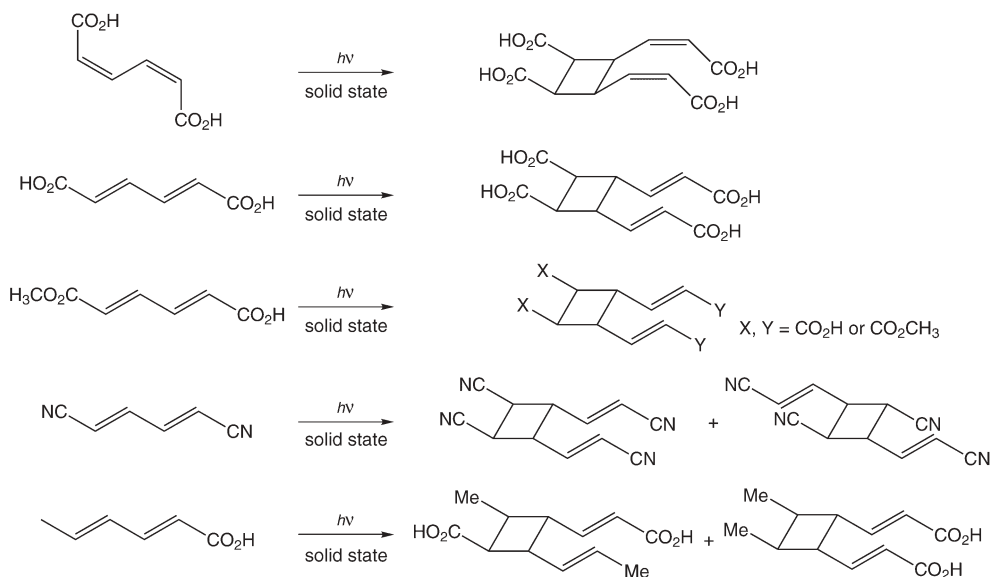
2 Photodimerization

2.1 Crystal Engineering Renaissance

The first recognition of the importance of solid-state organic reactions dates back to the 1960s–1970s. The crystallographic investigation of topologically controlled chemical reactions started during the early 1960s [17], and the

concept of crystal engineering was already established in 1971 [9, 18]. The first studies on topochemistry, pioneered and brilliantly exploited by Schmidt and coworkers, were focused on the photoreactions of cinnamic acid crystals as crystalline-lattice-controlled reactions.

[2+2] Photodimerization is one of the most typical and classic organic solid-state reactions. Continuous and numerous studies have been carried out, supported by advanced molecular design using crystal engineering and by progress in experimental apparatus and circumstance. In the early works of topochemistry, Schmidt et al. pointed out that [2+2] photodimerization proceeds not only for olefins such as cinnamic derivatives but also for some 1,3-diene compounds. They reported the formation of a *syn*-type cycloproduct by the photoreaction of (*Z,Z*)- or (*E,E*)-muconic acids in the crystals (Scheme 2) [19]. Similar reactions also proceeded for the monomethyl ester and the nitrile derivative of (*E,E*)-muconic acid, or (*E,E*)-sorbic acid and its amide derivative, but the structure of the product was more complicated, depending on the molecular stacking fashion in the crystals [20]. The derivatives of 5-phenylpentadienoic acid provide a single stereo- and regioisomer, but with different starting compounds leading to the formation of different types of cyclodimers as the products [20].



Scheme 2 Solid-state photoreactions of some muconic and sorbic derivatives reported in 1967 and 1971 [19, 20]

In a series of papers published in the 1960s by Schmidt and coworkers, there is no description of any successful and stereospecific reaction of 1,3-diene compounds, e.g., topochemical polymerization, other than cyclodimerization. They

analyzed the crystal structure of the reactant and the chemical structure of the product to discuss the topochemical rules for the reactions (the Schmidt rule) [9]. After the discovery of the topochemical polymerization of diacetylenes and diolefins in the 1960s, many researchers devoted themselves to studies on the solid-state polymerization of vinyl and diene monomers, only to later conclude that the topochemical polymerization of vinyl and diene monomers is impossible. Schmidt and coworkers reported that some 1,3-diene carboxylic acids and their ester, amide, and nitrile derivatives provided a stereospecific cyclobutane as the [2+2] cycloaddition product under crystal lattice control, but they found no successful example for the topochemical polymerization of 1,3-diene compounds.

Later, Tieke reported the UV- and γ -irradiation polymerization of butadiene derivatives crystallized in perovskite-type layer structures [21, 22]. He reported the solid-state polymerization of butadienes containing aminomethyl groups as pendant substituents that form layered perovskite halide salts to yield *erythro*-diisotactic 1,4-*trans* polymers. Interestingly, Tieke and his coworker determined the crystal structure of the polymerized compounds of some derivatives by X-ray diffraction [23, 24]. From comparative X-ray studies of monomeric and polymeric crystals, a contraction of the lattice constant parallel to the polymer chain direction by approximately 8% is evident. Both the carboxylic acid and aminomethyl substituent groups are in an isotactic arrangement, resulting in diisotactic polymer chains. He also referred to the γ -radiation polymerization of molecular crystals of the sorbic acid derivatives with a long alkyl chain as the N-substituent [25]. More recently, Schlitter and Beck reported the solid-state polymerization of lithium sorbate [26]. However, the details of topochemical polymerization of 1,3-diene monomers were not revealed until very recently.

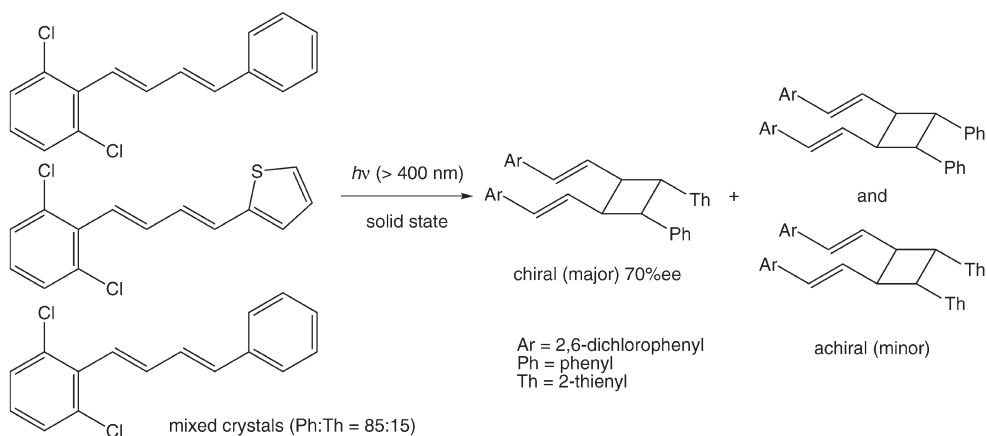
Since the 1990s, the crystal engineering approach has changed and renewed as a strategy for the rational design of organic solid architecture utilizing supramolecular chemistry [18, 27–31]. Furthermore, during the last decade, studies on organic solid-state reactions and crystal structure analysis have been accelerated by the development of methods and apparatus for static and dynamic crystal structure analyses using a two-dimensional detector such as an imaging plate or a CCD camera, as well as by striking improvements in both hardware and software for computation. Now, we face a new stage of studies on solid-state organic chemistry and crystal engineering, there being a world of difference in the study conditions between the old days in the 1960s to 1970s and the present day. A new approach may give new insight even into the same target molecules and reactions. Furthermore, in recent years, the concept of green sustainable chemistry and approaches to environmentally benign organic synthesis have accelerated progress in the research of solid-state organic chemistry [32, 33]. A solvent-free process for organic synthesis, including solid-state reactions of unsaturated compounds, will inevitably become more important in the environmental aspects of chemistry in the future. Namely, we can consider the present as the Renaissance period of crystal engineering.

2.2

Photodimerization of 1,3-Diene Compounds

Since the work of Schmidt, many chemists have designed [2+2] photodimerizations of olefins to control solid-state reactivity by molecular design [6] or using host–guest inclusion crystals [32], mixed crystals [34, 35], and linear templates [36]. Molecular design includes the introduction of appropriate functional groups or atoms [37–39], which interact with each other to make a desired molecular assembly in the crystals. For example, Cl–Cl, donor–acceptor, and phenyl–perfluorophenyl interactions or hydrogen bonds are used to control the organization of reacting olefins. Another approach is the method using an auxiliary component in the form of a molecule or cavity, as is seen in inclusion crystals [40] or templates [41].

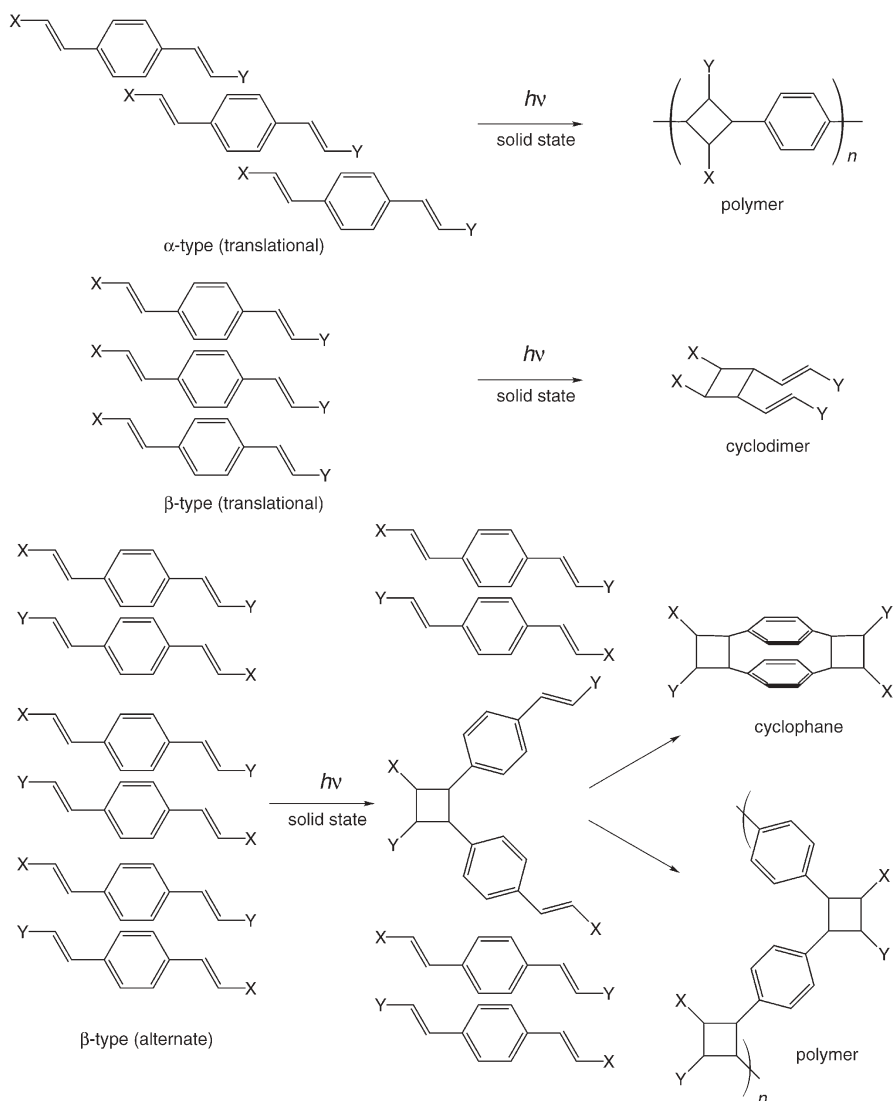
The photodimerization of 1,3-diene compounds is well known as the most typical example for controlling the asymmetric structure of the heterocyclo-dimer as the photoproduct [42]. 1-(2,6-Dichlorophenyl)-4-phenyl-(*E,E*)-butadiene and the 4-thienyl analogue (Scheme 3) crystallize in an isostructural arrangement in the same space group ($P2_12_12_1$). They form mixed crystals (solid solutions) when cooled from the melt or solution of both components. Photoirradiation resulted in a mixture of enantiomeric heterodimers and achiral homodimers of each component. Selective excitation of the thiophene moieties, which absorb light at a longer wavelength, led to a reduction in the formation of achiral homodimers and reached a high optical yield with an enantiomeric excess of approximately 70%.



Scheme 3 Asymmetric [2+2] photodimerization of 1,3-butadiene derivatives in the mixed crystals [42]

Hasegawa et al. established the four-center-type photopolymerization of diolefin crystals, in which diolefin molecules are superimposed in the direction of the long molecular axes displaced by about half a molecule, as shown in

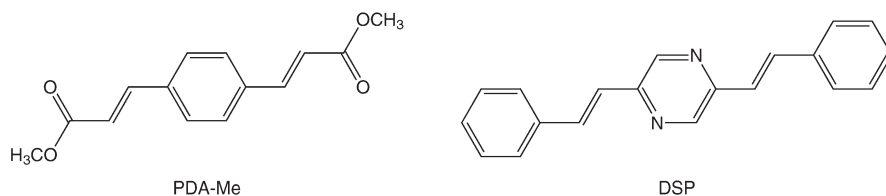
α -type crystal packing in Scheme 4, or arranged without displacement as shown in β -type crystal packing [11]. The former crystals often provide a linear high molecular weight polymer in nearly quantitative yield, and the latter generally result in dimer formation. In the plane-to-plane stack of diolefin crystals with β -type packing, two molecules sometimes make a pair separated from another pair. Some compounds can provide cyclophane derivatives through cycloaddition between the olefin moieties of two molecules [43]. There is a possibility



Scheme 4 Stacking of diolefin compounds and the formation of cyclobutane, cyclophane, and polymers as the photoproducts

of the formation of zigzag-type polymer through V-shaped dimer formation, but only a few cases have been reported. In the crystals of 1,4-dicinnamoylbenzene, both reaction pathways may occur competitively at the initial stage of reaction [11].

In general, when diolefin derivatives polymerize successively by [2+2] cycloaddition, their bulk crystals become polycrystals, even when started from a monomer single crystal, because of the accumulation of strains during the polymerization [44, 45]. Recently, the polymerization behavior of two kinds of derivatives as typical diolefin compounds was investigated again in both bulk crystals and nanocrystals, and the characteristics of diolefin nanocrystals were explored [46]. Nanocrystals of PDA-Me and DSP were prepared by the reprecipitation



method as follows: 200 μL of a diolefin tetrahydrofuran solution (5.0 mmol/L) was injected using a microsyringe into 10 mL of pure water and stirred vigorously [47]. Immediately their nanocrystals were produced in an aqueous medium.

The morphology of the nanocrystals was observed before and after UV irradiation using SEM. Interestingly, the shape of PDA-Me nanocrystals, which were platelike and about 500 nm a side, and of DSP nanocrystals, which were rod-shaped and of length from 150 nm to about 400 nm, were almost the same as those of the corresponding monomers and no cracks were recognized, while a PDA-Me bulk crystal is broken into fragments during polymerization. Solid-state photopolymerization of these nanocrystals in water was confirmed by UV-visible and IR spectra. All these data support quantitative conversion of monomers to the corresponding polymers. Strain accumulated in the nanocrystals can be easily released by deforming the crystal shape. Actually, the larger interior angle of developed parallelogram surfaces of PDA-Me monomer nanocrystals seems to become smaller in the polymer nanocrystals. This change is possibly related to a change in the lattice parameter. Thus, the nanocrystals of two diolefin derivatives were successfully prepared, and these nanocrystals were found to transform from a monomer single crystal to a polymer single crystal.

Very recently, MacGillivray et al. succeeded in the supramolecular construction of molecular ladders in the solid state using a linear template approach [48]. They designed the cocrystals 1,3-benzenediol (resorcinol) or a derivative with an all-*trans*-bis(4-pyridyl)butadiene or hexatriene, in which two resorcinol molecules preorganize two polyene molecules through two hydrogen bond interactions, for [2+2] photoaddition (Scheme 5). In this design, two polyenes would



be positioned by the templates such that the carbon-to-carbon double bonds lie parallel and separated by $<4.2 \text{ \AA}$, a position suitable for the photoreaction leading to the production of the targeted ladderane with the fused cyclobutane framework. The remarkable efficiency of this intermolecular process is exemplified by the fact that the polyenes are converted to the ladderanes stereospecifically, in gram quantities, and in 100% yield.

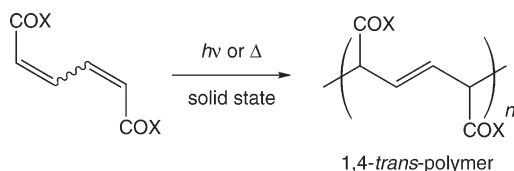
3

Topochemical Polymerization

3.1

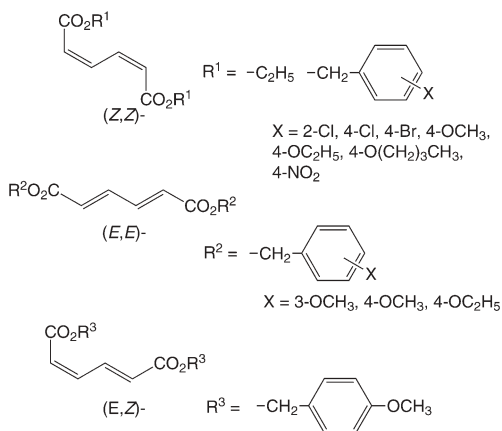
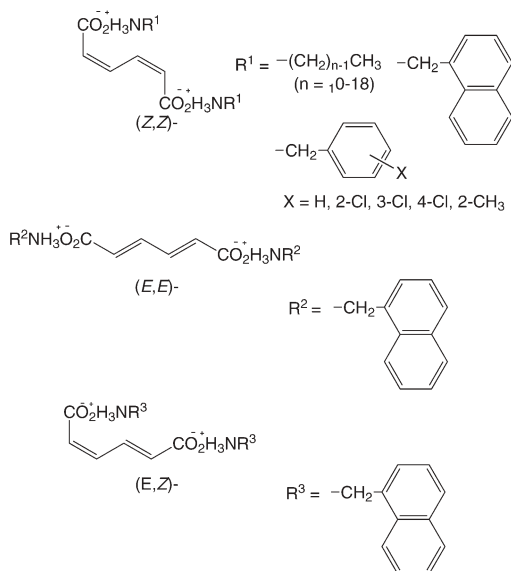
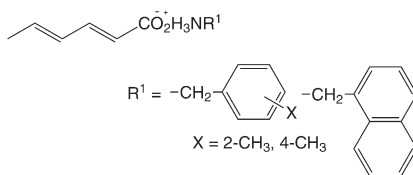
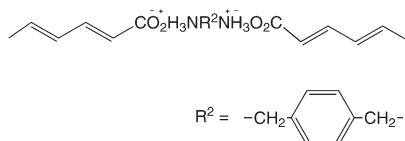
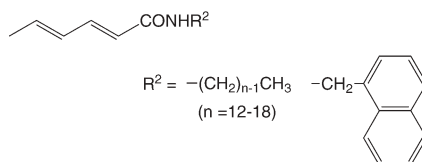
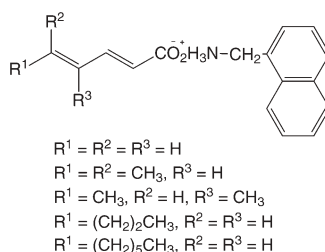
Features and Mechanism of Polymerization of 1,3-Diene Compounds

Figure 1 summarizes the chemical structures of the topochemically polymerizable 1,3-diene monomers providing stereoregular 1,4-*trans* polymer (Scheme 6) [16]. Most of the polymerizable monomers contain benzyl, naphthylmethyl, and long alkyl-chain substituents in their chemical structures. The (*Z,Z*)-, (*E,Z*)-, and (*E,E*)-muconic and sorbic acids as well as the other diene carboxylic acids are used as the ester, amide, and ammonium derivatives. In contrast to this, the carboxylic acids themselves have crystal structures unfavorable for polymerization while they undergo [2+2] photodimerization, as has already been described in the preceding sections.



Scheme 6 Solid-state polymerization of 1,3-diene compounds providing 1,4-*trans* polymers

The polymerization proceeds under photo- [49, 50], X-ray [51], and γ -ray [52] irradiation in the dark in vacuo, in air, or even in water or organic solvent as the dispersant (nonsolvent) for the crystals, similar to the solid-state polymerization of diacetylene compounds [12]. The process of topochemical polymerization of 1,3-diene monomers is also independent of the environment surrounding the crystals. Recently, the thermally induced topochemical polymerization of several monomers with a high decomposition and melting point was confirmed [53]. The polymer yield increases as the reaction temperature increases during the thermal polymerization. IR and NMR spectroscopies certified that the polymers obtained from the thermally induced polymerization in the dark have a stereoregular repeating structure identical to those of the photopolymers produced by UV or γ -ray irradiation.

Dialkyl MuconatesDi(alkylammonium) MuconatesAlkylammonium SorbatesAlkylenediammonium DisorbatesN-AlkylsorbamidesOther 1,3-Diene Monomers**Fig. 1** Chemical structures of topochemically polymerizable 1,3-diene monomers

The polymerization proceeds via a radical chain-reaction mechanism, judging from some features of the polymerization: initiation by irradiation or upon heating, no formation of oligomers, and polymer formation irrespective of the medium or atmosphere. The propagating radicals are readily detected by ESR spectroscopy during polymerization in the crystalline state (Fig. 2), because termination between the propagating radicals occurs less frequently in the solid state [50].

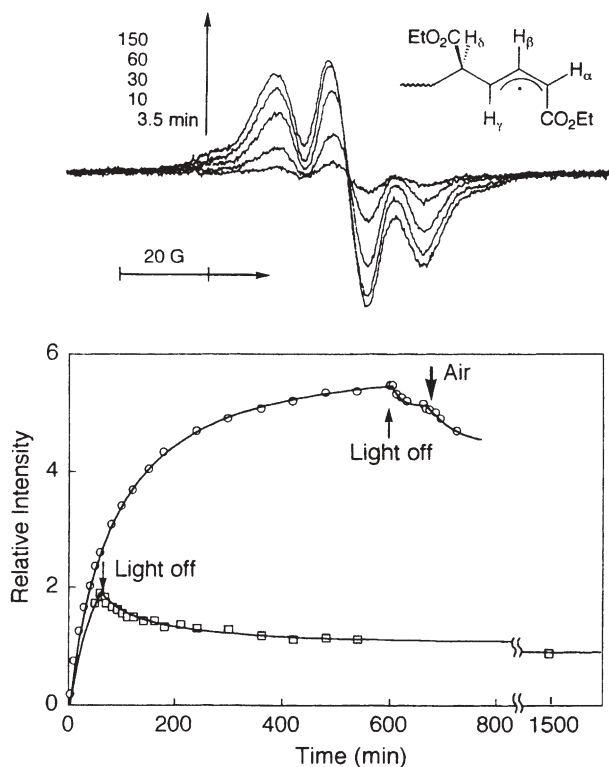
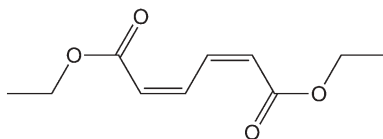


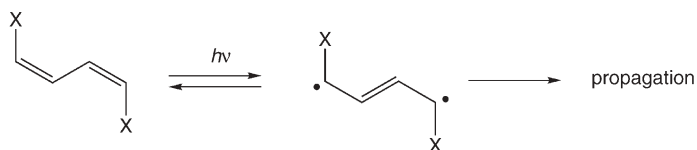
Fig. 2 ESR spectrum of the propagating radical of 1 during solid-state polymerization, and change in the concentration under continuous UV irradiation and after interruption of the irradiation [50]

The rate of photopolymerization depends on the polymerization temperature, despite the photoinitiating system of the polymerization [50]. The polymer yield becomes quantitative during UV irradiation over several hours at a relatively high temperature, but it gradually decreases with decreasing polymerization temperature. The polymer yield of the photoradiation below room temperature was very low. The overall activation energy was large at approximately 55 kJ/mol for the photopolymerization of diethyl (*Z,Z*)-muconate (1). The activation energy for the propagating reaction is assumed to be small because an ultrahigh molecular weight polymer is produced independent of the

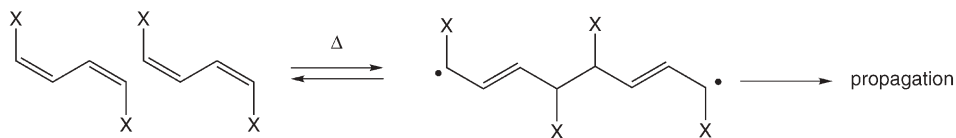


polymerization temperature. This suggests another type of initiation in addition to the photochemical initiation. Strain accumulated in the monomer crystals may initiate new propagation along with polymer formation. It was confirmed that the overall activation energy for thermal polymerization in the dark is much greater than that for the photopolymerization. For the thermally induced and photoinduced polymerization, a similar heterogeneous reaction is involved as the propagation process, but the initiation steps are different from each other. During the photoinduced polymerization, a unimolecular initiation is caused by excitation of the diene part, and a bimolecular initiation is also possibly included due to the crystal-lattice strain. The thermally induced polymerization has only a bimolecular reaction as the initiation step for producing two free radicals (Scheme 7). The polymerization kinetics have been investigated in detail by IR and Raman spectroscopies [51, 54].

Unimolecular initiation (photochemical)



Bimolecular initiation (thermal)



Scheme 7 Unimolecular and bimolecular initiation mechanisms induced by photochemical and thermal processes, respectively

During topochemical polymerization, the molecular arrangement of monomers determines polymerization reactivity in the crystalline state. Therefore, crystal structure analysis is a key to understanding the nature of the topochemical polymerization and designing the structure of polymerizable monomer crystals. Tashiro et al. successfully determined the crystal structure of **1** using a CCD camera system, which can quickly collect the X-ray diffraction data with a sufficient quantitative intensity [55]. A single crystal of poly(**1**) was obtained with less strain and fewer defects by the X- and γ -ray radiation polymerizations of the single crystal of **1**. The crystallographic parameters of **1** and poly(**1**) are very similar to each other. The crystal structures of other polymerizable monomers were also determined in a similar way using a CCD camera system. Figure 3 shows the crystal structures of di(4-chlorobenzyl) (*Z,Z*)-muconate (**2**) and poly(**2**) [56].

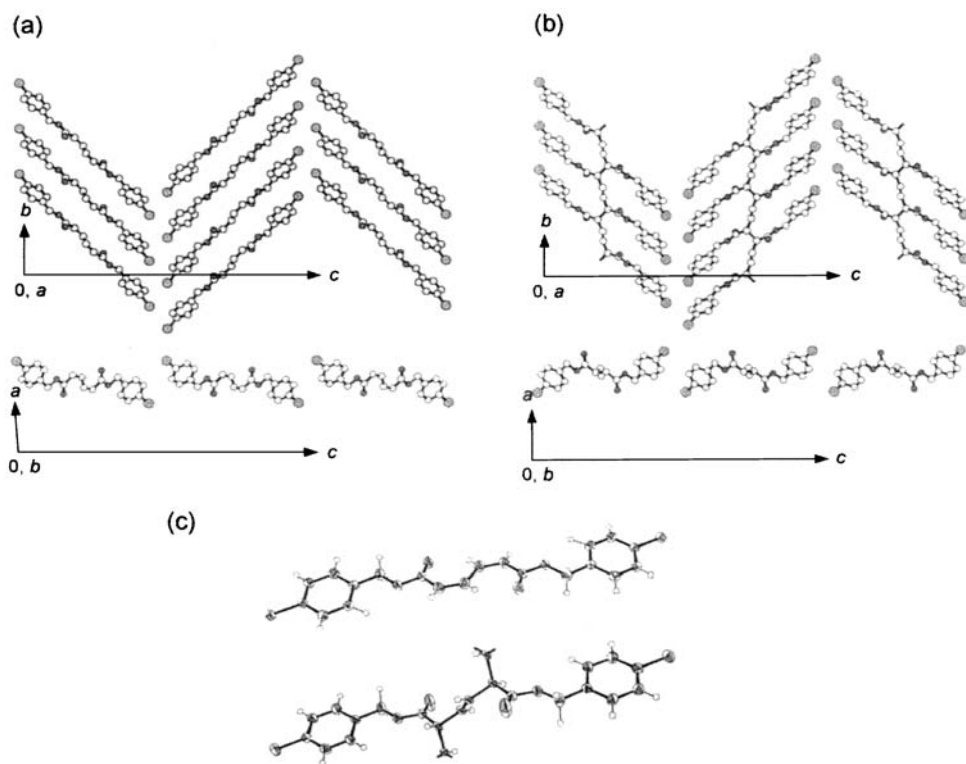
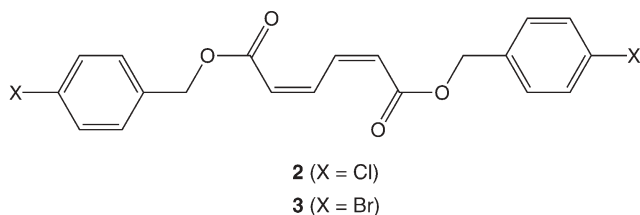


Fig. 3a, b Crystal structures of **2** and poly(**2**) viewed down along the crystallographic *a*- and *b*-axes at the top and bottom, respectively. Hydrogen atoms are omitted for clarity. **c** ORTEP drawing for **2** (−120 °C) and repeating unit of poly(**2**). Thermal ellipsoids are plotted at the 50% probability level [56]



The collection of reflection data from the monomer crystal was carried out within 10 min to avoid the effect of the polymerization. Crystals of both the monomer and polymer have identical space groups and similar cell parameters: monoclinic, $P2_1/c$, $a=5.629(6)$ Å, $b=5.122(6)$ Å, $c=32.08(2)$ Å, $\beta=93.712(1)^\circ$, $V=923.0(4)$ Å³, $Z=2$ for the **2** crystal; and monoclinic, $P2_1/c$, $a=5.6796(3)$ Å, $b=4.8631(1)$ Å, $c=32.097(1)$ Å, $\beta=90.185(2)^\circ$, $V=886.54(5)$ Å³, $Z=2$ for the poly(**2**) crystal. The same space group before and after the polymerization indicated that this polymerization is really a topochemical polymerization. The reflection

from the monomer crystals observed at room temperature was somewhat insufficient for least-squares refinement. Enough reflections could be successfully collected at $-120\text{ }^{\circ}\text{C}$ without the effect of structural change using an imaging plate detector, due to the suppressed polymerization at a lower temperature. The structure agreed well with that at room temperature except for a slight change in the lattice parameters dependent on the temperature: $a=5.6457(2)\text{ }\text{\AA}$, $b=5.0639(3)\text{ }\text{\AA}$, $c=31.685(4)\text{ }\text{\AA}$, $\beta=92.746(4)^{\circ}$, $V=904.82(8)\text{ }\text{\AA}^3$ at $-120\text{ }^{\circ}\text{C}$.

The successful determination of the crystal structure of the polymer provides direct and reliable evidence for the stereochemical structure of the resulting polymer. In the monomer crystals, the monomer molecules stack along the a - and b -axes in a column structure. A polymer chain is produced along the b -axis from the consideration of the overlap of the π -orbitals of the reacting moieties, which is in good agreement with the polymer crystal structure. The 4-chlorobenzyl moiety as the side chain has no significant change in its orientation during polymerization. The polymerization proceeds with only rotation of the diene moiety and with no large movement of the center of mass. The topochemical polymerization of **2** undergoes an accompanying change in the type of chemical bond with a minimum movement of atoms to produce a polymer chain in the crystals. Poly(**3**) has a similar crystal structure.

Novel phase transition was observed for organic polymer crystals, which were directly fabricated by the topochemical polymerization of **2** and **3** in the crystalline state [57]. The obtained polymers were thermally stable and their crystal structures reversibly changed in two steps according to the temperature. The phase transition of these organic polymer crystals has been revealed based on the results of thermal analyses including thermogravimetric and differential thermal analyses, and differential scanning calorimetry, as well as powder X-ray diffraction (XRD), single crystal structure analysis, and IR spectroscopy under temperature control. A change in cell lengths was evaluated from d -spacing values observed by XRD at various temperatures. It was concluded that the conformational change in the ester moiety of the polymer side chain induces a noncontinuous change in the crystal structures as the phase transition in a thermodynamic equilibrium, which can be detected by X-ray diffraction measurement and thermal analyses. The highly regular crystalline structure of the polymer crystals has provided a new insight into organic crystalline materials in terms of the thermal stability of the polymer crystals, which is much superior to that of organic crystals consisting of low molecular weight molecules. A change in several physical properties of the polymer crystals accompanying the phase transitions is now being investigated.

Interestingly, a change in the crystal lattice from the monomer to the polymer during topochemical polymerization can be observed macroscopically [58]. Figure 4a, b shows optical photographs of the giant crystals of the monomer **2**, and the polymer crystal obtained by γ -radiation polymerization. Several monomer single crystals with a small size provide the corresponding polymer single crystals with a high quality, which can be used for crystal structure analysis (see also Fig. 3). In contrast, during the photoirradiation of the

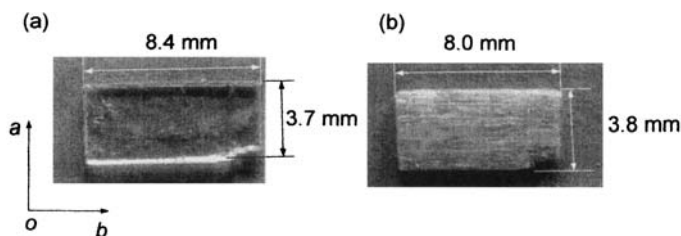


Fig. 4 Photographs of the crystals of **a** **2** and **b** poly(**2**). The polymer crystal was obtained by γ -radiation polymerization

giant crystals, cracks were formed and subsequently the transparency of the crystals was reduced, as shown in the photographs in Fig. 4b. This is due to the formation of successive covalent bonds along the specific crystal axis, e.g., the *b*-axis in the crystal of **2**. A macroscopic shrinkage is observed for the crystal during polymerization, in good agreement with the change in the crystallographic lattice, i.e., 5.122 to 4.863 Å in the *b*-axis length for the monomer and polymer crystals of **2**, together with a reduction of 5.1%. In general, solid-state reactions include any movement or rearrangement of atoms in the crystals. Structural strain formed during the reaction may be released by a change in the shape and volume of void space between the reacting molecules. Due to the presence of long and covalent-bonded chains in the polymer crystals, a few single-crystal-to-single-crystal polymerization reactions have been reported. When a change in the axis length is small, polymer single crystals are more favorably produced without defects and collapse in the crystals.

We can learn the structural change in the crystals during topochemical polymerization by powder X-ray diffraction measurements. X-ray diffraction profiles continuously changed during the polymerization of **1** under the irradiation of an X-ray beam (Fig. 5) [51]. The reflections shifted and approached the reflection position of the polymer. This suggests that the polymerization

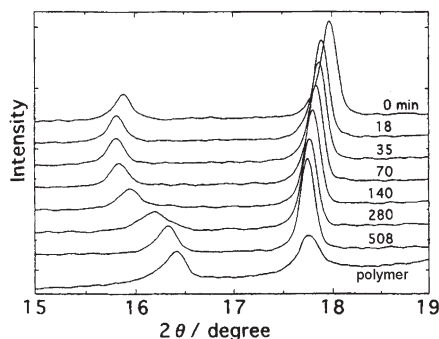


Fig. 5 Time dependence of X-ray diffraction profiles measured for the powder crystals of **1** at room temperature [51]

occurs gradually but continuously while generating some strains in the crystal lattice, where both the monomer and polymer species are coexistent. The X-ray diffraction may occur coherently from both the domains of monomers and polymers, which are not separated from each other on a macroscopic scale.

3.2

The 5 Å Rule as the Polymerization Principle

Crystal engineering is the planning of the properties and functions of crystalline materials using preorganized molecules [27]. This process involves the control of crystal packing on the basis of information from the chemical structure of the molecules and is required for clarification of the correlation between the structure and functions. It is important to investigate the molecular packing in the crystals of diene monomers that can or cannot undergo topochemical polymerization, in order to understand the crystal structure and polymerization reactivity relationship.

Muconic and sorbic acid derivatives, independent of their *EZ* configurations, have similar molecular conformations in the crystalline state. All the diene

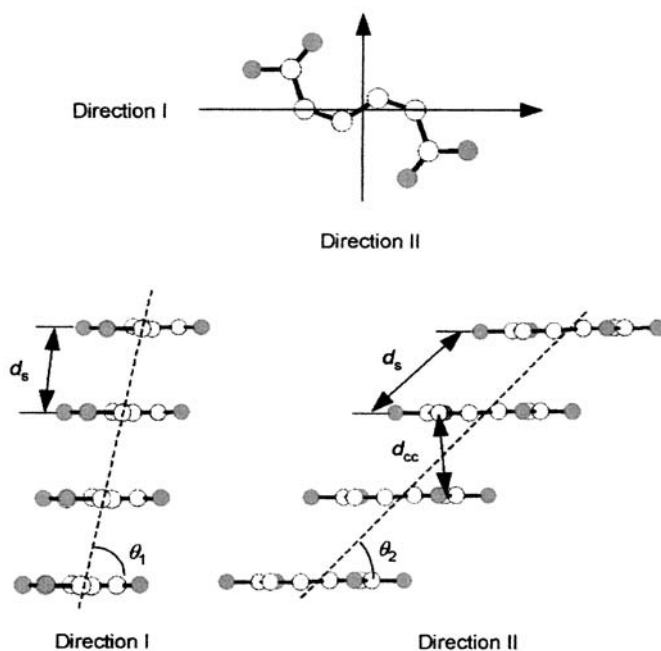


Fig. 6 Stacking model for the muconate derivatives in the crystalline state and the definition of stacking parameters used for the prediction of the topochemical polymerization reactivity. d_{cc} is the intermolecular distance between the 2 and 5' carbons. d_s is the stacking distance between the adjacent monomers in a column. θ_1 and θ_2 are the angles between the stacking direction and the molecular plane in orthogonally different directions [59]

Table 2 Monomer stacking parameters for the crystals of topochemically polymerizable 1,3-diene mono- and dicarboxylic acid derivatives^a [16]

| Monomer | Space group ^b | Temp. (°C) | d_s (Å) | d_{cc} (Å) | θ_1 (°) | θ_2 (°) |
|--|--------------------------|------------|------------------------|--------------|----------------|----------------|
| <i>Dialkyl (Z,Z)-muconates</i> | | | | | | |
| R=ethyl (1) | $P2_1/c$ | 25 | 4.9310(6) | 3.79 | 79 | 49 |
| 4-chlorobenzyl (2) | $P2_1/c$ | 25 | 5.122(6) | 3.56 | 82 | 44 |
| 4-chlorobenzyl (2) | $P2_1/c$ | -120 | 5.0639(3) | 3.48 | 78 | 43 |
| 4-bromobenzyl (3) | $P2_1/c$ | 25 | 5.21(1) | 3.89 | 72 | 49 |
| 4-methoxybenzyl (4) | $C2/c$ | -70 | 9.4840(7) ^c | 3.44 | ^d | ^d |
| <i>Dialkyl (E,E)-muconate</i> | | | | | | |
| R=4-methoxybenzyl (5) | $C2/c$ | -70 | 9.7803(6) ^c | 3.32 | ^d | ^d |
| <i>Di(alkylammonium) (Z,Z)-muconates</i> | | | | | | |
| R=benzyl | $P2_1/a$ | -63 | 4.862(2) | 4.24 | 67 | 55 |
| 2-chlorobenzyl | $P2_1/a$ | 23 | 4.9360(8) | 4.19 | 62 | 52 |
| <i>Alkylammonium (E,E)-sorbrates</i> | | | | | | |
| R=2-methylbenzyl | $P2_1/a$ | 23 | 4.9958(8) | 5.35 | 28 | 60 |
| 4-methylbenzyl | $P\bar{1}$ | 23 | 4.932(1) | 5.43 | 24 | 61 |
| 1-naphthylmethyl | $C2/c$ | 23 | 4.9909(1) | 5.35 | 29 | 61 |
| <i>p</i> -xylylene | $P\bar{1}$ | 23 | 4.9876(5) | 5.47 | 25 | 60 |
| <i>Other dienes</i> | | | | | | |
| Lithium (E,E)-sorbrates | $C2/c$ | 21 | 5.037(2) | 5.69 | 7 | 32 |
| 1-Naphthylmethyl (E)-pentadienoate | $Pca2_1$ | -70 | 4.9472(5) | 5.31 | 29 | 61 |
| 1-Naphthylmethyl 5-methyl-(E)-hexadienoate | $C2/c$ | 23 | 4.9006(5) | 3.30 | 87 | 42 |

^a d_{cc} : distance between the reacting C₂ and C₅' carbons; d_s : stacking distance; θ_1 , θ_2 : tilt angles of the molecular plane.

^b References to X-ray single crystal structure.

^c Twice d_s values due to the alternate molecular stacking in a column.

^d Not determined.

monomers favor an *s-trans* conformation with a highly planar structure. The stacking structure of the monomers can be evaluated using the following parameters [59]: the intermolecular distance between carbons that react to form a new bond during the topochemical polymerization (d_{cc}), the stacking distance along the column (d_s), and the angles between the stacking direction and the molecular plane in orthogonally different directions (θ_1 and θ_2). The view from direction I is parallel to a vector through the 2 and 5 carbon atoms of the diene moieties. The definition is shown in Fig. 6. Table 2 summarizes the molecular stacking parameters determined for the crystals of topochemically polymerizable 1,3-diene monomers [16].

The polymerizable monomer crystals exhibit d_{cc} values over a relatively wide range of 3.3–5.7 Å. The θ_1 and θ_2 values are also dependent on the monomer structure. The θ_1 values for the sorbates ($\theta_1=24\text{--}29^\circ$) are much smaller than those for the salts ($\theta_1=52\text{--}55^\circ$) and esters ($\theta_1=72\text{--}82^\circ$) of muconates. The diene plane of the sorbates leans in a polymerizable direction in the column. This offset stacking includes a structure that has an unfavorable overlap of the π -orbitals. However, because the sorbate anions are fixed on the sheet of the hydrogen bond network only at one side, the diene parts of the sorbates can twist and revolve easily to change molecular conformation suitable for the polymerization.

In contrast, all the d_s values are in an exclusively limited region of 4.74–5.21 Å. The average d_s value is 5.0 Å for the polymerizable monomers. Figure 7 shows the relationship between the d_s and θ_2 values. Closed and open symbols represent polymerizable and nonpolymerizable monomers, respectively. The curve drawn in this figure is calculated for the closest packing of the planar molecules with a thickness of 3.5 Å and a θ_1 value of 90° . The muconic ester monomers favor the closest packing structure of the planar molecules in the crystals, while the ammonium derivatives often favor various structures, not a columnar structure, resulting in scattered plots far from the calculated curve. This is due to the diversity in the hydrogen bond pattern including 1D ladders and 2D sheets, depending on the structure of the *N*-substituted groups, as is discussed in a later section.

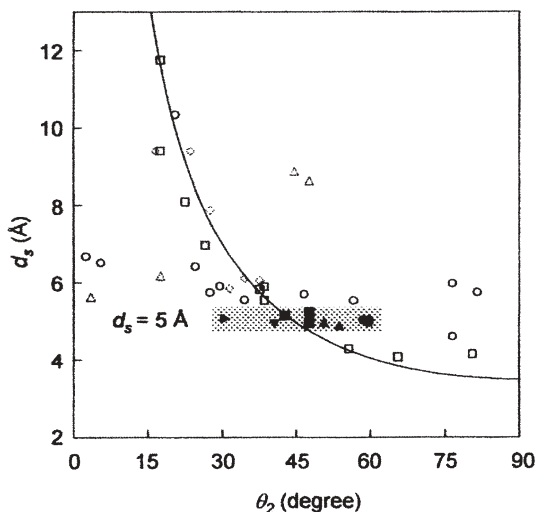


Fig. 7 Relationship between the d_s and θ_2 values for the 1,3-diene monomers in the crystals. Closed and open symbols represent polymerizable and nonpolymerizable monomers, respectively. Different symbols correspond to the different series of monomers. The curve is calculated for the closed packing of planar monomers with a thickness of 3.5 Å and θ_1 of 90° [59]

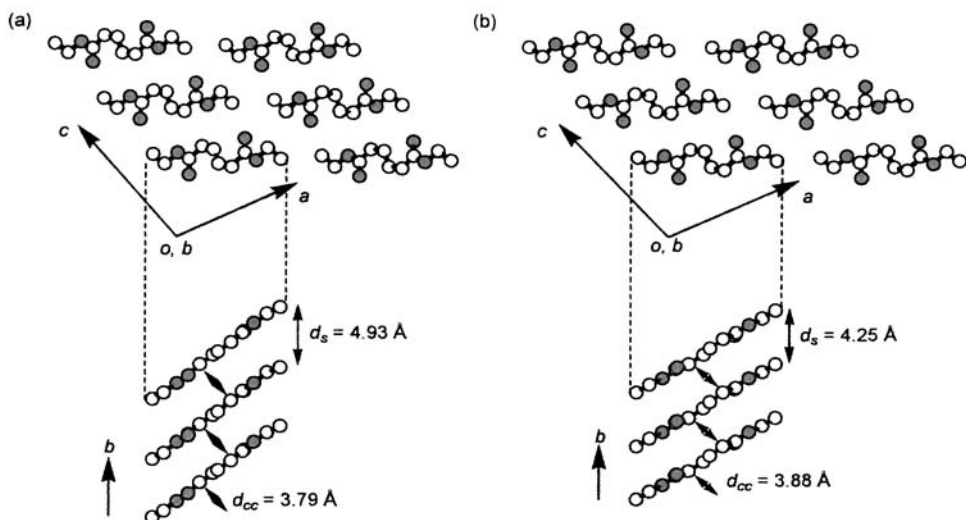
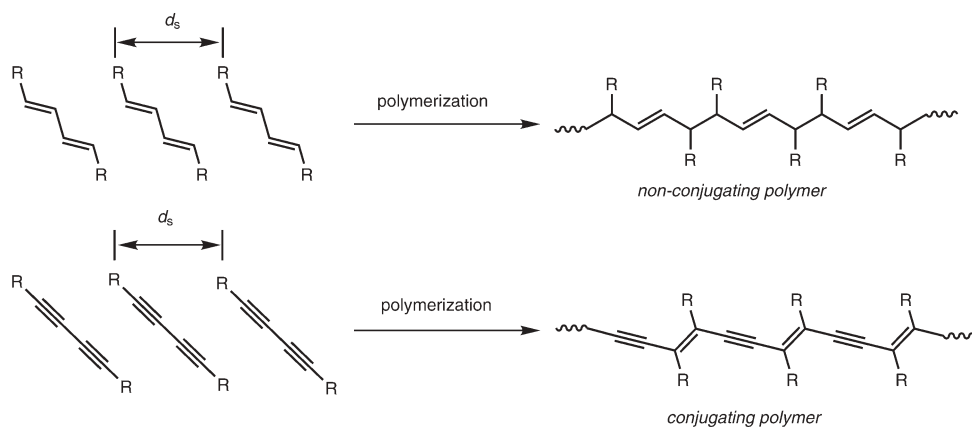


Fig. 8 Crystal structure of 1 at room temperature (a) and -80 °C (b) [60]

Several monomers have shorter d_{cc} and d_s values, and they are actually non-polymerizable although this appears to be advantageous for the polymerization. For example, 1 has an alternative crystal structure at a low temperature due to the first-order phase transition, which seriously affects the polymerization reactivity. Compound 1 polymerizes quite rapidly at room temperature, but not at all below -45 °C. Figure 8 shows the crystal structure of 1 at room temperature and -80 °C. The stacking parameters determined at low temperature are as follows: d_{cc} =3.88 Å, d_s =4.25 Å, θ_1 =80°, and θ_2 =57° [60], which are very similar to those for the polymerizable structure at room temperature: d_{cc} =3.79 Å, d_s =4.93 Å, θ_1 =79°, and θ_2 =49°. In this way, a slight change in the d_s value from 4.93 to 4.25 Å or a deviation from the limited zone appropriate for the polymerization in Fig. 7 diminishes the polymerization reactivity of 1. We emphasize the importance of the d_s value for the topochemical polymerization process. The stacking distances of the polymerizable monomers are close to the values of the repeating unit, i.e., a fiber period of polymer chains with a fully stretched conformation, produced along with a crystallographic axis in the crystals. The fiber period for poly(1) and poly(2) was experimentally determined to be 4.84 Å from the X-ray diffraction of the polymer single crystals [55, 56]. If the polymerization proceeds for d_s values greater or smaller than 5 Å, then monomer molecules have to translate along the stacking axis during polymerization. When the d_s value is close to the fiber period of the resulting polymer, monomer molecules rotate with the minimum translational movement and form a bond between the 2 and 5' carbon atoms.

The present polymerization principle (the 5 Å rule) for the 1,3-diene monomers seems to have features similar to the empirical rules for the polymerization of diacetylene compounds reported in the literature: d_s ~5 Å and θ ~45°

[10, 12]. Currently, topochemical polymerization is opened not only to the diacetylene library but also to the diene library, which is more popular and a larger collection. Diene polymerization has the potential of being applied to the construction of advanced organic materials in the solid state, because the topochemical polymerization of diacetylene and diene monomers provides different types of polymers, that is, conjugate and nonconjugate polymers, respectively (Scheme 8) [16, 61].



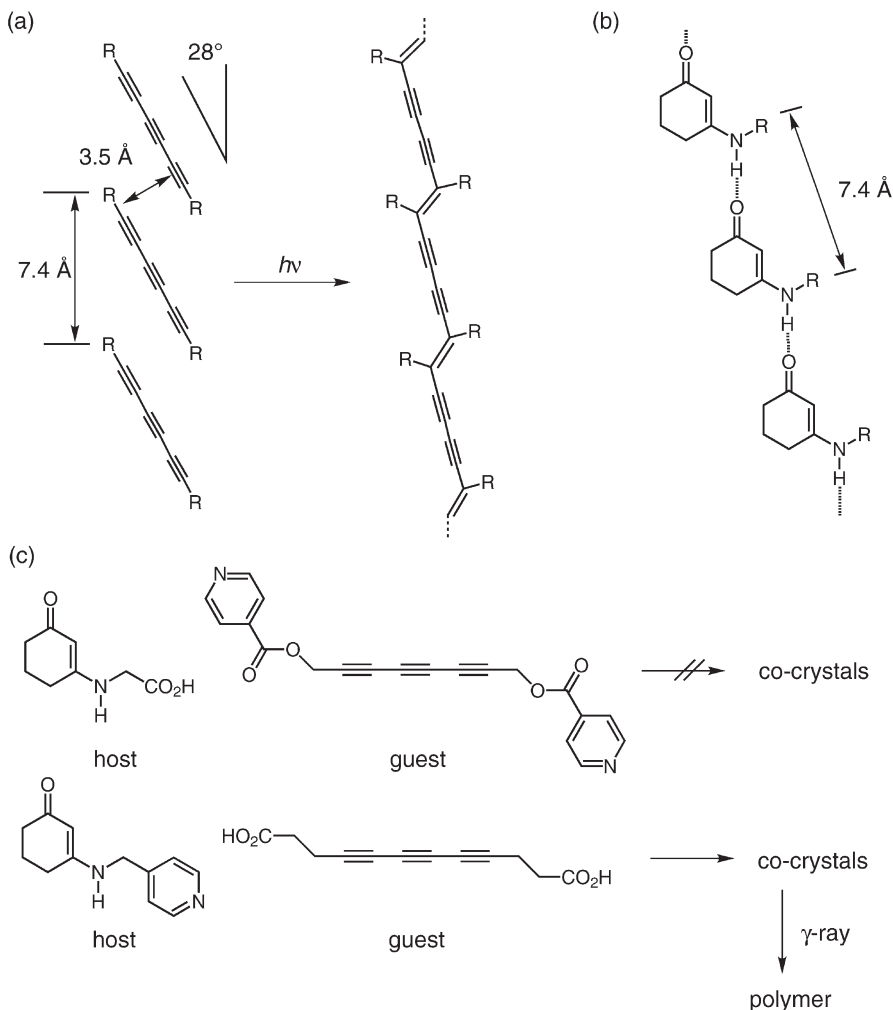
Scheme 8 Nonconjugating and conjugating polymer formation through topochemical polymerization of 1,3-diene and 1,3-diyne compounds

The rules for diene polymerization are more sensitive to a slight change in the monomer crystal structure. In other words, for the polymerizable 1,3-diene monomers, the tolerable range in the d_s values is very narrow and the regions for the polymerizable and nonpolymerizable monomers are clearly divided. On the other hand, the plots for polymerizable and nonpolymerizable diacetylene monomers are mingled even in an ideal zone around a d_s value of 5 Å and a θ value of 45° [12]. Because of the more limited conditions of structural factors for diene polymerization in the crystalline state, the discovery and generalization of this type of diene polymerization has greatly lagged behind [14]. It is also noteworthy that polymorphism is important as another factor for the diacetylene polymerization relationship. Regarding the literature values of crystal structures, the conditions for crystallization (for example, temperature, solvents, etc.) are not always the same for structure determination and the polymerization test, because of some limits in the conditions for single crystal structure analysis with a classic apparatus, such as a four-circle diffractometer for several days at a low temperature, that was used in the 1970s to 1980s. The experimental conditions are required to be the same, as much as possible, for crystal fabrication and handling during both the X-ray crystal structure analysis and the topochemical polymerization experiments.

3.3

Topochemical Polymerization of Other Monomers

Lauher and Fowler et al. have proposed an elegant strategy for the control of topochemical polymerization based on the host–guest cocrystal concept. They used the ureylene and oxalamide functionality to form layered supramolecular structures for the topochemically controlled polymerization of diacetylenes and 1,3-butadienes in the solid state [62, 63].

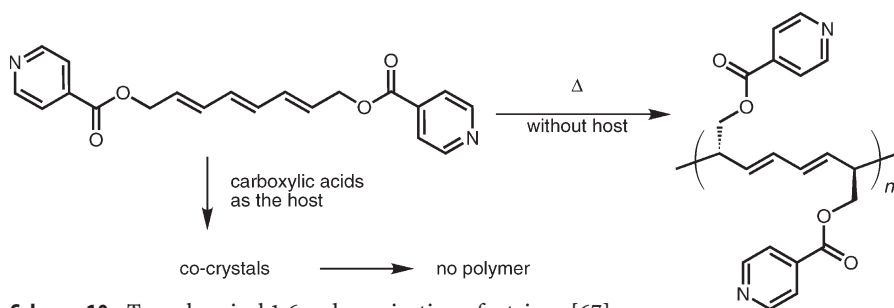


Scheme 9 Strategy for the 1,6-polymerization of triacetylene. **a** Polymerization principles for triacetylene. **b** Supramolecular synthon as the host to arrange triacetylene molecules as the guest with a stacking distance of 7.4 Å. **c** Successful and unsuccessful examples for the combination of host and guest molecules with carboxylic acid or pyridine moieties [63]

The 1,6-polymerization of triacetylene was an unknown transformation for a long time [64, 65]. Enkelmann provided a complete analysis of the criteria necessary for successful polymerization, but although it was a long-standing synthetic problem of considerable interest and the requirements were very well defined, no one had been able to devise a successful synthesis. Lauher et al. solved this problem by the designed 1,6-polymerization, which served as a significant test for supramolecular synthesis, as is shown in Scheme 9 [66]. Preliminary attempts to grow cocrystals between the carboxylic acid host and the dipyridine guest were not promising due to the solubility differences. Subsequently, the researchers turned their attention to the pyridine host, which readily cocrystallized with simple dicarboxylic acids such as succinic and adipic acids. A single crystal X-ray structure of the host–guest compound clearly showed that the molecules had self-assembled in accordance with their design: a stacking distance of 7.143 Å and tilt angle of 29.2°. The exposure of the host–guest crystals to γ -radiation resulted in the crystals becoming dark red. The Raman spectrum of the polytriacetylene showed only two intense bands, which can be assigned to the $C\equiv C$ and $C=C$ bonds.

The topochemical 1,6-polymerization of a triene was also an unknown transformation until recently. In addition to the tacticity problems associated with 1,6-substituted trienes, competition between the 1,2-, 1,4-, and 1,6-polymer reaction pathways is to be anticipated. For a successful topochemical polymerization, molecular modeling suggested the trienes should be translationally spaced with a repeat distance of about 7.2 Å. If the trienes also are aligned with a tilt angle of about 29°, the reacting carbon atoms (C1–C6) of adjacent π -systems will approach each other to within a close contact (3.5 Å). Since these supramolecular structural features are very similar to those previously used for the triacetylene polymerization, Lauher and Fowler et al. decided again to explore the same strategy for a 1,6-triene polymerization [67]. This approach involves the use of two molecules; one acts as the host, controlling the supramolecular structure and establishing the 7.2 Å translational repeat distance, and the other, the guest, is the intended triene monomer. Several different host and guest molecules have been synthesized, but such combinations resulted in an unsuccessful polymerization.

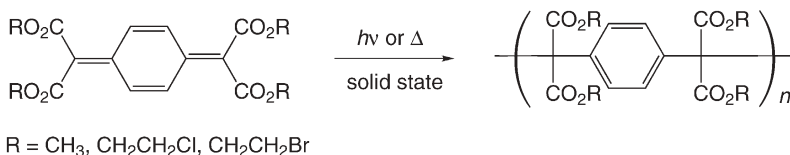
One of the intended triene guest molecules, shown in Scheme 10, was prepared and its crystal structure revealed a supramolecular structure that might



Scheme 10 Topochemical 1,6-polymerization of a triene [67]

be suitable for a topochemical polymerization. When the single crystal was heated to 110 °C for 8 h, this process resulted in a smooth transformation to a new material whose X-ray crystal structure clearly demonstrated that a topochemical 1,6-polymerization of the triene to a polytriene had occurred. Although the polymerization of the triene was a serendipitous discovery, it clearly demonstrates that the topochemical polymerization of a triene is possible, thus adding it to the small but growing number of important topochemical reactions.

The novel highly conjugated monomers 7,7,8,8-tetrakis(alkoxycarbonyl)quinodimethanes, with methoxy, ethoxy, isopropoxy, benzyloxy, chloroethoxy, and bromoethoxy as the alkoxy group, were synthesized and their polymerizations in the crystalline state were investigated by Itoh et al. [68, 69] (Scheme 11). The recrystallizations of these quinodimethanes yielded several kinds of crystal forms (prisms, needles, or plates) for each compound. They have different molecular packing modes by X-ray crystal structure analysis, indicating that the crystals are polymorphic. In the photopolymerizations of these monomer crystals in the solid state, some crystals polymerized topochemically to give crystalline polymers. For their thermal polymerizations in the solid state, the other two crystals also polymerized. The packing of quinodimethane molecules in the crystals was defined by four kinds of parameters: stacking distance (d_s), the distance between the reacting exomethylene carbon atoms (d_{cc}), and the angles formed between the stacking axis and longer axis of the monomer molecule (θ_1) and the shorter axis of the monomer molecule (θ_2). The polymerization reactivity of these quinodimethanes in the solid state was discussed on the basis of these parameters, similar to the 1,3-diene polymerization [59]. It was found that topochemical polymerizations of the quinodimethane monomers might take place when they are packed in crystals with parameters of $\theta_1 = 30\text{--}33^\circ$, $\theta_2 = 83\text{--}89^\circ$, $d_s = 7.0\text{--}7.6 \text{ \AA}$, and $d_{cc} = 3.8\text{--}4.2 \text{ \AA}$.



Scheme 11 Topochemical polymerization of 7,7,8,8-tetrakis(alkoxycarbonyl)quinodimethanes in the solid state under photoirradiation or upon heating

3.4

Stacking Control in the Crystals

Most of the topochemical reactions, including the first finding of the topochemical polymerization of **1**, were found accidentally or beyond any expectation [14]. During subsequent and extensive investigation, numerous studies have been carried out by trial-and-error approaches to establish any empirical rule accounting for a correlation between the geometry of functional moieties and reactions in the solid

state. Recent ideas based on crystal engineering and supramolecular chemistry have been leading us to a fruitful design and control of the crystal structures, the properties, and the reactivity of organic molecules in the solid state to overcome difficulty in prediction of the crystal packing of organic molecules [70–72].

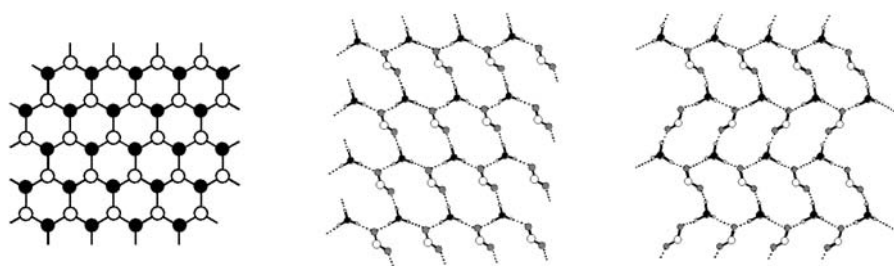
Some supramolecular synthons are available for the topochemical polymerization of the 1,3-diene carboxylic acid derivatives; for example, a 2D hydrogen bond network, aromatic ring stacking, and CH/ π , CH/O, and halogen–halogen interactions [59]. In the 2D hydrogen bond network formed between primary ammoniums and carboxylates, the ammonium and carboxylate groups act as triple hydrogen bond donors and acceptors, respectively. Regarding the close stacking of aromatic rings, the benzyl and naphthylmethyl moieties are packed in the crystals with a herringbone or γ -type structure [27]. The CH/ π interaction between aromatic groups is also important. It is noteworthy that a naphthylmethylammonium as the counteranion is well known for forming a robust layer structure, in which diene carboxylic acid molecules are arranged in a fashion appropriate for polymerization as a result of the synergetic effects of the 2D hydrogen bond network, aromatic stacking, and CH/ π interaction. This has already been proved by the polymerization reactivity of several kinds of diene carboxylic acids, i.e., not only the muconic and sorbic acid derivatives but also other diene and diyne monomers [59, 73]. Their crystal structure and molecular packing are similar to those of the other polymerizable sorbate and muconate monomers, indicating that the polymerization principles are valid for a variety of monomers other than the muconates and sorbates.

3.5

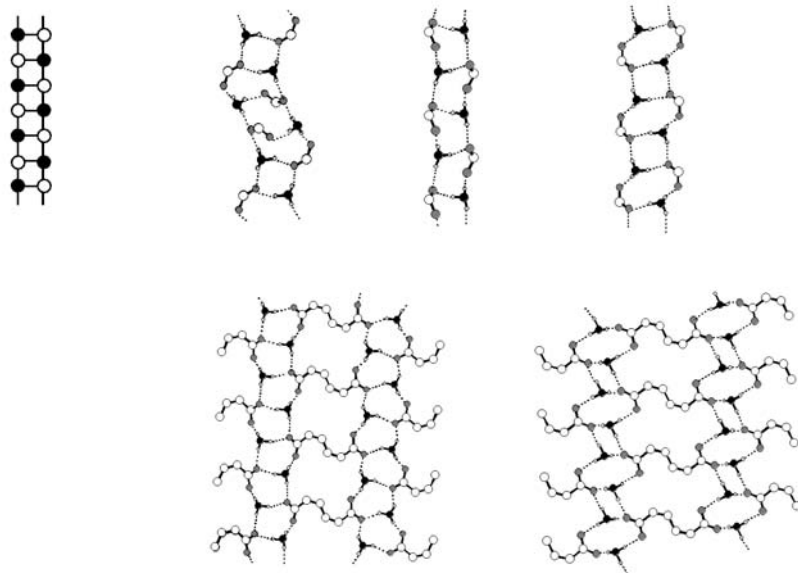
Hydrogen Bond Network

For the crystal structure design of ammonium derivatives using the hydrogen bond network, the diversity and isomerism of hydrogen bond networks are a problem to be overcome [74–80]. The 2D hydrogen bond networks for polymerizable monomers involve two kinds of pattern as shown in Fig. 9a [81, 82]. In the schematic models (left), open and closed circles represent the carboxylate and ammonium groups as the triple hydrogen bond donors and acceptors, respectively. In the crystal structures (right), the small circles show hydrogen atoms attached to nitrogen atoms, and dotted lines show hydrogen bonds. The other hydrogen atoms and substituents are omitted for clarity. The sorbate or muconate anions and the primary ammonium cations are linked to each other through hydrogen bond networks. The primary ammonium cations form hydrogen bonds with three neighboring carboxylate anions, and, in turn, the carboxylate groups with three neighboring ammonium cations. Irrespective of the molecular structure, all of the polymerizable monomers have an identical hydrogen bond network structure; 16-membered rings are the repeating units in the 2D sheet [83, 84]. The 2D hydrogen bond networks run perpendicular to the molecular plane of the dienes and support a suitable columnar structure for topochemical polymerization. They include two types of arrangement of the

(a) polymerizable 2D network



(b) 1D ladder



(c) non-polymerizable 2D network

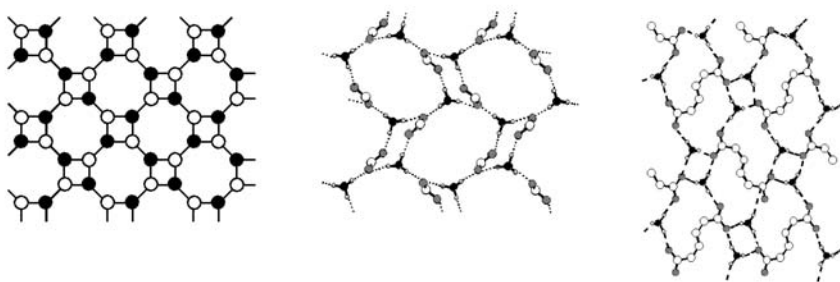


Fig. 9 Classification of the patterns of the hydrogen bond networks. **a** Polymerizable 2D network, **b** 1D ladder, and **c** nonpolymerizable 2D network

columns: one is a parallel arrangement in which they run in the same direction, and the other is an antiparallel arrangement in which all the columns run alternately in the opposite direction.

The nonpolymerizable salts have a variety of hydrogen bond networks. As shown in Fig. 9b, c, they are divided into several categories on the basis of unit hydrogen bond cycles and the numbers of the incorporated atoms. 1D ladders are built up to the successive 8-, 10-, or 12-membered rings. In the case of the muconates, the 10 ladders are further bridged by the diene moieties as the bifunctional triple hydrogen bond acceptors. As discussed earlier, a stacking distance of 5 Å is the most important factor for the polymerizable monomer crystals. However, the distance values for these stacking styles are greater than the ideal one (~5 Å) for polymerization, or the hydrogen bond network runs parallel to the molecular plane of the muconates, which are aligned in a sheet.

The polymerization proceeds via a radical chain-reaction mechanism, judging by some features of the polymerization: initiation by irradiation or upon heating, no formation of oligomers, and polymer formation irrespective of the medium or atmosphere. The propagating radicals are readily detected by ESR spectroscopy during polymerization in the crystalline state (Fig. 2), because termination between the propagating radicals occurs less frequently in the solid state [50].

It is well known that the primary and secondary amides form robust hydrogen-bonded ribbons, tapes, and sheets as the structural motifs for crystal engineering [75, 76]. It is possible that the secondary amides of muconic and sorbic acids form linear hydrogen bonds via bidentate interaction between the N–H and C=O groups at the ideal stacking distance of 5 Å. In contrast to the results of the successful polymerization of the ammonium and ester derivatives during the last decade, no polymerization has been reported for the amide derivatives of the 1,3-diene carboxylic acids, except for the case of *N*-octadecylsorbamide [25]. Recently, Matsumoto et al. confirmed that the topochemical polymerization proceeds under UV and γ -ray irradiation in the crystalline state when naphthylmethyl and higher *n*-alkyl groups are introduced as the N-substituent of the amide derivatives as expected [85]. During polymerization of the sorbamides, polymerization proceeded in a direction different from that of the 1D hydrogen bond chain despite the appropriate stacking distance. This is due to the unfavorable direction of the diene moieties for the π – π stacking of the diene moieties. A sheet-type arrangement in the crystals of the sorbamide derivatives was revealed, in which linear hydrogen bonds supported the sheet structure and the polymerization occurred between the sheets by the introduction of a naphthylmethyl and long alkyl groups as the N-substituents, resulting in the situation of the diene moieties by the stacking of the sheets in an appropriate sheet-to-sheet distance and phase.

3.6

Halogen–Halogen Interactions

Halogen–halogen interaction as the supramolecular synthon has a significant potential in the presence of other weak interactions (for example, CH/ π inter-

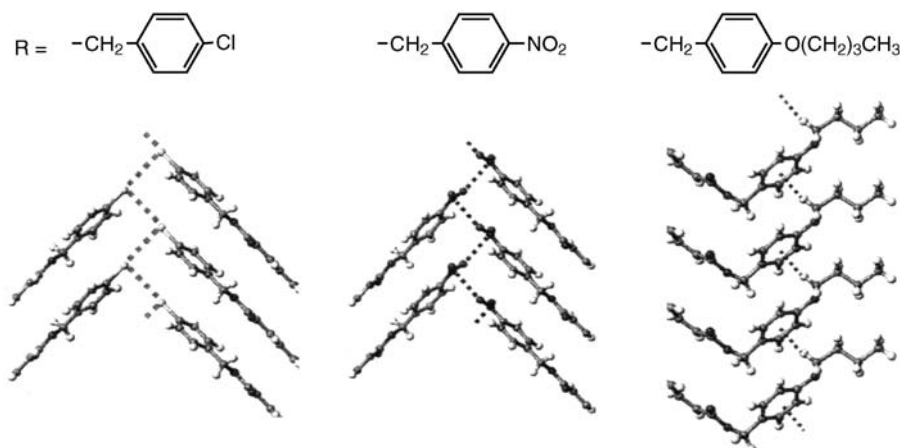


Fig. 10 Translational molecular stacking of 4-substituted benzyl (*Z,Z*)-muconates in the crystals. R is the ester alkyl group. Dotted lines indicate intermolecular interactions in a column to translationally arrange monomer molecules at a stacking distance of 5 Å

actions) and is used for rational crystal design of diene monomers other than the ammonium derivatives (Fig. 10). The control of the molecular alignment through a halogen–halogen interaction is effective when any robust interaction such as a hydrogen bond is absent, as seen in the case of the ester derivatives.

From the viewpoint of intermolecular force for the monomer stacking, the following facts support the existence of a halogen–halogen interaction in the crystals of several muconic ester compounds [56]. Initially, the distances between the nonbonding halogen atoms (for example, 3.57 and 3.63 Å in the crystals of **2** and **3**, respectively) are shorter than the sum of the corresponding van der Waals radii. Secondly, the Kitaigorodskii rule [70] breaks down in this case, despite its validity for a large number of other crystals of nonpolar and various shaped aliphatic molecules. The replacement of one by the other would not change their crystal structure when packing is governed by the Kitaigorodskii rule. The substituent groups have no significant difference in their volumes (20 Å³ for Cl, 26 Å³ for Br, and 24 Å³ for CH₃). Nevertheless, the crystal structure of the 4-methyl-substituted monomer is completely different from those of the 4-chloro- and 4-bromo-substituted derivatives. The alignment of the dibenzyl muconate monomers in the crystals is regulated by the characteristic halogen zigzag chains as a supramolecular synthon, which may be applicable for the crystal design of halogen-containing ester derivatives. In the crystals of **2** and **3**, the molecules are connected by a CH/π interaction as well as halogen chains, which strengthen the columnar structure appropriate for the polymerization. The control of the molecular alignment through a halogen–halogen interaction is effective in combination with any other weak interaction. Similar translational stacking of monomer molecules in the crystals is also observed for the nitro- or *n*-butoxy-benzyl-substituted esters, as shown in Fig. 10.

3.7

CH/ π Interactions

Weak hydrogen bonds including CH/ π interactions are important for controlling a molecular packing structure in the crystals [86–88]. Figure 11 shows the crystal structure of a polymerizable ammonium monomer with 1-naphthylmethylammonium as the counteranion. The side view of the stacking structure of the anion and cation layers indicates an alternating lamellar packing. For the construction of such a lamellar structure, π – π stacking and CH/ π interaction are important for packing in the lipophilic layer. Figure 11 also represents CH/ π interaction between the primary ammonium cations in a cation layer. A similar structure and interaction are observed for the crystals of both sorbates and muconates, irrespective of their mono- and dianion structures [82].

A similar sandwiched structure formed by alternating stacks of hydrogen-bonded, naphthalene, and alkyl layers is also observed for various 1-naphthylmethylammonium *n*-alkanoates [89]. The hydrogen bond pattern is again that of the typical example of primary ammonium carboxylates. In order to confirm the robustness of the trilayer structure, powder X-ray diffraction patterns were examined. As a result, a series of 1-naphthylmethylammonium *n*-alkanoates from acetate to tridecanoate produced isomorphous layered structures with the interlayer distances, *d* spacings, proportional to the lengths of the alkyl chains. This is attributed to synergistic intermolecular interactions: π – π and CH/ π interactions of the naphthalene rings between the cations, hydrophobic interactions of the alkyl chains, and 2D hydrogen bond networks between the primary ammonium cations and the carboxylate anions.

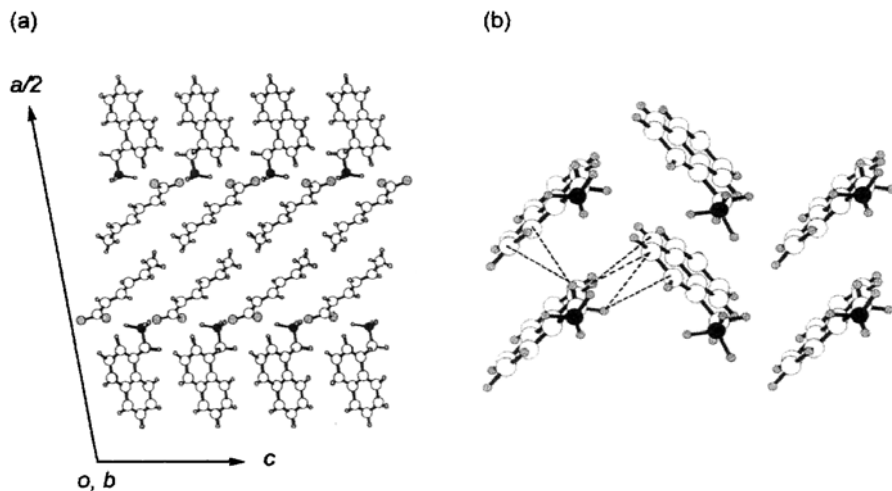


Fig. 11 a Side view of an anion layer sandwiched between cation layers viewed down along the crystallographic *a*-axis. b CH/ π interactions between the aromatic groups in the ammonium cation layers for 1-naphthylmethylammonium (*E,E*)-sorbate [82]

The robust trilayer structures of 1-naphthylmethylammonium *n*-alkanotes are constructed by summation of the characteristic robust motifs of the individual intermolecular interactions. This is attributed to agreement of the repeating distances among the three supramolecular synthons, in particular, the synergy of the steric dimensions of the alkyl groups and the repeating distances of the hydrogen bond networks within the robust layered crystal structures. Therefore, understanding the steric dimensions, geometries of interactions, and characteristic repeating distances of the supramolecular synthons is essential for elucidating the crystal structures from molecular structures, designing robust structural motifs, and predicting isomerism of the hydrogen bond networks. Moreover, this system provides unique organic robust layer structures with adjustable interlayer spacing controlled by the number of methylene units. The linear relationship between the interlayer spacing and the methylene carbon number is rare for organic crystalline materials, but ubiquitous in the organic–inorganic hybrid layered crystals.

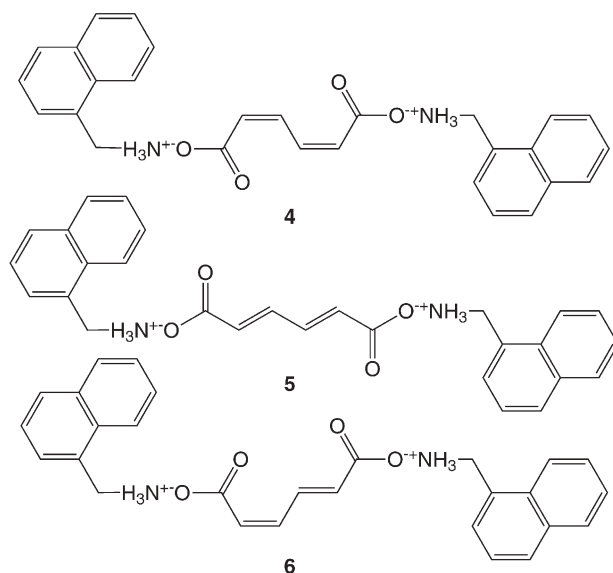
3.8

Supramolecular Control of Stereochemistry of Polymers

Topochemical polymerization in the crystalline state is the most promising method for controlling the stereochemistry of polymers. Polymers with different properties can be derived from the same starting monomers by changing the way of connecting the repeating units during polymer formation. The stereochemistry of polymers, i.e., tacticity, is one of the most important factors for determining the properties of polymeric materials, as well as the repeating unit structure, molecular weight, and molecular weight distribution. The syntheses of isotactic and syndiotactic polypropylenes and other stereoregular polymers from vinyl and diene monomers have been developed by Natta and coworkers since the 1950s and by other groups thereafter [90]. However, the precise control of the stereoregularity of diene polymers, including the polymers of muconic and sorbic derivatives, was still difficult using catalytic controls, i.e., ionic and coordination polymerizations [91–93] and also by radical polymerization with Lewis acid and other additives [94].

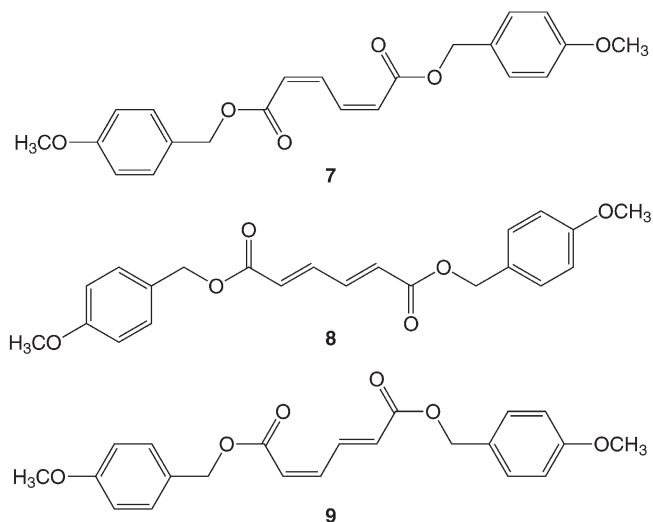
Molecular alignment in the monomer crystals is controlled by several intermolecular interactions, such as strong and weak hydrogen bonds, leading to the formation of various types of stereoregular polymers via a topochemical polymerization process. This approach to the stereocontrol of polymers differs from other conventional ways in the control of the propagating chain end using catalysts or additives in solution polymerization.

1-Naphthylmethylammonium (*Z,Z*)- and (*E,E*)-muconates (**4** and **5**, respectively) with C_2 symmetry favor a translational molecular packing in the crystals. The reacting diene moieties stack in a columnar structure with the aid of 2D hydrogen bond networks at the interface of the muconate anion and counteranion layers in the lamellar crystals [83]. The structures of monomer packing and the hydrogen bond networks of **4** and **5** are judged from powder X-ray diffraction



data to be similar to these for other related benzyl- or naphthylmethylammonium monomers [81, 84]. In fact, 4 and 5 produce the same stereoregular polymer with a *meso*-diisotactic structure by topochemical polymerization under UV irradiation in the crystalline state.

On the other hand, it was found that the 4-methoxybenzyl (*Z,Z*)- and (*E,E*)-muconates (7 and 8, respectively) alternately stack in a column by a CH/π interaction between the methoxy hydrogens and the π electrons of the phenyl



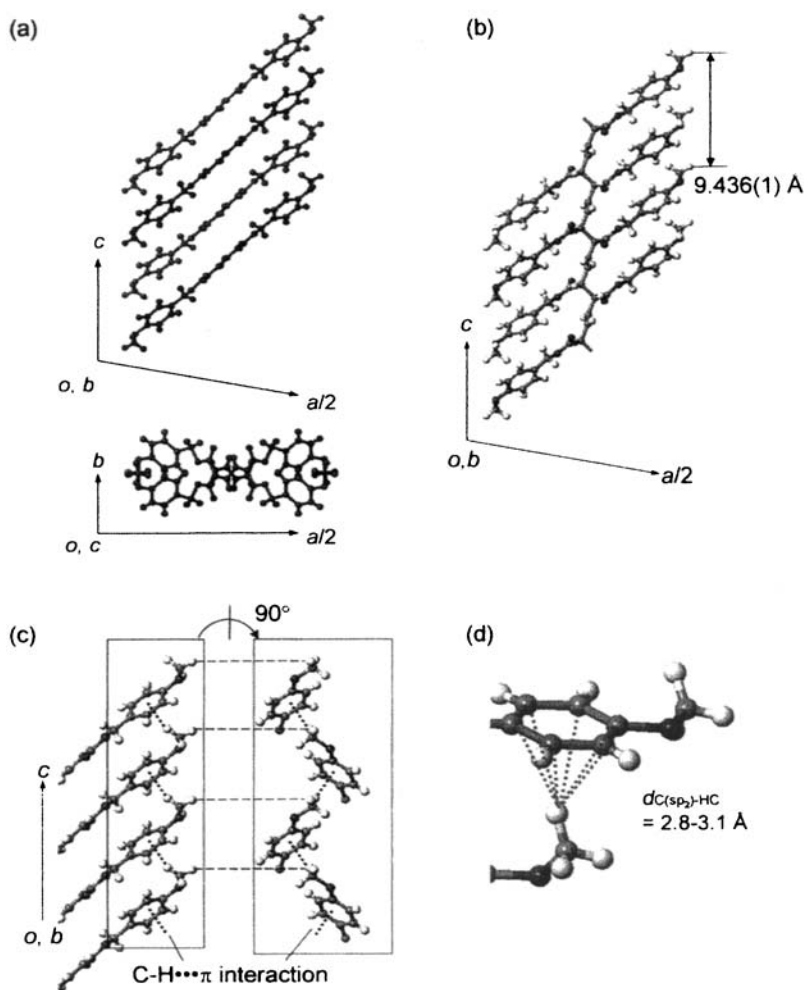


Fig. 12a, b Crystal structures of **7** and poly(**7**). Monomer crystal: monoclinic, $C2/c$, $a = 36.026(3)$ Å, $b = 5.6019(4)$ Å, $c = 9.4840(7)$ Å, $\beta = 100.27(1)^\circ$, $V = 1,883.4(2)$ Å³, $Z = 4$. Polymer crystal: monoclinic, $C2/c$, $a = 35.117(4)$ Å, $b = 5.7980(6)$ Å, $c = 9.436(1)$ Å, $\beta = 99.321(2)^\circ$, $V = 1,895.9(3)$ Å³, $Z = 4$. **c** Alternating molecular stacking of **7**. **d** CH/ π intermolecular interaction in a column

group, resulting in the formation of a different type of stereoregular polymer upon photoirradiation. The monomers **7** and **8** provide a 2,5-*trans* racemo-disyndiotactic polymer under photoirradiation in the crystalline state, as a result of the alternating molecular stacking in a column formed in the crystals with the aid of weak hydrogen bonds such as CH/ π and CH/O intermolecular interactions (Fig. 12) [95], while di(4-halobenzyl) (*Z,Z*)-muconates (**2** and **3**) provide diisotactic polymers due to the translational molecular stacking supported by the CH/ π and halogen–halogen interactions (Fig. 3) [56].

The single crystal structures of **7** and **8** revealed that the monomer molecules are packed in a column in an alternating fashion. The stacking distance of monomer molecules, d_s , which was evaluated as the distance between the mass centers of adjacent monomer molecules, is 4.74 and 4.87 Å, and the carbon-to-carbon distance between C2 and C5' carbons is 3.44 and 3.32 Å for **7** and **8**, respectively (Fig. 12). These values are very similar to those reported for other diene monomers providing isotactic polymers (See Table 2). The conformational structure is similar in each case before and after polymerization, being supported by the weak intermolecular interaction between adjacent monomer molecules within a column and inter-columns. The adjacent columns are linked to each other by the CH/O interaction between the methoxy groups to form a sheet structure, and between the carbonyl oxygen and the hydrogen of a butadiene moiety. The molecular sheets stack alternately to fabricate the molecular stacking structure appropriate for syndiotactic polymerization in the crystals. In the column, close CH/ π contact (e.g., 2.84–3.06 Å) is observed between the benzene ring and the methoxy group. The CH/O and CH/ π interactions are maintained during the polymerization [58].

There are four types of possible stereoregular structures for each *trans*-1,4 polymer of 1,4-disubstituted butadiene (Fig. 13). The stereochemistry of polymers is represented by two kinds of relationship as follows, one of which is the relative configuration between the two repeating monomer units. When all the

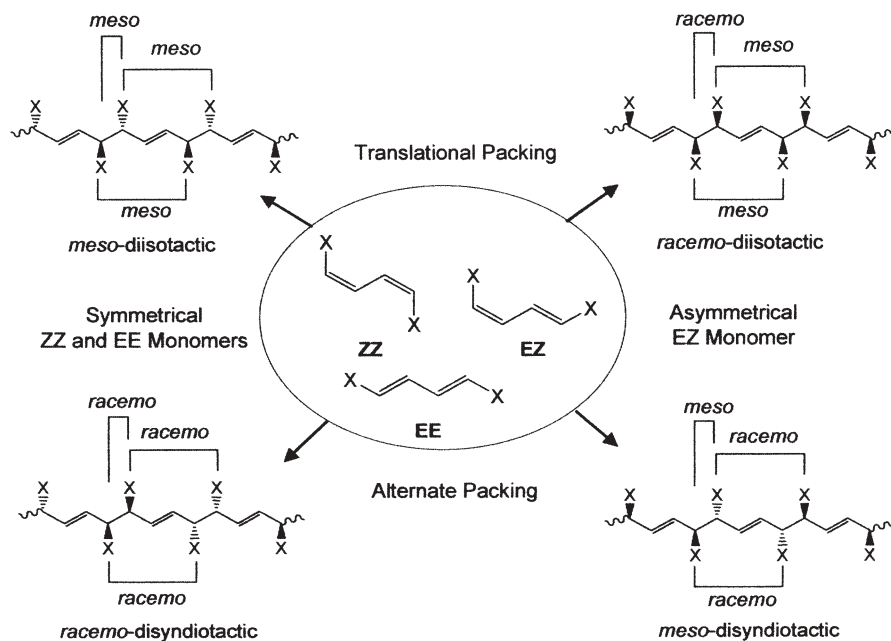


Fig. 13 Stereoregular polymer sequences for *trans*-1,4 polymers obtained from 1,3-diene dicarboxylic acid derivatives

repeating relations are *meso*, the polymer is diisotactic, and when they are *racemo*, it is disyndiotactic. Another relationship is the relative configuration between the vicinal carbon centers, which are also represented by the same terms, *meso* and *racemo* for a symmetrical structure such as poly(muconate)s, or by other terms, *erythro* and *threo* for an asymmetric structure such as poly(sorbates) [90, 94]. The stereochemical structure of the polymers produced during the topochemical polymerization is designed on the basis of the *EZ* configuration and the stacking of the monomers [96].

If the corresponding *EZ* monomers with a different symmetrical structure undergo topochemical polymerization, the polymer produced is a new type of stereoregular polymer. The translational molecular packing of 1-naphthyl-methylammonium (*E,Z*)-muconate (**6**) by the interaction of 2D hydrogen bond networks gives a *racemo*-diisotactic polymer. Similarly, the alternate stacking of 4-methoxybenzyl (*E,Z*)-muconate (**9**) results in the formation of a *meso*-disyndiotactic polymer. Actually, a successful synthesis was reported for the preparation of all four kinds of stereoregular polymers by the stacking control of symmetrical and asymmetrical monomers [96].

Under UV irradiation of the crystals, **6** provided an atactic polymer due to the simultaneous occurrence of isomerization and polymerization, while **9** had no reaction. However, it has recently been revealed that γ -radiation polymerization provides polymers of **6** and **9** without any isomerization to the *EE* isomers. The powder X-ray diffraction profiles of the monomers and polymers indicated that all the polymerizations proceed via a topochemical reaction process keeping a similar and highly crystalline structure. The diffraction pattern of **6** also suggests translational molecular packing in the crystals supported by 2D hydrogen bond networks, being very close to those for **4** and **5**. The structure of the *racemo*-diisotactic polymer obtained from **6** was confirmed by the reaction of the corresponding poly(muconic acid) derived from the ammonium polymers via a solid-state hydrolysis. A pair of adjacent carboxyl groups of the *racemo*-diisotactic poly(muconic acid), which was derived from the polymer of **6**, is located in the same direction along the main chain, while the carboxyl groups of the *meso*-diisotactic polymer are in the opposite direction to the polymer chain. This structural difference is distinguished as a difference in the thermal properties of both polymers.

The polymer obtained from **9** by γ -radiation was soluble in chloroform despite a high crystallinity. The alternating molecular stacking of **9** led to stereoregular polymer formation with a disyndiotactic structure. The *racemo* and *meso* structures of the resulting polymers were confirmed by ^{13}C NMR spectroscopy. A comparison of the NMR data of related polymers concludes that the chemical shifts for a series of the polymers are predominantly determined by the *meso*–*racemo* structure rather than the diisotactic–disyndiotactic one.

Thus, it has been demonstrated that the combination of weak interactions is useful for the design of topochemical polymerization to yield a new type of stereoregular polymer. The weak intermolecular interactions are tolerant of a variety of crystal structure formations and induce a different molecular stack-

ing leading to the different tacticity of polymers. This differs from the strong hydrogen bond network, which is robust and credible but inflexible, for the ammonium derivatives. Historically, syndiotactic and disyndiotactic polymerizations of olefins and polar vinyl monomers have followed isotactic and diisotactic polymerizations, as seen in the polymerizations of styrene, propylene, methacrylates, and crotonates, because well-designed and more sophisticated catalysts are required for the control of syndiotactic propagation [97–99].

The synthesis of *cis*-1,4 polymers was also tried by the use of monomers with an *s-cis* conformation. The solid-state photopolymerization of pyridone derivatives, which is a six-membered cyclic diene amide and is a tautomer of 2-hydroxypyridine, was attempted [100]. Pyridones make hydrogen-bonded cocrystals with a carboxylic acid in the crystalline state. Because the cyclic structure fixes its *s-cis* conformation, if the polymerization proceeds, a *cis*-2,5 polymer would be obtained. Actually, however, the photopolymerization did not occur, contrary to our expectation, but [4+4] photodimerization proceeded when the carbon-to-carbon distance for the dimerization was small (less than 4 Å) [101]. A closer stacking distance of the 2-pyridone moieties might be required for the topochemical polymerization of cyclic diene monomers.

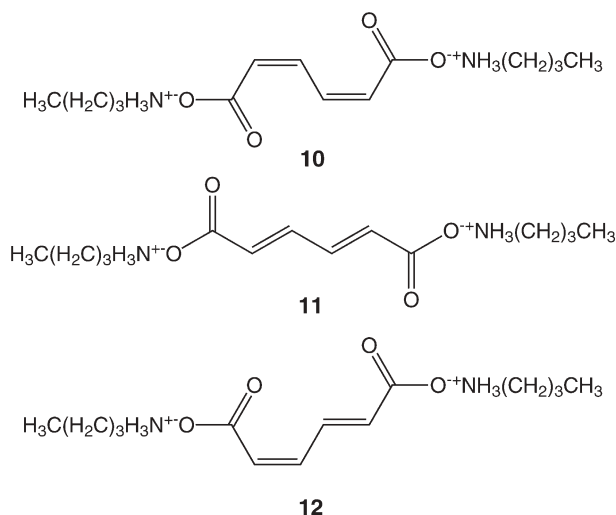
The topochemical polymerization of 1,3-diene monomers based on polymer crystal engineering can be used not only for tacticity but also for the other chain structures such as molecular weight [102], ladder [84] or sheet [103] structures, and also polymer layer structures using intercalation reactions [104–107]. Some mechanical and structural properties have already been revealed with well-defined and highly or partly crystalline polymers [108–111]. A totally solvent-free system for the synthesis of layered polymer crystals was also reported [112].

4 Photoisomerization

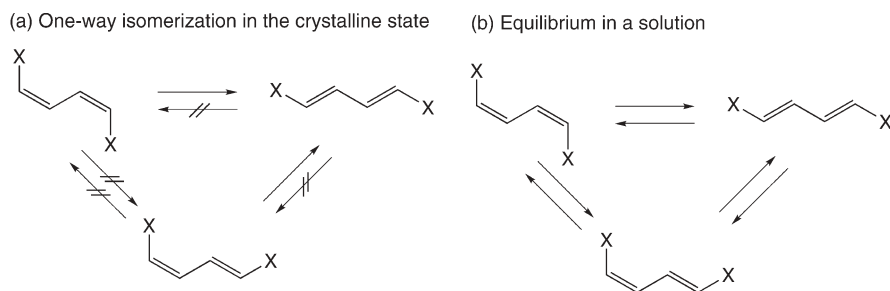
4.1 One-Way *EZ* Photoisomerization of 1,3-Diene Compounds

In contrast to cyclization and rearrangement as the unimolecular reaction, the *EZ* isomerization of olefins is difficult due to a drastic and unenviable change in the size and shape of the occupied space by substituents on the double bond during isomerization in the crystalline state. Some (*Z,Z*)-muconic derivatives provide a geometrical isomer as the photoproduct in a high yield, but not a polymer, under UV irradiation in the crystalline state, as is described in the Introduction (Scheme 1 and Table 1). This isomerization is a crystal-to-crystal reaction with an excellent selectivity, which is completely different from ordinary photoisomerizations.

When crystals of di(*n*-butylammonium) (*Z,Z*)-muconate (**10**) are photoirradiated, isomerization to di(*n*-butylammonium) (*E,E*)-muconate (**11**) proceeds [113]. In this system, no polymer is produced due to the absence of a columnar



structure appropriate for the topochemical polymerization in the crystals. ^1H NMR spectroscopy evidenced that the solid-state photoisomerization is highly stereoselective, i.e., no *E,Z* isomer (**12**) formed during photoirradiation in the crystalline state, in contrast to the photoirradiation in solution resulting in a mixture of three kinds of isomers, and complementary to the exclusive formation of **12** during thermal isomerization in solution (Scheme 12). As summarized in Table 3, the conversion of **10** to **11** achieved 98% for the 10-h irradiation. When **11** was irradiated in the crystalline state under similar conditions, unreacted **11** was recovered. Thus, the isomerization occurs solely one-way from **10** to **11** in the crystalline state. Similar one-way isomerization was observed for a series of muconic acid derivatives, e.g., *n*-alkyl- and branched alkylammonium salts, alkyl esters, and *N*-alkylamides [114]. Monoolefins and azo compounds generally induce reversible *EZ* isomerization in solution and the photoproducts are



Scheme 12 Photoisomerization of 1,3-diene compounds in the crystalline state and solution. **a** One-way isomerization to *EE* isomer in the crystalline state. **b** Usual isomerization in equilibrium observed in solution

Table 3 Photoisomerization of (*Z,Z*)- and (*E,E*)-muconates under irradiation with a high-pressure mercury lamp in the crystalline state or in solution

| Substrate | Temp (°C) | Time (h) | Composition after photoirradiation | | |
|-----------|-----------------|----------|------------------------------------|-----------|-----------|
| | | | <i>ZZ</i> | <i>EE</i> | <i>EZ</i> |
| 10 | 30 | 2 | 79 | 21 | 0 |
| | | 4 | 44 | 58 | 0 |
| | | 6 | 30 | 70 | 0 |
| | | 8 | 5 | 95 | 0 |
| | | 10 | 2 | 98 | 0 |
| 11 | 30 | 8 | 0 | 100 | 0 |
| 10 | 80 ^a | 2 | 60 | 0 | 40 |
| 10 | 30 ^b | 8 | 24 | 33 | 43 |
| 13 | 30 | 24 | 96 | 4 | 0 |
| 15 | 30 | 24 | 59 | 41 | 0 |

^a Thermal isomerization in D₂O.^b Photoisomerization in D₂O.

isolated as a mixture of *cis* and *trans* isomers, whose composition is dependent on the wavelength of light used. Therefore, the one-way *EZ* isomerization of (*Z,Z*)-muconates to the corresponding *E,E* isomers is a new type of solid-state reaction.

4.2

Mechanism of *EZ* Isomerization in Constrained Media

Powder X-ray diffraction has verified that the isomerization occurs via a crystal-to-crystal reaction process, and that the diffraction profiles of the crystals after photoirradiation consist of overlapped patterns of diffraction due to the crystals of **10** and **11**. This indicates that the crystal domains of each isomer exist simultaneously in the crystals accompanied by crystal phase separation during the photoisomerization. Single crystal structure analysis has disclosed that the crystals of **11** as the photoproduct have a symmetry different from that of the starting crystals of **10** (Fig. 14).

The isomerization from **10** to **11** in the crystalline state requires not only the movements of atoms but also a change in the crystal symmetry and the reconstruction of the hydrogen bond network pattern. In the crystals of these primary ammonium carboxylates, 1D ladder-type hydrogen bonds are observed. The isomerization from the *ZZ* to *EE* form is associated with the rotation of carbonyl groups and the change in the hydrogen bond structure in this case. The quantitative transformation of **10** to **11** in the crystalline state suggests that the molecular motion in the crystals occurred cooperatively with the minimum movement of atoms in the crystals via a phase transition from the crystal of **10**

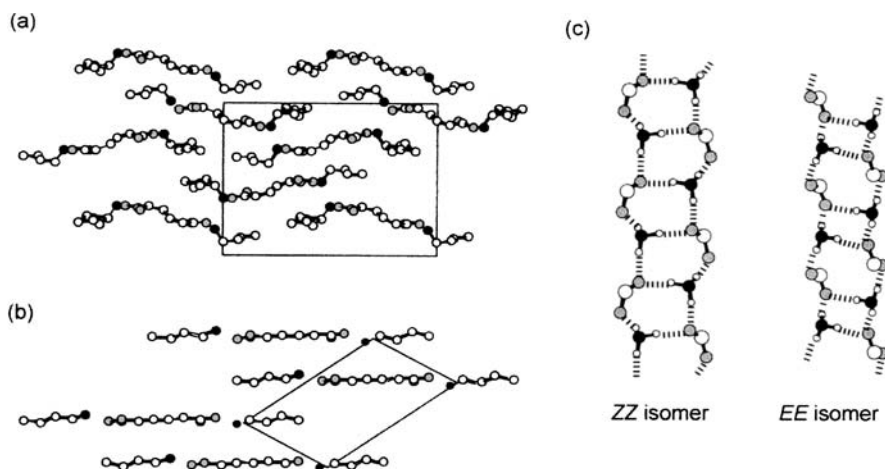
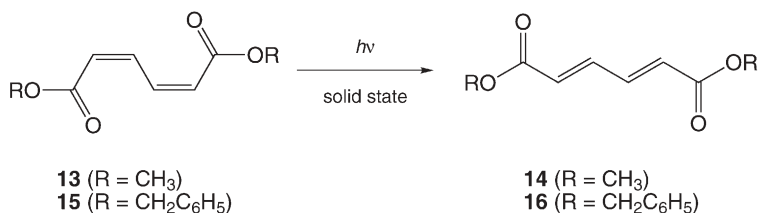


Fig. 14 Crystal structure of a di(*n*-butylammonium) (*Z,Z*)-muconate (**10**) and b di(*n*-butylammonium) (*E,E*)-muconate (**11**) viewed along the crystallographic *a*-axis. Hydrogen atoms are omitted. Hydrogen bond networks run along the crystallographic *a*-axis. Crystallographic data for **10**: monoclinic, $P2_1/n$, $a=5.7715(4)$ Å, $b=20.005(1)$ Å, $c=14.749(1)$ Å, $\beta=96.510(4)^\circ$, $V=1691.9(2)$ Å³, $Z=4$, $D_c=1.132$ g/cm³. A butyl group was disordered. **11**: triclinic, $P(-1)$, $a=5.5246(8)$ Å, $b=7.433(1)$ Å, $c=10.865(2)$ Å, $\alpha=98.88(1)^\circ$, $\beta=100.86(1)^\circ$, $\gamma=104.38(1)^\circ$, $V=414.8(1)$ Å³, $Z=2$, $D_c=1.154$ g/cm³. c One-dimensional ladder-type hydrogen bond networks

to that of **11**. The heterogeneous solid-state reaction is possibly accelerated in a boundary domain between the mutual crystal phases of **10** and **11**.

Thus, the solid-state photoisomerization of **10** proceeds via a topotactic reaction mechanism, while some (*Z,Z*)-muconic esters (e.g., **13** and **15**) can photoisomerize to the corresponding (*E,E*)-muconic esters (**14** and **16**) without any change in the space group, i.e., proceed via topochemical *EZ* isomerization (Scheme 13, Fig. 15) [115].



Scheme 13 Topochemical photoisomerization of dialkyl (*Z,Z*)-muconates **13** and **15** in the crystalline state in a one-way isomerization mechanism

The terms topochemical and topotactic reactions (or polymerizations) have been used in various situations with different meanings in different fields.

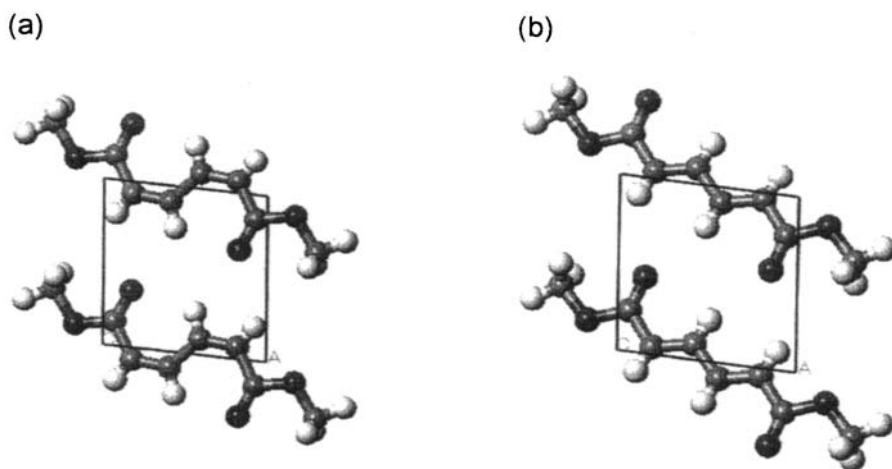


Fig. 15 Crystal structure of **a** dimethyl (*Z,Z*)-muconate (**13**) and **b** dimethyl (*E,E*)-muconate (**14**) viewed along the crystallographic *c*-axis. **13**: triclinic, *P*($\bar{1}$), $a=5.788(7)$ Å, $b=5.722(10)$ Å, $c=6.991(10)$ Å, $\alpha=93.08(4)^\circ$, $\beta=109.55(2)^\circ$, $V=94.79(3)$ Å³. **14**: triclinic, *P*($\bar{1}$), $a=5.81(8)$ Å, $b=5.820(6)$ Å, $c=6.804(13)$ Å, $\alpha=105.09(4)^\circ$, $\beta=106.33(7)^\circ$, $V=92.14(3)$ Å³

Their usage is not always uniform and often confuses our understanding of concepts [2]. In this context, we use the topochemical term in its simplest form as follows: a topochemical reaction is one that proceeds with the minimum movement of molecules and atoms in the solid state, and the symmetry of the product crystal is the same as that of the starting crystal [116].

Recently, Liu et al. proposed the hula-twist process as a volume-conserving *cis*–*trans* photoisomerization reaction mechanism, which is the preferred process for isomerization in confined media such as viscous fluid, rigid matrix, organic glass, and organic crystals, as well as the isomerization of olefins with bulky substituents [117–119]. For the topochemical isomerization process of the muconic derivatives in the solid state, a bicycle-pedal model is possibly preferred. During both bicycle-pedal and hula-twist processes, any change in the volume or shape of the isomerizing molecule is small compared with that of the conventional one-bond flip mechanism, which is usually observed during reactions in solution. Topotactic and topochemical *EZ* isomerizations are advantageous for 1,3-diene derivatives such as muconates, for which both isomers have similar molecular shapes, different from the case of monoolefins. As an exceptional event, unique one-way isomerization of an anthracene-substituted olefin with *Z* configuration has been reported [120, 121], in which the isomerization to the *E* derivative proceeds during photoirradiation in solution, but the reverse reaction hardly occurs due to the presence of the large aromatic substituent which changes its potential energy surfaces at the excited triplet state. Furthermore, several examples have also been found for *EZ* isomerization of olefins in the crystalline state, which seems to be a difficult process [119, 122].

5

Conclusions

Forty years ago, Schmidt first outlined topochemical postulates and pioneered the new field of solid-state organic chemistry. The goal of crystal engineering is the design of organic solids with a desired property or function. Therefore, crystal engineering is rapidly expanding to various fields of chemistry, physics, and biology as well as material sciences and nanotechnology. The solid-state reactions of 1,3-diene compounds have great potential for crystal engineering because they include not only [2+2] dimerization but also stereospecific reactions, such as polymerization and isomerization. Especially, the topochemical polymerization of 1,3-diene compounds is very useful for fabrication of new advanced organic solids. For the topochemical polymerization of 1,3-diene monomers, we are now able to access a rational design of the crystal structure and the crystalline-state polymerizations by the combination of several strong and weak intermolecular interactions. The principles proposed for the topochemical polymerization of 1,3-diene monomers are used in order to predict the polymerization reactivity and design crystalline polymer materials. Supramolecular synthons have been used for constructing the desired monomer stacking in the crystals using weak intermolecular interactions such as the 2D hydrogen bond network, aromatic ring stacking, and CH/ π , CH/O, and halogen–halogen interactions. Solvent-free organic and polymer syntheses including topochemical polymerization will become more important. It is expected that a new kind of organic and materials chemistry will be born from the present renaissance days of crystal engineering, and it will further grow up in the future.

Acknowledgements The author acknowledges Dr. Toshihiro Tanaka, Dr. Toru Odani, Dr. Sadamu Nagahama, and the other members of the research group of Osaka City University. He deeply thanks Prof. Kazuki Sada, Kyushu University, Prof. Mikiji Miyata, and Prof. Kohji Tashiro, Osaka University, for their continuous collaboration and invaluable discussions, and Prof. Kunio Oka, Osaka Prefecture University, for the radiation experiments. This work was financially supported by the Japan Science and Technology Corporation Agency (JST) and by Grants-in-Aid from the Ministry of Education, Culture, Sports, Science, and Technology of Japan.

References

1. Paul IC, Curtin DY (1973) *Acc Chem Res* 6:217
2. Thomas JM (1974) *Philos Trans R Soc Lond* 277:251
3. Cohen MD (1975) *Angew Chem Int Ed Engl* 14:386
4. Green BS, Arad-Yellin R, Cohen MD (1986) *Top Stereochem* 16:131
5. Toda F (1995) *Acc Chem Res* 28:480
6. Ramamurthy V (ed) (1991) *Photochemistry in organized and constrained media*. VCH, New York
7. Ohashi Y (ed) (1993) *Reactivity in molecular crystals*. Kodansha-VCH, Tokyo

8. Toda F (ed) (2002) Organic solid-state reactions. Kluwer, Dordrecht
9. Schmidt GMJ (1971) Pure Appl Chem 27:647
10. Wegner G (1977) Pure Appl Chem 49:443
11. Hasegawa M (1995) Adv Phys Org Chem 30:117
12. Enkelmann V (1984) Adv Polym Sci 63:91
13. Matsumoto A, Matsumura T, Aoki S (1994) J Chem Soc Chem Commun 138
14. Matsumoto A, Odani T (2001) Macromol Rapid Commun 22:1195
15. Matsumoto A (2001) Prog React Kinet Mech 26:59
16. Matsumoto A (2003) Polym J 35:93
17. Cohen MD, Schmidt GMJ (1964) J Chem Soc 1996
18. Braga D (2003) Chem Commun 2751
19. Lahav M, Schmidt GMJ (1967) J Chem Soc B 312
20. Green BS, Lahav, M, Schmidt GMJ (1971) J Chem Soc B 1552
21. Tieke B (1985) Adv Polym Sci 71:79
22. Tieke B (1992) In: Paleos CM (ed) Polymerization in organized media. Gordon and Breach, Philadelphia, p 105
23. Tieke B (1984) J Polym Sci Polym Chem 22:391
24. Tieke B, Chapuis G (1984) J Polym Sci Polym Chem 22:2895
25. Tieke B (1985) Colloid Polym Sci 263:965
26. Schlitter SM, Beck HP (1996) Chem Ber 129:1561
27. Desiraju GR (1989) Crystal engineering: the design of organic solids. Elsevier, Amsterdam
28. Desiraju GR (2001) Nature 412:397
29. Desiraju GR (2002) Nat Mater 1:77
30. MacNicol DD, Toda F, Bishop R (eds) (1996) Comprehensive supramolecular chemistry, vol 6. Solid-state supramolecular chemistry: crystal engineering. Pergamon, Oxford
31. Steed JW, Atwood JL (2000) Supramolecular chemistry. Wiley, Chichester, p 389
32. Tanaka K, Toda F (2000) Chem Rev 100:1025
33. Tanaka K (2003) Solvent-free organic synthesis. Wiley-VCH, Weinheim
34. Itoh Y (1999) In: Ramamurthy V, Schanze KS (eds) Organic molecular photochemistry. Marcel Dekker, New York, p 1
35. Koshima H (2002) In: Toda F (ed) Organic solid-state reactions. Kluwer, Dordrecht, p 189
36. MacGillivray LR (2002) CrystEngComm 4:37
37. Feldman KS, Campbell RF (1995) J Org Chem 60:1924
38. Coates GW, Dunn AR, Henling LM, Dougherty DA, Grubbs RH (1997) Angew Chem Int Ed 36:248
39. Coates GW, Dunn AR, Henling LM, Ziller JW, Lobkovsky EB, Grubbs RH (1998) J Am Chem Soc 120:3641
40. Tanaka K, Toda F, Mochizuki E, Yasui N, Kai Y, Miyahara I, Hirotsu K (1999) Angew Chem Int Ed Engl 38:3523
41. MacGillivray LR, Reid JL, Ripmeester JA (2000) J Am Chem Soc 122:7817
42. Elgavi A, Green BS, Schmidt GMJ (1973) J Am Chem Soc 95:2058
43. Hasegawa M, Saigo K, Mori T, Uno H, Nohira M, Nakanishi H (1985) J Am Chem Soc 107:2788
44. Hasegawa M (1983) Chem Rev 83:507
45. Nakanishi H, Hasegawa M, Kirihaara H, Yurugi M (1977) Nippon Kagaku Zasshi 7:1046
46. Takahashi S, Miura H, Kasai H, Okada S, Oikawa H, Nakanishi H (2002) J Am Chem Soc 124:10944
47. Kasai H, Nalwa HS, Oikawa H, Okada S, Matsuda H, Minami N, Kakuta A, Ono K, Mukoh A, Nakanishi H (1992) Jpn J Appl Phys 31: L1132

48. Goa X, Friscic T, MacGillivray LR (2003) *Angew Chem Int Ed* 43:232
49. Matsumoto A, Matsumura T, Aoki S (1996) *Macromolecules* 29:423
50. Matsumoto A, Yokoi K, Aoki S, Tashiro K, Kamae T, Kobayashi M (1998) *Macromolecules* 31:2129
51. Tashiro K, Kamae T, Kobayashi M, Matsumoto A, Yokoi K, Aoki S (1999) *Macromolecules* 32:2449
52. Matsumoto A, Katayama K, Odani T, Oka K, Tashiro K, Saragai S, Nakamoto S (2000) *Macromolecules* 33:7786
53. Nagahama S, Matsumoto A (2002) *Chem Lett* 1026
54. Tashiro K, Nakamoto S, Saragai S, Matsumoto A, Tsubouchi T (2001) *Polymer* 42:6747
55. Tashiro K, Zadorin AN, Saragai S, Kamae T, Matsumoto A, Yokoi K, Aoki S (1999) *Macromolecules* 32:7946
56. Matsumoto A, Tanaka T, Tsubouchi T, Tashiro K, Saragai S, Nakamoto S (2002) *J Am Chem Soc* 124:8891
57. Matsumoto A, Nakazawa H (2004) *Macromolecules* 37:8538
58. Matsumoto A, Tanaka T, Mori Y, Oka K (in preparation)
59. Matsumoto A, Sada K, Tashiro K, Miyata M, Tsubouchi T, Tanaka T, Odani T, Nagahama S, Tanaka T, Inoue K, Saragai S, Nakamoto S (2002) *Angew Chem Int Ed* 41:2502
60. Saragai S, Tashiro K, Nakamoto S, Kamae T, Matsumoto A, Tsubouchi T (2001) *Polym J* 33:199
61. Matsumoto A, Fujioka D, Kunisue T (2003) *Polym J* 35:652
62. Kane JJ, Liao RF, Lauher JW, Fowler FW (1995) *J Am Chem Soc* 117:12003
63. Dinkelmeier B, Lauher JW, Fowler FW (1998) *Mol Cryst Liq Cryst* 313:259
64. Enkelmann V (1994) *Chem Mater* 6:1337
65. Kiji J, Kaiser J, Wegner G, Schulz RC (1973) *Polymer* 14:433
66. Xiao J, Yang M, Lauher JW, Fowler FW (2000) *Angew Chem Int Ed* 39:2132
67. Hoang T, Lauher JW, Fowler FW (2002) *J Am Chem Soc* 124:10656
68. Itoh T, Nomura S, Uno T, Kubo M, Sada K, Miyata M (2002) *Angew Chem Int Ed* 41:4306
69. Nomura S, Itoh T, Nakasho H, Uno T, Kubo M, Sada K, Inoue K, Miyata M (2004) *J Am Chem Soc* 126:2035
70. Kitaigorodskii AI (1973) *Molecular crystals and molecules*. Academic, New York
71. Desiraju GR (1995) *Angew Chem Int Ed Engl* 34:2311
72. Gavezzotti A (2002) *Synlett* 201
73. Matsumoto A, Matsumoto A, Kunisue T, Tanaka A, Tohnai N, Sada K, Miyata M (2004) *Chem Lett* 33:96
74. Etter MC (1990) *Acc Chem Res* 23:120
75. MacDonald JC, Whitesides GM (1994) *Chem Rev* 94:2383
76. Kinbara K, Hashimoto Y, Sukegawa M, Nohira H, Saigo K (1996) *J Am Chem Soc* 118:3441
77. Meléndez RE, Hamilton AD (1998) *Top Curr Chem* 198:97
78. Aakeröy CB (1997) *Acta Crystallogr B* 53:569
79. Moulton B, Zaworotko MJ (2001) *Chem Rev* 101:1629
80. Holman KT, Pivovar AM, Swift JA, Ward MD (2001) *Acc Chem Res* 34:107
81. Matsumoto A, Odani T, Chikada M, Sada K, Miyata M (1999) *J Am Chem Soc* 121:11122
82. Nagahama S, Inoue K, Sada K, Miyata M, Matsumoto A (2003) *Cryst Growth Des* 3:247
83. Matsumoto A, Nagahama S, Odani T (2000) *J Am Chem Soc* 122:9109
84. Nagahama S, Matsumoto A (2001) *J Am Chem Soc* 123:12176
85. Matsumoto A, Chiba T, Oka K (2003) *Macromolecules* 36:2573
86. Desiraju GR, Steiner T (1999) *The weak hydrogen bond in structural chemistry and biology*. Oxford University Press, Oxford

87. Nishio M, Hirota M, Umezawa Y (1998) *The CH/ π interaction: evidence, nature, and consequences*. Wiley, New York
88. Nishio M (2004) *CrystEngComm* 6:130
89. Sada K, Inoue K, Tanaka T, Tanaka A, Epergyes A, Nagahama S, Matsumoto A, Miyata M (2004) *J Am Chem Soc* 126:1764
90. Farina M (1987) *Top Stereochem* 17:1
91. Farina M, Natta G, Allegra G, Löffelholz M (1967) *J Polym Sci C* 16:2517
92. Farina M, Audisio G, Natta G (1967) *J Am Chem Soc* 89:5071
93. Takasu A, Ishii M, Inai Y, Hirabayashi T, Inomata K (2003) *Macromolecules* 36:7055
94. Matsumoto A (2002) In: Matyjaszewski K, Davis TP (eds) *Handbook of radical polymerization*. Wiley, New York, p 691
95. Tanaka T, Matsumoto A (2002) *J Am Chem Soc* 124:9676
96. Nagahama S, Tanaka T, Matsumoto A (2004) *Angew Chem Int Ed* 43:3811
97. Hatada K, Kitayama T (2000) *Polym Int* 49:11
98. Soga K, Shiono T (1997) *Prog Polym Sci* 22:1503
99. Yasuda H, Ihara E (1997) *Adv Polym Sci* 133:53
100. Odani T, Matsumoto A (2002) *CrystEngComm* 4:467
101. Tanaka K, Toda F (1984) *Nippon Kagaku Kaishi* 141
102. Matsumoto A, Yokoi K (1998) *J Polym Sci A Polym Chem* 36:3147
103. Nagahama S, Matsumoto A (2004) *J Polym Sci A Polym Chem* 42:3922
104. Matsumoto A, Odani T, Sada K, Miyata M, Tashiro K (2000) *Nature* 405:328
105. Matsumoto A, Oshita S, Fujioka D (2002) *J Am Chem Soc* 124:13749
106. Oshita S, Matsumoto A (2003) *Chem Lett* 32:712
107. Matsumoto A, Odani T (2004) *Chem Lett* 33:42
108. Nakamoto S, Tashiro K, Matsumoto A (2003) *Macromolecules* 36:109
109. Nakamoto S, Tashiro K, Matsumoto A (2003) *J Polym Sci B Polym Phys* 41:444
110. Tashiro K, Nakamoto S, Fujii T, Matsumoto A (2003) *Polymer* 44:6043
111. Tashiro K, Kariyo S, Nishimori A, Fujii T, Saragai S, Nakamoto S, Kawaguchi T, Matsumoto A, Rangsiman O (2002) *J Polym Sci B Polym Phys* 40:495
112. Odani T, Matsumoto A (2002) *Polym J* 34:846
113. Odani T, Matsumoto A, Sada K, Miyata M (2001) *Chem Commun* 2004
114. Matsumoto A, Odani T, Yokoi K (1998) *Proc Jpn Acad Ser B* 74:110
115. Saragai S, Tashiro K, Nakamoto S, Matsumoto A, Tsubouchi T (2001) *J Phys Chem B* 105:4155
116. Thakur M (1989) In: Kroschwitz JI (ed) *Encyclopedia of polymer science and engineering*, vol 15. Wiley, New York, p 362
117. Liu RSH (2002) *Photochem Photobiol* 76:580
118. Liu RSH (2001) *Acc Chem Res* 34:555
119. Kaupp G (2002) *Photochem Photobiol* 76:590
120. Arai T, Tokumaru K (1993) *Chem Rev* 93:23
121. Arai T (1999) In: Ramamurthy V, Schanze KS (eds) *Organic molecular photochemistry*. Marcel Dekker, New York, p 131
122. Kaupp G (1995) *Adv Photochem* 19:119

Author Index Volumes 251–254

Author Index Vols. 26–50 see Vol. 50

Author Index Vols. 51–100 see Vol. 100

Author Index Vols. 101–150 see Vol. 150

Author Index Vols. 151–200 see Vol. 200

Author Index Vols. 201–250 see Vol. 250

The volume numbers are printed in italics

Alberto R (2005) New Organometallic Technetium Complexes for Radiopharmaceutical Imaging. 252: 1–44

Anderson CJ, see Li WP (2005) 252: 179–192

Armitage BA (2005) Cyanine Dye–DNA Interactions: Intercalation, Groove Binding and Aggregation. 253: 55–76

Arya DP (2005) Aminoglycoside–Nucleic Acid Interactions: The Case for Neomycin. 253: 149–178

Bailly C, see Dias N (2005) 253: 89–108

Barbieri CM, see Pilch DS (2005) 253: 179–204

Boschi A, Duatti A, Uccelli L (2005) Development of Technetium-99m and Rhenium-188 Radiopharmaceuticals Containing a Terminal Metal–Nitrido Multiple Bond for Diagnosis and Therapy. 252: 85–115

Braga D, D’Addario D, Giaffreda SL, Maini L, Polito M, Grepioni F (2005) Intra-Solid and Inter-Solid Reactions of Molecular Crystals: a Green Route to Crystal Engineering. 254: 71–94

Chaires JB (2005) Structural Selectivity of Drug–Nucleic Acid Interactions Probed by Competition Dialysis. 253: 33–53

Correia JDG, see Santos I (2005) 252: 45–84

D’Addario D, see Braga D (2005) 254: 71–94

Dervan PB, Poulin-Kerstien AT, Fechter EJ, Edelson BS (2005) Regulation of Gene Expression by Synthetic DNA-Binding Ligands. 253: 1–31

Dias N, Vezin H, Lansiaux A, Bailly C (2005) Topoisomerase Inhibitors of Marine Origin and Their Potential Use as Anticancer Agents. 253: 89–108

Duatti A, see Boschi A (2005) 252: 85–115

Edelson BS, see Dervan PB (2005) 253: 1–31

Edwards DS, see Liu S (2005) 252: 193–216

Escudé C, Sun J-S (2005) DNA Major Groove Binders: Triple Helix-Forming Oligonucleotides, Triple Helix-Specific DNA Ligands and Cleaving Agents. 253: 109–148

Fechter EJ, see Dervan PB (2005) 253: 1–31

Fujiwara S-i, Kambe N (2005) Thio-, Seleno-, and Telluro-Carboxylic Acid Esters. 251: 87–140

Giaffreda SL, see Braga D (2005) 254: 71–94

Grepioni F, see Braga D (2005) 254: 71–94

Ishii A, Nakayama J (2005) Carbodithioic Acid Esters. 251: 181–225

Ishii A, Nakayama J (2005) Carboselenothioic and Carbodiselenoic Acid Derivatives and Related Compounds. 251: 227–246

Jones W, see Trask AV (2005) 254: 41–70

Kambe N, see Fujiwara S-i (2005) 251: 87–140

- Kano N, Kawashima T (2005) Dithiocarboxylic Acid Salts of Group 1–17 Elements (Except for Carbon). 251: 141–180
- Kato S, Niyomura O (2005) Group 1–17 Element (Except Carbon) Derivatives of Thio-, Seleno- and Telluro-Carboxylic Acids. 251: 19–85
- Kato S, see Niyomura O (2005) 251: 1–12
- Kaul M, see Pilch DS (2005) 253: 179–204
- Kaupp G (2005) Organic Solid-State Reactions with 100% Yield. 254: 95–183
- Kawashima T, see Kano N (2005) 251: 141–180
- Komatsu K (2005) The Mechanochemical Solid-State Reaction of Fullerenes. 254: 185–206
- Lansiaux A, see Dias N (2005) 253: 89–108
- Li WP, Meyer LA, Anderson CJ (2005) Radiopharmaceuticals for Positron Emission Tomography Imaging of Somatostatin Receptor Positive Tumors. 252: 179–192
- Liu S (2005) 6-Hydrazinonicotinamide Derivatives as Bifunctional Coupling Agents for ^{99m}Tc -Labeling of Small Biomolecules. 252: 117–153
- Liu S, Robinson SP, Edwards DS (2005) Radiolabeled Integrin $\alpha_v\beta_3$ Antagonists as Radiopharmaceuticals for Tumor Radiotherapy. 252: 193–216
- Maini L, see Braga D (2005) 254: 71–94
- Matsumoto A (2005) Reactions of 1,3-Diene Compounds in the Crystalline State. 254: 263–305
- Meyer LA, see Li WP (2005) 252: 179–192
- Murai T (2005) Thio-, Seleno-, Telluro-Amides. 251: 247–272
- Nakayama J, see Ishii A (2005) 251: 181–225
- Nakayama J, see Ishii A (2005) 251: 227–246
- Niyomura O, Kato S (2005) Chalcogenocarboxylic Acids. 251: 1–12
- Niyomura O, see Kato S (2005) 251: 19–85
- Paulo A, see Santos I (2005) 252: 45–84
- Pilch DS, Kaul M, Barbieri CM (2005) Ribosomal RNA Recognition by Aminoglycoside Antibiotics. 253: 179–204
- Piwnica-Worms D, see Sharma V (2005) 252: 155–178
- Polito M, see Braga D (2005) 254: 71–94
- Poulin-Kerstien AT, see Dervan PB (2005) 253: 1–31
- Robinson SP, see Liu S (2005) 252: 193–216
- Sakamoto M (2005) Photochemical Aspects of Thiocarbonyl Compounds in the Solid-State. 254: 207–232
- Santos I, Paulo A, Correia JDG (2005) Rhenium and Technetium Complexes Anchored by Phosphines and Scorpionates for Radiopharmaceutical Applications. 252: 45–84
- Scheffer JR, Xia W (2005) Asymmetric Induction in Organic Photochemistry via the Solid-State Ionic Chiral Auxiliary Approach. 254: 233–262
- Sharma V, Piwnica-Worms D (2005) Monitoring Multidrug Resistance P-Glycoprotein Drug Transport Activity with Single-Photon-Emission Computed Tomography and Positron Emission Tomography Radiopharmaceuticals. 252: 155–178
- Sun J-S, see Escudé C (2005) 253: 109–148
- Toda F (2005) Thermal and Photochemical Reactions in the Solid-State. 254: 1–40
- Trask AV, Jones W (2005) Crystal Engineering of Organic Cocrystals by the Solid-State Grinding Approach. 254: 41–70
- Uccelli L, see Boschi A (2005) 252: 85–115
- Vezin H, see Dias N (2005) 253: 89–108
- Williams LD (2005) Between Objectivity and Whim: Nucleic Acid Structural Biology. 253: 77–88
- Xia W, see Scheffer JR (2005) 254: 233–262

Subject Index

- Acyl halides 172
Acyloin 170
Adiponitrile 17
Aldehydes, Knoevenagel condensation 161
Algorithm, genetic 65
Alkenes 120
–, bromination, gas-solid 235
Alkenyl carbon 230
Alkyl halogenides 135
N-Alkylfuran-2-carboxyanilides 32
Alkyl lithium 200
Alloxane hydrate 157
Amides 136
Amines 76
Amino acids 105, 116
Aminomethylations 128
4-Aminopyridine 189, 191
Ammonia 76–79
Aniline 144
Annealing, simulated 65
Anthracenes 167, 178, 193
Anthracenophane 168
Antipyrin 143
Aryl iodide 146
Arylamines 141
Asymmetric synthesis, absolute 234
Atom economy 96, 175
Azafullerene 198
Azines 154
Aziridines 222
Azo coupling 147
Azo dye 148
Azomethine ylide 175, 198

Ball milling 186, 187
Barbituric acids 140, 148, 161
Benzil 179
Benzocyclohexadiene 258
Benzodiazepine 159

Benzoin 179
Benzothiazoles 107
Benzoylation process, solvent-free 23
Benzoylation reactions 22
2-Benzoylbenzofuran 18
Benzylidene aniline 118
Bingel reaction 201, 202
Bisallenenes 168
Boronic esters 130
BrCN 77
Bromination, gas-solid, alkenes 235
–, stereoselective 3
Bromine 77, 98, 118
tert-Butyldimethylsilyl chloride 7

C₇₀ 188–191, 200–204
C₁₂₀ 188, 191, 199
Calixarene 187
Cambridge Structural Database 68
Cannizzarro reactions 9
Carbodiimide 165
Carbonic acid derivatives, cyclic 140
Carboxylic anhydrides, cyclic 140
Cascade reactions 159, 172
CCD camera 267
CH/ π interaction 290, 291
Chalcone, bromination 2
Charge-transfer complex 43, 44
Cinnamic acid 117, 120, 266
Claisen reactions 9
ClCN 77
Cleavage plane 54, 63
Cocrystal 41, 46, 54, 57, 58, 66
Complex, crystalline molecular 42
Conglomerate complex 25
Coordinatoclathrate compound,
optically pure 238
Crystal engineering 42, 68, 71, 264, 265,
287

- Crystal packing analyses 96
Crystal shearing 54
Crystals, chiral 207
–, single crystal-to-single crystal process 249, 251
Crystal-to-crystal reactions 25
Crystal-to-crystal transformation 212, 214
Cucurbit[7]uril 188
Cyanates 132
Cyanogen bromide 134
Cyanoguanidine 127
Cyclization 168
Cycloadditions 164
–, [2+2] 207, 209
 γ -Cyclodextrin 187, 188
Cyclodimerization, [2+2] 263
Cyclophane 269
Cyclopropanation 201
Cysteine 159, 177

DBU 201, 202
DDQ 178
Degrees of freedom 65
Deliquescent salts 130
Dendrimer 143
Diacetylene 283
Dialkylamines 136
Diamines 157
Diarylureas 139
Diazo compound 197
Diazonium salts 145
Diazotization 144
Dibenzobarrelene 246
Di(4-chlorobenzyl) (Z,Z)-muconate 275
Diels-Alder adducts 116, 167, 172
1,3-Diene compounds 263
Diethyl (Z,Z)-muconate 274
Diffusion 43, 54
Dihydrofuran 203
Dimedone 162
Dimer 188–192, 199, 204
Dimerization 264
–, linear 162, 163
Dimethylthiocarbamoyl chloride 121
Dinitriles 58
Diolefin crystals 268
Direct-space approach 65
Dithiazine 229
Dumbbell 191, 191

Electrochemical reduction 192
Electron transfer reactions 102
Enantiomerism, conformational 254
Enantioselectivity 228
Environmental protection 186
Equilibrium 189, 193
Ethyl 3-methylbutanoate 9

Faujasite type Y zeolites 242
Ferrocenyl dicarboxylic acid 84
Fiber period 282
Formic acid 81
1-Formylnaphthalene 10
Fulleroid 197
Fulleropyrazoline 197
Fulleropyrrolidine 199, 200
Fullerotriazoline 198

Gas sensors 110
Gas-solid reactions 5, 73, 100, 225
Glycine 197–199
Green chemistry 43, 53, 71
Grignard reagent 200
Grinding 41, 100
–, attractive aspects 43
–, competition experiment 49
–, displacement via 49
–, distinct cocrystal products 53
–, drawbacks 43
–, followed by heating 48
–, for preparation of cocrystal seeds 58
–, kinetics 59, 63
–, mechanism 43, 68
–, polymorph control 59
–, sublimation during 66

Halogen-halogen interaction 290
Halogenohydrides 121
Heterocumulenes 125
Hexadiynediols 113
Hexahydroanthracene 178
Host-guest cocrystal 284
HSVM 186–204
Hula-twist mechanism 115, 170, 301
Hydrazine derivatives 152
Hydriazines 154
Hydrogen abstraction 207, 218, 222, 230, 255
Hydrogen bond network 287, 299
Hydrogen bonding 42–51, 54, 57, 63–68, 83, 86

- Hydrogenations 117
Hydroquinone 126
2-Hydroxy-3-naphthyl-*p*-methylbenzoate 24
- Imbibitions 110
Imides, acyclic 57
Imines 18
–, formation 152
Iminium hydrohalogenides 108
Inclusion complex 4, 13
Inclusion compounds 1, 60, 61
Inclusion crystal 4
Inclusion efficiencies 111
Inductor, chiral 242
Initiation 275
Intercalation 297
Intrasolid reactions 101
Invertomers 170
Iodine 116
Ionic chiral auxiliaries 233, 244, 246, 259
Isomerization, one-way 298
Isothiocyanates 126
- Ketene iminium salts 132
Ketoalcohols 21
Kinetics 59, 63
Kitaigorodskii rule 290
Kneading 73, 87, 90
Knoevenagel condensation 161
- β -Lactams 222, 239
–, thietane 211
Ladder 297
Ladderane 272
Layered inorganic solids 49
- Malonic acid 87
Malonic acid ester 201
Malononitrile 162
Mannitol 131
Mechanical energy 185, 186
Mechanochemistry 43, 84, 109, 185
Meldrum acid 162
Melt reactions 100
Menthol 7
2-Mercaptobenzothiazole 105
2-Mercaptopyridine 30
Mesitylacetophenone derivatives, photocyclization 252
Methanofullerene 197
- Methyl iodide 129
p-Methylbenzonitrile 17
2-Methylcyclohexanone 11
Michael addition 162, 204
Microwave energy 48
Milling 100
Molecular ladders 270
Molecular packing 99
Molecular torsion 65, 66
Monothioimides 210
Monte Carlo 65
- N/O acetals 117
–, semi- 130
Nanocrystals 270
Naphthol 147
1-Naphthylmethylammonium *n*-alkanoates 291
Nitrations 143
Nitrosobenzenes 146
Nitrosonium nitrates 102, 177
Nitroxyls 102
Nonlinear optical (NLO) materials 45
Norrish/Yang type II reaction 248
- N*-Octadecyl-sorbamide 289
One-bond flip mechanism 301
One-electron transfer 193, 196
Organic azide 198
Organometallic cocrystal 53, 58
Organozinc reagent 201
Oxazolidines 117
Oxazolidinone 240
Oxidations 177
Oxiranes 123
 α -Oxoamides 239, 245
- Pasteur resolution procedure 258
Penicillamine 159
Pentacene 194, 195
Perovskite, layered 267
Phase rebuilding 96
Phenacyl bromides 19, 172
Phenanthroline 89
Phenolates 132
Phenoxides 130
Phenyl sulfide 16
Phenylboronic acid 139
Phenylboronic esters 130
Phenylenediamines 106
Phosgene 132

- Photochemistry, asymmetric induction 233
Photochrome 168
Photoconversion 114
Photocyclization 33
–, Yang 254
Photocycloaddition, [2+2], untermolecular 235
Photodimerization 37, 60, 83, 164, 265
–, [4+4] 297
Photodimers 115
Photoirradiation 32
Photoisomerization, *cis,trans*- 247, 301
–, one-way EZ 297
–, solid-state 298
Photopolymerization, [2+2], asymmetric 268
Photoreaction, solid-state 264
Photorearrangement, di- π -methane (Zimmermann) 236, 246
–, oxadi- π -methane 257
Photostationary state 229
Phthalazine 195
Phthalic anhydrides 141
Phthalimides 139
Physicochemical properties 43, 48
Pimelonitrile 18
Platinum 168
Polymerization 163, 188
–, topochemical 272
Polymers, stereochemistry 292
Polymorph control 59
Polymorphism 42, 43, 58, 62, 63, 84
Polyols 131
Prato reaction 199, 201
Pyrazoline 197
Pyrazolones 148
Pyrone 162

Quinhydrone 43, 44
Quinoxalinone 157

Racemic complex 25
Rap-Stoermer reactions 18
Reactions, enantioselective 1
–, photochemical 82
–, stereoselective 1
–, topochemical 82
Reactivity, chemical 53
Reductions 176
Reformatsky-type 200

Reprecipitation method 270
Rietveld refinement 66, 67
Robinson annelation, one-pot process 11

Salicylaldehydes 19
Sandmeyer reaction 146
Sandwich complexes 111
Schiff bases 108
Schmidt rule 267
Seeding 74, 85, 86
Semicarbazone 153
Sensitizer, chiral 257
O-Silyl ethers 8
O-Silylation reactions 6
SNOM 101, 177
Solid-gas reactions 75, 90
Solid-solid reactions 5, 73, 87, 90, 100
Solid-state reductions 176
Solution crystallisation 42
Solvent-drop grinding 59, 60–63
Solvent-free reactions 6, 100
Sorbic acid 266
Space groups 210, 228
– –, chiral 214, 216, 221, 229, 235
Stacking model 279
Stilbene 2
STM 191
Stobbe condensation 6
Stream bed 101
Sulfadimidine 48
Sulfamethazine 48
Sulfonamides 136, 141
Supermicroscopic studies 96
Surface passivation 113
Suspension medium 4
Synthons, supramolecular 287

TADDOLS 113
TEMPO 112
2,4,4,6-Tetrabromocyclohexa-2,5-dienone 5
Tetracene 194
7,7,8,8-Tetrakis(alkoxycarbonyl)-quinodimethanes 286
Tetrazine 195
Thietane 208, 210
Thioamides 209, 226
–, α,β -unsaturated 226
Thiobenzophenone 208, 224
Thiocarbamates 216
Thiocarbonyl compounds 207

- Thiocyanates 134
Thioglycolic acid 116
Thiohydantoin 105
Thioimides 209
Thioketene 230
Thioketones 209, 219, 225
Thiolactam 227, 229
Thiolactone 217
Thiolates 134
Thiols 134
Thiones 224, 225
–, conjugated 226
Thioureas 125
Thorpe reactions 16
Triacetylene, 1,6-polymerization 285
Tribochemistry 101
Triethylsilyl chloride 7
Trimer 188, 191
Trimethylamine 138
Tri-*o*-thymotide 124
Troeger's bases 128, 129
Tropolone alkyl ethers, photocyclization 238
Tyrosine, bromination 143
Ultrasound 48
UMW polymers 274
UV-irradiation 60
Vapors, separation 111
Verdazyl radicals 102
Vibration mixer-mill 186
Viehe salt 118–120, 134, 137
N-Vinylcarbazole 125
N-Vinylisatin 117
N-Vinylpyrrolidinone 122, 162
Volatility 48
Wagner-Meerwein rearrangement 170
Water medium 12
X-ray crystallography 190
XRD, powder 45, 49, 59, 60, 65–68
–, single crystal 43–46, 48, 51, 54, 59, 64, 65
Zeolites 109
–, chirally modified 241